Primitive magmas in convergent margins and at oceanic spreading ridges: evidence from early formed phenocryst phases and their melt inclusions

by

Ingvar Atli Sigurdsson
BSc. (Hons). University of Iceland

Submitted in fulfilment of the requirements
for the degree of
Doctor of Philosophy (Geology)
University of Tasmania

May, 1994

STATEMENT

This thesis contains the results of research done in the Geology Department, University of Tasmania between 1990 and 1994. Part of the material presented in chapter 3 has been published as:

Sigurdsson I.A., Kaminetsky V.S., Crawford A.J., Eggins S.M. and Zlobin S.K., 1993. Primitive island arc and oceanic lavas from the Hunter Ridge-Hunter fracture zone. Evidence from glass, olivine and spinel compositions. *Mineralogy and Petrology*, **47**: 149-169.

This thesis contains no material which has been accepted or submitted for the award of any other higher degree or graduated diploma in any tertiary institution an to the best of the author's knowledge and belief, the thesis contains no material previously published or written by another person, except where due reference is made in the text of the thesis.

(i) I agree/~~do not agree~~ that the thesis may be made available for loan.

(ii) I agree/~~do not agree~~ that the thesis may be made available for photocopying.

Ingvar A. Sigurdsson
University of Tasmania
May, 1994.

ABSTRACT

The Heating Stage, and Applications to Studies of Basalt Crystallization

Melt inclusions in early formed minerals in mantle-derived magmas can give vital information on the crystallization history of the magma. By carefully applying the microthermometric (heating stage) technique of homogenizing the inclusions under visual control, and taking into account the possible effects of processes such as Fe^{2+} - Mg re-equilibration and H_2 diffusion, both the crystallization temperature and the melt composition for that particular inclusion can be accurately estimated. The behaviour of melt inclusions upon heating in each magma suite studied must be tested via a series of kinetic experiments to estimate optimum heating rates; only after these have been done can the technique be applied with confidence. After the experiments, results are further tested and checked using established mineral-melt equilibria before they can be accepted as giving the true crystallization temperature and melt composition.

At the Australian-Antarctic Discordance (AAD) on the Southeast Indian Ridge spreading centre, a site proposed to be underlain by abnormally cold mantle, early formed phenocryst phases are as primitive as those found at "normal" segments of the oceanic spreading systems. Results from heating stage experiments give crystallization temperature of 1240°C for olivine $Fo_{89.7}$, which is the same temperature as obtained from olivine of the same composition from MORB at normal spreading segments. Similarly, the calculated parental melt composition in equilibrium with the most magnesian olivine ($Fo_{90.4}$) is similar to the parental melt calculated for other MORB suites (Dmitriev et al., 1985; Sobolev et al., 1989). This suggests that there is unlikely to be any significant temperature difference between the upper mantle beneath the AAD and normal sub-spreading ridge upper mantle.

The difference in glass compositions (e.g. generally higher K_2O contents) between the AAD and adjacent areas is most pronounced in the most evolved samples, and the geochemical trend defined by these glasses cannot be explained by crystal fractionation involving olivine, plagioclase or clinopyroxene. This difference is therefore likely to be caused by mixing of a normal MORB magma with a magma with low TiO_2 and FeO*, and high SiO_2, Na_2O and K_2O contents This mixing occurs early in the history of the magma suite, as these variations recorded from quenched pillow glasses are also present in melt inclusions in early formed olivine phenocrysts..

Magma Genesis in the North Fiji Basin and Hunter Ridge

At the southernmost part of the North Fiji Basin in an area around the mainly submarine Hunter Ridge, glass geochemistry of dredged rocks reflects the complexity of an area where a back-arc basin spreading ridge is transecting a youthful intra-oceanic island arc. Magma types identified from the glass geochemistry include boninites, island arc tholeiites, back-arc basin basalts, incompatible element enriched-basalts, and mixed magmas and rhyolites. Each magma group has olivine phenocrysts and spinel inclusions in olivine of distinct composition. Although most magma groups have similar CaO contents, CaO in olivine varies significantly between each group, being lowest in the boninites and highest in the back-arc basin basalts and the incompatible element enriched basalts, with the island arc tholeiites intermediate; this is likely to reflect the significantly different silica activity in melts from the different magma suites.

A new classification scheme is proposed for all available basalt glass analyses from the North Fiji Basin back-arc basin, using K_2O/TiO_2, K_2O/Al_2O_3 and TiO_2/Al_2O_3; this scheme effectively distinguishes between the N-MORB-like glasses and two groups of incompatible element-enriched back-arc basin basalt glasses. Two distinct enrichment trends are evident, suggesting mixing of N-MORB with two types of enriched magmas with different K_2O/TiO_2. One of these is likely to be related to ocean island basalts from the Rotuma-Samoan lineament, whereas the other could represent influences from E-MORB-like magmas believed from dredged seamount evidence to be present in the South Fiji Basin.

New whole-rock analyses of back-arc basin basalts from the North Fiji Basin show that the basalts are strongly depleted in the light rare earth elements and Nb, but enriched in Rb, Ba and K, suggesting that they are derived from a source more refractory than the N-MORB source, with the addition of a slab-derived fluid.

Melt inclusion studies of a single North Fiji Basin basalt sample indicate a simple evolutionary history from a single parental melt by fractionation of olivine only.

Andesites from dredge station 108 on the Hunter Ridge are distinct in composition from the other magma groups defined from this region during this study, and show strong mineralogical evidence for magma mixing. Olivine phenocrysts show bimodal compositional distribution ranging from Fo_{93-82}, and both olivine and clinopyroxene show complex zoning patterns; furthermore, two main groups of Cr-spinel inclusions occur in olivines. The most magnesian olivine crystallized at approximately 1350°C from a melt with approximately 17% MgO. Significant variations are evident in compositions of melt inclusions, indicating mixing between two or more magma types.

Melt inclusion studies, together with whole-rock major and trace element analyses, suggest that these mixed andesites evolved through open system fractionation, during which frequent magma mixing of cogenetic refractory island arc tholeiitic magmas and fractionation of olivine and clinopyroxene buffered the major element composition, but caused an increase in the incompatible minor elements and separated, for example, Y from Zr. Addition of back-arc basin basalt magmas to this system, when the southward propagating spreading centre in the North Fiji Basin transected the Hunter Ridge, provided this additional component to the mixing, as is evident from compositions of Cr-spinel inclusions in olivines and trace element contents of the andesites.

Primitive Basaltic Magmas in Iceland

Whole-rock compositions of the most magnesian tholeiites from Iceland are too magnesian to be in equilibrium with their most magnesian olivines, suggesting that they must have accumulated some olivine. Tholeiites with olivines > Fo_{90} are all depleted in the light rare earth elements, whereas the only light rare earth element enriched sample has no olivines more magnesian than $Fo_{84.6}$. Cr-spinel inclusions are also different in the enriched tholeiite, and no evidence for mixing between the enriched and depleted tholeiites was found. A single sample from the Krafla system in northern Iceland contains two populations of Cr-spinel inclusions in olivines, due to either mixing between the depleted Icelandic tholeiites and more typical N-MORB, or because of assimilation of clinopyroxene and plagioclase from entrained gabbroic xenoliths.

A review of published melt inclusion studies on phenocrysts in Icelandic tholeiites (Gurenko et al., 1988b; Hansteen, 1991) reveals that the calculated primary melts of Gurenko et al. (1988b), and a parental melt calculated herein from a composition from Hansteen (1991), are both too rich in diopside to be in equilibrium with a mantle residue. This is likely to be caused by assimilation of clinopyroxene, since both these studies were performed on samples containing abundant gabbroic xenoliths and resorbed clinopyroxene xenocrysts.

ACKNOWLEDGMENTS

A number of people have helped in many different ways during the course of this study. I therefore am pleased to acknowledge:

Professor David H. Green and Dr. Tony Crawford for supervision and support, and for keeping track of all aspects of this project throughout.

Dr. Leonid Danyushevsky for supervising parts of the project and for leading me into, and then out of, the abyss of melt inclusion studies. Leonid and Helena Psotova are thanked for providing me with a spare bed for the last few weeks of my time in Hobart.

Dr. Vadim (Dima) Kamenetsky for invaluable assistance, guidance and encouragement during data gathering. Dima Jr. and Maya Kamenetsky are thanked for their friendship during their time in Hobart.

Wieslaw Jablonski for keeping the Cameca microprobe running and finding solutions for all the problems I could confront him with.

Phil Robinson and Nilar Hlaing for instruction and assistance with sample preparation and the running of the XRF machine.

The post-doctoral and visiting fellows working in this department at various times over the last few years for friendship and encouragement, especially Drs. Steve Eggins, Trevor Falloon, Russell Sweeney, Chris Ballhaus, Bob Musgrave, Yoshi Tatsumi, Wayne Taylor, John Sinton, Alex Andronikov and many others.

Simon Stevens and Naomi Deards for lapidary work.

The secretaries, Jeanette Hankin and Julie Beattie for invaluable assistance.

All my fellow students in the Geology Department and in CODES through the years, especially Massimo Gasparon, Ruth Lanyon, Alicia Verbeeten, Fernando Della-Pasqua, Udi Hartono, Greg Yaxley, Geoff Nichols, Mike Seitz, Andrew McNeill, Marcel Kamperman, Sampan Singharajwarapan, Ai Yang, Aung Pwa, Mohammad Adabi, Paul Kitto, Steve Hunns, Mark Doyle and many, many others.

All the staff and students of the Geology Department and CODES for friendship over the years, and for introducing me to the magic world of Cricket.

The Icelandic Government Student Loan Fund for financial assistance.

The late George Wilson, and Ruth Dudgeon for renting out Rosebank, 11 Hampden Road, at very affordable price, but especially for their friendship.

All the occupants of Rosebank (including Rocket) through the years.

My parents, brothers and sister for support throughout this project and for financial support, especially during the last few months.

TABLE OF CONTENTS

LIST OF TABLES

Chapter 2

Chapter 3

Chapter 4

Chapter 5

Chapter 6

LIST OF FIGURES

Chapter 1

Chapter 2

Chapter 3

Chapter 4

Chapter 5

Chapter 6

INTRODUCTION

This thesis documents a study of aspects of the petrogenesis of three contrasting suites of mantle-derived magmas from oceanic regions, focussing on primitive phenocrysts (mainly olivine and spinel) and their melt inclusions, and the information they can yield about their source mantle compositions, conditions of partial melting, and subsequent magmatic evolution. In particular, some emphasis is placed on a microthermometric (heating stage) study of melt inclusions in olivines from these suites, a relatively new technique in igneous petrology studies of mantle-derived magmas.

Chapter 1 describes the heating stage apparatus, and the methodology employed in heating stage studies of inclusions in olivine phenocrysts, based on homogenization of inclusions under visual control. Experimental procedure, the treatment of the data obtained, and some common problems inherent in the technique (e.g. diffusion of volatiles, Fe^{2+}- Mg subsolidus re-equilibration, mass exchange between the host olivine and the melt inclusion) are discussed in some detail.

Chapter 2 reports a study of mid-ocean ridge basalts from the Australian-Antarctic Discordance segment of the Southeast Indian Ridge. This segment of the global spreading ridge system has been claimed to overlie abnormally cold upper mantle, due to downwelling induced here by the convergent interaction of two major mantle convection cells. The aim of this study is to test whether there are any indications from the mineralogy and melt inclusions for the existence of abnormally cold mantle beneath the Discordance. New analyses of quenched glasses, and mineral compositions in selected samples are detailed, and the heating stage technique is applied to establish the crystallization temperatures and the compositions of the melts from which the host minerals crystallized.

Chapter 3 provides an extensive set of glass analyses of a new series of magma suites dredged from the southernmost part of the North Fiji back-arc basin and adjacent Hunter Ridge. This area is of particular interest, as it contains a magmatic record of the products of (i) a newly-formed intra-oceanic arc (the Hunter Ridge, probably less than 5 Ma old), and (ii) interactions at the orthogonal intersection between the southern spreading segment in the North Fiji Basin and this new arc. Magma suites present in this region were found to include two suites of back-arc basin basalts, two suites of boninites, some complex magnesian andesites which show good evidence of magma mixing in their genesis, some basalts transitional between enriched MORB and ocean island basalts, and sodic rhyolites.

In chapter 4, all available basalt analyses from the North Fiji Basin are compiled and a classification scheme is suggested to distinguish between the several diverse magma suites present in this back-arc basin. New whole-rock major and trace element analyses are presented, and the heating stage technique is applied to basalts from a single dredge station.

Chapter 5 reports a heating stage study of the unusual magnesian andesites from the Hunter Ridge. These contain a wide range of olivine phenocryst compositions (to Fo_{94}); olivine phenocrysts, and the mineralogy and whole-rock geochemistry show strong evidence for magma mixing. The aim of this study was to use the heating stage technique to identify the magmatic components taking part in this magma mixing, to establish their crystallization temperatures, and to assess their tectono-magmatic significance.

Chapter 6 deals with a suite of primitive tholeiites from Iceland. Systematic analysis of olivine phenocrysts and their spinel inclusions enables confident identification of the most magnesian olivines in each sample. These are compared with olivine compositions calculated to be in equilibrium with the whole-rock compositions. Based on these data, an assessment is made of the cumulate versus liquid nature of these lavas, and the information they offer towards identifying their primary magma compositions is discussed. Published melt inclusion studies on Icelandic tholeiites are reviewed, and on the basis of all the foregoing work, the MgO content of the parental melt of the Icelandic tholeiites is estimated.

The main conclusions of this thesis are summarized in Chapter 7.

Chapter 1

USE OF MELT INCLUSIONS AS A PROBE INTO EARLY STAGES OF MAGMA EVOLUTION

1.1 Introduction

During the growth of minerals from a melt, it is not uncommon for the growing crystals to capture small crystals of co-precipitating phases, inclusions of silicate and/or sulfide melt, and inclusions of coexisting fluid. Thus the inclusions in phenocrysts provide a "snapshot" of a particular evolutionary stage of a magma, as sampled by a phenocryst at a particular time, place and host melt. The examination of melt inclusions has become potentially more rewarding with the availability of diverse microbeam techniques which include spectroscopic techniques and laser, electron and ion beam excitation or ablation to obtain a variety of chemical and isotopic information. As these techniques are applied, it is necessary to evaluate the information obtained against limitations to interpretations, imposed by "container issues", that is continuing reaction of included phases with the host crystal, continuing reaction of the host crystal with its surrounding (and changing) melt and questions of diffusions of components through the host crystal.

Successful data gathering from inclusions and appropriate interpretation offers particular insight into the presence or absence of magma mixing, the separation and loss of an immiscible sulfide melt or metal-rich brine, and additional insight into melt evolutionary paths, particularly in cases where reaction relations exist between early-formed phases, melt and later phases. Applied to the particular problem of identifying primitive magma of mantle derivation, the technique is particularly suited to investigation of magma mixing and thus whether geochemically-identified "end-members" are source characteristics prior to mantle up-welling and melting or whether they are mixing components assembled from physically separate sources by the process of mantle up-welling and melting itself (e.g. diapir and wall-rock components). Models of magma genesis which are currently favoured include concepts of porous flow and melt extraction from a melt column or more complex volume in which increments of melt from within the volume are pooled to define the characteristic N-MORB, E-MORB or "hot-spot" magma composition. It is conceivable that early-formed olivine crystals for example might entrap migratory melt increments. Even if such models, although mathematically satisfying, are physically unreliable due to continuous reaction and back-reaction during porous flow, the study of melt inclusions and early-formed phenocrysts addresses the only direct evidence in magmas

themselves of the process by which magmas are assembled in the earliest stages of their evolution.

It is for these reasons that the subject of melt inclusions in primitive olivines from basalts was chosen as the major theme. In recent years the subject has been developed principally by A.V. Sobolev and colleagues at Vernadsky Institute of Geochemistry, Moscow and this group has explored techniques and interpretations in considerable depth. The choice of samples for study was guided by the availability of dredged samples from the southern margin of the North Fiji Basin, where earlier work had clearly indicated the possibility of several complicated magmatic sources. However, as a new technique was to be used and understood, a preferred starting point was the "simple" mid-ocean ridge magmatism. Samples were available from the vicinity of the Australian-Antarctic Discordance and these were chosen for the initial study.

This chapter is an introduction to the study of the origin and post-entrapment history of melt inclusions in general, indicating the information which can be obtained from them. Melt inclusions can be used to help solve common petrological problems by applying a technique of homogenizing the inclusions under visual control. The heating stage, set up in the Geology Department at the University of Tasmania, will be described together with the technique and procedure developed to obtain reliable results.

The aim of melt inclusion studies is to establish the temperature of crystallization of host-minerals, and to establish the melt composition from which they crystallized. For a given magmatic suite, crystals formed at different stages of melt evolution can give information on the liquid line of descent and on the temperature interval of crystallization (Roedder, 1979). The technique is potentially very powerful in identifying magma mixing and characterizing the mixing components.

1.2 History of inclusion studies

Inclusions in minerals have been intensively studied during the last twenty years or so. Roedder (1979, 1984), Sobolev and Kostyuk (1975) and Clocchiatti (1975) presented reviews of the early history of melt inclusion studies and this will only be discussed briefly here. The first description of inclusions to appear in the literature is believed to be from the eleventh century (Lemmlein, 1950) but the first attempted analytical work to establish a composition of an inclusion is from the early eighteenth century (Roedder, 1984). Sorby (1858) was the first to show that the coefficients of thermal expansion for a variety of liquids, resembling the fluids in inclusions, were one or two orders of magnitude greater than for silicates. In applying the results to studies of inclusions in minerals he suggested that cooling after trapping should result in the formation of a shrinkage bubble in homogeneously trapped inclusions and he

also suggested that the temperature of trapping could be estimated by the disappearance of the shrinkage bubble upon heating. Further discussions will be concentrated on modern methods of melt inclusions studies.

1.2.1 Experimental approach

Two main methods exist in modern methods of melt inclusion studies. The experimental approach involves heating the inclusion and aims to obtain the crystallization temperature and the melt composition.

Sobolev et al., (1980) developed a high temperature heating stage with visual control and the techniques which are involved will be discussed later in this chapter. This heating stage differs from existing commercial heating stages in that it can provide very fast quenching and this is the reason why this particular apparatus was employed during this study. The heating stage with visual control has the advantage that it is possible to observe processes which occur within the inclusions during experiments and the temperature can be estimated with an accuracy of $\pm$ 20 °C.

An alternative technique applied, for example, by Hansteen (1991), Sinton et al. (1993) and Johnson et al. (in press), involves heating batches of crystals in a 1 atm vertical furnace under controlled oxygen fugacity. The batches are heated to different temperatures and the inclusions are examined by optical microscope and then analysed by electron microprobe. This technique is not discussed further here.

1.2.3 Non experimental approach

Melt inclusions have sometimes been analysed without first being homogenized (e.g. Watson, 1976; Donaldson and Brown, 1977; Dungan and Rhodes, 1978; Falloon and Green, 1986; Sigurdsson, 1989; Metrich et al., 1991; McDonough and Ireland, 1993). These studies are useful because ratios of elements that are incompatible in phases that have crystallized from the inclusion after trapping will not change and will thus preserve the geochemical signature of the parental melt. However, to estimate trapping temperature and melt composition is difficult, and sometimes erroneous, due to difficulties in obtaining accurate estimates of the amounts and compositions of daughter crystals/overgrowths that have formed after trapping (see for example discussion in Sobolev and Danyushevsky (in press) about possible causes of errors).

1.3 Melt inclusions

Inclusions in minerals are of four types; melt inclusions, solid inclusions, fluid inclusions, and combined inclusions consisting of any combination of the first three. Inclusions are then further subdivided into three groups, primary, pseudo-secondary and secondary inclusions. Secondary inclusions form by healing of late stage fractures

in the host crystal whereas pseudosecondary inclusions form by healing of fractures during crystal growth (Roedder, 1984). In this study, the focus is on the primary melt inclusions, as they give information on the melt from which the crystal grew.

Primary melt inclusions are formed when a melt is trapped in a growing crystal as a result of growth irregularities. Roedder (1979, 1984) lists several ways of trapping primary inclusions (Fig. 1.1), for example:

- Rapid skeletal or dendritic growth that is later covered by a solid growth.
- Resorption and then regrowth of an earlier formed crystal.
- Entrapment between different growth spirals or subparallel growths.
- Cracks in a growing crystal, leading to irregularities in subsequent growth.
- Entrapment of melt resulting from irregularities caused by solid inclusions such as spinel in olivine.

After a melt is trapped in a mineral as an inclusion, it becomes isolated from the surrounding melt and other crystallizing phases that may have been in equilibrium with the melt at the time of entrapment. Therefore inclusions trapped in crystals at different stages of evolution of the melt will record the liquid line of descent of the magmatic system (Roedder, 1984) and will correlate to magmatic temperatures.

During natural cooling after trapping each inclusion itself will undergo compositional changes and the number of phases present may change. Generally there is continued crystallization of the host mineral on the inclusion walls (Roedder, 1979). This may not be clearly visible when viewed under optical microscope. In some cases, especially if the trapped melt was in equilibrium with more than one mineral, other daughter minerals that are clearly visible will form inside the inclusion, as opposed to overgrowth on the inclusion walls. Because of differences in thermal expansion coefficients between the host mineral and melt inclusion, and because phases crystallizing from a basaltic melt at low pressures (<3-4 kbar) are generally denser than the melt (Wager and Brown, 1968), the cooling of an inclusion after trapping leads to formation of a shrinkage bubble in the inclusion. Note that pressure inside inclusions at room temperature is always lower than the trapping pressure. If the concentration of volatiles in the melt is negligible, then the shrinkage bubble approaches a vacuum, but if any volatile species are present in the melt they will be concentrated in the shrinkage bubble (Roedder, 1979). However there are some occurrences reported in the literature (e.g. Roedder, 1984) of glassy inclusions without a shrinkage bubble. The absence of a shrinkage bubble does not indicate that no crystals have been formed inside the inclusion, as inclusions always crystallize the host mineral on the inclusion walls (as there is no nucleation problem for the host mineral to crystallize) whereas formation of a shrinkage bubble does not always take place because of nucleation problems. Nucleation of shrinkage bubbles apparently relates to the size of the inclusion, with bubbles often absent from smaller inclusions. Nucleation of shrinkage

bubbles can also be inhibited by viscosity or rapid quenching of the inclusion (Roedder, 1979).

The assumption that the host crystal and inclusion remain a closed system is a first approach to interpretation of any data obtained from melt inclusion studies, but the possibility of diffusive exchange between inclusions and host phenocryst and the main body of melt/magma must be kept in mind. Similarly, changing fH_2, fO_2 in the enclosing magma may lead to H_2 diffusion from the inclusion (Roedder, 1979). In later sections, the issue of "open system" effects on host crystal and melt inclusions is discussed.

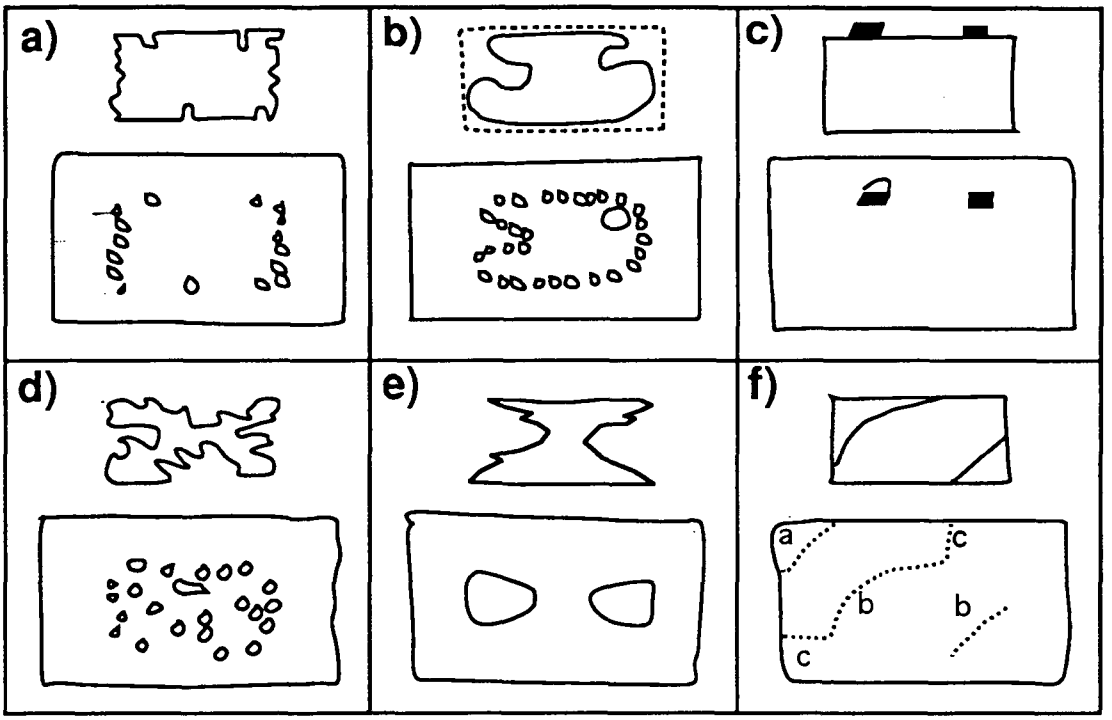

Figure 1.1: Methods of trapping primary inclusions. a) A sudden growth causes skeletal rim of a crystal, later solid growth then traps a zone of inclusions. b) Partial resorption of a crystal and later re-growth can trap both large inclusions and a zone of smaller inclusions. c) Inclusions are trapped because of irregularities caused by solid inclusion. d) Rapid skeletal or dendritic growth succeeded by solid growth results in a crystal core with many small inclusions. e) Solid growth over crystal grown rapidly in a hollow or tubular way traps two large inclusions. f) A crack in the surface of a growing crystal leads to trapping of primary inclusions in later solid growth as shown by (c). (a) shows secondary inclusions formed in a healed crack in the crystal whereas (b) shows pseudosecondary inclusions (Roedder, 1979; drawn from his Fig. 1).

1.4 Sample selection and sample preparation

In this study, the focus is on primitive melts and their phenocrysts, and therefore porphyritic and relatively primitive samples, with at least 4-5% MgO have been selected for melt inclusion research. If the suite contains phenocrysts of more than one

mineral phase it is important to know the order of crystallization and to compare compositions of inclusions in each mineral phase.

The sample is carefully crushed and sieved and phenocrysts are hand picked from the suitable size fraction using a binocular microscope. The mineral phases are then mounted separately into epoxy, polished and at least 25 minerals are analysed by the electron microprobe to determine the range of mineral compositions in the suite, the compositional distribution and to check for compositonal homogeneity in each of the crystals. Phenocrysts containing melt inclusions are extracted and polished individually on both sides and if suitable primary melt inclusions are wholly contained within the crystal, then they are ready for heating stage experiments.

1.5 Heating stage experiments

The heating stage used was set up in the Geology Department, University of Tasmania, and is the same as that designed and described by Sobolev et al. (1980). The heater, a 6 mm long vertical tube with a diameter of 2 mm, is made of $Pt_{90}Rh_{10}$ foil. The sample holder is located in the centre of the heater and is made of a 0.1 mm thick and 0.7 mm wide Pt ring with a diameter of 1 mm. The sample is placed on a 200-300 μm thick plate of mantle olivine, which is ideal as working platform because it is refractory enough to remain intact at high temperatures, it is free of inclusions and transparent. The olivine plate also protects the sample holder and the heater from interaction with melt if the sample contains melt inclusions that are open. The temperature is monitored by a Pt, $Pt_{90}Rh_{10}$ thermocouple that is welded to the heater. To establish the temperature gradient inside the working area two olivine plates, each with six pieces of Au distributed evenly on top, are placed on top of each other on the sample heater and heated up to the melting point of Au. As a result the vertical and horizontal temperature gradient was shown to be less than 10 °C, and to minimize this effect a piece of Au was put on top of the sample in each run, as close to the inclusion of interest as possible.

All experiments are run in an ultra-pure He atmosphere. He is used because of its very low thermal conductivity which provides for very low thermal inertia inside the sample chamber, and thus samples can be very efficiently quenched by switching off the power to the heater. In addition, the He flux is increased at the same time as the power is turned off.

The experimental procedures described below are those appropriate to fluid-saturated systems only and they cannot be readily applied to undersaturated systems. The easiest way to demonstrate fluid saturation is to find fluid inclusions in phenocrysts. Fluid inclusions were found in the most primitive phenocrysts in all samples used for melt inclusion studies here.

Fluid solubility is governed mainly by pressure (e.g. Burnham, 1979), and, for a fluid-saturated melt, as temperature and pressure inside an inclusion drop after trapping, it leads to the formation of a fluid bubble (See section 1.3). During heating in the experiment the fluid bubble will disappear when the pressure inside the inclusion is equal to the pressure of trapping and this moment corresponds to the disappearance of all daughter crystals that were formed during cooling. Thus the temperature at the moment of homogenization, which is the moment of disappearance of the fluid bubble, corresponds to the temperature of trapping, that is the crystallization temperature, and the composition of the melt at this moment corresponds to the composition of the trapped melt.

However, various problems can arise from kinetic effects in individual samples and there are many factors that need to be considered, such as the heating rate, duration of the experiment at high temperatures (>1100 °C) and the size of the inclusion. Below I consider processes that occur in inclusions in phenocrysts in primitive, mantle-derived magmas.

Dependence of the temperature of homogenization (T_h) on the heating rate was shown by Bakumenko (1975; see also Sobolev and Danyushevsky, in press). An increase in the heating rate at temperatures above 1100 °C leads to an exponential rise in T_h, but a decrease in the heating rate results in a decrease in T_h until it reaches a constant value that is taken to be the true temperature of trapping (Sobolev and Danyushevsky, in press).

Sobolev et al. (1983) showed that in the case of H_2O-bearing melts a continued increase in T_h occurs at temperatures above 1100 °C during the experiment, accompanied by crystallization of magnetite. This has been explained by dissociation of H_2O and H_2 diffusion through the host mineral driven by difference in fH_2 between the inclusion and the sample chamber. As the experiments are run at 1 atm pressure of pure He (with < 2ppm H_2) the partial pressure of H_2 in the sample chamber is less than ($2x10^{-6}$ atm). On the other hand, the pressure inside the inclusion at high temperature is close to the trapping pressure, which is usually more than 1 kbar. Even if the proportion of H_2 in the fluid is the same as in the ultra pure He (which is a minimum estimate, as H_2O is a common component of magmatic fluids) the H_2 partial pressure is at least 1000 times greater in the inclusion than in the sample chamber. O_2, however, does not diffuse as easily as H_2 and is left behind, causing oxidation of the melt in the inclusion (Roedder, 1979). Because Fe^{2+} is the main component in the melt that is easily oxidized, Sobolev and Danyushevsky (in press) suggest that the diffusion is limited by the availability of Fe^{2+} in the melt by the reactions:

$2H_2Om + 6FeOm = 2H_2 + 2Fe_3O_4$

or

$H_2Om + 2FeOm = H_2 + Fe_2O_3m$ (above magnetite stability)

The maximum amount of H_2O that can dissociate can then be calculated by the equation: $H_2O\% = 0.125 \times FeO\%$.

H_2O dissociation will cause a reduction of the volume of the melt due to the large molar volume of H_2O and the loss of water will increase the temperature of melting (Sobolev and Danyushevsky, in press). Both factors will increase the T_h as the reduction of volume means that more of the host mineral has to be melted to dissolve the fluid bubble and because of the effects of water on the temperature of melting (e.g. Yoder and Tilley, 1962).

Inclusions must be larger than 20 μm in diameter so that they can be analysed by the electron microprobe, and for the optical observation of phase changes during heating. Inclusions larger than 150 μm are rarely contained fully within the doubly polished host crystals. The size of inclusions used in this study was in the range 20-100 μm.

1.6 Kinetic experiments

Before starting heating stage experiments on phenocrysts from a particular suite of rocks it is necessary to do kinetic experiments to see if T_h increases with the duration of the experiment (Sobolev et al., 1983) and to decide on the heating rate to be used (Bakumenko, 1975).

To check for changes in T_h with time, the inclusions are first heated as quickly as possible up to 1100 °C. The temperature is then increased with a constant heating rate (100 °C/minute) until the inclusion has homogenized, and the temperature is taken down to 1100 °C again and kept at 1100 °C for 20-30 minutes before the inclusions are again homogenized using the same heating rate (100 °C/minute). If the T_h is higher during the second homogenization, this is repeated until T_h does not increase further. As was mentioned in the previous section, an increase in T_h has been explained by dissociation of H_2O and H_2 diffusion through the host mineral during experiments (Sobolev et al., 1983). This increase in T_h is limited by both the H_2O and FeO contents of the melt (Sobolev and Danyushevsky, in press) and should therefore reach a constant level.

Figure 1.2 shows the results of kinetic experiments done by Sobolev and Danyushevsky, (in press) on inclusions in olivine phenocrysts in boninites from Tonga. In the smaller inclusions (20-40 μm) the difference in T_h between the first homogenization (at t = 0) and the second homogenization of the same inclusions after it was kept at 1100 °C for 20 minutes (t = 0.33) is more than 140 °C. Homogenization, after 1 1/2 hour at a temperature of 1100 °C, occurs at a temperature almost 200 °C higher than the first homogenization. The increase in T_h in larger inclusions (100-120 μm) is much slower, homogenization after one hour at 1100 °C occurs at 40 °C higher

temperature than the first homogenization (at t = 0), and approximately 140 °C higher temperature after four hours at 1100 °C (Figure 1.2). In this particular case the most suitable size of the inclusions for experiments was 100-150 μm, and because of the increase in T_h with time, the duration of the experiments had to be as short as possible. The temperature was therefore raised quickly until the bubble had almost disappeared and then a heating rate of 30-40 °C/minute was used, with the duration of runs at temperature above 1100 °C reported to be less than 1 minute (Sobolev and Danyushevsky, in press). The results from kinetic experiments done during the course of this study are described in chapter 2 and chapter 5.

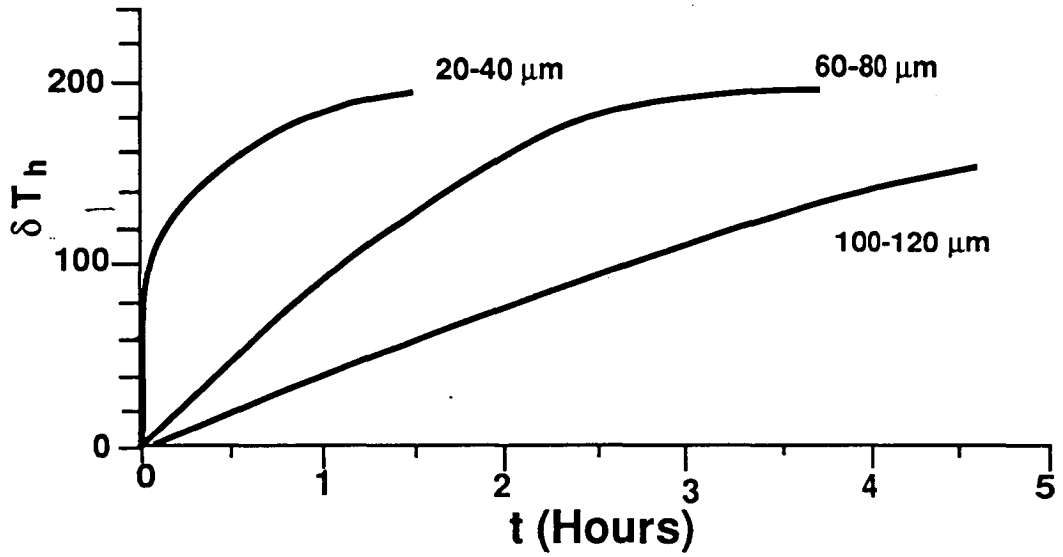

Figure 1.2: Correlation between temperature of homogenization (T_h), the inclusion size and run duration (t). δT_h is the difference between obtained T_h in the first experiment at t = 0, and T_h of subsequent experiments after the inclusions have been kept at 1100 °C for a given time. See text for discussion. (Sobolev and Danyushevsky, in press; part of their Fig. 5c).

If no increase is observed in the T_h with the duration of the experiments, the next set of kinetic experiments is done to establish the maximum heating rate that can be used to obtain equilibrium. However if there is a significant change in T_h with time these experiments to establish the heating rate can only be done after the T_h has stopped increasing. Danyushevsky et al. (1992) showed that for ultramafic to basaltic melt compositions the optimum heating rate is between 1 and 60 °C/minute. Therefore the samples are first homogenized using a heating rate of 60 °C/minute, then the temperature is taken down and when the inclusion is heterogeneous, as indicated by the formation of a bubble, the inclusion is homogenized again, using a lower heating rate each time. As the heating rate is lowered, T_h should reach a minimum value that is taken to be the true value that equals the temperature of trapping (Bakumenko, 1975).

Sobolev et al. (1989) showed that for a suite of mid-ocean ridge basalts they studied, experiments should not exceed 20-25 minutes at temperatures above 1100 °C,

to avoid H_2 diffusion and magnetite crystallization, and that the heating rate should not exceed 1-2 °C/minute at temperatures near the T_h, to give the inclusion time to reach equilibrium.

1.7 Assessment of experimental results

After the heating stage experiment on each inclusion, the host crystal is mounted in epoxy resin and polished to expose the inclusion. Both the crystal and the inclusion are then analysed by electron microprobe. To assess the quality of the experiments it is necessary to first evaluate if equilibrium has been achieved. This is checked by using mineral-melt thermometers (Roeder and Emslie, 1970; Drake, 1976; Nielsen and Drake, 1979, Ford et al., 1983; Ariskin et al., 1986; Ariskin and Barmina, 1990) which allow the liquidus temperatures to be calculated for the minerals of interest by using the composition of the melt inclusion. For a dry system the calculated liquidus temperature should be equal or close to the T_h. However if the melt contains significant amounts of H_2O the calculated temperatures may be higher than the T_h, since water lowers the temperature of melting. If the calculated temperature is significantly lower than the T_h it indicates bad quenching and crystallization of the host mineral on the inclusion walls. Crystallization of the host mineral will lead to a different melt composition that is more depleted in the host mineral component than the trapped melt and therefore the calculated liquidus temperature for this derivative melt will be lower. K_D relations between mineral and melt are also utilized to calculate the mineral composition that should be in equilibrium with the melt, and this composition should be equal to the host mineral composition.

The experimental reproduction of equilibrium between melt and host crystal is, nevertheless, not enough to guarantee that the original entrapment temperature has been established correctly, as it is possible that natural re-equilibrium of inclusions and their host mineral occurred at a different temperatures following entrapment. Independent criteria, such as correlation between T_h and the composition of the host mineral, which should exist if the type of crystallization was fractional, is then used to estimate the validity of the data obtained. The compositions of the homogenized melt inclusions also should give a liquid line of descent which is in agreement with the observed crystallization order, and comparable to the trend shown by natural rocks and glasses. These aspects of interpretation of the experimental and analytical data are discussed in following sections.

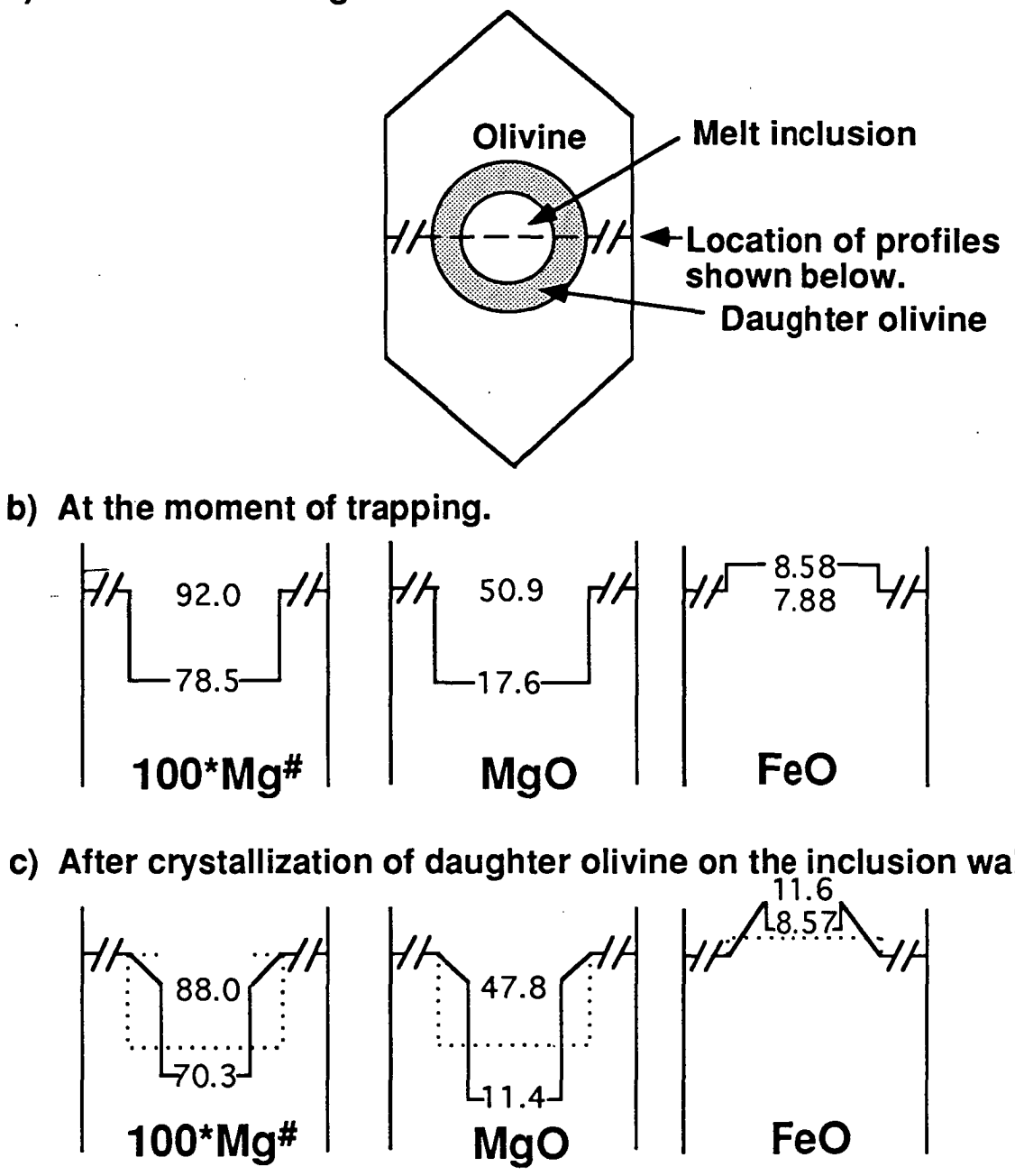

Figure 1.3: A diagram showing the re-equilibration of Mg^{2+} and Fe^{2+} in olivine and melt inclusions. a) Olivine phenocryst with a melt inclusion that has crystallized a daughter olivine on the inclusion walls. The dotted line shows the location of the compositional profiles in b-g. b) Olivine Fo_{92} traps a melt inclusion with Mg# = 78.5. The olivine contains 50.9% MgO and 7.88% FeO whereas the melt contains 17.6% MgO and 8.58% FeO. c) Shortly after entrapment the melt has crystallized daughter olivine on the inclusion walls. This olivine is zoned down to Fo_{88}, with 47.8% MgO and 11.6% FeO and it is in equilibrium with the remaining melt that now contains 11.4% MgO and 8.57% FeO.

d) After re-equilibration of melt and daughter olivine with the host olivine.

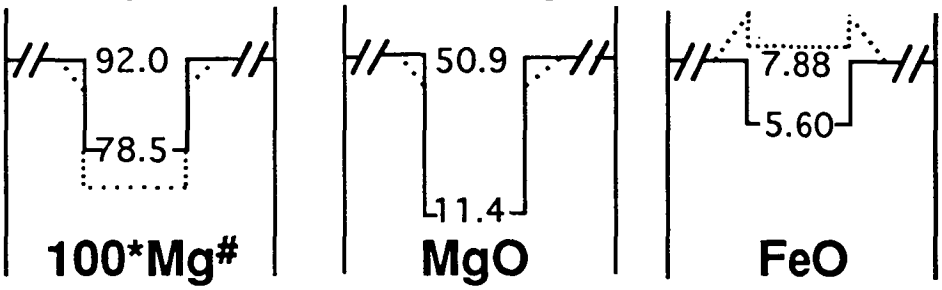

e) After homogenization.

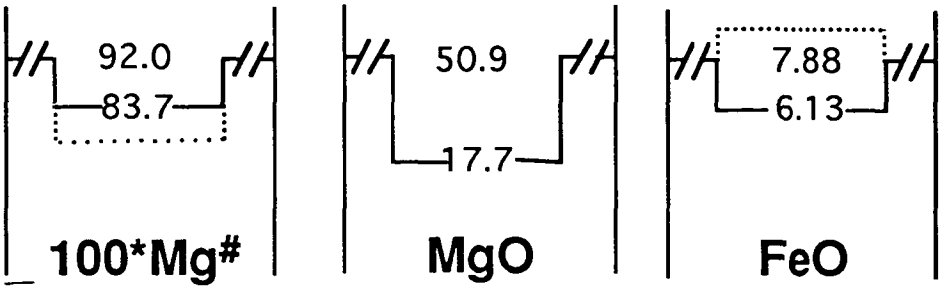

f) After re-equilibration of the host olivine down to Fo_{88}.

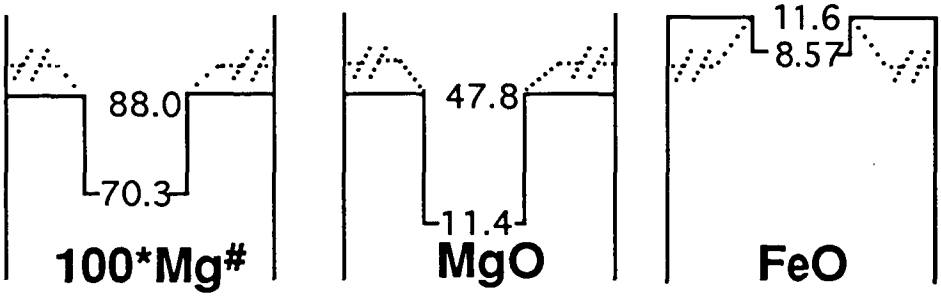

g) After homogenization.

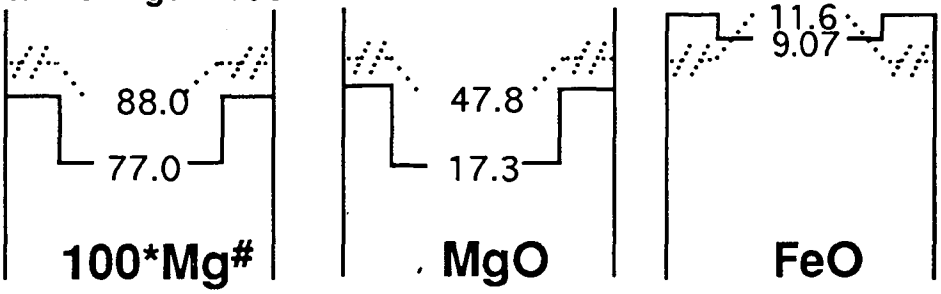

Figure 1.3 continued: d) The daughter olivine and the melt inclusion have re-equilibrated with the host olivine and the melt is now in equilibrium with Fo_{92}. MgO is buffered by temperature and is kept constant by some precipitation of olivine Fo_{92} but FeO drops significantly and is now 5.6% in the melts. e) When the inclusion is homogenized during the heating stage experiment the same amount of olivine still has to be incorporated back into the inclusion in order to homogenize it but now the daughter olivine has the composition Fo_{92} instead of being zoned down to Fo_{88}. After homogenization the melt inclusion has Mg# of 83.7 with 17.7 MgO and only 6.13% FeO. f) A scenario in which after crystallization of daughter olivine (Fig. 1.3c) the host olivine re-equilibrates down to Fo_{88}. In the case shown here the MgO and FeO do not change as the melt inclusion was already in equilibrium with Fo_{88}. g) After homogenization the addition of olivine Fo_{88} to a melt that was already in equilibrium with this olivine results in the melt having Mg# that is too high to be in equilibrium with the host olivine. The MgO and FeO contents are in fact close to the original contents in the melt that was trapped with MgO being 17.3% instead of 17.6% and FeO of 9.07% instead of 8.58%.

1.8 Complicating issues

Sometimes melt inclusions in olivine show abnormally low FeO contents when compared to compositions at similar MgO, CaO, Al_2O_3, SiO_2 etc. in natural rock suites, and this is associated with unrealistically high $K_D^{ol\text{-}liq}_{Fe\text{-}Mg}$ values between the host olivine and the inclusion (Sobolev and Danyushevsky, in press). This may be caused by Fe^{2+} and Mg^{2+} exchange between host olivine, the olivine that crystallized on the inclusion walls, and the melt inclusion (Fig. 1.3). After the inclusion is trapped, olivine continues to crystallize on the inclusion walls, but as this takes place in a closed system, this overgrowth olivine is more FeO-rich than the host olivine and the remaining melt will be in equilibrium with this olivine. As the volume of the melt inclusion and this more FeO-rich olivine is relatively small compared to the host olivine, it is susceptible to later re-equilibration if the olivine stays at high temperatures within the magma.

This involves Fe^{2+}-Mg^{2+} exchange, with Fe^{2+} diffusing into the host olivine until both the daughter olivine on the inclusion walls and the melt inclusions are in equilibrium with the more MgO-rich, FeO-poor host olivine. This results in lower FeO content inside the original volume of the melt inclusion. During the heating stage experiments the same volumes of olivine still needs to be incorporated back into the inclusion to achieve the pressure of trapping necessary to dissolve the fluid bubble, but as the inclusion has lost FeO during re-equilibration, the FeO content of the melt inclusion will be lower. The effects on MgO on the other hand will be less pronounced because the MgO content of olivine-saturated melt is largely controlled by temperature, and as a result the inclusions will have higher $Mg^{\#}$ ($Mg^{\#}$ = Mg/(Mg + Fe^{2+}), than required to be in equilibrium with the host mineral (Fig. 1.3e). This can be detected in the data and corrected for by recalculation. The program used for this recalculation (written by L.V. Danyushevsky) exchanges Mg^{2+} by Fe^{2+} until the inclusion reaches equilibrium with its host mineral.

The host olivine can also re-equilibrate to a different Fo-content, either because it is entrained in a melt with different $Mg^{\#}$, or during equilibrium crystallization where the olivine continuously adjusts its composition as the surrounding melt evolves. If for instance, an olivine of Fo_{92} containing a melt inclusion re-equilibrates to Fo_{88}, the melt inclusion would have to adjust its $Mg^{\#}$ as well to be in equilibrium with this new Fo value (Fig. 1.3f). During heating stage experiment, olivine still needs to be incorporated back into the inclusion in order to homogenize it, but as the inclusion was already in equilibrium with Fo_{88}, addition of more of this component would lead to a higher $Mg^{\#}$ for the inclusion than would be expected based on K_D relationships (Fig. 1.3g). Therefore, it would seem in this case that all the experiments were overheated, as overheating also leads to addition of extra olivine component to a melt that is already

in equilibrium with that olivine composition. This would not significantly change the T_h, which would be the same as the temperature of trapping in Fo_{92}. So if olivines with different forsterite content re-equilibrate to a constant value, results from heating stage experiments would give a range of T_h for that forsterite content. However, in this case the FeO content of the melt inclusion is not affected significantly, in contrast to the case described above and shown in Figure 1.3d-e.

1.9 Melt inclusion work in the course of this study

For several aspects of this study (chapters 2, 4 and 5), melt inclusion studies have been used together with more conventional mineralogical and petrological methods. The melt inclusion studies involved using the heating stage with visual control, described in this chapter, to homogenize the inclusions and thus obtain the crystallization temperature and the melt composition. In some cases the inclusions could not be homogenized and were therefore quenched after the disappearance of the last daughter phase inside the inclusion. In addition, naturally quenched glassy inclusions were analysed and though their compositions cannot be used directly as representing actual melt composition, due to overgrowth on host walls, the ratios of elements that are incompatible in the host mineral were used to help identify the chemical signature of the melt (chapter 5).

Chapter 2

THE AUSTRALIAN-ANTARCTIC DISCORDANCE

2.1 Introduction

The Southeast Indian Ridge (SEIR) extends from the Rodriguez triple junction in the Indian Ocean to the Macquarie triple junction in the Southwest Pacific Ocean. At approximately 50 °S, between Australia and Antarctica, a portion of the SEIR between 138 °E and 105 °E, has been divided into three zones, A, B, and C, of different geophysical and morphological properties (Weissel and Hayes, 1971). Zone B (~128 °E to ~120 °E) is the Australian-Antarctic Discordance (AAD) (Hayes and Conolly, 1972), whereas zones A and C are east and west off it respectively (Fig. 2.1). Zones A and B are further divided into spreading segments that are connected by transform faults or propagating rifts (Vogt et al. 1983).

The AAD, which is an anomalously deep and morphologically complex segment of the SEIR, has been interpreted as a zone of a down-welling mantle flow resulting in a colder mantle in this region (Hayes and Conolly, 1972; Weissel and Hayes, 1974; Forsyth et al., 1987). The depth of intersection of geotherm and solidus is thus believed to be shallower beneath the AAD than the adjacent regions. This allegedly leads to a smaller degree and lower mean pressure of melting, resulting in higher Na_2O and SiO_2 and lower FeO* in MORB lavas dredged from within the AAD compared to those in zones A or C (for example Klein et al., 1991). The AAD is also the boundary between Pacific and Indian isotopic provinces and Klein et al. (1988) suggested that it is a site of convergence between convective Pacific mantle flow from the east and Indian mantle flow from the west.

In this study, heating stage experiments were done on olivine phenocrysts from three basalts from within the AAD to establish the crystallization temperature and the melt composition from which these olivines crystallized. The crystallization temperature is then compared with crystallization temperatures obtained with the same method for other MORB suites to test the hypothesis that the AAD is a site of anomalously cold mantle. A parental magma composition is then calculated and the pressure and temperature of melt segregation is estimated.

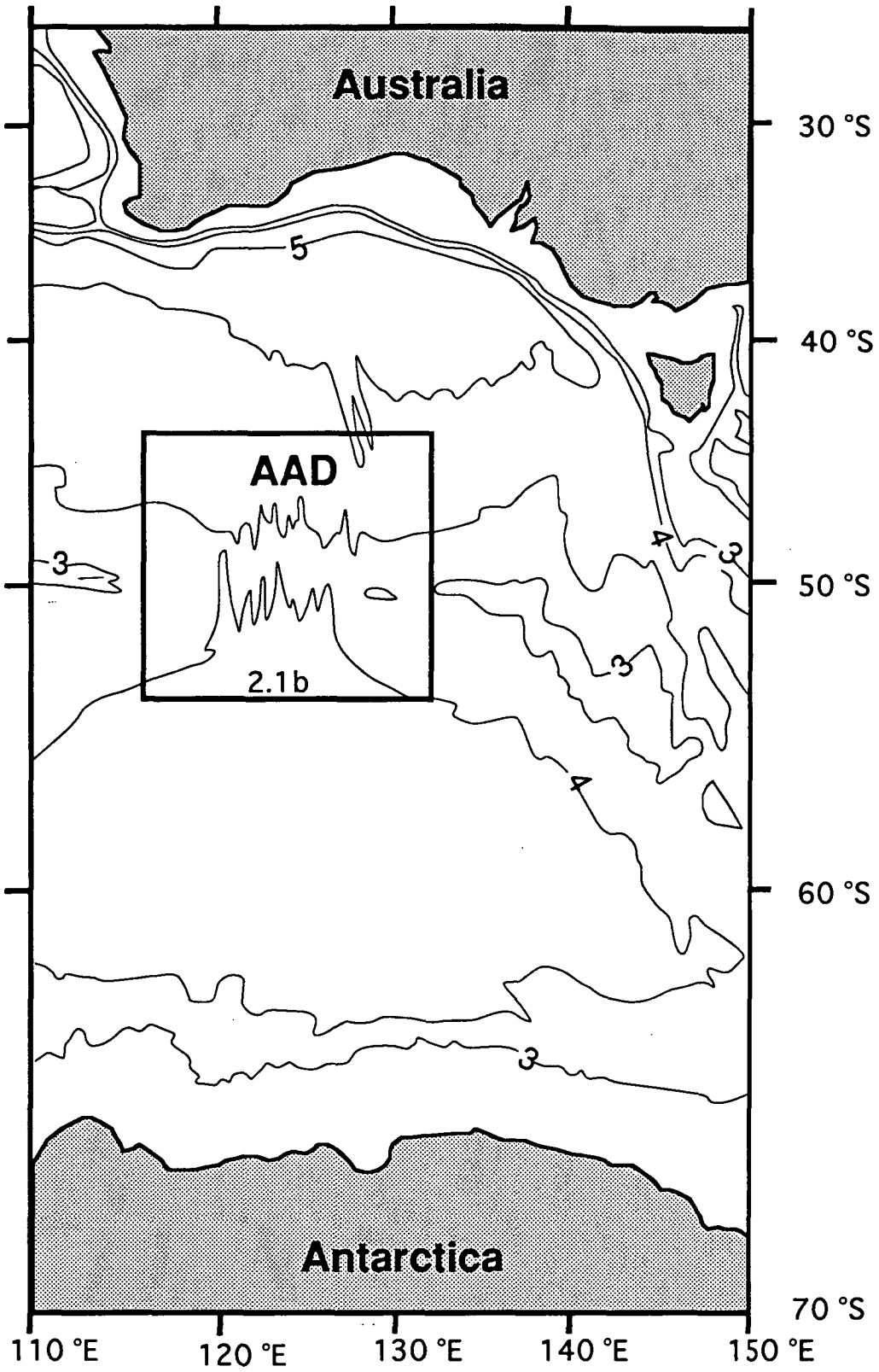

Figure 2.1a: The Southern Ocean between Australia and Antarctica. Numbers on contour lines indicate depth in thousand meters. The box shows the location of Figure 2.1b. Modified from Sempéré et al., (1991).

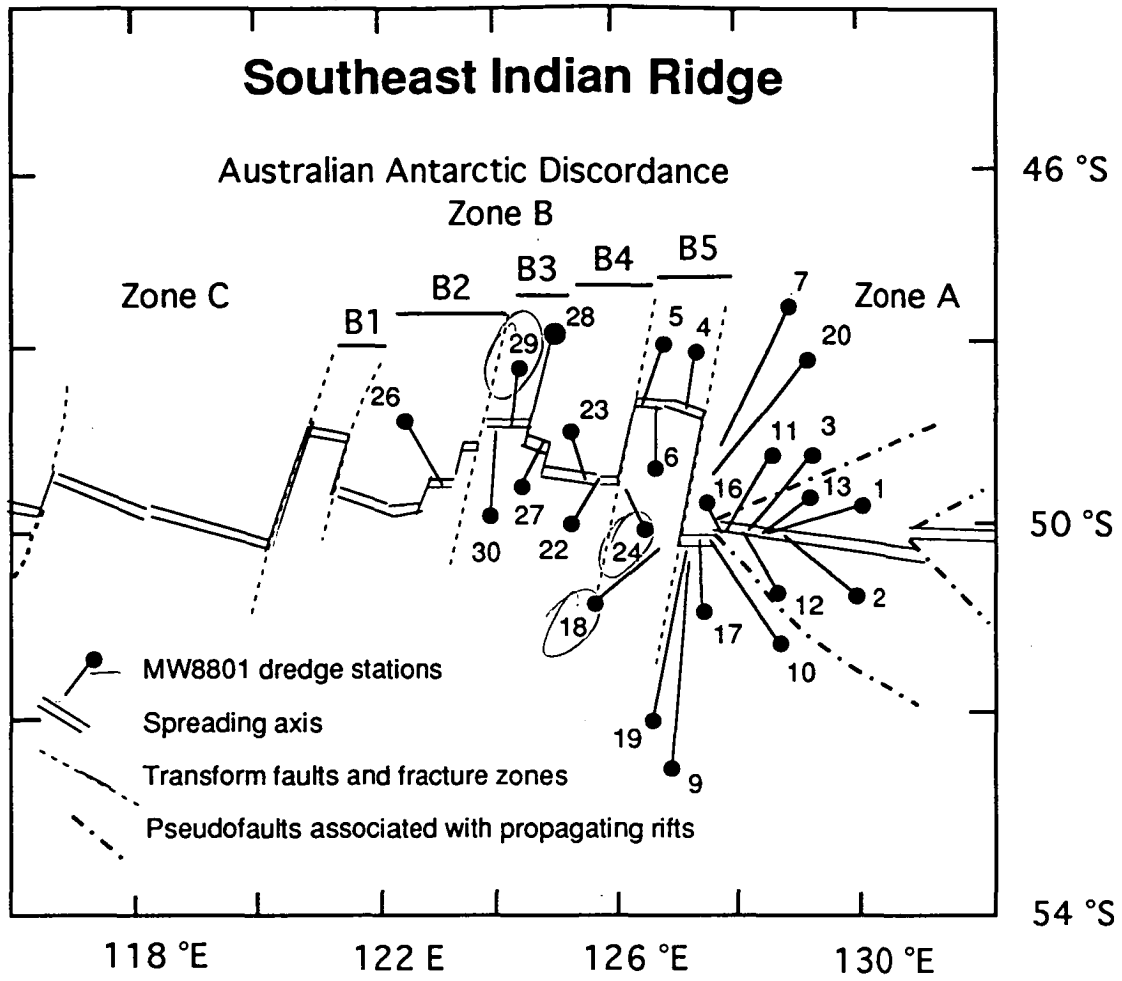

Figure 2.1b: The Southeast Indian Ridge between 116 and 132 °E showing the locations of dredge station from the MW8801 cruise of R/V Moana Wave in 1988. Locations of dredge stations are taken from Pyle et al., 1992. Modified from Sempéré et al., (1991).

The basaltic samples used were dredged from zone A and the AAD by R.V. Moana Wave in 1988 during the cruise MW8801 (Pyle et al., 1992). From the sample suite available (courtesy of Dr. D. Christie (O.S.U.)), at the University of Tasmania, it was possible to select many samples with glassy rims, or glassy fragments; these were analysed to form a data base for the sample selection for the more detailed study. Ninety four glasses were analysed for major elements using the electron microprobe and seventeen glasses had been previously analysed for major elements and H_2O by L.V. Danyushevsky (unpublished). Most of these samples are sparsely phyric but four samples were selected as having sufficient phenocrysts, potentially suitable for inclusion studies. (Table 1, samples 18-9, 18-17, 24-14, 29-2). Samples 18-9, 18-17 and 24-14 are from a single geochemical group (see section 2.2).

Table 2.1: Electron microprobe analyses of glasses from R/V Moana Wave, MW8801 cruise. Each analyses is an average of three spot analyses. FeO* denotes all Fe represented as FeO. H_2O was analysed by FTIR by L.V. Danyushevsky as well as major elements for those glasses where H_2O was analysed (L.V. Danyushevsky, unpublished).

	Group 1									
Sample	18-8	18-9	18-12	18-16	18-17	18-18	24-1	24-3	24-6	24-7
SiO_2	50.99	51.35	51.19	52.03	51.12	53.00	51.95	52.05	52.28	51.60
TiO_2	1.10	1.34	1.34	1.44	1.31	1.61	1.41	1.38	1.36	1.38
Al_2O_3	16.13	16.04	15.91	15.87	16.39	15.26	15.87	16.07	16.17	15.98
FeO*	7.86	8.47	8.19	8.45	7.83	8.69	8.18	8.13	8.09	8.16
MnO	0.10	0.16	0.15	0.16	0.10	0.17	0.14	0.09	0.12	0.13
MgO	8.07	7.47	7.37	7.31	7.58	6.39	7.06	7.09	7.20	7.14
CaO	11.49	11.07	11.08	11.20	10.84	10.28	10.69	10.53	10.67	10.70
Na_2O	2.87	3.30	3.12	3.19	3.62	3.46	3.55	3.52	3.48	3.50
K_2O	0.11	0.12	0.13	0.14	0.12	0.27	0.16	0.15	0.14	0.15
P_2O_5	0.08	0.11	0.07	0.12	0.10	0.17	0.15	0.12	0.16	0.12
Cr_2O_3	0.06	0.05	0.06	0.06	0.05	0.06	0.04	0.05	0.05	0.05
H_2O										
Sum	98.86	99.48	98.61	99.97	99.06	99.36	99.20	99.18	99.72	98.91

Sample	24-9	24-10	24-14	24-15	27-7	27-8	27-41	27-48	27-66	27-68
SiO_2	52.90	51.63	52.28	51.96	51.70	51.68	52.07	51.92	51.53	52.01
TiO_2	1.38	1.43	1.44	1.39	1.32	1.26	1.41	1.39	1.36	1.33
Al_2O_3	16.28	16.04	15.88	15.97	16.43	16.30	16.14	16.13	16.16	16.29
FeO*	8.11	8.13	8.22	7.93	8.00	7.94	7.96	7.97	7.93	8.13
MnO	0.14	0.08	0.21	0.12	0.14	0.10	0.12	0.19	0.13	0.15
MgO	7.30	7.26	7.04	7.18	7.60	7.58	7.22	7.22	7.24	7.28
CaO	10.77	10.60	10.56	10.72	10.91	11.04	10.60	10.65	10.62	10.66
Na_2O	3.61	3.49	3.44	3.48	3.29	3.35	3.52	3.48	3.48	3.50
K_2O	0.14	0.14	0.16	0.14	0.13	0.13	0.19	0.18	0.19	0.19
P_2O_5	0.16	0.12	0.13	0.14	0.08	0.11	0.13	0.12	0.10	0.14
Cr_2O_3	0.06	0.04	0.03	0.06	0.06	0.04	0.05	0.01	0.07	0.04
H_2O	0.24									
Sum	101.09	98.96	99.39	99.09	99.66	99.53	99.41	99.26	98.81	99.72

	Group 2									
Sample	29-1	29-2	29-3	29-5	29-29	30-2	30-5	30-6	30-15	30-24
SiO_2	51.83	51.60	51.76	52.51	51.80	52.62	51.56	51.66	51.83	52.01
TiO_2	1.21	1.19	1.22	1.21	1.19	1.24	1.23	1.23	1.35	1.21
Al_2O_3	16.32	16.57	16.31	16.85	16.29	16.76	16.21	16.32	16.39	16.44
FeO*	7.63	7.68	7.67	7.79	7.63	7.85	7.88	7.80	7.87	7.88
MnO	0.16	0.13	0.16	0.13	0.15	0.17	0.13	0.15	0.14	0.07
MgO	7.84	7.91	7.88	8.10	7.91	7.79	7.61	7.64	7.40	7.74
CaO	10.93	10.87	10.89	11.06	10.85	11.11	11.10	11.16	10.91	11.15
Na_2O	3.21	3.18	3.22	3.22	3.22	3.36	3.19	3.23	3.30	3.22
K_2O	0.17	0.17	0.17	0.17	0.17	0.16	0.15	0.14	0.28	0.16
P_2O_5	0.11	0.11	0.11	0.13	0.13	0.14	0.08	0.09	0.13	0.12
Cr_2O_3	0.06	0.01	0.07	0.05	0.03	0.07	0.05	0.06	0.10	0.07
H_2O				0.22		0.22				
Sum	99.47	99.42	99.46	101.44	99.37	101.49	99.19	99.48	99.70	100.07

			Group 3			Group 4			Group 5	
Sample	22-4	22-11	22-18	22-26	22-32	23-1	23-3	23-4	5-1	6-1
SiO_2	50.75	50.32	50.68	50.74	51.48	51.18	51.05	51.22	51.40	51.61
TiO_2	0.98	1.00	0.99	1.03	0.98	1.08	1.08	1.08	1.47	1.43
Al_2O_3	16.69	16.62	16.66	16.77	17.05	16.24	16.46	16.25	15.91	15.95
FeO*	8.18	8.34	8.44	8.20	8.21	9.42	9.44	9.31	8.91	8.86
MnO	0.07	0.14	0.12	0.13	0.11	0.12	0.10	0.18	0.14	0.09
MgO	8.11	8.08	8.15	8.16	8.32	7.72	7.91	7.75	7.65	7.80
CaO	11.21	11.15	11.20	11.25	11.40	10.99	10.94	11.02	11.33	11.31
Na_2O	2.98	3.05	3.01	3.05	3.11	2.72	2.82	2.75	2.93	2.88
K_2O	0.09	0.10	0.08	0.09	0.08	0.07	0.07	0.09	0.13	0.09
P_2O_5	0.13	0.06	0.08	0.06	0.11	0.09	0.08	0.09	0.12	0.13
Cr_2O_3	0.06	0.04	0.07	0.04	0.09	0.04	0.04	0.04	0.05	0.02
H_2O					0.19	0.18				
Sum	99.25	98.90	99.48	99.52	101.13	99.85	99.99	99.78	100.04	100.17

Table 2.1: continued.

			Group 6	Group 7	Group 8					
Sample	6-2	6-3	4-2	27-52	1-1	1-2	1-7	1-11	1-13	1-15
SiO_2	51.71	51.27	50.15	51.67	51.11	50.82	50.24	50.02	50.19	50.76
TiO_2	1.48	1.36	1.44	1.46	2.39	2.48	2.52	2.44	2.41	2.44
Al_2O_3	15.86	15.61	16.29	17.45	13.99	13.74	13.61	13.85	13.86	13.97
FeO*	8.84	8.81	8.88	8.28	12.02	12.44	12.71	12.09	11.98	12.00
MnO	0.17	0.10	0.10	0.14	0.17	0.21	0.16	0.11	0.19	0.21
MgO	7.86	7.67	7.25	7.27	6.62	6.42	6.35	6.64	6.63	6.63
CaO	11.44	11.77	11.82	9.97	10.84	10.65	10.56	10.87	10.71	10.86
Na_2O	2.90	2.74	3.18	3.61	2.60	2.74	2.80	2.67	2.62	2.66
K_2O	0.08	0.08	0.06	0.66	0.12	0.11	0.11	0.12	0.13	0.13
P_2O_5	0.13	0.12	0.12	0.26	0.23	0.23	0.23	0.21	0.26	0.22
Cr_2O_3	0.05	0.09	0.07	0.06	0.03	0.01	0.05	0.01	0.04	0.04
H_2O		0.24	0.45	0.40						
Sum	100.52	99.86	99.81	101.23	100.12	99.85	99.34	99.03	99.02	99.92

Sample	1-25	1-26	1-27	1-38	1-47	1-55	1-59	2-1	3-2	3-3
SiO_2	50.77	50.38	51.11	51.77	50.91	50.41	51.52	50.52	50.76	50.66
TiO_2	2.52	2.41	2.42	2.71	2.60	2.41	2.42	1.96	3.15	3.05
Al_2O_3	13.62	13.89	13.96	14.03	13.70	13.83	14.16	14.42	12.68	12.82
FeO*	12.33	11.95	12.03	12.96	12.54	12.02	11.90	10.74	14.63	14.42
MnO	0.13	0.18	0.23	0.17	0.22	0.18	0.25	0.21	0.19	0.19
MgO	5.86	6.69	6.64	6.39	6.28	6.64	6.72	6.78	5.29	5.44
CaO	9.91	10.85	10.90	10.58	10.41	10.89	10.92	11.54	9.45	9.51
Na_2O	3.13	2.71	2.62	2.20	2.84	2.64	2.68	2.85	2.88	2.89
K_2O	0.15	0.10	0.12	0.12	0.11	0.12	0.12	0.08	0.15	0.14
P_2O_5	0.26	0.23	0.23	0.25	0.25	0.23	0.22	0.15	0.29	0.29
Cr_2O_3	0.03	0.03	0.05	0.05	0.03	0.04	0.02	0.05	0.03	0.01
H_2O							0.34	0.30		
Sum	98.71	99.42	100.31	101.23	99.89	99.41	101.27	99.60	99.50	99.42

									Group 9	
Sample	3-10	3-17	3-18	3-21	12-1	13-A	13-20	13-30	9-11	9-13
SiO_2	51.75	51.11	51.09	50.66	50.72	50.61	50.21	50.41	50.75	50.63
TiO_2	3.01	3.04	3.17	3.25	3.07	2.67	2.58	2.80	2.00	1.96
Al_2O_3	13.04	12.99	12.90	12.64	13.32	13.54	13.58	13.51	14.64	14.63
FeO*	14.29	14.35	14.52	14.70	13.64	12.81	12.74	13.01	10.26	10.28
MnO	0.22	0.18	0.19	0.21	0.21	0.27	0.21	0.16	0.12	0.19
MgO	5.32	5.32	5.27	5.27	5.56	5.97	6.21	6.04	7.15	7.16
CaO	9.74	9.47	9.45	9.35	9.81	10.39	10.45	10.40	11.33	11.50
Na_2O	2.71	2.92	2.94	2.85	3.05	2.94	2.85	2.88	2.96	2.91
K_2O	0.16	0.14	0.14	0.14	0.17	0.12	0.11	0.12	0.09	0.08
P_2O_5	0.31	0.28	0.30	0.31	0.34	0.26	0.26	0.26	0.19	0.15
Cr_2O_3	0.04	0.02	0.04	0.02	0.03	0.03	0.01	0.03	0.06	0.03
H_2O	0.17									
Sum	100.76	99.82	100.01	99.40	99.92	99.61	99.21	99.62	99.55	99.52

Sample	9-14	9-17	9-18	9-20	9-22	9-23	9-26	9-29	9-31	9-42
SiO_2	50.52	50.38	50.67	50.47	50.16	50.54	50.32	50.25	50.51	50.35
TiO_2	1.95	1.96	2.02	2.03	1.97	2.03	1.95	1.97	1.93	1.99
Al_2O_3	14.67	14.70	14.54	14.39	14.63	14.63	14.65	14.56	14.65	14.47
FeO*	10.30	10.24	10.49	10.59	10.42	10.34	10.40	10.35	10.43	10.38
MnO	0.18	0.15	0.15	0.15	0.16	0.17	0.18	0.13	0.15	0.20
MgO	7.20	7.18	7.11	7.05	7.19	7.18	7.19	7.20	7.20	7.13
CaO	11.41	11.35	11.33	11.42	11.39	11.42	11.36	11.54	11.35	11.36
Na_2O	3.00	2.92	2.94	2.92	2.99	2.94	2.97	2.94	2.97	3.01
K_2O	0.08	0.08	0.09	0.09	0.09	0.08	0.08	0.09	0.08	0.09
P_2O_5	0.18	0.19	0.18	0.18	0.15	0.20	0.19	0.18	0.18	0.16
Cr_2O_3	0.03	0.04	0.06	0.03	0.04	0.06	0.05	0.07	0.07	0.07
H_2O										
Sum	99.52	99.19	99.58	99.32	99.19	99.59	99.34	99.28	99.52	99.21

Table 2.1: continued.

Sample	9-49	9-51	10-2	10-3	10-4	10-5	10-8	10-10	10-13	11-5
SiO_2	50.47	51.52	51.59	50.86	50.68	50.09	50.41	50.42	50.56	50.37
TiO_2	1.98	2.00	2.48	2.52	2.50	2.52	2.52	2.59	2.51	1.93
Al_2O_3	14.52	14.86	14.03	14.06	13.95	13.88	13.89	13.95	13.95	14.91
FeO*	10.26	10.12	11.70	11.65	11.64	11.82	11.66	11.68	11.58	10.62
MnO	0.20	0.17	0.17	0.18	0.16	0.12	0.19	0.21	0.14	0.15
MgO	7.16	7.18	6.49	6.26	6.16	6.30	6.26	6.27	6.14	7.15
CaO	11.48	11.56	10.56	10.59	10.62	10.58	10.59	10.62	10.54	11.22
Na_2O	2.91	2.90	2.94	2.93	3.13	3.16	3.11	3.12	3.05	2.90
K_2O	0.09	0.08	0.11	0.14	0.15	0.12	0.13	0.11	0.13	0.08
P_2O_5	0.18	0.17	0.27	0.27	0.26	0.26	0.26	0.28	0.25	0.14
Cr_2O_3	0.06	0.03	0.04	0.03	0.01	0.01	0.02	0.05	0.02	0.04
H_2O		0.34	0.26							
Sum	99.31	100.93	100.64	99.49	99.26	98.86	99.04	99.30	98.87	99.51

Sample	11-8	11-9	11-24	16-9	16-20	16-24	16-28	19-32	19-41	19-45
SiO_2	50.99	50.64	50.38	50.34	50.54	51.02	50.62	50.57	51.35	50.95
TiO_2	1.97	1.90	1.99	1.40	1.48	1.47	1.46	2.38	2.23	2.47
Al_2O_3	15.08	14.54	14.91	15.78	15.49	15.60	15.49	14.08	14.79	13.79
FeO*	10.62	10.72	10.58	9.02	9.27	9.23	9.14	11.36	10.80	12.20
MnO	0.17	0.18	0.12	0.16	0.19	0.14	0.17	0.21	0.15	0.18
MgO	7.23	7.16	7.17	7.70	7.55	7.60	7.63	6.44	6.90	6.27
CaO	11.28	11.21	11.25	12.16	12.10	12.18	12.12	10.76	11.18	10.39
Na_2O	2.90	2.88	2.85	2.97	2.96	2.98	2.96	3.08	2.98	3.13
K_2O	0.08	0.06	0.08	0.08	0.07	0.07	0.06	0.13	0.16	0.12
P_2O_5	0.19	0.12	0.18	0.11	0.14	0.13	0.14	0.25	0.22	0.23
Cr_2O_3	0.05	0.03	0.07	0.04	0.06	0.04	0.04	0.03	0.06	0.02
H_2O	0.26								0.34	
Sum	100.82	99.44	99.58	99.76	99.85	100.46	99.83	99.29	101.06	99.75

			Group 10				Group 11	Group 12		
Sample	19-52	19-54	17-1	17-18	17-31	17-45	20-1	16-2	16-3	16-12
SiO_2	50.87	50.61	50.72	50.84	50.98	51.28	51.75	49.77	50.65	50.06
TiO_2	2.61	2.52	1.29	1.32	1.32	1.57	1.94	1.67	1.66	1.64
Al_2O_3	13.82	14.10	15.83	15.97	15.85	15.25	14.79	16.91	16.97	16.77
FeO*	12.23	11.72	8.93	8.94	8.91	9.81	10.89	8.80	8.77	8.73
MnO	0.17	0.13	0.17	0.14	0.13	0.15	0.17	0.11	0.12	0.14
MgO	6.19	6.58	8.40	8.37	7.92	7.67	7.42	7.84	7.91	7.79
CaO	10.43	10.75	11.82	11.82	11.88	11.76	10.79	11.23	11.38	11.24
Na_2O	3.11	2.91	2.72	2.79	2.82	2.66	2.78	3.08	2.97	3.07
K_2O	0.12	0.13	0.04	0.03	0.03	0.05	0.10	0.20	0.21	0.19
P_2O_5	0.26	0.25	0.11	0.09	0.11	0.13	0.19	0.20	0.23	0.23
Cr_2O_3	0.03	0.03	0.05	0.06	0.07	0.06	0.03	0.03	0.08	0.02
H_2O							0.25		0.33	
Sum	99.84	99.73	100.08	100.37	100.02	100.39	101.10	99.84	101.28	99.88

2.2 Major element glass compositions

The glasses from dredges within the AAD differ significantly from glasses from zone A, having higher SiO_2, Al_2O_3, Na_2O and K_2O and lower TiO_2, FeO* and CaO for a given MgO. Glasses from the AAD are further divided into seven geochemical groups (Groups 1-7) based on major element compositions and the zone A glasses are divided into five groups (Groups 8-12). Two groups were dredged from both station 16 and station 27 but other dredge station ~~are composed of~~ yielded a single geochemical group. This is in an agreement with the studies of Pyle et al. (1992). Some neighbouring stations belong to the same geochemical group e.g. 5 and 6; 9, 10, 11, 19 and part of 16. In Figure 2.2 the major elements are conventionally plotted against MgO.

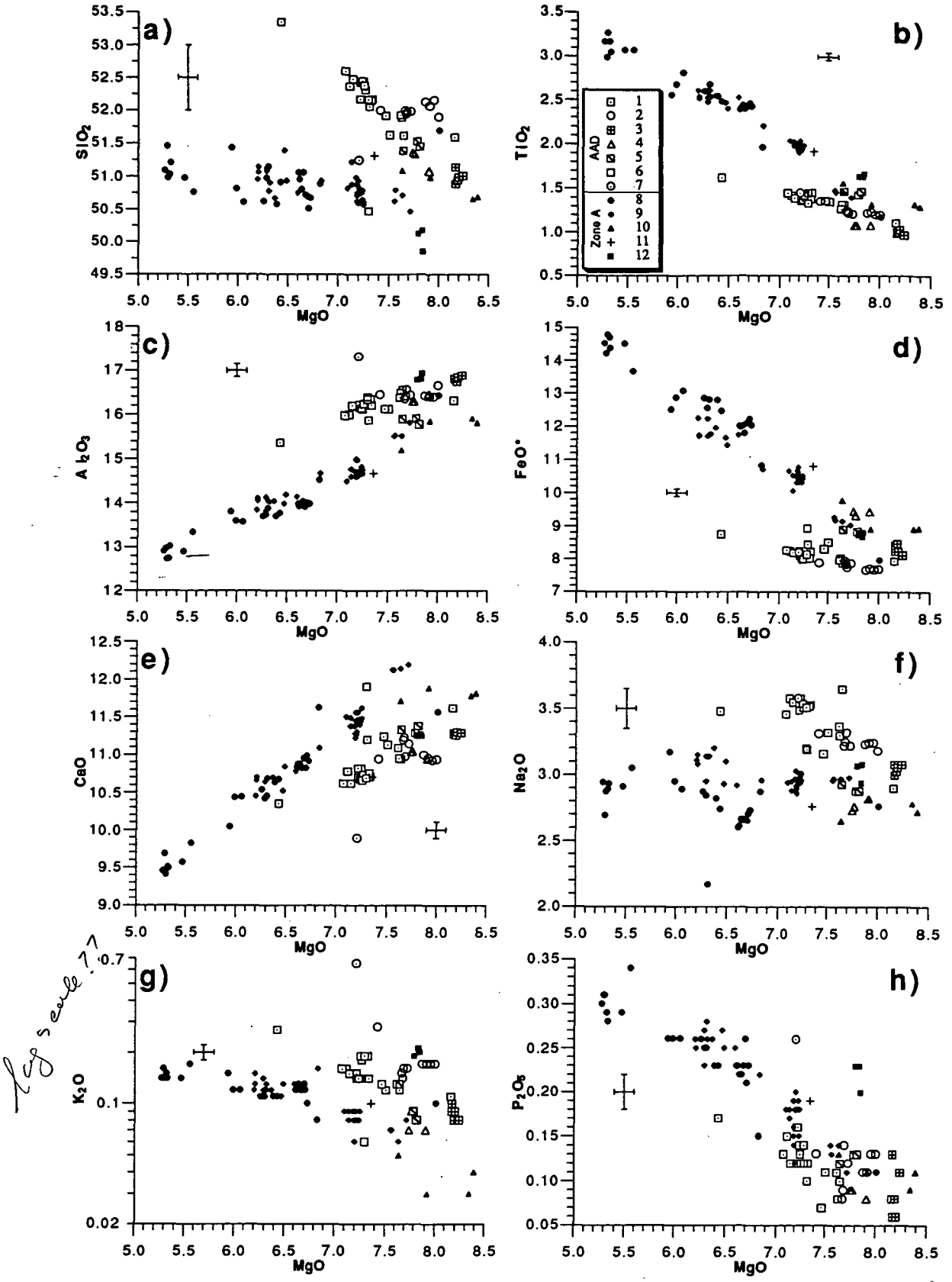

Figure 2.2: Major elements plotted as oxides against MgO for glasses from the Southeast Indian Ridge. 1 = Dredge stations 18, 24 and 27. 2 = Dredge stations 29 and 30. 3 = Dredge station 22. 4 = Dredge station 23. 5 = Dredge stations 5 and 6. 6 = Sample 4-2. 7 = Sample 27-52. 8 = Dredge stations 1, 2, 3, 12 and 13. 9 = Dredge stations 9, 10, 11, 16 and 19. 10 = Dredge station 17. 11 = Sample 20-1. 12 = Samples 2, 3 and 12 from dredge station 16. Groups 1-7 are from the AAD whereas groups 8-12 are from zone A. The crosses show the average standard deviation of the microprobe analyses.

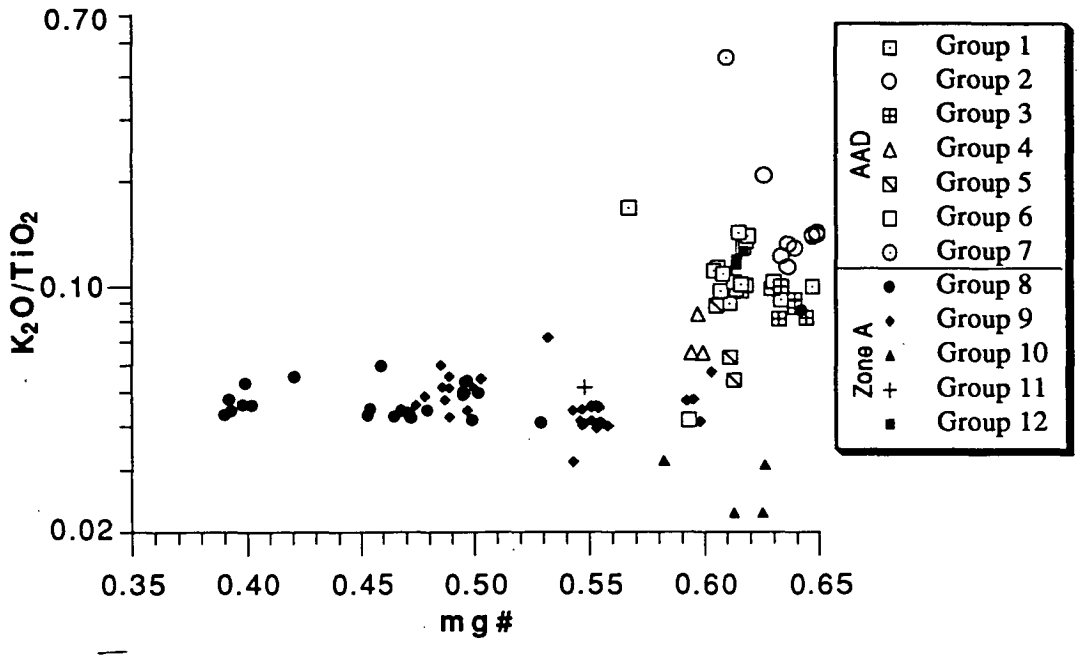

Figure 2.3: K_2O/TiO_2 plotted against the mg# for glasses from the Southeast Indian Ridge.

Group 1 consists of twenty glasses from stations 18, 24 and 27 that define the main trend for the AAD (Fig. 2.2). MgO varies from 8.1 to 6.4% but FeO* shows small variations, ranging from 7.9 to 8.7%. SiO_2 and Na_2O rise sharply over this MgO interval, TiO_2 and K_2O rise and Al_2O_3 and CaO decrease. Other glasses from the AAD show in general the same behaviour. Group 2 is composed of nine glasses from stations 29 and 30 and differs from group 1 by having higher SiO_2 and K_2O and slightly lower FeO*. Five glasses from station 22 (Group 3) and three glasses from station 23 (Group 4) are similar in almost all major elements but there is a clear difference between the two stations in Na_2O content. Compared to the main trend (Group 1) these glasses have lower TiO_2, Al_2O_3, CaO and K_2O and higher FeO*. Three glasses from stations 5 and 6 (Group 5) have high TiO_2 and FeO* and low Al_2O_3 and Na_2O, whereas one sample from station 4 (Group 6) has very low SiO_2 and K_2O and high CaO. Finally sample 27-52 (Group 7) has high Al_2O_3, K_2O and P_2O_5 and low SiO_2 and CaO compared to the other AAD samples.

Groups 8 and 9, from stations 1, 2, 3, 12 and 13 on one hand and stations 9, 10, 11, 16 and 19 on the other hand, form the main trend for the zone A glasses but are separated by some minor differences in Al_2O_3, FeO* and Na_2O content. Glasses from station 17 (Group 10) are grouped separately because of their low K_2O content and a single glass from station 20 (Group 11) because of its low CaO content. Three glasses from station 16 (Group 12) are distinguished by having low SiO_2 and CaO, and high Al_2O_3, K_2O and P_2O_5.

In Figure 2.3, K_2O/TiO_2, a ratio which does not change substantially with crystallization of olivine, spinel, plagioclase or clinopyroxene, is plotted against the

mg# value (mg# = Mg/(Mg + Fe^{2+}); all iron calculated as Fe^{2+}). Most AAD glasses are relatively primitive (mg# > 0.60), so the variable K_2O/TiO_2 (0.03-0.5) cannot be explained by crystal fractionation. Glasses from zone A have a wider range of mg# (0.64-0.39) and the majority of glasses have almost constant K_2O/TiO_2, between 0.04-0.06. Glasses from station 17 have lower K_2O/TiO_2 (0.02-0.03) and plot below all the other samples whereas group 12 has K_2O/TiO_2 above 0.1 and plots together with the AAD samples.

Glass 27-52 (Group 7) from the AAD has E-MORB like composition, with low SiO_2 and CaO and high K_2O and P_2O_5. An E-MORB signature is also evident in some glasses from zone A, with those from group 12 showing low SiO_2 and CaO and high K_2O and P_2O_5 compared to all the other zone A glasses (Fig 2.2).

Thus the data for naturally quenched glasses suggests that there are several magma types available in both the AAD and in the eastern zone A, and that these magma types are not related by simple crystal fractionation and re-mixing. To a first approximation, magmas from zone A have a dominant magma type with $K_2O/TiO_2 \sim 0.05$ but more depleted ($K_2O/TiO_2 \sim 0.02$) and enriched ($K_2O/TiO_2 \sim 0.13$) types do occur. Within the AAD, K_2O/TiO_2 ranges from that of zone A ($K_2O/TiO_2 \sim 0.04$) to more enriched ($K_2O/TiO_2 \sim 0.6$), all within relatively unfractionated magmas.

2.3 Samples suitable for melt inclusion studies

As noted above, only four rock samples were sufficiently phyric for separation of phenocrysts for melt inclusion work. Samples 18-9, 18-17 and 24-14 are from Group 1 and their glass compositions are among the least evolved with MgO = 7.47 (Mg# = 0.64; Mg# = Mg/(Mg + Fe^{2+}) with assumed $Fe^{2+}/(Fe^{2+} + Fe^{3+})$= 0.9) in sample 18-9, MgO = 7.58 (Mg# = 0.66) in sample 18-17 and MgO = 7.30 (Mg# = 0.64) in sample 24-14. Sample 29-2 is from Group 2 and again is relatively primitive with MgO = 7.91 (Mg# = 0.67). This sample has higher SiO_2 and K_2O and lower CaO than the Group 1 samples.

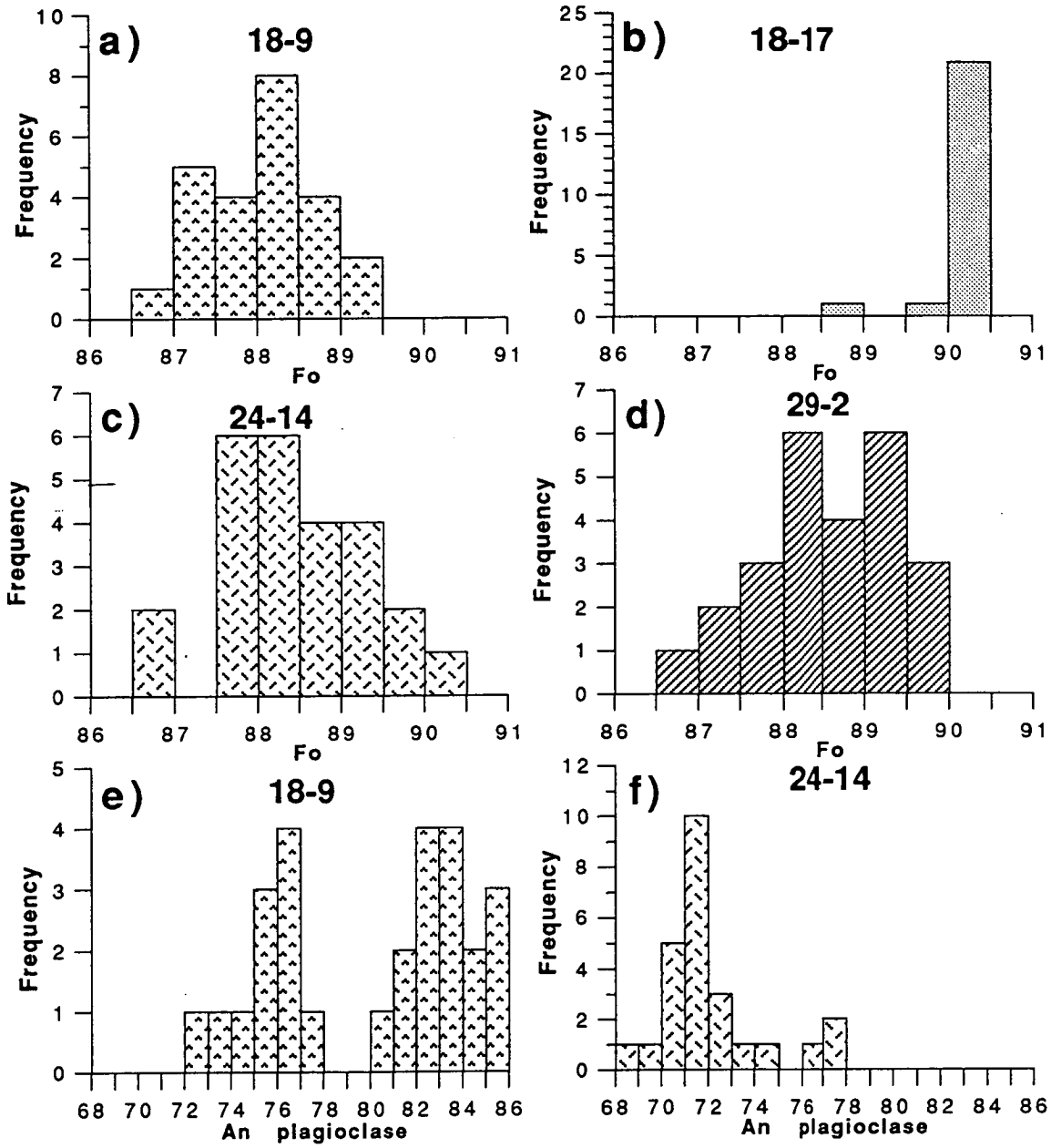

Figure 2.4: Histograms showing the composition of olivine and plagioclase. a) Olivine in sample 18-9. b) Olivine in sample 18-17. c) Olivine in sample 24-14. d) Olivine in sample 29-2. e) Plagioclase in sample 18-9. f) Plagioclase in sample 24-14.

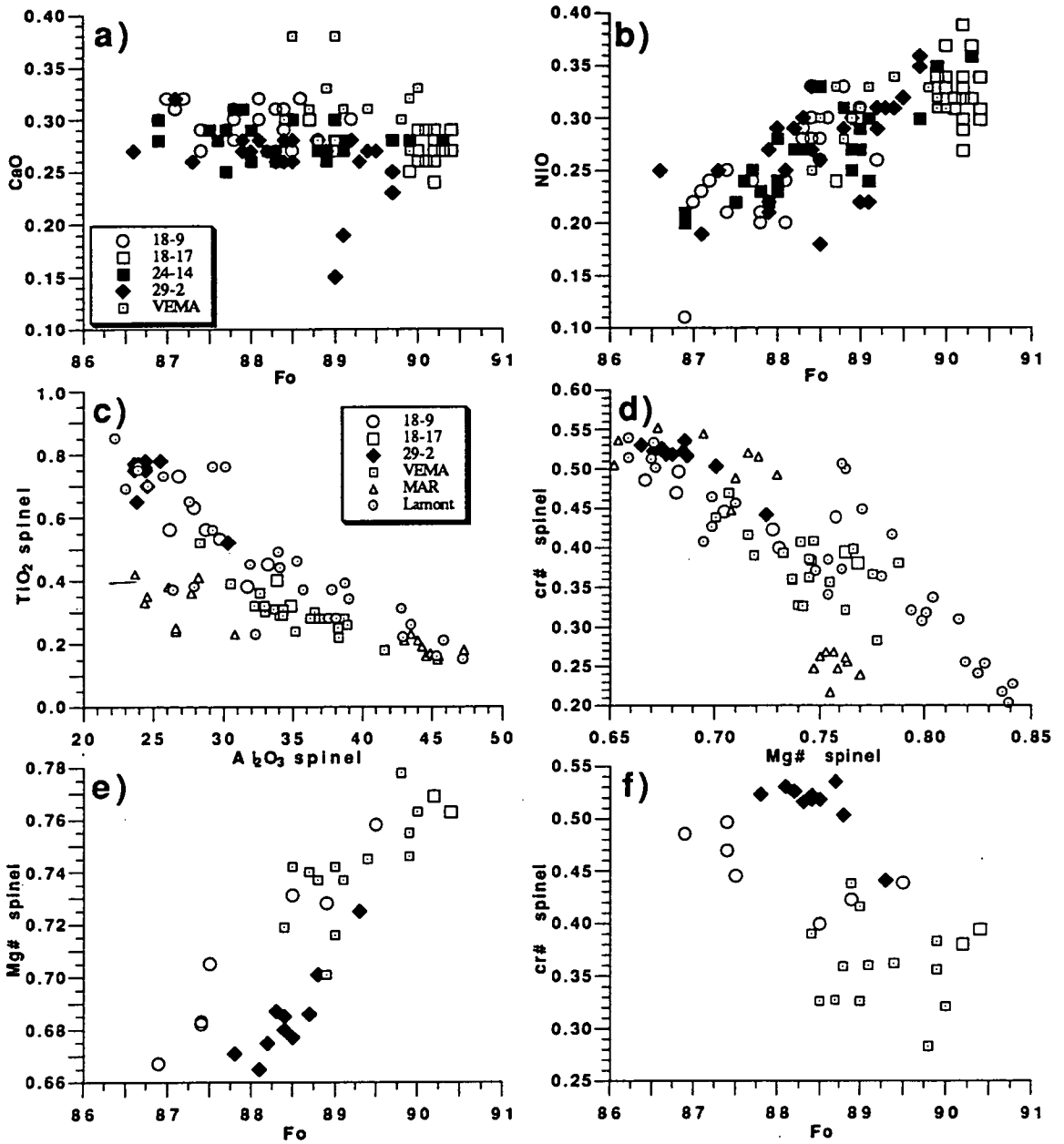

Figure 2.5: Diagrams showing compositions of olivine and spinel. a) CaO in olivine vs Fo. b) NiO in olivine vs Fo. c) TiO_2 vs Al_2O_3 in spinel. d) $cr^{\#}$ vs $Mg^{\#}$ in spinel. e) $Mg^{\#}$ in spinel vs Fo in host olivine. f) $cr^{\#}$ in spinel vs Fo in host olivine. Also shown for comparison are compositions of olivine and spinels from VEMA fracture zone at 10 °N on the Mid-Atlantic Ridge (Sobolev et al., 1989), and spinels from the Mid-Atlantic Ridge (Sigurdsson and Schilling, 1976) and from the East Pacific Rise and Lamont Seamounts (Allan et al., 1988).

2.4 Olivine, spinel and plagioclase compositions

Compositions of olivine from each of the four samples and plagioclase from samples 18-09 and 24-14 are shown in Figure 2.4, and in Appendix 3. No plagioclase was analysed from samples 18-17 and 29-02. Olivine and spinel relationships are shown in Figure 2.5 and in Appendix 4.

Olivine in sample 18-17 has a narrow compositional range between $Fo_{90.5-90}$ whereas olivine compositions in the other samples vary from $Fo_{90.5-86.5}$ (Fig. 2.4a-d). Profiles through individual phenocrysts show that zoning is less than half a Fo and An unit in all cases. CaO in olivine is almost constant (0.25-0.30) in the range Fo_{90-87} whereas NiO decreases from 0.35-0.20 (Fig. 2.5).

No spinels were found as discrete phenocrysts and only few spinels were found as inclusions in olivine. These spinels are plotted in Figure 2.5c-f. Also shown in Figure 2.5 are compositions of spinel phenocrysts and spinel inclusions from MORB samples from the Mid-Atlantic ridge (Sigurdsson and Schilling, 1976; Sobolev et al., 1989) and from the East Pacific Rise and Lamont seamounts (Allan et al., 1988). The spinels from sample 18-17, with a very restricted olivine composition range, have the highest Al_2O_3 and $mg^{\#}$ and lowest TiO_2 and $cr^{\#}$. If plagioclase is crystallizing together with olivine and spinel in MORB then spinels become less aluminous with increasing crystallization, and therefore have higher $cr^{\#}$ accompanying the increase in TiO_2 (Allan et al., 1988, Fig. 2.5). This is because Mg and Al decrease in the fractionating magma and Fe and Cr substitute for Mg + Al in spinel respectively. For example spinel in olivine Fo_{89} from sample 18-9 has 31.8% Al_2O_3, 0.38% TiO_2 and $cr^{\#}$ of 0.42 whereas spinel in olivine Fo_{87} in the same sample has 26.8% Al_2O_3, 0.73% TiO_2 and $cr^{\#} = 0.49$. This evolutionary trend is consistent with the trend shown by the spinels in other MORB samples (Fig. 2.5c-d). Thus the spinel data indicate that plagioclase accompanied olivine + spinel as a high-temperature or near-liquidus phase in these basalts.

Plagioclase compositions in sample 18-9 show a bimodal distribution, with one group having composition between An_{86-80} and another group between An_{78-72}. Plagioclase in sample 24-14 has the compositional range An_{78-68} with most plagioclases around An_{72} (Fig. 2.4e, f).

2.5 Heating stage experiments

Experiments were only carried out on inclusions in olivine phenocrysts, as the inclusions in plagioclase phenocrysts were too small for inclusion studies (< 20 μm).

2.5.1 Kinetic experiments

Kinetic experiments were done on inclusions in olivine phenocrysts from sample 18-9 to check for changes in T_h with time at high temperatures (see chapter 1) and establish the heating rate that should be used during experiments. No rise was observed in T_h with time but magnetite started to crystallize in the inclusion after just over one hour at T > 1000 °C. This indicates the presence of some H_2O in the melt and H_2 diffusion during the experiment (Sobolev et al., 1983). However, this effect

should be negligible if the duration of the experiments at temperatures above 1000 °C is less than half an hour.

No change was observed in the T_h during the experiments and therefore it was possible to do a series of kinetic experiments on a single inclusion, starting with a heating rate of 60 °C/minute and using a slower heating rate each time. The result showed that the T_h decreases until a heating rate of 5 °C/minute is used. A heating rate of 1 °C/minute did not lower the observed T_h but when the inclusion was left at a temperature 5 °C below the T_h for a heating rate of 5°C/ minute, it homogenized after 20 minutes. During all experiments a heating rate of 5 °C/minute was used, but close to the homogenization temperature the heating rate was lowered to 1 °C/minute. This should minimize, though not exclude, the risk of overheating the inclusions and thus overshooting the homogenization temperature.

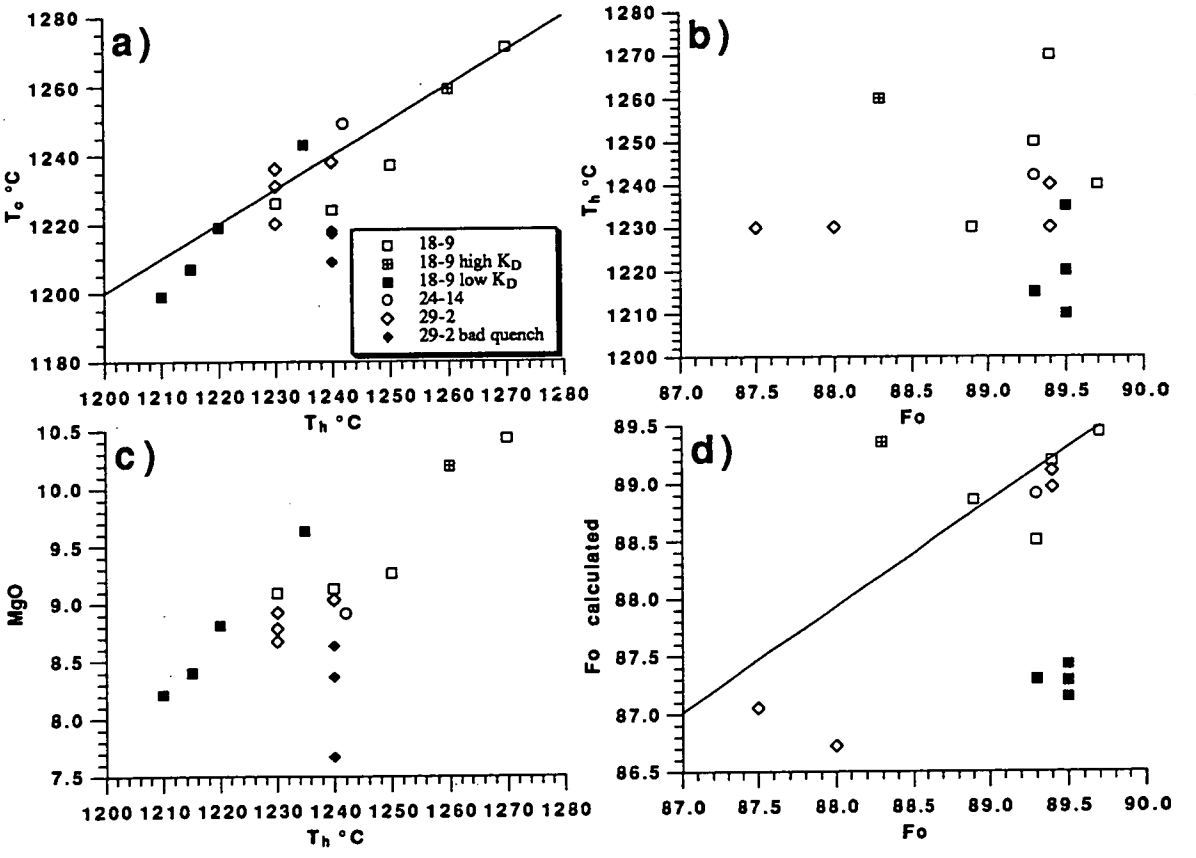

Figure 2.6: a) Calculated dry equilibrium liquidus temperature (T_C) vs temperature of homogenization (T_h) for all the inclusions. b) T_h vs Fo content of the host olivine. c) MgO content of the melt inclusion vs T_h. d) Calculated Fo content in equilibrium with the melt inclusion vs the Fo content of the host olivine. T_c and Fo content were calculated using the model of Ford et al., (1983).

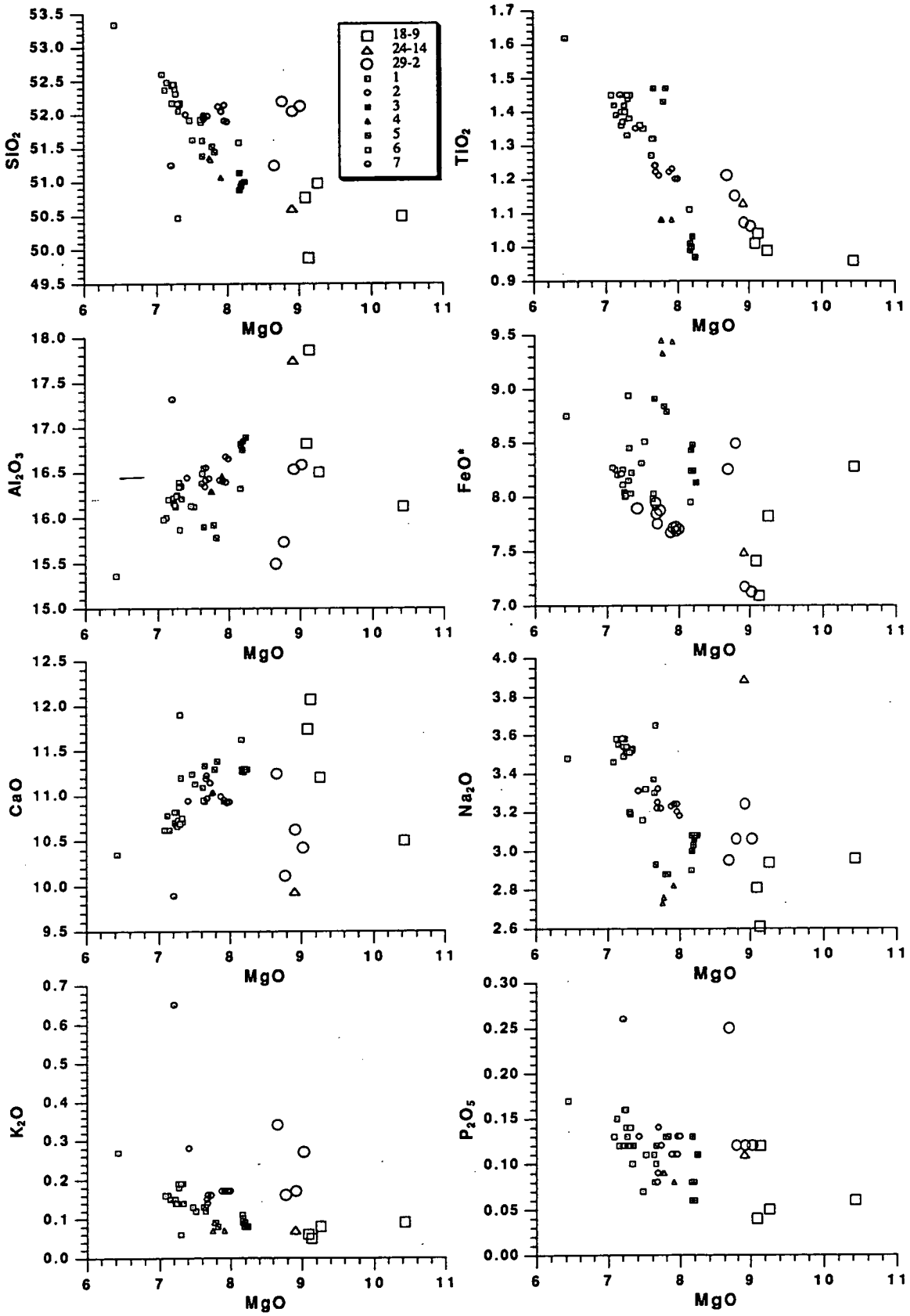

Figure 2.7: The compositions of melt inclusions from the heating stage experiments plotted as oxides against MgO, together with the seven groups of matrix glasses from the AAD.

Table 2.2: The compositions of the nine melt inclusions, and their host olivine, that were accepted as representing true melt compositions. T_c is olivine temperature calculated using the model of Ford et al., 1983 and Fo_c is the calculated Fo content of the liquidus olivine for the melt inclusion.

Sample	18-9	18-9	18-9	18-9	24-14	29-2.	29-2.	29-2.	29-2.
Olivine	295	209	87	2	201	1	2	5	42
SiO_2	40.73	40.31	40.11	40.33	40.99	40.40	40.93	40.48	40.05
Cr_2O_3	0.07	0.06	0.04		0.06				
FeO	10.51	10.00	10.41	10.68	10.58	11.87	10.40	10.19	12.09
MnO	0.16	0.12	0.16		0.18				
MgO	49.59	49.07	48.99	48.14	49.36	48.87	49.46	48.48	47.64
CaO	0.29	0.29	0.29	0.25	0.27	0.26	0.24	0.29	0.31
NiO	0.28	0.28	0.35		0.30				
Sum	101.63	100.13	100.35	99.40	101.74	101.40	101.03	99.45	100.10
Fo	89.4	89.7	89.3	88.9	89.3	88.0	89.5	89.5	87.5
Inclusion	295	209	87	2	201	1	2	5	42
SiO_2	50.81	49.64	51.03	51.09	51.28	52.70	53.02	51.79	51.67
TiO_2	0.97	1.04	0.99	1.02	1.14	1.16	1.09	1.05	1.22
Al_2O_3	16.22	17.77	16.52	16.92	17.98	15.88	16.84	16.48	15.62
FeO*	8.34	7.05	7.82	7.46	7.59	8.57	7.31	7.07	8.32
MnO	0.08	0.11	0.13	0.21	0.07	0.08	0.01	0.12	0.11
MgO	10.50	9.09	9.27	9.15	9.03	8.87	9.09	8.97	8.74
CaO	10.57	12.01	11.21	11.81	10.07	10.21	10.82	10.35	11.33
Na_2O	2.98	2.60	2.94	2.83	3.94	3.09	3.30	3.04	2.97
K_2O	0.09	0.05	0.08	0.06	0.07	0.16	0.17	0.27	0.34
P_2O_5	0.06	0.12	0.05	0.04	0.11	0.12	0.12	0.12	0.25
Cr_2O_3	0.02	0.04	0.05	0.04	0.04	0.12	0.12	0.11	0.26
Sum	100.64	99.52	100.09	100.62	101.32	100.97	101.89	99.37	100.83
T_h °C	1270	1240	1250	1230	1242	1230	1230	1240	1230
K_D	0.30	0.29	0.28	0.30	0.28	0.28	0.29	0.30	0.30
T_c °C	1271	1224	1237	1226	1249	1231	1236	1238	1220
Fo_c	89.2	89.5	88.5	88.9	88.9	86.7	89.0	89.1	87.1

2.5.2 Results from heating stage experiments

The first four experiments were quenched at temperatures between 1210-1240 °C, before homogenization, but homogenization was achieved in nine experiments at temperatures between 1240-1270 °C. Seventeen inclusions were analysed from those experiments. The dry equilibrium liquidus temperature (T_c) calculated using the model of Ford et al. (1983) is plotted against the T_h in Figure 2.6a. T_c is close to T_h in most cases but three inclusions, all in the same olivine grain, lie significantly below the 1:1 line which indicates bad quenching in that experiment. In Figure 2.6b, Fo of the host olivine is plotted against T_h (temperature of quenching for four inclusions). Most olivines have compositions between $Fo_{89-89.5}$ and the T_h for that compositional range is 1210-1270 °C. This temperature range is greater than the uncertainty of the technique, so there has to be another explanation for this temperature range. In Figure 2.6c, MgO shows a good correlation with T_h as expected, since the MgO content of an

olivine-saturated melt is controlled by temperature. The three inclusions with the low T_c fall off the trend in Figure 2.6c supporting that the quenching was bad in this experiment. These three inclusions were therefore discarded and they will not be discussed any further here. The calculated forsterite content of olivine in equilibrium with the homogenized melt inclusions (calculated using the model of Ford et al., 1983) is in most cases lower than the actual forsterite content of the host olivine (Fig. 2.6d). In most cases the difference is less than one forsterite unit, with $K_{D_{Fe\text{-}Mg}}^{ol\text{-}liq} = 0.27\text{-}0.30$, but in the four inclusions that were quenched before homogenization, the difference is more than two forsterite units and the $K_{D_{Fe\text{-}Mg}}^{ol\text{-}liq} = 0.24\text{-}0.25$. This indicates that these inclusions were significantly removed from homogenization and they will therefore not be discussed further. One inclusion in olivine $Fo_{88.3}$ has calculated forsterite content higher than the actual forsterite content, $K_{D_{Fe\text{-}Mg}}^{ol\text{-}liq} = 0.34$, indicating that this inclusion was over heated. This leaves nine inclusions, with homogenization temperature in the range 1230-1270 °C, which pass the various tests as outlined in chapter 1. Their major element compositions are shown in Table 2.2 and plotted in Figure 2.7 together with the natural glasses from groups 1-7 from within the AAD.

The homogenized melt inclusions have MgO in the range 10.4-8.6%. Three inclusions from sample 18-9 form an extension of the trend shown by group 1 on the SiO_2 and TiO_2 vs MgO diagram, but do not lie on the Al_2O_3 and CaO trends. They have lower Al_2O_3 and CaO contents suggesting either that olivine (± spinel) was the only liquidus phase when these three inclusions were trapped or that these inclusions were overheated, resulting in the addition of olivine component. FeO* content is not consistent with crystal fractionation of a single melt and the variations in other oxides in the inclusions is similar to the variations shown by group 1 as a whole. The fourth melt inclusion from sample 18-9 (209) has lower SiO_2, Na_2O and FeO* and higher Al_2O_3 and CaO. It extends the trends shown by Al_2O_3 to significantly higher Al_2O_3, which indicates that both olivine and plagioclase were on the liquidus when this inclusion was trapped. Although it is not the most MgO-rich of the homogenized melts, inclusion 209 is in a more forsteritic olivine than the other three inclusions from sample 18-9, but it has relatively low T_h (1240 °C). Because this inclusion contains high Al_2O_3 together with high MgO, whereas the other three inclusions fall on an olivine-addition vector, there remains the possibility that all the melt inclusions, except for inclusion 209, were over heated. However differences in K_2O/TiO_2, K_2O/Na_2O and K_2O/P_2O_5 among these four homogenized inclusions also show that they do represent different melt lineages and furthermore that some were evolving on olivine + plagioclase + spinel cotectic while others were evolving only on olivine + spinel cotectic. The more limited data set of more primitive liquids obtained by the melt inclusion experiments is re-inforced by the matrix glasses, which indicate a spread of parental melt compositions being pooled. However, because overheating cannot be

ruled out in the compositions lying at higher MgO but lower Al_2O_3, this must be kept in mind before these inclusions are used to infer the parental magma composition.

The single inclusion from sample 24-14 also has high Al_2O_3 content but it differs from inclusion 209 by significantly lower CaO and higher Na_2O contents. Again these differences point to differences in parent magma compositions.

The four inclusions from sample 29-2, (which belongs to group 2), have higher SiO_2 than all the other inclusions and show a wide range of Al_2O_3, FeO*, CaO and K_2O contents. Their high SiO_2 and K_2O, and low CaO contents compared to the inclusions from sample 18-9 are all consistent with the differences that separate group 1 from group 2.

In general the inclusions from each sample show variations in most major elements that are greater than can be explained by evolution via crystal fractionation from a single parental melt. The study of melt inclusions and of their homogenization temperatures shows that in the AAD, magma mixing occurs very early in the magma evolution path. The individual melt components include olivine + plagioclase + spinel saturated melts and olivine + spinel saturated melts but they also have different K_2O, TiO_2, Na_2O etc.

2.5 Discussion

By using the concentration of SiO_2, FeO and Na_2O normalized to 8% MgO ($Si_{8.0}$, $Fe_{8.0}$, $Na_{8.0}$) together with CaO/Al_2O_3 and axial depth, Klein and Langmuir (1987; 1989) suggested that these parameters might give information on the temperature, mean pressure and extent of partial melting.

Figure 2.8 shows that the lowest CaO/Al_2O_3, $Fe_{8.0}$ and the highest $Si_{8.0}$ and $Na_{8.0}$ occur in samples from the AAD where the depth to the ridge axis is greater than in zone A. Klein et al. (1991) used this observation to infer that magmas beneath the AAD were generated at lower pressure and by lesser extent of melting because the mantle was significantly cooler beneath the AAD than beneath zone A. The heating stage experiments on olivine in sample 18-9 from the AAD show that the crystallization temperature for olivine $Fo_{89.5}$ was approximately 1240 °C which is the same (1220-1240 °C) as for olivine Fo_{89-90} in typical N-MORB from 10 °N on the Mid-Atlantic Ridge studied by the same method (Sobolev et al., 1989). Also the composition of olivine in samples 18-9, 18-17, 24-9 and 29-2 and plagioclase in sample 18-9 (Fig. 2.4) is comparable to the most primitive compositions found in N-MORB samples in general (e.g. Dmitriev et al., 1985; Sobolev et al., 1989), showing that the crystallization temperature at least was not much different in the AAD samples from typical N-MORB.

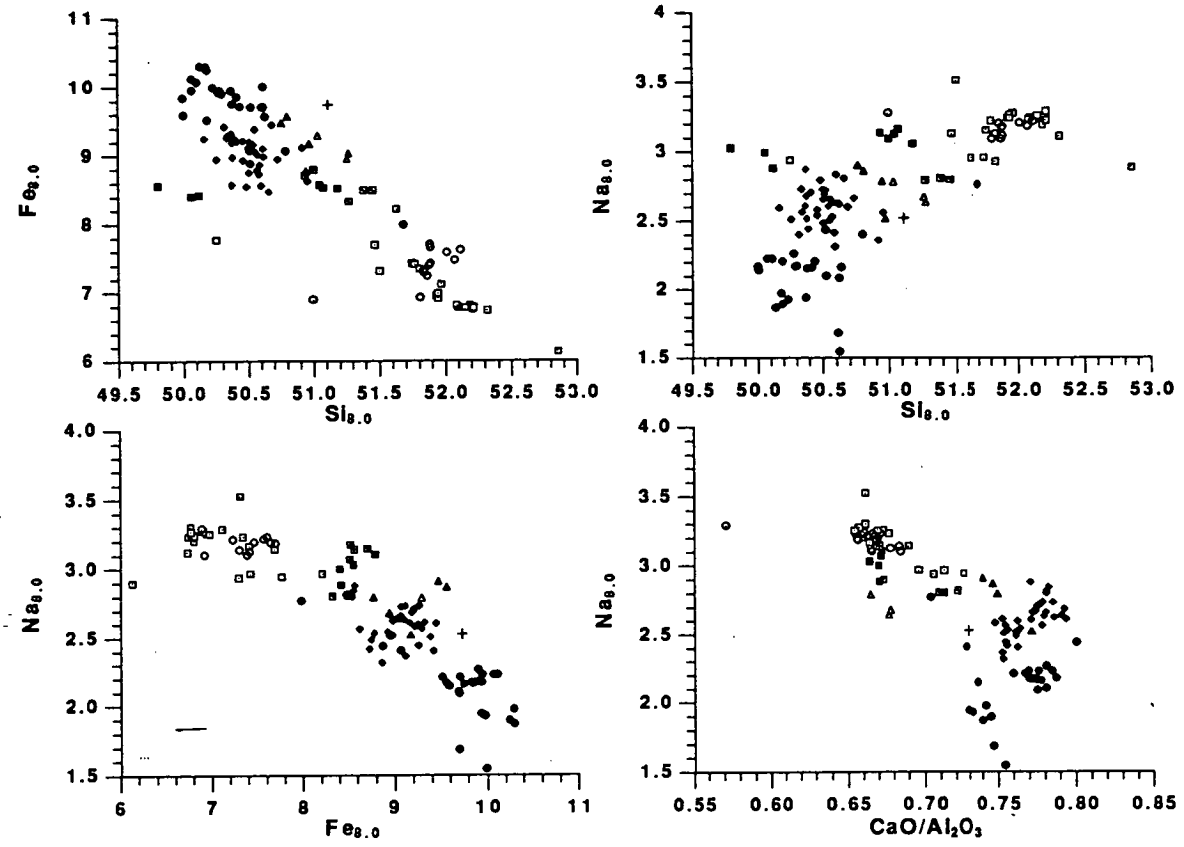

Figure 2.8: Relations between CaO/Al_2O_3 and SiO_2, FeO* and Na_2O calculated to 8 % MgO ($Si_{8.0}$, $Fe_{8.0}$ and $Na_{8.0}$) according to the method of Klein and Langmuir (1987, 1989). Samples and legend to symbols same as for Figure 2.2.

The method Klein and Langmuir (1987; 1989) used to calculate SiO_2, FeO* and Na_2O back to 8.0% MgO projects these elements along subparallel vectors using the equations:

$$Na_{8.0} = Na_2O + 0.373MgO - 2.98$$

$$Fe_{8.0} = FeO + 1.664MgO - 13.313$$

$$Si_{8.0} = SiO_2 + 0.31MgO - 2.48$$

These equations are used for samples containing 5.0-8.5% MgO.

In light of the different behaviour of SiO_2, FeO* and Na_2O shown by the AAD and zone A samples (Fig. 2.2) this calculation method gives very biased results. Because of their contrasting trends, it is obviously inappropriate to use the same extrapolation relationship for both groups of compositions. In Figure 2.9, in which $Si_{8.0}$, $Fe_{8.0}$, $Na_{8.0}$ and CaO/Al_2O_3 are plotted against the $mg^{\#}$ of the glasses, it is obvious that the most evolved samples are calculated to the lowest $Na_{8.0}$ and highest $Fe_{8.0}$ because of the difference between the slopes of the calculation vector and the slope of the actual trend shown by the glasses (Fig. 2.2). It is quite possible though that the apparent constant Na_2O in the zone A glasses in Figure 2.2f could be a combination of subparallel trends, as fractionation of olivine, plagioclase and clinopyroxene leads to an increase in Na_2O.

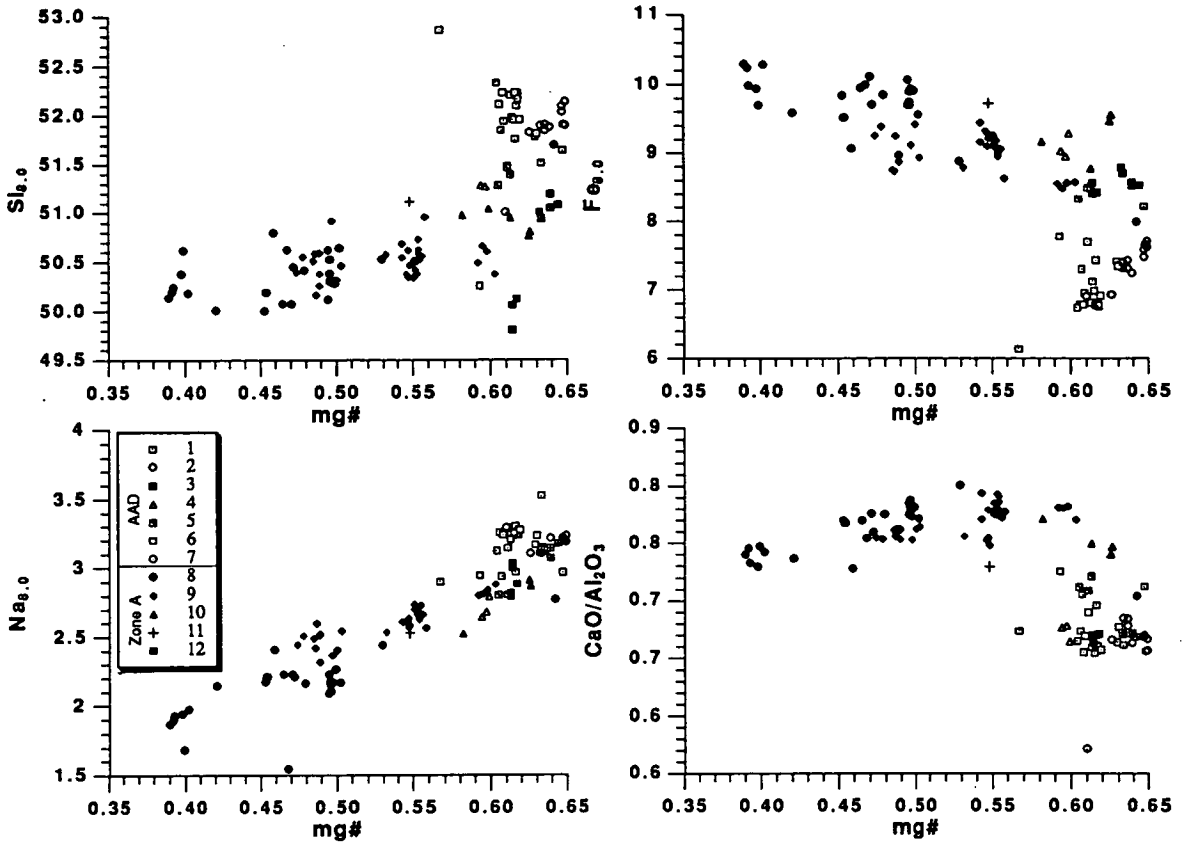

Figure 2.9: $Si_{8.0}$, $Fe_{8.0}$ and $Na_{8.0}$ and CaO/Al_2O_3 vs $mg^{\#}$ for the matrix glasses form the AAD and zone A. Legend to symbols same as for Figure 2.2.

For a given MgO the basalts from the AAD have higher SiO_2 and Na_2O and lower FeO* than the basalts from zone A. Therefore if both basaltic suites are derived from a similar mantle source, the behaviour of SiO_2, FeO* and Na_2O in the experiments of Jaques and Green (1980) would suggest that the AAD basalts were derived by lower degree of melting and at lower pressure than the zone A basalts. It is not clear though whether these variations are caused by differences in melting systematics or by some other factors such as crystal fractionation or magma mixing. For example, at approximately 8% MgO there does not seem to be much difference between the AAD and zone A glasses in almost all the major elements (Fig. 2.2).

In Figure 2.10 the major elements of all the matrix glasses are plotted together with the glass inclusions from the experiments, this time using $mg^{\#}$ as an abscissa instead of MgO. Because of the lower FeO* content for a given MgO in the AAD glasses they plot at higher $mg^{\#}$ than the zone A glasses and on the TiO_2 and Al_2O_3 diagrams the AAD trend overprints the zone A trend. The matrix glasses from groups 3 and 4 plot at lower TiO_2 for a given $mg^{\#}$ and groups 3, 4 and 7 from the AAD and group 12 from zone A plot at higher Al_2O_3. The difference in Al_2O_3 is likely to be the result of a later appearance of plagioclase on the liquidus in these glasses whereas the difference in TiO_2 is harder to explain in terms of crystal fractionation. There is, though, a

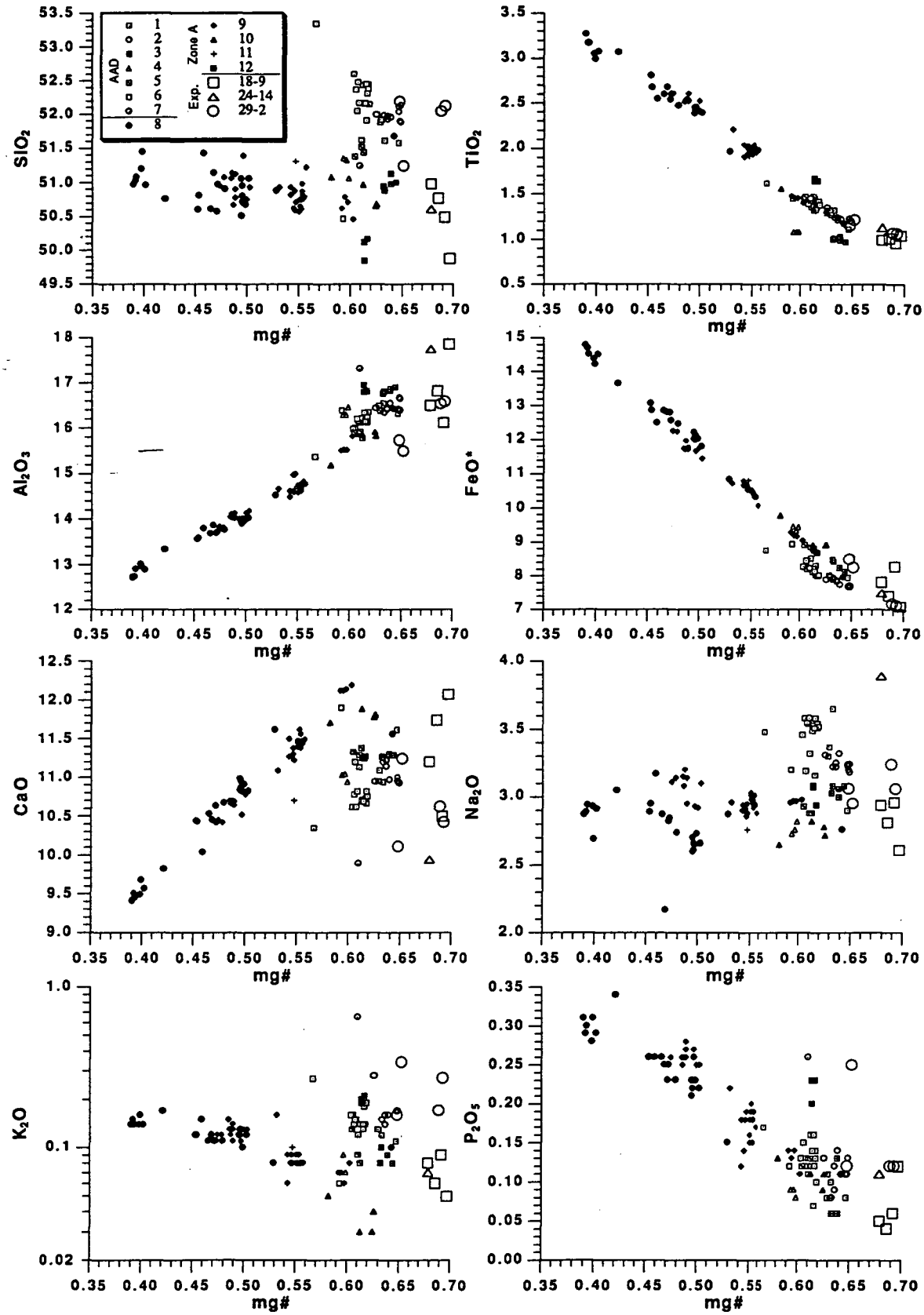

Figure 2.10: Compositions of the matrix glasses from the AAD and zone A and the inclusions vs mg#.

difference between the less primitive AAD glasses and the zone A glasses in all the other major elements, but on almost all plots the more primitive glasses seem to be similar. Examination and presentation of the data in this way suggests that the difference in AAD and zone A glasses are not mantle source differences but are differences generated in subjacent "intermediate" magma chambers, which may reflect different depths (olivine or olivine + plagioclase saturation), different wall-rock interaction and different mixing components entering the magma chamber. There is a significant difference in CaO contents between the AAD and zone A basalts although groups 11 and 12 and a single glass from group 8 approach the AAD samples. This could be because of earlier appearance of clinopyroxene in the AAD samples due to crystallization at higher pressures. This will be discussed in the next section.

2.5.1 Crystal fractionation models

The program Petrolog (Danyushevsky et al., 1990) was used to model the fractional crystallization down to 6% MgO to test if it was possible to reproduce the trend shown by groups 8 and 9 by fractionation of olivine, plagioclase and clinopyroxene. But first as a test case the program was tried on glasses from three MORB suites, ODP hole 896A (A. McNeill, unpublished), Galapagos Platform (Sinton et al., 1993) and VEMA on the Mid-Atlantic Ridge at 10 °N (Sobolev et al., 1989). The results from the modelling are shown in Figure 2.11.

The program uses the model of Ford et al. (1983) for olivine, Ariskin et al. (1986) for clinopyroxene and either Ariskin and Barmina (1990) or Drake (1976) for plagioclase. When the Ariskin and Barmina (1990) model for plagioclase is used the liquid line of descent has similar slope for most major elements but it is displaced somewhat from the actual trends because the program calculates plagioclase alone on the liquidus for the first few percent of crystallization before plagioclase is joined by olivine and later by clinopyroxene. This causes MgO to rise initially, thus the shift in the trend to higher MgO (Fig. 2.11). The Drake (1976) model on the other hand gives fractionation paths that have different slopes from the actual trends shown by the samples (Fig. 2.11). The model thus gives reasonable fractionation trends if the model of Ariskin and Barmina (1990) is used for plagioclase together with the models of Ford et al. (1983) for olivine and Ariskin et al. (1986) for clinopyroxene.

For modelling of the zone A glasses, sample 16-9 from group 9 was first chosen as a starting compositions (Fig. 2.12). Like in the examples above, the program initially calculates plagioclase alone on the liquidus, causing MgO to rise from 7.7-8.1% until olivine joins plagioclase on the liquidus, followed shortly after by clinopyroxene. When the liquid reaches 6% MgO over 50% has crystallized. The modelled crystallization path is in reasonable agreement with the trend shown by groups 8 and 9, apart from the shift to higher MgO caused by the initial plagioclase fractionation.

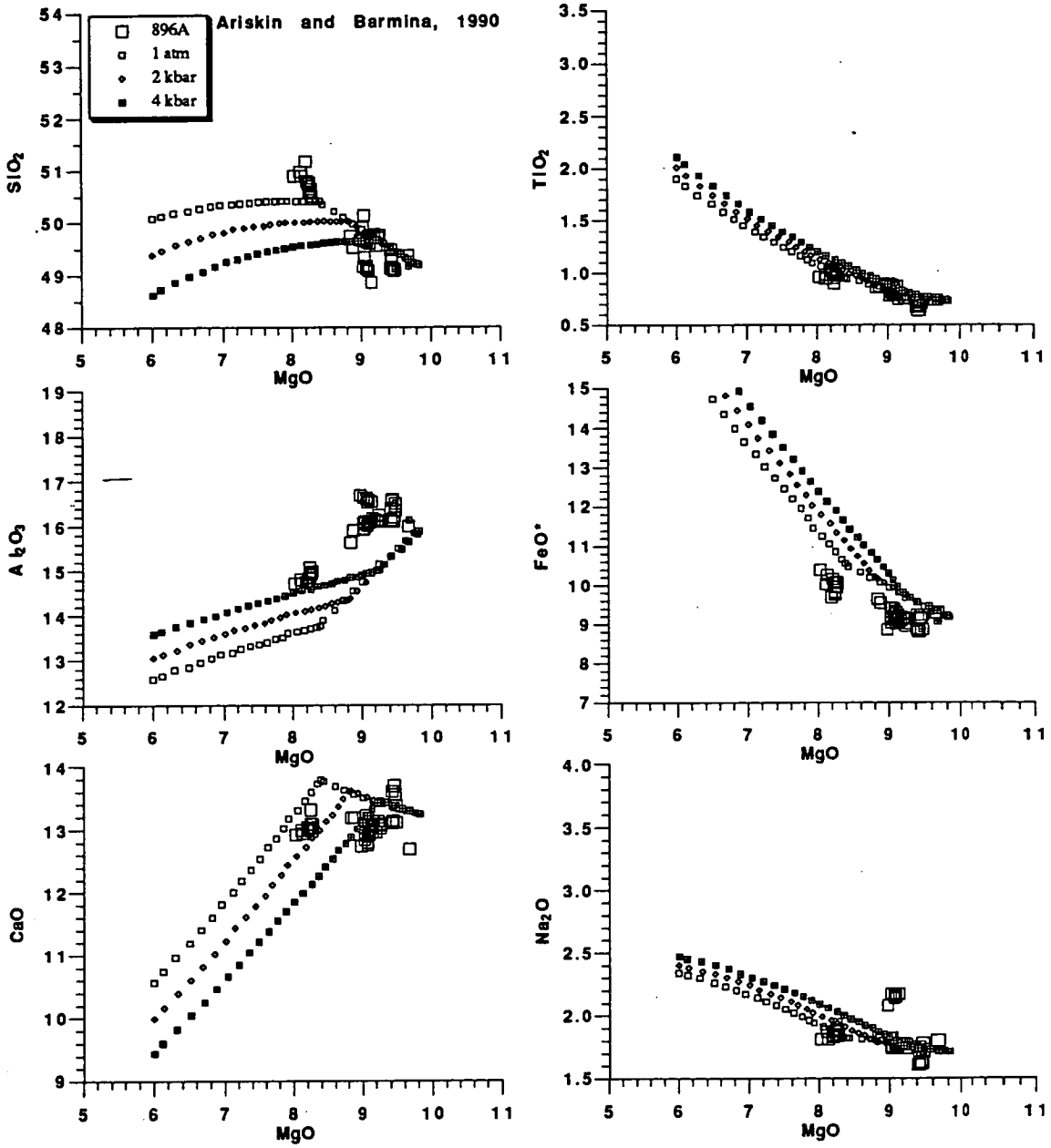

Figure 2.11: Calculated crystal fractionation paths for a primitive glass from three suites of basaltic glasses using the program Petrolog (Danyushevsky et al., 1990). The program used the models of Ford et al., (1983) for olivine, Ariskin (1986) for pyroxene and either Drake (1976) or Ariskin and Barmina (1990) for plagioclase. a) Glasses from ODP hole 896A (A. McNeill, unpublished) and calculated fractionation paths at 1 atm, 2 kbar and 4 kbar, using the model of Ariskin and Barmina (1990) for plagioclase.

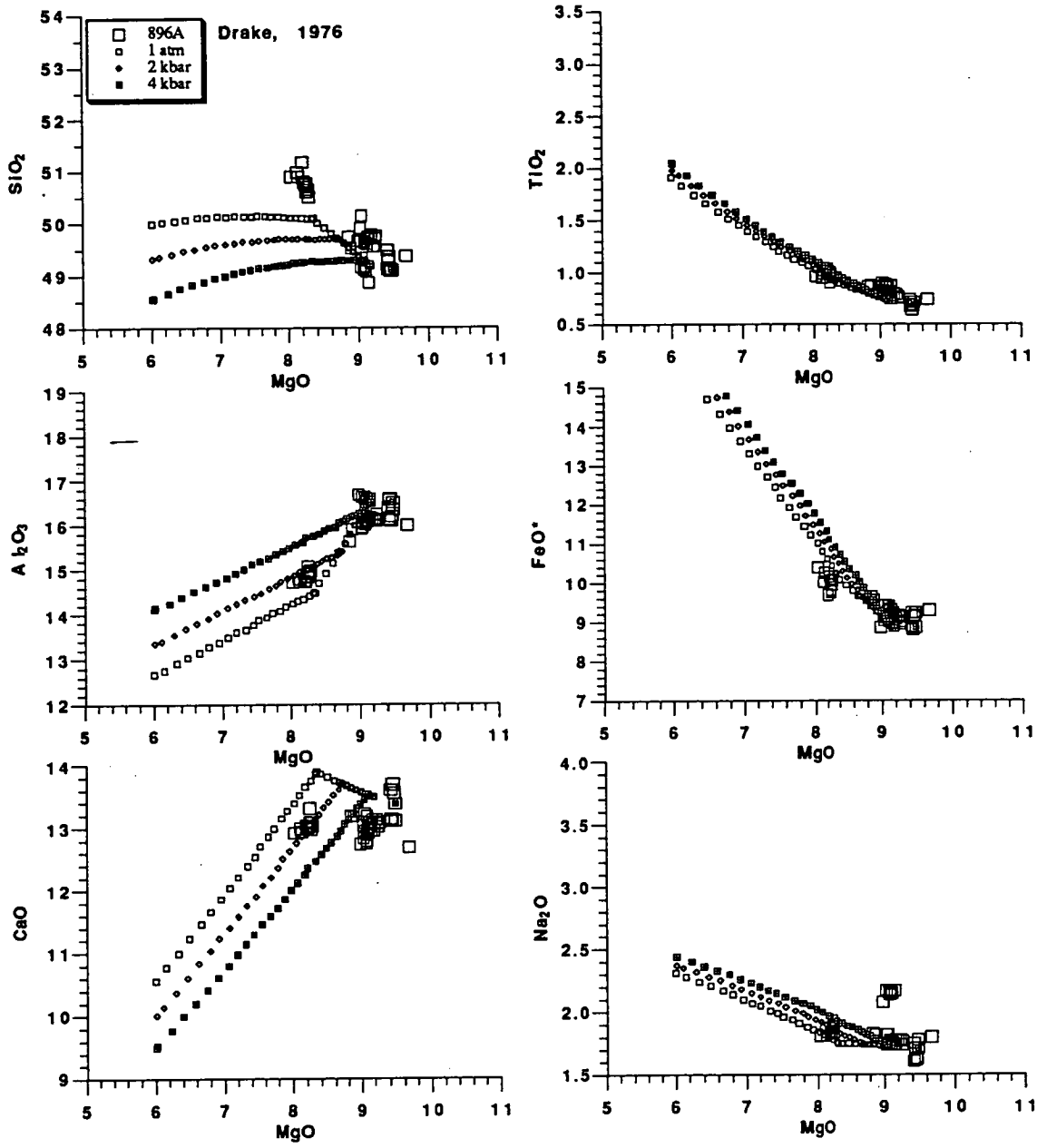

Figure 2.11 continued: b) Glasses from ODP hole 896A (A. McNeill, unpublished) and calculated fractionation paths at 1 atm, 2 kbar and 4 kbar, with the model of Drake (1976) used for plagioclase.

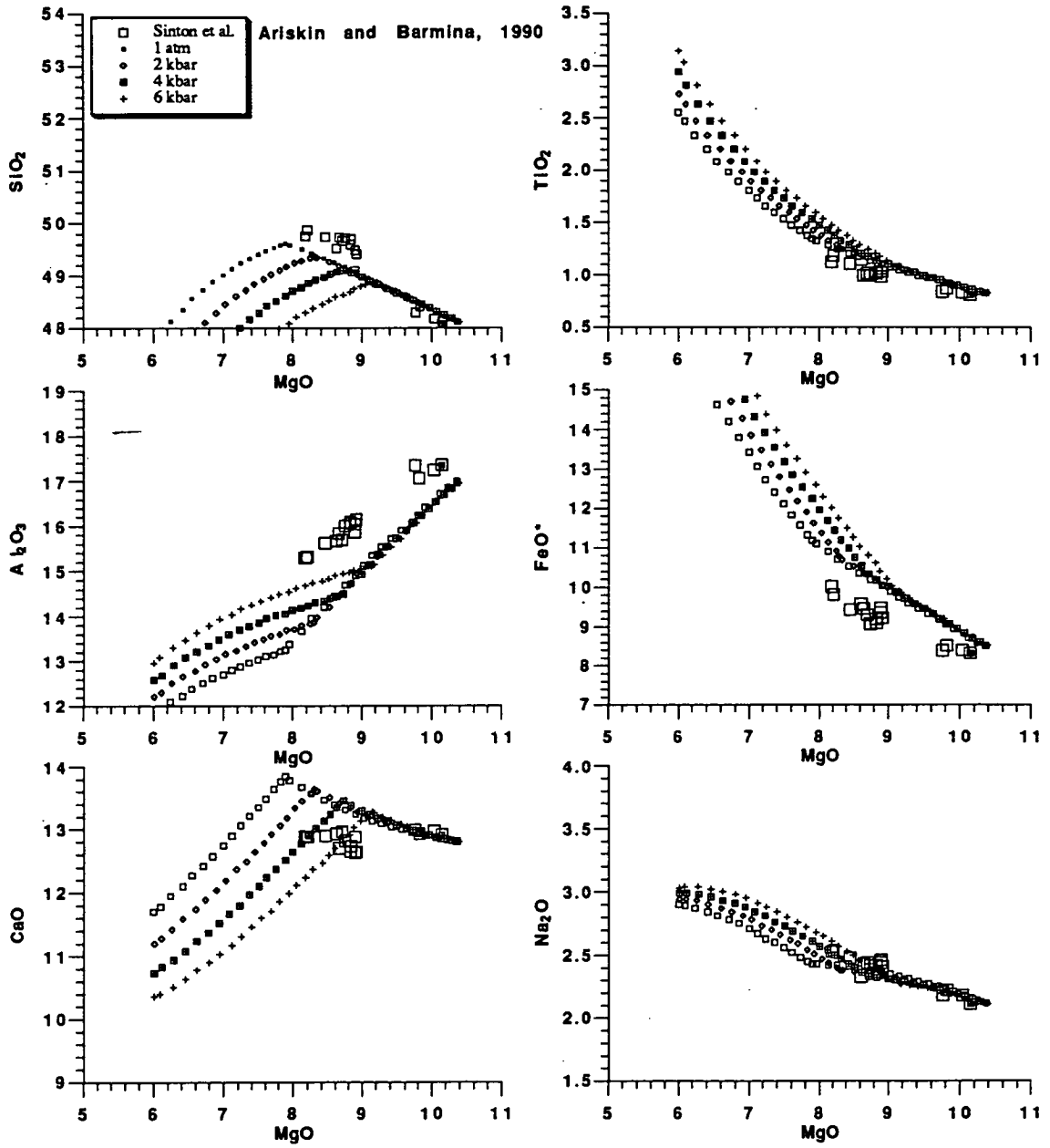

Figure 2.11 continued: c) Glasses from the Galapagos Platform (Sinton et al., 1993) and calculated fractionation paths for the most MgO rich glass at 1 atm, 2 kbar, 4 kbar and 6 kbar, with the model of Ariskin and Barmina (1990) used for plagioclase.

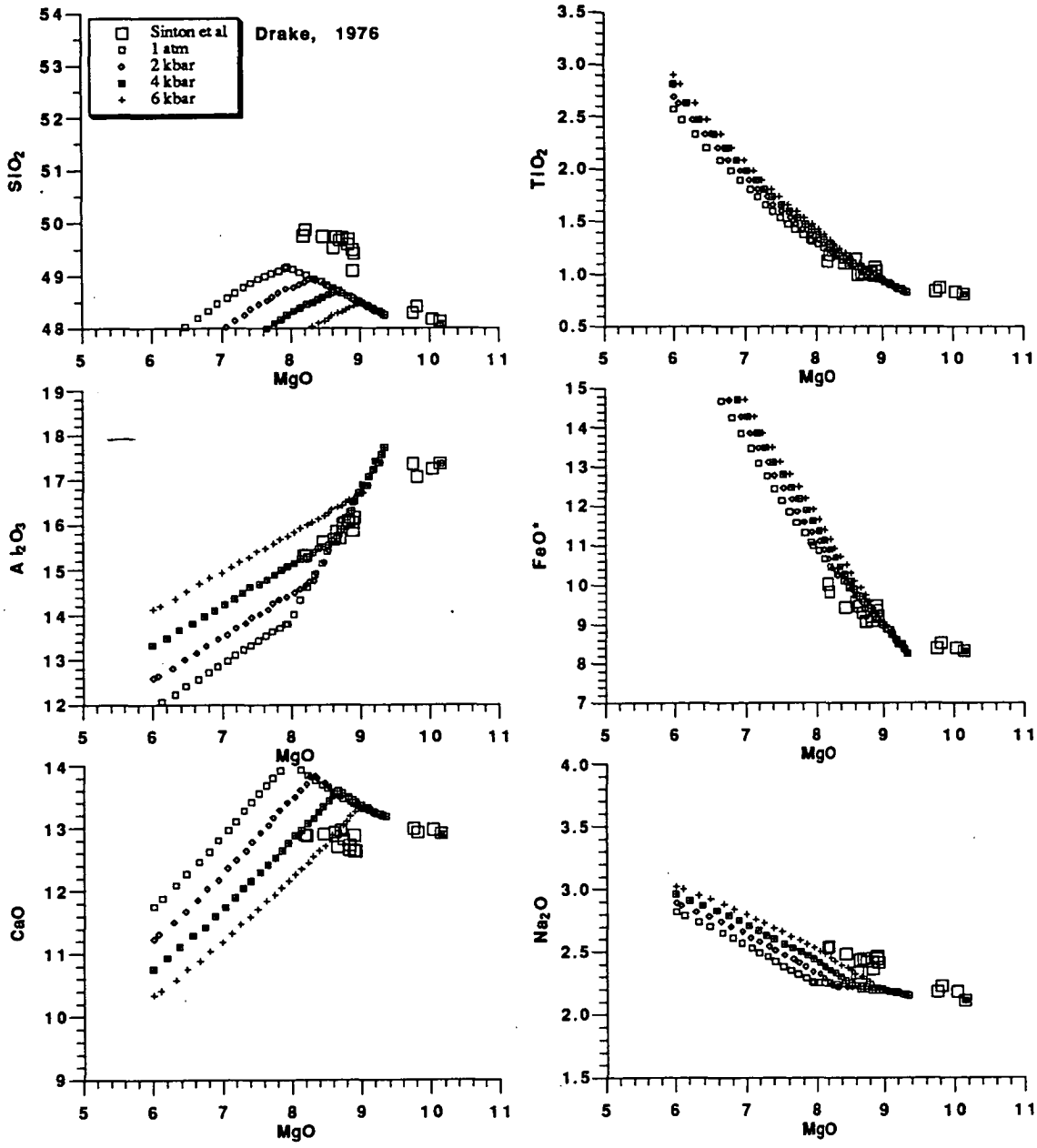

Figure 2.11 continued: d) Glasses from the Galapagos Platform (Sinton et al., 1993) and calculated fractionation paths for the most MgO rich glass at 1 atm, 2 kbar, 4 kbar and 6 kbar, with the model of Drake (1976) used for plagioclase.

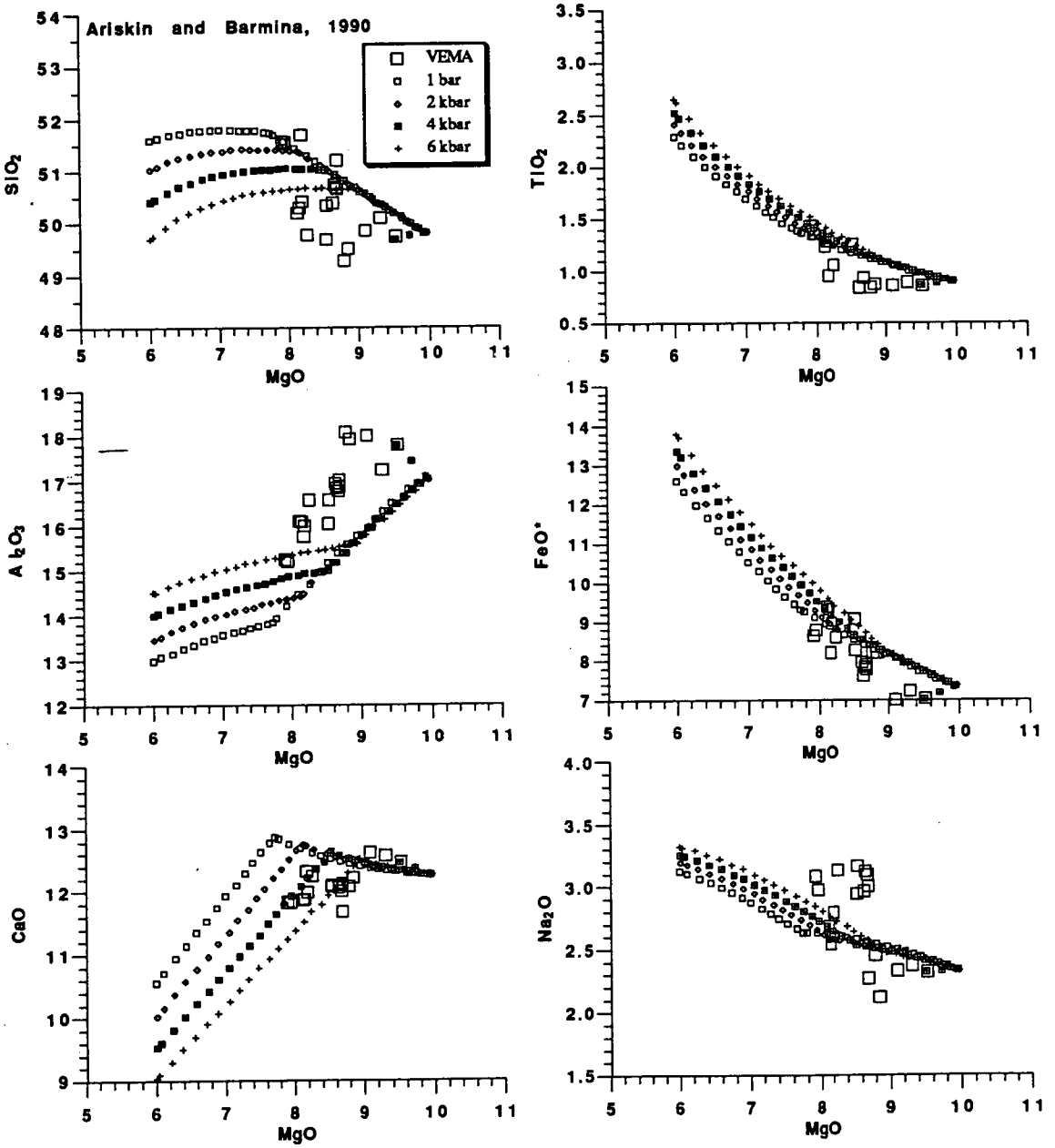

Figure 2.11 continued: e) Glasses from VEMA fracture zone (Sobolev et al., 1989) and calculated fractionation paths for the most MgO rich glass at 1 atm, 2 kbar, 4 kbar and 6 kbar, with the model of Ariskin and Barmina (1990) used for plagioclase.

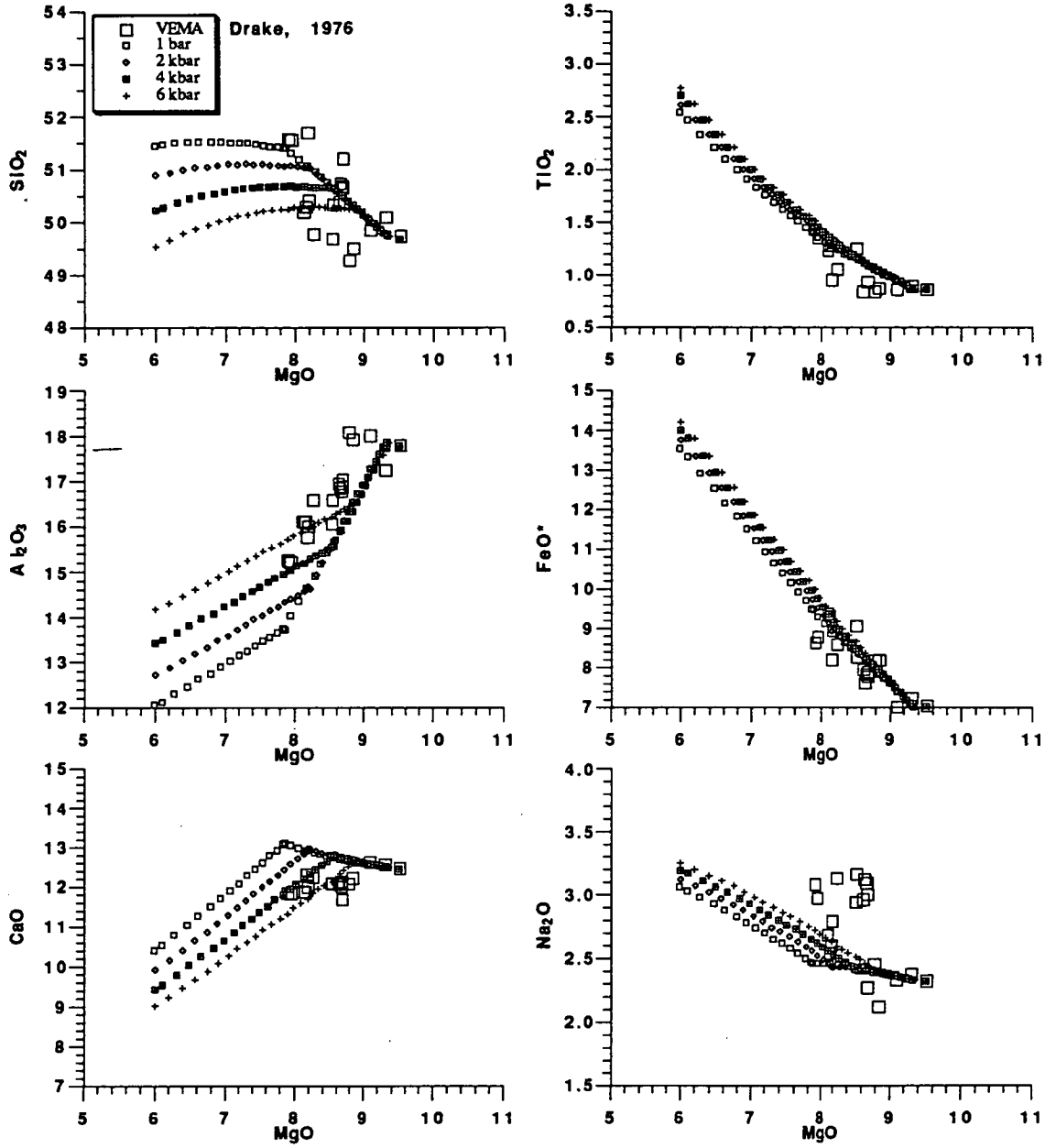

Figure 2.11 continued: f) Glasses from VEMA fracture zone (Sobolev et al., 1989) and calculated fractionation paths for the most MgO rich glass at 1 atm, 2 kbar, 4 kbar and 6 kbar, with the model of Drake (1976) used for plagioclase.

Sample 17-1 from group 10 was modelled at 4 and 6 kbars. At 4 kbars both olivine and plagioclase are on the liquidus and CaO rises initially until clinopyroxene joins the crystallization assemblage, and then the crystallization path is subparallel to the trend shown by groups 8 and 9. Crystallization at lower pressure (2-4 kbars) would cause clinopyroxene to join the liquidus at lower MgO and the crystallization path for group 10 would therefore follow the trend shown by groups 8 and 9. If sample 17-1 on the other hand crystallizes at pressure around 6 kbars, then clinopyroxene joins on the liquidus almost immediately, causing CaO to drop earlier. Group 11 could therefore be related to groups 8-10 by crystallization at higher pressures. It therefore looks likely, based on major elements, that groups 8-11 could all be derived from a similar mantle source and that the differences that can be seen are caused by variation in crystallization pressure. Group 12 however cannot be related to the other groups from zone A by crystallization processes, as it has lower SiO_2 and CaO together with higher Al_2O_3, K_2O and P_2O_5.

The elements that do not fit the calculated fractionation paths from samples 16-9 and 17-1, are SiO_2 and Na_2O. The zone A glasses show almost constant Na_2O content around 3% from 8 to 5.5% MgO whereas all calculated crystal fractionation paths cause Na_2O to rise. It is therefore likely that there are some differences in the initial Na_2O content and that the apparent trend is in fact a combination of several subparallel trends with increasing Na_2O with decreasing MgO. A similar explanation may account for the SiO_2-variation although the adequacy of the model calculations and the absence of oxide phases may be questioned.

In contrast to the zone A glasses, this modelling also shows that it is not possible to produce the trend shown by the AAD glasses by crystal fractionation. This is particularly evident in the SiO_2 and FeO* data. If the trend was caused by crystal fractionation, the decrease in CaO shows that clinopyroxene would have to be a liquidus phase. This would cause a significant increase in FeO* and would restrict the SiO_2 increase, effects not seen in the data. Differences in melting systematics or magma mixing are therefore more likely explanation for the variations seen in the AAD glasses.

2.5.2 Parental magma composition for the AAD basalts

In Figure 2.13 the glasses with $Mg^{\#} > 64$, plus three glasses from group 12 ($Mg^{\#} > 63$) and four glasses from group 9 ($Mg^{\#} > 61$) are plotted in the CIPW normative projection from diopside and plagioclase. Both the AAD and the zone A glasses plot within or close to the fields for primitive MORB glasses as plotted by Falloon and Green (1988). These authors argued that such liquids were not primary magmas and that most of them have fractionated olivine and possibly plagioclase and clinopyroxene, since they were in equilibrium with mantle residue. Groups 1, 2 and 10 on one hand and 3 and 12 on the other hand plot very close together on both projections showing

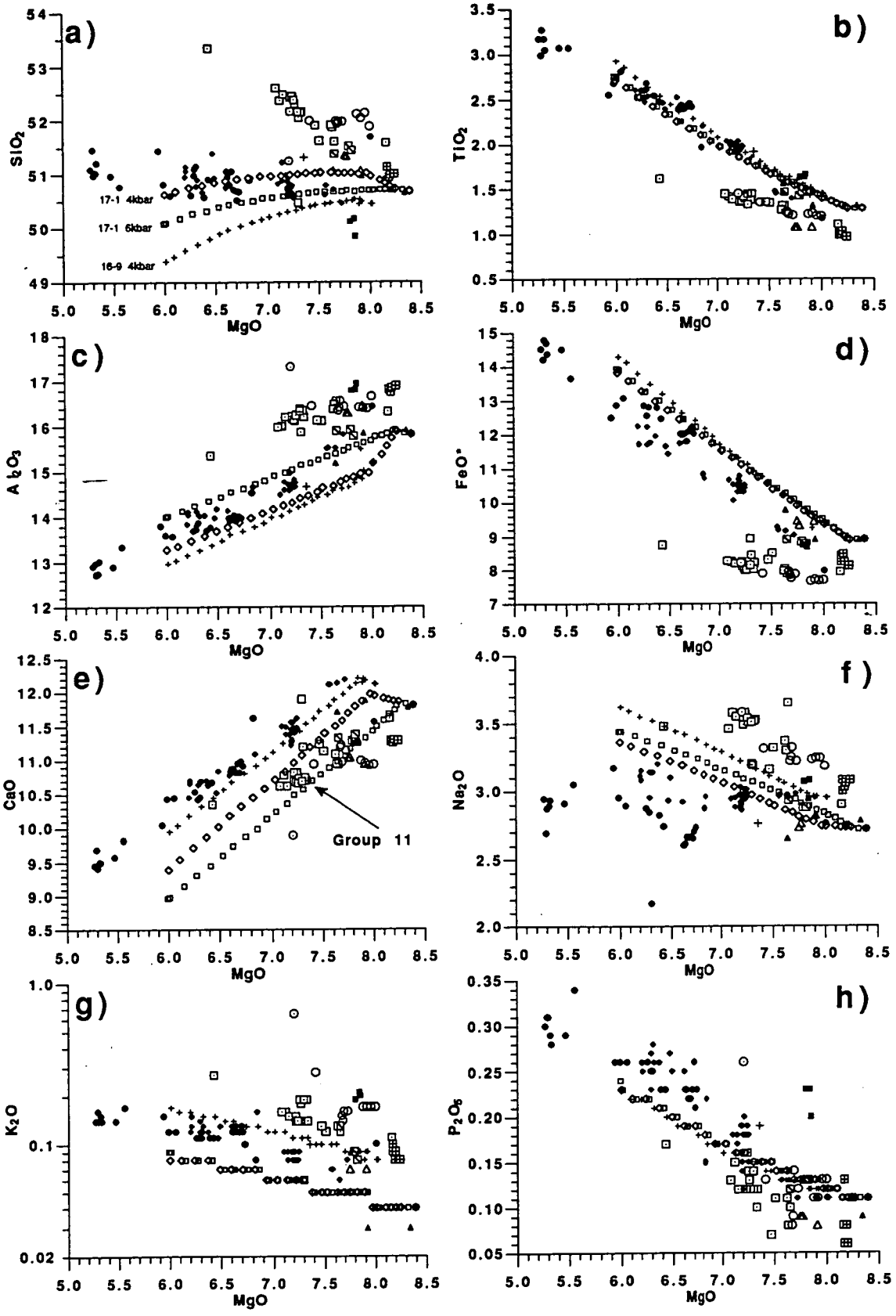

Figure 2.12: Calculated crystal fractionation paths for sample 16-9 at 4 kbars (crosses), and for sample 17-1 at 4 (open diamonds) and 6 kbar (open squares). Other symbols as in Figure 2.2.

that there is not much difference between the most primitive samples from the AAD and zone A.

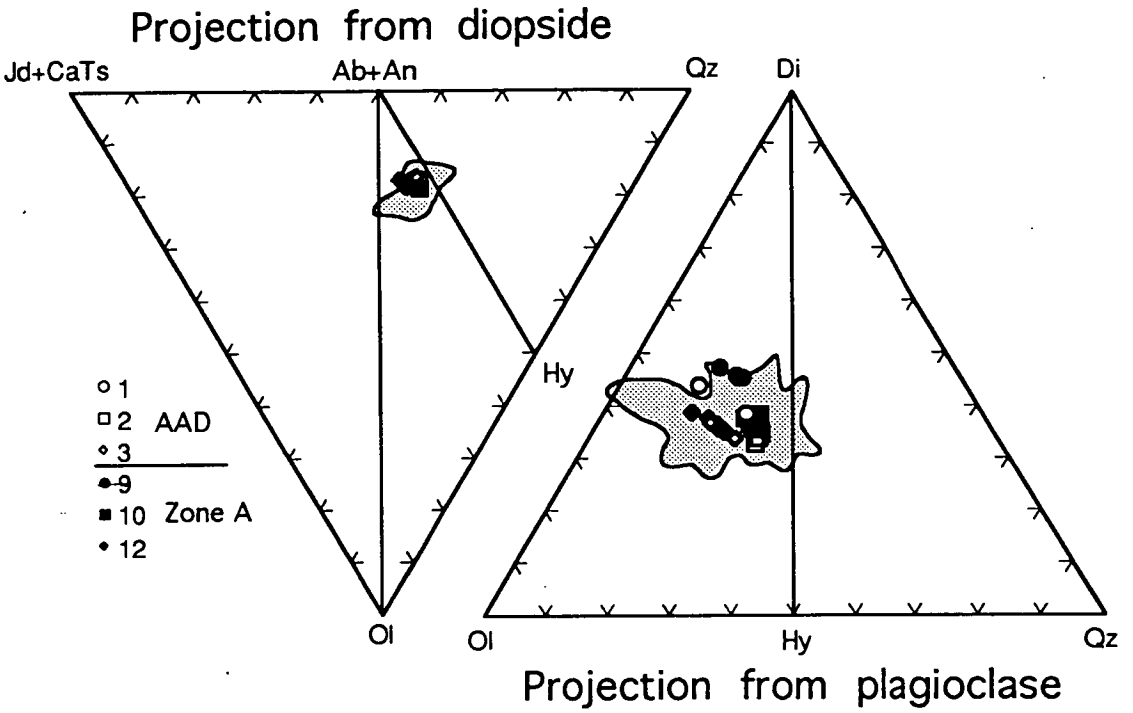

Figure 2.13: The most primitive glasses from the AAD and zone A plotted in the CIPW molecular normative basalt tetrahedron. Shaded area shows the field of primitive MORB glasses taken from Falloon and Green, (1988).

It is likely that the basalts from the AAD are derived from more than one parental magma based on compositional variations seen in both the matrix glasses and the homogenized melt inclusions. One melt inclusion, 18-9/209, was chosen to calculate a possible parental magma composition for some of the AAD samples. It occurs in olivine of the composition $Fo_{89.7}$ and it has an homogenization temperature of 1240 °C. It is clear from Figure 2.7 that this inclusion was not overheated as it has high Al_2O_3 together with high MgO and it falls on an extension of the trend shown by group 1 matrix glasses, it is therefore ideal for this purpose. Using the program Petrolog (Danyushevsky et al., 1990), calculations were run until this inclusion was in equilibrium with olivine $Fo_{90.4}$ which is the most magnesian olivine found in the AAD samples. There is no evidence for crystallization of a more magnesian olivine from the AAD basalts and therefore, there is no reason to calculate a parental magma in equilibrium with more forsteritic olivine. Two possible parental melt compositions were calculated, one on an olivine-plagioclase cotectic and one in equilibrium with olivine only. These parental melt compositions are shown in Table 2.3 and plotted on a CIPW normative tetrahedron in Figure 2.14. In the projection from diopside these

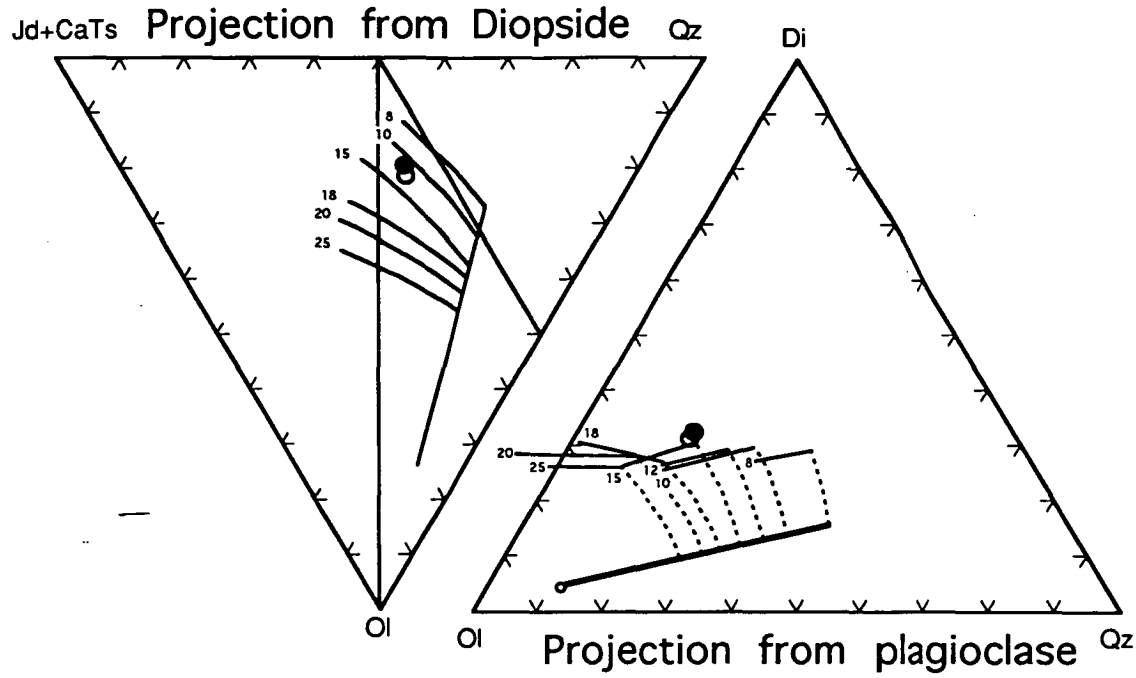

Figure 2.14: Calculated parental melt plotted in the CIPW molecular normative basalt tetrahedron. The lines show the cotectics for melts in equilibrium with MORB pyrolite at pressures indicated by small numbers (Falloon and Green, 1988). Filled circle shows parental melt calculated from inclusion 18-9/209 on a olivine-plagioclase cotectic, to be in equilibrium with olivine $Fo_{90.4}$ whereas the open circle shows melt calculated by addition of olivine only.

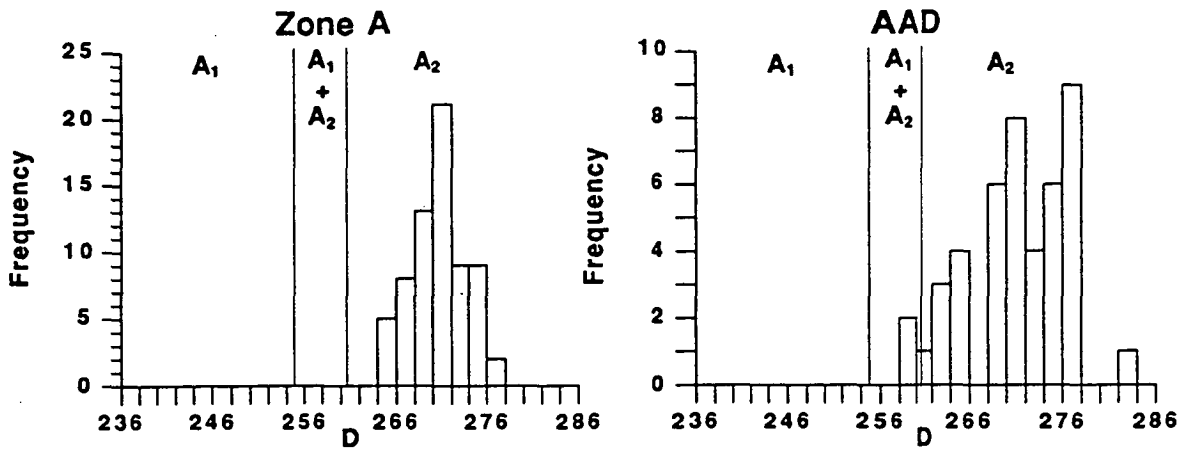

Figure 2.15: Histogram showing values for the discriminating function D for AAD and zone A glasses. This discriminating function D (D = $16.53Na_2O$ + $16.19TiO_2$ + $3.114SiO_2$ + 2.93MgO + 1.45CaO + $0.92Al_2O_3$ - $32.94K_2O$ - 1.46FeO*) was used by Dmitriev et al., (1985) to identify two groups (A_1 and A_2) of Atlantic MORB glasses.

Table 2.3: Calculated parental melt compositions. 18-9/209a is calculated parental melt in equilibrium with olivine Fo90.4, assuming the melt composition was on an olivine-plagioclase cotectic, whereas 18-9/209b is calculated parental melt in equilibrium with olivine only. A2 and ORT-2 are calculated primary melts for Atlantic MORB, from Dmitriev et al., (1985) and Sobolev et al., (1989), respectively.

Sample	18-9/209a	18-9/209b	A2	ORT-2
SiO_2	49.54	49.59	49.70	49.60
TiO_2	0.93	1.01	0.90	0.90
Al_2O_3	18.57	17.37	18.00	18.60
Fe_2O_3	0.73	0.88	1.30	
FeO	5.94	6.36	6.30	7.20
MnO	0.10	0.11		
MgO	9.40	10.19	9.50	9.40
CaO	12.05	11.74	11.90	12.00
Na_2O	2.54	2.54	2.30	2.30
K_2O	0.04	0.05	0.04	0.04
P_2O_5	0.11	0.12		
Sum	99.95	99.96	99.94	100.04

calculated parental melt compositions fall between the 10 and 15 kbar cotectics for MORB pyrolite (Falloon and Green, 1988) and are slightly more diopside-rich than the cotectics on the projection from plagioclase. Calculated liquidus temperatures at 10 kbar pressure indicate that this melt is close to multiple saturation with olivine, temperature 1277 °C (Ford et al., 1983), plagioclase, 1278 °C (Drake, 1976), clinopyroxene, 1275 °C (Ariskin et al., 1986) and orthopyroxene, 1266 °C (Nielsen and Drake, 1979). The comparison with Falloon and Green's (1988) data suggests that the compositions should be close to olivine + orthopyroxene + clinopyroxene ± spinel cotectic at 12-13 kbars.

2.5.3 Comparison with other N-MORB magmas

Dmitriev et al. (1985) distinguished two main compositional MORB groups from a large database of Atlantic glasses using an eight-component discrimination factor. They inferred that the compositional difference reflected the depth of separation of primary melts from the mantle, with group A_1 separating at depths between 30-60 km and group A_2 at depths from 15-30 km. When this discrimination factor is used on the AAD and zone A glasses, both suites fall within the field for group A_2 (Fig. 1.15). Dmitriev et al. (1985) calculated a primary melt for both groups and their primary melt composition for group A_2 and a primary melt calculated for MORB by Sobolev et al. (1989) are almost identical to the parental melt calculated for inclusion 18-9/209. This demonstrates that the parental melt for the AAD glasses is in no sense different from parental melts at normal mid-ocean ridges and there is therefore no evidence for an abnormally cold mantle beneath the AAD.

2.6. Conclusions

Major element glass compositions of 111 glasses dredged from the Southeast Indian Ridge reveal a compositional difference between glasses from the AAD and glasses from zone A to the east of the AAD. In general the glasses from the AAD are more primitive and they show greater variations in incompatible elements (e.g. in K_2O/TiO_2) than can be explained by crystal fractionation. The variations are likely to be caused by magma mixing. The variation in the glasses from zone A on the other hand are result of crystal fractionation of olivine (± spinel), plagioclase and clinopyroxene, super-imposed on minor variations, particularly in Na_2O and SiO_2 among parental magmas.

The most primitive phenocrysts found in the AAD basalts are similar to the most primitive phenocrysts found in MORB from the Mid-Atlantic Ridge. Melt inclusion studies demonstrate that the olivine phenocrysts in the AAD basalts crystallized at temperatures comparable to the crystallization temperature for olivines in N-MORB and from similar parental melt. This suggests that the parental melts for the AAD basalts were generated at pressure and temperature comparable to those for N-MORB and by similar extent of melting. Therefore neither mineralogy nor geochemistry support the hypothesis that the AAD basalts were generated from an abnormally cold mantle.

An E-MORB was dredged from station 27 within the AAD and an E-MORB-like signature can be seen in three samples from station 16 from zone A. Involvement of E-MORB is however not enough to explain the variations seen in the AAD basalts and an additional factor is, for example, needed to explain the variations in SiO_2, Na_2O and FeO* in the AAD basalts. If magma mixing is an explanation for this variation, then the nature and origin of the mixing component cannot be interpreted from this study. However, the study of melt inclusions in early-formed phenocrysts does offer the possibility of identifying this end-member if samples rich in highly forsteritic olivine can be collected.

Chapter 3

PRIMITIVE ISLAND ARC AND OCEANIC LAVAS FROM THE HUNTER RIDGE-HUNTER FRACTURE ZONE. GLASS, OLIVINE AND SPINEL COMPOSITIONS

3.1 Introduction

In 1990, the Soviet research vessel "Academician A. Nesmeyanov" dredged the southernmost part of the North Fiji Basin (NFB). Locations of the 26 dredge stations from which volcanic rocks were recovered are shown in Figure 3.1 and listed in Table 3.1. The diverse assemblage of rocks recovered includes several suites of primitive arc tholeiites, boninites, back-arc basin basalts, incompatible element enriched basalts and sodic rhyolites, plus a variety of peridotites. This remarkable diversity of lithologies reflects the complex tectonic setting of the dredged area.

The area sampled lies at the southern margin of the NFB, east of Matthew and Hunter Islands, and overlaps the Hunter Ridge in the area where it abuts the southern end of the NFB main spreading ridge (Fig. 3.1). Maillet et al. (1989) produced a new bathymetric map, and described the regional structure and geodynamic development of this area. They suggested that the NFB spreading ridge in this region is propagating southward into the Hunter Ridge, and that a small pull-apart basin may be developing south of the Hunter Ridge, linked to the spreading ridge that is presently transecting the Hunter Ridge by an ENE-trending transform fault zone (Fig. 3.1).

For this study, natural glasses from pillow rims and hyaloclastites from all the dredges were analysed, and they are described in this chapter together with an assessment of the compositions of olivine and spinel pairs from selected samples from each of the geochemical groups identified. Chapter 4 then deals further with the back-arc basin basalts and E-MORB-like samples that occur at seven dredge stations both within the NFB and south of the Hunter Ridge, and in chapter 5 andesites and sodic rhyolites from the Hunter Ridge are described in detail and compared to other samples from the Hunter Ridge.

All samples from R/V A. A. Nesmeyanov cruise were examined under a binocular microscope, and fresh glass, where present, was hand picked and prepared for major element analysis using the electron microprobe. Most of the glasses contain some quenched crystals, but these were easily avoided during microprobe analysis. Each reported glass composition consists of an average of at least three points.

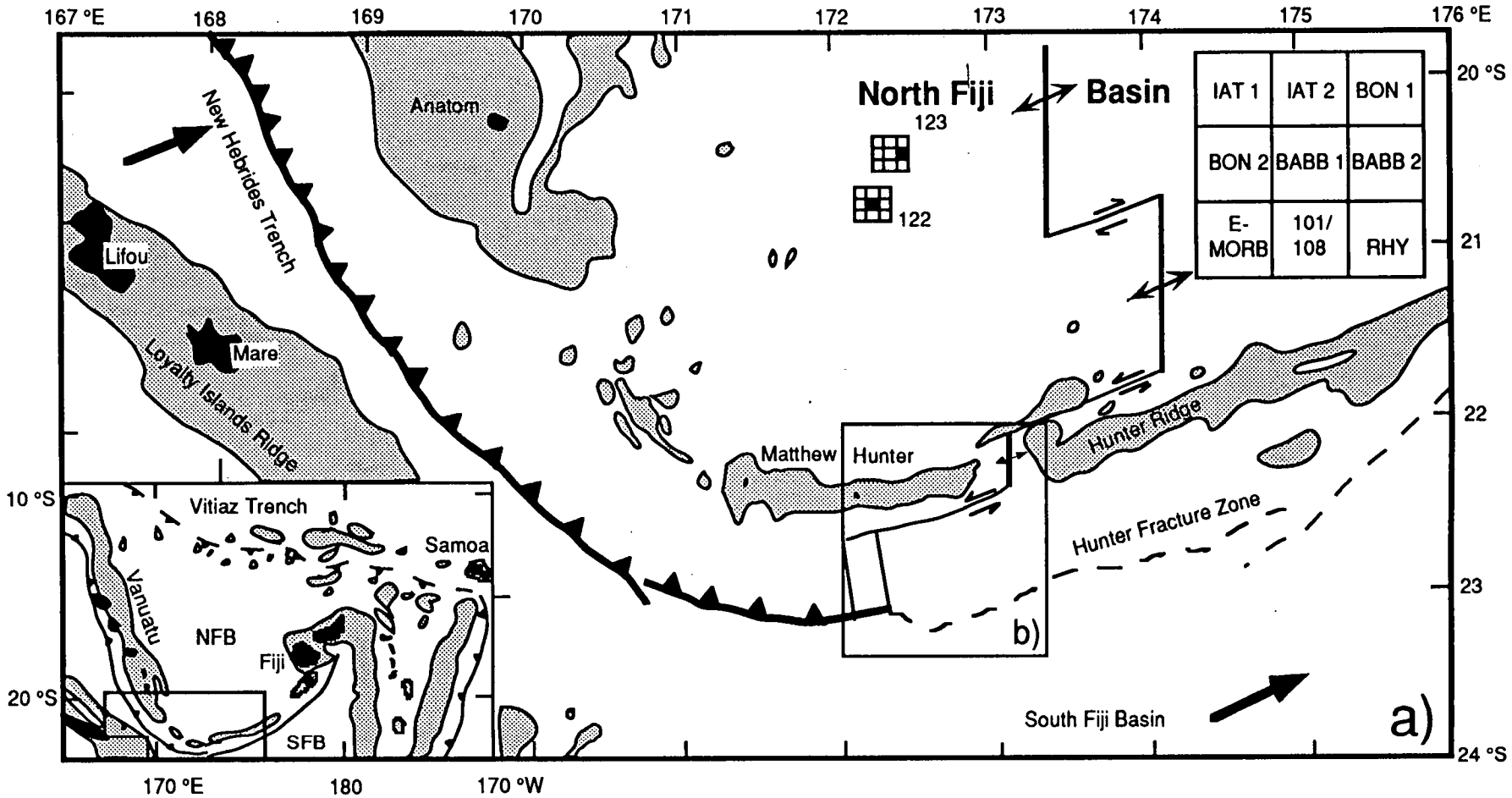

Figure 3.1: a) Location map of the southern part of the North Fiji Basin showing tectonic configuration and location of dredges122 and 123. Filled boxes indicate magma groups identified from major element glass compositions (see key in the top right hand corner). Shaded areas show water depth between 0-2000m. Drawn from a map by Maillet et al. (1989).

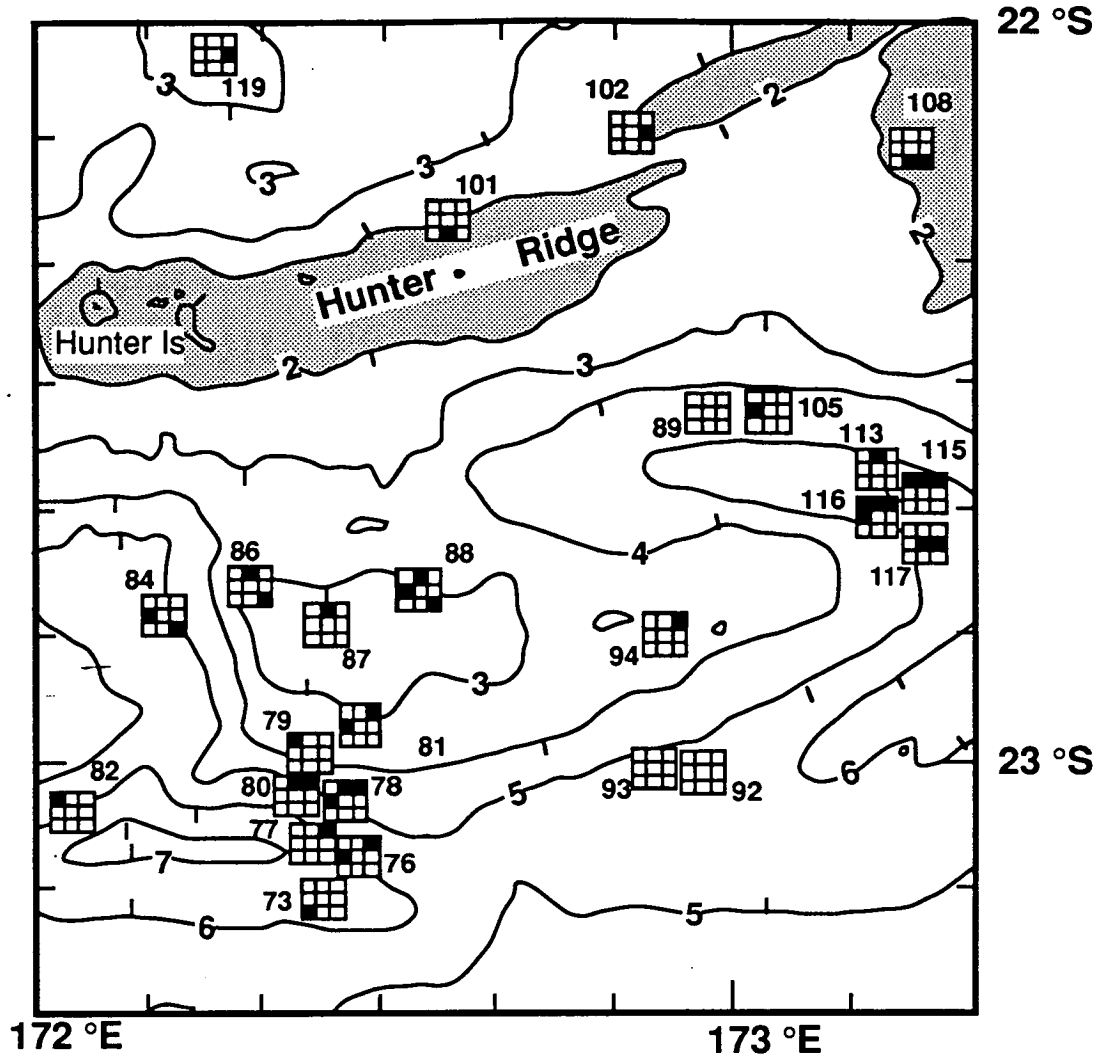

Figure 3.1 continued: b) Bathymetric map of the dredged area, showing locations of dredge stations and magma groups occurring at each dredge station (for key see Fig. 3.1a). No glasses were present at stations 89, 92 and 93. The map is drawn from a map by Maillet et al. (1989).

Selected samples were crushed by hand with pestle and mortar, sieved, and olivine crystals picked from the size fractions between 0.3 and 1.0 mm. Approximately 250 olivine grains from each sample were glued in epoxy and polished for microprobe analyses. Olivine-spinel pairs were analysed wherever spinel inclusions were exposed on the polished surface. Only SiO_2, MgO, FeO and CaO were analysed in olivine.

Analytical conditions were 15 kV accelerating voltage and 20 nA beam current. Significant Na-loss was detected in the rhyolitic glasses at these conditions but was minimized by using a slightly defocussed beam and 8 nA beam current. Analyses of natural obsidian glass (Astimex Scientific Limited) and Soda-Lime Flat Glass (National Bureau of Standards, Standard Reference Material 620) showed Na-loss to be less than 3% relative using these conditions.

Table 3.1. Location of dredge stations and magma groups identified from glass compositions.

Dredge	Latitude	Longitude	Water depth, m	Magma groups.
N17-73	23°10'	172°26'	6500-6120	E-MORB
N17-76	23°06'	172°28'	6280-6200	Boninite 1/2.
N17-77	23°05'	172°26'	5960-5840	Boninite 1.
N17-78	23°04'	172°26'	5280-4650	IAT 2, boninite 1/2.
N17-79	23°01'	172°24'	4650-4400	IAT 1.
N17-80	23°02'	172°24'	4400-4250	IAT 2, boninite 1.
N17-81	22°58'	172°27'	3480-3040	Boninite 1/2.
N17-82	23°05'	172°02'	6920-6840	IAT 1.
N17-84	22°48'	172°12'	5200-4700	Boninite 2, rhyolite.
N17-86	22°47'	172°18'	3160-2900	IAT 2, rhyolite.
N17-87	22°48'	172°24'	2630-2260	IAT 2.
N17-88	22°46'	172°32'	2600-2360	IAT 2, boninite 2, rhyolite.
N17-89	22°32'	172°54'	4300-4240	No glass present.
N17-92	23°01'	172°54'	6000-5600	No glass present.
N17-93	23°00'	172°50'	5220-4900	No glass present.
N17-94*	22°46'	172°50'	3360	Boninite 1.
N17-101*	22°15'	172°45'	2000	Basaltic andesite.
N17-102*	22°11'	172°51'	1940-1840	BABB 2.
N17-105	22°32'	172°59'	4620-4040	Boninite 2.
N17-108	22°10'	173°13'	1520-1320	Andesite, rhyolite.
N17-113	22°37'	173°13'	5560-5160	IAT 2.
N17-115	22°39'	173°13'	5880-5560	IAT 1/2, boninite 1.
N17-116	22°41'	173°13'	5400-5000	IAT 1/2, boninite 1/2.
N17-117	22°42'	173°13'	4800-4480	BABB 1/2.
N17-119*	22°03'	172°54'	1960	BABB 2.
N17-122	20°31'	172°14'	3400-3200	BABB 1.
N17-123	20°29'	172°15'	2800-2620	BABB 2.

* Gravity corer.

3.2 Major element geochemistry

Based on major elements, the glasses are divided into eight groups (Fig. 3.2). These include two groups of island arc tholeiites, two groups of boninites, two groups of back-arc basin basalts (BABB), one group similar to enriched mid-ocean ridge basalt (E-MORB) and one of sodic rhyolites. Glasses from stations 101 and 108 on the Hunter Ridge could not be classified with any of those groups and are therefore treated separately. All the analyses are given in Table 3.2.

3.2.1 Island arc tholeiites (IAT 1 and IAT 2)

Forty two glasses from ten dredge stations are island arc tholeiites (Jakes and Gill, 1970; Miyashiro,1974). MgO contents range from 7.4-2.8% with SiO_2 content from 51-59%. TiO_2 increases significantly with fractionation from 0.4-1.1% and K_2O from 0.2-0.6% whereas Al_2O_3 is almost constant at 15.0-16.5%. FeO* shows a small increase with fractionation. The distinction between the two arc tholeiite groups is made on differences in K_2O content. IAT 2 has higher K_2O contents and also slightly higher FeO* and lower SiO_2 than IAT 1 at a given MgO content (Fig. 3.2).

Table 3.2: Electron microprobe analyses of the glasses from R/V A.A. Nesmeyanov cruise. Each analyses is an average of at least three spot analyses. FeO* denotes all Fe represented as FeO.

Island Arc Tholeiite 1:

Sample	79/8	79/9	79/16	79/19	79/20	82/21a	82/21b	115/4	115/23
SiO_2	57.07	57.23	55.78	55.71	56.12	56.17	55.62	51.23	51.64
TiO_2	1.03	1.09	0.92	0.90	0.89	0.78	0.76	0.42	0.43
Al_2O_3	15.05	15.96	15.36	15.34	15.52	15.58	15.37	15.74	15.25
FeO*	9.93	9.56	10.15	10.14	10.01	9.67	9.39	9.25	9.57
MnO	0.15	0.15	0.15	0.10	0.14	0.13	0.17	0.17	0.21
MgO	3.11	2.69	4.13	4.17	4.18	4.36	4.51	7.09	6.81
CaO	7.68	6.98	8.65	8.63	8.66	8.58	8.98	12.69	12.19
Na_2O	2.76	2.71	2.71	2.74	2.81	1.75	2.29	1.47	1.31
K_2O	0.39	0.45	0.34	0.33	0.32	0.24	0.30	0.22	0.22
P_2O_5	0.12	0.14	0.07	0.08	0.09	0.07	0.07	0.05	0.03
Sum	97.29	96.96	98.26	98.14	98.74	97.33	97.46	98.33	97.65

Sample	115/25	115/31	115/37	115/39	115/39b	115/40	115/41b	115/42	116/28
SiO_2	52.36	51.79	52.04	51.67	52.11	51.38	51.00	51.94	51.78
TiO_2	0.47	0.44	0.45	0.43	0.40	0.42	0.40	0.46	0.57
Al_2O_3	15.05	15.37	15.42	15.55	15.49	15.16	15.69	15.36	15.33
FeO*	10.40	9.93	10.13	8.99	9.18	9.30	9.24	9.44	10.80
MnO	0.13	0.12	0.13	0.15	0.15	0.14	0.11	0.13	0.16
MgO	6.64	6.81	6.90	7.09	6.86	7.11	7.24	6.85	6.06
CaO	12.06	12.37	12.43	12.52	12.00	12.37	12.92	12.05	11.59
Na_2O	1.44	1.41	1.48	1.44	1.48	1.41	1.34	1.34	1.77
K_2O	0.21	0.22	0.20	0.21	0.27	0.27	0.25	0.24	0.27
P_2O_5	0.07	0.04	0.01	0.01	0.03	0.04	0.03	0.05	0.07
Sum	98.82	98.50	99.19	98.05	97.97	97.60	98.23	97.87	98.42

Island Arc Tholeiite 2:

Sample	78/62	78/64	80/39	80/53	86/6	87/7	87/8	87/11	87/13
SiO_2	54.67	56.68	54.65	54.72	56.79	55.07	51.51	55.36	55.07
TiO_2	0.82	0.80	0.73	0.89	0.81	0.93	0.55	0.91	0.90
Al_2O_3	14.93	16.08	15.24	15.08	15.62	14.81	15.32	15.04	14.93
FeO*	11.86	10.70	10.51	11.22	11.02	11.26	11.50	11.10	10.93
MnO	0.20	0.16	0.23	0.17	0.16	0.21	0.21	0.14	0.14
MgO	4.39	3.60	4.81	4.39	3.90	4.39	6.33	4.60	4.47
CaO	9.06	8.26	9.51	8.85	8.46	8.88	11.74	8.81	8.71
Na_2O	2.66	2.55	2.51	2.75	2.58	2.68	1.96	2.88	2.81
K_2O	0.51	0.51	0.50	0.58	0.50	0.44	0.39	0.48	0.46
P_2O_5	0.10	0.15	0.10	0.10	0.14	0.09	0.05	0.08	0.07
Sum	99.21	99.49	98.78	98.75	99.97	98.76	99.56	99.40	98.50

Sample	87/15	87/16	87/34	87/35	87/36	88/9	113/1	113/3	113/8
SiO_2	55.29	55.34	51.05	50.81	50.46	54.61	53.15	53.16	52.41
TiO_2	0.90	0.93	0.50	0.50	0.50	0.81	0.61	0.55	0.57
Al_2O_3	14.78	15.02	15.21	15.58	15.27	15.14	15.36	16.41	15.32
FeO*	11.16	11.21	11.33	11.18	11.35	11.02	9.89	9.55	9.93
MnO	0.19	0.20	0.18	0.18	0.14	0.13	0.15	0.16	0.18
MgO	4.46	4.56	6.33	6.65	6.34	4.63	5.96	6.32	6.46
CaO	8.58	8.71	12.04	12.37	12.27	9.11	11.13	11.56	11.34
Na_2O	2.52	2.77	1.82	1.82	1.83	2.75	2.14	2.20	2.03
K_2O	0.46	0.48	0.36	0.34	0.33	0.57	0.41	0.36	0.44
P_2O_5	0.09	0.07	0.07	0.06	0.04	0.11	0.06	0.03	0.06
Sum	98.42	99.29	98.89	99.49	98.53	98.88	98.87	100.32	98.75

Table 3.2 continued:

Boninite 1:

Sample	115/6	115/7	115/38	115/39c	115/66	116/29	76/35	76/38	76/41
SiO_2	53.04	54.71	53.02	53.09	55.79	53.69	56.09	58.84	56.61
TiO_2	0.49	0.85	0.48	0.56	0.85	0.70	0.17	0.21	0.17
Al_2O_3	15.56	15.32	15.49	15.26	14.64	15.55	15.03	16.73	13.88
FeO*	10.23	11.05	10.30	10.76	11.15	10.16	8.00	8.30	8.23
MnO	0.16	0.19	0.19	0.20	0.19	0.19	0.13	0.13	0.12
MgO	6.30	4.36	6.27	5.40	3.27	5.26	5.82	3.80	7.66
CaO	11.62	9.07	11.55	10.73	7.63	10.06	11.22	9.31	11.35
Na_2O	1.62	2.69	1.61	1.80	2.60	2.42	1.06	1.13	1.02
K_2O	0.34	0.52	0.36	0.42	0.64	0.45	0.28	0.34	0.25
P_2O_5	0.05	0.08	0.06	0.11	0.13	0.05	0.00	0.02	0.00
Sum	99.41	98.84	99.33	98.33	96.89	98.53	97.81	98.81	99.29

Sample	76/43	76/65	77/28	78/66	78/73a	78/73b	78/83	80/51	80/54
SiO_2	56.33	61.87	56.83	55.83	55.55	55.60	56.04	54.72	56.64
TiO_2	0.19	0.48	0.14	0.19	0.24	0.25	0.26	0.33	0.16
Al_2O_3	13.67	15.50	13.63	13.85	14.97	15.22	15.88	15.99	13.35
FeO*	8.05	7.71	8.43	8.30	8.90	8.90	8.68	7.79	7.96
MnO	0.12	0.08	0.15	0.08	0.19	0.25	0.12	0.14	0.12
MgO	7.93	2.14	6.95	8.07	5.99	6.03	5.90	6.87	7.74
CaO	11.41	5.94	11.85	12.30	13.07	12.78	10.97	11.78	11.39
Na_2O	1.18	2.36	0.78	0.88	0.92	0.93	0.94	1.44	0.89
K_2O	0.30	0.67	0.20	0.22	0.19	0.18	0.24	0.26	0.21
P_2O_5	0.01	0.07	0.00	0.00	0.02	0.03	0.00	0.03	0.00
Sum	99.19	96.83	98.97	99.73	100.03	100.18	99.04	99.34	98.48

Sample	80/55	81/18	94/1	115/24	115/41	115/41a	115/41b	115/43	115/59
SiO_2	56.08	57.32	55.27	54.19	57.24	55.44	54.46	54.66	57.47
TiO_2	0.18	0.23	0.27	0.44	0.27	0.28	0.23	0.45	0.58
Al_2O_3	14.55	17.72	14.14	15.07	16.14	15.81	15.82	15.75	14.32
FeO*	7.88	8.51	8.30	9.53	8.66	8.13	8.02	9.64	9.62
MnO	0.11	0.10	0.15	0.16	0.15	0.13	0.04	0.18	0.13
MgO	6.67	3.12	7.41	6.03	5.18	5.51	6.43	5.57	3.89
CaO	11.67	9.39	12.00	11.14	10.76	10.86	11.77	11.28	8.60
Na_2O	1.18	1.34	1.15	1.35	1.10	1.16	1.04	1.50	1.79
K_2O	0.29	0.29	0.29	0.26	0.25	0.21	0.21	0.23	0.36
P_2O_5	0.00	0.03	0.00	0.03	0.00	0.03	0.01	0.01	0.05
Sum	98.60	98.06	98.98	98.21	99.75	97.56	98.03	99.27	96.81

Boninite 2:

Sample	116/26	116/36	76/39	76/59	78/X	81/17	84/5	88/14	105/1
SiO_2	53.57	55.92	59.72	60.42	61.00	57.94	59.11	68.87	54.82
TiO_2	0.38	0.25	0.49	0.49	0.44	0.46	0.31	0.73	0.42
Al_2O_3	15.30	16.16	14.87	15.23	15.50	15.39	15.84	14.61	13.71
FeO*	9.09	8.39	8.74	9.20	8.26	8.98	8.62	5.48	9.55
MnO	0.17	0.12	0.10	0.14	0.13	0.15	0.17	0.14	0.18
MgO	5.96	5.34	3.46	3.08	3.03	3.81	5.21	1.28	6.76
CaO	10.93	10.85	8.00	7.56	7.11	8.35	8.25	4.84	10.99
Na_2O	1.28	1.10	2.76	2.68	2.74	2.55	2.67	3.63	1.90
K_2O	0.31	0.22	0.54	0.61	0.49	0.49	0.38	1.07	0.44
P_2O_5	0.03	0.02	0.08	0.03	0.05	0.07	0.03	0.19	0.05
Sum	97.01	98.35	98.77	99.44	98.77	98.18	100.59	100.84	98.82

Table 3.2 continued:

Back-arc Basin Basalt 1:

Sample	116/33	117/1	117/4	117/13	117/16	122/8	122/11	122/13
SiO_2	57.63	49.89	50.25	49.54	50.44	50.78	50.53	50.10
TiO_2	0.53	1.49	1.33	2.15	2.36	1.41	1.40	2.20
Al_2O_3	14.80	14.65	15.03	13.09	13.05	15.02	14.91	13.16
FeO*	9.02	10.51	10.67	13.57	14.06	10.95	10.65	14.41
MnO	0.16	0.17	0.19	0.18	0.18	0.17	0.11	0.22
MgO	3.59	7.59	7.88	6.05	5.90	7.71	7.75	5.92
CaO	8.30	11.94	12.22	10.30	10.19	12.09	12.33	10.27
Na_2O	2.30	2.27	2.29	2.47	2.17	2.38	2.26	2.59
K_2O	0.46	0.06	0.05	0.09	0.09	0.06	0.06	0.10
P_2O_5	0.06	0.07	0.11	0.14	0.17	0.08	0.08	0.11
Sum	96.85	98.65	100.03	97.59	98.61	100.65	100.08	99.08

Back-arc Basin Basalt 2: E-MORB:

Sample	102/1	117/2	117/5	119/1	123/1	123/2	123/3	73/1	73/2
SiO_2	50.00	48.76	48.76	48.11	48.69	50.15	48.77	48.63	49.51
TiO_2	1.33	1.56	1.50	1.30	1.38	1.21	1.36	2.07	2.15
Al_2O_3	16.22	17.00	17.25	17.41	17.37	18.71	17.93	16.50	16.83
FeO*	9.68	9.32	9.15	9.13	8.83	7.97	8.79	9.25	9.05
MnO	0.18	0.19	0.10	0.15	0.12	0.07	0.12	0.16	0.15
MgO	7.39	8.18	7.96	8.26	8.29	7.92	8.29	7.31	7.19
CaO	11.48	11.86	11.74	12.19	12.13	11.24	12.02	10.63	10.69
Na_2O	3.30	3.26	3.26	3.00	3.07	3.05	3.08	3.52	3.56
K_2O	0.05	0.02	0.02	0.05	0.13	0.10	0.12	0.59	0.59
P_2O_5	0.03	0.11	0.05	0.00	0.06	0.07	0.05	0.37	0.41
Sum	99.66	100.26	99.79	99.60	100.07	100.49	100.53	99.03	100.13

Stations 101 and 101: Rhyolites:

Sample	73/8	101/1	108/5	108/6	108/7	108/8	108/14	84/6	84/10
SiO_2	49.19	53.14	57.62	58.42	58.11	57.79	58.42	71.53	74.05
TiO_2	2.05	0.99	0.84	0.81	0.80	0.84	0.87	0.53	0.37
Al_2O_3	16.57	16.40	16.11	15.28	16.04	16.18	15.86	14.25	11.67
FeO*	9.14	8.02	7.12	7.16	6.96	6.84	7.09	3.45	2.53
MnO	0.12	0.10	0.11	0.12	0.12	0.07	0.06	0.10	0.08
MgO	7.16	5.18	4.11	4.77	4.51	4.16	4.01	0.16	0.30
CaO	10.68	10.55	8.35	8.04	8.29	8.35	7.87	3.46	2.20
Na_2O	3.23	3.10	3.61	3.49	3.65	3.59	3.60	4.84	4.00
K_2O	0.58	0.29	0.67	0.70	0.67	0.67	0.71	1.03	0.98
P_2O_5	0.41	0.11	0.11	0.10	0.12	0.12	0.14	0.19	0.06
Sum	99.13	97.87	98.65	98.90	99.28	98.62	98.63	99.54	96.24

Sample	84/11	84/13	86/8	86/9	108/1	108/4	108/16
SiO_2	74.42	71.99	71.39	69.84	71.76	73.72	72.87
TiO_2	0.37	0.74	0.73	0.72	0.30	0.32	0.32
Al_2O_3	12.76	12.02	12.46	12.25	15.08	14.86	13.76
FeO*	2.92	5.19	4.72	6.31	1.53	1.50	1.94
MnO	0.09	0.14	0.11	0.18	0.06	0.05	0.15
MgO	0.33	0.19	0.23	0.70	0.28	0.20	0.71
CaO	2.80	2.52	2.60	3.18	2.02	1.86	1.68
Na_2O	4.22	4.66	5.00	4.60	6.36	6.29	5.89
K_2O	0.95	1.12	0.85	0.98	1.48	1.48	1.55
P_2O_5	0.08	0.19	0.18	0.22	0.05	0.04	0.06
Sum	98.94	98.76	98.27	98.98	98.92	100.32	98.93

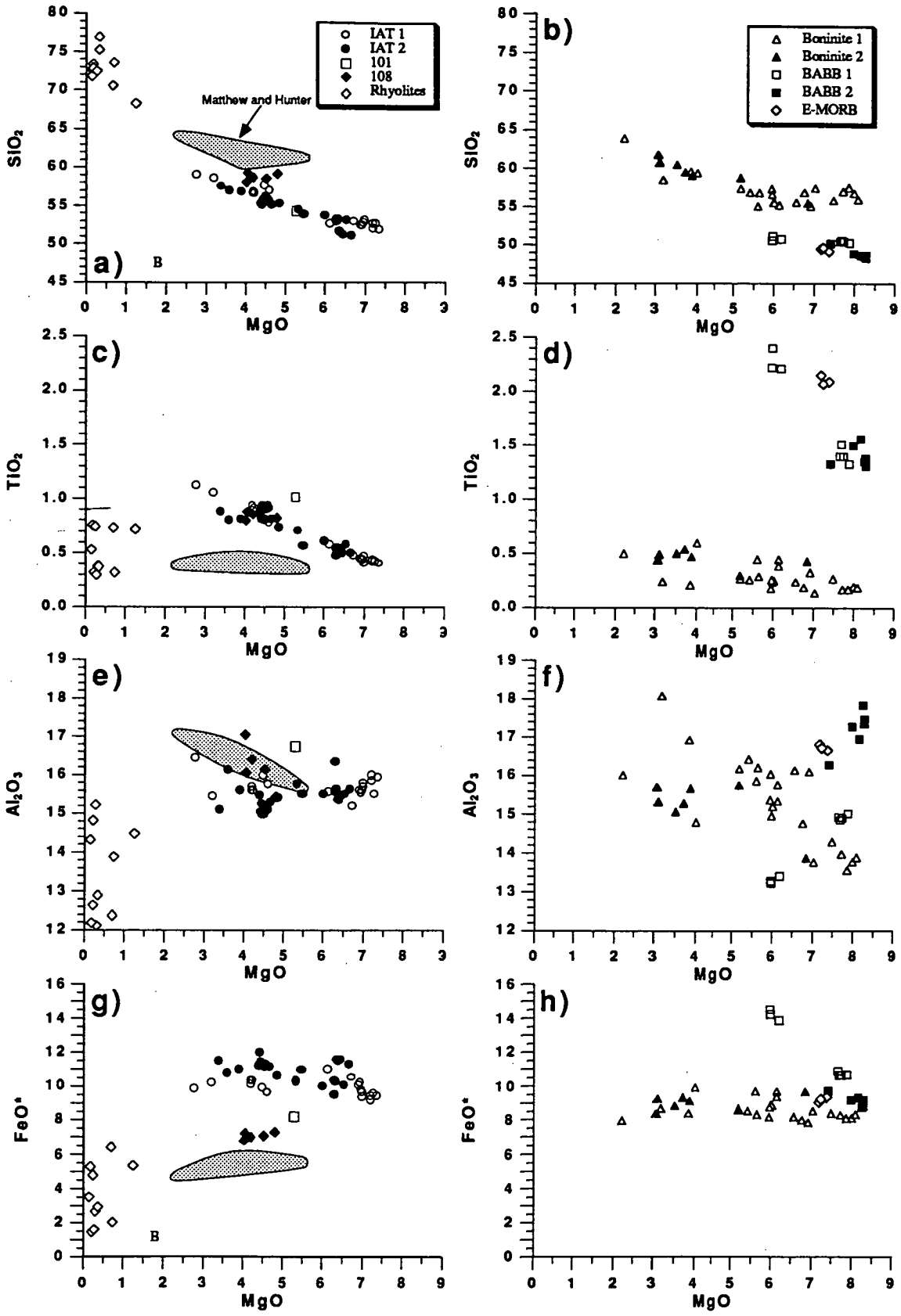

Figure 3.2: MgO variation diagrams for the NFB-glasses, all elements are in wt%, normalized anhydrous to 100%. Also shown is the field for whole-rock compositions of Matthew and Hunter andesites (Maillet et al., 1986).

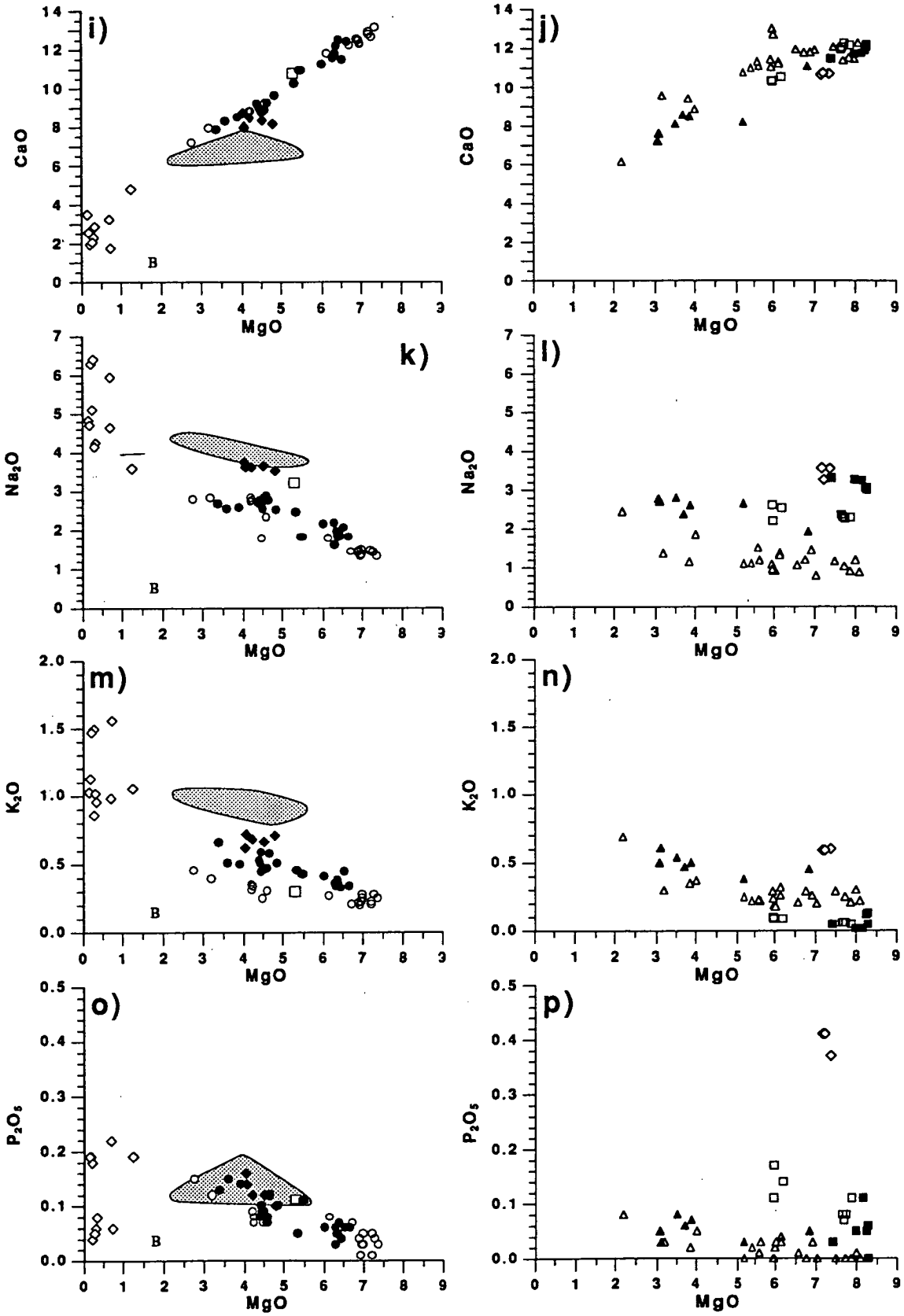

Figure 3.2 continued:

3.2.2 Boninites (BON 1 and BON 2)

Twenty nine samples from eleven dredge stations are high-Ca boninites, or derived from a high-Ca boninite parent (Crawford et al., 1989). Compared to the island arc tholeiites, the boninites have higher SiO_2 contents and lower FeO*, TiO_2 and P_2O_5 contents. MgO contents range from 8.1-2.1%. The boninites are further divided into two groups, with BON 2 having significantly higher Na_2O and slightly higher SiO_2, K_2O and P_2O_5 and lower Al_2O_3 and CaO contents than BON 1 (Fig. 3.2).

3.2.3 Back-arc basin basalts (BABB 1 and BABB 2)

Thirteen samples from five dredge stations constitute the two groups of back-arc basin basalts (BABB). Four of these dredge stations are located north of the Hunter Ridge but interestingly, BABB were also found at station 117 south of the Hunter Ridge in close proximity to island arc tholeiites and boninites. BABB glasses have 8.3-5.9% MgO, relatively high TiO_2 (>1.2%) and Na_2O (>2%) contents and low K_2O (<0.13%). BABB 2 is distinguished from BABB 1 by higher Al_2O_3 and Na_2O and lower FeO* and CaO at any MgO level (Fig. 3.2). BABB 2 is similar, in major element compositions, to "typical" BABB (Sinton and Fryer, 1987) whereas BABB 1 is more like typical N-MORB from the East Pacific Rise (e.g. Fryer et al., 1981). Trace element data (chapter 4) show that both groups are slightly enriched over N-MORB in most large ion lithophile elements (LILE).

3.2.4 Incompatible element enriched basalts (E-MORB)

Three glasses from dredge station 73 on the South Fiji Basin (SFB) crust south of the HFZ are notably enriched in TiO_2, Na_2O, K_2O and P_2O_5 compared to all the other groups and resemble E-MORB (Sun and McDonough, 1989). Though these lavas do not occur in a mid-ocean ridge setting the name E-MORB will be used for this group here based on compositional similarities. Significantly, whole-rock data show that similar rocks (lacking glass) also occur at dredge stations 87 (A.J. Crawford, pers. comm.) and 92 between the Hunter Ridge and HFZ (Fig. 3.1).

3.2.5 Stations 101 and 108

Six glasses from dredge stations 101 and 108 could not be grouped with other samples. Although there are similarities between samples from these two stations, such as high SiO_2 and Na_2O, and low FeO* content at a given MgO content, K_2O contents are very different (Fig. 3.2).

Glass samples from station 108 have MgO from 4.0-4.8%, whereas sample 101/1 has 5.18% MgO, and on all major element plots except TiO_2 (Fig. 3.1) these samples deviate from the other groups towards compositions similar to the low TiO_2 andesites of nearby Matthew and Hunter Islands (Maillet et al., 1986). Highly magnesian

olivine (up to Fo_{93}) and pyroxene phenocrysts ($mg^{\#}$=90), often showing reverse zoning, and a wide compositional range of resorbed plagioclase phenocrysts suggest a complex evolutionary history for these samples.

3.2.6 Sodic rhyolites

Eleven glasses from four dredge stations are low-K rhyolites (Ewart, 1979) with 1.3-0.2% MgO and 68.3-74.4% SiO_2. Na_2O is high but quite variable, ranging from 3.6-6.4% whereas K_2O varies from 0.85-1.55%. The rhyolites are found together with island arc tholeiites (Station 86 and 88), boninites (Station 84 and 88), and at station 108, and could therefore represent highly fractionated end members of any of these groups.

3.3 Olivine compositions and olivine-spinel pairs

All glass-defined compositional groups, except for the rhyolites, contain olivine-phyric samples, and twenty-eight samples were chosen for analysis of olivines and olivine-spinel pairs. For nine of those olivine-phyric samples no glass rims were present, so either naturally quenched melt inclusions in olivine or whole-rock analyses were used to group them. The range in Fo content in phenocrysts from the samples selected from each group is shown in Figure 3.3 and the compsitions of olivines and their spinel inclusions are given in Appendix 4. Compositional relationships of olivine-spinel pairs for each group are presented in Figure 3.4.

The phenocrystic (as opposed to xenocrystic) nature of the olivines is clearly demonstrated by the Fo vs CaO data. CaO in olivine is lowest in the boninites and highest in the E-MORB and it correlates well with the SiO_2 content of the glasses (the lower the SiO_2 in the melt, the higher the CaO in the olivine) The island arc tholeiite olivines show characteristics transitional between BABB and boninites. Within the boninite group, boninite 2 is more refractory as suggested by higher $cr^{\#}$ in spinel. Similarly the E-MORB spinels have higher $cr^{\#}$ than BABB 2 spinels, but the E-MORB spinels occur in less forsteritic olivines, so the difference in $cr^{\#}$ between these two groups could be explained by co-fractionation of olivine and plagioclase that depletes the melt in Al_2O_3 relatively to Cr_2O_3. Although Dick and Bullen (1984) stated that olivine and plagioclase fractionation did not cause large increase in $cr^{\#}$ of spinel before the disappearance of spinel from the liquidus of abyssal basalts, Allan et al. (1988) showed for MORB lavas that spinels become more and more Cr-rich with increasing fractionation of the host lava. As olivine and plagioclase fractionate, Fe^{2+} in the magma will increase while Mg and Al decrease, and due to combined

substitution of Cr and Fe^{2+} for Mg and Al in spinel, this will result in the crystallization of spinels with higher $cr^{\#}$ and lower $Mg^{\#}$ (Allan et al., 1988).

The island arc tholeiite (IAT 1 and 2) spinels most resemble those of boninites, whereas olivine phenocrysts have higher CaO content, reflecting higher CaO in the arc tholeiite melts. Magnetite solid solution in spinel is indicative of the oxidation state of the melt (e.g. Ballhaus et al., 1991) and shows boninites as more oxidized than BABB, with E-MORB as intermediate. TiO_2 and Al_2O_3 in spinel are particularly distinctive, separating E-MORB, BABB, boninite 1 and boninite 2 and suggesting mixing between boninite-like signatures and E-MORB or BABB 2 for producing 101 and 108.

3.3.1 Island arc tholeiites

Olivine phenocrysts in IAT range from $Fo_{94.3-80}$ (Fig. 3.3a, b). Most samples show variations of 4-5 Fo units, except for sample 115/3 that covers the range from $Fo_{94.3-82}$. CaO contents in olivine vary from 0.15-0.34% with maximum values around Fo_{90}, where clinopyroxene joins olivine as a liquidus phase (Fig. 3.4a).

Most spinels have $Mg^{\#}$ and $cr^{\#}$ higher than 0.5 (Fig. 3.4c, e, g), with only a few spinels in the least forsteritic olivines having $Mg^{\#} < 0.5$ (Fig. 3.4c). In IAT 1, no spinels were found in olivines with Fo < 83, but IAT 2 have spinels in olivines down to Fo_{80}. A few spinels with $cr^{\#} < 0.5$ are also present in some samples (Fig. 3.4e, g), mostly in sample 116/28.

TiO_2 contents of the spinels vary from 0.08-0.40% and Al_2O_3 varies from 5-26% (Fig. 3.4k). There is an overlap between IAT 1 and IAT 2 spinel compositions, but IAT 2 spinels tend to have higher TiO_2 contents (Fig. 3.4k) and higher $cr^{\#}$ (Fig. 3.4e, g), and to be more oxidized than IAT 1 spinels (Fig. 3.4i).

3.3.2 Boninites

Olivine compositions in the boninites vary from Fo_{93-80} (Fig. 3.3c, d) and they have lower CaO contents than IAT olivines, mainly from 0.10-0.25 % CaO (Fig. 3.4b). Coexisting spinels always have $cr^{\#}$ >0.70 (Fig. 3.4f) and there is no systematic change in $cr^{\#}$ with falling $Mg^{\#}$ (Fig. 3.4h). BON 2 spinels are generally distinct from those in BON 1 by their lower Al_2O_3 and higher TiO_2 contents (Fig 3.4l), higher $cr^{\#}$ (Fig. 3.4f, h) and higher Fe^{3+} (Fig. 3.4j).

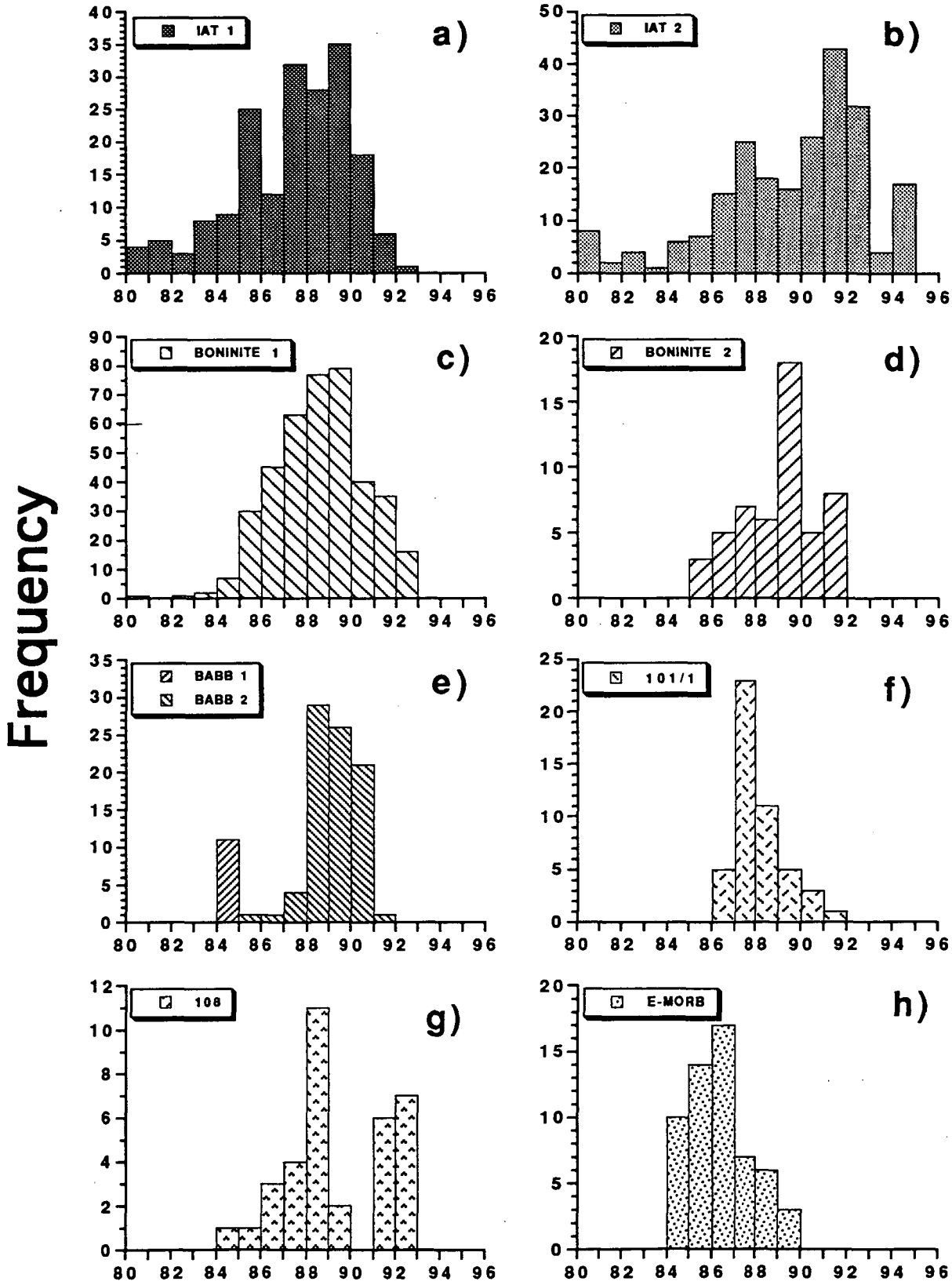

Figure 3.3: Histograms showing Fo-content of olivine phenocrysts in the compositional groups identified.

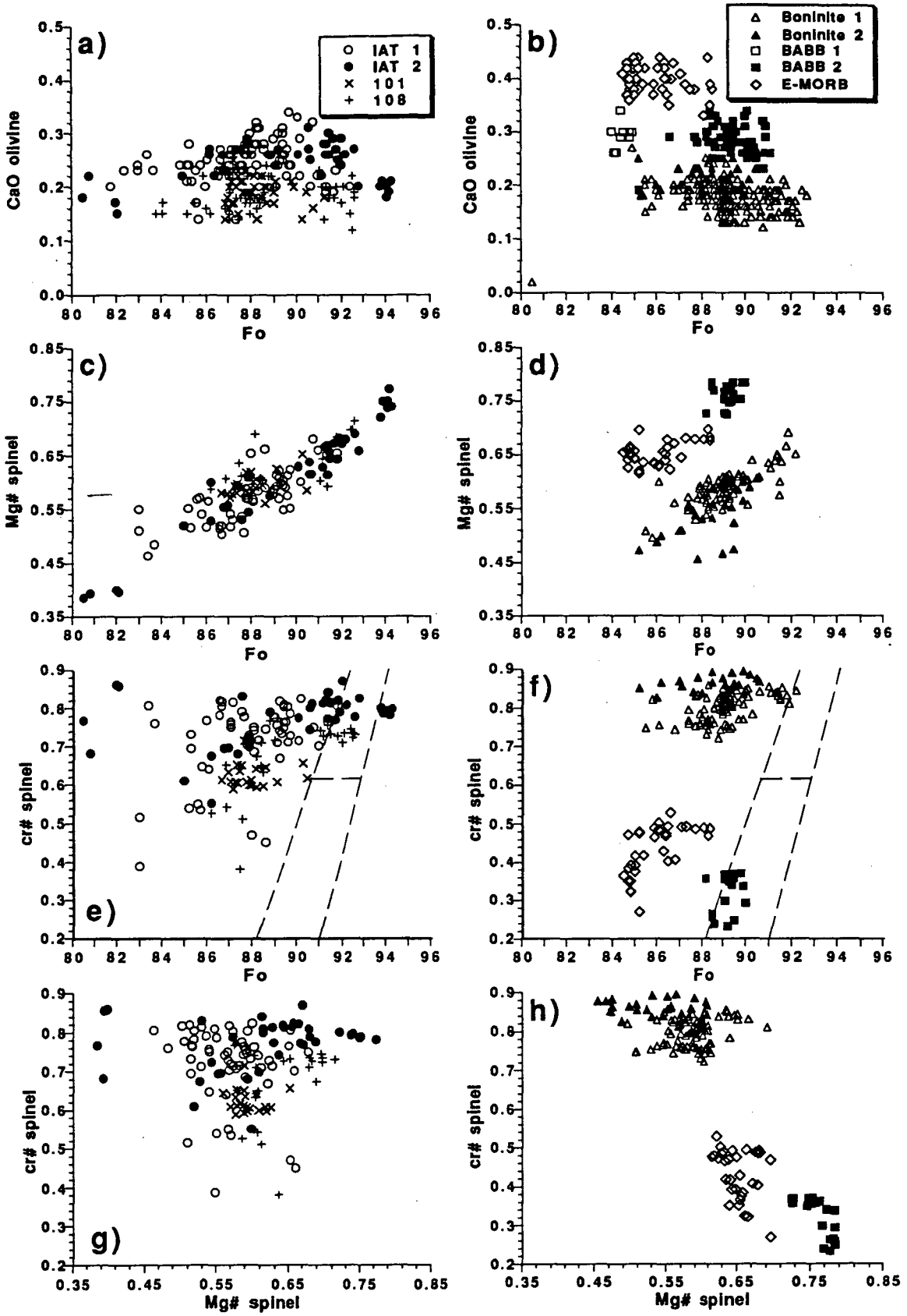

Figure 3.4. Compositional variations of olivine phenocrysts and spinel inclusions. a-b) CaO in olivine vs. Fo content of the olivine. c-d) $Mg^{\#}$ of spinel inclusions vs. Fo content of the host olivine. e-f) $cr^{\#}$ of spinel inclusion vs. Fo content of the host olivine. The broken lines show the mantle array from Arai (1987). g-h) $cr^{\#}$ vs. $Mg^{\#}$ of spinel.

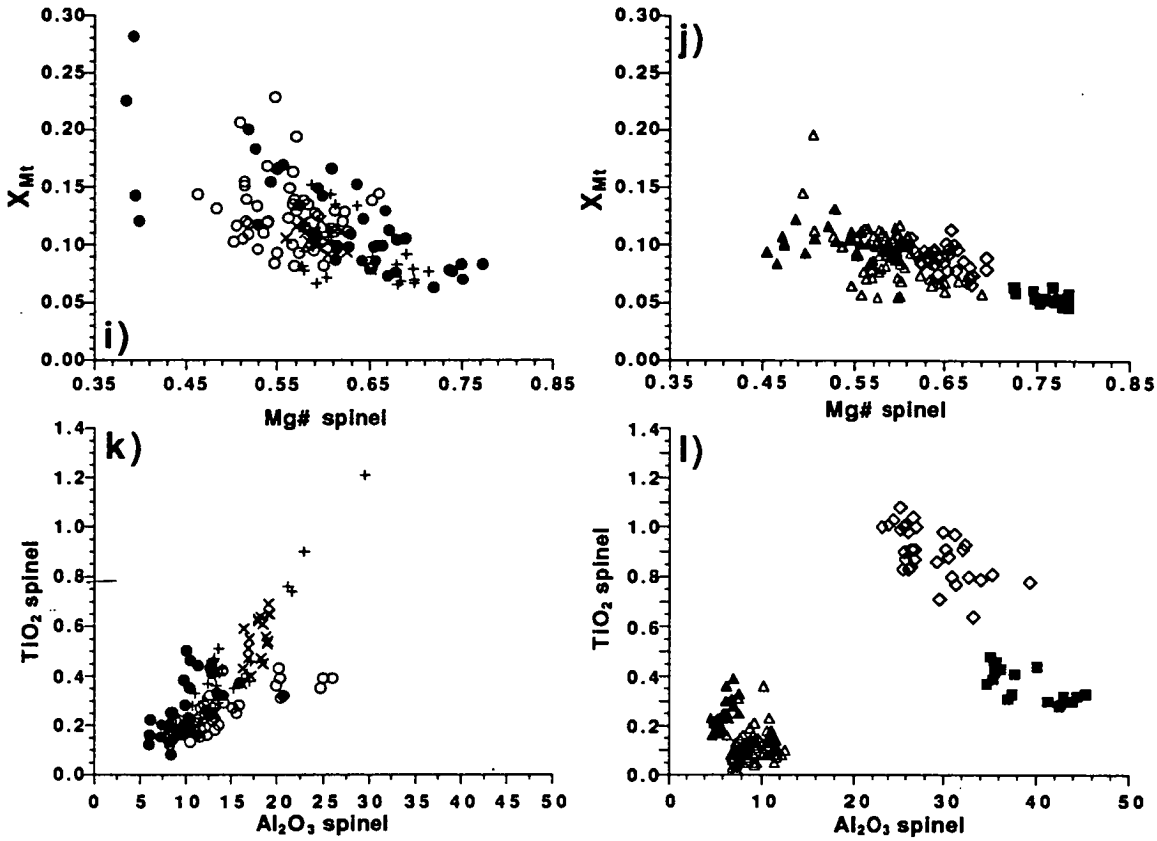

Figure 3.4 continued: i-j) The magnetite component (X_{mt} = Fe^{3+}/ (Fe^{3+} + Al + Cr)) vs. $Mg^{\#}$ of spinel. k-l) TiO_2 in spinel vs. Al_2O_3 in spinel.

3.3.3 Back-arc basin basalts

Olivine in the BABB samples ranges from $Fo_{91.1\text{-}84}$ (Fig 3.3e) with CaO contents from 0.23-0.34% (Fig. 3.4b). Most BABB samples are aphyric, and only one sample from BABB 1 has olivine phenocrysts (< 1%, $Fo_{85\text{-}84}$), but these lack spinel inclusions. In BABB 2 samples, spinel inclusions were only found in olivine within the compositonal range $Fo_{90\text{-}88}$. These spinels all have $Mg^{\#}$ > 0.72 and $cr^{\#}$ < 0.37 (Fig. 3.4d, f, h) and $Mg^{\#}$ is systematically higher than in spinel included in olivine of similar Fo content in both IAT and boninite samples (Fig 3.4c, d). Fe^{3+} contents are lower in BABB spinels than in all the other groups (Fig. 3.4i, j).

3.3.4 E-MORB

Samples from station 73 are all aphyric, so sample 92/37 was chosen, on the basis of whole-rock composition, to represent this group. Olivines vary from $Fo_{90\text{-}84}$ (Fig. 3.3h) and have higher CaO contents (0.33-0.44%) than olivine from the other groups (Fig. 3.4a, b). As for BABB spinels, E-MORB spinels have high $Mg^{\#}$ (Fig. 3.4c. d)

and low Fe^{3+} (Fig. 3.4i. j) compared to spinel in olivine of similar Fo content in IAT and boninite samples. $cr^{\#}$ is relatively low (0.25-0.55), although not as low as in BABB spinel (Fig. 3.4f, h).

3.3.5 Stations 101 and 108

Olivine compositions in samples from station 108 vary from Fo_{93-84} (Fig. 3.3g) and CaO contents of olivine are low (0.11-0.25%) , similar to those in the boninites (Fig. 3.4a) and in olivine from the andesites of Matthew and Hunter Island (Maillet et al., 1986). Olivines show a bimodal distribution, with no olivine between $Fo_{89.1}$ and Fo_{91}. Al_2O_3 and TiO_2 contents in spinels vary from levels similar to spinel in the IAT, with a few spinels having higher Al_2O_3 and TiO_2 contents, similar to those of the E-MORB spinels (Fig. 3.4k, l).

Olivine compositions in sample 101/1 vary from Fo_{92-86} and their CaO contents are similar to olivines in andesites from station 108. Spinels fall on the same trend as spinels from station 108 but show a more restricted compositional range (Fig. 3.4).

3.4 Discussion

3.4.1 Primitive boninite and island arc tholeiite glasses

Primitive basalts are rare in island arc settings, where basaltic andesites and more evolved compositions predominate (e.g. Ewart, 1976). Where primitive arc magmas do occur, in the Vanuatu arc for instance, (Gorton, 1977; Dupuy et al., 1982; Barsdell and Berry, 1990; Eggins, 1993), they are generally sub-aerial, highly porphyritic and lack quenched glassy rims. Most analyses reported are of whole-rock samples (occasionally with groundmass separates also analysed, e.g. Barsdell 1988) that do not necessarily represent liquid compositions. It is, therefore, particularly significant to find glasses from suites of primitive to evolved island arc tholeiites and boninites. The occurrence of fresh IAT and boninitic glasses on and south of the Hunter Ridge confirms that subduction has been active in this area. Auzende et al. (in press), suggested that the SFB started subducting under the Hunter Ridge-Hunter Fracture Zone approxemately 3 Ma ago. This is supported by results of a recent cruise between 174 °E and Kandavu Island in Fiji that recovered arc-related lithologies along the whole length of the Hunter Ridge-Hunter Fracture Zone, indicating active subduction under the Hunter Ridge during its formation (P. Maillet, A.C. Verbeeten and A.J. Crawford, pers. comm. 1994).

The discovery of boninites confirms a prediction that the juxtaposition of hot MORB-like upper mantle beneath the NFB spreading centre, and the sub-arc mantle beneath the Hunter Ridge, could produce boninitic magmas in this region (Crawford

et al., 1989). No further work was done on the IAT and boninite suites during this study, except for boninites from station 105, but whole-rock major and trace elements have recently been analysed in most samples from these suites (S.M. Eggins, unpublished; A.J. Crawford; unpublished) as well as Sr, Nd and Pb isotopes for selected samples (S.M. Eggins, unpublished).

3.4.2 Na-rhyolites (plagiogranites and trondhjemites)

High-Na, low-K silicic rocks have been described from various oceanic arc and back-arc basin settings (e.g. Bryan, 1979; Ikeda and Yuasa, 1989; Ishizuka et al., 1990; Fryer et al., 1990; Hochstaedter et al., 1990a, b) and from ophiolites (e.g. Coleman and Peterman, 1975; Gerlach et al., 1981; Coish et al., 1982; Pearcy et al., 1990). Some controversy surrounds interpretation of their origin, and primary magma composition. Alternatives include fractional crystallization from a more basaltic parent (e.g. Coleman and Peterman, 1975), formation as a late stage immiscible liquid during fractional crystallization (e.g. Dixon and Rutherford, 1979), hydrous partial melting of basalts (e.g. Gerlach et al., 1981), and metasomatic alteration of low-K dacites (e.g. Pearcy et al., 1990).

The excellent state of preservation of these glassy felsic lavas from the Nesmeyanov dredged suite rules out an origin via Na-metasomatism for these rocks. They show pronounced compositional similarities to high-Na rhyolites from the Sumisu Rift (Hochstaedter et al., 1990a). Hochstaedter et al. (1990b) showed that trace element (including REE) systematics of the Sumisu Rift Na-rhyolites supported their derivation from associated BABB, although they could not conclude whether by fractionation or partial melting. Fryer et al. (1990) concluded on the basis of trace element compositions and Nd-Sr isotopic data that the Sumisu Rift rhyolites are derived from the associated BABB by fractional crystallization.

In contrast, rhyolites are not present together with BABB group lavas at any of the dredged stations in the NFB, but occur instead with IAT, boninites, and the andesites at station 108. These rhyolites are therefore likely to be related to one of these groups. This will be discussed further in chapter 5.

3.4.3 Olivine and olivine-spinel pairs

CaO is an important minor element in olivine and its concentration is believed to reflect both the physical and chemical environment of crystallization. Simkin and Smith (1970) showed that CaO in olivine in plutonic rocks is generally less than 0.1% whereas olivines in extrusive rocks have CaO higher than 0.1%; they suggested that the depth (pressure) of crystallization had a strong influence on CaO concentration in olivine. Jurewicz and Watson (1988) showed experimentally that above solidus, olivine CaO contents are dependent on the equilibrium melt composition (mainly CaO

content), but are almost independent of temperature, fO_2 and pressure, at least below 2.0 GPa. Besides CaO, of the major elements, SiO_2 is believed to have the greatest influence on the CaO concentration in olivine (Stormer, 1973).

Olivines in the E-MORB sample have the highest CaO contents whereas olivines in the boninites and andesites have the lowest CaO contents (Fig. 3.4a, b). This is not simply due to CaO differences between the melts because all the groups have similar CaO contents at a given MgO (Fig. 3.2i, j). On the other hand, SiO_2 content and normative compositions are very different between the groups, with SiO_2 content being lowest in the E-MORB and highest in the boninites and andesites, supporting the implied strong influence of melt SiO_2 on olivine CaO content.

All magmatic groups identified here include samples that have olivine compositions that are as, or more, magnesian than reported in the literature for similar magma series. For example, BABB 2 have olivine as magnesian as Fo_{92} whereas Dmitriev et al. (1985) found no olivine more magnesian than Fo_{90} in a compilation from the literature of N-MORB samples with similar major element glass compositions. Highly forsteritic olivines ($Fo_{91.3}$) have been reported from the Lau Basin (e.g. Sunkel, 1990) whereas olivines from other back-arc basins are generally less forsteritic than Fo_{88-89} (e.g. Ridley et al., 1974; Saunders and Tarney, 1979; Mattey et al., 1981; Beccaluva et al., 1990). The most magnesian olivines ($Fo_{94.3}$) are found in IAT 2 (Fig. 3.3), even though these glasses have the highest FeO* at a given MgO content (Fig. 3.2g, h). Since the olivine-hosted spinels in these rocks have the highest Fe^{3+} values among the magmatic groups identified (Fig. 3.4k, l), the olivine and spinel in the IAT 2 magma probably crystallized under more oxidized conditions than the other magmatic groups.

All magma groups show a strong linear relationship between Fo content of olivine and $mg^{\#}$ of coexisting spinel because of Fe-Mg exchange between olivine and spinel to low temperature (e.g. Dick and Bullen, 1984; Ballhaus et al., 1991) (Fig. 3.4c, d), but at any given Fo content BON 2 spinels (High $cr^{\#}$) have the lowest $Mg^{\#}$ and BABB 2 (Low $cr^{\#}$) the highest, as increasing $cr^{\#}$ shifts the coexisting spinel to more Fe-rich compositions (Dick and Bullen, 1984). Most magmatic groups have a limited range in spinel Al_2O_3 and TiO_2 compositions and in Figure 3.41 spinels in the boninite, E-MORB and BABB suites form discrete, coherent groups. Spinels in the IAT and andesites, on the other hand, show more compositional spread and overlap with the boninite groups (Fig. 3.4k, l). The andesite spinel compositions form a mixing trend between either boninite or IAT compositions towards more fertile spinel compositions (eg. E-MORB), whereas IAT 1 spinel compositions show a mixing trend towards the BABB spinel field, indicating that magma mixing probably played an important role in magma generation in this area.

The $cr^{\#}$ of spinel in high Fo olivines (>Fo_{87}) is a useful indicator of the degree of melting, or extent of depletion, of the mantle source (Dick and Bullen, 1984; Duncan and Green, 1987) and in Figures 3.4e and f, $cr^{\#}$ is plotted against Fo-content of the host olivine. The mantle array of olivine-spinel systematics, defined by Arai (1987; 1992), from spinel lherzolites and spinel harzburgites is shown for comparison. Spinels in the boninites have the highest $cr^{\#}$, indicating the most refractory source composition for these magmas, whereas the BABB have the lowest $cr^{\#}$ and presumably derive from the least depleted magma source. Spinels in primitive MORB generally have $cr^{\#} < 0.3$, but plagioclase co-fractionation with olivine in typical MORB pushes spinel $cr^{\#}$ values into the range 0.4-0.6 (Sigurdsson and Schilling, 1976). This indicates either a less depleted lherzolitic mantle source or lower degree of melting to produce BABB 2 liquidus spinel, in comparison with that for the E-MORB spinel. Spinels from the other groups suggest harzburgitic mantle sources. Although many of the lavas are evolved, they still have primitive phenocrysts that may provide information on the compositions of primitive magmas from which these lavas evolved.

3.4.4 Back-arc basin basalts, E-MORB and stations 101 and 108

The back-arc basin basalt and E-MORB glasses will be further discussed together with whole-rock major and trace elements in chapter 4, whereas the andesites from station 108 are discussed in detail in chapter 5 together with whole-rock major and trace element geochemistry of samples from stations 89, 101 and 105.

3.5 Conclusions

Major element analyses of over 100 glasses from the southernmost part of the North Fiji Basin show that this area contains an exceptionally diverse spectrum of magma types. Eight magmatic groups are recognized, including island arc tholeiites, boninites, BABB and E-MORB. Highly forsteritic olivine, often exceeding values previously reported for these magma series, confirm the near-primary nature of some of these samples. Extensive crystal fractionation from either island arc tholeiites or high-Ca boninites is the most likely scenario for generation of the Na-rhyolites, though other possibilities could not be ruled out.

CaO in olivines differs between the magmatic groups and correlates strongly with the SiO_2 content of the magmas, the higher the SiO_2 of the melt the lower is CaO in olivine.

Glasses of island arc tholeiite composition are rarely reported, and trace element and isotopic studies of these rocks (S.M. Eggins, unpublished) should offer important

constraints on magma genesis in young, primitive intra-oceanic areas, and clarify the relationships, if any, between arc tholeiites and high-Ca boninites.

Primitive BABB, containing highly forsteritic olivine and high alumina spinels, were found not only in the North Fiji Basin proper, but also perhaps unexpectedly, south of the Hunter Ridge, in close proximity to both the island arc tholeiites and boninites. This probably confirms the tectonic scenario put forward by Maillet et al. (1989) in which the break in the Hunter Ridge in this area is interpreted to be a pull-apart structure due to southward propagation of the main North Fiji Basin spreading centre through the Hunter Ridge.

Chapter 4

NORTH FIJI BASIN BASALTS

4.1 Introduction

This chapter deals with the three basaltic groups, BABB-1, BABB-2 and E-MORB, identified from the glass compositions described in chapter 3. First I will briefly discuss back-arc basins and magma generation in back-arcs in general and then describe the geological setting in the NFB. Based on a review of published and new basaltic compositions from the NFB I propose a new classification scheme to distinguish between N-MORB like basalts (BABB) and more alkali-enriched basalts that occur together with BABB in most areas previously studied in the NFB. Finally, I present new whole-rock major and trace element analyses from BABB and E-MORB-like lavas dredged by R/V A.A. Nesmeyanov from the southernmost part of the NFB, close to the Hunter fracture zone, and discuss magma generation and magma evolution in this area.

4.1.1 Back arc basins

Back-arc basins in intra-oceanic arcs are extensional features that develop via rifting within or just behind island arc volcanoes (e.g. Karig, 1974). Some basalts erupted in back-arc basins (BABB) show distinctive features when compared with typical N-MORB (Sinton and Fryer, 1987). This includes higher Al_2O_3, H_2O and total alkalis and lower FeO* and TiO_2 for a given MgO. These BABB are also enriched, relative to N-MORB, in large ion lithophile elements (LILE) and, in some cases, in the light rare earth elements (LREE) relative to the high field strength elements (HFSE). It has been suggested that the high Al_2O_3 content results from a displacement of the olivine-plagioclase cotectic, due to relatively high H_2O content of the melt, whereas the lower FeO* has been explained by lower pressure and temperature of generation of BABB compared to N-MORB (Fryer et al., 1981; Sinton and Fryer, 1987). BABB are considered to be intermediate in composition between N-MORB and island arc tholeiites (Gill, 1976; Volpe et al., 1987).

BABB with strong arc-like signatures (enrichment in LILE and LREE) are thought to be erupted close to the arc at the initiation of back arc opening (Gill, 1976; Saunders and Tarney, 1979; Crawford et al., 1981). As the basin widens and the ridge and the active arc become more widely separated, arc geochemical influences become less apparent, and BABB trend towards N-MORB compositions. This leads to a compositional zoning in mature basins where basalts with arc geochemical signature

are found on the flanks grading through BABB, to near N-MORB compositions in the central, youngest parts of the back-arc basin, furthest from the arc (Hawkins and Melchior, 1985; Stern et al., 1990).

However, recent studies on basalts from the Sumisu Rift, a back-arc basin behind the Izu arc, have shown that basalts erupting close (<20 km) to the arc are typical BABB without strong arc geochemical signature. Thus the simple model described above is not applicable to all back-arc basins (Fryer et al., 1990; Hochstaedter et al., 1990a, b).

An alternative model for BABB petrogenesis, based on a study of the North Fiji Basin (NFB), suggests that some BABB are generated by mixing between an N-MORB endmember and an ocean island basalt (OIB) endmember (Johnson and Sinton, 1990; Price et al., 1990; Sinton et al., 1991).

Presently, the best-known back-arc basins are the Lau and Mariana back-arc basins (e.g. Karig, 1971; Hawkins, 1974, 1976; Hawkins and Melchior, 1985; Hawkins et al., 1990; Sinton and Fryer, 1987; Falloon et al., 1987, 1992; Woodhead, 1989). In both basins, the arc is rifting essentially along its length parallel to the adjacent trench, and the new back-arc basin spreading centres develop by rifting of arc lithosphere. The terminations of these back-arc basins are poorly-known, except for the northernmost Lau basin. There, complex triple junction tectonics in the back-arc basin, involving one ridge segment propagating to the north-east into the tight northern corner of the Tongan arc system, have generated a diverse array of magmas, including boninites (Falloon et al. 1987, 1989; Falloon and Crawford 1991).

A near-mirror-image of the complex northern termination of the Tongan arc is present at the southern end of the Vanuatu arc in the southern NFB. There the southernmost ridge of the complex NFB back-arc spreading system is propagating into the Hunter Ridge. Crawford et al. (1989) suggested that the conjunction of hot MORB-type asthenosphere supplying the back-arc basin spreading ridge, and the cold (and presumably 'damp') arc lithosphere of the Hunter Ridge, should result in the production of boninitic magmas. Furthermore, this is one of the few locations on Earth in which a back-arc basin spreading centre is propagating almost perpendicularly into arc lithosphere, rather than subparallel to the arc opening, as is normally the case.

4.1.2 Geological setting

The NFB, an active back-arc basin located between the Pacific and India-Australian plates, is roughly triangular in shape and bounded to the north by the inactive (Falvey, 1975) Vitiaz trench, by the New Hebrides arc in the west and the Hunter Ridge-Hunter fracture zone and Fiji in the south and east respectively (Fig. 4.1). The basin is tectonically complex and unstable and it has formed during the last 8-10 Ma (Auzende

et al., 1988a; Malahoff et al., 1982a, b; Charvis and Pelletier, 1989; Louat and Pelletier, 1989; Eissen et al., 1991, in press).

Prior to the formation of the NFB, the Pacific plate was being subducted under the India-Australian plate along a continuous arc consisting of the Solomon, New Hebrides, Fiji and Lau Islands at the Vitiaz trench (Malahoff et al., 1982a), until the Ontong-Java plateau collided with the Vitiaz trench causing a reversal in subduction polarity around 10-12 Ma (Auzende et al., 1988a; Eissen et al., 1991). During the opening of the NFB, the New Hebrides arc rotated clockwise, while the Fiji Islands rotated anticlockwise (Gill and Gorton, 1973; Falvey, 1978; Malahoff et al., 1982a).

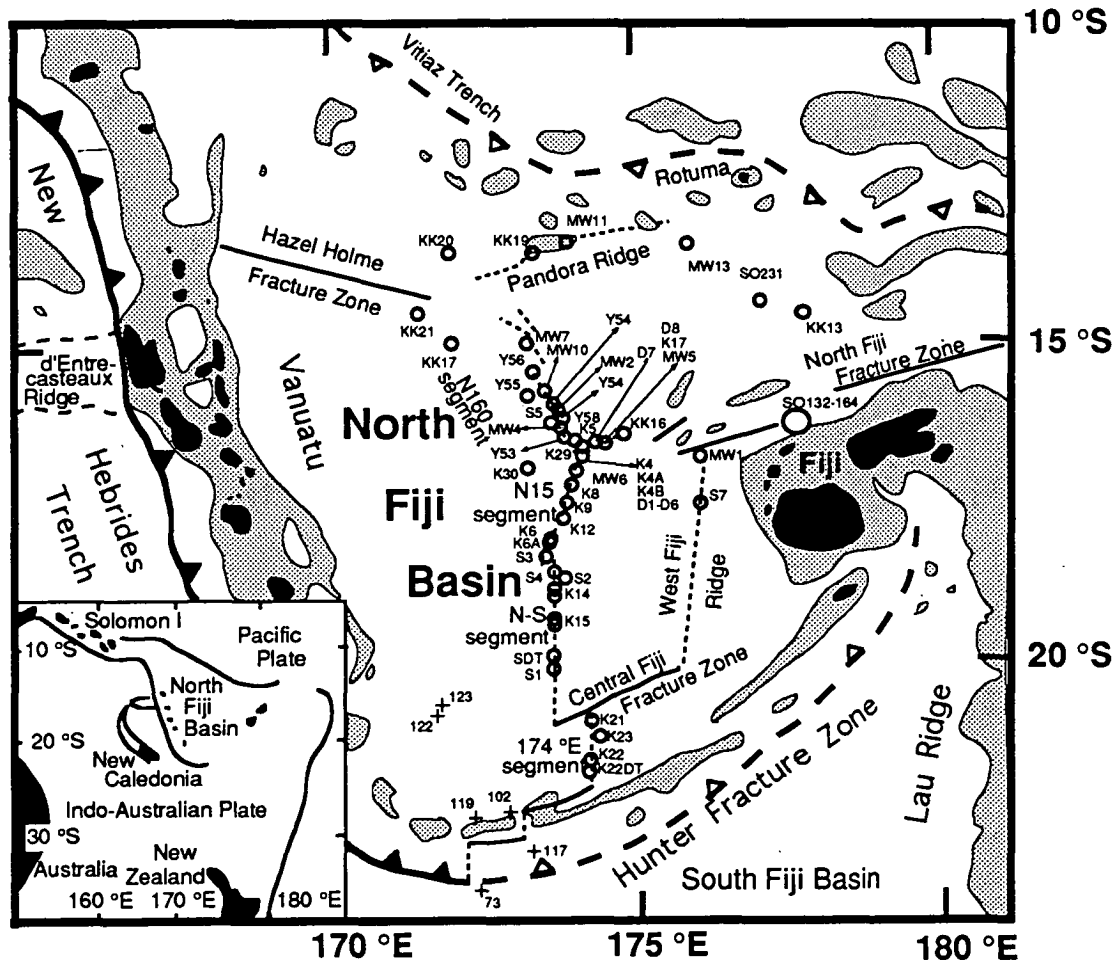

Figure 4.1: A map of the North Fiji Basin showing the location of the dredge stations where BABB and E-MORB-like lavas were recovered during the R/V A.A. Nesmeyanov cruise in 1989 (crosses). Thin dashed lines show the active spreading ridges and the circles show approximate locations of other samples discussed in this chapter. Modified from Eissen et al., 1993.

Currently the India-Australian plate is subducting under the NFB at a rate of 9-16 cm/yr, with a 70°E convergence direction. The subduction rate is lowest where the d'Entrecasteaux ridge collides with the arc at 15.5°S (Louat and Pelletier, 1989). South of 23°S the subduction becomes more oblique, eventually shifting to transform fault motion along the Hunter fracture zone, that extends north-eastward to Kandavu island in Fiji (Fig. 4.1). Although there is currently little or no apparent subduction beneath the Hunter Ridge, it is believed that subduction was taking place there since about 3 Ma and until recently (Auzende et al., in press).

At the present time, the most prominent active spreading ridge in the NFB is situated at 173°E between 16°S and 22°S (Auzende et al., 1988a, b), but other shorter spreading ridges have also been recognized (e.g., Price et al., 1990; Johnson and Sinton, 1990). The central ridge at 173°E consists of three connected ridge segments, from north to south, the N160 segment, the N15 segment and the N-S segment, and near 21°S a fourth segment is offset at 174 °E. The 174°E segment has been interpreted as a dying rift (Eissen et al., 1991), with active spreading shifting to the N-S segment which is propagating south, and a small rift segment is present at 173°E, 22°10'S that cuts through the Hunter Ridge (Fig. 4.1) (Maillet et al., 1989). At 16°50'S, the N160 segment, the N15 segment and the Fiji fracture zone form a ridge-ridge-fracture zone triple junction that represents the most elevated part of the NFB (Eissen et al., in press). Calculated spreading rate increases towards the south, from 4.6 cm/yr for the N15 segment to 7.8 cm/yr for the N-S segment at 20°S (Eissen et al. 1991).

Within the North Fiji Basin, fossil transform faults aligned 45°E, and magnetic anomalies oriented 135°E, are both believed to be linked to a 135°E spreading ridge that was active before the presently active ridge came into existence about 3 Ma ago. Since then, the subduction zone has propagated south from Anatom Island towards the Hunter Ridge, where subduction changes progressively over to a transform fault at the Hunter fracture zone (Maillet et al., 1989).

In the last ten years or so, French and Japanese workers have studied the NFB in detail, including bathymetry, geophysical profiles, water sampling, dredging and submersible dives (Auzende and Urabe, in press). As one of the results from that study, Auzende et al. (in press) have recently presented a detailed model for the opening and evolution of the NFB (Fig. 4.2).

4.1.3 Previous work

Previous work on basalts from the NFB spreading centres has revealed a spectrum of magma types, ranging from N-MORB like magmas to more alkali- and incompatible element enriched magmas.

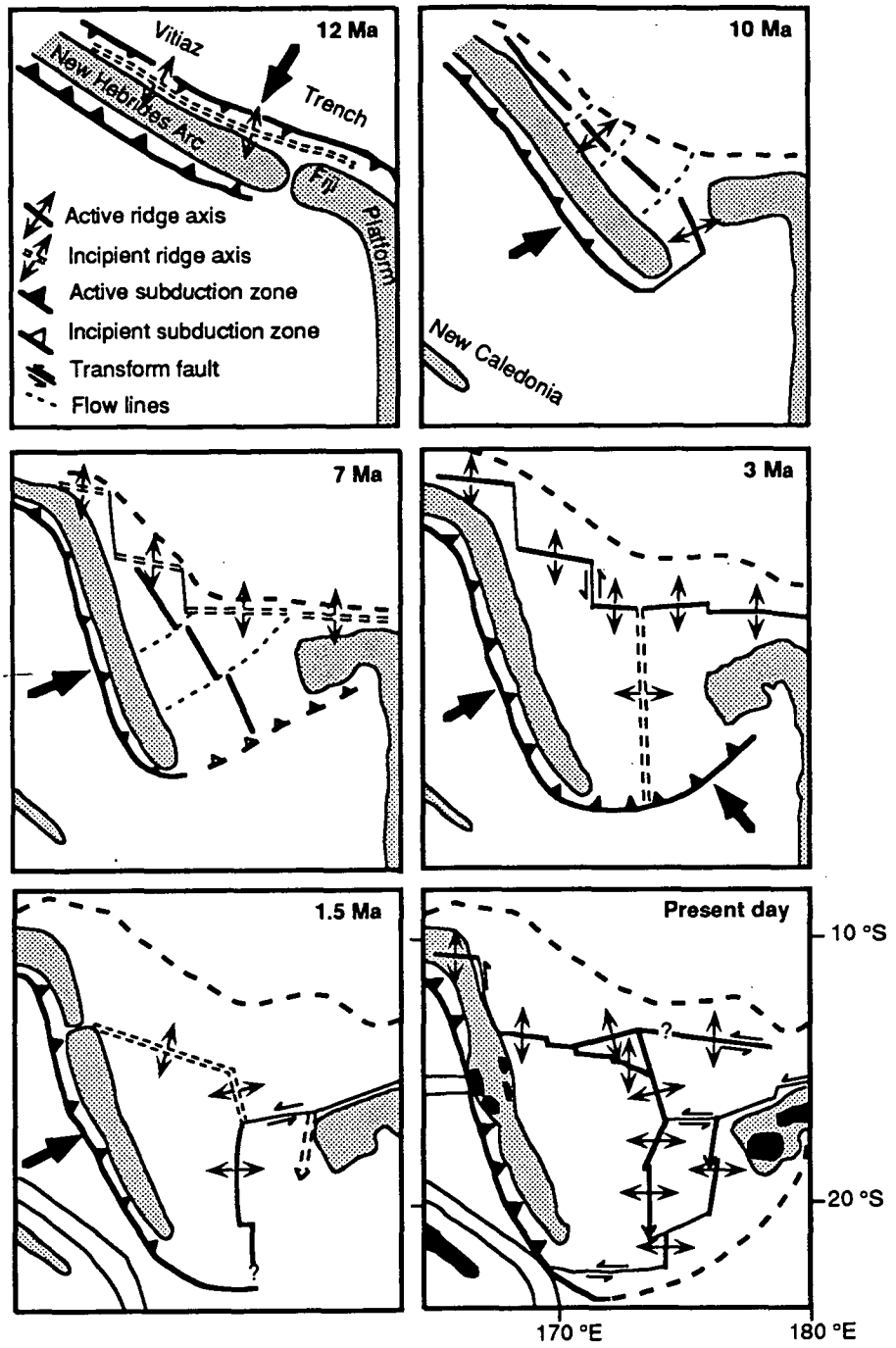

Figure 4.2: Diagram showing the evolution of the North Fiji Basin during the last 12 Ma. 12 Ma ago, the collition of the Ontong-Java Plateau causes a change in subduction polarity from the Vitiaz Trench over to the New Hebrides Trench. The Vitiaz-New Hebrides-Fiji-Lau-Tonga arc is split and spreading starts behind the New Hebrides arc. At 10 Ma spreading and the opening of the NFB causes a clockwise rotation of the NFB and anticlokckwise rotation of the Fiji Platform. 7 Ma ago spreding stops at the NW-SE ridge and an EW trending spreading start beween the northwestern tip of the basin and the Fiji Platform. This causes further anticlockwise rotation of the Fiji Platform and initiates a new subduction zone at the southern limit of the NFB. 3 Ma agao a triple junction was active between the EW axis and a new NS spreading axis. 1.5 Ma ago the EW axis was reorganized, the North Fiji Fracture zone is formed along the Fiji Platform and the West Fiji and Hasel Holme Ridges are formed. At present spreading is active along several complex spreading ridges connected by even more complex fracture zones. Redrawn from Auzende et al. (in press).

Based on K_2O versus H_2O relationships, Danyushevsky et al. (1993) demonstrated that basaltic glasses from back-arc basins, including five glasses from the NFB, show two distinct enrichment trends. All the back-arc basins which they studied contain glasses with compositions similar to N-MORB and they inferred that the compositional spectrum seen in each case results from mixing of this N-MORB component with either a subduction-related component, or with a non-subduction related component, the latter most likely an enriched alkaline magma. The glasses which they examined from the NFB were either geochemically similar to N-MORB or showed evidence for mixing with an enriched alkaline component of non-subduction related character.

Johnson and Sinton (1990) used a total alkalies vs $mg^{\#}$ diagram to define three magma types from analyses of basaltic glasses from the NFB. These three types are described briefly below and then all glass analyses available from the NFB are compared using this classification of Johnson and Sinton (1990). I then propose a more simplified classification, based on K_2O/TiO_2, that is consistent with trace element concentrations.

Johnson and Sinton (1990) described samples from a short spreading segment on the Fiji fracture zone and divided them into three types based on major element composition (Fig. 4.3a). Type 1 is most abundant and has major and trace element compositions similar to N-MORB. Type 2 is classified as BABB and is enriched in all incompatible elements compared to Type 1. It is believed to be formed by mixing between an N-MORB-like source (Type 1 source) and an enriched ocean island basalt (OIB) mantle component similar to the source for Samoan OIB. Type 3 is even more enriched in incompatible elements and more closely represents the enriched OIB endmember.

The three types defined by Sinton et al., (1991), from six dredge stations in the NFB and one station in the Lau basin (not shown in Fig. 4.3b), are consistent with this classification.

Price et al., (1990) also defined three basalt types in the NFB, based on trace elements. Type 1 is depleted in LREE similar to N-MORB, Type 3 has a LREE-enriched OIB-like composition, and Type 2 is intermediate between Types 1 and 3. These three types are not fully consistent with the classification into three types suggested by Johnson and Sinton (1990), in that several of Price et al's Type 2 lavas are as, or even more enriched in total alkalis than Johnson and Sinton's Type 3 (Fig. 4.3c).

Price et al. (1990) compared their Type 2 basalt with the average Mariana BABB, calculated from data taken from Sinton and Fryer (1987) and Hawkins and Melchior (1985). They found their Type 2 to be almost identical in incompatible elements to the average Mariana BABB. This led them to conclude that BABB in general might

simply be a part of a magma spectrum formed by mixing of N-MORB like basalts with more alkalic basalt (OIB) and that there was no need to involve subduction-related components in BABB genesis. However, Falloon et al., (1992) and this study, show that the conclusions of Price et al., (1990) cannot explain the apparent depletion of HFSE, such as Nb, in typical BABB. Compiling available data from the Mariana back-arc basin, it became apparent that earlier papers either did not report Nb values (Sinton and Fryer, 1987) or gave values between 5-11 ppm Nb (Hawkins and Melchior, 1985; Volpe et al., 1987) averaging 8.8 ppm. However, in a more recent paper by some of the same authors, the average Nb content of Mariana BABB is now reported as close to 1 ppm (Hawkins et al., 1990) and an average value for BABB in the Sumisu Rift is 1.5 ppm (Hochstaedter et al., 1990b). Therefore the Type 2 magmas in the NFB, containing 5-54 ppm Nb cannot be regarded as "typical" BABB magmas (Sinton and Fryer, 1987), if a trace element characterization of BABB is used, since the definition by Price et al., (1990) was based on incorrect, mistakenly high Nb values.

Auzende et al. (1988b) reported major element glass compositions of samples from six dredge stations in the central NFB, and concluded that these samples had a MORB-like composition with a small shift towards BABB. All the glasses have similar or lower $Na_2O + K_2O$ than the field for Type 1 from Johnson and Sinton (1990) (Fig. 4.3d).

Eissen et al., (1991) reported new petrological and geochemical data from the main spreading centres in the NFB and Eissen et al., (in press) presented new data and compared them with previously published analyses from the NFB. They concluded that the dominant magma type has largely a N-MORB-like signature. In the northernmost part of the basin, magmas resulting from mixing of N-MORB- and E-MORB-like sources become more abundant, whereas in the south both E-MORB and subduction-related signatures (i.e. enrichment in LILE relative to HFSE) can be detected in the lava compositions. The glass analyses reported by Eissen et al. (1991) do not fit well with the classification of Johnson and Sinton (1990) and fall to some extent outside the fields for the three types (Fig. 4.3e). This extends the fields from Johnson and Sinton (1990) for basaltic magmas present in the NFB but it also makes the boundaries between the three types unclear, suggesting that there is a continuous spectrum from N-MORB-like compositions through to more alkali-enriched magmas. Eissen et al's (1991) data are important in that they include a high proportion of more primitive glasses and demonstrate a spread of Na_2O and K_2O contents within primitive magma compositions. This data set has to be treated with caution though as one whole rock analysis contains 3% MnO and high water content (K12-2) and glass analysis S1-01 shows strong indications for plagioclase overlap during analyses.

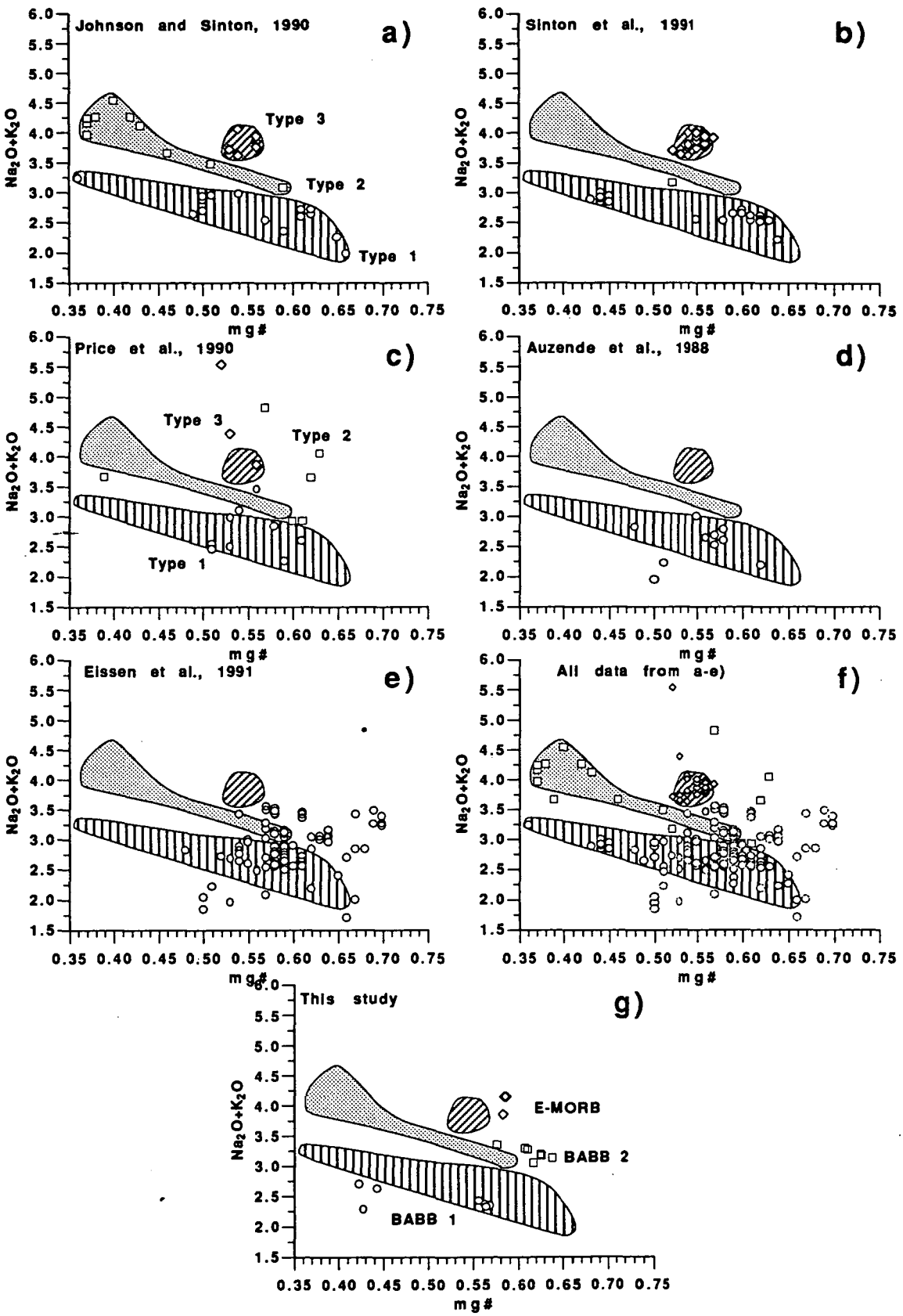

Figure 4.3: a) The three magma types from the NFB as they were defined by Johnson and Sinton (1990). b-e) Glass analyses from Sinton et al. (1991), Price et al. (1990), Auzende et al. (1988b) and Eissen et al. (1991) compared with the fields for the three types define by Johnson and Sinton (1990). f) All the glass analyses from (a-e) shown together. g) Glasses from this study.

4.1.4 Classification used in this study

When all available glass analyses from the NFB are compiled (Fig. 4.3f), it becomes impossible to simply classify them according to the three types defined by Johnson and Sinton (1990). In an attempt to separate the N-MORB-like glasses from the more incompatible element enriched glasses, the glasses are here divided into three groups based on their K_2O and TiO_2 contents, plotted in Figure 4.4 as K_2O/Al_2O_3 against TiO_2/Al_2O_3, and K_2O/TiO_2 against mg#. The rationale for using these ratios is that decrease in mg# indicates crystal fractionation but if olivine, pyroxene and plagioclase are fractionating phases in more primitive melts, then K_2O/TiO_2 will not change but K_2O/Al_2O_3 will increase and TiO_2/Al_2O_3 will increase with increasing fractionation. TiO_2/Al_2O_3 will vary with fractionation and ratios containing TiO_2 will be sensitive to the appearance of a Ti-Fe oxide phase in the crystallization interval. Thus Figure 4.4 is useful for distinguishing primary geochemical differences (major and minor elements) between magma series and separating these from concentration changes during crystal fractionation. The low K_2O (K_2O/Al_2O_3) group, representing the N-MORB like glasses, includes Types 1 from Johnson and Sinton (1990) and Sinton et al. (1991), most of Type 1 from Price et al. (1990) and the bulk of the glasses from both Auzende et al. (1988b) and Eissen et al. (1991). The more K_2O-rich glasses show two trends in Figure 4.4a, one subparallel to the N-MORB-like glasses but at higher K_2O/Al_2O_3 levels, whereas the other shows steep increase in K_2O/Al_2O_3 relative to TiO_2/Al_2O_3. There is no clear trend (Fig 4.4b) in K_2O/TiO_2 with crystal fractionation (decreasing mg#) suggesting similar bulk K_d's for K and Ti in the fractionating assemblages.

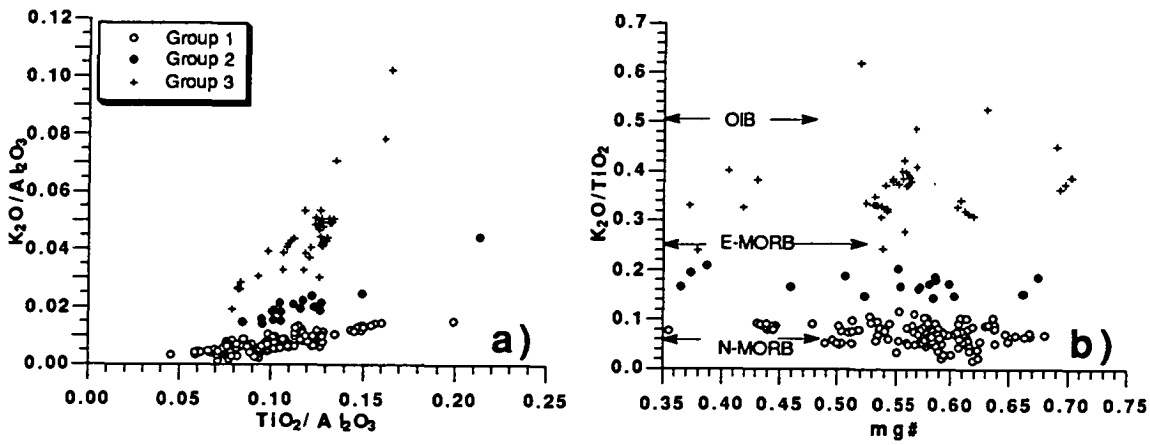

Figure 4.4: a) The three lava groups from the NFB, as defined in this study, shown on a K_2O/Al_2O_3 vs TiO_2/Al_2O_3 diagram and b) K_2O/TiO_2 vs mg#. The arrows show the K_2O/TiO_2 values in N-MORB, E-MORB and OIB, data from Sun and McDunough, 1989.

To test if this grouping also holds for the trace element compositions, trace element ratios (Zr/Y, Nb/La, La/Yb) normalized to N-MORB are plotted in Figure 4.5 for those glasses that have been analysed for trace elements and for those samples where both glasses and whole rock major and trace elements have been analysed. Trace element data from Eissen et al. (in press) may be plotted on the same figure and illustrate the same spread. However they cannot be split into groups based on glass chemistry because no major element glass analyses are available, so the distinction is made based on trace element ratios in the other groups.

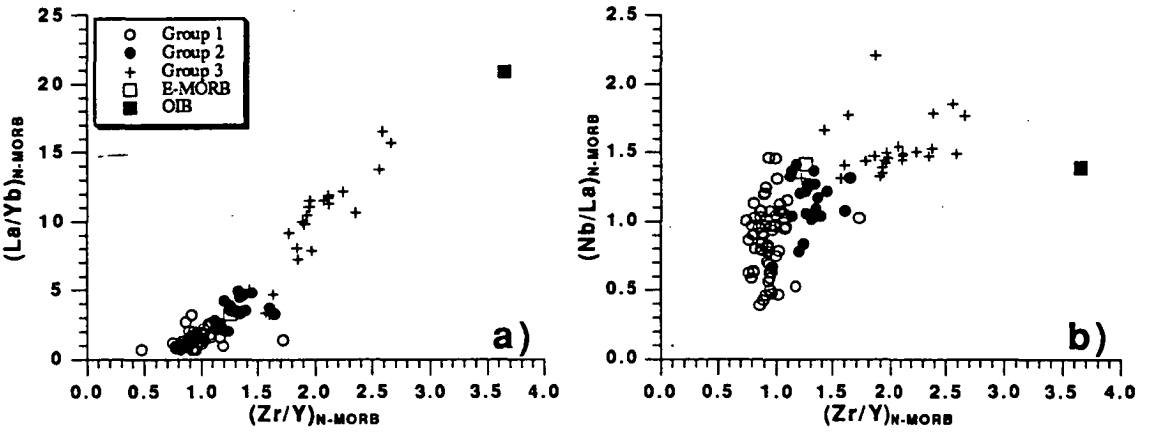

Figure 4.5: a) La/Yb and b) Nb/ La, normalized to N-MORB, vs Zr/Y, normalized to N-MORB, for the three magma groups as defined here. Also shown are the same normalized ratios in E-MORB and OIB. N-MORB, E-MORB and OIB values from Sun and McDunough, 1989.

Figure 4.5 shows that the low K_2O, N-MORB like glasses (Group 1) form a tight group based on the trace elements (except for sample 231/1 from Johnson and Sinton, (1990), which has abnormally high Zr content), although there is a continuous spectrum from N-MORB-like compositions to more incompatible element enriched compositions (Groups 2 and 3). Most N-MORB-like samples show depletion or slight enrichment in Zr/Y, Nb/La, and La/Yb, whereas Groups 2 and 3 show moderate to strong enrichment. This is further demonstrated in REE diagrams in Figure 4.6 in which five samples from each group are shown on chondrite normalized diagrams and in Figure 4.7 in which the element abundances are normalized to N-MORB. The enrichment trend for Group 3 (Fig. 4.5) is on a mixing line between N- or E-MORB and OIB (Sun and McDonough, 1989); Group 1 is similar to N-MORB although an arc signature can be seen in some samples (i.e. slight relative Nb depletion) whereas Group 2 is intermediate between Groups 1 and 3.

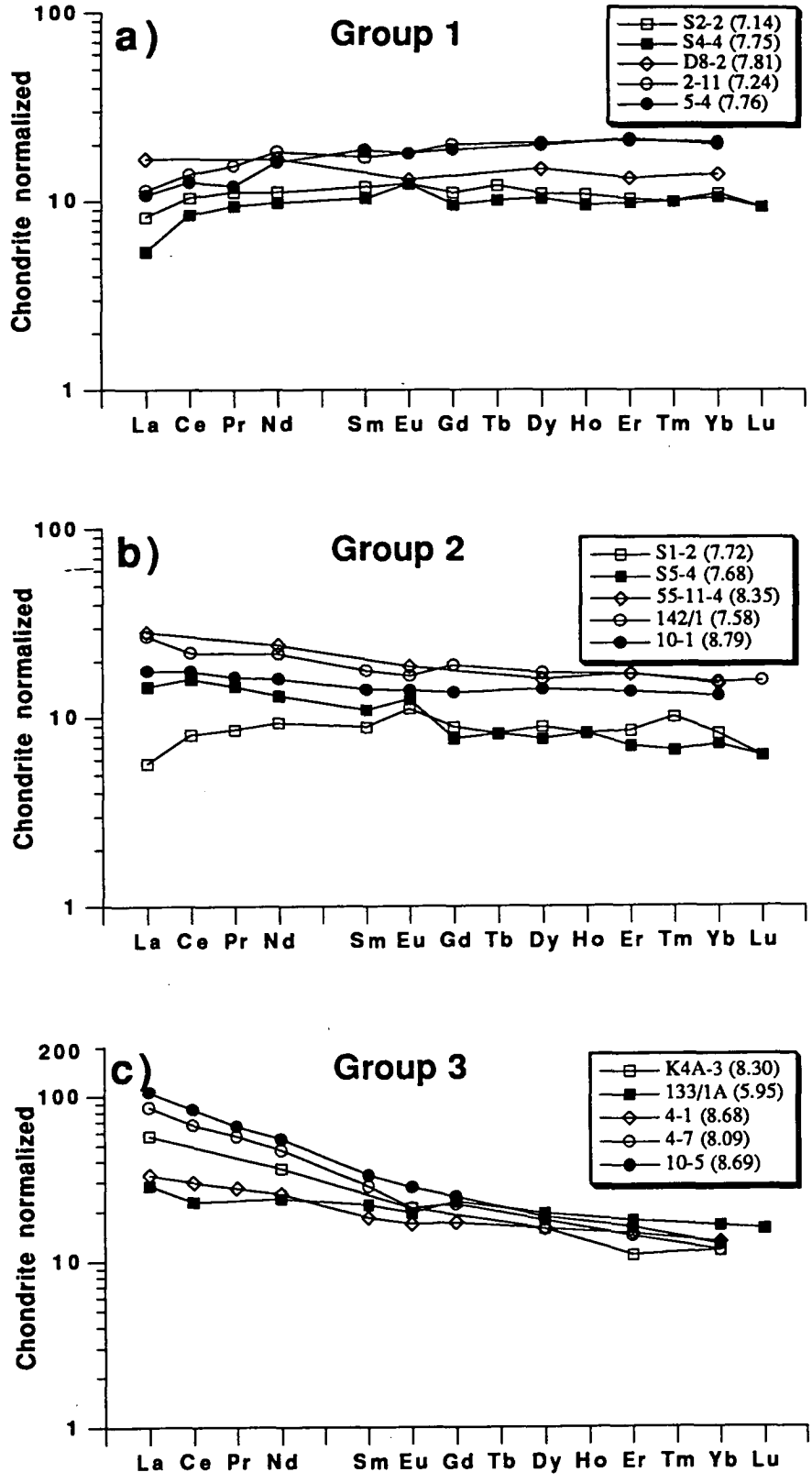

Figure 4.6: REE concentration, normalized to chondrite, for five samples from each of the three groups from the NFB. Chondrite values are taken from Taylor and Gorton, 1977.

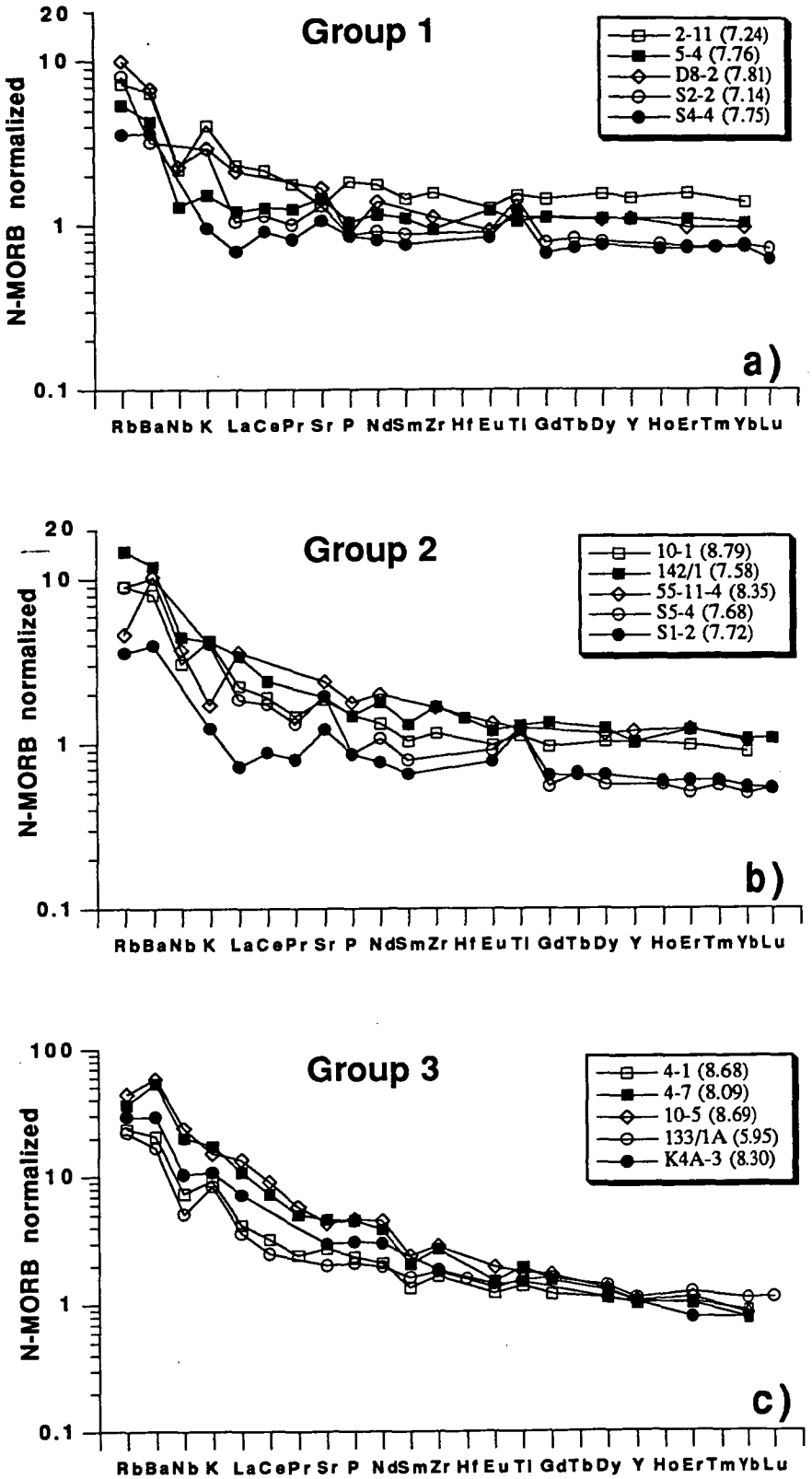

Figure 4.7: N-MORB normalized element diagram for five samples from each of the three groups from the NFB. Normalizing values from Sun and McDonough, 1989.

4.2 Basaltic lavas dredged by R/V A. A. Nesmeyanov

BABB lavas were dredged at stations 102, 117, 119, 122 and 123, and E-MORB-like lavas were dredged at stations 73 and 92. In chapter 3 the glass compositions and olivine-spinel systematics of some of these samples were described. Here I deal briefly with the petrography of lavas from stations 73, 102, 122 and 123, and whole-rock geochemistry of samples from all stations except for station 119 for which only a small glassy fragment was available.

4.2.1 Petrography

The E-MORB-like lava from station 73 is a glassy pillow fragment. The groundmass is glassy with microphenocrysts of skeletal olivine (<1 mm). The glass is largely devitrified and shows alteration in vesicles and around cracks. No thin section was made from sample 92/37, but it is picritic with approximately 40% olivine phenocrysts (Fo_{90-84}).

BABB 102/1 is aphyric with the groundmass consisting of plagioclase laths separated by devitrified glass or clinopyroxene. BABB 122/1 and 122/2 are fine- and medium-grained dolerites respectively, with plagioclase laths subophitically enclosed by clinopyroxene and minor interstitial devitrified glass and magnetite. BABB 122/5 is aphyric with plagioclase and clinopyroxene microlites set in a groundmass of devitrified glass and interstitial magnetite. BABB 122/8 contains rare euhedral olivine phenocrysts, (<2 mm) that contain numerous small euhedral plagioclase inclusions, and euhedral plagioclase (<1 mm) phenocrysts in a groundmass consisting of plagioclase laths and interstitial clinopyroxene set in devitrified glass.

BABB 123/1 and 123/2 are olivine- and plagioclase-phyric (An_{77-69}) with the olivines (Fo_{91-88}) commonly containing cr-spinel inclusions (see chapter 3). The groundmass consists of plagioclase laths surrounded by devitrified glass, olivine and cr-spinel. All BABB samples show some alteration in the groundmass.

4.2.2 Major element glass geochemistry

The major element glass geochemistry was reported in chapter 3 together with other glasses from the R/V A. A. Nesmeyanov cruise. Two types of BABB were identified, with BABB 1 having lower Al_2O_3 and Na_2O and higher FeO* than BABB 2. Glasses from dredge 73 showed similarities to E-MORB, with low CaO and high TiO_2, K_2O and P_2O_5. In Figure 4.8 the BABB and E-MORB-like glasses are plotted together with fields for all the glass analyses available from the NFB that have MgO > 5%. Group 1 and Group 3 glasses form a tight trend on all plots whereas Group 2 is transitional between groups 1 and 3. A single Group 1 glass (S1-1 from Eissen et al., (1991)) has abnormally high Al_2O_3 and CaO, and low TiO_2, MgO and FeO*

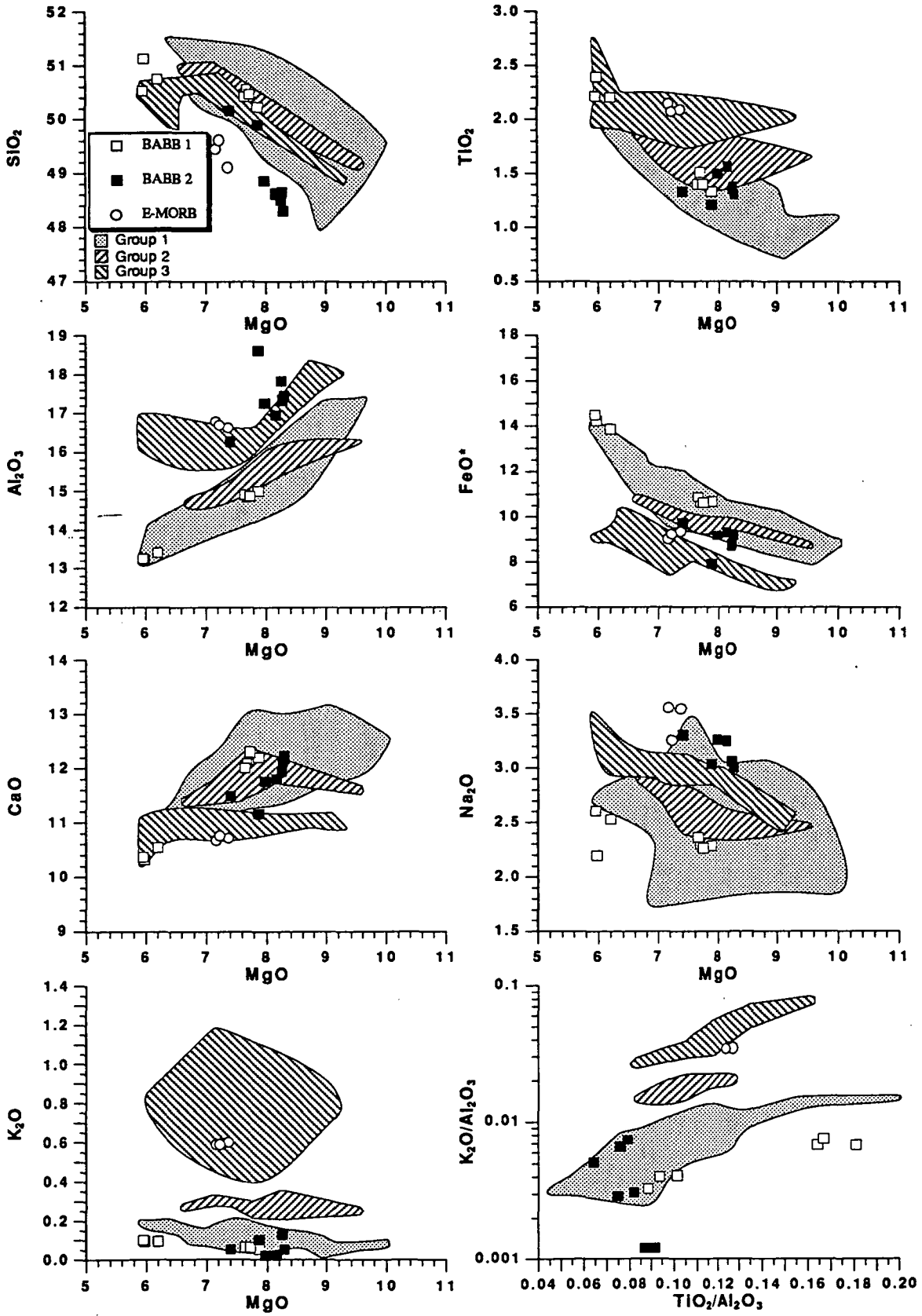

Figure 4.8: The major element glass compositions for the BABB 1, BABB 2 and E-MORB groups from chapter 3 plotted together with fields for the three basalt groups from the NFB on conventional MgO variations diagrams and K_2O/Al_2O_3 versus TiO_2/Al_2O_3 diagram.

Table 4.1: Whole-rock major and trace element compositions of the basalts from the NFB. Major and trace elements were analysed by XRF except for Th and Hf by INAA. REE were analysed by XRF ion exchange technique (Robinson et al., 1986) except for basalts 117/1, 117/13, 117/2 and 92/37 by INAA.

Group	BABB 1						
Sample#	122/1	122/2	122/5	122/8	117/1	117/4	117/13
SiO_2	48.33	48.27	49.91	49.11	49.22	47.31	49.69
TiO_2	1.33	1.12	2.14	1.33	1.42	1.32	2.13
Al_2O_3	14.75	15.45	13.28	14.99	15.15	14.49	13.16
Fe_2O_3	11.80	10.90	14.19	11.80	11.67	11.07	15.20
MnO	0.18	0.17	0.21	0.19	0.19	0.17	0.23
MgO	6.74	6.83	5.89	7.50	7.20	7.50	6.36
CaO	11.87	11.76	10.19	11.78	12.16	11.65	10.39
Na_2O	3.05	2.95	2.99	2.50	2.43	2.38	2.45
K_2O	0.26	0.30	0.33	0.11	0.11	0.19	0.11
P_2O_5	0.15	0.15	0.20	0.14	0.13	0.12	0.18
LOI	1.04	1.79	1.15	0.00	0.41	1.43	-0.45
Sum	99.50	99.69	100.48	99.45	100.09	97.63	99.45
Trace elements (ppm)							
Pb	7	8	5	<2	1	4	1.5
Ba	19	20	30	19	13.5	11.5	19
Sr	91	118	96	87	89	87	82.5
La	3.41	2.76	4.03	2.00	2.29	3.2	4.23
Ce	8.34	6.63	14.60	8.24	7.82	9.9	12.2
Pr	1.64	1.24	2.60	1.53			
Nd	9.00	7.24	15.40	8.85	7.27	8.4	11.3
Sm	3.52	2.82	6.33	4.01	3.27		5.3
Eu	1.07	0.92	2.02	1.48	1.28		1.67
Gd	4.95	4.10	8.67	5.28			
Tb					0.82		1.41
Dy	6.09	4.77	10.30	6.08			
Ho					1.32		2.27
Er	3.98	3.23	6.81	3.95			
Yb	3.76	2.79	6.39	3.76	3.84		6.4
Lu					0.59		1.06
Y	37	31	59	36	37.6	37	56.6
Th	0.14	0.24	0.26	0.2	0.42		0.73
Zr	80	68	133	79	78	76	123
Hf	2.11	1.89	3.54	2.14	2.29		3.68
Nb	1	1	2	1	1.2	1.3	2.8
Sc	43	33	45	53	45.2	47.1	48.6
V	366	274	533	384	362.4	345	500.9
Cr	87	98	56	112	357	361.1	120.3
Ni	341	299	118	379	104	114	64
Ga							

Table 4.1: continued.

Group	BABB 2					E-MORB	
Sample	123/1	123/2	117/2	117/5	102/1	73/8	92/37
SiO_2	46.89	47.46	47.49	47.62	49.77	47.84	40.61
TiO_2	1.18	1.16	1.33	1.36	1.29	2.09	0.95
Al_2O_3	15.67	15.79	16.42	16.50	15.77	16.11	9.08
Fe_2O_3	9.92	9.71	9.77	9.76	10.49	10.17	11.60
MnO	0.16	0.14	0.15	0.16	0.19	0.17	0.20
MgO	11.54	11.75	10.18	10.80	7.09	8.16	21.11
CaO	10.68	10.65	10.90	10.89	11.27	10.21	8.99
Na_2O	2.85	2.69	3.25	3.16	3.55	3.43	1.16
K_2O	0.21	0.19	0.15	0.05	0.24	0.64	0.28
P_2O_5	0.10	0.10	0.10	0.10	0.09	0.41	0.16
LOI	0.34	0.70	-0.05	-0.44	0.24	1.12	6.00
Sum	99.54	100.34	99.69	99.96	99.99	100.35	100.14
Trace elements (ppm)							
Rb	3.5	3.5	4.5	1	3	4	6
Ba	20	18	9	4.5	14	49	65
Sr	166	165	136.5	133.5	116	342	160.5
La	2.29	2.81	1.34	0.5	1.55	14.50	9.8
Ce	8.03	9.39	6.74	8.7	6.74	37.70	20.4
Pr	1.23	1.64			1.46	4.99	
Nd	8.49	9.46	8.86	8.9	9.91	23.00	12.2
Sm	3.02	3.49	3.07		3.64	5.67	2.64
Eu	1.18	1.32	1.09		1.48	1.92	0.88
Gd	3.92	4.34			5.31	6.17	
Tb			0.7				0.45
Dy	4.21	4.67			5.69	5.83	
Ho			0.96				0.51
Er	2.67	2.70			3.62	3.22	
Yb	2.34	2.47	2.7		3.26	2.97	1.18
Lu			0.4				0.17
Y	26	25	29.6	29.1	31	36	13.9
Th	0.18	0.2	0.38		0.15	1.05	1.21
Zr	82	81	83.5	81.5	71	234	67
Hf	2.1	2.05	1.94		4.27	4.47	1.39
Nb	2	2	0.4	0.8	<1	17	15.4
Sc	37	39	36.6	35.6	40	36	26.1
V	208	218	211.9	207.6	282	275	161
Cr	346	368	544.2	535.9	59	158	1193.3
Ni	794	853	264	271	111	376	589
Ga					18.1	18.2	

compared with all the other group 1 glasses, which suggests plagioclase overlap in that analysis. The E-MORB-like glasses plot together with Group 3 glasses from the NFB on all the plots and similarly BABB 1 glasses plot together with Group 1 glasses. The BABB 2 glasses on the other hand, which according to the classification used here, are of Group 1 because of their low K_2O and K_2O/Al_2O_3, have lower SiO_2 than most group 1 glasses as well as higher Al_2O_3. This will be discussed further in a later section.

4.2.3 Whole-rock major and trace element compositions

Seven whole-rock samples from BABB 1, five from BABB 2 and two from the E-MORB-like group were analysed for major and trace elements, including REE for all but two samples. The analytical techniques are described in Appendix 2. The reported analyses of 92/37 is of a sieved fraction > 0.3 mm, and is significantly olivine (MgO) enriched due to selective removal of the fine, phenocryst poor fraction (Table 4.1). This analysis is therefore not shown on major element plots but it is included in the trace element plots. Major element whole-rock analyses of all other analysed basalts are shown in Figure 4.9 together with fields for the whole-rock analyses from the three groups from the NFB. Samples from these three groups with MgO lower than 5% were left out as well as three samples with Al_2O_3 higher than 18% that are likely to be plagioclase-accumulative. Most Group 1 basalts form a tight group at 6 to 8% MgO on most plots and some of the spread in the data, especially in Al_2O_3 (Fig 4.9c), is likely to be caused by plagioclase accumulation. Group 3 plots systematically at higher TiO_2, Al_2O_3 and K_2O, and lower FeO* and Na_2O than the other groups, with Group 2 largely plotting between the other two groups.

The olivine-phyric samples from dredges 117 and 123 (BABB-2) are more MgO-rich than any other samples from the NFB and from 11.8 to 10% MgO, Al_2O_3 and CaO rise, indicating olivine only fractionation. At 7% MgO, Al_2O_3 has decreased slightly, so if all BABB-2 samples are related by crystal fractionation plagioclase must have joined olivine on the liquidus before this stage.

The trend shown by BABB 1, between 8 and 6% MgO indicates fractionation of olivine, plagioclase and clinopyroxene, as FeO* increases and Al_2O_3 and CaO decrease with decreasing MgO. Na_2O shows significant variations in the NFB basalts, both for the glass and whole-rock analyses, with BABB 1 having low Na_2O and BABB 2 high Na_2O. Basalt 73/8 plots together with Group 3 basalts except that it has lower SiO_2 and higher FeO* than most Group 3 basalts.

In Figure 4.10 the trace element analyses from this study have been added to the data from Figure 4.5 but this time on a log-log plot because of low La/Yb and Nb/La in both BABB 1 and BABB 2. BABB 1 plots within the field of Group 1 basalts on both plots but they have the strongest relative Nb depletion. BABB 2 have similar

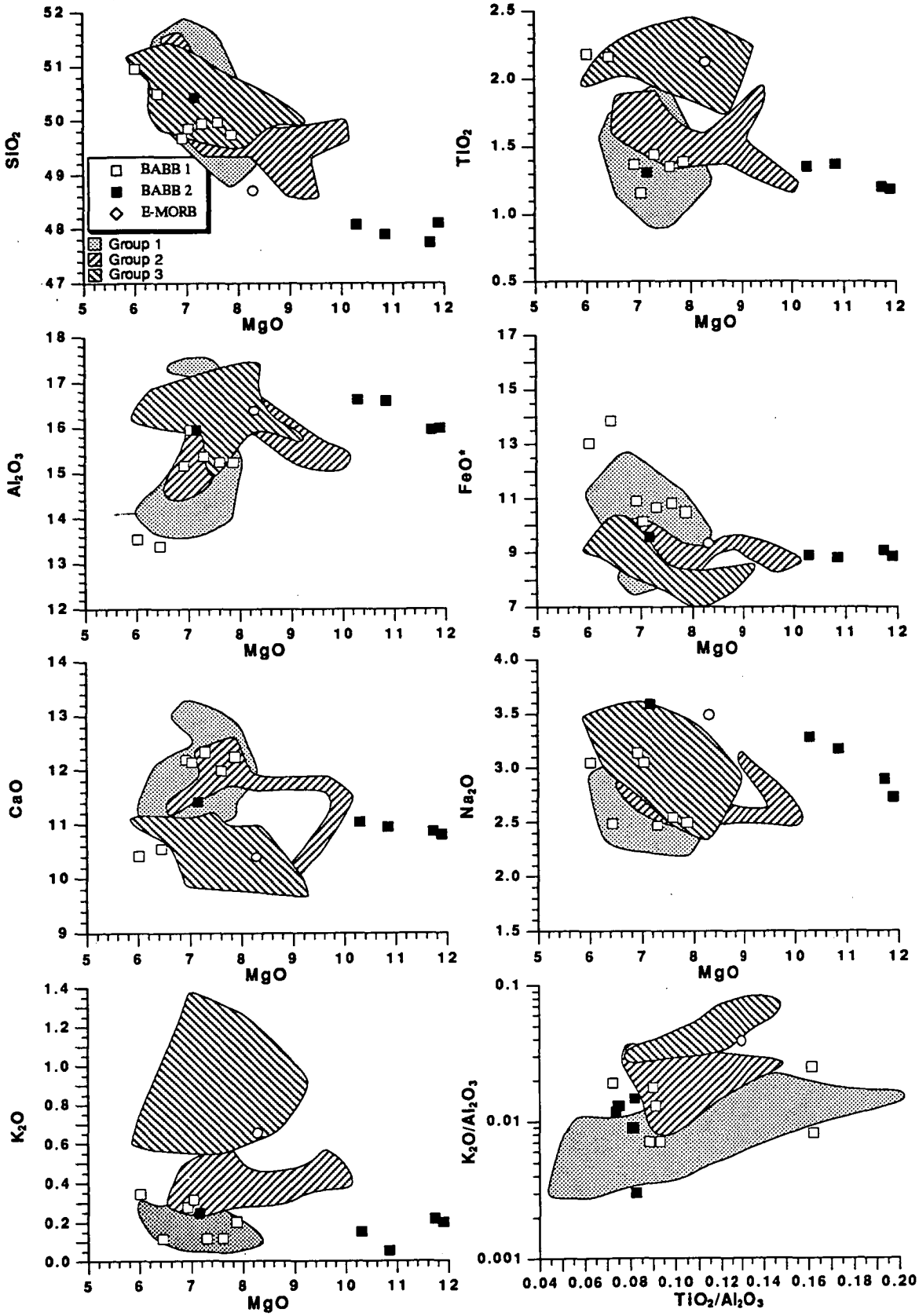

Figure 4.9: The major element whole-rock compositions for the BABB 1, BABB 2 and E-MORB groups plotted together with fields for the three basalt groups from the NFB, on conventional MgO variations diagrams and K_2O/Al_2O_3 versus TiO_2/Al_2O_3 diagram.

La/Yb and Nb/La as group 1 but they have higher Zr/Y. Both BABB 1 and BABB 2 show moderate to strong depletion in the LREE whereas the E-MORB-like samples are LREE-enriched and plot in-between E-MORB and OIB (Figs. 4.11 and 4.12).

Negative Eu-anomalies can be seen in BABB-1 basalts (Fig. 4.11) with MgO = 6.02-7.06% but it is absent in BABB-1 with MgO higher than 7.31% and from BABB-2 basalts which have MgO = 7.18-11.75%).

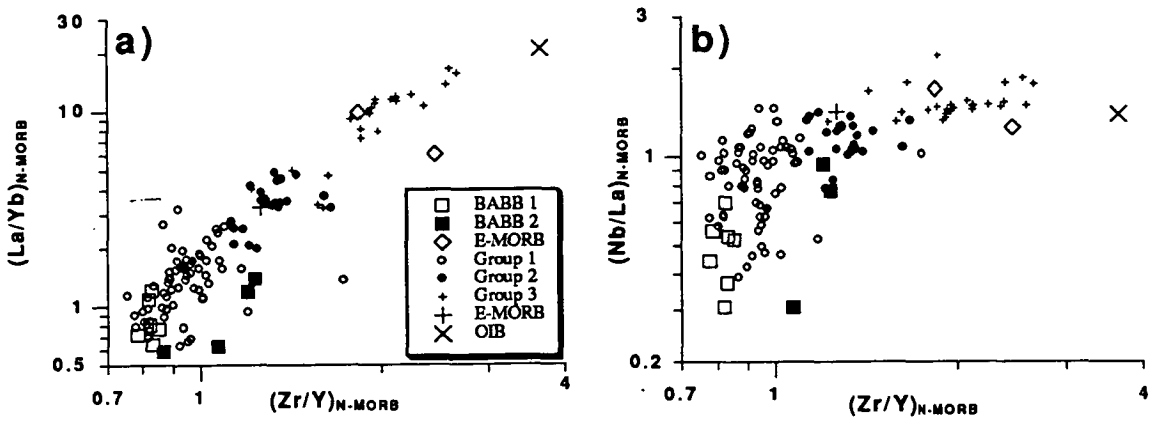

Figure 4.10: a) La/Yb and b) Nb/ La, normalized to N-MORB, vs Zr/Y, normalized to N-MORB, for the BABB 1, BABB 2 and E-MORB groups from the NFB together with the three magma groups from NFB as defined here. Also shown are the same normalized ratios in E-MORB and OIB. N-MORB, E-MORB and OIB values from Sun and McDunough, 1989.

4.3 Melt inclusions

Heating stage experiments have been performed on olivine phenocrysts ($Fo_{89.7-90.9}$) in three basalts from station 123. The inclusions did not homogenize but were quenched at temperatures between 1250 or 1270 °C after melting all the crystals inside the inclusions. The composition of these inclusions cannot, therefore, be used directly as representing true melt compositions, but the ratios of elements that are incompatible in olivine should not be affected.

In Figure 4.13 ratios of elements incompatible in olivine are plotted for these melt inclusions versus Fo content of the host olivine; also shown are the three natural glasses from station 123 with the equilibrium olivine compositions calculated using the model of Ford et al. (1983), with Fe^{2+}/Fe^{3+} = 8.41 based on Fe^{2+}/Fe^{3+} in spinel (Maurel and Maurel, 1982a). Also shown for comparison are ratios for inclusions in olivines from andesites from dredge 108 (chapter 5) and from basalts from the AAD (chapter 2). Figure 4.13 shows that the natural glasses have not fractionated

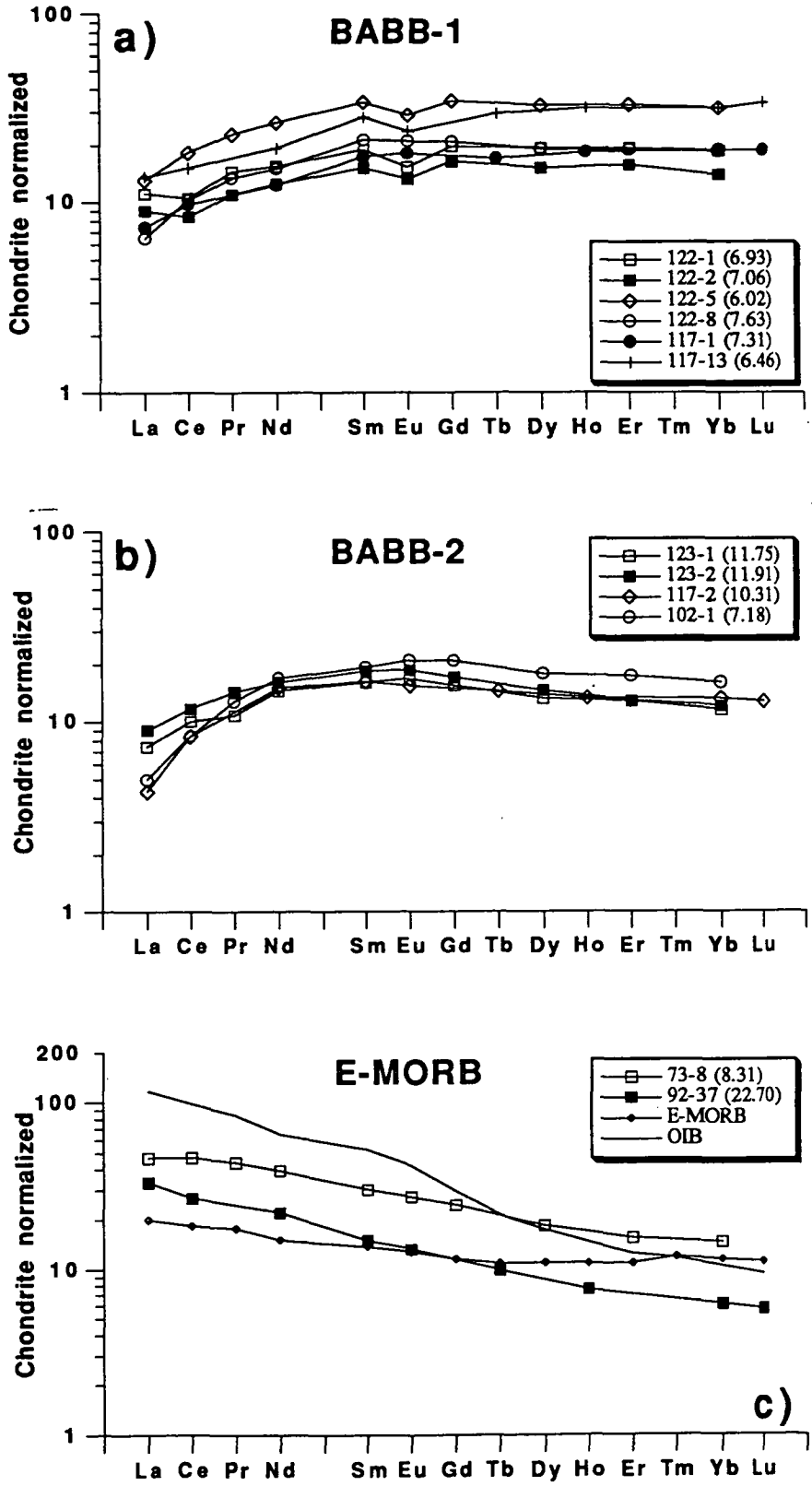

Figure 4.11: REE concentration, normalized to chondrite, for the analysed samples from the NFB. Chondrite values are taken from Taylor and Gorton, 1977.

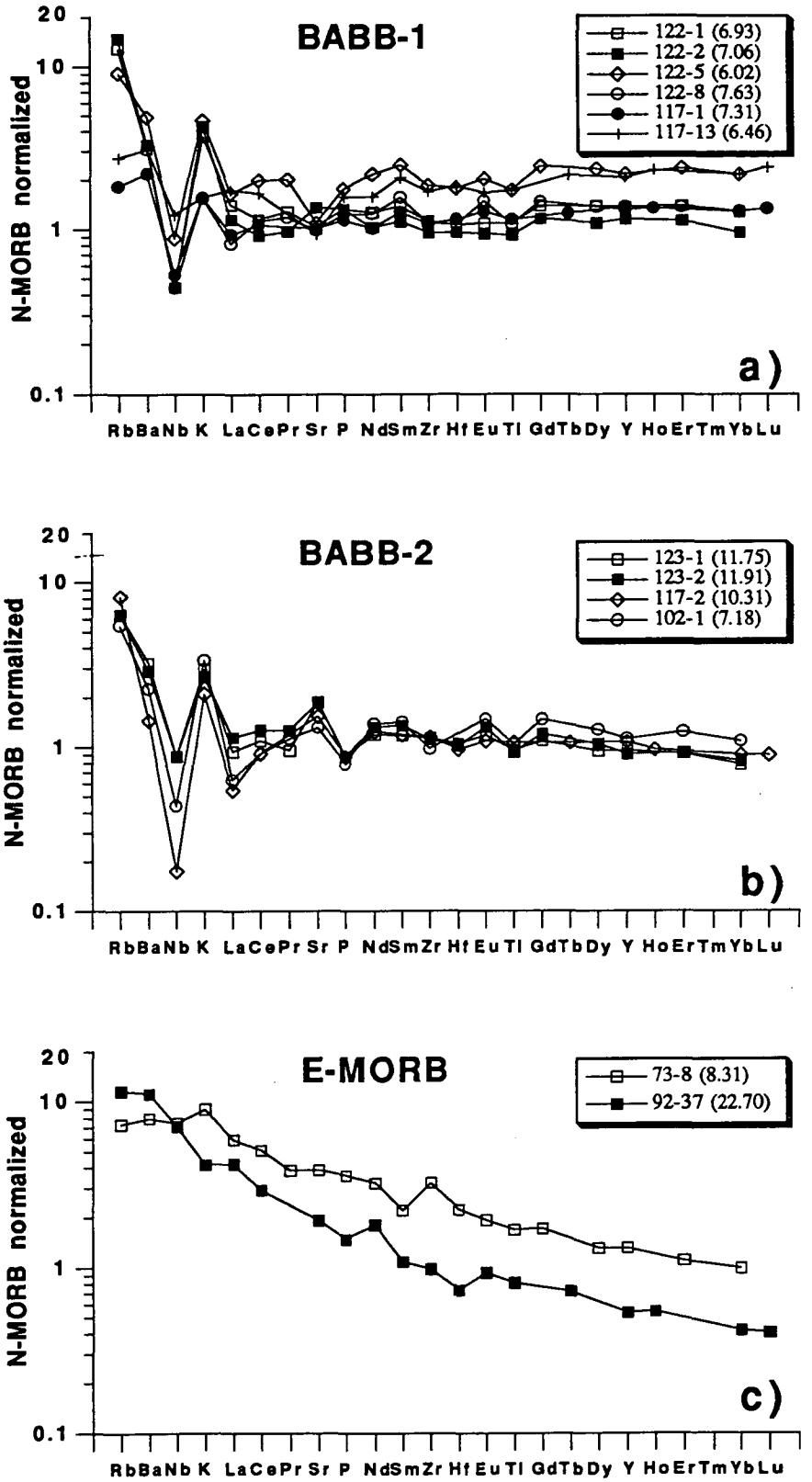

Figure 4.12: N-MORB normalized element diagram for the analysed samples the NFB. Normalizing values from Sun and McDonough, 1989.

plagioclase or clinopyroxene since they were in equilibrium with olivine Fo_{91}, as no differences can be seen in these elements between the inclusions and the natural glasses, and plagioclase crystallization would cause an increase in K_2O/Al_2O_3, and clinopyroxene crystallization would cause an increase in K_2O/CaO. The range in these ratios in the inclusions is also very small compared to the other suites (AAD and dredge 108) where mixing between geochemically distinct magmas is demonstrated (chapter 2 and chapter 5).

In short, the compositions of these melt inclusions show no evidence for magma mixing during evolution of the BABB from dredge 123 and olivine ± spinel was the only liquidus phase.

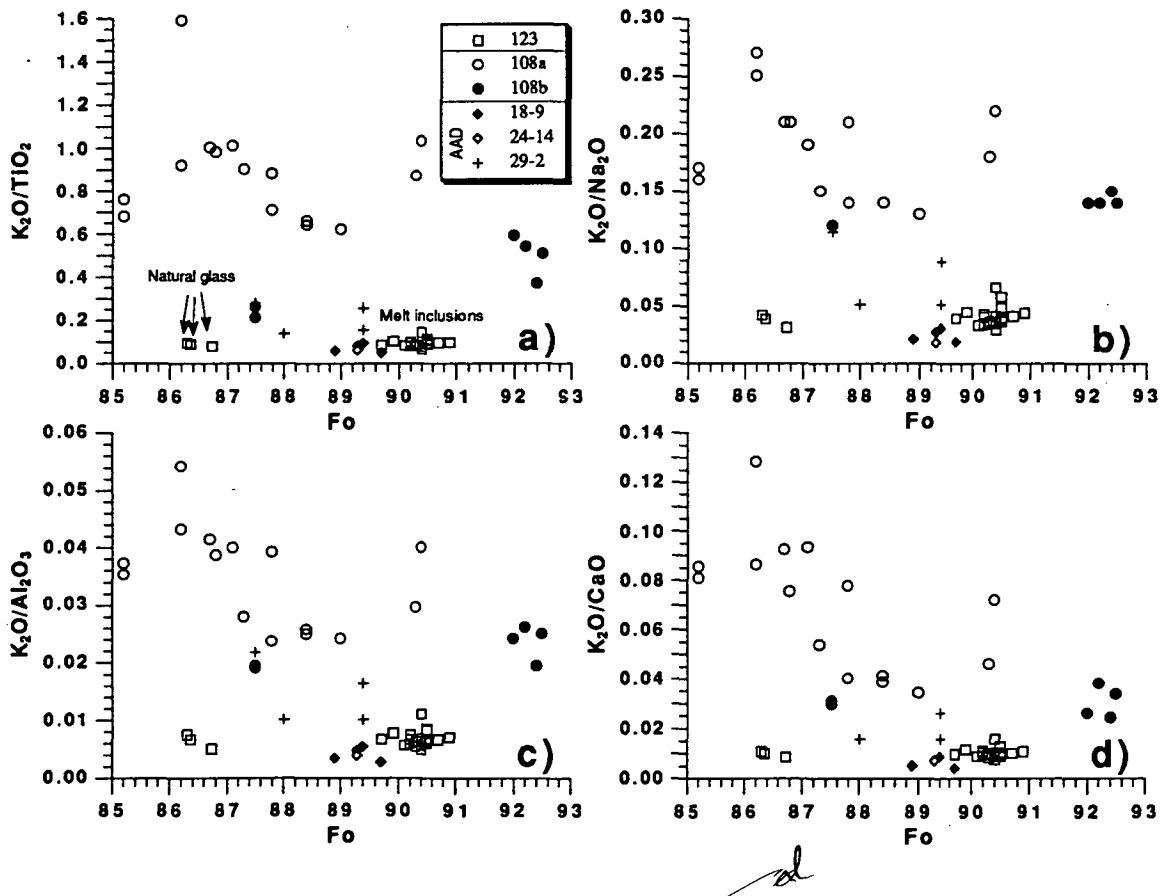

Figure 4.13: K_2O/TiO_2, K_2O/Na_2O, K_2O/Al_2O_3 and K_2O/CaO for the melt inclusions in olivines from BABB from dredge 123 plotted versus Fo-content of the host olivine. Also shown are the same ratios in the natural glasses, with equilibrium olivine calculated using the method of Ford et al., (1983) and inclusions from olivines in andesites from dredge 108 (chapter 5) and from basalts from the AAD (chapter 2).

4.4 Discussion

Eissen et al. (in press), compiled all available analyses from the NFB and showed that the dominant magma source is similar to N-MORB, with subduction-related contamination evident in some samples (enrichment in LILE/LREE over HFSE/HREE relative to N-MORB, see Figure 4.7). In the northernmost part of the basin, E-MORB-like influences become more prominent towards the Rotuma-Samoan lineament, whereas E-MORB-like signatures are absent on the N-S segment in the central NFB. However, the E-MORB like signature appears again in the 174 °E segment between the N-S segment and the Hunter Ridge (Fig. 4.1).

Dredge 73, which is located on a seamount south of the trench on old South Fiji Basin (SFB) crust, shows that E-MORB-like samples were erupted in the SFB. E-MORB-like lavas where also dredged from the forearc at station 92, as well as at stations 93 and 87 (S.M. Eggins, pers. comm., 1993, A.J. Crawford, pers. comm. 1993). It is not clear however, whether the occurrence of E-MORB-like lavas in the NFB in this area represents a continuation of the SFB occurrence in the south, having been trapped by the southward-stepping growth of the NFB over the last 7 Ma (Fig. 4.2), or in situ E-MORB magmatism in the NFB. Radiometric age determinations are required to clarify which of these alternatives is more likely to be correct.

4.4.1 Back-arc basin basalts

The two BABB groups identified from glass compositions are both of Group 1, as defined here. They also occur closer to the arc than any of the previously analysed samples from the main spreading centres in the NFB, and they show the strongest arc signature. On the other hand most of the basalts from the main spreading centres in the mature NFB lack the arc signature, but show instead evidence for mixing with E-MORB-like magmas. The basalts from dredge 123 are the most primitive in terms of whole-rock major element and olivine compositions and do not show any evidence for magma mixing. The component causing the LILE enrichment in dredge 123 basalts must therefore be added to the source prior to melting. When basalts 122/8 and 123/1 are compared to BABB from the Mariana Trough (Hawkins et al., 1990) on a N-MORB normalized element diagram (Fig. 4.14), these samples have similar patterns except that the NFB samples lack (or show less) enrichment in the LREE. However, at similar degrees of fractionation the NFB have higher absolute trace element concentrations (Fig. 4.14).

Both BABB groups are derived from a mantle source that was even more depleted in the LREE than N-MORB and the component that caused the enrichment in the LILE elements did not cause any enrichment in the LREE. Similar LILE enrichment in

strongly LREE-depleted tholeiites from the Mariana arc, was described by Crawford et al., (1986).

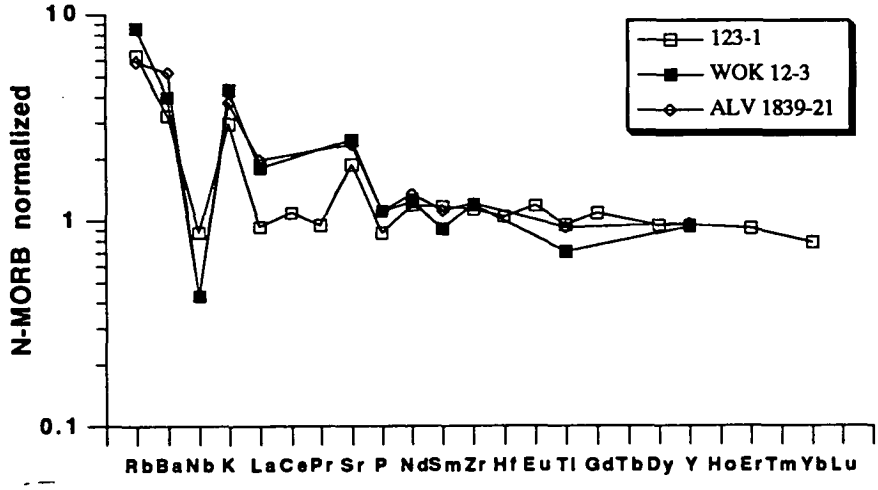

Figure 4.14: N-MORB normalized incompatible element diagram for sample 122/8 (BABB 1) and 123/1 (BABB 2) compared with two samples from the Mariana Rift (Hawkins et al., 1990). Normalizing values from Sun and McDonough, 1989.

4.5 Conclusions

Basalts from the main spreading centres in the mature NFB have previously been divided into three types based either on total alkalies (Johnson and Sinton, 1990; Sinton et al., 1991) or trace element contents (Price et al., 1991). These classifications are not internally consistent, so a new classification, based on K_2O/TiO_2, K_2O/Al_2O_3 and TiO_2/Al_2O_3, is suggested to separate the N-MORB-like lavas from those that show evidence for involvement of an E-MORB-like source. This classification is also consistent with the trace element contents. Group 1 is similar to N-MORB but some arc-like influences are still evident (e.g. low Nb/La). Both Groups 2 and 3 are enriched in all incompatible elements and the distinction between them is based on two apparent enrichment trends in Figure 4.4a, suggesting mixing with two distinct enriched components with different K_2O/TiO_2.

The E-MORB like influences in the northern part of the NFB have been associated with mixing of N-MORB like lavas with incompatible element-enriched lavas from the Rotuma-Samoan lineament (e.g. Johnson and Sinton, 1990; Price et al., 1990; Eissen et al., 1993), whereas the E-MORB-like influences in the southernmost part of the basin are more puzzling. E-MORB-like lavas were recovered at one dredge station in the SFB as well as three dredge stations in the forearc south of the Hunter Ridge. The E-MORB-like influences seen in the forearc could therefore result from interactions with enriched mantle in parts of the SFB due to southward growth of the NFB.

Two sub-types of BABB were identified in the course of this study, but both are of Group 1 as identified here. BABB 1 has major element compositions similar to N-MORB whereas BABB 2 have higher Al_2O_3 and Na_2O and lower FeO*, all of which are characteristics that separate BABB from N-MORB (Fryer et al., 1981). When those two sub-types are compared with Group 1 from the NFB, there is a continuous spectrum from N-MORB-like compositions to more typical BABB as represented by BABB 2, showing that the NFB has produced compositions ranging from typical BABB through to N-MORB-like compositions. No dating is available at present for these samples but the location of dredges 122 (BABB 1) and 123 (BABB 2) suggest that they were erupted when the N135°E spreading axis was active between 7-3 Ma ago. Dredges 102, 117 and 119 which also consist of both BABB 1 and 2, are, on the other hand, close to active spreading ridges. This suggest that both N-MORB-like lavas and more typical BABB have been erupting in the NFB through most of its history.

Chapter 5

PETROLOGY AND GEOCHEMISTRY OF PRIMITIVE ANDESITES AND SODIC RHYOLITES FROM THE HUNTER RIDGE

5.1 Introduction

The glass analyses of samples from the R/V A. A. Nesmeyanov cruise to the southernmost North Fiji Basin (chapter 3) revealed the existence of several magma groups occurring in close proximity to each other. These include groups of island arc tholeiites, boninites, back arc basin basalts and E-MORB, with rhyolitic compositions occurring at several dredge stations. Basaltic andesite from station 101 and andesites from station 108 on the Hunter Ridge are clearly distinct from these groups and compositions of their olivines and spinels suggest magma mixing involving two or more magma types.

This chapter deals with the origin of the andesites from station 108, through detailed studies combining heating stage experiments with conventional mineralogical and geochemical methods, and the relationship between the andesites and rhyolites at station 108 is discussed. The end members taking part in the mixing at station 108 are then evaluated and compared with other magmatic suites from this area, including high-Mg andesites from islands and seamounts on and just northwest of the Hunter Ridge (the HMA group of Monzier et al., 1993), back arc basin basalts (chapter 4) and samples from three dredge stations south and west of station 108, where small sample size did not allow detailed mineralogical and inclusion studies.

A marked topographic low occurs on the Hunter Ridge at 173 °E, interpreted to be a short N-S trending spreading centre crosscutting the Hunter Ridge (Maillet et al., 1989). Dredge station 108 is just east of this low whereas the other three stations discussed in this chapter are south and west of it (Fig. 5.1).

The crest of the Hunter Ridge generally lies around 2000m below sea-level but it is subaerial at Matthew and Hunter Islands (Maillet et al., 1986) and has numerous seamounts reaching shallow depths (Fig. 5.1), particularly near Matthew and Hunter Islands (Monzier et al., 1993).

Unusual low-K dacites hosting primitive olivine phenocrysts (Fo_{92}) and primitive dolerite inclusions of boninitic affinity occur on Matthew and Hunter Islands on the Hunter Ridge (Maillet et al., 1986), and high Mg-andesites and their fractionation products occur on various seamounts on the Hunter Ridge (Monzier et al., 1993).

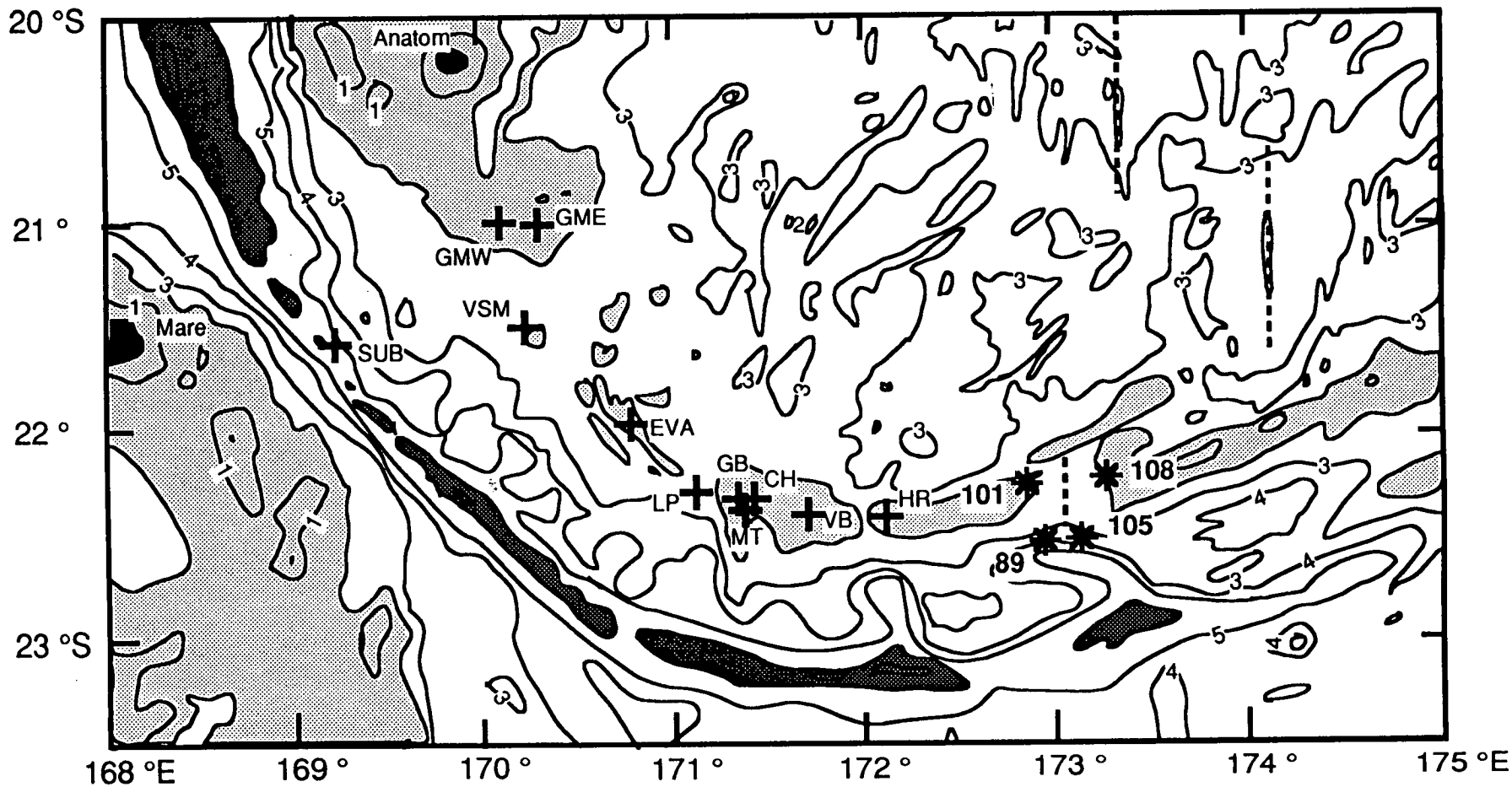

Figure 5.1: The Hunter Ridge and the southernmost part of the North Fiji Basin. Locations of dredge stations 89, 101, 105 and 108 are shown with an asterisk. Crosses show locations of samples described by Monzier et al., 1993. Dashed lines are the southernmost spreading ridges in the North Fiji Basin. Numbers on contour lines indicate depth in thousand meters, lightly shaded areas indicate water depth less than 2000 m, whereas dark shading indicates water depth greater than 6000 m. Modified from Monzier et al., 1993.

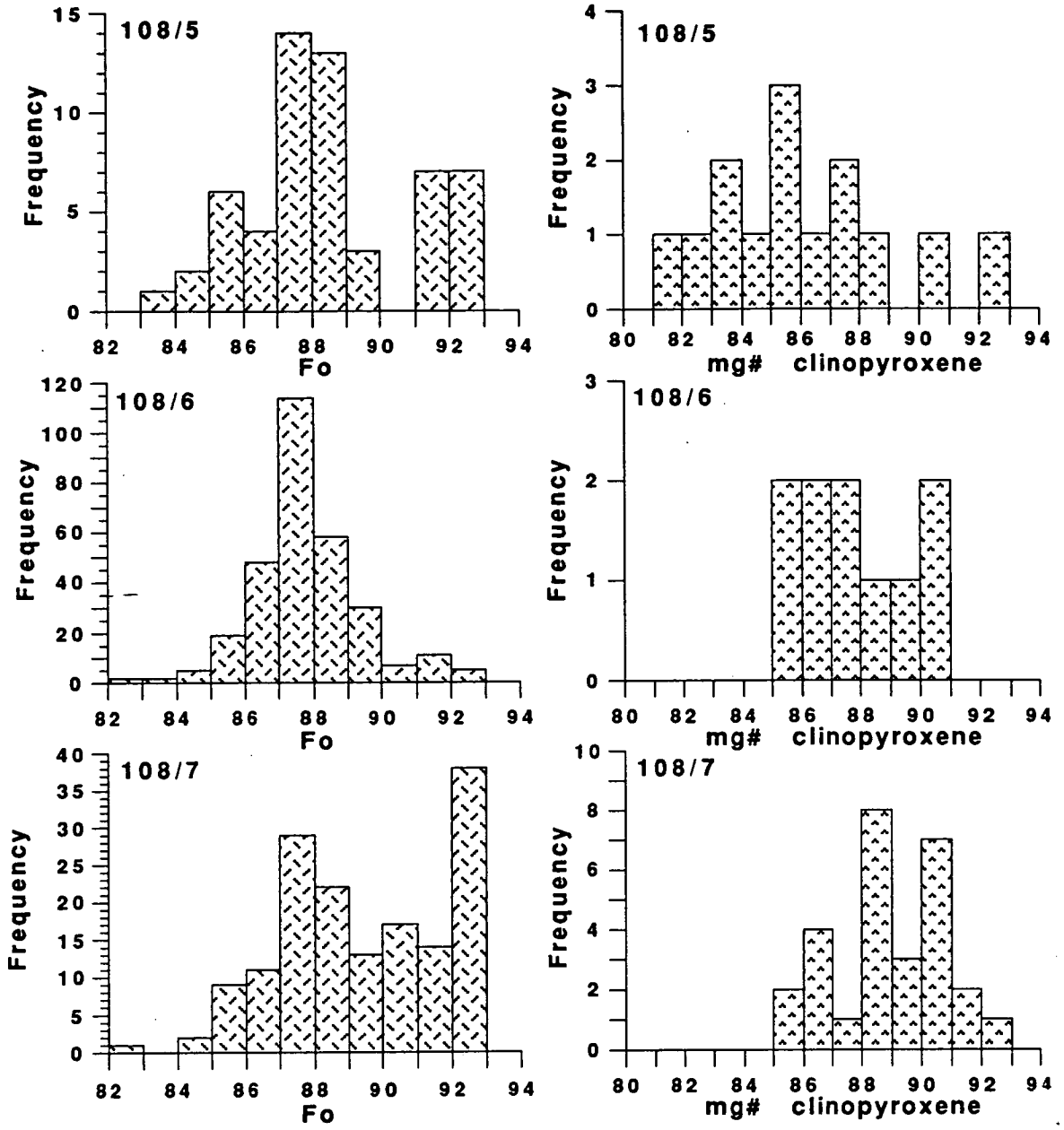

Figure 5.2: Fo content of olivine and mg# of clinopyroxene in andesite samples 108/5, 108/6 and 108/7 from station 108.

5.2 Evidence for magma mixing - petrography and mineralogy

The andesites from station 108 are described in detail below whereas andesite from stations 89, basaltic andesite from station 101 and high-Ca boninites from station 105 plus the rhyolites from station 108 are described more briefly. Finally the mineralogy of these samples is compared with samples HR11A from Hunter Island, LP34A from La Pérouse seamount and VB11C from Vauban seamount all on the Hunter Ridge, data taken from Monzier et al., (1993). Representative mineral analyses are in Appendix 3.

5.2.1 Andesite samples 108/5, 108/6 and 108/7

These samples have phenocrysts of olivine (3-5%), clinopyroxene (3-5%), and minor amounts of plagioclase, orthopyroxene, and titanomagnetite, and Cr-Al-spinel commonly occurs as inclusions in olivine but rarely in clinopyroxene. The groundmass is glassy with abundant small clinopyroxene, plagioclase and magnetite crystals and relatively uncommon skeletal olivine.

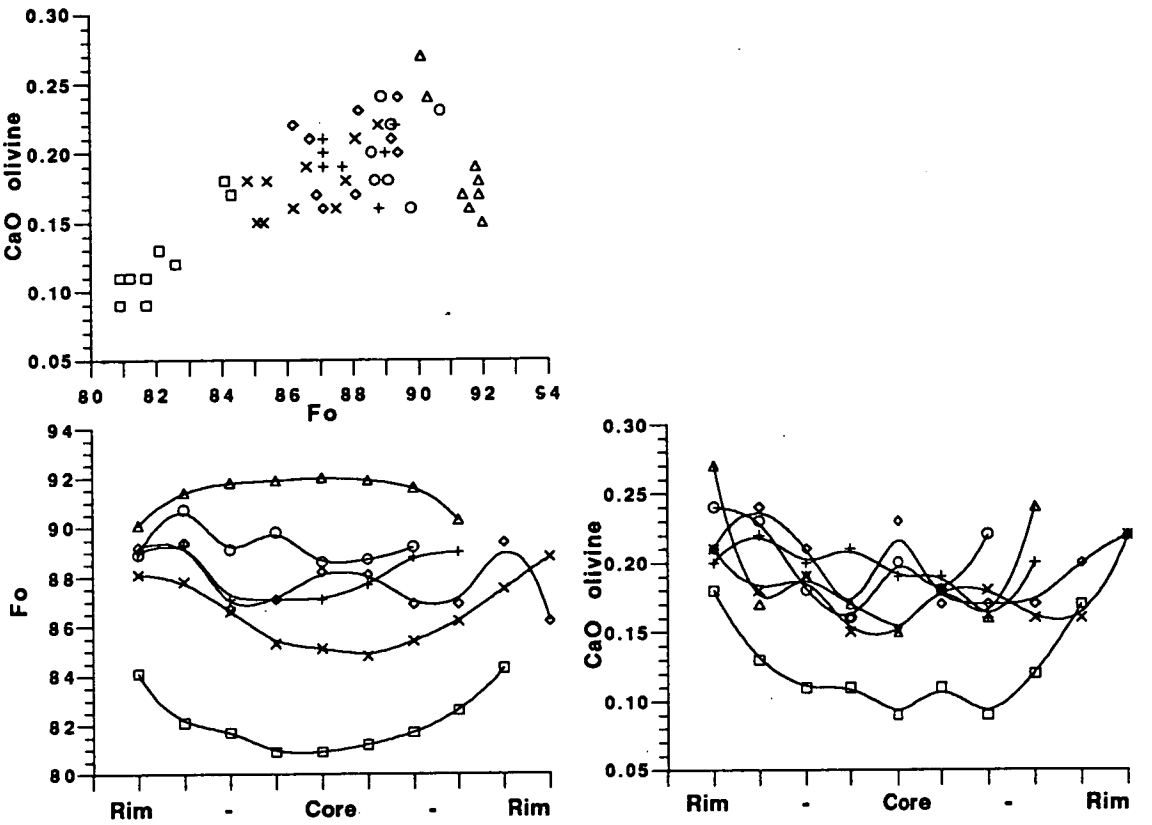

Figure 5.3: Zoning profiles for Fo and CaO from rim to rim in six olivine phenocrysts in andesite 108/7 and the relationship between Fo and CaO in zoned olivines.

5.2.1.a Olivine

Olivine generally forms euhedral crystals although anhedral crystals also occur. Individual phenocrysts reach more than 1.0 mm in size but average 0.2-0.4 mm. Many olivines contain spinel and melt inclusions. Olivine core compositions range from Fo_{82} to Fo_{93}. Andesite 108/6 shows a normal distribution of olivine core compositions with maxima at Fo_{87-88}, whereas andesites 108/5 and 108/7 have a bimodal distribution with maxima at Fo_{88} and Fo_{91-93} (Fig. 5.2). Zoning occurs in all olivine grains analysed in thin section (25 grains in sample 108/5 and 108/6). Figure 5.3 shows zoning profiles through six olivine grains. The low-Mg olivines (Fo_{82-86}) show reverse zoning whereas the high-Mg olivines (>Fo_{92}) show normal zoning. Olivines of intermediate compositions show quite complex zoning patterns which suggest several growth zones. Zoning is also evident in the CaO content of the olivines. In olivine Fo_{92} CaO increases towards the rim as the Fo content

decreases indicating that clinopyroxene was not a liquidus phase during that stage of crystallization. Similarly CaO also increases in the reversely zoned low-Mg olivine, showing that the rim crystallized after the crystal came in contact with a melt with higher larnite (Ca_2SiO_4) activity than that from which the more Fe-rich core crystallized. Again the intermediate compositions (Fo_{87-90}) show the most complex zoning patterns. Most olivines have narrow (<20 μm) rims (not shown in Figure 5.3) with compositions in the range Fo_{83-86}, which match those of groundmass olivines. CaO content decreases with decreasing Fo in these rims.

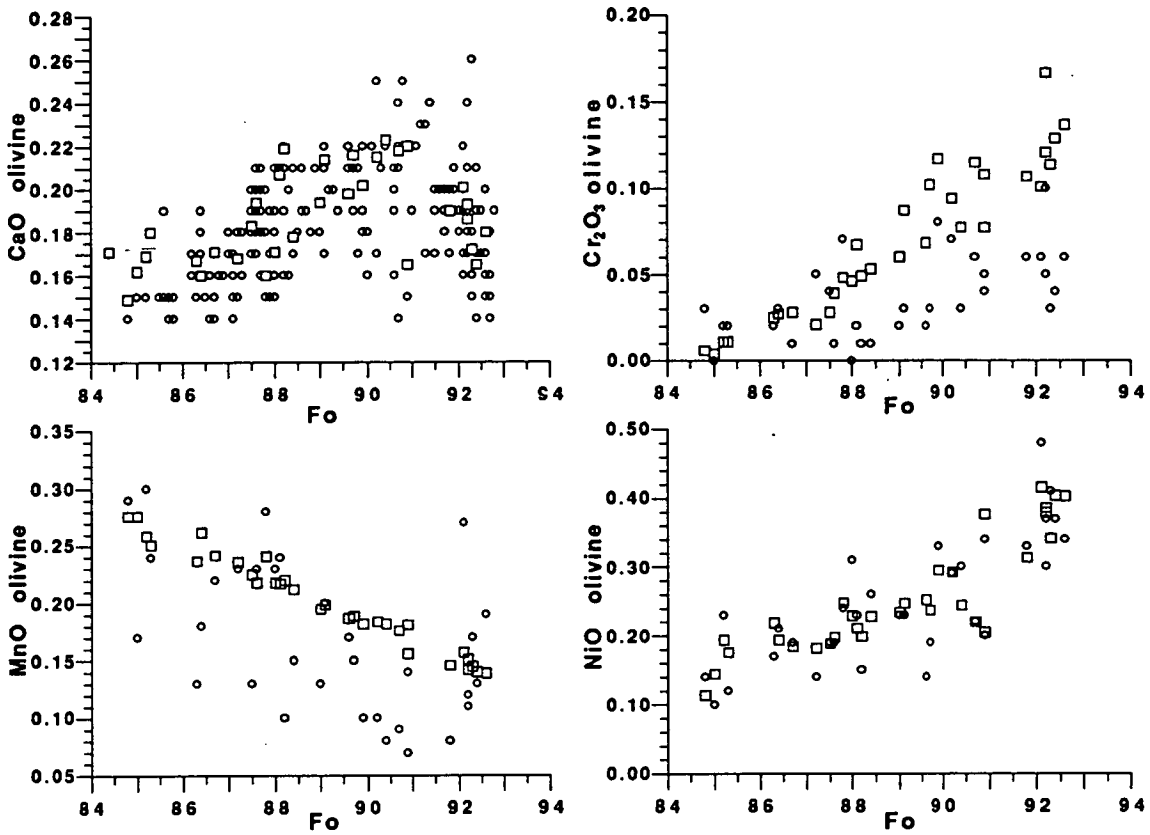

Figure 5.4: The minor elements in olivine from sample 108/7. These elements were analysed using long counting times and high voltage and high current (squares). Additional analyses of CaO using normal analytical conditions are included (circles) whereas the circles in the Cr_2O_3, MnO and NiO diagrams show the average of three analyses of the same spot using normal analytical conditions. CaO and NiO can be analysed accurately, but with lower precision, using normal analytical conditions whereas analyses of Cr_2O_3 and MnO require the longer counting times. Analyses with normal analytical conditions show consistently lower Cr_2O_3 and MnO contents and much lower precision. For description of analytical conditions see Appendix 2.

The minor elements in olivine were analysed in 32 crystals from sample 108/7, representing the whole range of compositions (Appendix 5). The minor elements vary systematically with Fo content (Fig. 5.4), in the interval Fo_{93-84} MnO increases (0.139-0.290%) and NiO and Cr_2O_3 decrease (0.416-0.114% and 0.167-0.004% respectively), whereas CaO varies from 0.165 to 0.201% between Fo_{93-92} but

decreases from 0.223-0.149% in the range Fo_{91-84}. CaO in the olivine cores shows behaviour that is closely matched by the zoned olivines (Figs. 5.3 and 5.4).

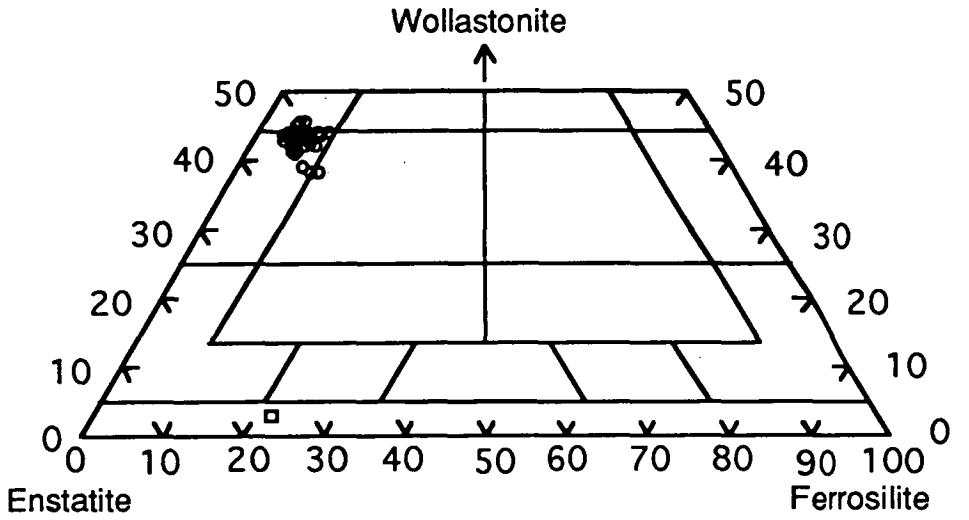

Figure 5.5: Compositions of pyroxenes in the andesites from station 108 shown in the system $CaMgSiO_6$-$CaFeSi_2O_6$-$Mg_2Si_2O_6$-$Fe_2Si_2O_6$.

5.2.1.b Clinopyroxene

The sub-anhedral clinopyroxene phenocrysts are mostly endiopsides (Fig. 5.5) with few crystals falling into the diopside and augite fields (Poldervaart and Hess 1951) with mg# ranging from 81 to 93 (Fig. 5.2). TiO_2 increases from 0.1-0.66% whereas Cr_2O_3 decreases from 1.1 to below detection limit (~0.1%) (Fig. 5.6). As for olivine, the compositional profiles show quite complex zoning, both normal and reverse (Fig 5.7). The most magnesian phenocrysts (mg# = 90) show normal zoning whereas others show reverse or complex zoning patterns.

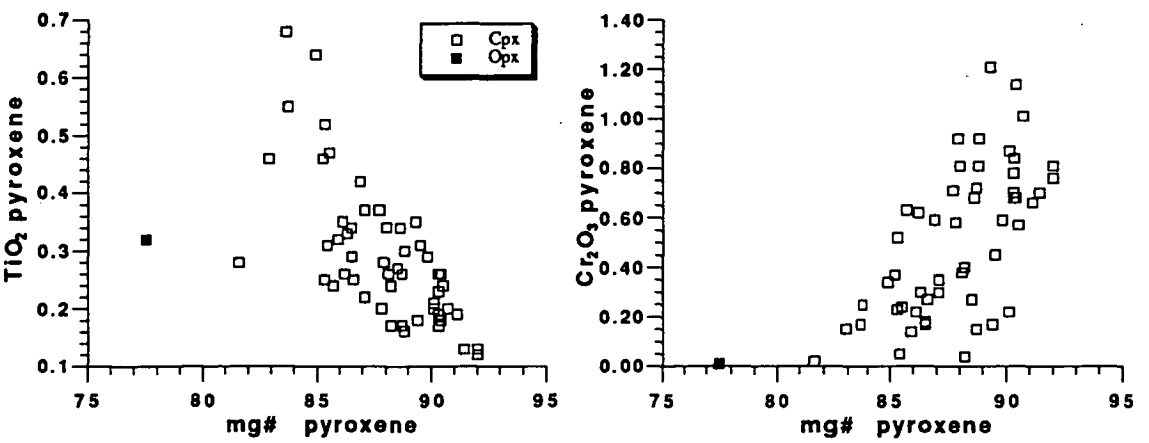

Figure 5.6: TiO_2 and Na_2O in pyroxenes in the andesites from station 108.

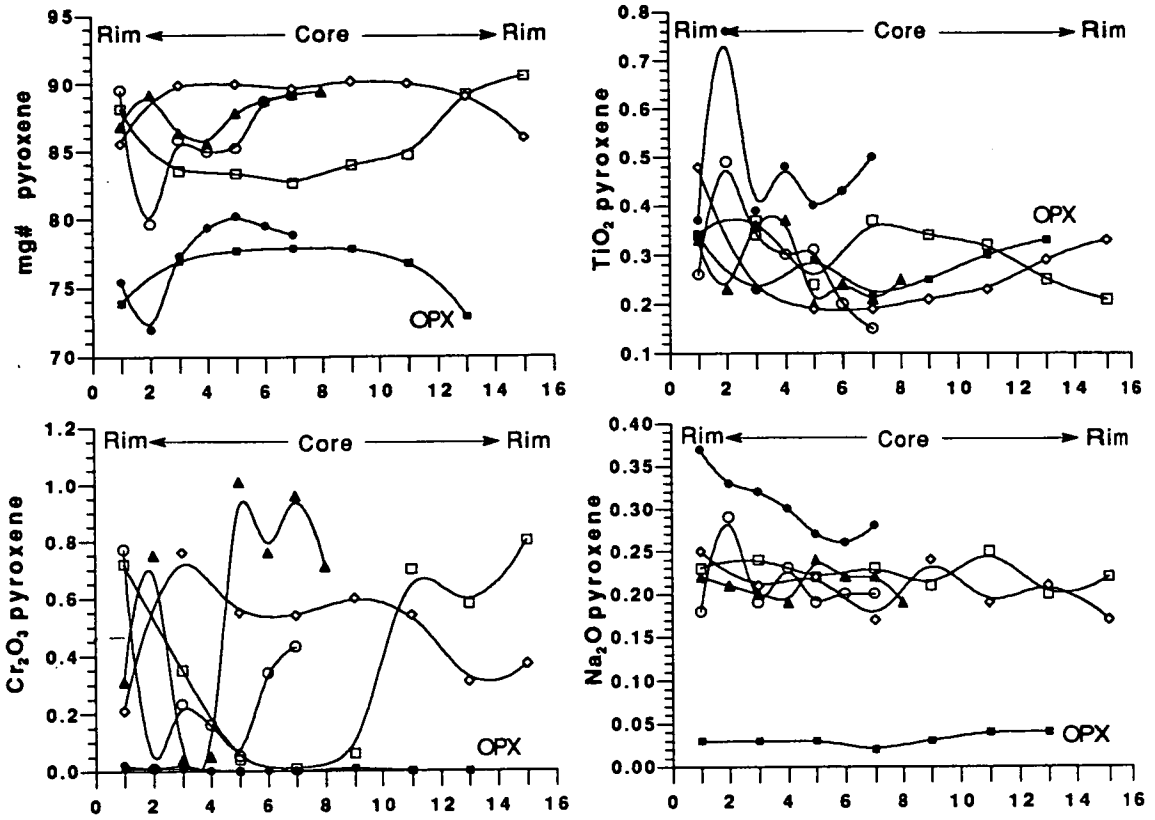

Figure 5.7: Zoning profiles for mg#, TiO_2, Cr_2O_3 and Na_2O in pyroxenes from station 108 andesites.

5.2.1.c Spinel

Cr-Al-spinels occur as common inclusions in olivine phenocrysts but are rare in clinopyroxene. They are usually euhedral and up to 60 μm in size. Their colour varies from reddish-brown (Cr-rich) through to yellowish-green (Al-rich). The spinels have been divided into two main groups (Fig. 5.8). Most spinels have Al_2O_3 less than 18% and TiO_2 less than 0.6% and are here called Cr-spinels. The second group has Al_2O_3 higher than 18% or TiO_2 higher than 0.6%, and is here called Al-Cr-spinels. A subgroup of the Al-Cr-spinels has Al_2O_3 less than 30% and TiO_2 higher than 2%, and is herein referred to as Al-Ti-spinels. The Cr-spinels are found in olivines $Fo_{86.5-93}$ whereas the Al-Cr- and Al-Ti-spinels are restricted to olivines less magnesian than $Fo_{88.5}$. The Cr-spinels have a $cr^{\#}$ between 65-80 with $Mg^{\#}$ between 55-73; the Al-Cr-spinels on the other hand, show negative correlation of $cr^{\#}$ with $Mg^{\#}$ (Fig. 5.8). This trend is typical for spinel in MORB and BABB for which co-fractionation of plagioclase causes an increase in $cr^{\#}$ with a decrease in $Mg^{\#}$ (see chapter 3), but it is not common in island arc lavas where olivine and clinopyroxene fractionation predominates. $Mg^{\#}$ of both Cr- and Al-Cr-spinels show positive correlations with Fo content of host olivine, though the slope is much steeper for the Al-Cr-spinels (Fig. 5.8). Fe^{3+}, calculated assuming perfect stoichiometry, is

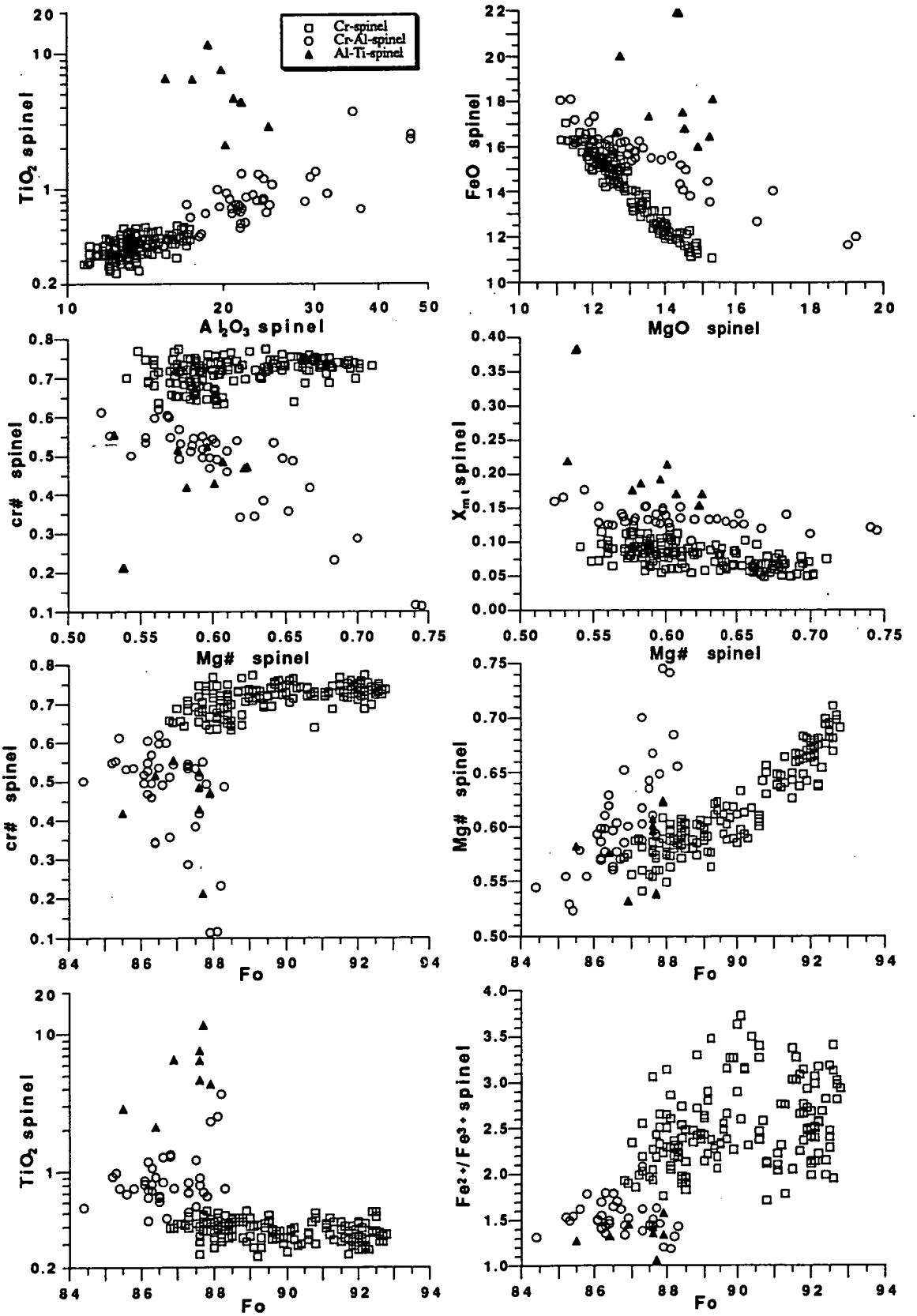

Figure 5.8: Compositions of spinels and olivine and spinel relationships in station 108 andesites.

considerably lower in the Cr-spinels than in the Al-Cr-spinels. In olivines less magnesian than Fo_{91}, Fe^{2+}/Fe^{3+} shows a steady decrease and there appears to be a break at around Fo_{91} that results in an increase in the slope on the diagram $Mg^{\#}$ of spinel versus Fo. In general there is a good separation between the groups in all the plots in Figure 5.8.

5.2.1.d Plagioclase, orthopyroxene, and Ti-magnetite

These phases occur in minor amounts and the crystals are always resorbed. The plagioclase phenocrysts (<0.3 mm) are normally zoned and have compositions between An_{86-63}; they often contain a large number of devitrified, irregular glass inclusions. Ti-magnetite crystals are less than 0.2 mm in diameter. A single orthopyroxene found in thin section is 0.3 mm in size and normally zoned with $mg^{\#}$ = 77-73 (Fig. 5.7).

5.2.1.e Groundmass minerals

Groundmass olivine varies between Fo_{84-88}, groundmass clinopyroxenes have $mg^{\#}$ between 83-86, and groundmass plagioclases have compositions of An_{70-68}.

5.2.2 Station 108 rhyolites

The rhyolites contain two populations of plagioclase phenocrysts with quite variable compositions (An_{66-59} and An_{43-27}) and trace amounts of small, euhedral orthopyroxene ($mg^{\#}$ = 72-70) and amphibole ($mg^{\#}$ = 72-60) plus magnetite and ilmenite. Apatite occurs as an inclusion in magnetite.

5.2.3 Stations 89, 101 and 105

Sample 89/1 is an andesite with skeletal olivine (Fo_{91-84}), strongly resorbed plagioclase (An_{64-43}) with devitrified glass and clinopyroxene inclusions, and ortho- and clinopyroxene phenocrysts ($mg^{\#}$ = 70 and 75 respectively) . Both olivines and plagioclase show slight normal zoning whereas both ortho- and clinopyroxenes are reversely zoned.

Basaltic andesite 101/1 contains euhedral phenocrysts of olivine (Fo_{92-86}), commonly with cr-spinel inclusions and both normally and reversely zoned clinopyroxene phenocrysts ($mg^{\#}$ = 80-89), and plagioclase (An_{76}) and pyroxene microphenocrysts ($mg^{\#}$ = 89).

Station 105 samples are high-Ca boninites. Sample 105/1 contains phenocrysts of both ortho- and clinopyroxene ($mg^{\#}$ = 90-78 and 85-78 respectively) whereas sample 105/2 has olivine ($Fo_{90.5-85.2}$) and orthopyroxene ($mg^{\#}$ = 89-82) phenocrysts set in a groundmass of quenched glass with abundant microlites of both ortho- and

clinopyroxene. Orthopyroxene phenocrysts are frequently rimmed by clinopyroxene. Cr-spinel inclusions in olivine have very low Al_2O_3 (4.5-8.0%) and TiO_2 (0.1-0.4%) and high $cr^{\#}$ (80-90), matching these from other boninites from this area (chapter 3).

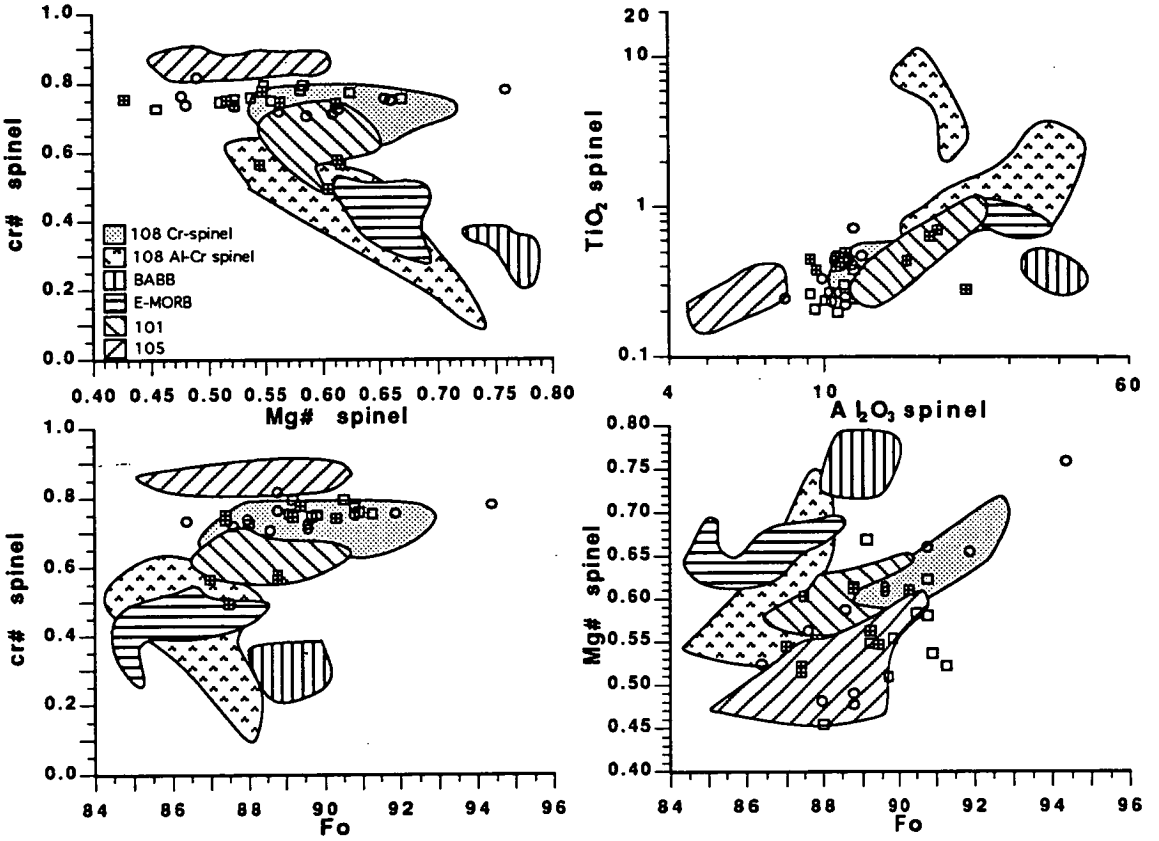

Figure 5.9: Compositions of spinels and olivine and spinel relationships in station 108 andesites compared to spinels in basaltic andesite 101/1, boninite 105/2, back arc basin basalts, E-MORB and samples HR11A (squares with crosses), LP34A (open squares) and VB11C (open circles). HR, LP and VB data are from Monzier et al. (1993).

5.2.4 Station 108 andesites compared to samples 89/1, 101/1, 105/2 and high magnesian andesites HR11A, LP34A and VB11C from the Hunter Ridge

Excluding some low CaO olivines (CaO<0.10%) in sample LP34A that are likely to be of xenocrystic origin (Monzier et al., 1993), there are no significant differences in minor elements in olivines. As an example, CaO varies between 0.15-0.25% in all samples, including the boninites from station 105 and NiO is the same for a given Fo content in station 108 andesites and samples HR11A, LP34A and VB11C.

Figure 5.9 shows olivine and spinel relationships for all the samples discussed here. The fields for 108 andesites are taken from Figure 5.8, whereas the fields for sample 101 and 105 plus BABB and E-MORB are taken from chapter 4. The Al-Cr spinels overlap most of the field for E-MORB spinels and extend to even lower $cr^{\#}$ than the BABB spinels. Most of the spinels from samples HR11A, LP34A and

VB11C fall within the fields for spinels from the 108 andesites though they have generally lower Al_2O_3 content and they extend to lower $Mg^{\#}$.

The pyroxenes in HR, LP and VB samples have lower $mg^{\#}$ than station 108 samples but they have similar Na_2O and TiO_2 and higher Cr_2O_3 for a given $mg^{\#}$. The pyroxenes in the boninites differ from the pyroxenes in all the other samples, as orthopyroxene starts to crystallize before clinopyroxene. This results in higher Cr_2O_3 in the orthopyroxenes and lower Cr_2O_3 in the clinopyroxenes. Na_2O and TiO_2 in pyroxenes are also lower in the boninites.

5.3 Evidence for magma mixing - geochemistry of station 108 andesites compared to other samples from the Hunter Ridge

5.3.1 Major elements

Major and trace element compositions of the analysed samples are shown in Table 5.1 and in Figure 5.10 major elements for wholerock compositions and glasses are plotted against MgO. Also shown for comparison in Figure 5.10 are the wholerock compositions of low-Ti andesites and related rocks from Matthew and Hunter Islands, and from seamounts on and just northwest of the Hunter Ridge that belong to the high-Mg group of Monzier et al. (1993).

The andesite glasses are similar to the wholerock samples from Gilbert seamount except for their higher TiO_2 and CaO. The basaltic andesite 101/1 differs from the other samples by its lower SiO_2 and K_2O, and higher TiO_2, Al_2O_3, FeO* and CaO. Andesite 89/1 also has high TiO_2 and significantly higher K_2O than all the other samples except for the subgroup of high K_2O lavas from Vauban seamount (Monzier et al., 1993). The boninites from station 105 have higher SiO_2 and lower TiO_2, Al_2O_3, Na_2O and P_2O_5 than all the other samples in Figure 5.10.

5.3.2 Rare earth elements

REE analyses, normalized to chondrite abundances are presented in Figure 5.11a. Andesite 108/5 and basaltic andesite 101/1 have similar HREE contents but 108/5 is slightly more LREE-enriched. Andesite 89/1 has higher HREE content than 108/5 and 101/1 and the pattern shows a steady increase from the HREE through the LREE. The boninites from station 105 have the lowest REE concentrations (4-7 times chondrite) and flat REE patterns. Finally the rhyolites from station 108 have the highest REE concentrations with flat HREE and strong enrichment in the LREE.

Compared to andesites from further west on the Hunter Ridge (Monzier et al., 1993), andesite 108/5 has identical HREE concentration to sample GB29B from Gilbert seamount but it is not as enriched in the LREE (Figure 5.11b).

Table 5.1: Whole-rock major and trace element compositions of analysed samples from stations 89, 101, 108 and 105. All elements were analysed by XRF except for Cs, Hf and Th; and REE in samples 89/1, 101/1. 105/2 and 105/1 by INAA. Isotope analyses are from S.M. Eggins, unpublished.

Sample	89/1	101/1	108/5	108/1	108/4	108/10	108/15	108/16	105/2	105/1
SiO_2	54.78	50.54	54.75	70.93	71.00	71.14	70.38	70.94	56.56	56.41
TiO_2	0.78	0.69	0.60	0.39	0.39	0.39	0.39	0.42	0.17	0.13
Al_2O_3	15.44	14.61	16.63	14.23	14.00	13.97	14.02	14.26	12.04	11.39
Fe_2O_3	7.13	8.77	6.38	2.30	2.25	2.28	2.24	2.33	8.48	9.62
MnO	0.11	0.18	0.10	0.09	0.09	0.09	0.09	0.10	0.15	0.17
MgO	6.13	11.34	5.27	0.53	0.53	0.51	0.52	0.54	10.42	9.84
CaO	6.78	10.13	9.06	1.80	1.83	1.81	1.79	1.82	8.67	9.30
Na_2O	3.72	2.60	3.73	5.92	6.42	6.08	6.00	6.10	1.34	1.59
K_2O	1.51	0.25	0.56	1.52	1.53	1.62	1.79	1.51	0.34	0.32
P_2O_5	0.16	0.05	0.13	0.09	0.08	0.05	0.07	0.09	0.00	0.00
LOI	3.62	0.92	2.66	1.65	1.76	2.02	2.70	1.56	1.70	1.08
Sum	100.16	100.08	99.87	99.45	99.88	99.96	99.99	99.67	99.87	99.85
Trace elements(ppm)										
Cs	<0.8	<0.8	<0.2		0.22			0.21	<1	<0.8
Pb	<1.5	3	2	4	5	4	4	4	<1.5	<1.5
Rb	21	3	4.5	20	19	20	21	19	5	4
Ba	136	57	114	288	286	288	277	290	68	39
Sr	319	184	441	266	265	266	265	268	111	115
La	8.34	3.05	4.67		18.00			18.60	1.46	0.90
Ce	18.60	8.82	12.40		43.70			47.20	4.04	2.25
Pr			2.00		5.73			6.29		
Nd	12.90	7.04	8.82		26.80			27.60	2.89	1.74
Sm	3.85	2.15	2.35		5.78			5.86	0.80	0.59
Eu	1.27	0.70	0.79		1.52			1.45	0.32	0.20
Gd			2.73		5.32			5.39		
Tb	0.70	0.48							0.20	0.13
Dy			2.83		5.00			5.43		
Ho	0.90	0.62							0.31	0.20
Er			1.84		3.57			3.80		
Yb	2.40	1.72	1.67		3.64			3.63	0.86	0.54
Lu	0.38	0.22							0.12	0.08
Y	23	19	17	34	34	35	33	34	8	6
Th	1.35	<0.4	0.79	4	3.61	3	3	3.55	<0.4	0.34
Zr	122	63	75	250	248	252	244	247	23	13
Hf	3.57	1.62	2.04		6.55			6.42	<0.5	0.57
Nb	1	<1	<1	2.5	2.5	2.5	2	2	<1	<1
Ga	16.2	14.5	16.4	17.5					9.5	11.3
Sc	22	40	33	6	4.5	6	5	6	41	48
V	175	236	188	21	18	19	19	17	223	259
Cr	144	246	41	<1	<1	<1	<1	<1	187	97
Ni	300	246	90	<2	2	2	2	3	719	511
87Sr/86Sr		0.702740						0.702776		
143Nd/144Nd		0.513128						0.513122		

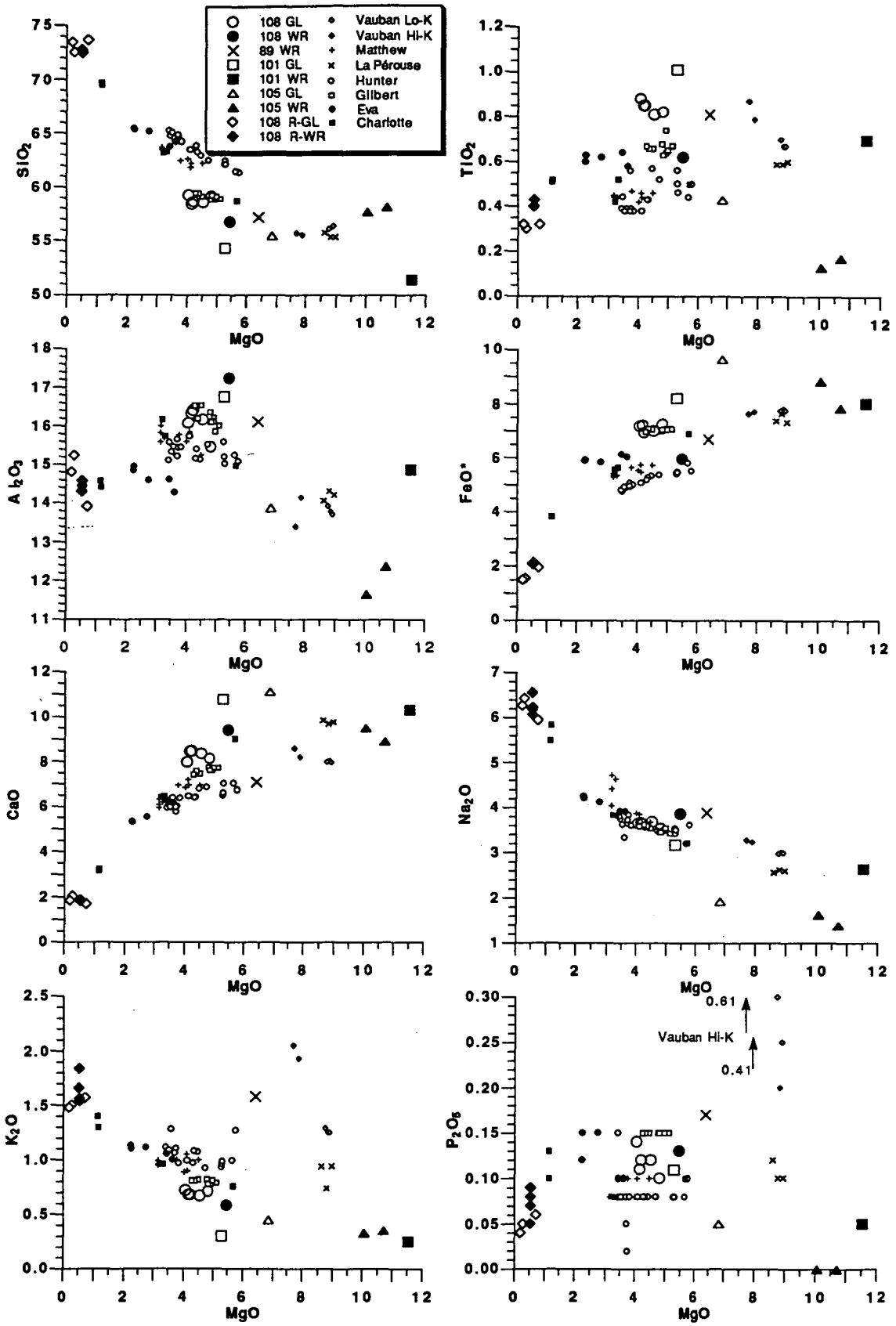

Figure 5.10: Glass and whole rock major elements plotted versus MgO for the analysed samples. Also shown are samples from the high magnesian andesite (HMA) group of Monzier et al., (1993).

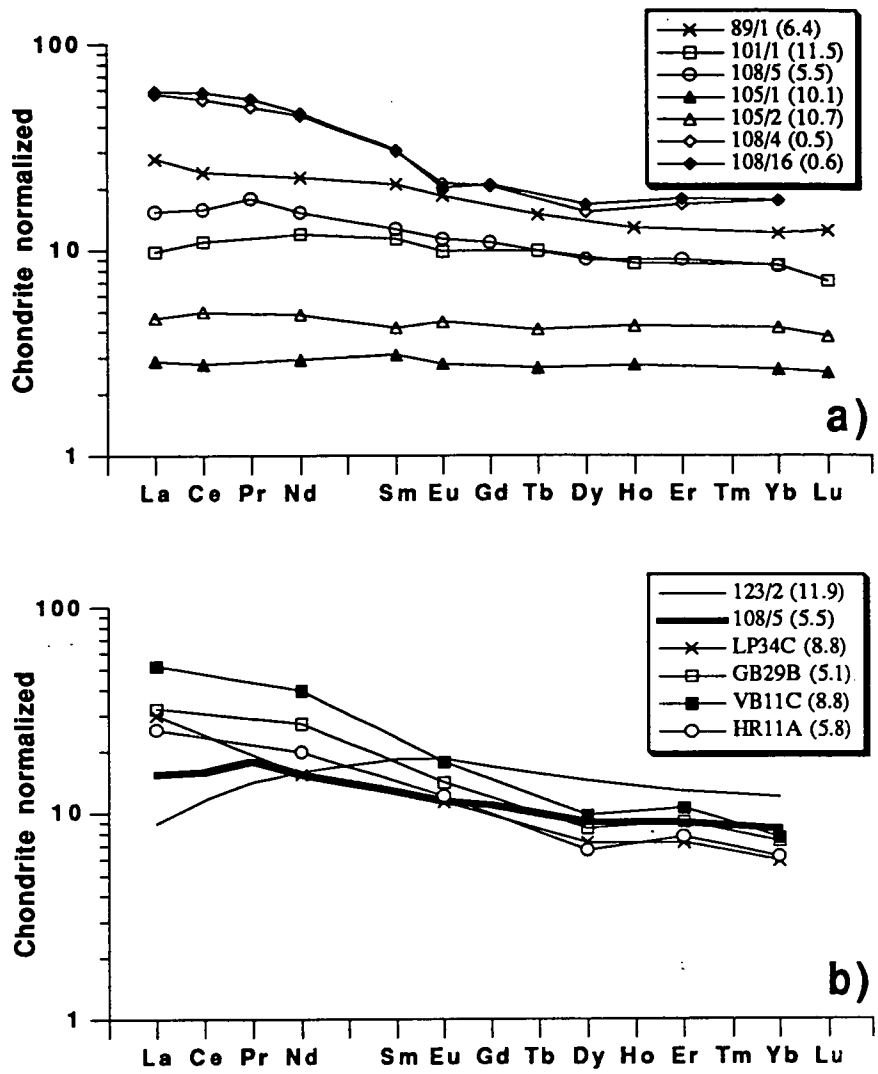

Figure 5.11: a) Chondrite normalized REE abundances for the analysed samples. b) REE in sample 108/5 compared to four andesites from the Hunter Ridge (Monzier et al., 1993) and BABB sample 123-2 from the NFB (chapter 4). Normalizing values are from Taylor and Gorton, (1977). The numbers in brackets behind the sample number indicate the MgO content, normalized anhydrous to 100%.

5.3.3 Trace elements

Trace elements, normalized to primitive mantle abundances (Sun and McDonough, 1989), are shown in Figure 5.12. All analysed samples, as well as the samples from Monzier et al., (1993) show typical island arc related patterns with an enrichment in the LILE and depletion in the HFSE. Nb is below the detection limit (1 ppm) for all samples apart from the rhyolites and P_2O_5 is below the detection limit (0.03%) in the boninites. Figure 5.12 reports values at the detection limit for these to indicate the maximum value and minimum relative depletion. Andesite 108/5 shows the same pattern and similar concentrations of incompatible elements as andesite GB29B from Gilbert seamount, excluding the LREE as mentioned above. The

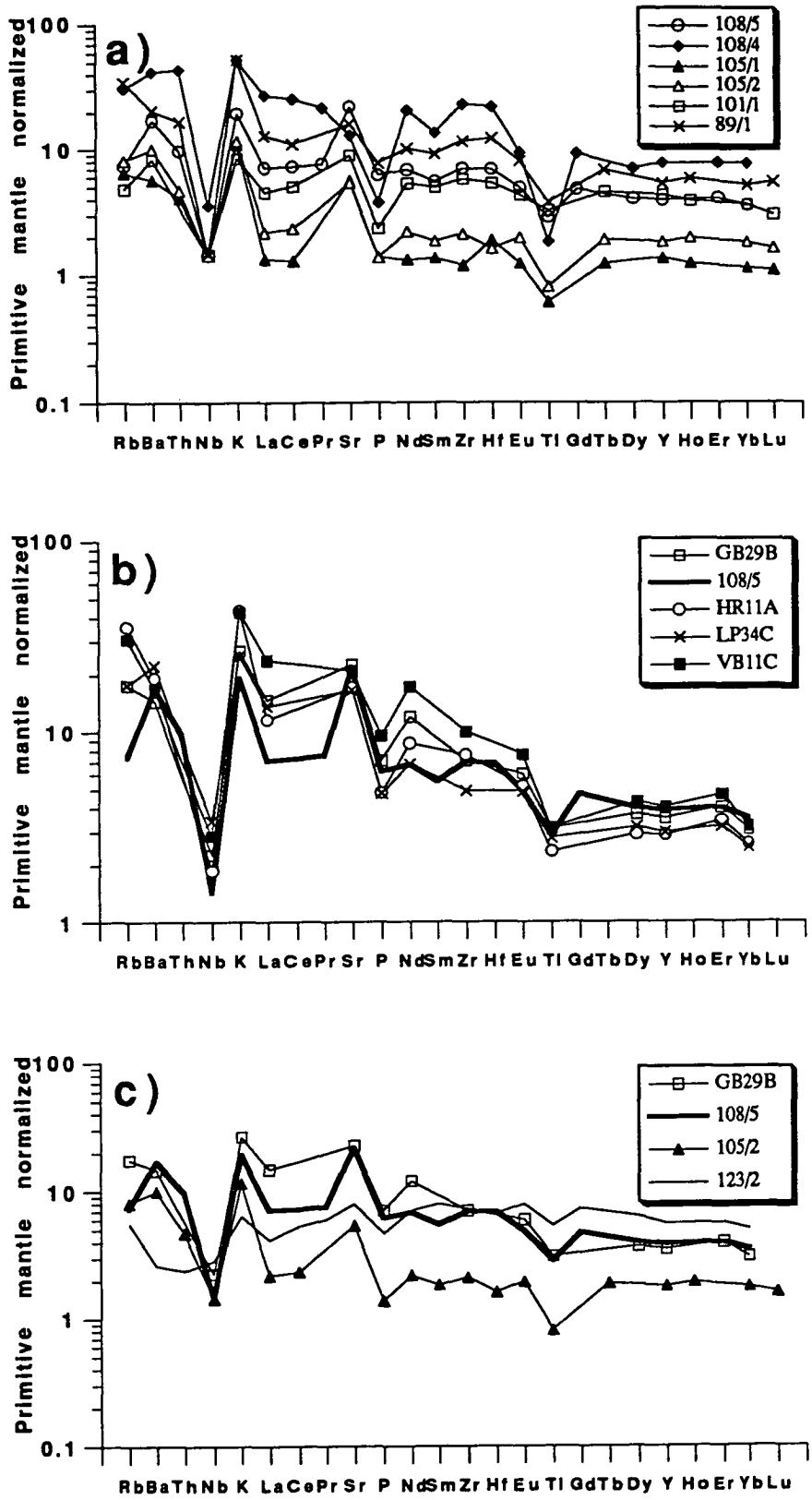

Figure 5.12: a) Primitive mantle normalized element concentrations for the analysed samples. b) Sample 108/5 compared to four samples from the Hunter Ridge (Monzier et al., in press). c) Samples 108/5 and 105/2 compared to back arc basin basalt sample 123/2 (chapter 4) and sample GB29B from Gilbert seamount on the Hunter Ridge (Monzier et al., 1993). Normalizing values are from Sun and McDonough, (1989).

boninites have the lowest concentrations for all incompatible elements and the most pronounced negative anomaly for Ti and presumably also P and Nb. The rhyolites have patterns similar to andesite 108/5 but at higher absolute values. These samples therefore are likely to be related by crystal fractionation, and the increase in Ti and P anomalies and the absence of the Sr anomaly results from fractionation of titanomagnetite, ilmenite, apatite and plagioclase, all of which occur as phenocryst phases in the rhyolites.

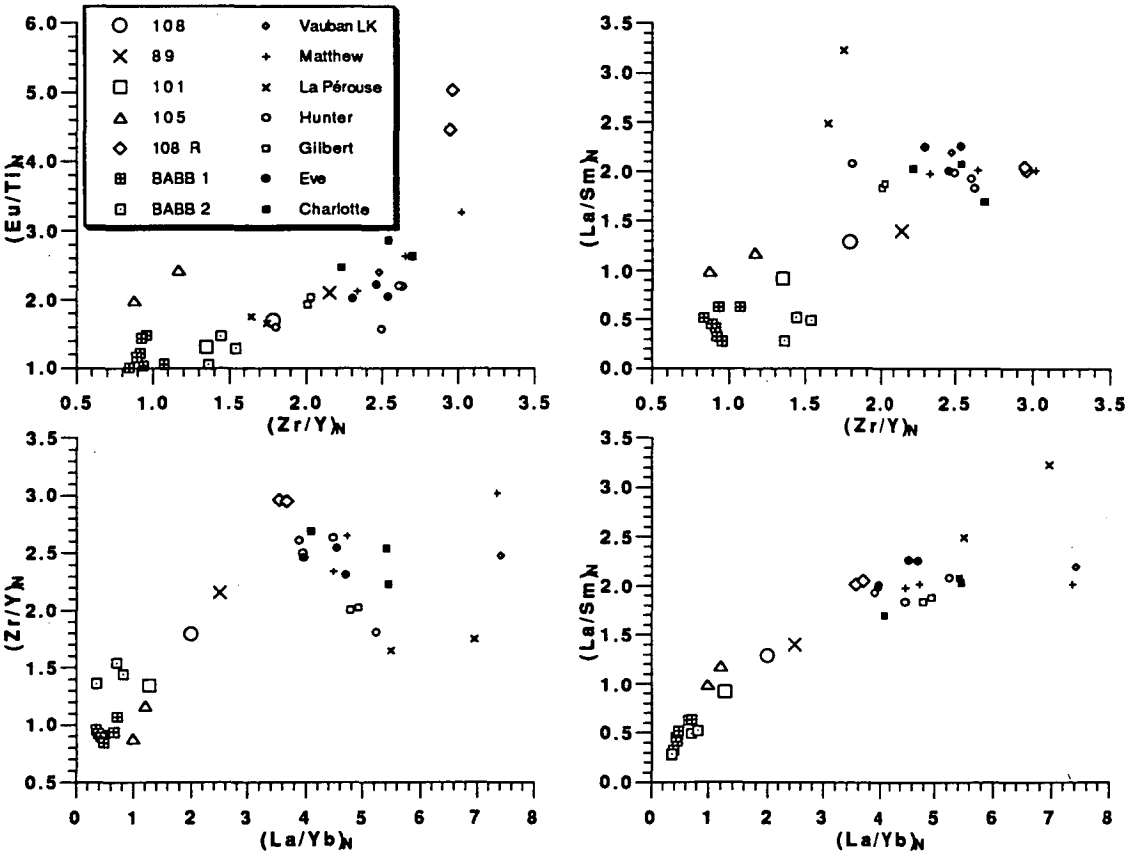

Figure 5.13: Primitive mantle normalized trace element ratios for the analysed samples together with back arc basin basalt basalts (chapter 4) and high magnesian andesites (HMA) from the Hunter Ridge (Monzier et al., 1993).

Figure 5.13 shows the relationships between some primitive mantle normalized trace element ratios (Sun and McDonough, 1989). Also shown for comparison are samples from the Hunter Ridge, (Monzier et al., 1993) and BABB from this area (chapter 4). Station 108 andesites differ from most other Hunter Ridge samples, including sample GB29B that has almost identical major element composition, by lower degrees of LREE and HFSE enrichment over the HREE (shown by differences in $(La/Yb)_N$ and $(Zr/Y)_N$, respectively), and they approach the BABB samples in this aspect.

5.3.4 Water content of the melt

Sobolev and Chaussidon (submitted) measured the water content of both natural glass and glass inclusions in andesite 108/5 with an ion microprobe technique. The matrix glass contains 1.47% H_2O whereas the average H_2O content of naturally quenched inclusions, corrected for olivine crystallization on the walls, is 2.51% (Sobolev and Chaussidon, submitted). The average of sums of electron microprobe analyses of matrix glasses and melt inclusions are in good agreement with this H_2O content. For natural glasses the average is 98.81% ± 0.28 and for homogenized and naturally quenched inclusions the totals are 97.28 ± 0.9 and 97.30 ± 1.19 respectively.

5.3.5 Fe^{2+}/Fe^{3+} in the melt

Maurel and Maurel (1982a) investigated experimentally the relationship between Fe^{2+}/Fe^{3+} in Cr-spinel and in basic silicate melt. In the temperature range 1180-1300 °C, at 1 atm total pressure and oxygen fugacity of 10^{-9}-10^{-3} the relationship is expressed by the equation:

$$\log_{10}(Fe^{2+}/Fe^{3+})_{sp} = 0.764 \log_{10}(Fe^{2+}/Fe^{3+})_{liq} - 0.343$$

Danyushevsky and Sobolev (submitted) have recently shown that this model gives accurate $(Fe^{2+}/Fe^{3+})_{liq}$ if the liquidus spinels have $TiO_2 < 2.5$ and $Cr_2O_3 > 13\%$, for crystallization temperature in the range 1000-1350 °C and $H_2O < 6\%$ in the melt.

The average (Fe^{2+}/Fe^{3+}) for the Cr-spinels, excluding the Cr-Al and Al-Ti spinels which are significantly more oxidized (Fig. 5.8), is 2.47 giving (Fe^{2+}/Fe^{3+}) in the melt of 9.2. This value is used in K_D calculations and calculations of liquidus mineral assemblages in later sections.

5.4 Summary

The mineralogy and geochemistry of station 108 andesites suggest that they were formed by complex magma mixing evolving two or more components. Spinel compositions and geochemistry suggest that both island arc related magmas (tholeiites and/or boninites) and back-arc magmas took part in this mixing. This is not unexpected as station 108 occurs where a back-arc spreading ridge is cutting through the Hunter Ridge and propagating into the fore-arc and thus providing the extra heat needed to form boninites by melting a refractory island arc source in this region, as was suggested by Crawford et al. (1989). In the next section the nature of these components will be studied further with aid of melt inclusions in olivine phenocrysts.

5.5 Melt inclusions in olivines from the andesites at station 108

From the lavas from stations 89, 101, 105 and 108 the andesites at station 108 were the only olivine phyric lavas for which sufficient material was available for detailed study of phenocryst phases and their melt inclusions. As both mineral phases and wholerock geochemistry suggest a complex history, possibly involving mixing between primitive magmas, there is the potential in the study of melt inclusions in the phenocrysts to identify liquid compositions of end members in the mixing process. Heating stage experiments were done to establish the crystallization history of these samples, the temperature of crystallization and the melt compositions from which the phenocrysts crystallized.

Melt inclusions occur in most olivine grains. They are rounded in shape, due to post-trapping crystallization on inclusion walls, and range in size from <20 to 200 μm. They vary from glassy to partly crystalline and most contain a low-density fluid bubble in shrinkage cavities. Separate fluid inclusions also occur in olivines, indicating that melts were fluid saturated during the crystallization of at least some of the olivine population.

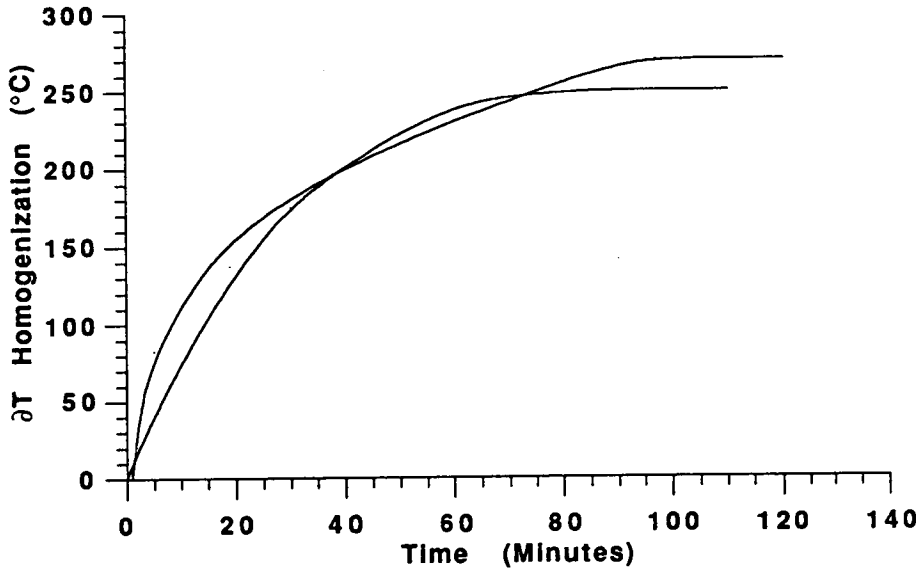

Figure 5.14: The correlation between the temperature of homogenization (T_h) and the duration of the run. ∂T is the difference between the real T_h and the actual homogenization temperature after a given time at temperatures above 1000 °C.

5.5.1 Kinetics experiments

The high water content in the melt causes some problems as H_2 diffuses very quickly through the host mineral at high temperatures. Figure 5.14 shows the results of two kinetic experiments. Within five minutes the T_h rises approximately 50 °C and after 1 hour the T_h has increased approximately 250 °C This is attributed to both

H_2-loss and resulting oxidation, as in long experiments a spinel phase becomes the most persistent daughter phase to very high temperatures. The experiments were therefore kept as short as possible and the duration of most runs was less than one or two minutes at temperatures above 1000 °C.

5.5.2 Heating stage experiments

Successful homogenization in olivine was achieved in 17 out of approximately 50 experiments at temperatures between 1120-1350 °C. Other experiments either failed to homogenize within the time taken for the experiment or the inclusion burst during heating. In Figure 5.15 temperature of homogenization (T_h) and MgO are plotted against Fo of the host olivine, together with data, obtained by the same method, from Tongan boninites (Sobolev and Danyushevsky, in press) and low-Ti ultramafic lavas from the Margi area, Troodos (Sobolev et al. 1991).

Because of the technique used to homogenize the inclusions, the experiments that give the lowest T_h for a given Fo content are taken to be closest to the real T_h (Sobolev and Danyushevsky, in press). Therefore the experiments are divided into two groups and only those with the lowest T_h for a given Fo are taken to give the true temperature of homogenization (Table 5.2). Those experiments give lower T_h and MgO than both Tonga and Margi for a given Fo. In all the experiments, calculated dry temperature (Ford et al., 1983) is significantly higher than T_h (Fig. 5.16), reflecting the high H_2O in the melts (Sobolev et al., 1991; Sobolev and Danyushevsky, in press; Sobolev and Chaussidon, submitted).

The K_D between host olivine and melt, for the homogenized inclusions is between 0.30-0.48 in the experiments that are accepted as not being overheated, and 0.31-0.45 in the overheated experiments. Many values are thus too high compared with the experimentally determined value 0.3 ± 0.03 (Roeder and Emslie, 1970). This is because most of the inclusions have relatively low FeO* (5.5-6.6), compared with the natural matrix glass (6.9-7.2). This is attributed to post-trapping re-equilibration and FeO-MgO exchange between olivine and melt inclusions (Sobolev and Danyushevsky, in press). All the melt compositions that were accepted as not being overheated were therefore recalculated using a program written by L. V. Danyushevsky. The method adjusts the homogenized liquid to an $Mg^{\#}$ consistent with $K_D = 0.3 \pm 0.03$ (see chapter 1). Compositions of recalculated melt inclusions are shown in Figure 5.17.

The inclusions show a reasonable liquid line of descent for SiO_2 and Al_2O_3 but other elements show greater variations than can be explained by crystal fractionation from a single homogeneous parental magma. These variations are greatest at approximately 9% MgO with CaO between 8.2-10.5, K_2O between 0.4-0.7 and TiO_2

Table 5.2: Results from the heating stage experiments that were accepted as not being overheated, including composition of the host olivine, composition of the melt inclusion, compositions of the melt inclusion after FeO/MgO re-calculations with Fe^{2+}/Fe^{3+} = 9.2, temperature of homogenization; and calculated dry liquidus temperature and calculated Fo content in equilibrium with the melt (Ford et al., 1983).

Olivine

	1	2a	2b	3	9	9b	4E6	15C2	1C3	7	E1	E2
SiO_2	39.78	39.89	39.98	40.07	40.23	40.23	40.51	40.94	40.91	39.69	41.09	41.28
Cr_2O_3							0.05	0.07	0.07		0.08	0.08
FeO	13.16	12.7	12.33	10.59	11.31	11.31	9.45	7.95	7.53	11.65	7.46	7.66
NiO							0.25	0.31	0.29		0.33	0.34
MnO							0.22	0.10	0.12		0.14	0.10
MgO	46.27	46.37	46.69	47.91	48.16	48.16	49.74	51.36	51.07	47.18	51.32	51.07
CaO	0.16	0.14	0.15	0.20	0.18	0.18	0.18	0.24	0.21	0.18	0.19	0.18
Sum	99.37	99.10	99.16	98.77	99.88	99.88	100.4	101.0	100.2	98.70	100.6	100.7
Fo	86.2	86.7	87.1	89.0	88.4	88.4	90.4	92.0	92.4	87.8	92.5	92.2

Melt inclusion

	1	2a	2b	3	9a	9b	4E6	15C2	1C3	7	E1	E2
SiO_2	58.05	56.68	57.00	53.29	53.58	53.10	53.11	53.08	51.18	53.39	51.78	50.98
TiO_2	0.56	0.67	0.66	0.56	0.57	0.61	0.59	0.47	0.68	0.72	0.58	0.58
Al_2O_3	16.67	16.18	16.6	14.66	15.14	14.99	15.14	11.56	12.85	15.99	12.06	11.85
FeO	5.40	6.05	5.94	6.28	5.95	6.06	5.75	5.69	6.15	6.40	5.69	5.80
MnO	0.00	0.06	0.07	0.10	0.07	0.00	0.10	0.05	0.13	0.09	0.06	0.04
MgO	5.39	6.15	6.11	8.77	8.66	8.78	10.53	13.87	13.58	8.36	15.43	16.55
CaO	7.05	7.25	7.14	10.29	9.85	9.41	8.42	10.75	10.3	8.06	8.92	8.15
Na_2O	3.41	3.14	3.46	2.63	2.70	2.79	2.79	1.93	1.63	3.01	2.09	2.17
K_2O	0.90	0.67	0.67	0.35	0.38	0.39	0.61	0.28	0.25	0.63	0.30	0.31
P_2O_5	0.15	0.14	0.10	0.04	0.03	0.05	0.12	0.04	0.04	0.12	0.01	0.03
Sum	97.58	96.99	97.74	96.97	96.93	96.18	97.17	97.73	96.78	96.77	96.92	96.45
mg#	64.0	64.4	64.7	71.3	72.2	72.1	76.5	81.3	79.7	69.9	82.9	83.6
T_h °C	1120	1130	1130	1190	1185	11.85	1240	1320	1325	1180	1350	1350
K_D	0.32	0.31	0.30	0.34	0.38	0.38	0.39	0.42	0.36	0.36	0.44	0.48

FeO/MgO recalculated

	1	2a	2b	3	9a	9b	4E6	15C2	1C3	7	E1	E2
SiO_2	59.42	58.39	58.27	54.67	54.68	54.57	53.91	53.34	52.43	54.63	52.20	51.17
TiO_2	0.57	0.69	0.67	0.57	0.57	0.62	0.59	0.46	0.69	0.73	0.56	0.55
Al_2O_3	17.05	16.66	16.97	14.94	15.23	15.16	15.05	11.29	12.99	16.20	11.67	11.18
Fe_2O_3	0.61	0.68	0.66	0.76	0.80	0.82	0.80	0.85	0.79	0.82	0.90	1.02
FeO	5.04	5.64	5.49	6.30	6.60	6.79	6.65	7.01	6.55	6.83	7.45	8.42
MnO	0.00	0.06	0.07	0.10	0.07	0.00	0.10	0.05	0.13	0.09	0.06	0.04
MgO	5.53	6.35	6.25	9.10	9.02	9.25	11.05	14.31	14.07	8.73	16.21	17.56
CaO	7.21	7.47	7.30	10.49	9.91	9.52	8.37	10.50	10.41	8.17	8.63	7.69
Na_2O	3.49	3.23	3.54	2.68	2.72	2.82	2.77	1.89	1.65	3.05	2.02	2.05
K_2O	0.92	0.69	0.68	0.36	0.38	0.39	0.61	0.27	0.25	0.64	0.29	0.29
P_2O_5	0.15	0.14	0.10	0.04	0.03	0.05	0.12	0.04	0.04	0.12	0.01	0.03
K_D	0.31	0.31	0.30	0.31	0.31	0.32	0.32	0.31	0.32	0.32	0.32	0.31
T_c °C	1195	1207	1211	1240	1242	1252	1301	1345	1335	1253	1385	1409
Ol_c	86.2	86.7	87.1	89.0	88.4	88.4	90.4	92.0	92.4	87.8	92.5	92.2

between 0.56-0.74. This causes large variations in ratios involving these elements (Fig. 5.18).

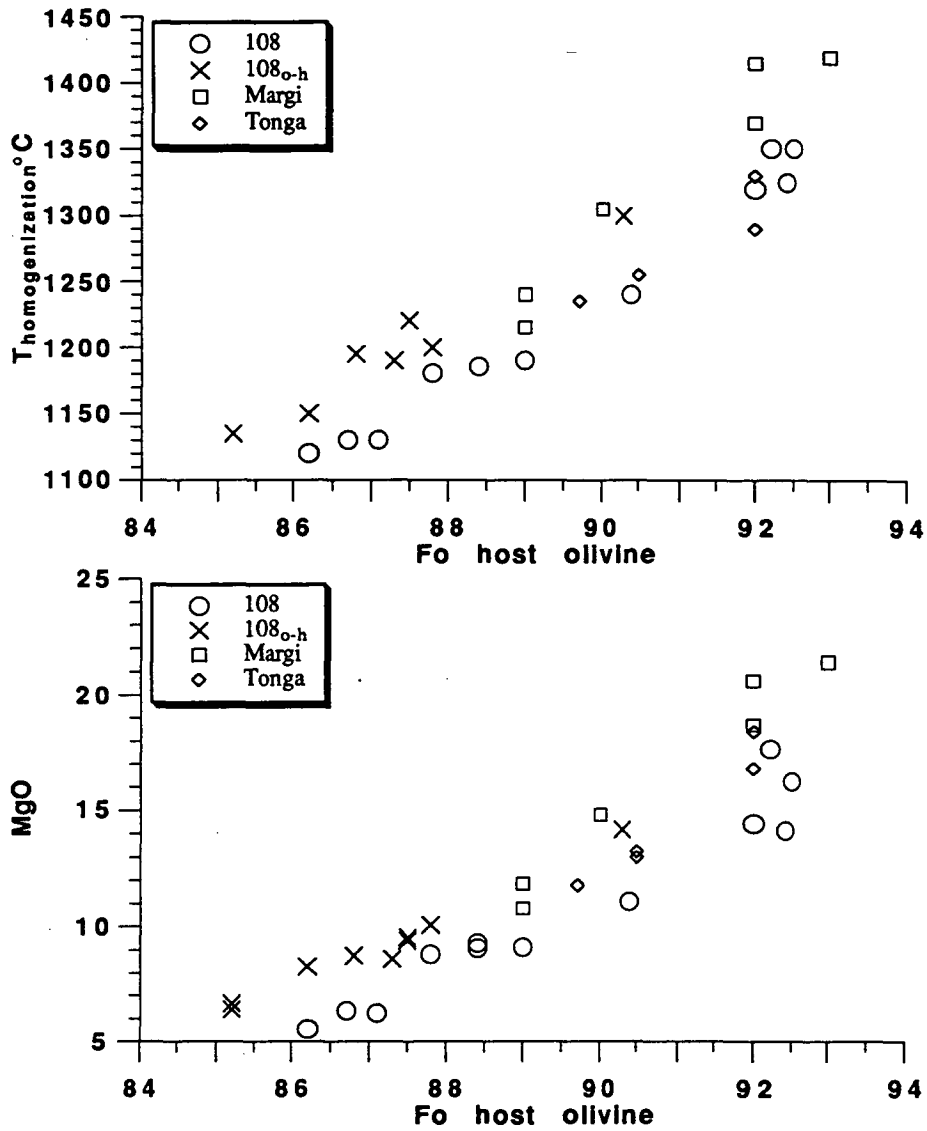

Figure 5.15: Temperature of homogenization and MgO content of the melt inclusions plotted against the Fo content of the host olivine for all the experiments from sample 108. The open circles show experiments that represent the true T_h and the actual melt composition whereas the crosses show experiments that where overheated. Also shown for comparison are data obtained by the same method from Margi (Sobolev et al., 1991) and Tonga (Sobolev and Danyushevsky, in press).

5.5.3 Naturally quenched inclusions in olivine and clinopyroxene

For additional data, seventy naturally-quenched inclusions in olivine phenocrysts were analysed (Table 5.3). Because of olivine crystallization on the inclusion walls and possible later re-equilibration the composition of those inclusions cannot be used directly as entrapped melt compositions. However, the ratio between elements that are incompatible in olivine (TiO_2, Al_2O_3, CaO, Na_2O and K_2O), should be

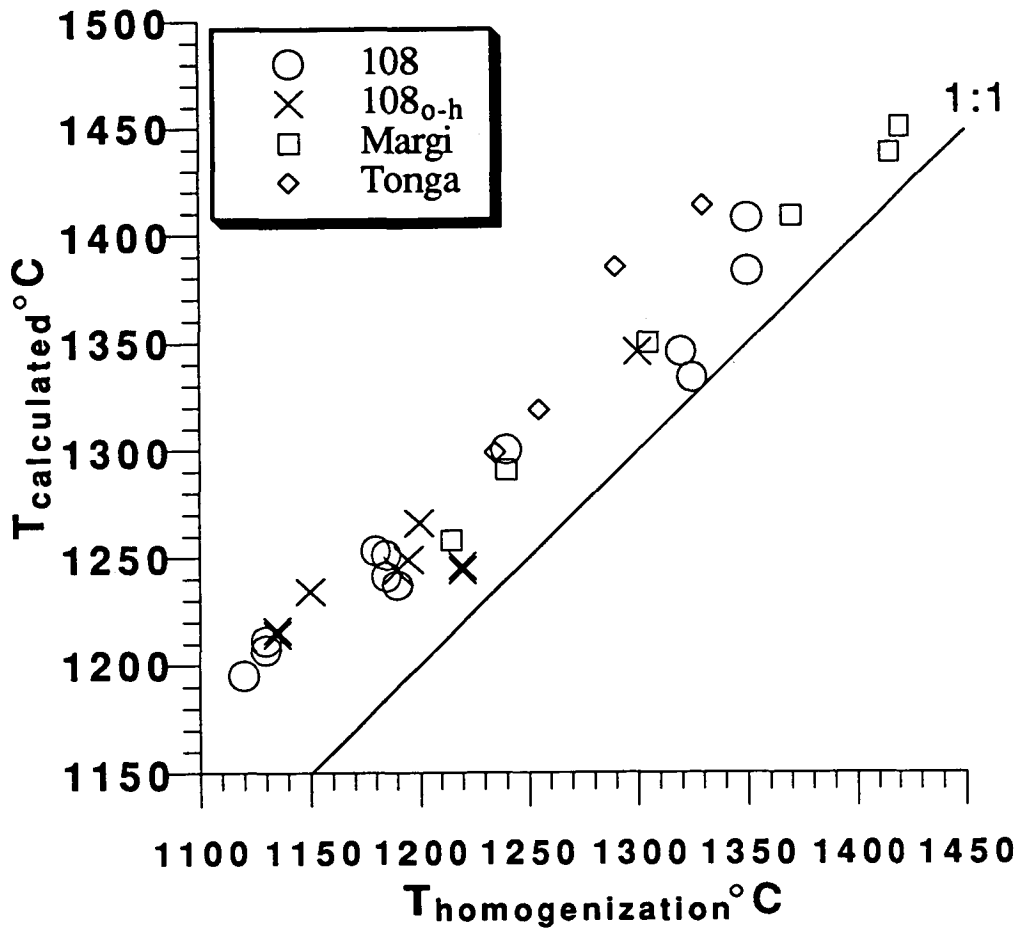

Figure 5.16: Calculated dry liquidus temperature (Ford et al., 1983) versus temperature of homogenization for the experiments on samples from station 108 together with samples from Margi (Sobolev et al., 1991) and Troodos (Sobolev and Danyushevsky, in press). The line shows 1:1 relationship.

components involved in magma generation at station 108. Eleven inclusions were analysed in clinopyroxene phenocrysts (Table 5.3) and they are plotted together with other inclusions as no systematic difference was seen between inclusions in olivine and those in clinopyroxene.

In Figure 5.18, various element ratios are plotted versus TiO_2/Al_2O_3 for the experimentally and naturally quenched inclusions together with the natural matrix glass. A field for glass inclusions in BABB sample 123 from the NFB (chapter 4) and fields for Hunter Ridge boninite (Boninite 1 and 2) and island arc tholeiite glasses (IAT 1 and 2) are shown for comparison (chapter 3). The scatter in these ratios for sample 108 is far greater than can be explained by crystal fractionation alone so that processes such as mixing between two or more components need to be evaluated.

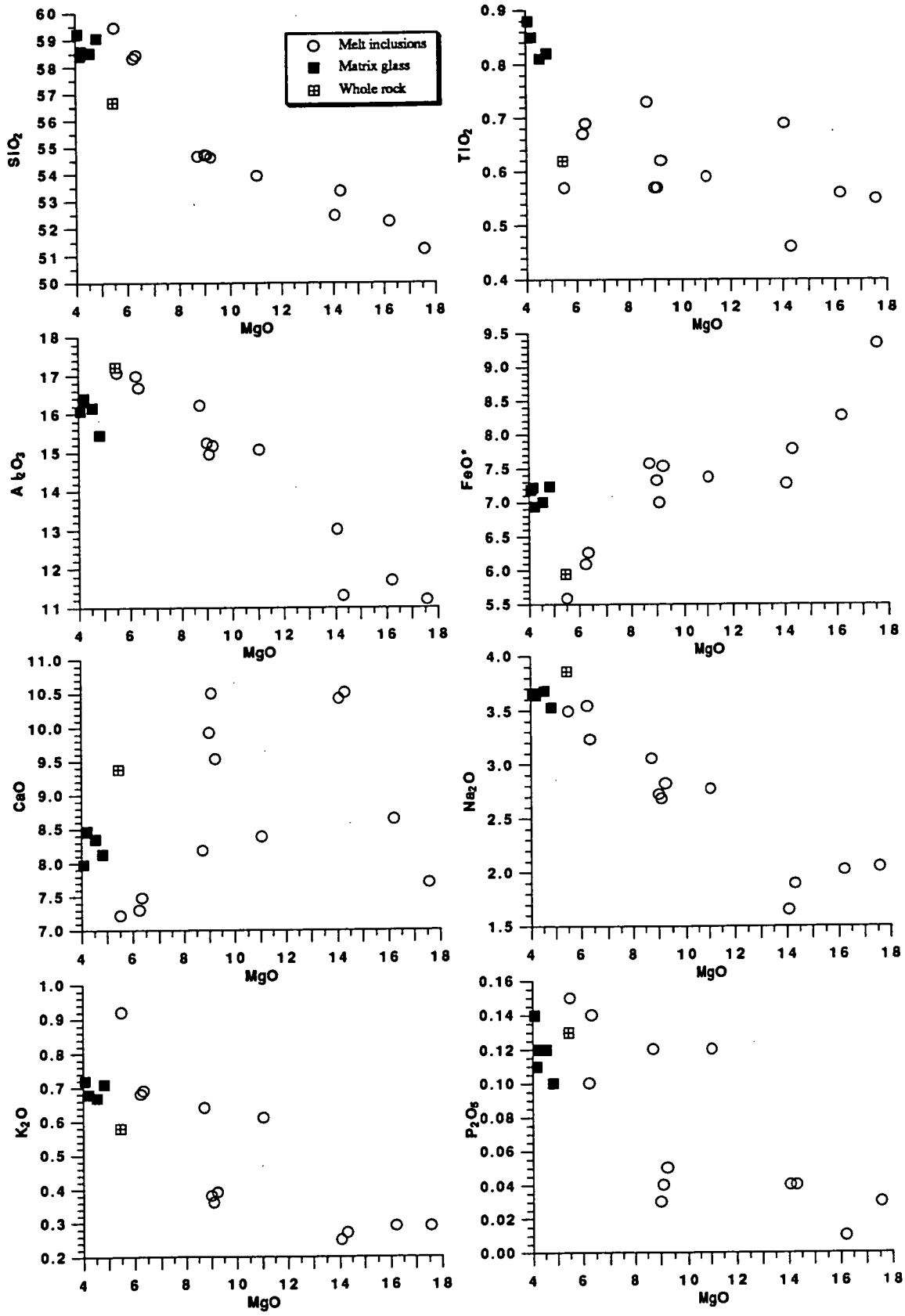

Figure 5.17: Major element compositions of recalculated melt inclusions in olivine from the andesites from station 108 plotted against MgO content together with whole rock and glass compositions.

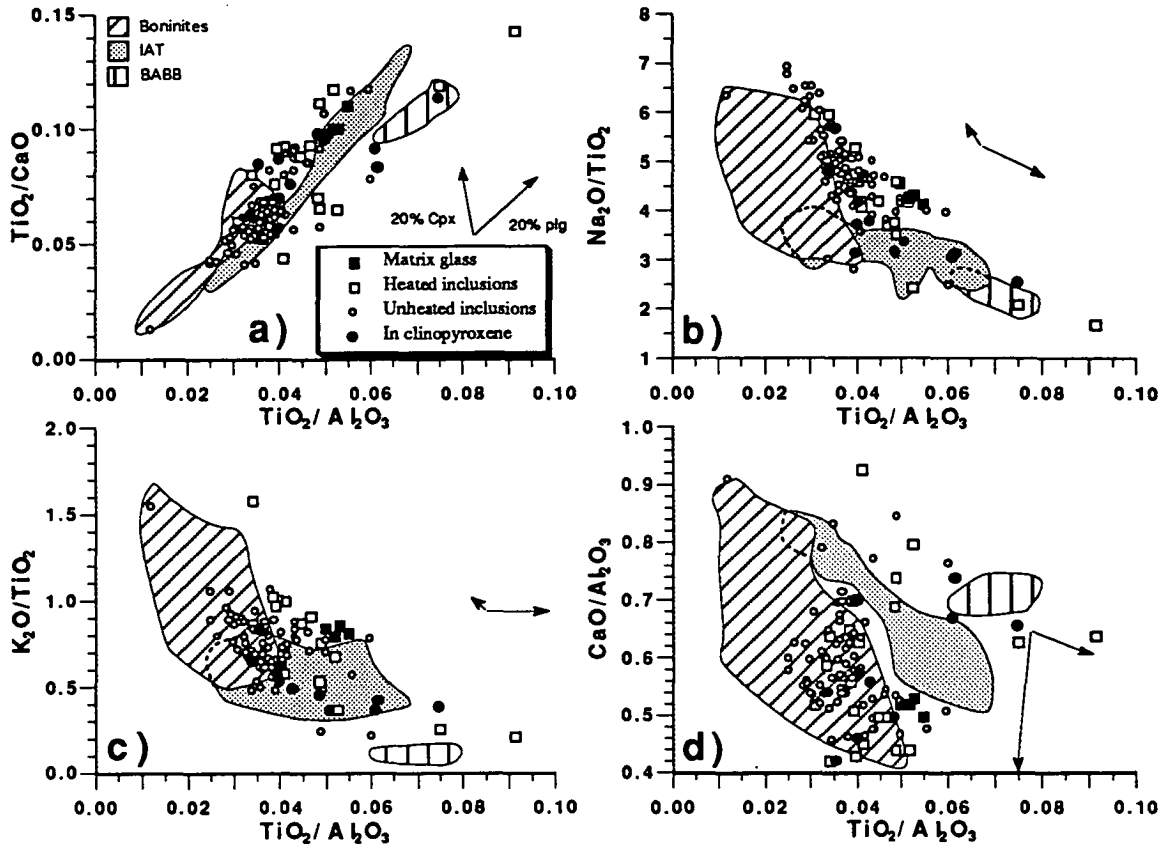

Figure 5.18: Various major element ratios plotted against TiO_2/Al_2O_3 for matrix glass and inclusions in olivine and clinopyroxene from the andesites from station 108. Also shown are the fields for boninite and island arc tholeiite matrix glasses (Chapter 3), glass inclusions in olivines from BABB sample 123/1 (Chapter 4) and vectors showing variations caused by 20% crystal fractionation of olivine and clinopyroxene calculated for an inclusion with $TiO_2/Al_2O_3 = 0.04$ and $TiO_2/CaO = 0.06$.

Variations, such as in TiO_2/CaO at the same TiO_2/Al_2O_3, can be caused by clinopyroxene fractionation (see vectors in Figure 5.18) but simple fractionation of olivine and clinopyroxene is not enough to explain the large variations in TiO_2/Al_2O_3. For example, inclusions from 108 andesites show greater variation in both TiO_2/CaO and TiO_2/Al_2O_3 than both the groups of boninite and island arc tholeiite glasses, and extend to higher values than the inclusions in the BABB from station 123. In addition, a group of inclusions occurring both among heated and unheated inclusions in olivine, as well as in inclusions in clinopyroxene, has relatively high CaO, causing this group to plot below the fields for island arc tholeiite and boninite glasses in Figure 5.18a, and above the fields in Figure 5.18c. This group also extends to higher TiO_2/Al_2O_3 and shows some affinities to BABB in all the ratios shown in Figure 5.18.

Table 5.3: Microprobe analyses of unheated melt inclusions in olivine and clinopyroxene from dredge 108 andesites. Fo and mg# are the forsterite content and mg# of host olivine and clinopyroxene respectively.

Inclusions in olivine

Number	191	159	215	160/3	100	256	62	210	173	102
SiO_2	55.57	53.37	52.83	52.88	55.03	51.28	54.19	56.12	54.66	56.66
TiO_2	0.84	0.77	0.71	0.66	0.47	0.68	0.56	0.99	0.75	0.61
Al_2O_3	16.79	18.56	18.49	17.97	16.17	17.36	17.42	17.69	18.00	17.58
FeO*	7.13	6.07	6.70	6.46	6.31	6.52	6.19	5.58	5.99	5.61
MnO	0.01	0.15	0.05	0.05	0.15	0.14	0.07	0.04	0.12	0.06
MgO	4.09	2.05	4.12	5.09	5.28	5.82	4.92	2.83	3.67	3.76
CaO	7.84	9.62	8.57	9.87	9.09	10.07	9.65	8.42	8.37	8.07
Na_2O	3.56	3.26	3.37	3.43	3.11	2.79	3.58	3.95	3.56	3.51
K_2O	0.59	0.55	0.76	0.48	0.51	0.45	0.49	0.57	0.56	0.58
P_2O_5	0.14	0.10	0.16	0.02	0.06	0.13	0.03	0.16	0.11	0.10
Sum	96.56	94.50	95.75	96.90	96.18	95.24	97.11	96.33	95.80	96.52
Fo	84.4	84.5	84.9	84.9	85.2	85.4	85.5	85.8	86.1	86.2

Number	160	160/2	60/1	60/2	184	15	219	245	125	54
SiO_2	54.28	53.74	53.82	55.38	52.78	54.90	55.44	53.80	56.52	53.57
TiO_2	0.66	0.58	0.83	0.68	0.75	0.54	0.44	0.85	0.77	0.62
Al_2O_3	18.20	17.87	16.96	18.38	18.34	18.91	17.53	18.26	16.73	17.10
FeO*	6.40	6.01	6.64	6.15	6.62	5.64	5.80	5.83	6.75	6.47
MnO	0.05	0.09	0.06	0.03	0.11	0.07	0.15	0.00	0.09	0.03
MgO	4.70	5.06	5.39	5.02	4.13	2.25	3.50	3.27	4.64	5.07
CaO	9.52	9.30	9.08	10.44	10.68	10.44	10.53	9.96	9.00	10.82
Na_2O	3.38	3.47	3.29	3.43	2.65	3.27	2.99	3.24	3.62	2.73
K_2O	0.45	0.46	0.38	0.50	0.55	0.52	0.47	0.61	0.63	0.40
P_2O_5	0.10	0.00	0.15	0.10	0.17	0.03	0.00	0.13	0.17	0.12
Sum	97.75	96.57	96.60	100.1	96.79	96.57	96.84	95.95	98.92	96.93
Fo	86.3	86.3	86.4	86.4	86.6	86.8	86.8	87.0	87.0	87.0

Number	38	74/2L	63	276	51	179/1	179/2	21	272	70
SiO_2	55.29	54.13	54.83	55.94	54.00	55.08	56.47	56.40	57.31	54.27
TiO_2	0.59	0.60	0.63	0.61	0.54	0.65	0.84	0.82	0.79	0.53
Al_2O_3	19.32	18.10	16.72	18.50	17.89	17.85	16.82	18.85	18.29	17.88
FeO*	5.50	6.17	6.34	5.35	5.62	6.61	6.99	5.11	4.42	6.72
MnO	0.00	0.09	0.07	0.13	0.15	0.07	0.10	0.12	0.10	0.12
MgO	2.33	4.60	5.72	4.19	5.16	5.18	4.57	2.37	1.57	4.87
CaO	10.40	10.96	10.32	9.96	9.65	10.23	8.88	9.98	9.04	9.97
Na_2O	3.85	3.07	3.08	3.38	3.43	3.25	3.50	3.51	3.98	3.27
K_2O	0.54	0.41	0.42	0.43	0.47	0.49	0.66	0.72	0.63	0.49
P_2O_5	0.09	0.08	0.00	0.09	0.07	0.06	0.03	0.08	0.24	0.07
Sum	97.90	98.20	98.13	98.59	96.96	99.45	98.86	97.95	96.37	98.20
Fo	87.0	87.2	87.2	87.3	87.3	87.3	87.3	87.3	87.3	87.4

Number	296	64a	64b	31	263	288	201	306	279	203
SiO_2	57.33	54.25	54.58	55.46	56.26	54.19	53.26	58.01	52.68	54.38
TiO_2	0.81	0.67	0.71	0.68	0.63	0.62	0.47	0.94	0.50	0.60
Al_2O_3	18.47	17.46	18.10	17.57	18.46	18.49	17.58	15.80	17.38	18.33
FeO*	4.83	5.55	6.78	5.80	5.22	5.46	6.51	7.11	6.15	6.37
MnO	0.00	0.05	0.06	0.02	0.21	0.13	0.21	0.18	0.23	0.07
MgO	2.18	3.40	4.65	3.30	1.63	3.32	5.39	4.13	5.43	3.44
CaO	8.81	10.93	10.94	11.26	9.47	11.13	11.03	8.02	10.86	11.20
Na_2O	3.83	2.93	3.12	2.95	3.61	2.85	3.01	3.75	3.15	3.39
K_2O	0.63	0.44	0.42	0.40	0.53	0.42	0.37	0.74	0.45	0.45
P_2O_5	0.07	0.07	0.07	0.02	0.10	0.01	0.11	0.11	0.13	0.12
Sum	96.97	95.76	99.43	97.47	96.12	96.61	97.94	98.78	96.95	98.35
Fo	87.5	87.5	87.5	87.6	87.6	87.7	87.7	87.8	87.8	87.9

Table 5.3 continued:

Number	134	221	170/1	170/2	297/1	297/2	199	242	48/1	48/2
SiO_2	54.20	53.58	55.90	54.02	53.19	53.20	56.21	54.70	55.21	54.97
TiO_2	0.54	0.63	0.69	0.46	0.79	1.00	0.65	0.62	0.65	0.57
Al_2O_3	17.59	17.51	18.26	18.43	16.10	16.65	16.82	17.31	17.78	19.03
FeO*	5.71	6.17	4.94	6.35	6.26	6.41	6.61	5.47	5.10	4.74
MnO	0.07	0.06	0.19	0.00	0.20	0.00	0.02	0.07	0.18	0.05
MgO	2.96	4.91	2.37	4.27	4.53	4.30	4.65	3.01	3.09	2.52
CaO	11.99	10.96	9.85	10.68	13.66	12.75	9.55	12.09	11.85	11.37
Na_2O	2.96	3.11	3.54	3.20	2.44	2.47	3.31	2.63	2.93	3.09
K_2O	0.40	0.39	0.55	0.41	0.19	0.22	0.58	0.31	0.39	0.44
P_2O_5	0.05	0.00	0.06	0.04	0.13	0.14	0.07	0.20	0.04	0.03
Sum	96.46	97.31	96.35	97.86	97.49	97.13	98.46	96.42	97.21	96.80
Fo	88.0	88.1	88.1	88.1	88.1	88.1	88.1	88.3	88.4	88.4

Number	48/3	77	309	15	292	164	110	255	1a	1b
SiO_2	55.37	56.05	57.95	57.33	55.11	55.05	55.18	56.96	54.56	56.40
TiO_2	0.70	0.59	0.67	0.75	0.62	0.67	0.70	0.78	0.68	0.63
Al_2O_3	18.60	16.23	18.08	18.24	16.90	17.39	16.77	17.99	17.86	18.21
FeO*	4.40	5.62	3.95	4.56	5.13	5.26	4.66	5.18	6.86	6.51
MnO	0.02	0.07	0.00	0.02	0.04	0.05	0.03	0.06	0.18	0.07
MgO	2.43	4.87	1.77	2.08	2.84	3.06	3.70	2.62	4.91	4.85
CaO	10.99	10.98	9.77	11.59	12.08	12.17	11.10	8.58	11.22	10.31
Na_2O	3.63	3.08	3.60	3.40	2.97	3.12	3.26	3.55	3.21	3.24
K_2O	0.52	0.41	0.55	0.49	0.38	0.41	0.48	0.66	0.39	0.44
P_2O_5	0.06	0.04	0.00	0.07	0.04	0.14	0.05	0.09	0.08	0.03
Sum	96.72	97.94	96.33	98.52	96.12	97.32	95.94	96.47	99.95	100.7
Fo	88.4	88.5	88.6	88.7	88.7	88.8	88.9	89.1	89.2	89.2

Number	50	239	62	150	27	1Sob	3Sob	4Sob	a	d
SiO_2	55.57	54.97	56.73	54.10	57.87	54.78	57.36	56.50	57.21	57.25
TiO_2	0.74	0.55	0.67	0.56	0.70	0.60	0.16	0.61	0.70	0.60
Al_2O_3	17.11	16.97	16.64	15.96	17.43	16.73	13.31	16.51	17.71	17.68
FeO*	4.78	4.91	3.88	6.57	3.57	6.30	6.86	4.22	5.02	5.23
MnO	0.04	0.09	0.09	0.20	0.06	0.20	0.12	0.08	0.12	0.17
MgO	2.28	2.49	3.96	4.78	2.22	5.88	5.70	4.27	2.70	2.59
CaO	13.27	13.48	11.66	13.34	12.28	10.01	12.16	11.57	11.39	11.5
Na_2O	2.92	2.81	3.42	2.41	3.38	2.89	1.02	3.31	1.94	1.8
K_2O	0.37	0.39	0.55	0.30	0.49	0.39	0.25	0.54	0.34	0.29
P_2O_5	0.05	0.10	0.02	0.09	0.05	0.08	0.03	0.10	0.01	0.01
Sum	97.13	96.75	97.63	98.30	98.07	97.86	96.97	97.71	97.14	97.12
Fo	89.4	89.6	91.4	91.5	92.0	86.8	89.2	91.9	87.6	87.6

Inclusions in clinopyroxene

Number	12	13	34	34	32	28	23	3	5	14	11
SiO_2	52.74	53.77	54.07	52.98	54.72	53.61	53.20	53.3	54.71	53.2	52.34
TiO_2	0.72	0.61	0.72	0.84	0.68	0.67	0.87	0.89	0.61	1.10	0.94
Al_2O_3	16.76	18.09	17.92	17.25	18.93	16.45	17.01	14.39	15.37	14.69	15.31
FeO*	7.70	6.17	6.73	6.86	5.55	6.89	7.06	7.63	6.21	10.03	9.03
MnO	0.27	0.09	0.12	0.10	0.22	0.03	0.10	0.08	0.05	0.10	0.20
MgO	5.70	5.65	5.21	5.32	3.88	5.58	5.37	6.94	6.64	5.87	5.94
CaO	9.35	9.80	8.25	8.57	7.98	9.45	8.81	10.64	10.78	9.66	10.25
Na_2O	2.71	2.95	2.67	2.64	3.84	2.79	2.91	2.78	1.91	2.79	2.84
K_2O	0.35	0.40	0.39	0.38	0.57	0.42	0.32	0.38	0.35	0.43	0.35
P_2O_5	0.07	0.10	0.07	0.01	0.07	0.08	0.12	0.03	0.06	0.07	0.03
Sum	96.37	97.63	96.14	94.96	96.43	95.95	95.75	97.05	96.69	97.95	97.23
mg#	87.1	88.3	82.9	82.9	90.4	85.2	87.9	85.9	88.4	81.9	83.0

5.6 Discussion

The observed diversity of phenocrysts including three types of spinels in olivines, the wide range of olivine compositions and complex zoning patterns in both olivine and clinopyroxene; together with the variability of melt compositions at each fractionation range suggests a scenario in which an andesite magma is made up of a mixture of crystals and geochemically distinct melts.

5.6.1 Crystallization history of station 108 andesites

From the data on mineral chemistry and homogenized melt inclusions, it is possible to characterize the temperature of crystallization of components of 108 andesite, the compositions of melt components and their liquidus phases, and their evolution during fractional crystallization.

The relationship between Fo content of the most magnesian olivines and the $cr^{\#}$ of their spinel inclusions (Fig. 5.8) indicates a mantle origin for a parental magma crystallizing Cr-rich spinels and > Fo_{89} olivine. Those olivine and spinel pairs fall into the mantle array of Arai (1987) and are comparable to those found in island arc tholeiites and boninites from this area (chapter 3). The most magnesian homogenized melt inclusion, with MgO content above 17%, in equilibrium with highly forsteritic olivine ($Fo_{92.2}$) suggests that it is close to a primary melt.

The temperature interval of crystallization for this melt, determined by the method of homogenization, is from 1350-1120 °C, which is very close to temperatures for Tongan boninites studied by the same method (Sobolev and Danyushevsky, in press). Tongan boninites show the same correlation between composition of olivine and their temperature of homogenization (Fig 5.15). On the other hand, the crystallization of olivine in low-Ti ultramafic lavas from Margi occurred at significantly higher temperature for any given olivine composition (Sobolev et al. 1991). This difference in temperature reflects difference in melt composition, mainly H_2O, which is similar in the studied Hunter Ridge mixed andesites and Tongan boninites (Sobolev and Chaussidon, submitted.; Sobolev and Danyushevsky, in press) but exceeds those in the Margi samples by up to 1% (Sobolev et al., 1991; Sobolev and Danyushevsky, in press).

CaO in olivines from sample 108/7 starts to decrease at approximately Fo_{91} (Fig. 5.3), which marks the appearance of clinopyroxene on the liquidus. Similarly, the CaO in the melt inclusions starts to decrease at MgO between 10 and 14% (Figure 5.17). This Fo and MgO is in agreement with the trend shown by MgO and Fo in Figure 5.15 and this should result in an increase in the slope of this trend at Fo_{91}.

Melt inclusion studies show that the main type of crystallization was fractional, as seen by the good correlation between Fo and T_h. The compositions of melt

inclusions demonstrate fractionation of olivine, ± cr-spinel, and clinopyroxene joining as a liquidus phase at MgO = 10-14%. However, from Figure 5.17 it is obvious that TiO_2, P_2O_5, Na_2O, K_2O and CaO vary greatly for a given MgO content. This is more evident when the unheated inclusions, both in olivine and clinopyroxene, are taken together with homogenized inclusions and the ratios between these elements are considered (Fig. 5.18). There is no difference between the heated and unheated inclusions, but two groups are recognized based on their CaO contents. Variations within each group that exceed the error of microprobe analyses cannot be explained on the basis of single stage fractionation, that is, crystallization from a single batch of melt with subsequent isolation of the crystals from the melt. Moreover, the wide range of Al_2O_3 in spinel, normal and reverse zoning in phenocrysts, and bimodal distribution of olivine compositions, all suggest magma mixing and multi-stage fractionation.

It is evident from Figure 5.18 that the inclusions in the andesites from station 108 show much more variation in TiO_2/CaO for a given TiO_2/Al_2O_3 than the IAT from south of the Hunter Ridge, and cover the whole range in TiO_2/Al_2O_3 shown by the boninites and IAT from this area. As the inclusions are at different stages of a complex evolution, and the absolute values of the incompatible elements in the naturally quenched inclusions are not known, it is difficult to determine the causes of these variations. To give an idea of the absolute values, least square calculations were used to add olivine back into both the heated and unheated inclusions in olivine until they had the same MgO content as the most MgO-rich inclusion (17.6% MgO). This is an arbitrary approximation as there is no necessity for all mixing components to have come from primitive melts with high MgO content. Nevertheless it does provide a basis for comparison. This gives an estimation of the fractionation of the original liquid and a model parental composition with lower incompatible elements can be calculated. As mentioned earlier, most inclusions suffered re-equilibration and FeO-MgO, exchange but this does not have any significant effects on the calculations. For example an increase in FeO from 6 to 8% causes less than 2% relative change in the incompatible elements.

In Figure 5.19 TiO_2, Al_2O_3, CaO, Na_2O and K_2O recalculated to MgO = 17.6% are plotted against the forsterite content of the host olivine. The general decrease in $CaO_{17.6}$ can be explained by crystallization of clinopyroxene, which was not taken into account in the calculations, but the variations at a given Fo content and the variation in other elements need some other explanations. Open system fractionation (O'Hara and Matthews, 1981) is one scenario in which a steady build up of the more incompatible elements can result from repeated replenishment and fractionation in a steady state magma chamber. If this was the case, the greatest enrichment would be expected in the less forsteritic olivines crystallized when the system reaches a steady

state just before an injection of a new magma batch. $K_2O_{17.6}$ shows greatest variations in olivines of compositions between Fo_{86-88}, but variations in olivines of Fo_{92} are greater than can be explained by mixing between primitive and evolved co-genetic magmas. This is also demonstrated in Figure 5.20 in which the compositions of the melt inclusions are shown together with calculated fractionation paths for the two most magnesian inclusions, calculated using the program Petrolog (Danyushevsky et al., 1990). The program removes 0.1% of the calculated dry liquidus mineral assemblage in each calculation step. The melt inclusions were modelled for olivine fractionation until clinopyroxene comes on the liquidus because this program, which simulates a dry system was not able to remove olivine and clinopyroxene simultaneously. Figure 5.20 shows that it is not possible to get the compositional spread shown by the melt inclusions by olivine fractionation from a single parental melt, and that more than one magma type must have been involved in magma generation at station 108.

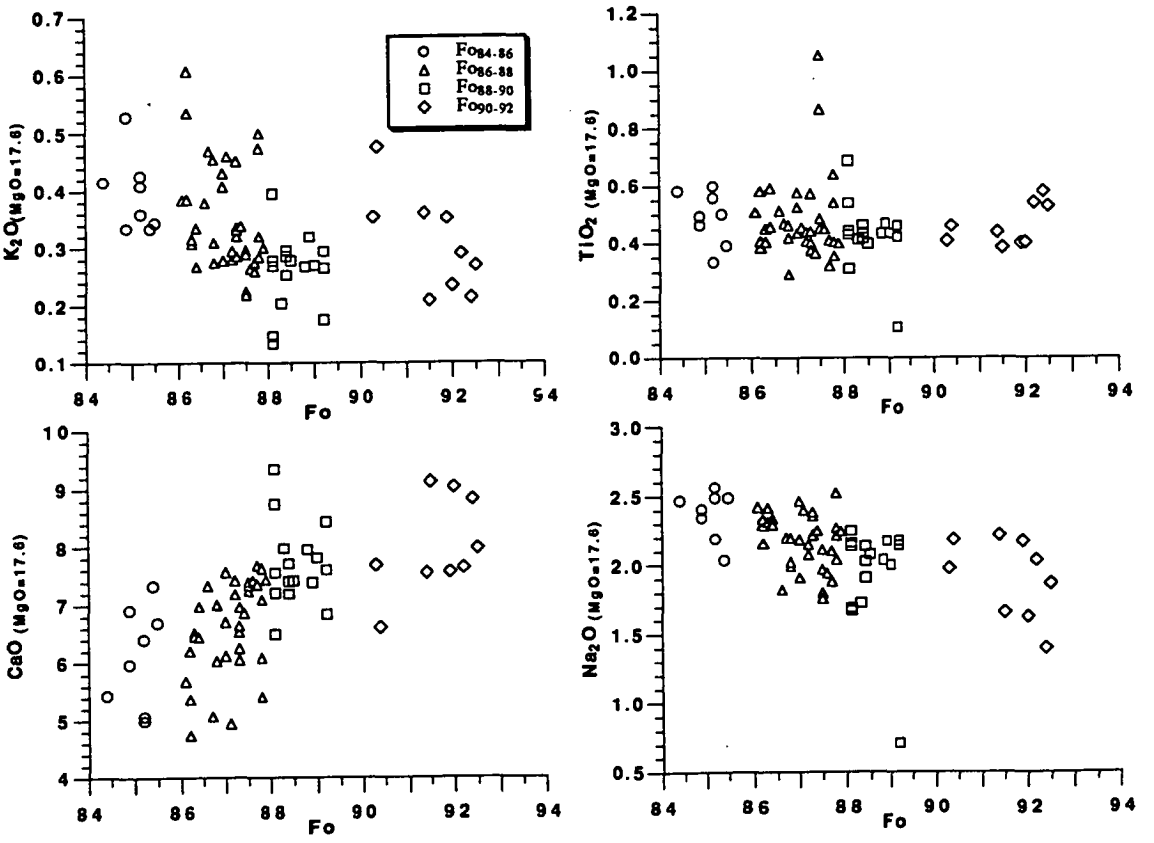

Figure 5.19: K_2O, TiO_2,CaO and Na_2O, calculated to 17.6% MgO for inclusions in olivine plotted against Fo of the host olivine.

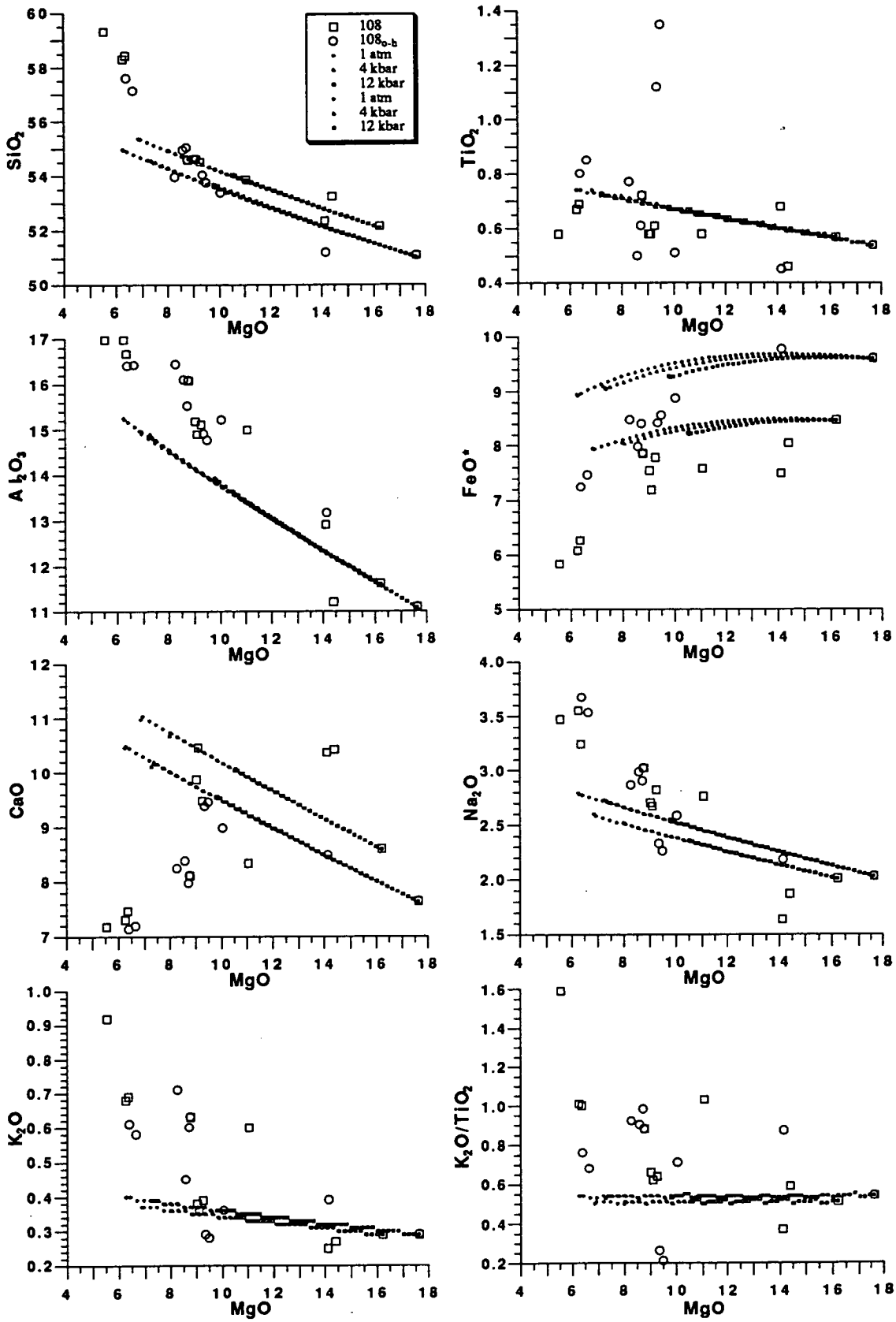

Figure 5.20: Same as Figure 5.17 with calculated fractionation paths for the two most magnesian inclusions.

5.6.2 Inferences on magma mixing in the generation of station 108 andesites

The zoning shown by olivine of compositions Fo_{88-90} (Fig. 5.3) and clinopyroxene with $mg^{\#}$ between 80 and 88 (Fig. 5.7) suggest several events where magmas at different stages of evolution are mixed. The two main groups of spinel inclusions in olivine also suggest magma mixing (Fig. 5.8). The Cr-spinels show an identical trend to the island arc tholeiites (chapter 3), whereas the Al-Cr-spinels form a trend that is more akin to spinels from BABB or E-MORB (Fig. 5.9). There is an important difference though as three of the 108 Al-Cr-spinels have high Al_2O_3 together with high TiO_2 contents (Fig. 5.8). However, spinels with Al_2O_3 content between 25-40% suggest that over this composition interval TiO_2 increases with decreasing Al_2O_3. In the BABB samples, $cr^{\#}$ increases with decreasing $Mg^{\#}$ due to crystallization of plagioclase, and as Al_2O_3 decreases, so TiO_2 increases.

The relationship between Al_2O_3 in spinel and melt has been studied experimentally by Maurel and Maurel (1982b, 1983). The range of Al_2O_3 observed in melt-inclusions (10.80-16.52%) can crystallize spinel with Al_2O_3 between 11 and 31%. In fact most of the spinel analyses fall within this range with only few spinels having higher Al_2O_3 (up to 46.5%). These high Al_2O_3 contents of spinel require melt with 19.5% Al_2O_3, and if a melt of this type did exist in the system it was not trapped by any of the crystallising olivines that were analysed. H_2O in melt is known to suppress the plagioclase liquidus (e.g. Yoder and Tilley, 1962), hence the steady increase in Al_2O_3 with decreasing MgO (Fig. 5.17). Plagioclase however, occurs as both microphenocrysts and resorbed phenocrysts in those samples, indicating plagioclase saturation and the difficulty of melt compositions evolving to much higher Al_2O_3 contents.

As can be seen in figure 5.9, the Al-Cr spinels form a trend extending from the Cr spinels that are similar to the spinels in IAT towards the field for spinels in BABB or E-MORB in this area. This suggests the involvement of both IAT and BABB or E-MORB-like magmas in the evolution of the andesites from station 108.

Incompatible element concentrations also support involvement of BABB in the evolution of station 108 andesites. Mixing with magmas similar to BABB sample 123 would not have much effect on any incompatible elements apart from lowering the LREE, as can indeed be seen when andesite 108/5 is compared with andesite GB29B which is otherwise very similar (Fig. 5.11b and 5.12c), but it may explain the variations in major elements seen in some of the melt inclusions, for example the high TiO_2/Al_2O_3 and TiO_2/CaO inclusions (Fig. 5.18). The more evolved BABB, e.g. sample 117/16, have TiO_2/Al_2O_3 up to 0.18 and TiO_2/CaO up to 0.23 (chapter 3), so some of the inclusions could be explained by mixing with similarly evolved BABB. In Figure 5.18 more inclusions plot in the field for boninitic glasses than in that for IAT but still the compositions of the homogenized inclusions are not

boninitic, though they show some boninitic affinities (e.g. high SiO_2 and low TiO_2). Some of these variations can be explained by clinopyroxene fractionation and mixing of evolved and primitive IAT melts, resulting in an increase in Al_2O_3 and a decrease in CaO.

Repeated mixing between evolved and primitive IAT and BABB magmas cannot explain all the variations observed and an additional component is needed to explain the range in K_2O contents in the melt inclusions (Fig 5.19). This component has not been identified in the course of this study but it is most likely to be a slab derived fluid.

5.6.3 The Hunter Ridge compared to adjacent areas

Monzier et al. (1993) showed that lavas from seamounts in the southernmost part of Vanuatu (their island arc basalt (IAB) group) differ from Hunter Ridge lavas (their high-Mg andesites (HMA) group) in both major and trace elements. Interestingly boninites, tholeiites and BABB from south of the Hunter Ridge show similarities to the IAB group in some trace element ratios, so the difference seen in these ratios in the Hunter Ridge samples is likely to be process rather than source related. In Figure 5.21 in which Y and Zr/Y are plotted against Zr, the more primitive magmas have similar Zr/Y. But the IAB group together with IAT and boninites, from south of the Hunter Ridge (Eggins, unpublished analyses), including rhyolitic compositions, as well as BABB from this area, define a clear grouping distinct from all the Hunter Ridge samples which have lower Y for a given Zr, and therefore higher Zr/Y. Andesite 108/5, like the andesite and basaltic andesite from stations 89 and 101, plot between the two groups which could indicate mixing of an evolving HMA magma suite with influx of BABB magma as suggested by melt inclusions and spinel compositions.

The IAB lavas from Monzier et al., (1993) and the IAT and boninites from south of the Hunter Ridge are tholeiitic according to the classification of Gill (1981), with plagioclase the dominant phenocryst phase whereas the Hunter Ridge lavas are calc-alkaline with olivine and clinopyroxene dominant as phenocryst phases. In Figure 5.21 three vectors show what effect repeated 20% plagioclase, 20% olivine and 20% clinopyroxene fractionation and then mixing of the remaining magma with 20% of the parental magma (with 15 ppm Y and 30 ppm Zr) would have on fractionating Y (and the HREE) from Zr (each arrow represents twelve fractionation and mixing cycles). Olivine and plagioclase fractionation and subsequent mixing has almost no effect on Zr/Y, whereas clinopyroxene fractionation is capable of effectively separating Y from Zr and thus increasing Zr/Y. Therefore the lower Y and HREE element concentration and the increase seen in the Zr/Y with increasing Zr can be explained by fractionation of clinopyroxene and frequent injections of new batches

of primitive magmas into the system, with subsequent mixing and continued clinopyroxene fractionation. Clinopyroxene fractionation can also cause the early increase of Zr/Y in the boninites and tholeiites from south of the Hunter Ridge before plagioclase takes over as the dominant crystallizing mineral in the more evolved samples. However, because of frequent magma injections and mixing occurring in the Hunter Ridge suite, clinopyroxene stays on the liquidus.

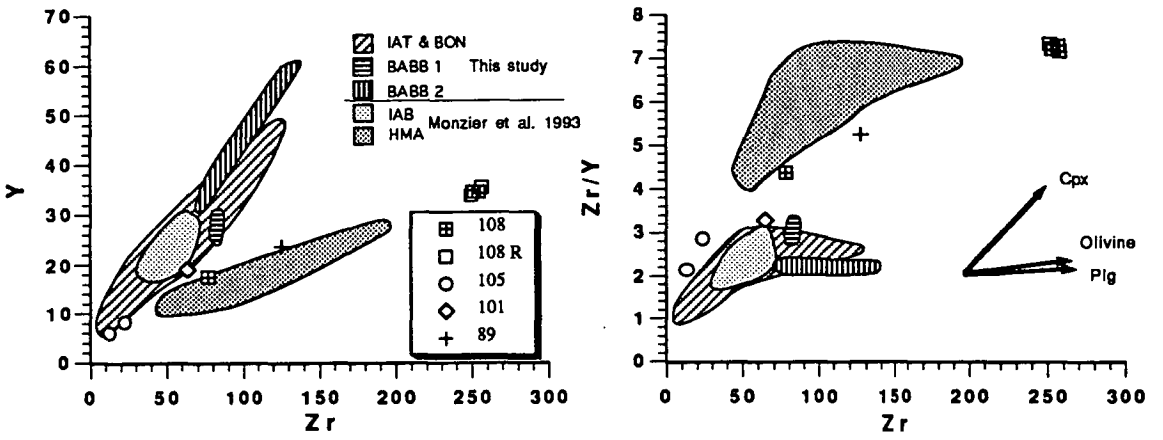

Figure 5.21: Y ppm and Zr/Y versus Zr ppm for analysed samples. Also shown are fields for island arc tholeiites and boninites from the fore arc south of the Hunter Ridge (Eggins, unpublished analyses), the island arc basalts (IAB) and high magnesian andesite (HMA) groups from Monzier et al., (1993) and back arc basin basalts from the North Fiji Basin (Chapter 4). The vectors show changes caused by repeated fractionation and mixing of new batch of primitive magma, 20% fractionation and then mixing of the remaining liquid, 80%, with 20% of the original liquid that contained 15 ppm Y and 30 ppm Zr. The vectors represent 12 such cycles. Partition coefficients were taken form Ewart and Hawkesworth (1987).

5.6.4 Relationship between the rhyolites and andesites at station 108

Fresh sodic rhyolites similar to the rhyolites at station 108 have been described from the Izu-Ogasawara arc and the Sumisu and Torishima back arc rifts (Ikeda and Yuasa, 1989; Fryer et al., 1990; Hochstaedter et al., 1990a, b). In Figure 5.22 major element compositions of these rhyolites are plotted against SiO_2 and in Figure 5.23 sample 108/4 is compared to sample 1880-10 from the Sumisu rift and sample D641 from the Shichito Ridge on a primitive mantle normalized incompatible element diagram. The station 108 rhyolites are almost identical to the back arc rift rhyolites in major elements but differ from the arc rhyolites by higher Al_2O_3, Na_2O and K_2O and lower FeO*, MgO and CaO for a given SiO_2. In incompatible trace elements, dredge 108 rhyolites have the same pattern as Sumisu Rift rhyolites 1880-10, and similar absolute concentrations except for slightly lower HREE. Sample D641 from Shichito Ridge, which has significantly lower SiO_2 content than the other samples, shows similar pattern but it does not show the strong titanium and phosphorous anomalies. Overall station 108 are more like the rhyolites from the back arc rifts than the arc rhyolites.

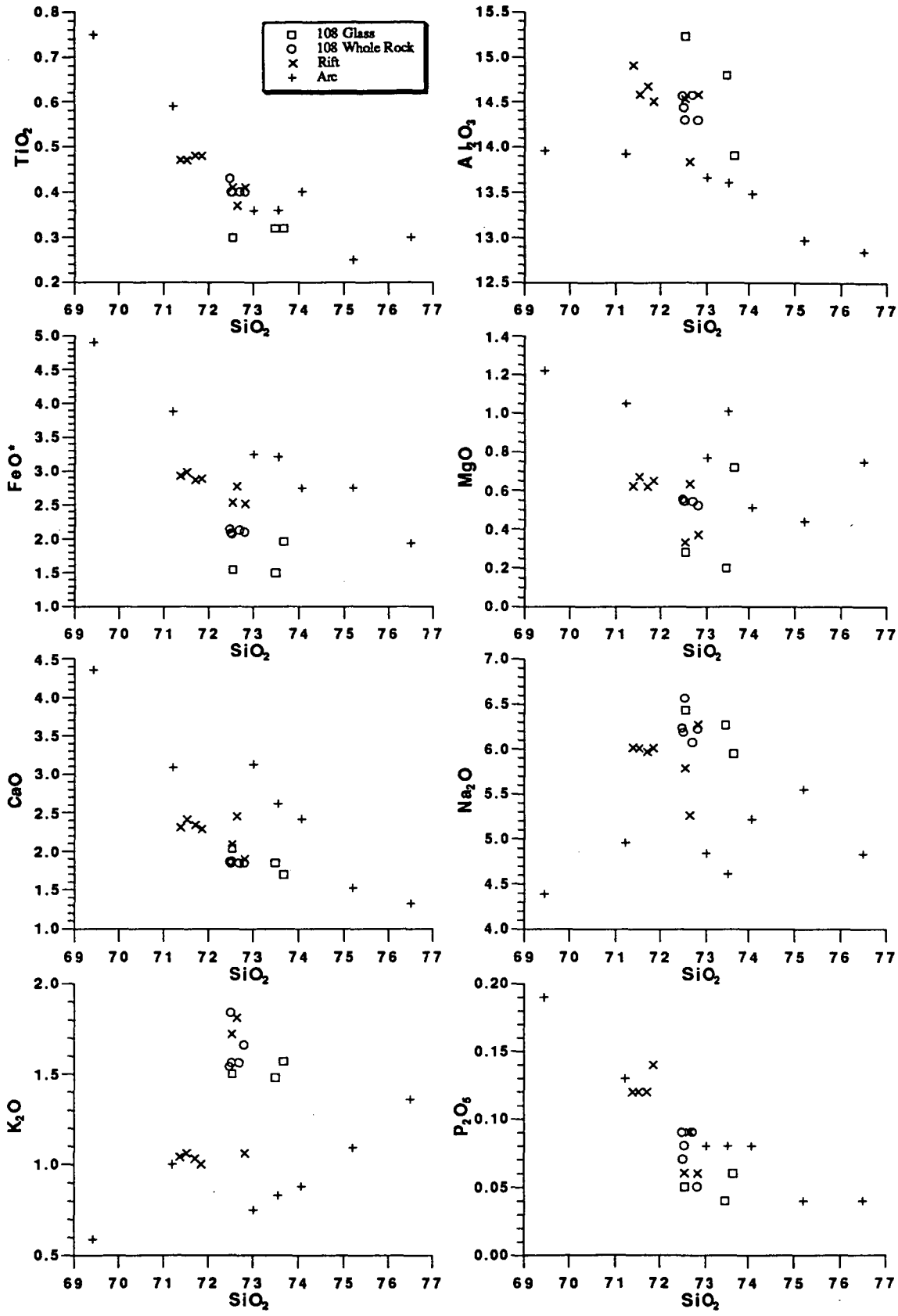

Figure 5.22: Whole -rock and glass major element compositions of the rhyolites from station 108 plotted together with rhyolites from the Shichito Ridge and the Sumisu and Torishima rifts.

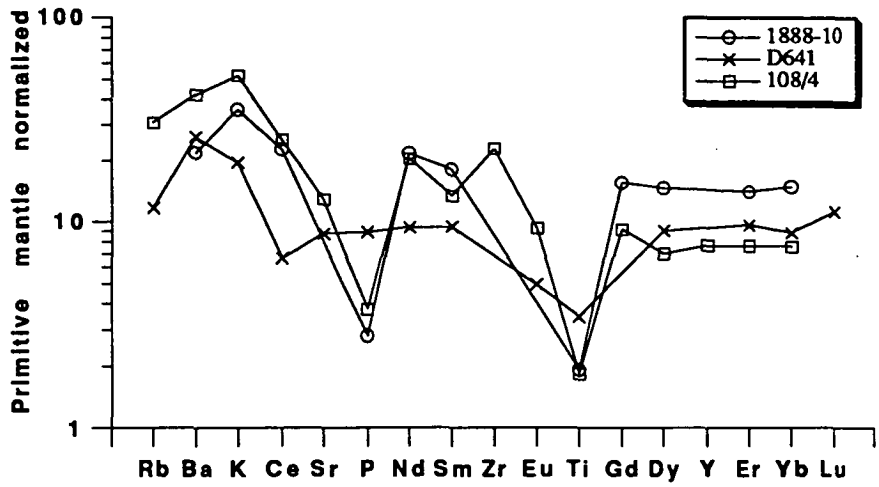

Figure 5.23: Primitive mantle normalized incompatible elements in sample rhyolite compared with rhyolites from the Sumisu rift and Shichito Ridge.

Least square calculations show that the rhyolites can be derived from the andesites by fractionation of olivine, clinopyroxene, plagioclase and magnetite (Table 5.4). Trace element modelling (Shaw, 1970) shows that the incompatible element concentration can be closely matched by using the mineral proportions from the least square calculations and partition coefficients from Ewart and Hawkesworth (1987). Sr is the only element that varies significantly (Figure 5.24), but that can be explained if the partition coefficient between plagioclase and melt is too low. The value given by Ewart and Hawkesworth (1987) is 1.2 whereas a compilation of values from the literature gives a range from 1.3-2.9 with an average of 1.8 (Henderson, 1982). It is therefore most likely that the rhyolites are derived from the dredge 108 andesites by crystal fractionation; this is also supported by Sr and Nd isotopes (Table 5.1) which are almost identical in the rhyolites and the andesites (S.M. Eggins, unpublished analyses).

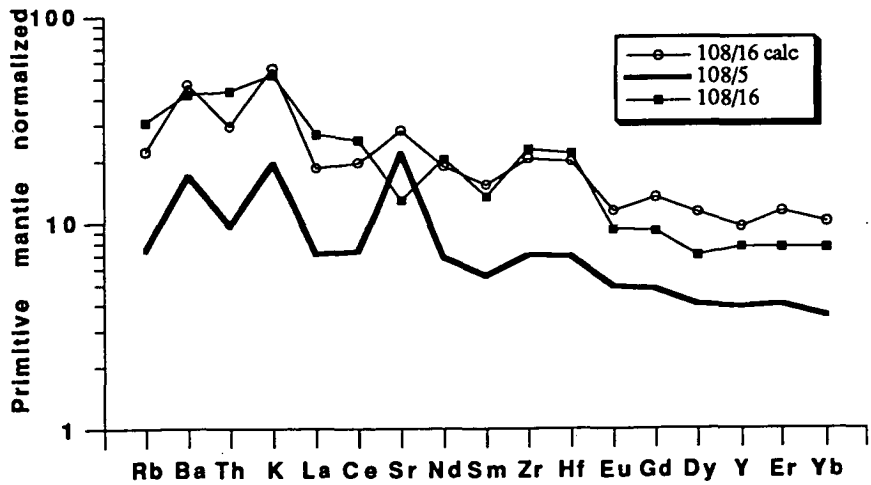

Figure 5.24: Calculated trace element composition (normalized to primitive mantle values of Sun and McDonough, 1989) of the rhyolites using the results from the least square calculations and partition coefficients from Ewart and Hawkesworth (1987).

Table 5.4: Results from least square calculations.

Reactants	%	SiO_2	TiO_2	Al_2O_3	FeO*	MgO	CaO	Na_2O	K_2O	P_2O_5	Sum
108/16	32.44	72.48	0.43	14.57	2.14	0.55	1.86	9.23	1.54	0.09	99.89
Olivine	5.86	39.87			15.40	44.19	0.19				99.65
Cpx	14.96	52.78	0.32	2.16	4.72	16.93	22.03	0.23			99.17
Plg	42.52	54.05		28.51	0.62	0.22	12.91	4.12	0.11		100.5
Mt	4.22	0.05	7.47	1.77	81.38	1.97					92.64
108/5	100	56.69	0.62	17.22	5.95	5.46	9.38	3.86	0.58	0.13	99.89
Reactants		56.73	0.50	17.25	6.00	5.48	9.40	3.81	0.55	0.03	
Product		56.69	0.62	17.22	5.95	5.46	9.38	3.86	0.58	0.13	99.89
Differences		0.04	-0.12	0.03	0.05	0.02	0.02	-0.05	-0.03	-0.10	
Residual Sum Squares			0.03								
Distance			0.18								

5.7 Conclusions

At the southern end of the New Hebrides island arc, in an area extending from Eva seamount to Hunter Island on the Hunter Ridge, a high magnesian andesite (HMA) suite has been described recently. HMA from Matthew and Hunter Islands are believed to have evolved by a combination of fractional crystallization and mixing of co-genetic mafic and more evolved magmas with some boninitic affinities (Monzier et al., 1993).

Detailed study of andesite lavas dredged close to a topographic depression, interpreted to be a spreading ridge linked to the back-arc spreading in the NFB that cuts through the Hunter Ridge, shows that these lavas have strong petrological and geochemical similarities to the HMA suite from the emergent volcanoes and seamounts further west on the Hunter Ridge. These station 108-andesites show clear evidence of magma mixing including both primitive (IAT and BABB) and fractionated melts. Repeated injections of primitive IAT magmas into an open magmatic system buffer the concentration of major elements that are compatible in the major fractionating phases (olivine and clinopyroxene) but cause significant variations in the more incompatible elements. BABB magmas supplied by the NFB spreading centre, that cuts through the Hunter Ridge in the vicinity of station 108, provided a further component that was involved in this mixing.

The most magnesian olivines ($Fo_{92.5}$) crystallized at 1350 °C from a melt containing 16.2% MgO and 0.54% TiO_2. This melt represents one possible endmember taking part in the evolution of station 108 andesites. Two olivine crystals Fo_{92} and $Fo_{92.4}$ crystallized at 1320-1325 °C from melts with approximately 14% MgO and 0.46 and 0.68% TiO_2, respectively. At temperatures around 1200 °C

melts with 8-10% MgO contain quite variable TiO_2, CaO, Na_2O, K_2O and P_2O_5 contents due to mixing between melts at different stages of evolution, increasing effects of clinopyroxene fractionation and the introduction of BABB into the magmatic system. Injection of a new magma batch probably occurred when the system contained approximately 8% MgO, as the greatest variations occur in melts with MgO content just above 8%. Mixing between cogenetic IAT melts and the addition of BABB magmas can explain most of the variations seen in the compositions of melt inclusions and phenocryst phases but an additional high-K component is needed to explain the large variations in K_2O in the melt inclusions. This component is most likely a slab-derived fluid.

Compositions of magmas erupted at the Hunter Ridge differ from magmas erupted north and south of the Ridge. This is likely to be caused by differences in magmatism as more frequent magma mixing at the Hunter Ridge buffers the magmas at compositions where clinopyroxene is a fractionating phase leading to a relative depletion in Y and the HREE compared to the more incompatible elements.

The sodic rhyolites are derived from the andesites by crystal fractionation.

Chapter 6

SOME CONSTRAINTS ON THE MGO CONTENT OF THE PRIMARY MELT FOR HIGH-MGO THOLEIITES FROM ICELAND

6.1 Introduction

Iceland is an oceanic plateau at the intersection of the Greenland-Faeroe Ridge and the Mid-Atlantic Ridge system. The Greenland-Faeroe Ridge is commonly interpreted as the productivity trail of the Iceland hotspot which at present is located approximately beneath the Grímsvötn area (Fig. 6.1). As the Mid-Atlantic Ridge system is moving WNW relative to the hotspot, the rift zone maintains its position over the hotspot by forming new spreading centres at its east margin (Oskarsson et al., 1985).

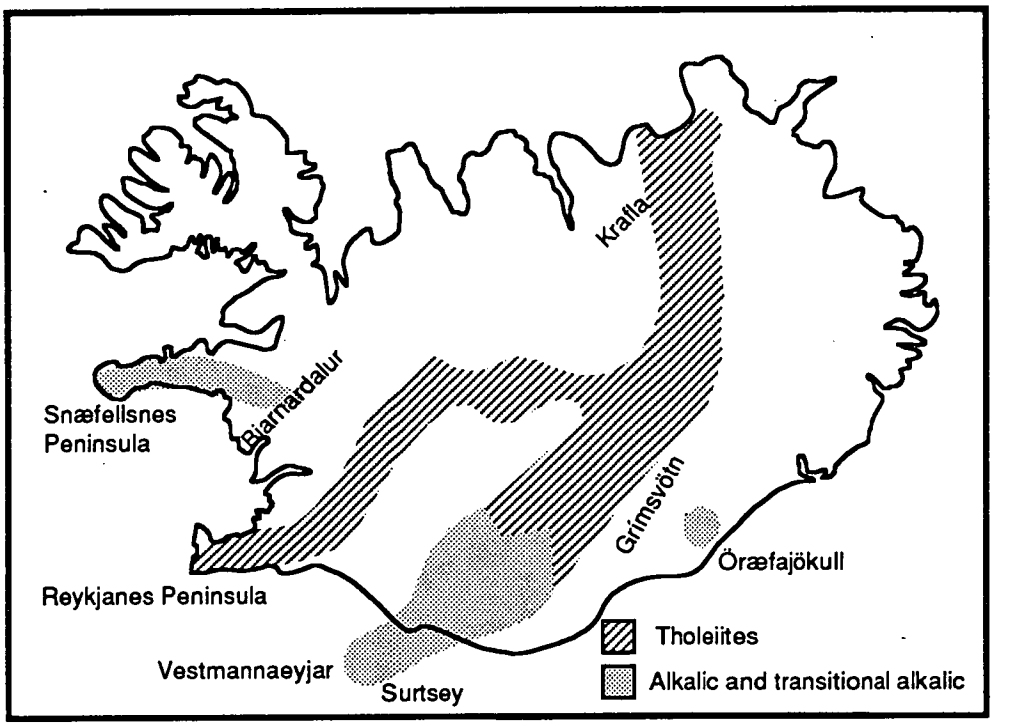

Figure 6.1: The active volcanic zones in Iceland and the distribution of tholeiitic and alkalic and transitional alkalic basalts. Modified from Jakobsson, 1979.

Jakobsson (1979) divided the active volcanic zones in Iceland (Figure 6.1) into volcanic systems, consisting of volcanic fissure swarms with or without a central volcano (Figure 6.2). Three main rock series occur in the volcanic zones, tholeiitic series, transitional alkalic series and alkalic series (Jakobsson, 1972). The tholeiites occur in the active rift zones, the onland continuation of the Mid-Atlantic spreading ridges (the Reykjanes and the Kolbeinsey Ridges), whereas the alkalic series is found off rift on the Snæfellsnes Peninsula, and in Vestmannaeyjar. The transitional alkalic

series occurs in the southern part of the Eastern Volcanic Zone (Figure 6.1) and the silicic Öræfajökull complex most likely belongs to this series as well (Jakobsson; 1979, Prestvik, 1979).

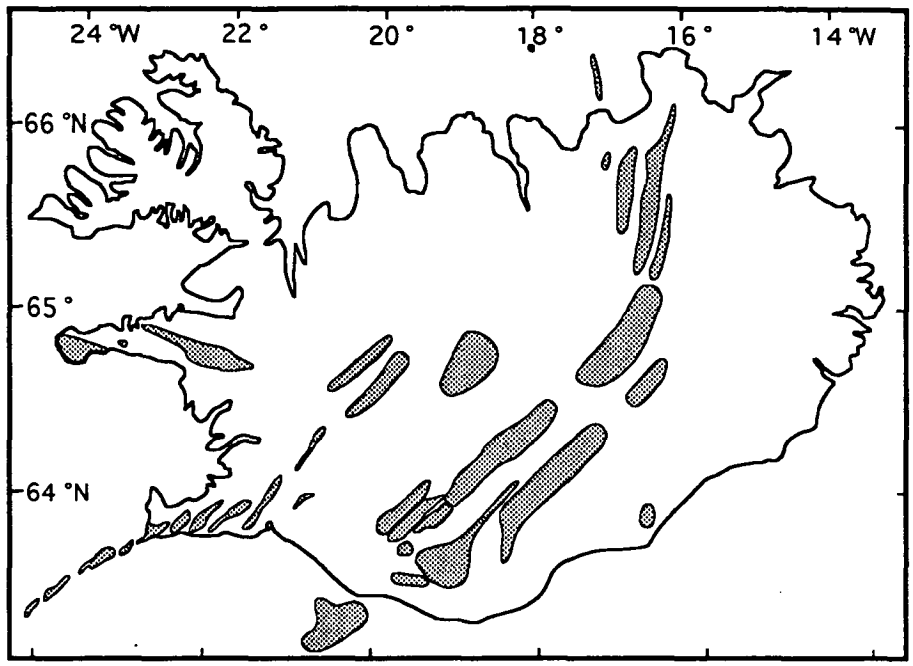

Figure 6.2: The active volcanic systems in Iceland. Modified from Jakobsson, 1979.

Several models have been proposed to explain the geochemical and isotopic variations in Icelandic basalts, which compared to N-MORB are enriched in incompatible trace elements, have higher $^{87}Sr/^{86}Sr$, lower $^{143}Nd/^{144}Nd$ and more radiogenic Pb (e.g. Hart et al., 1973; Sun and Jahn, 1975; O'Nions et al., 1977; Zindler et al., 1979; Hemond et al., 1993). Low $\delta^{18}O$ values of Icelandic tholeiites (Muehlenbachs et al., 1974) suggest interaction with meteoric water and this led to petrogenic models in which magmas from a homogeneous mantle interacted with hydrothermally altered crust to produce the entire spectrum of magma compositions in Iceland (Oskarsson et al., 1982; Steinthorsson et al., 1985; Hemond et al., 1988; Nicholson et al., 1991). However, more recent studies have shown that the range in isotopic compositions, especially Nd, is far greater than can be explained by interaction of magmas from an homogeneous source with hydrothermally altered crust (Hemond et al., 1993). Other models have suggested heterogeneous mantle beneath Iceland and/or interaction between a plume source and N-MORB source (e.g. Schilling, 1973; Hart et al., 1973; Langmuir et al., 1978; Zindler et al., 1979; Hemond et al., 1993).

The most magnesian tholeiites are also the most geochemically and isotopically depleted magmas occurring in Iceland. This was explained by Elliott et al., (1991)

using a dynamic melting model in which the more depleted tholeiites were generated as the last melt fraction at the top of a melting column. If melt is continuously extracted from the upwelling mantle and mixed to form a point and depth average (McKenzie and Bickle, 1988), this last melt fraction will be the most depleted if it can avoid mixing with the more enriched melts, generated at greater depths in the melting column (Elliott et al., 1991).

Maaløe and Jakobsson (1980), concluded based on experimental phase relations that Icelandic tholeiite RE 78 with 18% MgO was close to a primary magma, generated at 25 kbar pressure and 1580 °C from a garnet-bearing lherzolite. Hardardóttir (1986) also suggested that the parental liquid for Mælifell has approximately 18% MgO. However, a melt with such a high MgO, and Fe^{2+}/Fe^{3+} in the range 5-8, would crystallize olivine with compositions above Fo_{93} (Table 6.3), but the most magnesian olivine reported from Icelandic basalts to date is $Fo_{92.2}$ (Gurenko et al., 1988b).

In this study, olivine-phyric tholeiites from the Reykjanes Peninsula and the Krafla volcanic system were analysed for major and trace elements, and olivine phenocrysts and their spinel inclusions were analysed to establish the compositions of the most magnesian olivine phenocrysts occurring in each sample and to look for evidence for magma mixing. For comparison, olivines and spinels were also analysed for comparison in two alkaline basalts from Surtsey. Recent studies of melt inclusions in Icelandic samples are then reviewed and used together with compositions of the most magnesian olivine phenocrysts to estimate the MgO content of the primary magmas for the high-MgO tholeiites.

6.2 Samples selected for this study

The 14 basalts studied here were provided by Dr. S.P. Jakobsson, at the Icelandic Museum of Natural History; all the basalts are olivine-phyric except for HP-8 which is aphyric but contains numerous gabbroic xenoliths (Sigurdsson, 1989). Nine are from the Reykjanes Peninsula (RE prefix), two from the Krafla system (NO prefix), two from Surtsey (SU prefix) and one is from Bjarnardalur (1977 A:4). RE 78 was analysed previously for major elements by Jakobsson et al., (1978) and trace elements by Zindler et al., (1979) and it is the same composition as studied experimentally by Maaløe and Jakobsson (1980). Other basalts have not been analysed before, though in some cases analyses have been done on the same lava flow. The two alkaline olivine-basalts from Surtsey were not analysed as they were analysed recently by Furman et al., (1991) for trace elements and S.P. Jakobsson (unpublished) for major elements.

6.2.1 Petrography

The tholeiites from the Reykjanes Peninsula all contain olivine (< 10 mm) and Cr-spinel (<0.5 mm) phenocrysts but plagioclase phenocrysts (< 5 mm) occur only in RE 78 and RE 185. No clinopyroxene phenocrysts were observed in the thin sections. Cr-spinel occurs both as inclusions in olivine and in the groundmass. Some of the plagioclase phenocrysts in both RE 78 and RE 185 contain irregular, devitrified glass inclusions. The glass inclusions in olivines are partly crystalline and usually rounded in shape. The groundmass usually consist of an ophitic or subophitic intergrowth of plagioclase laths and clinopyroxene with interstitial magnetite. Minor deuteric alteration can be seen in olivines and in the groundmass of RE 36 and RE 217, other basalts are completely fresh.

NO 42 and NO 58 from the Krafla volcanic system are olivine- and plagioclase-phyric with Cr-spinel occurring as inclusions in olivine, as well as discrete phenocrysts. A few dark-green pyroxenes (xenocrysts?) occur in NO 42, as well as small gabbroic xenoliths, consisting of olivine, clinopyroxene and plagioclase. The groundmass is as for the Reykjanes Peninsula samples. Both samples are fresh.

The alkaline basalts, SU 18II and SU 24, from Surtsey contain olivine and plagioclase phenocrysts. Cr-spinel occurs as inclusions in olivines and in the groundmass. The texture is intergranular and quite distinct from the tholeiitic lavas.

Sample 1977:A4 from Bjarnardalur is an olivine accumulate, with interstitial patches of plagioclase sub-ophitically enclosed by clinopyroxene and interstitial magnetite. The olivines often contain magnetite inclusions. No Cr-spinels were observed in this sample.

6. 3 Geochemistry

6.3.1 Major elements

The geochemistry of tholeiites from Iceland has been the focus of studies by numerous workers in the last twenty years or so (e.g. Sigvaldason, 1974; Sun et al., 1975; Jakobsson et al., 1978; Zindler et al., 1979; Wood et al., 1979; Wood, 1981; Oskarsson et al., 1982; Meyer et al., 1985; Steinthorsson et al., 1985; Elliott et al., 1991; Hemond et al., 1993). New whole-rock major element compositions of the studied tholeiites are presented in Table 6.1 and Figure 6.3. Also shown in Figure 6.3 for comparison are analyses from Elliott et al., (1991) from Theistareykir and Reykjanes Peninsula, Jakobsson et al., (1978) from Reykjanes Peninsula and the two analyses of the alkaline basalts from Surtsey, (S.P. Jakobsson, unpublished).

1977:A4 from Bjarnardalur is not shown here as it is obviously olivine accumulate (Table 6.1), with over 22 % MgO and very low Al_2O_3 (8%) and CaO (7%).

Table 6.1: Major and trace element compositions of the analysed basalts. All elements were analysed by XRF, except REE, Th and Hf by INAA.

Sample	NO 42	NO 58	RE 36	RE 78	RE 120	RE 154	RE 185	RE 217	RE 286	RE 291	HP-8	1977 A:4
SiO_2	48.33	48.86	47.6	45.92	46.68	47.6	46.9	47.66	46.94	46.99	48.48	43.52
TiO_2	0.63	0.71	0.45	0.37	0.4	0.51	0.33	0.51	1.45	0.4	0.75	1.25
Al_2O_3	14.78	15.51	14.27	13.57	12.04	15.55	15.32	15.38	14.45	13.62	15.04	7.89
Fe_2O_3	10.07	10.41	9.07	9.43	9.82	9.16	8.89	9.28	12.95	9.25	10.83	15.92
MnO	0.16	0.17	0.14	0.14	0.16	0.15	0.14	0.15	0.19	0.14	0.17	0.22
MgO	12.21	10.49	14.41	18.82	19.23	13.02	15.1	13.45	11.44	17.55	10.86	22.26
CaO	13.01	12.7	12.99	10.89	10.86	12.9	12.47	12.72	11.17	11.64	12.92	7.1
Na_2O	1.63	1.82	1.42	1.35	1.13	1.59	1.17	1.58	1.94	1.26	1.58	1.29
K_2O	0.06	0.08	0.01	0.01	0.02	0.02	0.01	0.02	0.15	0.01	0.06	0.19
P_2O_5	0.07	0.07	0.04	0.03	0.04	0.05	0.04	0.05	0.14	0.04	0.08	0.13
LOI	-0.60	-0.62	-0.32	-0.52	-0.57	-0.44	-0.24	-0.54	-0.52	-0.42	-0.44	0.63
Sum	100.35	100.20	100.08	100.01	99.81	100.11	100.13	100.26	100.30	100.48	100.33	100.40
Trace elements ppm												
Rb	1	2	<1	<1	1	<1	<1	1	3	1	1	4
Ba	15.5	24.5	4	4	8	6	4.5	7	45.5	3	18	49
Sr	87.5	115.5	44	56	36.3	62	42	61.5	160.5	52.5	72	126
La	1.2	1.89		0.28		0.57		0.7	5.05	0.45		
Ce	3.52	5.85		1.74		2.77		2.18	13.9	1.27		
Nd	3.11	4.65		1.99		3.28		2.7	9.69	1.38		
Sm	1.24	1.52		0.78		1.07		1.12	2.82	0.72		
Eu	0.54	0.69		0.22		0.37		0.44	1.01	0.26		
Tb	0.36	0.4		0.21		0.31		0.32	0.57	0.19		
Ho	0.55	0.57		0.33		0.49		0.51	0.82	0.29		
Yb	1.37	1.62		1.21		1.73		1.73	2.16	1.14		
Lu	0.21	0.23		0.21		0.29		0.29	0.31	0.21		
Y	15.2	15.1	13.9	11.9	11.5	15.4	9.9	16.5	21.8	11	17.8	16.9
Th	<0.2	0.4		<0.2		0.2		0.64	<0.2	<0.2		
Zr	26	30.5	14.7	10.5	14	17	11	17.5	65	13.5	36	65
Hf									1.74			
Nb	1.3	2.2	1.2	0.8	1.6	0.75	0.9	1.1	7.5	1.2	3.4	8.1
Sc	42.9	42.4	38.3	33.4	35.9	39.6	33	41.6	38.1	34	42.1	27.3
V	231.7	242	195.8	161.9	200.2	210.9	179.2	213	296.7	164.6	256.3	209.2
Cr	645.4	390.5	1681	1575	1890	875.6	1395	922.9	520.4	1615	630.8	539.9
Ni	274	187	411	593	755	352	461	379	267	621	217	667

The Reykjanes Peninsula tholeiites have MgO from 19-11% and are among the most magnesian analysed from that area. RE 286 differs from all other analysed tholeiites by its lower SiO_2 and CaO and higher TiO_2, FeO*, Na_2O, K_2O and P_2O_5 indicating a transitionsl alkaline affinity for this sample. The two samples from the Krafla volcanic system have 10.5 and 12.2% MgO and are similar in all major elements to the tholeiites from Reykjanes Peninsula.

The general trends indicate olivine control down to approximately 11% Mgo where plagioclase joins the liquidus, followed shortly after by clinopyroxene. RE 286 is clearly distinct from other tholeiites and cannot be related to the more magnesian tholeiites by removal of olivine or plagioclase.

6.3.2 Trace elements

All samples were analysed for ten trace elements by XRF and seven samples were analysed for REE, Th and Hf by INAA (Table 6.1). On a N-MORB normalized element variation diagram (Figure 6.4) NO 42 and NO 58 have lower levels than N-MORB due to higher MgO content but have broadly similar patterns apart from

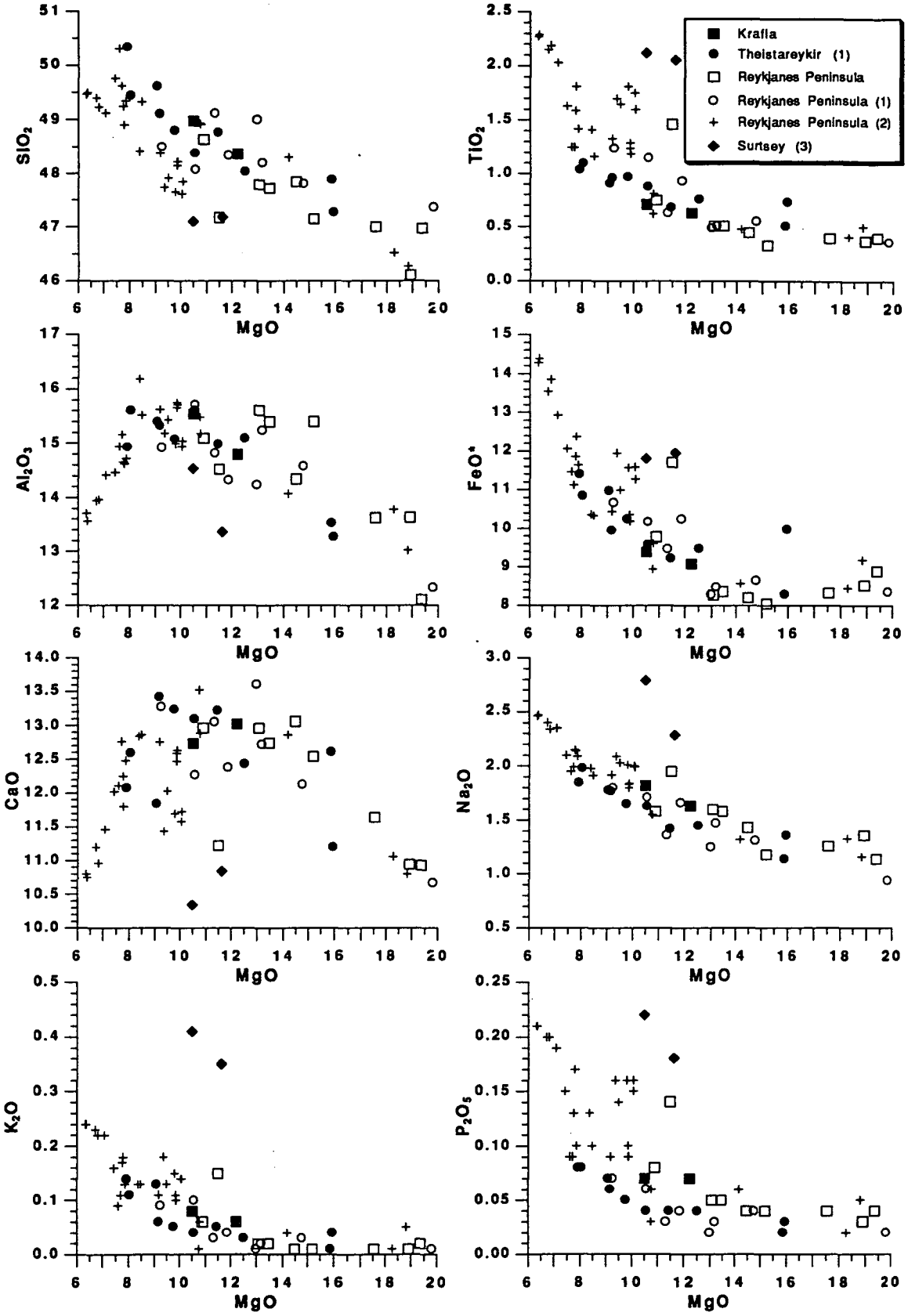

Figure 6.3: MgO variation diagrams for the tholeiites from Iceland. The two alkaline basalts from Surtsey (S.P. Jakobsson, unpublished) are shown for comparison. Additional data from Reykjanes and Theistareykir come from (1) Elliott et al., (1991) and (2) Jakobsson et al., (1978).

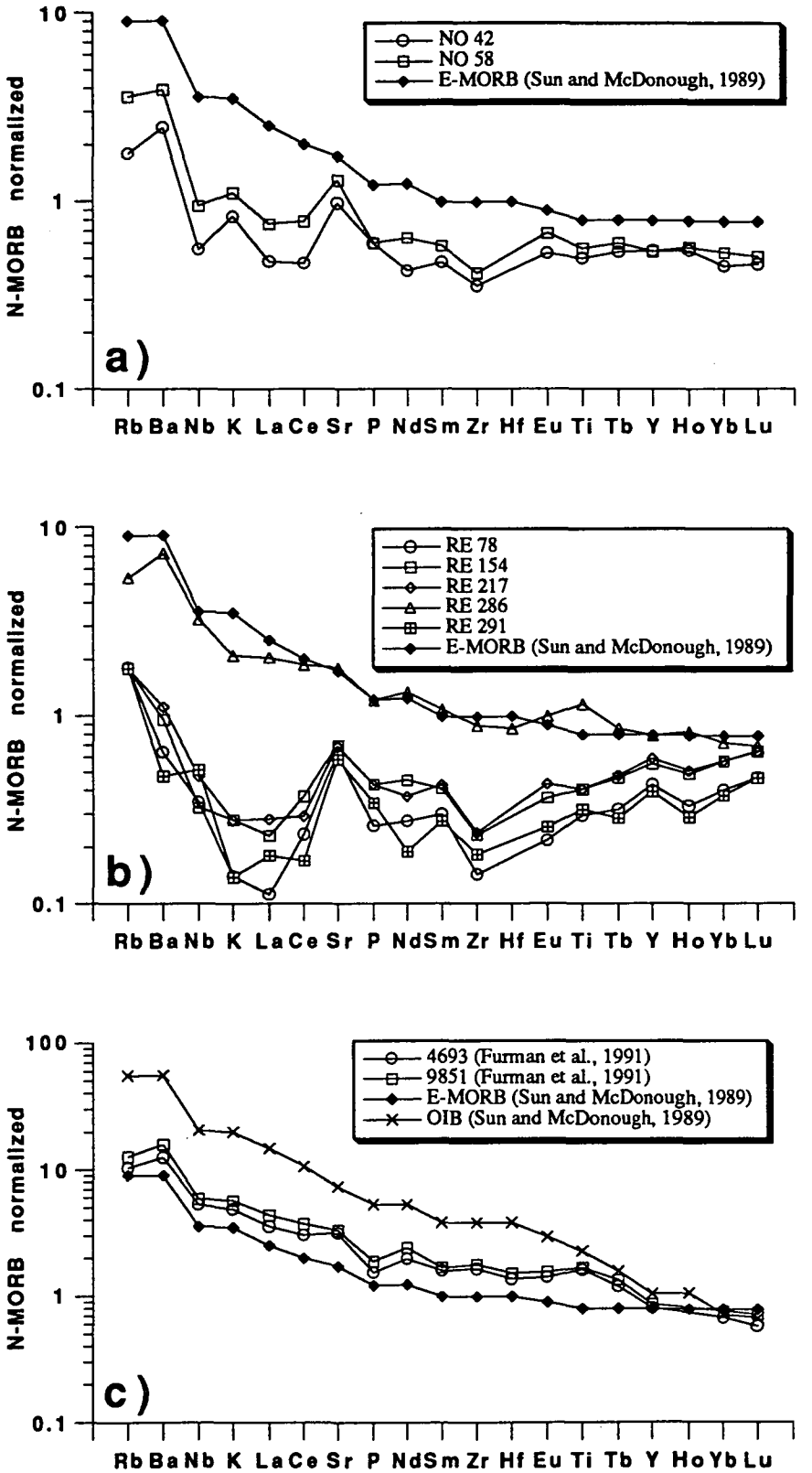

Figure 6.4: N-MORB normalized element diagrams for the Krafla tholeiites (a) and Reykjanes Peninsula tholeiites (b). c) The two samples from Surtsey (Furman et al., 1991; K, P and Ti from S.P. Jakobsson (unpublished)). Normalizing values and E-MORB and OIB compositions are taken from Sun and McDonough, (1989).

enrichment in K, Sr, Ba and Rb (Fig. 6.4a). RE 286 shows enrichment in all incompatible elements relative to N-MORB and is almost identical to an average E-MORB (Sun and McDonough, 1989). All other Reykjanes Peninsula tholeiites show strong depletion, compared to N-MORB, in almost all the incompatible elements. However they have a positive Sr spike, and relative enrichment in Rb, Ba, Nb and K (Fig. 6.4b). The two samples from Surtsey (Furman et al., 1991) show enriched patterns intermediate between E-MORB and OIB (Fig. 6.4c).

Relative enrichment in Rb, Ba and Sr is characteristic of the most primitive tholeiites in Iceland and this has been explained by contamination from hydrothermally altered crust (Hemond et al., 1993). This contamination is thought to affect all Icelandic lavas but it is most clearly visible in the most magnesian tholeiites, as they have the lowest concentration of these and adjacent elements of similar incompatibility (Hemond et al., 1993).

6.4 Olivine and spinel compositions

6.4.1 Forsterite content of olivine

Olivines were hand picked from each sample and analysed with an electron microprobe. Spinel inclusions were analysed wherever they were exposed on the surface. In Figure 6.5 the compositional range of olivine in each sample is shown as series of histograms, together with olivine compositions calculated to be in equilibrium with the whole-rock compositions using the model of Ford et al., (1983) and Fe2+/Fe3+ as calulated from Fe2+/Fe3+ in Cr-spinels (Table 6.1) using the model of Maurel and Maurel, 1982a).

The most magnesian olivines previously reported from Icelandic lavas come from Mælifell in the Hengill volcanic system ($Fo_{91.7}$, Hansteen, 1991) and from a lava flow 30 km north of Lúdent in the Krafla system ($Fo_{92.2}$, Gurenko et al., 1988b). Olivine microphenocrysts as magnesian as $Fo_{98.8}$ were reported from Kolbeinsey, north of Iceland, but they were found to occur in a highly oxidised lava with $Fe_2O_3/FeO = 23.6$ (Sigurdsson and Brown, 1970). The most magnesian olivines ($Fo_{92.5}$) found during this study come from sample NO 42 from Randahraun (Fig 6.5i), which almost certainly is the same lava flow as that studied by Gurenko et al. (1988b). The most magnesian olivines found in samples from the Reykjanes Peninsula during this study come from RE 120 (Fig. 6.5c) and have compositions of $Fo_{91.6}$. RE 286, which is the only incompatible element-enriched sample from Reykjanes Peninsula studied here, has no olivine phenocrysts more magnesian than $Fo_{84.6}$ (Fig. 6.5g). The alkaline samples from Surtsey (Fig. 6.5k, l) have olivines up to $Fo_{86.1}$.

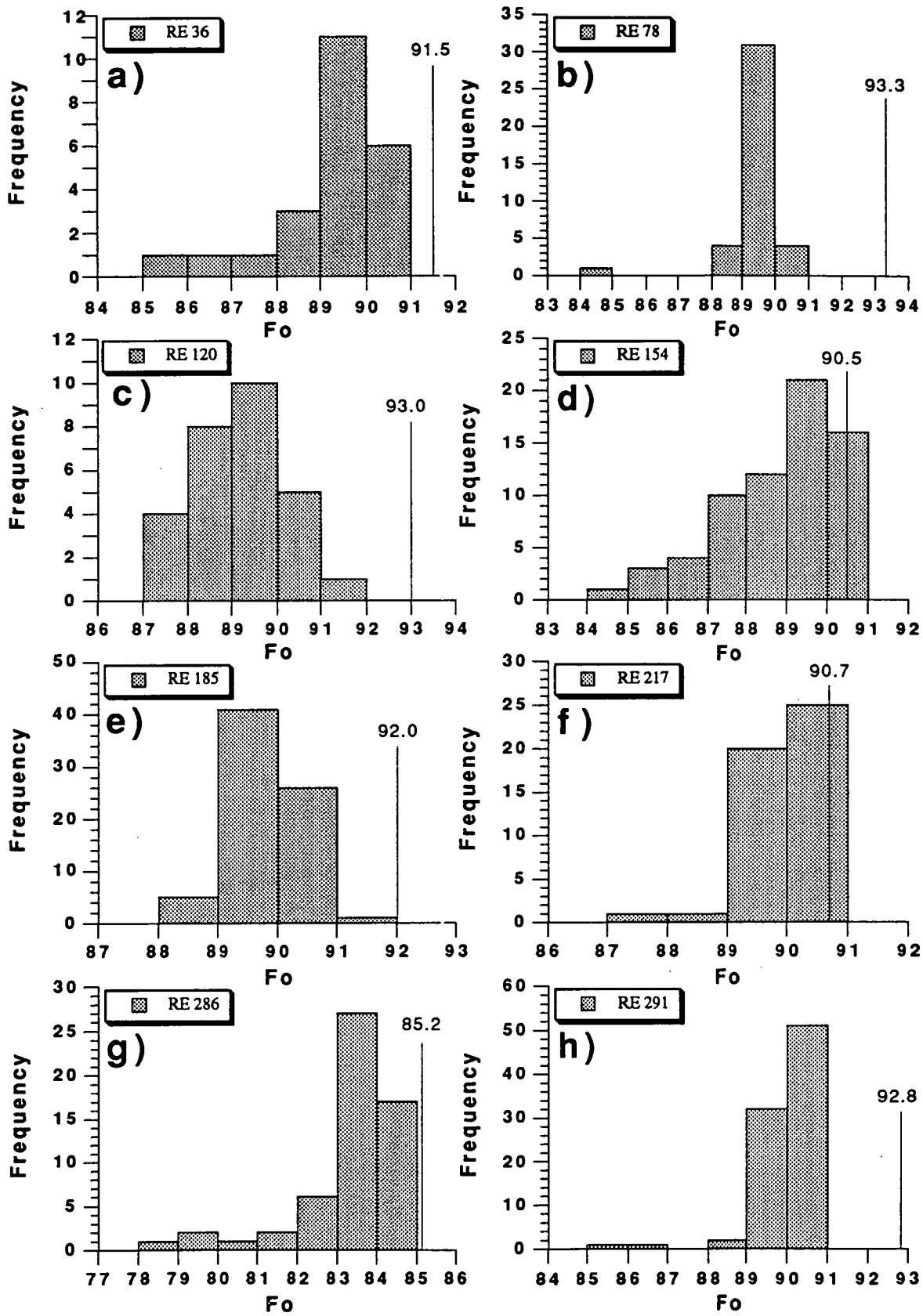

Figure 6.5: Histograms showing olivine compositions in the analysed basalts and the xenolith from NO 42. The lines and numbers in each histogram indicate calculated Fo value (Ford et al., 1983) for olivine in equilibrium with the whole-rock composition.

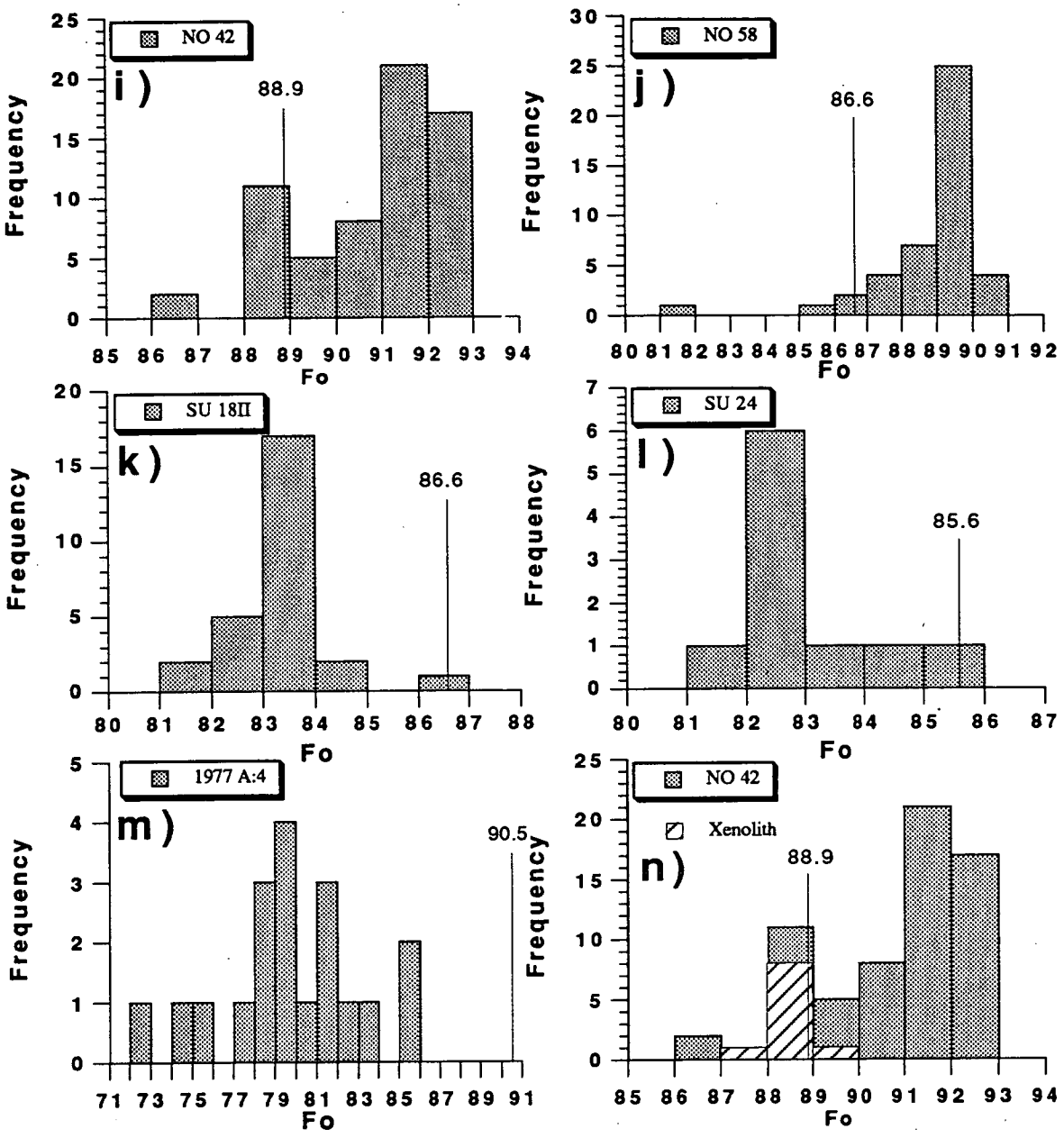

Figure 6.5 continued:

If actual Fo contents of olivines are compared to the calculated Fo value predicted from the whole rock compositions (Fig. 6.5 and Fig. 6.6), calculated equilibrium olivines for 1977 A:4, RE 78, RE 120 and RE 291 are considerably more magnesian than the most magnesian olivine found in these samples. This strongly suggests that these samples have accumulated some olivine and that their compositions, with 17.6 - 22% MgO, do not represent true liquid composition. Calculated liquidus olivine for other samples from Reykjanes Peninsula (MgO = 11.4 - 15.1%) are equal to or less than one Fo unit higher than the most magnesian olivine found in these samples. NO

42 and NO 58, on the other hand, contain olivines that are more magnesian (~ 4 Fo units) than the calculated liquidus olivine.

Calculated equilibrium olivine (Ford et al., 1983) for both NO 42 and NO 58 is 3-4 Fo units lower than olivines occurring in these samples. This indicates either that the most magnesian olivines are xenocrysts or that these samples have lost some of their phenocrysts.

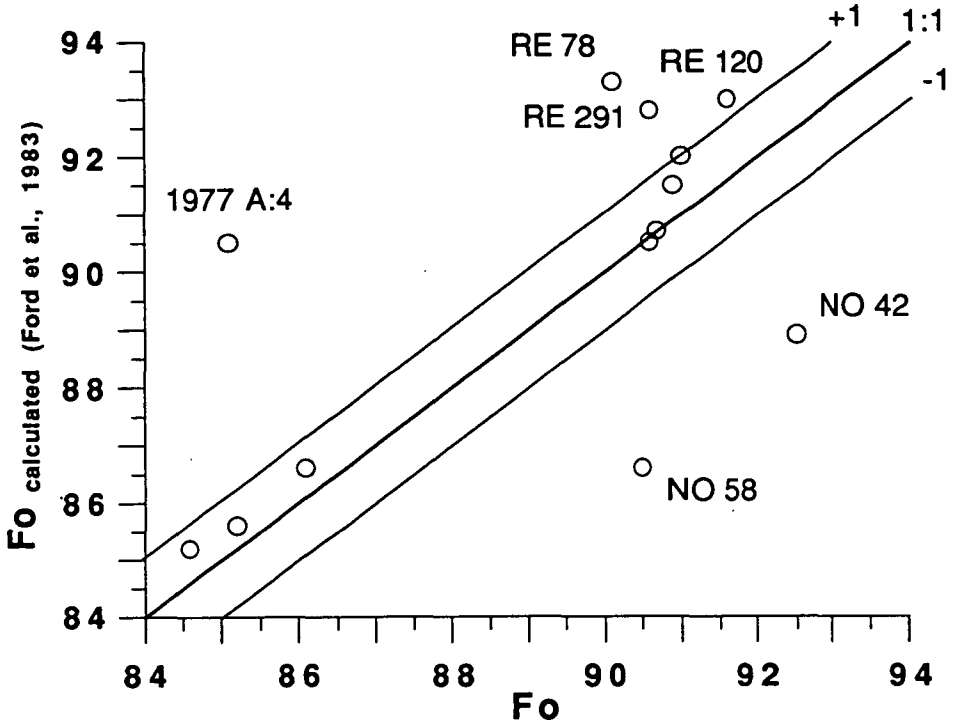

Figure 6.6: Comparison between the Fo value of the most magnesian olivine occurring in each sample and the calculated Fo value (Ford et al., 1983) of olivine in equilibrium with the whole-rock composition.

6.4.2 Cr_2O_3, MnO, CaO and NiO in olivine

The minor elements in olivine phenocrysts were analysed carefully with the electron microprobe, using long counting times and a high beam current (Appendix 5).

The Cr_2O_3 content in olivine decreases systematically with decreasing Fo content in most samples (Fig. 6.7a-c). For example in SU18II Cr_2O_3 falls from 0.07-0.03 in olivines Fo_{87-83} and from 0.15-0.06 for $Fo_{92-88.5}$ in RE 120.NO 42 has the highest Cr_2O_3 (0.20%) in $Fo_{92.5}$, and in Fo88 Cr_2O_3 is 0.02%. There is a distinct break in the Cr_2O_3 in NO 42 at Fo_{90}, with less forsteritic olivines having $Cr_2O_3 < 0.08$ and all but one olivine > Fo90 with $Cr_2O_3 > 0.12$.

MnO increases steadily with decreasing Fo (Fig. 6.7d-f). All tholeiitic samples have similar MnO for a given Fo content whereas the trend for the alkalic SU18II is at approximately 0.03% lower MnO for a given Fo.

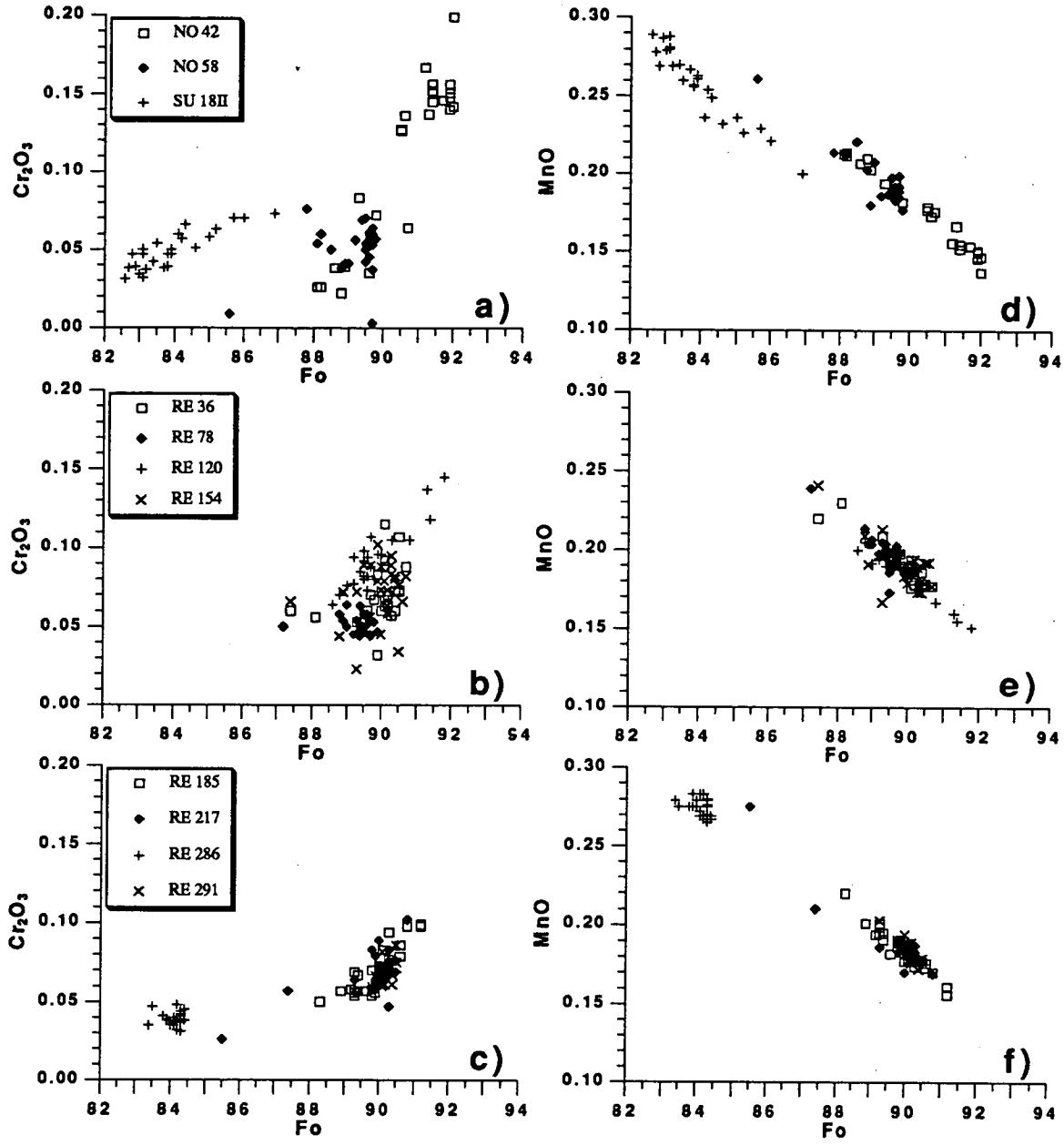

Figure 6.7: The minor elements in olivine plotted against the Fo content.

CaO is constant or increases slightly with decreasing Fo in most samples (Fig. 6.7g-i). There appear to be two groups of olivine with slightly different CaO in NO 42 and few olivines fall away from the main groups in RE 36 and RE 154. Although RE 36 and RE 154 have almost identical CaO and SiO2 contents, which are believed to have the greatest influence on CaO in olivine (Jurewicz and Watson, 1988; Stormer 1973), CaO in olivine is about 0.05% higher in RE 36 for the same Fo content.

NiO decreases with decreasing Fo (Fig. 6.7j-l) but the slope is different between individual samples. For example NiO decreases more rapidly in RE 185 than in RE 217. In NO 42 and RE 36 NiO shows more variation for a given Fo than in any other samples.

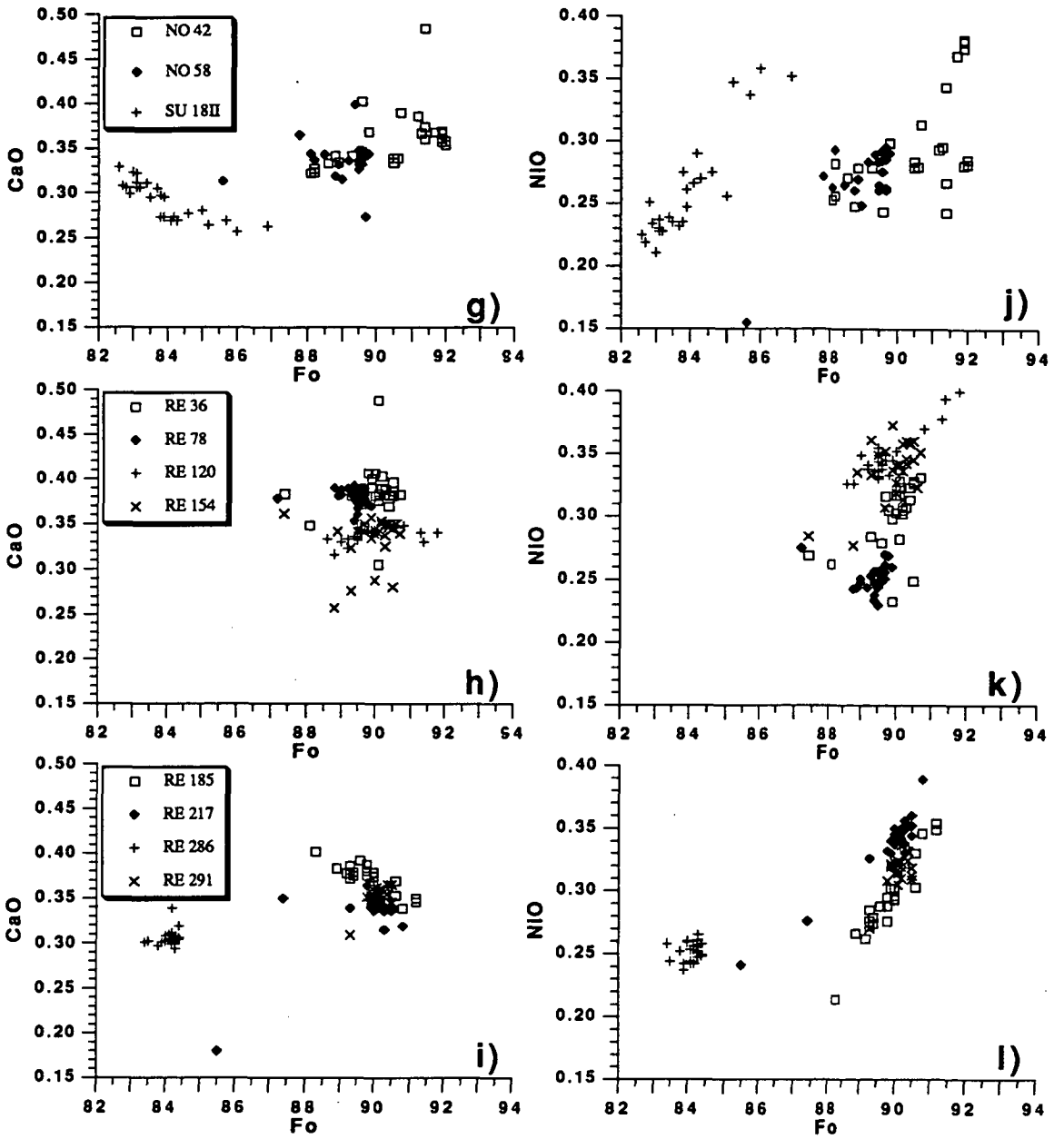

Figure 6.7 continued:

6.4.3 Spinel compositions and olivine and spinel relations

Between twenty and one hundred Cr-spinel inclusions were analysed in olivine phenocrysts from each sample, except for 1977 A:4 in which only magnetite inclusions occur in olivines. The olivine and Cr-spinel compositions are shown in Figure 6.8 and listed in Appendix 4.

Most Cr-spinels in the Reykjanes Peninsula samples and NO 58 have Al_2O_3 between 20 and 40% and TiO_2 between 0.1 and 0.5%, with TiO_2 rising with decreasing Al_2O_3 (Fig. 6.8a-c). Cr-spinels in RE 286 have significantly higher TiO_2

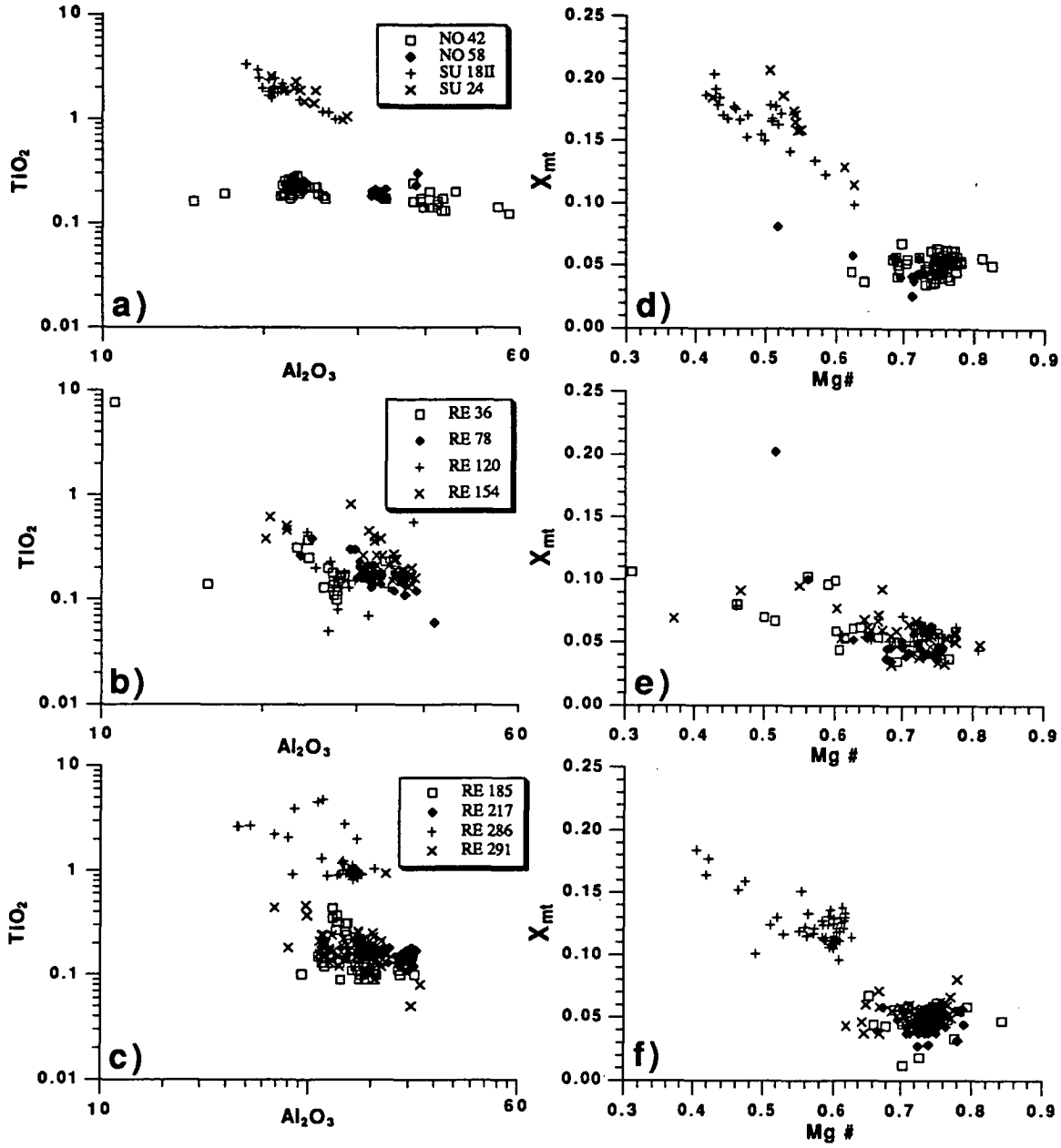

Figure 6.8: Compositions of spinels and relations between olivine phenocrysts and their spinel inclusions.

(1-8%) as do the cr-spinels in the alkaline samples from Surtsey. Cr-spinels in NO 42 show the greatest range in Al_2O_3 (15-57%) but TiO_2 is fairly constant (0.1-0.3).

$Mg^{\#}$ in the majority of cr-spinels in the Reykjanes Peninsula is between 0.8 and 0.6 and over this interval the magnetite component (X_{mt}) is in the range 0.03-0.07. Few cr-spinels, mostly from RE 36 and RE 154, have $Mg^{\#}$ lower than 0.6 and X_{mt} as high as 0.11. Cr-spinels in RE 286 and the Surtsey samples have Mg# from 0.64-0.4 and over this interval X_{mt} increases from 0.10-0.20 (Fig. 6.8d-f). The $cr^{\#}$ for all samples except NO 42 generally increases slightly with decreasing $Mg^{\#}$ and is in the range 0.35-0.55 (Fig. 6.8g-i). The Cr-spinels in NO 42 can be split into two groups based

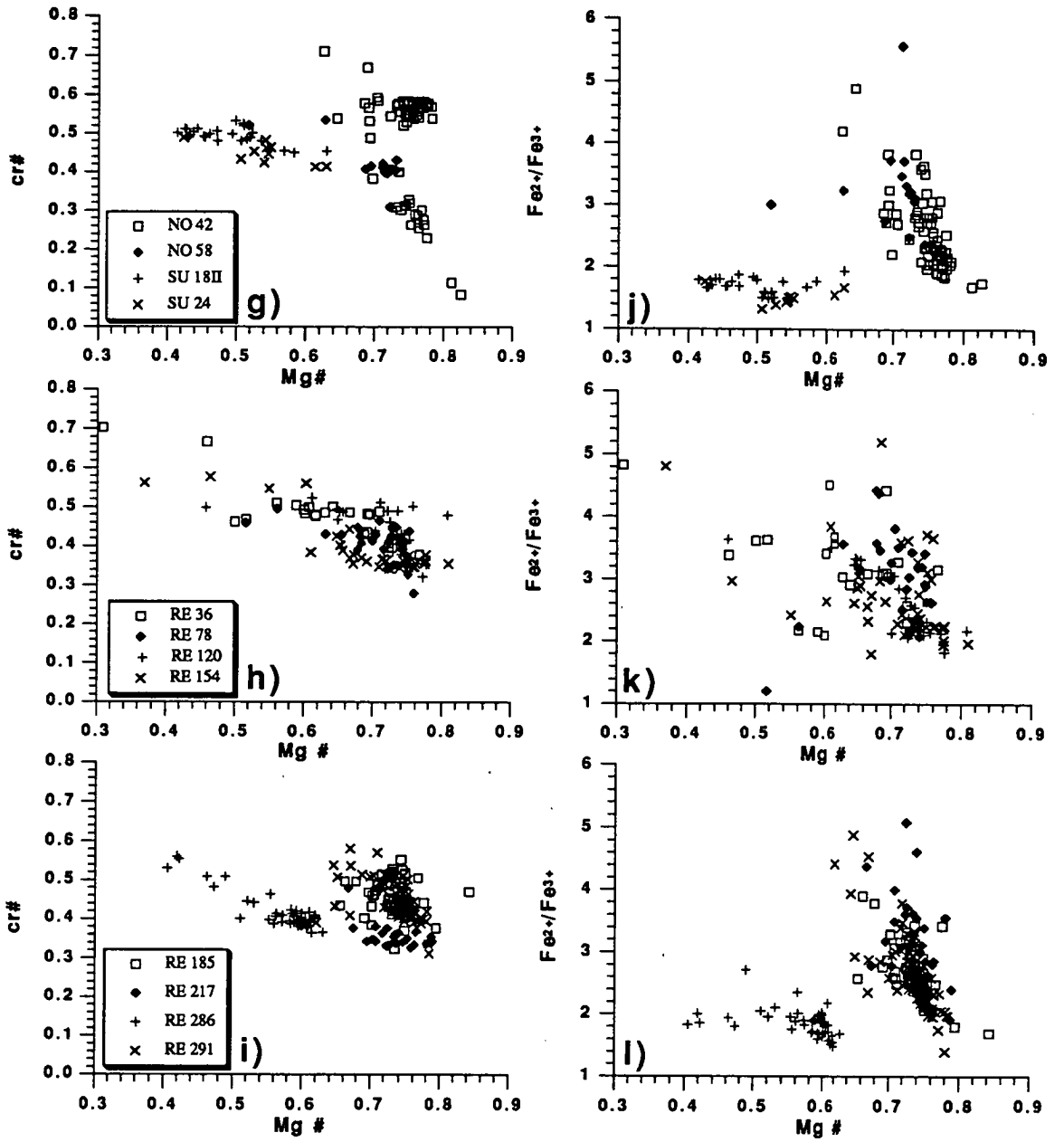

Figure 6.8 continued:

on their cr#. One group has cr# 0.5-0.6 at Mg# 0.8-0.65 whereas the other group has Mg# 0.84-0.70 and over this interval cr# increases from 0.08-0.40 (Fig. 6.8g). Fe^{2+}/Fe^{3+} is lowest in RE 286 and the alkaline samples (1.4-2), but it is quite variable in all the other samples but mostly between 2 and 4. No clear trend can be seen in Figure 6.8j-l, but if anything Fe^{2+}/Fe^{3+} increases with decreasing Mg#.

Mg# of Cr-spinel decreases with decreasing Fo content of the host olivine except for NO 42 where Mg# does not appear to have any correlation with the Fo content of the host olivine (Fig. 6.8m-o). This is because the high Al_2O_3, low cr# spinels which occur in olivines <Fo90 have the same Mg# as the spinels with the high cr#.

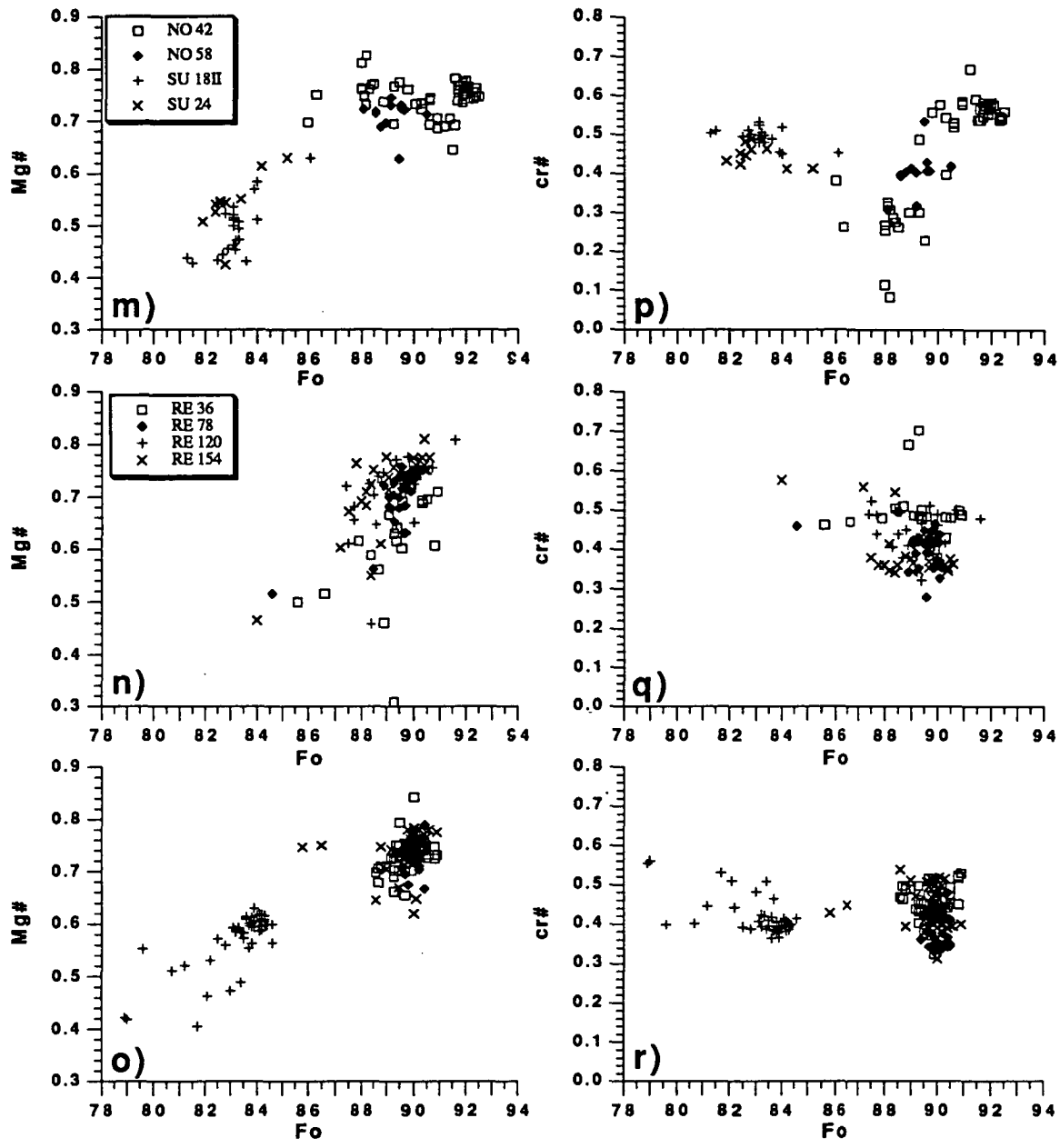

Figure 6.8 continued:

The $cr^{\#}$ values show no clear correlation with Fo content of the host olivine, except for NO 42, in which the Cr-spinels with the lowest $cr^{\#}$ occur in low Fo olivines but are absent from olivines more magnesian than Fo_{90} (Fig. 6.8p-r).

In summary, Cr-spinels in the alkaline Surtsey samples and in enriched tholeiite RE 286 differ from Cr-spinels in all other tholeiitic samples by their higher TiO_2 and X_{mt}, and lower $Mg^{\#}$ and Fe^{2+}/Fe^{3+}. The host olivines for these cr-spinels are also less magnesian than in any other samples (< Fo_{86}). NO 42 contains two populations of cr-spinels, one with Al_2O_3 from 15-26% and another with Al_2O_3 from 32-57%. The more Al_2O_3 spinels are restricted to olivines < Fo_{90}.

The Cr-spinels in the Reykjanes Peninsula tholeiites form a tight compositional groups for each sample, with those in the incompatible element-enriched RE 286 plotting clearly away from cr-spinels in the depleted samples. Significantly, there is no evidence for the more depleted tholeiites entraining spinels (or olivines, though olivines may be more susceptible to re-equilibration) from the more enriched tholeiites. Similarly, RE 286 does not contain any spinels from the more depleted samples even though all these samples occur in close proximity to each other. Most spinels in the Reykjanes Peninsula samples have almost constant $cr^{\#}$ with a decrease in $Mg^{\#}$, the $cr^{\#}$ though increases in both RE 185 and RE 291 and starts to increase at $Mg^{\#} = 0.55$ in RE 286 suggesting plagioclase crystallization together with olivine and spinel in these samples. Plagioclase does occur as phenocrysts in RE 185 but no phenocrysts were seen in the thin sections from either RE 186 or RE 291.

Table 6.2: Comparison between clinopyroxene and plagioclase in NO 42 and the xenolith in NO 42.

Clinopyroxene in the lava:					Clinopyroxene in the xenolith:					
Number	2	3	4	6	20	1	5	6	7	16
SiO_2	51.46	52.94	51.23	51.11	51.70	51.32	51.96	50.83	50.93	51.23
TiO2	0.17	0.10	0.18	0.17	0.16	0.16	0.13	0.18	0.19	0.19
Al_2O_2	6.11	4.74	6.14	6.10	5.70	4.66	3.77	4.80	5.23	4.72
Cr_2O_2	1.24	0.64	1.27	1.33	1.00	0.54	0.39	0.43	0.50	0.40
FeO*	3.87	3.45	3.80	3.93	3.96	4.39	4.30	4.30	4.47	4.06
MnO	0.05	0.10	0.05	0.06	0.03	0.12	0.16	0.08	0.15	0.09
MgO	17.72	19.00	17.50	17.64	17.90	18.59	18.82	18.35	18.02	18.20
CaO	19.88	19.92	19.99	19.73	19.81	19.62	19.88	20.01	20.00	20.40
Na_2O	0.24	0.16	0.23	0.23	0.23	0.22	0.24	0.21	0.22	0.22
Sum	100.74	101.05	100.39	100.30	100.49	99.62	99.65	99.19	99.71	99.51
mg	89.0	90.8	89.1	88.9	89.0	88.3	88.6	88.4	87.8	88.9
En	51.8	53.9	51.5	51.8	52.1	52.9	53.0	52.2	51.6	51.8
Fe	6.4	5.5	6.3	6.5	6.5	7.0	6.8	6.9	7.2	6.5
Wo	41.8	40.6	42.3	41.7	41.4	40.1	40.2	40.9	41.2	41.7

Plagioclase in the lava:					Plagioclase in the xenolith:					
Number	92	93	94	95	87	1	4	5	7	10
SiO_2	45.68	46.57	47.51	46.83	46.45	46.47	47.76	48.09	46.73	46.35
Al_2O_3	34.76	33.88	33.10	33.84	34.09	34.04	33.06	33.06	33.74	34.12
FeO	0.26	0.34	0.30	0.33	0.47	0.34	0.38	0.32	0.32	0.34
MgO	0.20	0.20	0.25	0.24	0.25	0.25	0.31	0.26	0.23	0.22
CaO	18.35	17.51	16.84	17.52	17.85	17.32	16.50	16.18	17.03	17.30
Na_2O	1.15	1.53	1.89	1.57	1.47	1.23	1.74	1.85	1.38	1.20
K_2O	0.01	0.01	0.01	0.01	0.01	0.02	0.01	0.03	0.03	0.01
Sum	100.41	100.04	99.90	100.34	100.59	99.67	99.76	99.79	99.46	99.54
Ab	10.2	13.6	16.9	13.9	13.0	11.4	16.0	17.1	12.8	11.1
An	89.8	86.3	83.1	86.0	87.0	88.5	83.9	82.7	87.1	88.8
Or	0.1	0.1	0.1	0.1	0.1	0.1	0.1	0.2	0.2	0.1

6.5 Pyroxene, plagioclase and gabbroic xenoliths in NO 42

NO 42 is the only sample studied that contains clinopyroxene but it also contains numerous small gabbroic xenoliths. One small xenolith available for this study is composed of olivine, clinopyroxene and plagioclase. The composition of clinopyroxene and plagioclase in the xenolith are identical to the those in the lava (Table 6.2) which suggest that both the clinopyroxenes and plagioclases in the lava are xenocrysts. The olivines in the xenolith have compositions from $Fo_{87.9-89}$ (Fig. 6.5n) which suggests that small peak seen in olivine Fo values of the lava (Fig 6.5i) is caused by xenocrystic olivines from disintegrated xenoliths. No cr-spinels were found in the xenolith but magnetite occurs as inclusions in plagioclase.

6.6 Review of melt inclusion studies on Icelandic samples

Russian workers used a high temperature heating stage with visual control to homogenize melt inclusions in early formed phenocrysts in both alkaline and tholeiitic samples from Iceland. The results were first published in the Russian literature (Gurenko et al., 1988a; 1991) but later translated into English (Gurenko et al., 1988b;, 1992).

The alkaline samples they studied came from Búdahraun and Sydri Raudamelskúlur on the Snæfellsnes peninsula. Successful homogenization was achieved for inclusions in both clinopyroxene and plagioclase whereas inclusions in olivine phenocrysts did not homogenize completely, as the fluid bubble could not be dissolved back into the melt inclusion (Gurenko et al., 1992). Inclusions in olivine were therefore quenched after the disappearance of the last daughter phase in the inclusions. In addition,inclusions in olivines had suffered FeO-loss and equilibrium compositions had to be recalculated (see chapter 1). As a result of these studies, Gurenko et al., (1992) calculated two possible primary melts for the alkali basalts, one in equilibrium with olivine Fo_{90} and the other in equilibrium with olivine Fo_{91}.

Gurenko et al., (1988b) did heating stage experiments on one tholeiite from Theistareykir. They managed to homogenize inclusions in olivine, plagioclase and clinopyroxene, but in olivine the fluid bubble disappeared 15-20 °C before the melting of daughter clinopyroxenes inside the inclusions. These inclusions were therefore quenched after the melting of the last clinopyroxene. The reason for this early disappearance of the fluid bubble is believed to be because the melt was not fluid saturated (Gurenko et al., 1988b). Comparison between melt inclusions in different mineral phases and utilization of mineral-melt equilibrium models indicated that all the inclusions where systematically underheated, and therefore not all the host mineral that

had crystallized on the inclusion walls after trapping, had been melted during the experiments. Gurenko et al, (1988b) therefore recalculated all the inclusions until they were in equilibrium with the host mineral and the inclusion in the most magnesian olivine ($Fo_{91.8}$) was used to calculate a primary melt in equilibrium with the most magnesian olivine found in this sample ($Fo_{92.2}$). The composition of this melt in shown in Table 6.3.

Table 6.3: Calculated primary melt compositions for the high magnesian tholeiites from Iceland. 1 = Calculated primary melt for tholeiite 11898 in equilibrium with olivine $Fo_{92.2}$ Gurenko et al., (1988b). 2 = Calculated primary melt from inclusion i20 from Hansteen (1991) for Mælifell in equilibrium with olivine $Fo_{91.7}$, assuming that no Fe^{2+}/Mg re-equilibration has taken place after trapping. 3 = Calculated primary melt from inclusion i20 from Hansteen (1991) for Mælifell in equilibrium with olivine $Fo_{91.7}$, assuming Fe^{2+}/Mg re-equilibration. 4 = Liquid composition for Mælifell from Hardardóttir (1986). 5 = Liquid composition from Mælifell from Hardardóttir (1986), using Fe2+/Fe3+ = 5.14 as calculated using the model of Maurel and Maurel (1982a) from the four spinel analyses reported in Hardardóttir (1986). 6 = RE 78 after subtraction of 9.4% of olivine $Fo_{89.4}$. 7 = RE 291 after subtraction of 9.4% olivine $Fo_{89.9}$.

	1	2	3	4	5	6	7
Sample	11898	i20	i20	Mælifell	Mælifell	"RE 78"	'RE 291"
SiO_2	48.8	47.96	47.39	46.8	46.8	46.32	47.64
TiO_2	0.5	0.90	0.85	0.8	0.8	0.41	0.44
Al_2O_3	14.1	15.02	14.14	11.7	11.7	14.90	15.02
Fe_2O_3	0.9	1.43	1.60	1.1	1.65	0.79	0.83
FeO	7.0	6.48	7.29	8.1	7.61	8.26	7.38
MnO		0.14	0.13	0.17	0.17	0.15	0.15
MgO	14.0	11.78	13.27	18.0	18.0	15.73	14.31
CaO	13.2	14.50	13.65	11.6	11.6	11.92	12.79
Na_2O	1.4	1.69	1.59	1.14	1.14	1.48	1.39
K_2O	0.02	0.03	0.03	0.03	0.03	0.01	0.01
P_2O_5		0.07	0.06	0.03	0.03	0.03	0.04
Sum	99.92	100.00	100.00	99.47	99.53	100.00	100.00
T_c°C	1325	1275	1310	1407	1404	1366	1332
Fo	92.2	91.7	91.7	93.2	93.5	92.2	92.2

Hansteen (1991) did heating stage experiments on melt inclusions in olivines from high magnesian tholeiites from Mælifell in the Hengill volcanic system, southwest Iceland. These experiments were complemented by batch heating of olivine crystals in a vertically oriented tube furnace. The heating stage used by Hansteen (1991) is a Linkam TH1500 model and differs in several aspects from the heating stage used by Gurenko et al. (1988b, 1992), which is of the same type as described in chapter 1, so the main differences will be discussed briefly here.

The experiments were run in commercial grade N atmosphere with the oxygen fugacity buffered at the C-CO-CO_2 buffer with a spec pure C disc (Hansteen, 1991; Oskarsson and Hansteen, 1992). The use of N atmosphere instead of He, and the presence of a hot spec pure C disc in the heating chamber, makes it impossible to

quench the inclusions fast enough after the experiments, and Hansteen (1991) does not mention anything about quenching of the heating stage experiments. It is therefore assumed that all the inclusions he analysed were from the batch heating experiments and that the heating stage experiments where done to establish the temperature range to be used in the batch heating experiments. The batch heating experiments were quenched by dropping the run into water, but if the 10 seconds reported as the time it took to quench the sample from run temperature to below 100 °C is correct, it gives ample time for crystallization of the host mineral on the inclusion walls. This might not be noticed during later microscopic examination of the inclusions.

The compositions of the five homogenized inclusions reported in Hansteen (1991) occur in olivines of compositions $Fo_{86.9-89.4}$, were quenched at temperatures between 1231-1238 °C, and have MgO contents varying from 9.36-10.25%. As MgO is largely controlled by temperature this range indicates bad quenching, crystallization of olivine on the inclusion walls in some of the runs, and therefore variable loss of an olivine component (MgO) from the inclusion. Calculated dry equilibrium temperature for the melt compositions (Ford et al., 1983) is slightly lower than quenching temperature, or from 1206-1235 °C, which further supports the suggestion that some olivine crystallization took place during quenching.

The inclusion with the highest MgO has a quenching temperature very close to the calculated dry temperature (Ford et al., 1983) and it was chosen here to calculate a parental melt composition in equilibrium with the most magnesian olivine of $Fo_{91.7}$ (Hansteen, 1991). For calculating the Fe_2O_3 in the melt, Fe_2O_3 in the six spinels reported in Hansteen (1991) and the model of Maurel and Maurel (1982a) were used, giving a value of 5.05 for Fe^{2+}/Fe^{3+}. This value gives a calculated equilibrium olivine composition of $Fo_{90.5}$ for this inclusion which occurs in olivine $Fo_{89.4}$. This difference in Fo value could represent overheating in the experiment, too low Fe^{2+}/Fe^{3+} used for the calculations, Fe^{2+} - Mg re-equilibration at high temperatures (chapter 1) or that the model of Ford et al (1983) gives too high Fo value. Assuming that the model of Ford et al. (1983) gives reliable results for these almost anhydrous Icelandic tholeiites (e.g. Gurenko et al., 1988b) and that no overheating took place, two possible parental melt compositions were calculated. The first one was calculated by stepwise addition of equilibrium olivine component (Danyushevsky et al., 1990) to the melt inclusion until it was in equilibrium with $Fo_{91.7}$, whereas the other was calculated by first re-adjusting the Fe^{2+}/Mg ratio (using a program written by L.V. Danyushevsky) in the melt, at 1235 °C, until it was in equilibrium with the host olivine $Fo_{89.4}$ and then adding equilibrium olivine component until the inclusion was in equilibrium with $Fo_{91.7}$. These two calculated primary melts are shown in Table 6.3. Also shown in Table 6.3 is calculated parental liquid composition for Mælifell taken from Hardardóttir (1986).

6.7 Discussion

The most magnesian olivine analysed in the Reykjanes tholeiites has the composition $Fo_{91.6}$ which is significantly less magnesian than the equilibrium olivine calculated for the most magnesian whole-rock samples with 17-19% MgO (Ford et al., 1983). This suggest either that these samples have accumulated some olivine and do therefore not represent a true liquid composition or that the more magnesian olivines are either fractionated out or re-equilibrated. RE 154 and RE 217 with 13-13.5% MgO on the other hand have olivine phenocrysts that are in equilibrium with the whole-rock compositions.

As mentioned earlier, sample NO 42 contains two populations of cr-spinels, the more magnesian olivines contain the most refractory spinels with $cr^{\#}$ between 0.55-0.60 whereas in olivines Fo_{86-90} the $cr^{\#}$ is 0.08-0.50. The olivines (Fo_{87-90}) from the gabbroic xenolith in NO 42 on the other hand do not contain any cr-spinel, so it is unlikely that the spinels with the low $cr^{\#}$ were derived directly from the xenoliths. The olivines in NO 42 are the most magnesian analysed from the Icelandic samples and their spinel inclusions have the highest $cr^{\#}$ of all the cr-spinels analysed here. The low $cr^{\#}$ spinels on the other hand are more like spinels in N-MORB, in which co-fractionation of plagioclase causes $cr^{\#}$ to increase with falling $Mg^{\#}$. This, therefore, suggests mixing between an high magnesian melt and an N-MORB-like melt, but the presence of the gabbroic xenoliths and xenocrystic clinopyroxene and plagioclase in NO 42 points to another possible mechanism to crystallize these more Al_2O_3 rich spinels. When gabbroic xenoliths composed of olivine, plagioclase and clinopyroxene are entrained in high magnesian tholeiite in which olivine and cr-spinel are on the liquidus, breakdown of plagioclase and clinopyroxene leads to an increase in Al_2O_3 in the melt causing crystallization of cr-spinel with lower $cr^{\#}$ and higher $mg^{\#}$. At this stage the liquidus olivine composition was ~Fo_{90}, which may explain why no low $cr^{\#}$ spinels are found in the more magnesian olivines. At this stage, it is not clear though whether mixing with N-MORB, or assimilation, is the more viable option.

6.7.1 Primary magma compositions for Icelandic tholeiites

Estimates of the MgO content of primary melts for Icelandic tholeiites vary significantly. Maaløe and Jakobsson (1980) and Hardardóttir (1986) suggest MgO of approximately 18% whereas calculated primary melt from Gurenko et al., (1988b) has 14% MgO and primary melt compositions calculated here from a composition of a melt inclusion from Hansteen (1991) have 11.8-13.3% MgO. There is also significant difference, for example, in TiO_2 contents of calculated primary melts (compare 1 and 3 in Table 6.3). This may suggest that the melt calculated from Gurenko (1988b)

represents a higher degree melt than the melts calculated from the inclusions from Hansteen (1991).

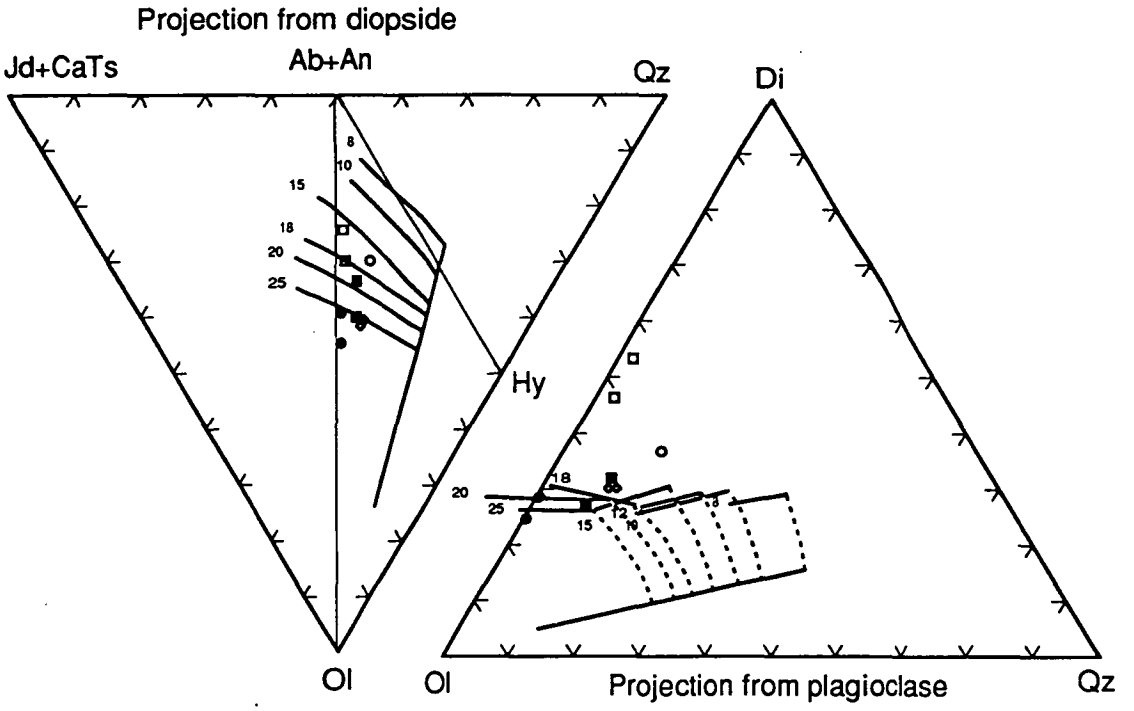

Figure 6.9: Calculated melt compositions from table 6.3 plotted in the normative projection of Falloon and Green, (1988). Open circle is calculated primary melt from Gurenko et al., (1988b), open squares are melt compositions in equilibrium with olivine $Fo_{91.7}$, calculated from inclusion i20 from Hansteen (1991), the less olivine normative point is calculated by adding equilibrium olivine whereas the more olivine normative composition is calculated by first re-adjusting the Fe^{2+}/Mg ratio. Open diamonds are the calculated melt composition from Hardardóttir (1986), and the same melt composition with the Fe_2O_3 content calculated from the spinel compositions given in Hardardóttir (1986). Filled circles and filled squares are the whole-rock compositions and the whole-rock compositions minus 9.4 equilibrium olivine for RE 78 and RE 291. Fe_2O_3 was calculated from the average Fe_2O_3 in cr-spinels in these samples (Maurel and Maurel, 1982a).

In Figure 6.9 the "primary" tholeiite melt compositions from Table 6.3 are plotted in the normative projection of Falloon and Green (1980), together with the whole-rock compositions of RE 78 with 18.8% MgO and RE 291 with 17.6% MgO. The "primary" melt composition of Gurenko et al., (1988b) and the melts calculated here from the inclusion from Hansteen (1991) have high normative diopside content and plot well away from the cotectics for primary melts from MORB pyrolite and are not in equilibrium with mantle residue. On the other hand, the whole-rock compositions and the calculated melt composition of Hardardóttir (1986) plot close to the cotectic at 25 kbar. However, the whole-rock samples have obviously accumulated some olivine as melts with these compositions would crystallize olivine > Fo93, but there are no evidence for such highly magnesian olivines having crystallized from these magmas.

For comparison with the melt calculated by Gurenko et al., (1988b), the average olivine composition occurring in RE 78 and RE 291, was subtracted from these samples until they were in equilibrium with $Fo_{92.2}$. This required subtraction of 9.4% of $Fo_{89.9}$ from RE 291 and 9.4% of $Fo_{89.4}$ from RE 78. These re-calculated compositions with 14.3-15.7 are shown in Table 6.3 and Figure 6.9 and are much closer to the cotectics for primary melts than the calculated "primary" melt from Gurenko et al., (1988b) and the melts calculated here from the inclusions from Hansteen (1991).

The heating stage experiments by Gurenko et al., (1988b) and Hansteen (1991) were done on crystals from lavas that contain numerous gabbroic xenoliths, composed of plagioclase, clinopyroxene and olivine. Both also contain clinopyroxene and plagioclase that are likely to be xenocrystic. It is therefore possible that the melt trapped by the inclusions had assimilated some gabbroic xenoliths before it was trapped and that it does not represent melt that was in equilibrium with mantle residue. Studies by Trønnes (1990) indicate that the most primitive glasses from the Hengill area could be derived by fractionation of olivine and plagioclase combined with 5-30% assimilation of clinopyroxene. The inclusions from both Gurenko et al., (1988b) and Hansteen also have higher CaO/Al_2O3 than the all the whole-rock analyses from the Reykjanes Peninsula which further supports the likelyhood that some assimilation of clinopyroxene has taken place.

The model preferred here is that the primary melt for these magmas segregated from a mantle residue at pressure above 20 kbar and had > 16% MgO. Some fractional crystallization must have occurred at high pressure before the melt was erupted at the surface. Assimilation of hydrothermally altered basaltic crust probably occurred either in deep seated magma chambers or during ascent (Hemond et al., 1993), and in addition, some samples show evidence of further assimilation of unaltered gabbroic xenoliths. The most magnesian samples so far analysed with > 16% MgO have all accumulated some olivine, possibly through flow differentiation, since individual samples from a single lava flow often vary greatly in MgO content (Jakobsson et al., 1978).

No direct evidence is available for the early fractionation history of these lavas. Melt inclusion studies to date (Gurenko et al., 1988b; Hansteen, 1991) have been unable to homogenize unmodified melt that can be linked to primary melt through olivine-only fractionation. However, most of the tholeiites studied here are potentially suitable for melt inclusion studies, as they contain a high proportion of highly magnesian olivines; furthermore as there is no evidence in most of the samples for assimilation of clinopyroxenes from gabbroic xenoliths, melt compositions determined via heating stage studies could be directly compared to experimental melt compositions. NO 42, which has the most magnesian olivines in addition to gabbroic xenoliths, could also

give direct evidence for the assimilation, as melt compositions in olivines of different composition should contain different amounts of the assimilant, and inclusions in minerals from the xenoliths could provide constraints to the origin of the xenoliths.

6.8 Conclusions

Most high magnesian tholeiites from Iceland are too magnesian to be in equilibrium with their most magnesian olivine phenocrysts, which strongly suggests that these samples have accumulated some olivine. Cr-spinel inclusions in olivines generally show a limited compositional range and there is a clear compositional distinction between cr-spinels in incompatible element depleted tholeiites and those in the more enriched tholeiites, with no signs of mixing between enriched and depleted tholeiites. Two populations of spinels can be seen in tholeiite NO 42 from Randahraun. Cr-rich spinels occur in olivines > Fo_{90} whereas more Al_2O_3-rich spinels occur in olivines < Fo_{90}. The more Al_2O_3 spinels either crystallized from a melt that has been enriched in Al_2O_3 due to assimilation of plagioclase from gabbroic xenoliths that are common in this lava flow, or they are from a N-MORB magma (with plagioclase on the liquidus) that mixed with high magnesian tholeiite.

Melt inclusion studies have so far only been done on Icelandic tholeiites that contain numerous gabbroic xenoliths (Gurenko et al., 1988b; Hansteen, 1991), and calculated primary melts obtained from these studies with 12-14% MgO have relatively high CaO and are not consistent with experimentally derived primary melt compositions (e.g. Falloon and Green, 1988) of typical oceanic peridotitic mantle.

Subtraction of the average olivine composition from the most magnesian tholeiites from Reykjanes Peninsula until they are in equilibrium with olivine $Fo_{92.2}$ gives melt compositions with 14-3-15.7% MgO. These calculated melts have lower CaO content than the melts calculated from the heating stage experiments and are more compatible with the experimentally-derived primary melt compositions.

Chapter 7

SYNTHESIS

This thesis has focussed on early formed phenocrysts (mainly olivine and spinel) in mantle-derived magmas, and the information that can be obtained from them and the melt inclusions that they host. A microthermometric technique involving homogenizing inclusions under visual control is described, and then used to provide information on magma compositions and temperatures of crystallization. This technique has been applied to several diverse suites of mantle-derived magmas to clarify different aspects of their petrogenetic histories.

The first application of the heating stage study of melt inclusions is to rocks dredged from the Australia-Antarctic Discordance (AAD), which is a proposed site of downwelling, abnormally cold mantle (Hayes and Conolly, 1972; Weissel and Hayes, 1974; Forsyth et al., 1987; Klein et al., 1991). However, the present study finds no evidence from the near-liquidus phenocrysts and their melt inclusions supporting the existence of colder mantle beneath this unusual segment of the global ridge system. The compositions of olivine and plagioclase phenocrysts are as primitive as previously reported from "normal" areas of mid-ocean ridges, and their crystallization temperatures are very close to those for typical N-MORB from the Mid-Atlantic Ridge (Sobolev et al., 1989).

The matrix glasses from the AAD basalts show a wider range of compositions (e.g. K_2O/TiO_2) than matrix glasses from adjacent spreading ridge segments, indicating a more complex evolutionary history for the AAD lavas, involving mixing between significantly different magma types. The same compositional range is recorded in melt inclusions in early formed phenocrysts, indicating that mixing is taking place early in the crystallization history of these magmas. One of the melts involved in this mixing process is derived from a typical N-MORB mantle. Another component has notably higher K_2O/TiO_2, high SiO_2 and Na_2O and low FeO*, but the origin of this component was not identified during the course of this study. Further studies focussing on melt inclusions should be able to identify this melt, and better constrain the petrogenesis of AAD magmas.

The second application of this study centred on an extensive and diverse suite of lavas dredged from a small area in the southernmost part of the North Fiji Basin and along the Hunter Ridge. The particular values of this suite is the large number of glasses of primitive (high $mg^{\#}$) character and containing phenocrysts of highly forsteritic olivine and magnesian and chromium rich spinel. Several magmatic suites have been identified from matrix glass compositions and distinctive olivine-spinel relations. These include island arc tholeiites, boninites, back-arc basin basalts and

incompatible-element enriched basalts transitional between T-MORB and E-MORB. Olivine phenocryst CaO contents demonstrate their phenocrystic (as opposed to xenocrystic) origin, and CaO contents are shown to be related to both CaO and SiO_2 in the respective magma types (ie. to notional activity of Ca_2SiO_4). Cr-spinels in the Hunter Ridge boninites are the most refractory Cr-spinels of all the magmatic suites identified in this region, groups, and crystallized from a magma produced as a partial melt of a harzburgitic mantle. In contrast, Cr-spinels in E-MORB-like and BABB magmas in this region have lower $cr^{\#}$, indicating crystallization from magmas derived from more fertile lherzolitic mantle sources.

Detailed heating stage experiments were used to identify mixing components involved in the genesis of a complex mixed-magma high-Mg andesite suite from the Hunter Ridge. Andesite samples from station 108 show strong mineralogical evidence (complex zoning patterns in olivine and clinopyroxene phenocrysts, bimodal olivine compositions and at least two distinct groups of Cr-spinel inclusions in olivine) for magma mixing. Heating stage experiments demonstrate that the most magnesian olivine phenocrysts crystallized from a melt with approximately 17% MgO at 1350 °C. Compositions of homogenized melt inclusions, together with selected ratios of elements incompatible in olivine in unheated, glassy inclusions demonstrate a complex history of magma mixing in this area. This, together with the mineralogy and whole-rock geochemistry, indicates open system crystal fractionation of refractory boninitic or IAT magma, with additional mixing in of BABB magmas from the small adjacent NFB spreading centre. Mixing of primitive IAT or boninitic magma with primitive BABB with concurrent crystal fractionation, appears to produce sufficient homogenization that consequent magmatic evolution produces reasonably coherent magmatic lineages documented as island arc basalt or high magnesian andesite suites.

At station 123 in the NFB, melt inclusions in olivine demonstrate a more simple petrogenetic scenario for these back-arc basin basalts. These inclusions did not homogenize, as the fluid bubble could not be dissolved back into the melt; they were therefore quenched after the disappearance of the last daughter phase. Although compositions of these quenched melt inclusions do not represent true liquid compositions, as olivine ($<Fo_{91}$) and Cr-spinel were the only crystallizing phases in the samples of this BABB suite, ratios of elements incompatible in olivine are used to identify the geochemical signature of the parental melt(s). These ratios are essentially identical in all analysed inclusions, as well as in the matrix glasses, and clearly document the evolution of a single homogeneous magma.

The last suite of rocks studied for this thesis comes from Iceland. Whole-rock compositions of high-Mg tholeiites shows that, if they represent liquid compositions, then they should crystallize olivines with compositions of $Fo>93$. Systematic study of compositions of olivine phenocrysts and their spinel inclusions from some high-Mg,

incompatible element depleted tholeiites from the Reykjanes Peninsula found no olivines more magnesian than $Fo_{91.6}$. Similarly, the most magnesian olivines occurring in high-Mg tholeiites from the Krafla system have compositions $Fo_{92.5}$. Therefore, those whole-rock compositions with 16-18% MgO must have accumulated olivine. Only one of these Icelandic tholeiites is enriched in incompatible elements, and the most magnesian olivines in that sample have the composition $Fo_{84.6}$ which is similar to the alkaline basalts studied from Surtsey.

A review of two published melt inclusion studies on Icelandic tholeiites, and primary melt compositions calculated from these studies, demonstrates that these compositions cannot represent liquids in equilibrium with mantle peridotite residues (e.g. Falloon and Green, 1988), since they contain considerably higher molecular normative Di than peridotite partial melts. One possible explanation for this is that these primitive Icelandic melts have assimilated some clinopyroxene prior to entrapment in olivine phenocrysts, since both tholeiitic lavas chosen to date for melt inclusion studies contain abundant gabbroic xenoliths.

Compositions of olivines and their Cr-spinels inclusions are clearly different between the incompatible element depleted tholeiites and the incompatible element enriched tholeiite, and no evidence was noted for mixing between these two magma types, despite their close proximity on the Reykjanes Peninsula. A single sample (NO 42) from the Krafla system contains two populations of Cr-spinels, indicating either mixing of this primitive Icelandic tholeiite with a typical N-MORB, or increasing Al_2O_3 in spinels with fractionation due to resorption of plagioclase from gabbroic xenoliths entrained in the magma.

This study shows that melt inclusions can give valuable information on the early crystallization history and petrogenesis of mantle-derived magma suites. However, it is emphasized that thorough heating stage thermometric studies towards achieving these aims must carefully take into consideration complications such as Fe^{2+} - Mg re-equilibration, between the melt inclusion and host olivine, and H_2 diffusion from the melt inclusions, with subsequent changes of ambient fO_2. This requires detailed and time consuming studies on the behaviour of melt inclusions during heating in <u>each</u> rock suite, through series of kinetic experiments. Having met these prerequisites, it is possible then to obtain the crystallization temperature and the compositions of the trapped (parental) melts, and to reconstruct these back to primary melt compositions. Although only electron microprobe studies of major and minor element contents have been used in the course of this study, recent advances in other micro-beam techniques have demonstrated that it is possible to accurately determine H_2O and trace element contents in homogenized melt inclusions (e.g. Sobolev and Shimizu, 1993; Sobolev and Chaussidon, submitted; McDonough and Ireland, 1993). This will open a new chapter in the study of mantle-derived magmas, and complemented by high-pressure

experiments of melt compositions determined in this manner, will greatly increase our understanding of the mechanisms and processes accompanying generation and extraction of magmas from the upper mantle.

REFERENCES

Allan J.F., Sack R.O. and Batiza R., 1988. Cr-rich spinels as petrogenetic indicators: MORB-type lavas from the Lamont seamount chain, eastern Pacific. *Am. Mineral.*, **73**: 741-753.

Arai S., 1987. An estimation of the least depleted spinel peridotite on the basis of olivine-spinel mantle array. *N. Jb. Miner. Mh.*, **8**: 347-354.

Arai S., 1992. Chemistry of chromian spinel in volcanic rocks as a potential guide to magma chemistry. *Min. Mag.*, **56**: 173-184.

Ariskin A.A. and Barmina G.S., 1990. Plagioclase-melt thermometry for basaltic and andesitic systems. *Geokhimiya*, **N3**: 441-446 (in Russian).

Ariskin A.A., Barmina G.S. and Frenkel M.Ya., 1986. Computer simulation of basaltic melt crystallization under controled fO_2. *Geokhimiya*, **N11**: 1614-1627 (in Russian).

Auzende J.M. and Urabe T., in press. *Marine Geology*, STARMER Special Issue.

Auzende J.M., Eissen J.P., Lafoy Y., Gente P. and Charlou J.L., 1988b. Seafloor spreading in the North Fiji Basin (Southwest Pacific). *Tectonophysics*, **146**: 317-351.

Auzende J.M., Lafoy Y. and Marsset B., 1988a. Recent geodynamic evolutuion of the North Fiji Basin (southwest Pacific). *Geology*, **16**: 925-989.

Auzende J.M., Pelletier B. and Eissen J.P., in press. The North Fiji Basin: Geology, structure and geodynamic evolution. **In**: Auzende J.M. and Urabe T. (eds). *Marine Geology*, STARMER Special Issue.

Bakumenko I.T., 1975. Inclusions in minerals of ultrabasic nodules as indictors of their origin. **In:** D. N. L. a. S. N. V. Sobolev V.S. (ed). *Deepseated xenoliths and the upper mantle*. Novosibirsk. Nauka, Siberian Branch. 231-235. (In Russian).

Ballhaus C., Berry R.F. and Green D.H., 1991. High pressure experimental calibration of the olivine-orthopyroxene-spinel oxygen geobarometer: implications for the oxidation state of the upper mantle. *Contrib. Mineral. Petrol.*, **107**: 27-40.

Barsdell M., 1988. Petrology and petrogenesis of clinopyroxene-rich tholeiitic lavas. Merelava volcano, Vanuatu. *J. Petrol.*, **29**: 927-964.

Barsdell M. and Berry R.F., 1990. Origin and evolution of primitive island arc ankaramites from Western Epi, Vanuatu. *J. Petrol.*, **31**: 747-777.

Beccaluva L., Bonatti E., Dupoy C., Ferrara G., Innocenti F., Lucchini F., Macera P., Petrini R., Rossi P.L., Serri G., Seyler M. and Siena F., 1990. Geochemistry and mineralogy of volcanic rocks from ODP sites 650, 651, 655, and 654 in the Tyrrhenian Sea. **In:** Kastens K.A., Mascle J. et al., (ed). *Proc. ODP, Sci. Results, vol. 107.* College Station, Texas (Ocean Drilling Program). 49-74.

Bryan W.B., 1979. Low-K_2O dacite from the Tonga-Kermadec island arc: petrography, chemistry and petrogenesis. **In:** Barker F. (ed). *Trondhjemites, dacites and related volcanic rocks*. Amsterdam. Elsevier. 581-600.

Burnham C.W., 1979. Magmas and hydrothermal fluids. **In:** Barnes H.L. (ed). *Geochemistry of Hydrothermal ore deposits. 2nd ed.* New York. John Wiley and Sons. 71-136.

Charvis P. and Pelletier B., 1989. The northern New Hebrides back-arc troughs: history and relation with the North Fiji Basin. *Tectonophysics*, **170**: 259-277.

Clocchiatti R., 1975. Glassy inclusions in crystals of quartz; optical, thermo-optical and chemical studies, and geological applications. *Soc. Géol. France, Memories, New Series,* , **54**: 96p., (in French).

Coish R.A., Hickey R. and Frey F.A., 1982. Rare earth element geochemistry of the Betts Cove ophiolite, Newfoundland: complexities in ophiolite formation. *Geochim. Cosmochim. Acta*, **46**: 2117-2134.

Coleman R.G. and Peterman Z.E., 1975. Oceanic plagiogranite. *J. Geophys. Res.*, **80**: 1099-1108.

Crawford A.J., Beccaluva L., Serri G. and Dostal J., 1986. Petrology, geochemistry and tectonic implications of volcanics dredged from the intersection of the Yap and Mariana trenches. *Earth Planet. Sci. Lett.*, **80**: 265-280.

Crawford A.J., Beccaluva L. and Serri G., 1981. Tectono-magmatic evolution of the West Philippine-Mariana region and the origin of boninites. *Earth Planet. Sci. Lett.*, **54**: 346-356.

Crawford A.J., Falloon T.J. and Green D.H., 1989. Classification, petrogenesis and tectonic setting of boninites. **In:** Crawford A.J. (ed). *Boninites and related rocks*. London. Unwin Hyman. 1-49.

Danyushevsky L.V. and Sobolev A.V., submitted. Oxygen fugacity calculations for primitive mantle-derived melts: a new methodology. Manuscript submitted to American Mineralogist, March 1994.

Danyushevsky L.V., Chizhov S., Kuzmin V., Pugachov R. and Sobolev A.V., 1990. Petrolog. 1.01. SeLeSoft Co. Moscow.

Danyushevsky L.V., Falloon T.J., Sobolev A.V., Crawford A.J., Carroll M. and Price R.C., 1993. The H_2O content of basalt glasses from Southwest Pacific back-arc basins. *Earth Planet. Sci. Lett.*, **117**: 347-362.

Danyushevsky L.V., Sobolev A.V. and Kononkova N.N., 1992. Methods of studying melt inclusions in minerals during investigations on water-bearing primitive mantle melts (Tonga trench boninites). *Geochem. Int.*, **29**: 48-62.

Dick H.J.B. and Bullen T., 1984. Chromian spinel as a petrogenetic indicator in abyssal and alpine-type peridotites and spatially associated lavas. *Contrib. Mineral. Petrol.*, **86**: 54-76.

Dixon S. and Rutherford M.J., 1979. Plagiogranites as a late-stage immiscible liquids in opholite and mid-ocean ridge suites: an experimental study. *Earth Planet. Sci. Lett.*, **45**: 45-60.

Dmitriev L.V., Sobolev A.V., Suschevskaya N.M and Zapunny S.A., 1985. Abyssal glasses, petrologic mapping of the ocean floor and "geochemical leg"

82. **In:** Bougault H., Cande S.C., et al. (ed). *Init. Repts. DSDP 82.* Washington. U.S. Govt. Printing Office. 509-518.

Donaldsson C.H. and Brown R.W., 1977. Refractory megacrysts and magnesium-rich melt inclusions within spinel in oceanic tholeiites: indicators of magma mixing and parental magma composition. *Earth Planet. Sci. Lett.*, **37**: 81-89.

Drake M.J., 1976. Plagioclase-melt equilibria. *Geochim. Cosmochim. Acta*, **40**: 457-465.

Duncan R.A. and Green D.H., 1987. The genesis of refractory melts in the formation of oceanic crust. *Contrib. Mineral. Petrol.*, **96**: 326-342.

Dungan M.A. and Rhodes J.M., 1978. Residual glasses and melt inclusions in basalts from DSDP Legs 45 and 46: evidence for magma mixing. *Contrib. Mineral. Petrol.*, **67**: 417-431.

Dypuy C., Dostal J., Marcelot G., Bougault H., Jorun J.L. and Treuil M., 1982. Geochemistry of basalts from the central and southern New Hebrides arc: implication for their source rock composition. *Earth Planet. Sci. Lett.*, **60**: 207-225.

Eggins S.M., 1993. Origin and differentiation of picritic arc magmas, Ambae (Aoba), Vanuatu. *Contrib. Mineral. Petrol.*, **114**: 79-100.

Eissen J-P., Lefèvre C., Maillet P., Morvan G. and Nohara M., 1991. Petrology and geochemistry of the central North Fiji Basin spreading centre (Southwest Pacific) between 16°S and 22°S. *Marine Geology*, **98**: 201-239.

Eissen J.-P., Nohara M. and Cotten J., in press. The North Fiji Basin basalts and their magma sources: part I. Trace and rare earth elements constraints. **In:** Auzende J.M. and Urabe T. (eds). *Marine Geology*, STARMER Special Issue.

Elliott T.R., Hawkesworth C.J. and Grönvold K., 1991. Dynamic melting of the Iceland plume. *Nature*, **351**: 201-206.

Ewart A., 1976. Mineralogy and chemistry of modern orogenic lavas - some statistics and implications. *Earth Planet. Sci. Lett.*, **31**: 417-432.

Ewart A., 1979. A review of the mineralogy and chemistry of Tertiary-Recent dacitic, latitic, rhyolitic, and related salic volcanic rocks. **In:** Barker F. (ed). *Trondhjemites, dacites and related volcanic rocks.* Amsterdam. Elsevier. 13-121.

Ewart A. and Hawkesworth C.J., 1987. The Pleistocene-Recent Tonga-Kermadec arc lavas: interpretation of new isotopic and rare earth data in terms of depleted mantle source model. *J. Petrol.*, **28**: 495-530.

Falloon T.J. and Crawford A.J., 1991. The petrogenesis of high-calcium boninite lavas dredged from the northern Tongan ridge. *Earth Planet. Sci. Lett.*, **102**: 375-394.

Falloon T.J. and Green D.H., 1986. Glass inclusions in magnesian olivine phemocrysts from Tonga: evidence for highly refractory parental magmas in the Tongan arc. *Earth Planet. Sci. Lett.*, **81**: 95-103.

Falloon T.J. and Green D.H., 1988. Anhydrous partial melting of peridotite from 8 to 35 kb and the petrogenesis of MORB. *J. Petrology*, **Special Lithosphere Issue**: 379-414.

Falloon T.J., Green D.H. and Crawford A.J., 1987. Dredged igneous rocks from the northern termination of the Tofua magmatic arc, Tonga and adjacent Lau Basin. *Austral. J. Earth Sci.*, **34**: 487-506.

Falloon T.J., Malahoff A., Zonenshain L.P. and Bogdanov Y., 1992. Petrology and geochemistry of back-arc basin basalts from Lau Basin spreading ridges at 15°, 18° and 19°S. *Mineralogy and Petrology*, **47**: 1-35.

Falvey D., 1975. Arc reversals, and a tectonic model for the North Fiji Basin. *Bull. Aust. Soc. Explor. Geophys.*, **6**: 47-49.

Falvey D., 1978. Analysis of palaeomagnetic data from the New Hebrides. *Bull. Aust. Soc. Explor. Geophys.*, **9**: 117-123.

Ford C.E., Russell D.G., Craven J.A. and Fisk M.R., 1983. Olivine-liquid equilibria: temperature, pressure and composition dependence of the crystal/liquid cation partition coefficients for Mg, Fe^{2+},Ca and Mn. *J. Petrol.*, **24**: 256-265.

Forsyth D.W., Ehrenbard R.L. and Chapin S., 1987. Anomalous upper mantle beneath the Australian-Antarctic discordance. *Earth Planet. Sci. Lett.*, **84**: 471-478.

Fryer P., Sinton J.M. and Philpotts J.A., 1981. Basaltic glasses from the Mariana Trough. **In:** Hussong D.M., Uyeda S., et al., (ed). *Init. Repts. DSDP 60.* Washington. U.S. Govt. Printing Office. 601-609.

Fryer P., Taylor B., Langmuir C.H. and Hochstaedter A.G., 1990. Petrology and geochemistry of lavas from the Sumisu and Torishima backarc rifts. *Earth Planet. Sci. Lett.*, **100**: 161-178.

Furman T., Frey F.A. and Park K-H., 1991. Chemical constraints on the petrogenesis of mildly alkaline lavas from Vestmannaeyjar, Iceland: the Eldfell (1973) and Surtsey (1963-1967) eruptions. *Contrib. Mineral. Petrol.*, **109**: 19-37.

Gerlach D.C., Leeman W.P. and Avé Lallemant H.G., 1981. Petrology and geochemistry of plagiogranite in the Canyon Mountain Ophiolite, Oregon. *Contrib. Mineral. Petrol.*, **77**: 82-92.

Gill J.B., 1976. Composition and age of Lau Basin and Ridge volcanic rocks: Implications for evolution of an interarc basin and remnant arc. *Geol. Soc. Am. Bull.*, **87**: 1384-1395.

Gill J.B., 1981. Orogenic andesites and plate tectonics. Springer-Verlag. New York. 390p.

Gill J.B. and Gorton M., 1973. A proposed geological and geochemical history of eastern Melanesia. **In:** Coleman P.J. (ed). *The Western Pacific: Island Arcs, Marginal Seas, and Geochemistry.* Nedlands. Western Australia University Press. 543-566.

Gorton M.P., 1977. The geochemistry and origin of quaternary volcanism in the New Hebrides. *Geochim. Cosmochim. Acta*, **41**: 1257-1270.

Gurenko A.A., Sobolev A.V., Polyakov A.I. and Kononkova N.N., 1988a. Pervichnyy rasplav riftogennykh toleitov Islandii: sostav i usloviya kristallizatsiya. Doklady Akademii Nauk. SSSR, 301: 179-184.

Gurenko A.A., Sobolev A.V., Polyakov A.I. and Kononkova N.N., 1988b. Primary melt of rift tholeiites of Iceland: composition and conditions of crystallization. *Trans. (Doklady) USSR Acad. Sci.*, **301**: 109-113.

Gurenko A.A., Sobolev A.V. and Kononkova N.N., 1991. Alkaline rift basalts of the Island: new data on petrology. *Geokhimiya*, **9**: 1262-1274 (In Russian).

Gurenko A.A., Sobolev A.V. and Kononkova N.N., 1992. New petrological data on Icelandic rift alkali basalts. *Geochem. Int.*, **29**: 41-53.

Hansteen T.H., 1991. Multi-stage evolution of the picritic Mælifell rocks, SW Iceland: constraints from mineralogy and inclusions of glass and fluid in olivine. *Contrib. Mineral. Petrol.*, **109**: 225-239.

Hardardóttir V., 1986. The petrology of the Mælifell picrite basalt, southern Iceland. *Jökull*, **36**: 31-40.

Hart S.R., Schilling J.G. and Powell J.L., 1973. Basalts from Iceland and along the Reykjanes ridge: Sr isotope geochemistry. *Nature*, **246**: 104-107.

Hawkins J.W., 1974. Geology of the Lau Basin, a marginal sea behind the Tonga Arc. **In:** Burk C. and Drake C. (ed). *Geology of Continental Margins*. New York. Springer. 505-520.

Hawkins J.W., 1976. Petrology and geochemistry of basaltic rocks of the Lau Basin. *Earth Planet. Sci. Lett.*, **28**: 283-298.

Hawkins J.W. and Melchior J.T., 1985. Petrology of Mariana Trough and Lau Basin Basalts. *J. Geophys. Res.*, **90**: 11431-11468.

Hawkins J.W., Lonsdale P.F., Macdougall J.D., and Volpe A.M., 1990. Petrology of the axial ridge of the Mariana Trough backarc spreading center. *Earth Planet. Sci. Lett.*, **100**: 226-250.

Hayes D.E. and Conolly J.R., 1972. Morphology of the southeast Indian Ocean. **In:** Hayes D.E. (ed). *Antarctic Oceanology II: The Australian-New Zealand Sector*. Washington D.C. American Geophysical Uninon Antarctic Research Series., 19: 125-145.

Hemond C., Arndt N.T., Lichtenstein U., Hofmann A.W., Oskarsson N. and Steinthorsson S., 1993. The heterogeneous Iceland plume: Nd-Sr-O isotopes and trace element constraints. *J. Geophys. Res.*, **98**: 15833-15850.

Hemond C., Condomines M., Fourcade S., Allègre C.J., Oskarsson N. and Javoy M., 1988. Thorium, strontium and oxygen isotopic geochemistry in recent tholeiites from Iceland: crustal influence on mantle-derived magmas. *Earth Planet. Sci. Lett.*, **87**: 273-285.

Henderson P., 1982. Inorganic geochemistry. Pergamon Press. Oxford. 353p.

Hochstaedter A.G., Gill J.B., Kusakabe M., Newman S., Pringle M., Taylor B. and Fryer P., 1990a. Volcanism in the Sumisu Rift, I. Major element, volatile and stable isotope geochemistry. *Earth Planet. Sci. Lett.*, **100**: 179-194.

Hochstaedter A.G., Gill J.G. and Morris J.D., 1990b. Volcanism in the Sumisu Rift, II. Subduction and non-subduction related components. *Earth Planet. Sci. Lett.*, **100**: 195-209.

Ikeda Y. and Yuasa M., 1989. Volcanism in nascent back-arc basin behind the Shichito Ridge and adjacent areas in the Izu-Ogazawara arc, northwest Pacific: evidence for mixing between E-type MORB and island arc magmas at the initiation of back-arc rifting. *Contrib. Mineral. Petrol.*, **101**: 377-393.

Ishizuka H., Kawanobe Y. and Sakai H., 1990. Petrology and geochemistry of volcanic rocks dredged from the Okinawa Trough, an active back-arc basin. *Geochem. J.*, **24**: 75-92.

Jakes P. and Gill J., 1970. Rare earth elememts and the island arc tholeiitic series. *Earth Planet. Sci. Lett.*, **9**: 17-28.

Jakobsson S.P., 1972. Chemistry and distribution pattern of Recent basaltic rocks in Iceland. *Lithos*, **5**: 365-386.

Jakobsson S.P., 1979. Petrology of Recent basalts of the Eastern Volcanic Zone, Iceland. *Acta Nat. Is.*, **26**: 1-103.

Jakobsson S.P., Jónsson J. and Shido F., 1978. Petrology of the western Reykjanes Peninsula, Iceland. *J. Petrol.*, **19**: 669-705.

Jaques A.L. and Green D.H., 1980. Anhydrous melting of peridotite at 0-15 Kb pressure and the genesis of tholeiitic basalts. *Contrib. Mineral. Petrol.*, **73**: 287-310.

Jarosewich E.J., Nelen J.A., Norberg J.A., 1980. Reference samples for electron microprobe analysis. *Geostandards Newsletter*, **4**: 43-47.

Johnson K.T.M. and Sinton J.M., 1990. Petrology, tectonic setting, and the formation of back-arc basin basalts in the North Fiji Basin. *Geol. Jb.*, **D92**: 517-545.

Johnson K.T.M., Fisk M.R. and Naslund H.R., in press. Geochemical characteristics of refractory silicate melt inclusions from Leg 140 basalts. **In:** Stokking L., Dick H.J., Erzinger J., et al., (ed). *Proc. ODP Sci. Results 140.* College Station Tx (Ocean Drilling Program).

Jurewicz A.J.G. and Watson E.B., 1988. Cations in olivine, Part 1: calcium partitioning and calcium-magnesium distribution between olivines and coexisting melts, with petrologic applications. *Contrib. Mineral. Petrol.*, **99**: 176-185.

Karig D.E., 1971. Structural history of the Mariana island arc system. *Geol. Soc. Am. Bull.*, **82**: 323-344.

Karig D.E., 1974. Evolution of arc systems in the western Pacific. *A. Rev. Earth Planet. Sci.*, **2**: 51-75.

Klein E.M. and Langmuir C.H., 1987. Global correlations of ocean ridge basalt chemistry with axial depth and crustal thickness. *J. Geophys. Res.*, **92**: 8089-8115.

Klein E.M. and Langmuir C.H., 1989. Local versus global variations in ocean ridge basalt composition: A reply. *J. Geophys. Res.*, **94**: 4241-4252.

Klein E.M., Langmuir C.H., Zindler A., Stautigel H. and Hamelin B., 1988. Isotope evidence of a mantle convection boundary at the Australian-Antarctic Discordance. *Nature*, **333**: 623-629.

Klein E.M., Langmuir C.H. and Staudigel H., 1991. Geochemistry of basalts from the southeast Indian Ridge, 115°E-138°E. *J. Geophys. Res.*, **96**: 2089-2107.

Langmuir C.H., Vocke R.D., Jr and Hanson G.N., 1978. A general mixing equation with applications to Icelandic basalt. *Earth Planet. Sci. Lett.*, **37**: 380-392.

Lavrentev Y.G., Pospelova L.N. and Sobolev A.V., 1974. Rock-forming mineral compositions determination by X-ray microanalysis. *Zavodskaya Laboratoria*, **40**: 657-666 (in Russian).

Lemmlein G.G., 1950. Al-Biruni's mineralogical information. Moscow-Leningrad, Sbornik Biruni *[collected papers], 106-127* (in Russian).

Louat R. and Pelletier B., 1989. Seismotectonics and present-day relative plate motions in the New Hebrides-North Fiji Basin region. *Tectonophysics*, **167**: 41-55.

Maaløe S. and Jakobsson S.P., 1980. The PT phase relations of a primary oceanite from the Reykjanes peninsula, Iceland. *Lithos*, **13**: 237-246.

Maillet P., Monzier M., Eissen J.P. and Louat R., 1989. Geodynamics of an arc-ridge junction: the case of the New Hebrides Arc/North Fiji Basin. *Tectonophysics*, **165**: 251-268.

Maillet P., Monzier M. and Lefevre C., 1986. Petrology of Matthew and Hunter volcanoes, south New Hebrides island arc (southwest Pacific). *J. Volcanol. Geotherm. Res.*, **30**: 1-27.

Malahoff A., Feden R.H. and Fleming H.S., 1982a. Magnetic anomalies and tectonic fabric of marginal basins north of New Zealand. *J. Geophys. Res.*, **87**: 4109-4125.

Malahoff A., Hammond S.R., Naughton J.J., Keeling D.L. and Richmond R.N., 1982b. Geophysical evidence for post-Miocene rotation of the island of Viti Levu, Fiji, and its relationship to the tectonic development of the North Fiji Basin. *Earth Planet. Sci. Lett.*, **57**: 398-414.

Mattey D.P., Marsh N.G. and Tarney J., 1981. The geochemistry, mineralogy , and petrology of basalts from the west Philippine and Parece Vela basins and from the Palau-Kyushu and west Mariana ridges Deep Sea Drilling Project Leg 59. **In:** (ed). *Deep Sea Drilling Project, Leg 59. Initial Rpts. DSDP 59.* 753-800.

Maurel C. and Maurel P., 1982a. Étude expérimentale de l'éauilibre Fe^{2+}-Fe^{3+} dans le spinelles chromifères et les liquides silicatés basiques coexistants, à 1 atm. *C.R. Acad. Sc. Paris*, **295**: 209-212.

Maurel C. and Maurel P., 1982b. Étude expérimentale de la distribution de l'aluminium entre bain silicaté basique et spinelle chromifère. Implications pétrogénétiques: teneur en chrome des spinelles. *Bull. Minéral.*, **105**: 197-202.

Maurel C. and Maurel P., 1983. Influence du fer ferrique sur la distribution de l'aluminium entre bain silicaté basique et spinelle chromifère. *Bull. Minéral.*, **106**: 623-624.

McDonough W.F. and Ireland T.R., 1993. Intraplate origin of komatiites inferred from trace elements in glass inclusions. *Nature*, **365**: 432-434.

McKenzie D. and Bickle M.J., 1988. The volume and composition of melt generated by extension of the lithosphere. *J. Petrol.*, **29**: 625-679.

Metrich N., Sigurdsson H., Meyer P.S. and Devine J.D., 1991. The 1783 Lakagigar eruption in Iceland: geochemistry, CO_2 and sulfur degassing. *Contrib. Mineral. Petrol.*, **107**: 435-447.

Meyer P.S., Sigurdsson H. and Schilling J.-G., 1985. Petrological and geochemical variations along Iceland's Neovolcanic zones. *J. Geophys. Res.*, **90**: 10043-10072.

Miyashiro A., 1974. Volcanic rock series in island arcs and active continental margins. *Am. Journal Sci.*, **274**: 321-355.

Monzier M., Danyushevsky L.V., Crawford A.J., Bellon H. and Cotten J., 1993. High-Mg andesites from the southern termination of the New Hebrides island arc (SW Pacific). *J. Volcanol. Geotherm. Res.*, **57**: 193-217.

Muehlenbachs K., Anderson A.T. and Sigvaldason G.E., 1974. Low $\partial^{18}O$ basalts from Iceland. *Geochim. Cosmochim. Acta*, **38**: 577-588.

Nicholson H., Condomines M., Fitton J.G., Fallick A.E., Grönvold K. and Rogers G., 1991. Geochemical and isotopic evidence for crustal assimilation beneath Krafla, Iceland. *J. Petrol.*, **32**: 1005-1020.

Nielsen R.L. and Drake M.J., 1979. Pyrexene-melt equilibria. *Geochim. Cosmochim. Acta*, **43**: 1259-1272.

Norrish K. and Chappell B.W., 1977. X-ray fluorescene spectrography. In: J. Zussman (ed). Physical methods in determinative mineralogy. Academic Press: 161-214.

Norrish K and Hutton J.T., 1969. An accurate X-ray spectrographic method for the analysis of a wide range of geological samples. *Geochim. Cosmochim. Acta*, **33**: 431-455.

O'Hara M.J. and Matthews R.E., 1981. Geochemical evolution in an advancing, periodically replenished, periodically tapped, continuously fractionated magma chamber. *J. Geol. Soc. London*, **138**: 237-277.

O'Nions R.K., Hamilton P.J. and Evensen N.M., 1977. Variations in $^{143}Nd/^{144}Nd$ and $^{87}Sr/^{86}Sr$ ratios in oceanic basalts. *Earth Planet. Sci. Lett.*, **34**: 13-22.

Oskarsson N. and Hansteen T.H., 1992. The use of graphite for the removal of oxygen from nitrogen purge gas in high temperature microthermometry using the Linkam® TH1500 stage. *Eur. J. Mineral.*, **4**: 865-871.

Oskarsson N., Sigvaldason G.E. and Steinthorsson S., 1982. A dynamic model of rift zone petrogenesis and the regional petrology of Iceland. *J. Petrol.*, **23**: 28-74.

Oskarsson N., Steinthorsson S. and Sigvaldason G.E., 1985. Iceland geochemical anomaly: Origin, volcanotectonics, chemical fractionation and isotope evolution of the crust. *J. Geophys. Res.*, **90**: 10011-10025.

Pearcy L.G., DeBari S.M. and Sleep N.H., 1990. Mass balance calculations for two sections of island arc crust and implications for the formation of continents. *Earth Planet. Sci. Lett.*, **96**: 427-442.

Poldervaart A. and Hess H.H., 1951. Pyroxenes in the crystallization of basaltic magma. *J. Geol.*, **59**: 472-489.

Prestvik T., 1979. Petrology of hybrid intermediate and silicic rocks from Öræfajökull, southeast Iceland. *Geol. Fören. Stockholm Förh.*, **101**: 299-307.

Price R.C., Johnson L.E. and Crawford A.J., 1990. Basalts of the North Fiji Basin: the generation of back arc basin magmas by mixing of depleted and enriched mantle sources. *Contrib. Mineral. Petrol.*, **105**: 106-121.

Pyle D.G., Christie D.M. and Mahoney J.J., 1992. Resolving an isotopic boundary within the Australian-Antarctic Discordance. *Earth Planet. Sci. Lett.*, **112**: 161-178.

Ridley W.I., Rhodes J.M., Reid A.M., Jakes P., Shih C. and Bass M.N., 1974. Basalts from Leg 6 of Deep-Sea Drilling Project. *J. Petrol.*, **15**: 140-159.

Robinson P., Higgins N.C. and Jenner G.A., 1986. Determination of rare-earth elements, yttrium and scandium in rocks by an ion exchange-X-ray fluorescence technique. *Cem. Geol.*, **55**: 121-137.

Roedder E., 1979. Origin and significance of magmatic inclusions. *Bull. Minéral.*, **102**: 487-510.

Roedder E., 1984. Fluid inclusions. *Min. Soc. Amer., Reviews in Mineralogy*, **12**: 644p.

Roeder P.L. and Emslie R.F., 1970. Olivine-liquid equilibrium. *Contrib. Mineral. Petrol.*, **29**: 275-289.

Saunders A.D. and Tarney J., 1979. The geochemistry of basalts from a back-arc spreading centre in the East Scotia Sea. *Geochim. Cosmochim. Acta*, **43**: 555-572.

Schilling J.-G., 1973. Iceland mantle plume: geochemical study of the Reykjanes Ridge. *Nature*, **242**: 565-571.

Sempéré J.-C., Palmer J., Christie D.M., Phipps Morgan J. and Shor A.N., 1992. Australian-Antarctic discordance. *Geology*, **19**: 429-432.

Shaw D.M., 1970. Trace element fractionation during anatexis. *Geochim. Cosmochim. Acta*, **34**: 237-243.

Sigurdsson H. and Brown G.M., 1970. An unusual enstatite-forsterite basalt from Kolbeinsey island, north of Iceland. *J. Petrol.*, **11**: 205-220.

Sigurdsson H. and Schilling J.-G., 1976. Spinels in Mid-Atlantic Ridge basalts: chemistry and occurrence. *Earth Planet. Sci. Lett.*, **29**: 7-20.

Sigurdsson I.A., 1989. *Gabbróhnydlingar í Hraunsvík á Reykjanesskaga.* Unpublished B.Sc. (Hon) thesis. University of Iceland. 67p.

Sigvaldason G.E., 1974. Basalts from the centre of the assumed Icelandic mantle plume. *J. Petrol.*, **15**: 497-524.

Simkin T. and Smith J.V., 1970. Minor-element distribution in olivine. *J. Geol.*, **78**: 304-325.

Sinton C.W., Cristie D.M., Coombs V.L., Nielsen R.L. and Fisk M.R., 1993. Near-primary melt inclusions in anorthite phenocrysts from the Galapagos Platform. *Earth Planet. Sci. Lett.*, **119**: 527-537.

Sinton J.M. and Fryer P., 1987. Mariana Trough lavas from 18°N: implications for the origin of back arc basin basalts. *J. Geophys. Res.*, **92**: 12782-12802.

Sinton J.M., Johnson K.T.M., Price R.C., Staudigel H. and Zindler A., 1991. Petrology and geochemistry of submarine lavas from the Lau and North Fiji back-arc basins. **In:** Kroenke L.W. (ed). *Basin formation ridge crest processes, and metallogenesis in the North Fiji Basin.* Circum-Pacific Council for Energy and Mineral Resources, Earth Science series 3.12. 155-177.

Sobolev A.V. and Chaussidon M., submitted. H_2O contents in the mantle derived melts included in high magnesium olivines. Manuscript submitted to Nature, January, 1993.

Sobolev A.V. and Danyushevsky L.V., in press. Petrology and geochemistry of the high-Ca boninites from the north termination of the Tonga Trench: constraints on high-Ca boninite primary magma generation conditions. *J. Petrol.*,

Sobolev A.V., Clocchiatti R. and Dhamelincourt P., 1983. Les variations la temperature de la pression partielle d'eau pendant la cristallisation de l'olivine dans les oceanites du Piton de la Fournaise (Reunion eruption de 1966). *C.R. Acad. Sci. Paris*, **296**: 275-280.

Sobolev A.V., Dmitriev L.V., Barsukov V.L., Nesorov V.N. and Slutsky A.B., 1980. The formation conditions of the high-magnesium olivines from the monomineralic fraction of Luna 24 regolith. *Proc. Lunar Planet. Sci. Conf.* **1**: 105-116.

Sobolev A.V., Danyushevsky L.V., Dmitiyev L.V. and Sushchevskaya N.M., 1989. High-alumina magnesian tholeiite as the primary basalt magma at midocean ridge. *Geochem. Int.*, **26**: 128-133.

Sobolev A.V., Dmitriev L.V., Tsameryan O.P., Kononkova N.N. and Robinson P.T., 1991. A possible primary melt composition for the ultramafic lavas of the Margi Area, Troodos ophiolite, Cyprus. **In:** Gibson I.L., Malpas J., Robinson P.T. and Xenophontus C. (ed). *Cyprus crustal study project: Initial report, holes CY-1 and 1a.* Paper 90-20. Geological Survey of Canada. 203-216.

Sobolev A.V. and Shimizu N., 1993. Ultra-depleted primary melt included in an olivine from the Mid-Atlantic Ridge. *Nature*, **363**: 151-154.

Sobolev V.S. and Kostyuk V.P., 1975. Magmatic crystalllization based on a study of melt inclusions. Nauka Press. Novosibirsk.

Sorby H.C., 1858. On the microscopical structure of crystals, indicating the origin of minerals and rocks. *Geol. Soc. London Quart. J.*, **14**: 453-500.

Steinthorsson S., Oskarsson N. and Sigvaldason G.E., 1985. Origin of alkali basalts in Iceland: A plate tectonic model. *J. Geophys. Res.*, **90**: 10027-10042.

Stern R.J., Lin P-N., Morris J.D., Jackson M.C., Fryer P., Bloomer S.H. and Ito E., 1990. Enriched back-arc basin basalt from the northern Mariana Trough: implications for the magmatic evolution of back-arc basins. *Earth Planet. Sci. Lett.*, **100**: 210-225.

Stormer J.C., Jr., 1973. Calcium zoning in olivine and its relationship to silica activity and pressure. *Geochim. Cosmochim. Acta*, **37**: 1815-1821.

Sun S.-S. and Jahn B., 1975. Lead and strontium isotopes in post-glacial basalts from Iceland. *Nature*, **255**: 527-530.

Sun S.-S. and McDonough W.F., 1989. Chemical and isotopic systematics of oceanic basalts: implications for mantle composition and processes. **In:** Saunders A.D. and Norry M.J. (ed). *Magmatism in the ocean basins*. Geological Society Special Publication 42. 313-345.

Sun S.-S., Tatsumoto M. and Schilling J.G., 1975. Mantle plume mixing along the Reykjanes Ridge axis: lead isotopic evidence. *Science*, **190**: 143-147.

Sunkel G., 1990. Origin of petrological and geochemical variations of Lau Basin lavas (SW Pacific). *Marine Mining*, **9**: 205-234.

Taylor S.R. and Gorton M.K., 1977. Geochemical application of spark-source mass spectrometry. III: element sensitivity, precision and accuracy. *Geochim. Cosmochim. Acta*, **41**: 1375-1380.

Trønnes R.G., 1990. Basaltic melt evolution of the Hengill volcanic system, SW Iceland, and evidence for clinopyroxene assimilation in primitive tholeiitic magmas. *J. Geophys. Res*, **95**: 15893-15910.

Vogt P.R., Cherkis N.Z. and Morgan G.A., 1983. Project Investigator - 1. Evolution af the Australia-Antarctic discordance deduced from a detailed aeromagnetic study. **In:** Olivier R.L., James P.R. and Jago J.B., (ed). *Antarctic Earth Science*. Canberra, A.C.T. Australian Academy of Science. 608-613.

Volpe A.M., Macdougall J.D. and Hawkins J.W., 1987. Mariana Trough basalts (MTB): trace element and Sr-Nd isotopic evidence for mixing between MORB-like and arc-like melts. *Earth Planet. Sci. Lett.*, **82**: 241-254.

Wager L.R. and Brown G.M., 1968. Layered igneous rocks. Oliver and Boyd. Edinburgh and London. 588p.

Watson E.B., 1976. Glass inclusions as samples of early magmatic liquid: determinative method and appilcation to a South Atlantic basalt. *J. Volcanol Geotherm. Res.*, **1**: 73-84.

Weissel J.K. and Hayes D.E., 1971. Asymmetric seafloor spreading south of Australia. *Nature*, **231**: 518-522.

Weissel J.K. and Hayes D.E., 1974. The Australian-Antarctic Discordance: new results and implications. *J. Geophys. Res.*, **79**: 2579-2587.

Wood D.A., 1981. Partial melting models for the petrogenesis of Reykjanes Peninsula basalts, Iceland: Implications for the use of trace elements and strontium and neodymium isotope ratios to record inhomogeneities in the upper mantle. *Earth Planet. Sci. Lett.*, **52**: 183-190.

Wood D.A., Joron J.-L., Treuil M., Norry M. and Tarney J., 1979. Elemental and Sr isotope variations in basic lavas from Iceland and surrounding ocean floor. *Contrib. Mineral. Petrol.*, **70**: 319-339.

Woodhead J.D., 1989. Geochemistry of the Mariana arc (western Pacific): Source composition and processes. *Chem. Geol.*, **76**: 1-24.

Yoder H.S. and Tilley C.E., 1962. Origin of basalt magmas: an experimental study of natural and synthetic rock systems. *J. Petrol.*, **3**: 342-532.

Zindler A., Hart S.R., Frey F.A. and Jakobsson S.P., 1979. Nd and Sr isotope ratios and rare earth element abundances in Reykjanes Peninsula basalts: Evidence for mantle heterogeneity beneath Iceland. *Earth Planet. Sci. Lett.*, **45**: 249-262.

Appendix 1

Catalogue of samples

The Australian-Antarctic Discordance:

UTAS#	Cruise	Sample no.	Latitude	Longitude	Depth, m	Group
78899	MW8801-	1-1	50.21°S	128.54°E	3200	8
78900	MW8801-	1-2	50.21°S	128.54°E	3200	8
78901	MW8801-	1-7	50.21°S	128.54°E	3200	8
78902	MW8801-	1-11	50.21°S	128.54°E	3200	8
78903	MW8801-	1-13	50.21°S	128.54°E	3200	8
78904	MW8801-	1-15	50.21°S	128.54°E	3200	8
78905	MW8801-	1-25	50.21°S	128.54°E	3200	8
78906	MW8801-	1-26	50.21°S	128.54°E	3200	8
78907	MW8801-	1-27	50.21°S	128.54°E	3200	8
78908	MW8801-	1-38	50.21°S	128.54°E	3200	8
78909	MW8801-	1-47	50.21°S	128.54°E	3200	8
78910	MW8801-	1-55	50.21°S	128.54°E	3200	8
78911	MW8801-	1-59	50.21°S	128.54°E	3200	8
78912	MW8801-	2-1	50.31°S	129.53°E	3200	8
78913	MW8801-	3-2	50.15°S	127.96°E	3600-3400	8
78914	MW8801-	3-3	50.15°S	127.96°E	3600-3400	8
78915	MW8801-	3-10	50.15°S	127.96°E	3600-3400	8
78916	MW8801-	3-17	50.15°S	127.96°E	3600-3400	8
78917	MW8801-	3-18	50.15°S	127.96°E	3600-3400	8
78918	MW8801-	3-21	50.15°S	127.96°E	3600-3400	8
78919	MW8801-	12-1	50.11°S	127.83°E	3600	8
78920	MW8801-	13-A	50.21°S	128.01°E	3400-3200	8
78921	MW8801-	13-20	50.21°S	128.01°E	3400-3200	8
78922	MW8801-	13-30	50.21°S	128.01°E	3400-3200	8
78923	MW8801-	16-2	50.16°S	127.58°E	3600-3500	12
78924	MW8801-	16-3	50.16°S	127.58°E	3600-3500	12
78925	MW8801-	16-12	50.16°S	127.58°E	3600-3500	12
78926	MW8801-	17-1	50.22°S	127.42°E	3400-3100	10
78927	MW8801-	17-18	50.22°S	127.42°E	3400-3100	10
78928	MW8801-	17-31	50.22°S	127.42°E	3400-3100	10
78929	MW8801-	17-45	50.22°S	127.42°E	3400-3100	10
78930	MW8801-	9-11	50.20°S	127.06°E	3400-3200	9
78931	MW8801-	9-13	50.20°S	127.06°E	3400-3200	9
78932	MW8801-	9-14	50.20°S	127.06°E	3400-3200	9
78933	MW8801-	9-17	50.20°S	127.06°E	3400-3200	9
78934	MW8801-	9-18	50.20°S	127.06°E	3400-3200	9
78935	MW8801-	9-20	50.20°S	127.06°E	3400-3200	9
78936	MW8801-	9-22	50.20°S	127.06°E	3400-3200	9
78937	MW8801-	9-23	50.20°S	127.06°E	3400-3200	9
78938	MW8801-	9-26	50.20°S	127.06°E	3400-3200	9
78939	MW8801-	9-29	50.20°S	127.06°E	3400-3200	9
78940	MW8801-	9-31	50.20°S	127.06°E	3400-3200	9
78941	MW8801-	9-42	50.20°S	127.06°E	3400-3200	9
78942	MW8801-	9-49	50.20°S	127.06°E	3400-3200	9
78943	MW8801-	9-51	50.20°S	127.06°E	3400-3200	9
78944	MW8801-	10-2	50.24°S	127.59°E	3200	9
78945	MW8801-	10-3	50.24°S	127.59°E	3200	9
78946	MW8801-	10-4	50.24°S	127.59°E	3200	9
78947	MW8801-	10-5	50.24°S	127.59°E	3200	9
78948	MW8801-	10-8	50.24°S	127.59°E	3200	9
78949	MW8801-	10-10	50.24°S	127.59°E	3200	9
78950	MW8801-	10-13	50.24°S	127.59°E	3200	9
78951	MW8801-	11-5	50.15°S	127.65°E	3400	9
78952	MW8801-	11-8	50.15°S	127.65°E	3400	9
78953	MW8801-	11-9	50.15°S	127.65°E	3400	9
78954	MW8801-	11-24	50.15°S	127.65°E	3400	9
78955	MW8801-	16-9	50.16°S	127.58°E	3600-3500	9
78956	MW8801-	16-20	50.16°S	127.58°E	3600-3500	9
78957	MW8801-	16-24	50.16°S	127.58°E	3600-3500	9
78958	MW8801-	16-28	50.16°S	127.58°E	3600-3500	9

UTAS#	Cruise	Sample no.	Latitude	Longitude	Depth, m	Group
78959	MW8801-	19-32	50.15°S	127.02°E	3200	9
78960	MW8801-	19-41	50.15°S	127.02°E	3200	9
78961	MW8801-	19-45	50.15°S	127.02°E	3200	9
78962	MW8801-	19-52	50.15°S	127.02°E	3200	9
78963	MW8801-	19-54	50.15°S	127.02°E	3200	9
78964	MW8801-	20-1	49.52°S	127.59°E	3300	11
78965	MW8801-	18-8	50.05°S	126.74°E	4600-4000	1
78966	MW8801-	18-9	50.05°S	126.74°E	4600-4000	1
78967	MW8801-	18-12	50.05°S	126.74°E	4600-4000	1
78968	MW8801-	18-16	50.05°S	126.74°E	4600-4000	1
78969	MW8801-	18-17	50.05°S	126.74°E	4600-4000	1
78970	MW8801-	18-18	50.05°S	126.74°E	4600-4000	1
78971	MW8801-	24-1	49.77°S	126.17°E	3600-3500	1
78972	MW8801-	24-3	49.77°S	126.17°E	3600-3500	1
78973	MW8801-	24-6	49.77°S	126.17°E	3600-3500	1
78974	MW8801-	24-7	49.77°S	126.17°E	3600-3500	1
78975	MW8801-	24-9	49.77°S	126.17°E	3600-3500	1
78976	MW8801-	24-10	49.77°S	126.17°E	3600-3500	1
78977	MW8801-	24-14	49.77°S	126.17°E	3600-3500	1
78978	MW8801-	24-15	49.77°S	126.17°E	3600-3500	1
78979	MW8801-	27-7	49.06°S	124.96°E	4200-4000	1
78980	MW8801-	27-8	49.06°S	124.96°E	4200-4000	1
78981	MW8801-	27-41	49.06°S	124.96°E	4200-4000	1
78982	MW8801-	27-48	49.06°S	124.96°E	4200-4000	1
78983	MW8801-	27-66	49.06°S	124.96°E	4200-4000	1
78984	MW8801-	27-68	49.06°S	124.96°E	4200-4000	1
78985	MW8801-	22-4	49.68°S	125.89°E	4000	3
78986	MW8801-	22-11	49.68°S	125.89°E	4000	3
78987	MW8801-	22-18	49.68°S	125.89°E	4000	3
78988	MW8801-	22-26	49.68°S	125.89°E	4000	3
78989	MW8801-	22-32	49.68°S	125.89°E	4000	3
78990	MW8801-	23-1	49.61°S	125.66°E	4000-3800	4
78991	MW8801-	23-3	49.61°S	125.66°E	4000-3800	4
78992	MW8801-	23-4	49.61°S	125.66°E	4000-3800	4
78993	MW8801-	29-1	48.91°S	124.47°E	4200-4600	2
78994	MW8801-	29-2	48.91°S	124.47°E	4200-4600	2
78995	MW8801-	29-3	48.91°S	124.47°E	4200-4600	2
78996	MW8801-	29-5	48.91°S	124.47°E	4200-4600	2
78997	MW8801-	29-29	48.91°S	124.47°E	4200-4600	2
78998	MW8801-	30-2	48.94°S	124.28°E	4400-4300	2
78999	MW8801-	30-5	49.68°S	125.89°E	4400-4300	2
79000	MW8801-	30-6	49.68°S	125.89°E	4400-4300	2
79001	MW8801-	30-15	49.68°S	125.89°E	4400-4300	2
79002	MW8801-	30-24	49.68°S	125.89°E	4400-4300	2
79003	MW8801-	5-1	48.68°S	126.52°E	4600-4800	5
79004	MW8801-	6-1	48.76°S	126.88°E	4400	5
79005	MW8801-	6-2	48.76°S	126.88°E	4400	5
79006	MW8801-	6-3	48.76°S	126.88°E	4400	5
79007	MW8801-	4-2	48.76°S	127.36°E	4000-3600	6
79008	MW8801-	27-52	49.06°S	124.96°E	4200-4000	7

North Fiji Basin-Hunter Ridge-Hunter fracture zone:

UTAS#	Cruise	Sample no	Latitude	Longitude	Depth, m	Group
74671	N-17-6	73/1	23°09.9'-23°10.3'S	172°26.3'-172°28.3'E	6500-6120	E-MORB
74672	N-17-6	73/2	23°09.9'-23°10.3'S	172°26.3'-172°28.3'E	6500-6120	E-MORB
74674	N-17-6	73/8	23°09.9'-23°10.3'S	172°26.3'-172°28.3'E	6500-6120	E-MORB
74698	N-17-6	76/35	23°05.6'-23°04.4'S	172°27.9'-172°27.5'E	6280-6200	Boninite 1
74700	N-17-6	76/38	23°05.6'-23°04.4'S	172°27.9'-172°27.5'E	6280-6200	Boninite 1
74701	N-17-6	76/39	23°05.6'-23°04.4'S	172°27.9'-172°27.5'E	6280-6200	Boninite 2
74703	N-17-6	76/41	23°05.6'-23°04.4'S	172°27.9'-172°27.5'E	6280-6200	Boninite 1
74704	N-17-6	76/43	23°05.6'-23°04.4'S	172°27.9'-172°27.5'E	6280-6200	Boninite 1
79009	N-17-6	76/59	23°05.6'-23°04.4'S	172°27.9'-172°27.5'E	6280-6200	Boninite 2
74711	N-17-6	76/65	23°05.6'-23°04.4'S	172°27.9'-172°27.5'E	6280-6200	Boninite 1
79010	N-17-6	77/28	23°04.5'-23°03.7'S	172°25.6'-172°26.6'E	5960-5840	Boninite 1
79011	N-17-6	78/62	23°03.9'-23°02.3'S	172°26.2'-172°28.4'E	5280-4650	IAT 2
74762	N-17-6	78/64	23°03.9'-23°02.3'S	172°26.2'-172°28.4'E	5280-4650	IAT 2
74764	N-17-6	78/66	23°03.9'-23°02.3'S	172°26.2'-172°28.4'E	5280-4650	Boninite 1
74766	N-17-6	78/73	23°03.9'-23°02.3'S	172°26.2'-172°28.4'E	5280-4650	Boninite 1
74767	N-17-6	78/83	23°03.9'-23°02.3'S	172°26.2'-172°28.4'E	5280-4650	Boninite 1
74773	N-17-6	79/8	23°01.7'-23°01.1'S	172°24.0'-172°24.5'E	4650-4440	IAT 1
74774	N-17-6	79/9	23°01.7'-23°01.1'S	172°24.0'-172°24.5'E	4650-4440	IAT 1
74778	N-17-6	79/16	23°01.7'-23°01.1'S	172°24.0'-172°24.5'E	4650-4440	IAT 1
79012	N-17-6	79/19	23°01.7'-23°01.1'S	172°24.0'-172°24.5'E	4650-4440	IAT 1
79013	N-17-6	79/20	23°01.7'-23°01.1'S	172°24.0'-172°24.5'E	4650-4440	IAT 1
74799	N-17-6	80/39	23°01.7'-23°01.1'S	172°24.0'-172°24.5'E	4400-4250	IAT 2
74805	N-17-6	80/51	23°01.7'-23°01.1'S	172°24.0'-172°24.5'E	4400-4250	Boninite 1
74806	N-17-6	80/53	23°01.7'-23°01.1'S	172°24.0'-172°24.5'E	4400-4250	IAT 2
74807	N-17-6	80/54	23°01.7'-23°01.1'S	172°24.0'-172°24.5'E	4400-4250	Boninite 1
74808	N-17-6	80/55	23°01.7'-23°01.1'S	172°24.0'-172°24.5'E	4400-4250	Boninite 1
74821	N-17-6	81/17	22°58.2'-22°58.4'S	172°26.8'-172°25.5'E	3480-3040	Boninite 2
74822	N-17-6	81/18	22°58.2'-22°58.4'S	172°26.8'-172°25.5'E	3480-3040	Boninite 1
79014	N-17-6	82/21	23°05.3'-23°06.1'S	172°02.1'-172°02.5'E	6920-6840	IAT 1
74844	N-17-6	84/5	22°47.8'-22°47.3'S	172°11.6'-172°14.8'E	5200-4700	Boninite 2
74845	N-17-6	84/6	22°47.8'-22°47.3'S	172°11.6'-172°14.8'E	5200-4700	Rhyolite
74847	N-17-6	84/10	22°47.8'-22°47.3'S	172°11.6'-172°14.8'E	5200-4700	Rhyolite
74848	N-17-6	84/11	22°47.8'-22°47.3'S	172°11.6'-172°14.8'E	5200-4700	Rhyolite
74850	N-17-6	84/13	22°47.8'-22°47.3'S	172°11.6'-172°14.8'E	5200-4700	Rhyolite
74863	N-17-6	86/6	22°46.9'-22°47.0'S	172°18.5'-172°19.4'E	3160-2900	IAT 2
74865	N-17-6	86/8	22°46.9'-22°47.0'S	172°18.5'-172°19.4'E	3160-2900	Rhyolite
74866	N-17-6	86/9	22°46.9'-22°47.0'S	172°18.5'-172°19.4'E	3160-2900	Rhyolite
74871	N-17-6	87/5	22°48.0'-22°48.0'S	172°24.1'-172°23.0'E	2630-2260	IAT 2
79015	N-17-6	87/7	22°48.0'-22°48.0'S	172°24.1'-172°23.0'E	2630-2260	IAT 2
74872	N-17-6	87/8	22°48.0'-22°48.0'S	172°24.1'-172°23.0'E	2630-2260	IAT 2
74875	N-17-6	87/11	22°48.0'-22°48.0'S	172°24.1'-172°23.0'E	2630-2260	IAT 2
74876	N-17-6	87/13	22°48.0'-22°48.0'S	172°24.1'-172°23.0'E	2630-2260	IAT 2
74878	N-17-6	87/15	22°48.0'-22°48.0'S	172°24.1'-172°23.0'E	2630-2260	IAT 2
79016	N-17-6	87/16	22°48.0'-22°48.0'S	172°24.1'-172°23.0'E	2630-2260	IAT 2
74882	N-17-6	87/21	22°48.0'-22°48.0'S	172°24.1'-172°23.0'E	2630-2260	IAT 2
74895	N-17-6	87/34	22°48.0'-22°48.0'S	172°24.1'-172°23.0'E	2630-2260	IAT 2
74896	N-17-6	87/35	22°48.0'-22°48.0'S	172°24.1'-172°23.0'E	2630-2260	IAT 2
79017	N-17-6	87/36	22°48.0'-22°48.0'S	172°24.1'-172°23.0'E	2630-2260	IAT 2
74913	N-17-6	88/9	22°45.9'-22°47.5'S	172°32.5'-172°31.4'E	2600-2360	IAT 2
74915	N-17-6	88/14	22°45.9'-22°47.5'S	172°32.5'-172°31.4'E	2600-2360	Boninite 2
74916	N-17-6	89/1	22°31.7'-22°31.7'S	172°54.1'-172°54.1'E	4300-4240	89
79018	N-17-6	92/37	23°01.4'-23°00.4'S	172°54.5'-172°52.9'E	6000-5600	E-MORB
74993	N-17-6	92/98	23°01.4'-23°00.4'S	172°54.5'-172°52.9'E	6000-5600	Boninite 1
79019	N-17-6	94/1	22°46'S	172°50'E	3360	Boninite 1
75016	N-17-6	101/1	22°15'S	172°45'S	2000	101
75017	N-17-6	102/1	22°11.5'-22°11.9'S	172°51.0'-172°52.0'E	1980-1840	BABB 2
75019	N-17-6	105/1	22°31.9'-22°30.1'S	172°59.5'-172°57.6'E	4620-4040	Boninite 2
75020	N-17-6	105/2	22°31.9'-22°30.1'S	172°59.5'-172°57.6'E	4620-4040	Boninite 2

UTAS#	Cruise	Sample no	Latitude	Longitude	Depth, m	Group
75021	N-17-6	108/1	22°09.9'-22°09.6'S	173°12.7'-173°12.9'E	1520-1320	Rhyolite
75024	N-17-6	108/4	22°09.9'-22°09.6'S	173°12.7'-173°12.9'E	1520-1320	Rhyolite
75025	N-17-6	108/5	22°09.9'-22°09.6'S	173°12.7'-173°12.9'E	1520-1320	108
75026	N-17-6	108/6	22°09.9'-22°09.6'S	173°12.7'-173°12.9'E	1520-1320	108
75027	N-17-6	108/7	22°09.9'-22°09.6'S	173°12.7'-173°12.9'E	1520-1320	108
75028	N-17-6	108/8	22°09.9'-22°09.6'S	173°12.7'-173°12.9'E	1520-1320	108
75030	N-17-6	108/10	22°09.9'-22°09.6'S	173°12.7'-173°12.9'E	1520-1320	Rhyolite
75034	N-17-6	108/14	22°09.9'-22°09.6'S	173°12.7'-173°12.9'E	1520-1320	108
75035	N-17-6	108/15	22°09.9'-22°09.6'S	173°12.7'-173°12.9'E	1520-1320	Rhyolite
75036	N-17-6	108/16	22°09.9'-22°09.6'S	173°12.7'-173°12.9'E	1520-1320	Rhyolite
75037	N-17-6	113/1	22°37.3'-22°36.4'S	173°12.8'-173°15.5'E	5560-5160	IAT 2
75039	N-17-6	113/3	22°37.3'-22°36.4'S	173°12.8'-173°15.5'E	5560-5160	IAT 2
75041	N-17-6	113/5	22°37.3'-22°36.4'S	173°12.8'-173°15.5'E	5560-5160	IAT 2
75042	N-17-6	113/6	22°37.3'-22°36.4'S	173°12.8'-173°15.5'E	5560-5160	IAT 2
75044	N-17-6	113/8	22°37.3'-22°36.4'S	173°12.8'-173°15.5'E	5560-5160	IAT 2
75058	N-17-6	115/3	22°39.5'-22°40.6'S	173°13.4'-173°15.1'E	5880-5560	IAT 2
75059	N-17-6	115/4	22°39.5'-22°40.6'S	173°13.4'-173°15.1'E	5880-5560	IAT 1
75061	N-17-6	115/6	22°39.5'-22°40.6'S	173°13.4'-173°15.1'E	5880-5560	IAT 2
75062	N-17-6	115/7	22°39.5'-22°40.6'S	173°13.4'-173°15.1'E	5880-5560	IAT 2
75078	N-17-6	115/23	22°39.5'-22°40.6'S	173°13.4'-173°15.1'E	5880-5560	IAT 1
75079	N-17-6	115/24	22°39.5'-22°40.6'S	173°13.4'-173°15.1'E	5880-5560	Boninite 1
75080	N-17-6	115/25	22°39.5'-22°40.6'S	173°13.4'-173°15.1'E	5880-5560	IAT 1
75085	N-17-6	115/31	22°39.5'-22°40.6'S	173°13.4'-173°15.1'E	5880-5560	IAT 1
79020	N-17-6	115/37	22°39.5'-22°40.6'S	173°13.4'-173°15.1'E	5880-5560	IAT 1
75089	N-17-6	115/38	22°39.5'-22°40.6'S	173°13.4'-173°15.1'E	5880-5560	IAT 2
75090	N-17-6	115/39	22°39.5'-22°40.6'S	173°13.4'-173°15.1'E	5880-5560	IAT 2
75091	N-17-6	115/40	22°39.5'-22°40.6'S	173°13.4'-173°15.1'E	5880-5560	IAT 1
75092	N-17-6	115/41	22°39.5'-22°40.6'S	173°13.4'-173°15.1'E	5880-5560	Boninite 1
75093	N-17-6	115/42	22°39.5'-22°40.6'S	173°13.4'-173°15.1'E	5880-5560	IAT 1
75094	N-17-6	115/43	22°39.5'-22°40.6'S	173°13.4'-173°15.1'E	5880-5560	Boninite 1
75098	N-17-6	115/47	22°39.5'-22°40.6'S	173°13.4'-173°15.1'E	5880-5560	IAT 1
75099	N-17-6	115/48	22°39.5'-22°40.6'S	173°13.4'-173°15.1'E	5880-5560	IAT 1
75110	N-17-6	115/59	22°39.5'-22°40.6'S	173°13.4'-173°15.1'E	5880-5560	Boninite 1
75117	N-17-6	115/66	22°39.5'-22°40.6'S	173°13.4'-173°15.1'E	5880-5560	IAT 2
75171	N-17-6	116/26	22°41'S	173°13'E	5400-5000	Boninite 1
75173	N-17-6	116/28	22°41'S	173°13'E	5400-5000	IAT 1
75174	N-17-6	116/29	22°41'S	173°13'E	5400-5000	IAT 2
75178	N-17-6	116/33	22°41'S	173°13'E	5400-5000	Boninite 2
75181	N-17-6	116/36	22°41'S	173°13'E	5400-5000	Boninite 1
75184	N-17-6	117/1	22°42'S	173°13'E	4800-4480	BABB 1
75185	N-17-6	117/2	22°42'S	173°13'E	4800-4480	BABB 2
75187	N-17-6	117/4	22°42'S	173°13'E	4800-4480	BABB 1
75188	N-17-6	117/5	22°42'S	173°13'E	4800-4480	BABB 2
75196	N-17-6	117/13	22°42'S	173°13'E	4800-4480	BABB 1
75199	N-17-6	117/16	22°42'S	173°13'E	4800-4480	BABB 1
79021	N-17-6	119/1	22°03'S	172°54'E	1960	BABB 2
75200	N-17-6	122/1	20°31'S	172°14'E	3400-3200	BABB 1
75201	N-17-6	122/2	20°31'S	172°14'E	3400-3200	BABB 1
75203	N-17-6	122/5	20°31'S	172°14'E	3400-3200	BABB 1
75206	N-17-6	122/8	20°31'S	172°14'E	3400-3200	BABB 1
75208	N-17-6	122/11	20°31'S	172°14'E	3400-3200	BABB 1
79022	N-17-6	122/13	20°31'S	172°14'E	3400-3200	BABB 1
75209	N-17-6	123/1	20°29'S	172°15'E	2800-2620	BABB 2
79023	N-17-6	123/2	20°29'S	172°15'E	2800-2620	BABB 2
79024	N-17-6	123/3	20°29'S	172°15'E	2800-2620	BABB 2

Iceland:

UTAS#	IMNH#	Sample no	Description	Locality
79025	9303	NO 42	Tholeiite (picrite)	N of Bæjarfjall, Randahraun, Krafla system
79026	5897	NO 42	Gabbroic xenolith in NO 42	N of Bæjarfjall, Randahraun, Krafla system
79027	9301	NO 58	Tholeiite (picrite)	V of Gæsafjöll, Bóndhólshraun, Krafla system
79028	8547	RE 36	Tholeiite (picrite)	Lágafellshraun, Reykjanes system
79029	4690	RE 78	Tholeiite (picrite)	Vatnsheidarhraun, Grindavík system
79030	8701	RE 120	Tholeiite (picrite)	Búrfellshraun, Hengill system
79031	8703	RE 154	Tholeiite (picrite)	Raufarhólshraun, Hengill system
79032	8592	RE 185	Tholeiite (picrite)	Fagradalshraun, Fagridalur, Grindavík system
79033	8702	RE 217	Tholeiite (picrite)	SE of Ásar, Ásar, Hengill system
79034	7996	RE 286	Tholeiite (olivine-tholeiite)	Stóru Eldborgarhraun, Krísuvík system
79035	8532	RE 291	Tholeiite (picrite)	Háleyjarbunga, Reykjanes system
79036		HP-8	Tholeiite (picrite)	Hrólfsvíkurhraun, Grindavík system
79037	6388	1977 A:4	Olivine accumulate	Skútagil, Bjarnardalur, of Nordurárdalur
79038	9847	SU 18II	Alkali-olivine basalt	NE part of Surtsey,
79039	9851	SU 24	Alkali-olivine basalt	E of the 1966 fissure, Surtsey

UTAS# = Catalogue number, University of Tasmania
IMNH# = Catalogue number, Icelandic Museum of Natural History

Appendix 2

Analytical techniques

A2.1 Microprobe analyses

Minerals were analysed either in thin section or more commonly in probe mounts with mineral separates. Whole-rock samples were carefully crushed and sieved and the phenocryst phases were picked from the suitable size fraction, glued in epoxy and polished. For glass analyses the glasses were carefully picked from pillow rims or chilled margins, glued in epoxy and polished.

The analyses were performed using a fully automated, three spectrometer Cameca SX 50 electron microprobe (Central Science Laboratory, University of Tasmania) calibrated with natural glass and mineral standards (PAP data reduction). In most instances three points were analysed and averaged, and during each session standards were analysed at the beginning and the end of each run, and at approximately three hours intervals in longer runs.

The standards used were San Carlos Olivine (USNM 111312/444), basaltic glass VG-2 (USNM 111249/52), plagioclase LPL (USNM 115900), Augite KA (USNM 122142) (Jarosewich et al., 1980), spinel UV-126 (Lavrentev et al., 1974) and natural obsidian glass (Astimex Scientific Limited). Analytical conditions and counting times for each analytical label used are given in Table A1 and representative averages of six standard analyses are given in Table A2. Matrix corrections, based on San Carlos Olivine, were applied while using the label KSPCOLTR.

Table A1: Analytical conditions and counting times for the analytical labels used during microprobe analyses.

		Label:							
Oxide	Spectrometer	Dima	Olivine	Leopyr	Lplg	Kspcoltr	Obsiglass	Glassleo	Uvspleo
SiO_2	TAP	10/5	10/5	10/5	10/5		10/5	10/5	10/5
TiO_2	PET			10/5			10/5	10/5	20/10
Al_2O_3	TAP			10/5	10/5		10/5	20/10	20/10
FeO	LIF	20/10	20/10	20/10	10/5		20/10	20/10	20/10
MnO	LIF		20/10	20/10		120/60	20/10	20/10	20/10
MgO	TAP	10/5	10/5	10/5	10/5		10/5	10/5	10/5
CaO	PET	20/10	20/10	10/5	10/5	120/60	10/5	10/5	(10/5)
Na_2O	TAP			20/10	20/10		20/10	20/10	
K_2O	PET				20/10		20/10	20/10	
P_2O_5	TAP						20/10	20/10	
Cr_2O_3	PET		20/10	20/10		120/60		20/10	10/5
NiO	LIF		20/10			120/60			10/5
ZnO	LIF								10/5
Accelerating voltage		15 kV	15 kV	15 kV	15 kV	20 kV	15 kV	15 kV	15 kV
Beam current		20 nA	20 nA	20 nA	20 nA	200 nA	8 nA	10 nA	20 nA
Beam size		5 µm	5 µm	5 µm	5 µm	20 µm	10 µm	5-10 µm	1 µm

Table A2: Standards and labels used for most of the microprobe analyses. The first column shows the average of six analyses, the second the standard deviation and the third the recomended values.

Label	UVSPLEO		
Oxide	UV-126	σ(n-1)	UV-126
SiO_2	0.31	0.06	0.30
TiO_2	4.75	0.10	4.61
Al_2O_3	8.77	0.11	8.79
Cr_2O_3	44.48	0.37	44.80
FeO*	26.08	0.24	26.30
MnO	0.23	0.06	0.29
NiO	0.24	0.05	0.32
MgO	14.10	0.19	14.10
ZnO	0.06	0.05	
Sum	100.12		99.51

Label	OLIVINE		
Oxide	SCOL	σ(n-1)	SCOL
SiO_2	40.48	0.33	40.81
Cr_2O_3	0.02	0.02	0.01
FeO	9.52	0.10	9.55
MnO	0.11	0.06	0.14
MgO	49.42	0.22	49.42
CaO	0.10	0.03	0.10
NiO	0.37	0.05	0.37
Sum	100.01		100.40

Label	LEOPYR		
Oxide	KA	σ(n-1)	KA
SiO_2	50.31	0.10	50.73
TiO_2	0.74	0.03	0.74
Al_2O_3	8.72	0.06	8.73
Cr_2O_3	0.14	0.03	
FeO*	6.37	0.10	6.37
MnO	0.09	0.03	0.13
MgO	16.64	0.07	16.65
CaO	15.82	0.09	15.82
Na_2O	1.27	0.03	1.27
Sum	100.28		100.44

Label	DIMA		
Oxide	Scol	σ(n-1)	SCOL
SiO_2	40.75	0.14	40.81
FeO	9.49	0.07	9.55
MgO	49.30	0.27	49.42
CaO	0.09	0.01	0.1
Sum	99.63		99.88

Label	LPLG		
Standard	LPL	σ(n-1)	LPL
SiO_2	51.14	0.25	51.25
Al_2O_3	30.59	0.14	30.91
FeO	0.43	0.06	0.46
MgO	0.13	0.02	0.14
CaO	13.56	0.04	13.64
Na_2O	3.54	0.03	3.45
K_2O	0.13	0.02	0.18
Sum	99.52		100.08

Label	KSPCOLTR		
Oxide	SCOL	σ(n-1)	SCOL
Cr_2O_3	0.013	0.002	
MnO	0.170	0.003	0.14
NiO	0.378	0.007	0.37
CaO	0.096	0.002	0.10

Label	OBSIGLASS		
Oxide	Obsidian	σ(n-1)	Obsidian
SiO_2	74.14	0.56	73.94
TiO_2	0.06	0.02	0.10
Al_2O_3	13.27	0.17	13.11
FeO*	1.58	0.10	1.72
MnO	0.05	0.05	0.06
MgO	0.04	0.01	0.07
CaO	0.81	0.01	0.76
Na_2O	3.96	0.06	4.06
K_2O	5.12	0.05	5.04
P_2O_5	0.02	0.02	
Sum	99.05		98.86

Label	GLASSLEO		
Oxide	VG2	σ(n-1)	VG2
SiO_2	50.71	0.23	50.81
TiO_2	1.85	0.06	1.85
Al_2O_3	14.07	0.08	14.06
FeO	11.90	0.14	11.84
MnO	0.25	0.03	0.22
MgO	6.82	0.05	6.71
CaO	11.03	0.09	11.12
Na_2O	2.58	0.05	2.62
K_2O	0.20	0.01	0.19
P_2O_5	0.17	0.03	0.20
Sum	99.58		99.62

A2.2 Whole-rock analyses

Samples were crushed in a steel jaw crusher and fresh chips were picked and washed in an ultrasonic bath before they were crushed to approximately 325 mesh in a tungsten carbide mill.

Major elements were analysed by XRF spectrometry in fused glass disks (Norrish and Hutton, 1969), and trace elements in pressed powder pellets cased in boric acid

(Norrish and Chappell, 1977), using an automated Philips PW1480 spectrometer at the Geology Department, University of Tasmania. Instrumental conditions are given in Table A3. Trace element concentrations were determined using mass absorption coefficients calculated from major element analyses and results were checked against internal standards.

Ignition loss (LOI) was determined on all samples by firing approximately 1 g of pre-dried sample at 1000 °C over night. Negative LOI indicates a gain in weight because oxidation of FeO to Fe_2O_3 was greater than the loss of volatiles.

Th, Hf and REE (where Lu is reported) were analysed by INAA (detection limits are given in Table A4) at the Becquerel Laboratories, Lucas Heights Research Laboratories, NSW (Dr Helen Waldron analyst); other REE were analysed by the ion exchange, XRF method of Robinson et al., (1986).

Table A3: Instrumental conditions for major and trace element analyses (Philips PW1480). Detection limits are 3 sigma (99%) confidence levels. Auxiliary collimator was used with the scintillation counter.

Oxide	Line	Tube	Crystal	Counter	Collimator	Vacuum	kV/mA	Det. limit (wt%)
SiO_2	K alpha	ScMo	PE	Flow	Coarse	YES	40/70	0.002
TiO_2	K alpha	ScMo	LiF200	Flow	Fine	YES	90/30	0.006
Al_2O_3	K alpha	ScMo	PE	Flow	Coarse	YES	40/70	0.008
Fe_2O_3	K alpha	ScMo	LiF200	Flow	Fine	YES	90/30	0.0041
MnO	K alpha	ScMo	LiF200	Flow	Fine	YES	90/30	0.0035
MgO	K alpha	ScMo	TLAP	Flow	Coarse	YES	40/70	0.011
CaO	K alpha	ScMo	LiF200	Flow	Fine	YES	40/70	0.0009
Na_2O	K alpha	ScMo	TLAP	Flow	Coarse	YES	40/70	0.024
K_2O	K alpha	ScMo	PE	Flow	Fine	YES	40/70	0.0004
P_2O_5	K alpha	ScMo	GE	Flow	Coarse	YES	40/70	0.0026
								(ppm)
Rb	K alpha	ScMo	LIF200	Scintillation	Fine	YES	90/30	1
Ba	L alpha	Au	LIF200	Flow	Fine	YES	47/70	4
Nb	K alpha	ScMo	LIF200	Scintillation	Fine	YES	80/38	1
Sr	K alpha	ScMo	LIF200	Scintillation	Fine	YES	80/35	1
Zr	K alpha	Au	LIF200	Scintillation	Fine	YES	80/35	1
Y	K alpha	ScMo	LIF200	Scintillation	Fine	YES	90/30	1
Sc	K alpha	Au	LIF200	Flow	Fine	YES	40/70	2
V	K alpha	Au	LIF200	Flow	Fine	YES	40/70	1.5
Cr	K alpha	Au	LIF200	Flow	Fine	YES	40/70	1
Ni	K alpha	ScMo	LIF200	Flow	Fine	YES	90/30	1

Table A4: Detection limits for Neutron Activation Analysis.

Element	ppm
La	0.1
Ce	1.0
Nd	2.0
Sm	0.05
Eu	0.1
Tb	0.3
Ho	0.3
Yb	0.1
Lu	0.05
Hf	0.2
Th	0.2

Appendix 3

Representative mineral analyses

Australian Antarctic Discordance

Olivine

Sample	18-9	18-9	18-9	18-9	18-9	18-9	18-9	18-9	18-9	18-9	18-9
Olivine	1	2	3	4	5	6	7	8	9	10	11
SiO_2	39.30	40.08	39.60	39.74	39.95	40.03	39.80	39.52	39.84	40.04	40.19
Cr_2O_3	0.04	0.04	0.06	0.08	0.05	0.07	0.06	0.08	0.06	0.09	0.06
FeO	12.16	12.41	11.70	11.74	10.58	11.38	11.05	12.39	12.05	11.85	11.15
MnO	0.18	0.16	0.14	0.11	0.12	0.16	0.12	0.18	0.14	0.10	0.12
MgO	46.33	46.94	47.31	47.25	48.13	47.46	47.66	46.41	47.09	47.33	47.33
CaO	0.31	0.31	0.28	0.30	0.27	0.30	0.27	0.32	0.29	0.29	0.27
NiO	0.24	0.23	0.20	0.21	0.31	0.24	0.27	0.22	0.21	0.24	0.29
Sum	98.56	100.17	99.29	99.43	99.41	99.65	99.24	99.11	99.67	99.93	99.39
Fo	87.2	87.1	87.8	87.8	89.0	88.1	88.5	87.0	87.4	87.7	88.3

Sample	18-9	18-9	18-9	18-9	18-9	18-9	18-9	18-9	18-9	18-9	18-9
Olivine	12	13	14	15	16	17	18	19	20	148	188
SiO_2	39.99	39.96	39.98	40.02	39.62	39.87	39.90	40.07	40.04	39.72	40.45
Cr_2O_3	0.06	0.06	0.07	0.07	0.08	0.09	0.07	0.03	0.03	0.07	0.03
FeO	11.19	11.30	11.13	10.98	11.08	11.14	11.41	10.41	12.08	12.51	10.82
MnO	0.12	0.11	0.11	0.19	0.08	0.11	0.14	0.11	0.12	0.12	0.10
MgO	47.41	47.77	47.73	47.99	47.41	47.61	47.37	48.26	47.19	46.53	48.35
CaO	0.31	0.27	0.29	0.32	0.31	0.31	0.32	0.30	0.27	0.30	0.28
NiO	0.28	0.28	0.33	0.30	0.30	0.28	0.20	0.26	0.25	0.11	0.33
Sum	99.36	99.73	99.63	99.86	98.86	99.40	99.39	99.43	99.96	99.35	100.35
Fo	88.3	88.3	88.4	88.6	88.4	88.4	88.1	89.2	87.4	86.9	88.8

Sample	18-9	18-9	18-17	18-17	18-17	18-17	18-17	18-17	18-17	18-17	18-17
Olivine	195	281	1	2	3	4	5	6	7	8	9
SiO_2	40.11	40.30	40.55	40.19	40.30	40.21	40.24	40.25	40.17	40.17	40.15
Cr_2O_3	0.07	0.05	0.04	0.08	0.05	0.06	0.05	0.04	0.07	0.05	0.07
FeO	11.15	11.77	9.75	9.53	9.67	9.32	9.60	9.62	9.67	9.47	9.47
MnO	0.12	0.15	0.11	0.09	0.14	0.12	0.15	0.17	0.12	0.15	0.16
MgO	47.99	47.61	49.30	49.24	49.09	49.42	49.28	49.24	49.08	49.31	49.14
CaO	0.30	0.32	0.26	0.28	0.29	0.27	0.26	0.29	0.27	0.28	0.29
NiO	0.26	0.21	0.37	0.39	0.34	0.31	0.31	0.32	0.33	0.37	0.33
Sum	99.98	100.39	100.38	99.80	99.88	99.69	99.89	99.94	99.71	99.79	99.59
Fo	88.5	87.8	90.0	90.2	90.0	90.4	90.1	90.1	90.0	90.3	90.2

Sample	18-17	18-17	18-17	18-17	18-17	18-17	18-17	18-17	18-17	18-17	18-17
Olivine	10	11	12	13	14	15	16	17	18	19	30
SiO_2	39.96	40.20	39.96	40.21	40.30	40.25	40.15	40.17	39.95	40.24	39.92
Cr_2O_3	0.06	0.05	0.05	0.06	0.08	0.09	0.04	0.07	0.07	0.06	0.08
FeO	9.47	9.57	9.78	9.47	9.46	9.50	9.52	9.47	9.63	9.39	10.96
MnO	0.11	0.13	0.09	0.14	0.11	0.12	0.12	0.17	0.10	0.12	0.16
MgO	48.95	49.22	48.89	49.20	49.12	49.17	49.14	49.12	48.73	49.45	48.10
CaO	0.28	0.28	0.25	0.27	0.26	0.27	0.27	0.24	0.25	0.29	0.30
NiO	0.31	0.34	0.34	0.32	0.30	0.29	0.34	0.33	0.34	0.34	0.24
Sum	99.14	99.79	99.35	99.68	99.63	99.69	99.58	99.58	99.07	99.89	99.76
Fo	90.2	90.2	89.9	90.3	90.2	90.2	90.2	90.2	90.0	90.4	88.7

Sample	18-17	18-17	18-17	24-14	24-14	24-14	24-14	24-14	24-14	24-14	24-14
Olivine	33	34	173	1	2	3	4	6	7	8	9
SiO_2	40.22	40.13	40.32	39.84	40.01	39.86	39.87	40.03	39.80	39.93	40.31
Cr_2O_3	0.03	0.16	0.07	0.06	0.05	0.03	0.04	0.06	0.05	0.06	0.05
FeO	9.61	9.46	9.33	11.65	11.83	12.39	11.49	11.50	10.69	10.98	9.99
MnO	0.14	0.13	0.15	0.16	0.18	0.21	0.18	0.18	0.12	0.17	0.15
MgO	49.47	49.04	49.05	47.10	47.13	46.15	47.33	46.96	47.79	47.60	48.81
CaO	0.27	0.26	0.27	0.31	0.25	0.28	0.29	0.30	0.27	0.29	0.28
NiO	0.34	0.27	0.30	0.23	0.25	0.19	0.28	0.22	0.30	0.33	0.30
Sum	100.08	99.45	99.48	99.35	99.70	99.12	99.48	99.25	99.02	99.36	99.88
Fo	90.2	90.2	90.4	87.8	87.7	86.9	88.0	87.9	88.8	88.5	89.7

Sample	24-14	24-14	24-14	24-14	24-14	24-14	24-14	24-14	24-14	24-14	24-14
Olivine	10	11	13	14	17	18	19	20	21	22	23
SiO_2	39.88	40.11	39.83	39.97	40.05	40.01	39.79	40.35	40.10	40.02	40.28
Cr_2O_3	0.06	0.06	0.08	0.08	0.07	0.06	0.06	0.04	0.05	0.05	0.09
FeO	12.53	10.55	11.58	10.52	11.24	10.68	11.78	9.41	11.22	11.48	9.78
MnO	0.19	0.15	0.15	0.13	0.17	0.15	0.16	0.14	0.16	0.19	0.13
MgO	46.45	48.09	47.48	48.07	47.59	48.20	46.84	49.22	47.26	47.18	48.80
CaO	0.30	0.28	0.26	0.27	0.27	0.27	0.28	0.28	0.27	0.29	0.28
NiO	0.21	0.27	0.24	0.24	0.27	0.27	0.23	0.36	0.27	0.23	0.35
Sum	99.62	99.51	99.61	99.28	99.66	99.63	99.14	99.79	99.32	99.44	99.71
Fo	86.9	89.0	88.0	89.1	88.3	88.9	87.6	90.3	88.2	88.0	89.9

Sample	24-14	24-14	24-14	24-14	24-14	24-14	29 - 2	29 - 2	29 - 2	29 - 2	29 - 2
Olivine	24	25	36	38	42	52	1	2	3	4	6
SiO_2	39.78	40.20	40.01	40.10	40.34	39.89	39.78	39.15	39.71	39.76	39.45
Cr_2O_3	0.05	0.04	0.06	0.05	0.05	0.07	0.05	0.04	0.05	0.06	0.06
FeO	11.90	10.73	10.41	11.19	10.59	11.76	10.15	12.64	11.62	11.21	10.76
MnO	0.20	0.15	0.14	0.18	0.13	0.16	0.12	0.15	0.14	0.16	0.16
MgO	46.73	48.04	47.81	47.40	48.18	47.25	48.30	45.83	47.33	48.06	47.93
CaO	0.29	0.26	0.27	0.26	0.30	0.29	0.27	0.27	0.27	0.26	0.28
NiO	0.21	0.25	0.29	0.27	0.29	0.25	0.32	0.25	0.22	0.27	0.29
Sum	99.15	99.65	98.98	99.45	99.88	99.68	98.98	98.33	99.34	99.77	98.92
Fo	87.5	88.9	89.1	88.3	89.0	87.7	89.5	86.6	87.9	88.4	88.8

Sample	29 - 2	29 - 2	29 - 2	29 - 2	29 - 2	29 - 2	29 - 2	29 - 2	29 - 2	29 - 2	29 - 2
Olivine	8	9	12	14	15	16	17	20	21	24	49
SiO_2	39.71	39.84	39.80	39.58	39.79	39.65	40.03	39.79	39.61	39.90	39.92
Cr_2O_3	0.05	0.07	0.04	0.04	0.05	0.07	0.06	0.06	0.04	0.05	0.05
FeO	11.33	11.06	11.62	11.54	10.38	9.98	11.42	11.40	10.62	10.54	10.20
MnO	0.18	0.18	0.16	0.17	0.15	0.16	0.14	0.18	0.14	0.15	0.06
MgO	47.55	47.68	47.37	47.10	48.23	48.65	47.48	47.03	47.76	48.31	48.20
CaO	0.27	0.27	0.28	0.28	0.27	0.22	0.28	0.26	0.27	0.19	0.27
NiO	0.28	0.18	0.21	0.27	0.29	0.35	0.25	0.29	0.30	0.22	0.31
Sum	99.38	99.27	99.47	98.97	99.17	99.08	99.67	99.01	98.74	99.35	99.01
Fo	88.2	88.5	87.9	87.9	89.2	89.7	88.1	88.0	88.9	89.1	89.4

Sample	29 - 2	29 - 2	29 - 2	29 - 2	29 - 2	29 - 2	29 - 2	29 - 2	29 - 2
Olivine	70	97	90	250	263	260	18	50	93
SiO_2	39.82	39.95	39.56	39.48	39.59	39.36	39.89	39.60	39.75
Cr_2O_3	0.07	0.04	0.07	0.05	0.07	0.37	0.05	0.04	0.05
FeO	12.09	10.25	12.24	11.09	11.27	10.99	9.93	10.59	10.33
MnO	0.20	0.14	0.20	0.15	0.18	0.12	0.12	0.17	0.14
MgO	46.54	48.20	46.36	47.42	47.61	47.29	48.60	47.97	48.02
CaO	0.26	0.26	0.32	0.28	0.25	0.26	0.25	0.15	0.27
NiO	0.24	0.31	0.19	0.32	0.30	0.25	0.35	0.22	0.30
Sum	99.23	99.15	98.93	98.80	99.26	98.64	99.19	98.73	98.86
Fo	87.3	89.3	87.1	88.4	88.3	88.5	89.7	89.0	89.2

Plagioclase

Sample	18 - 9	18 - 9	18 - 9	18 - 9	18 - 9	18 - 9	18 - 9	18 - 9	18 - 9	18 - 9	18 - 9	18 - 9
Plagioclase	282	281	280	279	278	277	275	274	273	270	269	268
SiO_2	46.81	46.81	48.71	45.84	47.89	48.48	48.80	46.14	47.11	48.88	46.63	49.38
Al_2O_3	32.71	32.55	30.90	33.23	31.69	31.51	31.26	32.68	31.97	31.00	32.65	30.79
FeO	0.24	0.29	0.27	0.28	0.28	0.30	0.28	0.27	0.30	0.31	0.31	0.29
MgO	0.20	0.17	0.20	0.16	0.21	0.23	0.23	0.16	0.21	0.21	0.16	0.20
CaO	16.83	16.96	14.95	17.42	15.67	15.33	15.07	17.16	16.40	15.13	16.91	14.70
Na_2O	1.90	1.84	2.80	1.58	2.44	2.59	2.70	1.74	2.07	2.74	1.89	2.99
K_2O	0.02	0.02	0.03	0.01	0.02	0.01	0.00	0.01	0.01	0.01	0.02	0.02
Sum	98.71	98.64	97.86	98.51	98.21	98.44	98.35	98.16	98.06	98.28	98.57	98.36
An	83.0	83.5	74.5	85.9	77.9	76.6	75.5	84.4	81.4	75.3	83.0	73.0
Ab	16.9	16.4	25.3	14.1	22.0	23.4	24.5	15.5	18.6	24.7	16.8	26.9
Or	0.1	0.1	0.2	0.0	0.1	0.1	0.0	0.1	0.0	0.1	0.1	0.1

Sample	18 - 9	18 - 9	18 - 9	18 - 9	18 - 9	18 - 9	18 - 9	18 - 9	18 - 9	18 - 9	18 - 9	18 - 9
Plagioclase	267	266	265	264	262	261	259	258	257	256	255	254
SiO_2	48.66	48.38	46.70	46.92	49.58	46.87	48.68	47.81	46.12	47.50	46.67	45.91
Al_2O_3	31.27	31.40	32.39	32.47	30.89	32.31	31.09	32.11	32.74	32.47	32.49	32.86
FeO	0.34	0.24	0.30	0.26	0.22	0.34	0.32	0.33	0.27	0.32	0.33	0.34
MgO	0.26	0.20	0.18	0.18	0.18	0.21	0.22	0.18	0.20	0.21	0.17	0.18
CaO	15.34	15.54	16.67	16.53	14.59	16.70	15.21	16.31	17.28	16.56	16.67	17.38
Na_2O	2.64	2.59	1.94	2.00	3.07	1.97	2.78	2.19	1.68	2.12	1.93	1.63
K_2O	0.01	0.03	0.03	0.02	0.03	0.02	0.01	0.02	0.01	0.02	0.03	0.01
Sum	98.51	98.37	98.22	98.38	98.56	98.43	98.30	98.94	98.29	99.20	98.28	98.31
An	76.2	76.7	82.5	82.0	72.3	82.3	75.1	80.3	85.0	81.1	82.6	85.5
Ab	23.8	23.1	17.4	17.9	27.5	17.6	24.8	19.5	15.0	18.8	17.3	14.5
Or	0.1	0.2	0.2	0.1	0.2	0.1	0.1	0.1	0.0	0.1	0.2	0.0

Sample	18 - 9	24-14	24-14	24-14	24-14	24-14	24-14	24-14	24-14	24-14	24-14	24-14
Plagioclase	250	23	28	1	2	3	4	5	6	7	8	9
SiO_2	46.18	49.86	48.12	50.51	50.14	49.98	49.49	49.48	48.38	49.72	50.04	48.17
Al_2O_3	32.88	30.97	31.85	29.97	30.41	30.83	31.01	30.91	31.64	30.64	30.60	31.65
FeO	0.23	0.24	0.29	0.26	0.30	0.30	0.25	0.30	0.33	0.29	0.27	0.25
MgO	0.19	0.21	0.17	0.21	0.23	0.17	0.20	0.21	0.17	0.17	0.22	0.18
CaO	17.21	14.60	15.81	13.79	14.19	14.61	14.67	14.77	15.51	14.56	14.59	15.74
Na_2O	1.69	3.07	2.52	3.49	3.30	3.20	3.11	2.99	2.65	3.19	3.17	2.58
K_2O	0.01	0.03	0.01	0.05	0.03	0.03	0.04	0.03	0.02	0.04	0.01	0.03
Sum	98.37	98.98	98.77	98.28	98.61	99.13	98.77	98.68	98.70	98.62	98.90	98.60
An	84.9	72.3	77.5	68.4	70.2	71.5	72.1	73.1	76.3	71.4	71.7	77.0
Ab	15.1	27.5	22.4	31.3	29.6	28.4	27.6	26.7	23.6	28.3	28.2	22.8
Or	0.1	0.2	0.1	0.3	0.2	0.2	0.3	0.2	0.1	0.2	0.1	0.2

Sample	24-14	24-14	24-14	24-14	24-14	24-14	24-14	24-14	24-14	24-14	24-14	24-14
Plagioclase	10	11	12	13	16	17	18	19	20	15	21	22
SiO_2	49.62	49.77	50.00	50.02	50.07	49.93	50.21	49.59	50.32	49.95	50.06	50.57
Al_2O_3	30.55	30.58	30.35	30.69	30.16	30.62	30.76	31.25	30.61	30.68	31.00	30.24
FeO	0.29	0.29	0.25	0.32	0.24	0.26	0.28	0.26	0.28	0.28	0.26	0.28
MgO	0.18	0.18	0.20	0.20	0.20	0.15	0.18	0.19	0.19	0.20	0.18	0.19
CaO	14.45	14.33	14.29	14.40	14.28	14.47	14.45	14.77	14.32	14.51	14.34	14.03
Na_2O	3.23	3.19	3.29	3.20	3.34	3.16	3.31	3.03	3.29	3.14	3.21	3.38
K_2O	0.04	0.05	0.02	0.02	0.01	0.03	0.02	0.02	0.04	0.04	0.03	0.03
Sum	98.35	98.38	98.41	98.85	98.31	98.62	99.22	99.12	99.06	98.79	99.09	98.73
An	71.1	71.1	70.5	71.2	70.2	71.6	70.6	72.8	70.4	71.7	71.0	69.5
Ab	28.7	28.6	29.4	28.7	29.7	28.3	29.3	27.1	29.3	28.1	28.8	30.3
Or	0.2	0.3	0.1	0.1	0.1	0.2	0.1	0.1	0.3	0.2	0.2	0.2

North Fiji Basin-Hunter Ridge-Hunter fracture zone

Clino-and orthopyroxene

Sample	89/1	89/1	89/1	89/1	89/1	89/1	89/1	89/1	101/1	101/1	101/1
Pyroxene	1	2	3	4	5	6	7	8	1	2	3
SiO_2	51.76	52.23	51.13	51.67	53.54	52.68	52.92	53.54	51.47	51.76	51.02
TiO_2	0.50	0.44	0.83	0.44	0.25	0.20	0.25	0.23	0.51	0.33	0.54
Al_2O_3	1.52	1.54	3.86	1.95	0.86	1.09	1.48	0.58	3.68	3.30	2.59
Cr_2O_3	0.01	0.02	0.16	0.02		0.01	0.01		0.57	0.95	0.03
FeO	8.99	9.09	6.71	8.70	19.05	19.29	16.94	17.79	5.24	3.94	7.54
MnO	0.44	0.47	0.13	0.32	0.67	0.72	0.26	0.74	0.12	0.08	0.26
MgO	14.58	14.85	16.34	15.02	24.59	24.32	25.74	25.38	16.47	16.54	16.09
CaO	21.08	21.12	20.59	21.35	1.31	1.28	1.70	1.46	22.37	23.16	21.18
Na_2O	0.48	0.40	0.29	0.45	0.02	0.02	0.02	0.05	0.23	0.19	0.23
K_2O	0.02	0.01	0.02		0.02	0.01	0.01	0.01			
Sum	99.38	100.17	100.06	99.92	100.31	99.62	99.33	99.78	100.66	100.25	99.48
mg#	74.3	74.4	81.3	75.5	69.7	69.2	73.0	71.8	84.9	88.2	79.2
En	41.9	42.3	46.8	42.6	67.9	67.4	70.6	69.7	46.4	46.7	45.3
Fs	14.5	14.5	10.8	13.8	29.5	30.0	26.1	27.4	8.3	6.2	11.9
Wo	43.6	43.2	42.4	43.5	2.6	2.6	3.4	2.9	45.3	47.0	42.8

Sample	101/1	101/1	101/1	101/1	101/1	101/1	101/1	101/1	105/1	105/1	105/1
Pyroxene	4	5	6	7	8	9	10	11	1	2	3
SiO_2	52.46	51.52	51.98	50.84	52.89	50.14	52.16	50.09	52.32	52.47	54.39
TiO_2	0.29	0.34	0.27	0.59	0.31	0.59	0.26	0.70	0.09	0.10	0.04
Al_2O_3	2.00	2.03	2.11	3.73	2.00	3.35	2.00	4.55	1.48	1.40	0.93
Cr_2O_3	0.64	0.50	0.63	0.35	0.49	0.17	0.61	0.81	0.24	0.06	0.28
FeO	4.10	4.26	4.05	6.00	4.22	6.80	4.27	5.59	5.62	6.10	10.43
MnO	0.15	0.15	0.09	0.14	0.16	0.12	0.19	0.06	0.17	0.12	0.24
MgO	17.69	17.78	18.04	16.16	17.98	15.82	17.81	16.38	17.46	17.55	29.26
CaO	22.50	22.47	22.21	22.15	22.55	22.20	22.75	21.64	21.04	20.77	2.12
Na_2O	0.15	0.15	0.18	0.25	0.14	0.24	0.19	0.23	0.14	0.15	
K_2O			0.02								
Sum	99.98	99.20	99.58	100.21	100.74	99.43	100.24	100.05	98.56	98.72	97.69
mg#	88.5	88.1	88.8	82.8	88.4	80.6	88.1	83.9	84.7	83.7	83.3
En	48.9	48.9	49.7	45.6	49.2	44.4	48.7	46.7	48.9	48.9	79.9
Fs	6.4	6.6	6.3	9.5	6.5	10.7	6.6	8.9	8.8	9.5	16.0
Wo	44.7	44.5	44.0	44.9	44.3	44.8	44.7	44.4	42.3	41.6	4.2

Sample	105/1	105/1	105/1	105/1	105/1	105/1	105/1	105/1	105/1	105/1	105/1
Pyroxene	4	5	6	7	8	9	10	11	12	13	14
SiO_2	50.34	51.62	51.09	51.83	52.74	53.72	53.13	54.59	51.22	50.28	50.42
TiO_2	0.09	0.05	0.04	0.05	0.04	0.03		0.06	0.02	0.09	0.12
Al_2O_3	1.76	1.43	1.70	0.84	0.93	0.64	0.95	1.29	1.09	1.58	1.44
Cr_2O_3	0.17	0.18	0.16	0.10	0.16	0.10	0.11	0.23	0.17	0.16	0.23
FeO	7.87	8.39	7.53	13.67	13.27	10.83	13.91	11.44	7.02	8.03	7.82
MnO	0.29	0.30	0.17	0.27	0.36	0.22	0.20	0.22	0.22	0.19	0.27
MgO	16.22	16.68	16.62	26.84	27.07	29.57	27.56	28.44	18.37	15.96	16.30
CaO	20.09	19.42	20.39	2.11	2.13	2.08	2.14	2.39	18.82	20.23	20.23
Na_2O	0.09	0.14	0.14				0.05	0.06	0.09	0.15	0.15
K_2O											
Sum	96.92	98.21	97.84	95.71	96.70	97.19	98.05	98.72	97.02	96.67	96.98
mg#	78.6	78.0	79.7	77.8	78.4	83.0	77.9	81.6	82.3	78.0	78.8
En	46.2	47.2	46.8	74.5	75.1	79.6	74.7	77.8	51.3	45.6	46.3
Fs	12.6	13.3	11.9	21.3	20.7	16.4	21.2	17.6	11.0	12.9	12.5
Wo	41.2	39.5	41.3	4.2	4.2	4.0	4.2	4.7	37.8	41.5	41.3

Sample	105/1	105/1	105/1	105/1	105/1	105/1	105/1	105/1	105/1	105/2	105/2
Pyroxene	16	17	18	19	20	21	22	23	24	1	2
SiO_2	51.19	50.73	50.35	55.96	55.27	55.15	54.64	53.86	53.76	55.98	56.59
TiO_2	0.09	0.09	0.15	0.03	0.03	0.08	0.04	0.03	0.03	0.06	
Al_2O_3	1.76	1.74	1.87	0.42	0.34	0.34	0.36	0.92	1.00	1.11	0.97
Cr_2O_3	0.19	0.20	0.07	0.32	0.34	0.33	0.32	0.38	0.29	0.55	0.59
FeO	8.14	8.40	10.21	6.56	8.42	7.78	8.82	11.59	12.66	8.36	8.10
MnO	0.13	0.15	0.24	0.16	0.20	0.18	0.20	0.21	0.29	0.16	0.19
MgO	16.16	16.25	14.44	33.13	31.35	31.91	31.13	28.66	28.12	32.02	32.18
CaO	20.26	19.31	20.46	1.41	1.50	1.30	1.42	1.85	1.95	1.93	2.05
Na_2O	0.15	0.15	0.15		0.04					0.02	0.02
K_2O											0.01
Sum	98.07	97.02	97.94	97.99	97.49	97.07	96.93	97.50	98.10	100.19	100.70
mg#	78.0	77.5	71.6	90.0	86.9	88.0	86.3	81.5	79.8	87.2	87.6
En	45.8	46.6	41.4	87.6	84.4	85.8	83.9	78.5	76.8	84.0	84.2
Fs	12.9	13.5	16.4	9.7	12.7	11.7	13.3	17.8	19.4	12.3	11.9
Wo	41.3	39.8	42.2	2.7	2.9	2.5	2.8	3.6	3.8	3.6	3.9

Sample	105/2	105/2	105/2	105/2	105/2	105/2	105/2	105/2	105/2	105/2	105/2
Pyroxene	3	4	5	6	7	8	9	10	11	12	13
SiO_2	55.29	55.34	55.48	55.57	56.24	49.81	48.23	55.53	50.82	46.97	55.52
TiO_2	0.01	0.03	0.03	0.09	0.06	0.19	0.31	0.08	0.15	0.36	0.02
Al_2O_3	1.89	0.92	0.93	1.04	0.68	4.04	5.79	0.90	3.35	6.77	0.65
Cr_2O_3	0.25	0.49	0.48	0.59	0.35	0.06		0.53	0.17		0.50
FeO	9.36	7.50	7.38	7.94	7.26	8.69	10.75	7.53	8.22	10.76	7.69
MnO	0.23	0.11	0.17	0.09	0.12	0.29	0.18	0.16	0.17	0.25	0.19
MgO	26.07	32.07	31.88	31.42	32.96	17.01	14.61	32.25	18.96	13.76	32.28
CaO	6.69	1.60	1.69	2.22	1.55	17.52	17.53	1.98	16.00	18.92	1.66
Na_2O	0.11					0.13	0.12		0.10	0.16	
K_2O	0.03										
Sum	99.93	98.06	98.04	98.96	99.22	97.74	97.52	98.96	97.94	97.95	98.51
mg#	83.2	88.4	88.5	87.6	89.0	77.7	70.8	88.4	80.4	69.5	88.2
En	72.2	85.7	85.6	83.8	86.4	49.3	43.9	85.1	54.1	41.2	85.4
Fs	14.5	11.2	11.1	11.9	10.7	14.1	18.1	11.1	13.2	18.1	11.4
Wo	13.3	3.1	3.3	4.3	2.9	36.5	37.9	3.8	32.8	40.7	3.2

Sample	105/2	105/2	105/2	105/2	105/2	105/2	105/2	105/2	105/2	105/2	105/2
Pyroxene	15	16	17	18	19	20	21	22	23	24	25
SiO_2	53.81	51.48	55.84	55.32	55.32	55.58	55.12	55.33	54.88	55.61	55.96
TiO_2	0.08	0.20	0.02	0.04		0.03	0.04		0.07		
Al_2O_3	1.87	3.08	0.67	0.72	0.67	1.04	0.96	1.23	0.92	0.87	0.87
Cr_2O_3	0.16	0.07	0.43	0.40	0.30	0.43	0.63	0.38	0.31	0.57	0.60
FeO	9.55	6.92	7.87	7.70	8.30	8.18	7.73	8.78	8.39	7.28	7.32
MnO	0.22	0.16	0.27	0.09	0.16	0.16	0.15	0.28	0.18	0.11	0.16
MgO	27.93	17.54	31.62	32.04	31.72	31.50	31.81	29.39	31.08	32.18	32.38
CaO	4.33	19.40	1.92	1.79	1.88	1.88	2.06	3.56	1.97	1.57	1.57
Na_2O	0.04	0.11						0.05	0.04		
K_2O											
Sum	97.99	98.96	98.64	98.10	98.35	98.80	98.50	99.00	97.84	98.19	98.86
mg#	83.9	81.9	87.7	88.1	87.2	87.3	88.0	85.6	86.8	88.7	88.7
En	76.7	49.6	84.5	85.1	84.1	84.1	84.5	79.7	83.5	86.1	86.1
Fs	14.7	11.0	11.8	11.5	12.3	12.3	11.5	13.4	12.7	10.9	10.9
Wo	8.6	39.4	3.7	3.4	3.6	3.6	3.9	6.9	3.8	3.0	3.0

Sample	105/2	105/2	105/2	108/5	108/5	108/5	108/5	108/5	108/5	108/5	108/5
Pyroxene	27	28	29	1	2	3	4	5	6	7	8
SiO_2	45.97	48.31	50.22	52.69	52.05	52.96	53.61	53.38	53.21	53.69	53.32
TiO_2	0.46	0.20	0.29	0.21	0.55	0.26	0.24	0.19	0.16	0.20	0.12
Al_2O_3	8.12	5.30	4.66	2.10	2.39	2.51	2.37	1.74	1.84	2.07	1.97
Cr_2O_3			0.06	0.42	0.04	0.46	0.62	0.64	0.81	0.79	0.83
FeO	12.60	9.27	7.98	3.78	6.98	3.97	3.46	3.49	3.38	3.33	3.39
MnO	0.17	0.23	0.26	0.07	0.15	0.08	0.06			0.06	0.02
MgO	12.28	15.00	16.05	17.49	16.00	17.54	17.76	18.18	18.14	18.13	17.95
CaO	18.60	18.75	20.27	22.94	21.78	22.86	22.63	22.03	22.55	22.34	22.90
Na_2O	0.21	0.17	0.15	0.18	0.32	0.21	0.19	0.19	0.22	0.19	0.17
K_2O						0.01	0.02		0.02		
Sum	98.41	97.23	99.94	99.88	100.26	100.86	100.96	99.84	100.33	100.80	100.67
mg#	63.5	74.2	78.2	89.2	80.3	88.7	90.1	90.3	90.5	90.7	90.4
En	37.5	44.5	45.7	48.4	45.0	48.4	49.4	50.5	50.0	50.3	49.4
Fs	21.6	15.4	12.8	5.9	11.0	6.2	5.4	5.4	5.2	5.2	5.2
Wo	40.9	40.0	41.5	45.7	44.0	45.4	45.2	44.0	44.7	44.5	45.3

Sample	108/5	108/5	108/5	108/5	108/5	108/5	108/5	108/4	108/4	108/4	108/4
Pyroxene	10	11	12	13	14	15	16	1	2	3	4
SiO_2	52.72	52.98	54.01	53.72	53.32	53.02	51.73	53.26	53.22	53.46	53.45
TiO_2	0.30	0.21	0.32	0.33	0.26	0.19	0.51	0.01	0.13	0.21	0.14
Al_2O_3	2.59	2.59	1.71	1.77	1.71	2.44	3.65	0.50	0.48	0.57	0.60
Cr_2O_3	0.48	0.57	0.04	0.01	0.07	1.09	0.10				
FeO	4.22	3.66	14.30	16.37	5.46	3.55	5.47	18.24	17.93	17.78	17.76
MnO	0.05		0.35	0.44	0.12	0.07	0.19	1.65	1.67	1.61	1.50
MgO	17.32	17.42	27.72	26.20	17.74	17.97	16.68	24.64	24.73	24.67	24.47
CaO	22.65	22.67	1.62	1.44	21.78	22.64	22.10	0.83	0.85	0.90	1.06
Na_2O	0.23	0.22	0.03	0.02	0.22	0.26	0.25				
K_2O	0.01		0.01		0.03	0.13	0.02				
Sum	100.57	100.32	100.11	100.30	100.71	101.36	100.70	99.13	99.01	99.20	98.98
mg#	88.0	89.5	77.5	74.0	85.3	90.0	84.5	70.7	71.1	71.2	71.1
En	48.1	48.7	75.1	71.9	48.7	49.6	46.8	69.5	69.9	69.9	69.5
Fs	6.6	5.7	21.7	25.2	8.4	5.5	8.6	28.9	28.4	28.3	28.3
Wo	45.3	45.6	3.2	2.8	42.9	44.9	44.6	1.7	1.7	1.8	2.2

Sample	108/4	108/4	108/4	108/4	108/4	108/4	108/16	108/16	108/16	108/16	108/16
Pyroxene	6	7	8	9	10	11	1	2	3	4	5
SiO_2	54.01	54.03	53.38	53.71	53.64	53.36	52.06	51.71	51.73	51.41	53.44
TiO_2	0.10	0.17	0.23	0.16	0.14	0.14	0.18	0.12	0.11	0.16	0.16
Al_2O_3	0.54	0.35	0.50	0.58	0.56	0.57	0.52	0.51	0.60	0.64	0.52
Cr_2O_3							0.02	0.03	0.04	0.04	0.03
FeO	18.15	18.17	18.46	18.25	18.16	17.79	18.18	17.73	18.04	18.10	18.07
MnO	1.57	1.55	1.49	1.62	1.52	1.65	1.71	1.44	1.75	1.57	1.64
MgO	24.43	24.48	24.30	24.36	24.60	24.49	24.40	24.81	24.64	24.21	24.86
CaO	0.86	0.88	0.87	0.93	0.92	0.92	0.87	0.95	0.81	0.99	0.83
Na_2O							0.02	0.02	0.02	0.03	0.03
K_2O										0.03	
Sum	99.66	99.63	99.23	99.61	99.54	98.92	97.96	97.32	97.74	97.18	99.58
mg#	70.6	70.6	70.1	70.4	70.7	71.0	70.5	71.4	70.9	70.4	71.0
En	69.3	69.3	68.9	69.1	69.4	69.7	69.3	70.0	69.7	69.0	69.8
Fs	28.9	28.9	29.4	29.0	28.7	28.4	29.0	28.1	28.6	29.0	28.5
Wo	1.8	1.8	1.8	1.9	1.9	1.9	1.8	1.9	1.6	2.0	1.7

Sample	108/16	108/16	108/16	78/73	78/73	77/28	77/28	77/28	77/28	77/28	81/18
Pyroxene	1	3	4	10	11	17	12	12	7	3	12
SiO_2	52.68	53.65	53.26	57.77	57.15	57.58	57.24	57.24	57.49	56.73	56.80
TiO_2	0.13	0.14	0.21	0.04	0.03		0.01	0.01	0.03	0.04	0.03
Al_2O_3	0.56	0.47	0.59	0.75	1.26	0.55	1.03	1.03	0.52	0.79	1.08
Cr_2O_3		0.03	0.03	0.28	0.68	0.42	0.70	0.70	0.32	0.49	0.61
FeO	17.08	17.80	18.18	7.74	7.96	6.84	7.95	7.95	8.31	9.12	8.17
MnO	1.44	1.53	1.56	0.04	0.19	0.11	0.22	0.22	0.20	0.29	0.15
MgO	25.14	24.48	24.14	33.91	33.74	34.00	32.85	32.85	32.91	32.01	31.16
CaO	0.95	0.87	0.80	2.10	2.03	2.19	1.80	1.80	1.99	2.07	2.59
Na_2O	0.02	0.04	0.01		0.01	0.02	0.01	0.01	0.01	0.00	0.02
K_2O			0.01								
Sum	98.00	99.01	98.79	102.63	103.07	101.72	101.81	101.81	101.78	101.55	100.60
mg#	72.4	71.0	70.3	88.7	88.3	89.9	88.0	88.0	87.6	86.2	87.2
En	71.0	69.8	69.1	85.3	85.0	86.3	85.1	85.1	84.4	82.9	82.9
Fs	27.1	28.5	29.2	10.9	11.3	9.7	11.6	11.6	12.0	13.3	12.2
Wo	1.9	1.8	1.6	3.8	3.7	4.0	3.4	3.4	3.7	3.9	4.9

Sample	115/41	115/41	115/41	115/41	115/41	115/43	115/43	115/43	115/43	115/43	115/43
Pyroxene	5	10	23	45	36	5	10	13	76	81	86
SiO_2	54.58	57.07	56.85	55.88	53.37	53.42	53.57	52.93	52.99	52.29	54.90
TiO_2			0.02		0.07	0.07	0.02	0.16	0.06	0.21	0.01
Al_2O_3	1.67	0.87	0.87	1.53	2.54	2.22	1.85	2.68	2.45	3.18	1.47
Cr_2O_3	0.66	0.26	0.29	0.58	0.81	0.75	0.73	0.41	0.24	0.39	
FeO	8.20	8.41	8.06	8.52	5.20	5.14	4.38	5.82	7.28	7.81	14.25
MnO	0.18	0.02	0.23	0.21	0.23	0.21	0.09	0.17	0.20	0.20	0.18
MgO	31.04	32.59	32.74	31.92	18.97	19.50	18.97	18.39	17.29	19.52	28.63
CaO	2.45	1.39	2.06	2.04	18.97	18.95	19.91	20.42	20.29	16.97	1.43
Na_2O	0.01	0.01	0.03	0.03	0.10	0.12	0.10	0.11	0.08	0.09	0.02
K_2O											
Sum	98.79	100.62	101.15	100.71	100.26	100.38	99.62	101.08	100.88	100.68	100.88
mg#	87.1	87.4	87.9	87.0	86.7	87.1	88.5	84.9	80.9	81.7	78.2
En	83.0	85.1	84.5	83.6	53.4	54.2	53.1	50.6	48.1	54.1	76.0
Fs	12.3	12.3	11.7	12.5	8.2	8.0	6.9	9.0	11.4	12.1	21.2
Wo	4.7	2.6	3.8	3.8	38.4	37.8	40.0	40.4	40.6	33.8	2.7

Sample	113/17	113/17	113/17	113/17	113/17	113/17	113/17	113/17	113/17	113/17	115/40
Pyroxene	13	14	15	16	17	19	21	20	18	22	122
SiO_2	53.66	53.51	52.61	52.62	53.14	52.21	52.47	53.07	52.36	53.74	52.82
TiO_2	0.15	0.13	0.21	0.13	0.15	0.26	0.15	0.12	0.20	0.06	0.11
Al_2O_3	2.09	1.93	3.40	2.73	2.29	3.03	2.94	2.09	2.64	1.90	2.87
Cr_2O_3	0.74	0.45	0.30	0.31	0.57	0.04	0.00	0.35	0.01	0.48	0.46
FeO	3.76	4.15	4.51	4.23	3.81	7.14	6.76	4.18	6.28	4.25	4.53
MnO	0.05	0.08	0.15	0.09	0.14	0.05	0.11	0.02	0.08	0.06	0.06
MgO	18.08	18.22	17.51	17.67	17.79	16.88	17.23	18.23	16.94	18.64	17.85
CaO	21.83	21.88	21.68	21.68	22.18	20.20	20.33	22.00	20.88	21.36	21.03
Na_2O	0.15	0.12	0.15	0.14	0.12	0.17	0.16	0.12	0.17	0.14	0.13
K_2O											
Sum	100.51	100.47	100.53	99.59	100.18	99.97	100.14	100.17	99.57	100.64	99.85
mg#	89.5	88.7	87.4	88.1	89.3	80.8	82.0	88.6	82.8	88.7	87.5
En	50.4	50.2	49.1	49.6	49.6	47.7	48.3	50.1	47.8	51.2	50.3
Fs	5.9	6.4	7.1	6.7	6.0	11.3	10.6	6.4	9.9	6.6	7.2
Wo	43.7	43.4	43.7	43.7	44.5	41.0	41.0	43.5	42.3	42.2	42.6

Plagioclase

Sample	89/1	89/1	89/1	89/1	89/1	89/1	89/1	89/1	101/1	101/1	101/1
Plagioclase	2	3	5	6	7	8	9	11	1	2	4
SiO_2	56.48	56.90	54.86	53.23	53.85	54.72	59.33	55.84	48.66	49.26	48.53
Al_2O_3	26.68	25.84	27.87	28.22	28.45	27.85	24.85	26.85	30.41	31.09	30.95
FeO	0.45	0.54	0.53	0.65	0.56	0.48	0.49	0.51	0.71	0.64	0.64
MgO	0.02	0.05	0.05	0.07	0.04	0.04	0.04	0.03	0.23	0.26	0.22
CaO	9.52	8.74	11.51	12.05	11.88	11.31	7.97	9.98	15.73	15.58	15.37
Na_2O	5.83	6.30	4.71	4.40	4.68	4.97	6.44	5.61	2.82	2.63	2.66
K_2O	0.14	0.16	0.10	0.12	0.10	0.10	0.21	0.15	0.02	0.02	0.03
Sum	99.12	98.53	99.63	98.74	99.56	99.47	99.33	98.97	98.58	99.48	98.40
An	47.0	43.0	57.1	59.8	58.0	55.4	40.1	49.1	75.4	76.5	76.0
Ab	52.1	56.1	42.3	39.5	41.4	44.0	58.6	50.0	24.5	23.4	23.8
Or	0.8	0.9	0.6	0.7	0.6	0.6	1.3	0.9	0.1	0.1	0.2

Sample	108/16	108/16	108/16	108/16	108/16	108/16	108/16	108/16	108/16	108/16	108/16
Plagioclase	1	3	4	7	8	11	13	18	19	20	21
SiO_2	52.99	51.35	51.65	51.51	60.69	62.50	62.62	63.92	62.21	61.48	58.50
Al_2O_3	28.48	29.67	29.70	29.61	24.81	24.07	23.75	23.57	23.76	24.30	24.88
FeO	0.44	0.59	0.49	0.55	0.32	0.26	0.32	0.40	0.39	0.79	0.35
MgO	0.04	0.06	0.05	0.05	0.01	0.00	0.00	0.00	0.00	0.00	0.01
CaO	12.00	13.29	13.59	13.40	7.00	6.09	5.97	5.33	5.95	6.78	7.30
Na_2O	4.53	3.96	3.84	3.53	7.34	7.80	7.78	8.03	7.74	7.41	6.76
K_2O	0.03	0.04	0.03	0.03	0.14	0.17	0.20	0.18	0.17	0.16	0.13
Sum	98.51	98.96	99.35	98.68	100.31	100.89	100.64	101.43	100.22	100.92	97.93
An	59.3	64.8	66.1	67.6	34.2	29.8	29.4	26.5	29.5	33.3	37.1
Ab	40.5	35.0	33.8	32.2	65.0	69.2	69.4	72.4	69.5	65.8	62.1
Or	0.2	0.2	0.2	0.2	0.8	1.0	1.2	1.1	1.0	0.9	0.8

Sample	108/16	108/4	108/4	108/4	108/4	108/4	108/4	108/4	108/4	108/4	108/4
Plagioclase	24	1	2	4	7	8	10	15	16	19	39
SiO_2	60.62	58.86	59.38	60.39	58.38	57.68	59.14	59.88	59.18	58.76	58.37
Al_2O_3	24.07	25.52	25.26	24.52	25.51	26.30	25.26	24.55	25.26	25.55	26.09
FeO	0.50	0.43	0.36	0.35	0.33	0.38	0.31	0.29	0.35	0.35	0.36
MgO	0.00	0.00	0.00	0.00	0.00	0.00	0.00	0.00	0.00	0.00	0.03
CaO	6.47	7.57	7.17	6.62	7.90	8.65	7.39	6.93	7.83	8.00	8.56
Na_2O	7.15	6.81	6.98	7.38	6.60	6.33	6.83	7.18	6.83	6.82	4.39
K_2O	0.17	0.13	0.12	0.15	0.12	0.09	0.16	0.15	0.10	0.10	0.10
Sum	98.98	99.32	99.27	99.41	98.84	99.43	99.09	98.98	99.55	99.58	97.90
An	33.0	37.8	36.0	32.8	39.5	42.8	37.1	34.5	38.6	39.1	51.5
Ab	66.0	61.5	63.3	66.3	59.8	56.7	62.0	64.6	60.9	60.3	47.8
Or	1.0	0.8	0.7	0.9	0.7	0.5	1.0	0.9	0.6	0.6	0.7

Sample	123/2	123/2	123/2	123/2	123/2	108/5	108/5	108/5	108/5	108/5	108/5
Plagioclase	2	3	5	7	9	1	2	3	4	5	6
SiO_2	51.11	49.70	49.47	49.08	50.49	51.03	53.40	46.63	46.00	47.73	54.05
Al_2O_3	29.02	31.31	31.33	31.55	30.20	30.04	28.48	32.99	33.46	32.12	28.51
FeO	0.75	0.57	0.46	0.38	0.67	0.61	0.68	0.39	0.34	0.51	0.62
MgO	0.40	0.25	0.22	0.24	0.40	0.09	0.05	0.13	0.12	0.11	0.22
CaO	14.33	15.37	15.59	15.79	14.93	14.03	12.26	17.78	18.24	16.76	12.91
Na_2O	3.61	2.86	2.73	2.63	3.14	3.43	4.43	1.55	1.41	2.19	4.12
K_2O	0.03	0.02	0.02	0.01	0.03	0.02	0.04	0.01	0.01	0.03	0.11
Sum	99.25	100.08	99.82	99.68	99.86	99.25	99.34	99.48	99.58	99.45	100.54
An	68.6	74.7	75.8	76.8	72.3	69.2	60.3	86.3	87.7	80.7	63.0
Ab	31.3	25.2	24.0	23.1	27.5	30.6	39.4	13.6	12.3	19.1	36.4
Or	0.2	0.1	0.1	0.1	0.2	0.1	0.2	0.1	0.1	0.2	0.6

Amphibole

Sample	108/4	108/4	108/4	108/4	108/4	108/16	108/16	108/16	108/16	108/16	108/16
Amphibole	1	5	6	8	9	3	5	7	9	10	12
SiO_2	44.56	42.98	41.80	42.48	42.71	43.26	43.53	45.55	43.60	44.41	49.52
TiO_2	2.62	2.74	3.20	2.88	2.72	2.73	2.75	2.01	2.91	2.53	1.62
Al_2O_3	9.03	10.32	10.68	10.19	10.00	10.08	10.01	7.90	10.11	10.49	7.56
Cr_2O_3			0.03	0.01	0.01		0.05		0.07	0.07	0.02
FeO	11.74	11.96	11.77	11.69	11.74	11.62	11.01	12.01	11.61	11.20	10.69
MnO	0.37	0.29	0.18	0.25	0.17	0.34	0.12	0.42	0.21	0.28	0.36
MgO	14.85	14.53	14.23	14.52	14.71	14.60	14.91	15.05	15.13	14.69	15.18
CaO	11.48	11.63	11.64	11.64	11.25	11.74	11.62	11.69	11.21	11.29	10.84
Na_2O	2.15	2.41	2.38	2.36	2.26	2.37	2.42	1.83	2.36	2.50	1.85
K_2O	0.18	0.17	0.17	0.20	0.17	0.17	0.15	0.19	0.19	0.18	0.21
Sum	96.98	97.03	96.08	96.22	95.74	96.91	96.57	96.65	97.40	97.64	97.85

Magnetite, ilmenite and apatite

Sample	108/5	108/4	108/16	108/4	108/16	108/4
Mineral	Magnetite	Magnetite	Magnetite	Ilmenite	Ilmenite	Apatite
SiO_2	0.07	0.05	0.08			
TiO_2	10.12	7.67	7.04	36.05	35.41	
Al_2O_3	2.94	1.79	1.60			
Cr_2O_3	0.12	0.07	0.09	0.05	0.02	
Fe_2O_3	47.36	52.14	52.78	33.41	34.29	
FeO	35.86	34.44	33.52	27.49	27.71	1.26
MnO	0.41	0.68	0.72	0.54	0.60	0.21
MgO	2.98	1.92	1.87	2.45	1.97	0.20
CaO						55.73
Na_2O						0.21
K_2O						0.01
P_2O_5						42.35
NiO	0.06					
Sum	99.91	98.76	97.70	100.00	100.00	99.97
$Mg^{\#}$	0.129	0.090	0.090			
$cr^{\#}$	0.027	0.026	0.036			
X_{mt}	0.909	0.948	0.953			
Fe^{2+}/Fe^{3+}	0.841	0.734	0.706			
ilmenite				0.579	0.586	
geikielite				0.092	0.074	
pyrophanite				0.012	0.013	
hematite				0.317	0.326	

Appendix 4

Olivine and spinel pairs

Australian Antarctic Discordance

Sample	18-09	18-09	18-09	18-09	18-09	18-09	18-09	18-17	18-17
Olivine	20-1	20-2	148	188	195	5	12	15	173
SiO_2	40.04	40.04	39.72	40.45	40.11	40.48	39.78	40.25	40.32
Cr_2O_3	0.03	0.03	0.07	0.03	0.07		0.18	0.09	0.07
FeO	12.08	12.08	12.51	10.82	11.15	10.19	11.87	9.50	9.33
MnO	0.12	0.12	0.12	0.10	0.12		0.19	0.12	0.15
MgO	47.19	47.19	46.53	48.35	47.99	48.48	46.60	49.17	49.05
CaO	0.27	0.27	0.30	0.28	0.30	0.29	0.30	0.27	0.27
NiO	0.25	0.25	0.11	0.33	0.26		0.27	0.29	0.30
Sum	99.96	99.96	99.35	100.35	99.98	99.45	99.19	99.69	99.48
Fo	87.4	87.4	86.9	88.9	88.5	89.5	87.5	90.2	90.4
Spinel	20-1	20-2	148	188	195	5	12	15	173
SiO_2	0.09	0.07	0.07	0.10	0.08	0.34	0.07	0.08	0.11
TiO_2	0.63	0.56	0.73	0.38	0.45	0.53	0.56	0.32	0.40
Al_2O_3	27.88	26.18	26.82	31.75	33.21	29.75	28.73	34.86	33.83
Cr_2O_3	36.65	38.44	37.62	34.61	32.88	34.58	34.31	31.84	32.74
Fe_2O_3	5.72	5.74	6.33	4.98	5.22	6.91	7.41	4.23	4.44
FeO	12.92	12.69	13.61	11.32	11.31	10.09	11.95	9.68	9.92
MnO	0.17	0.17	0.04	0.15	0.10	0.19	0.17	0.12	0.18
MgO	15.52	15.36	15.27	16.99	17.22	17.75	16.02	18.09	17.93
NiO	0.14	0.14	0.14	0.15	0.19	0.27	0.16	0.25	0.24
ZnO							0.15		
Sum	99.72	99.34	100.63	100.43	100.66	100.41	99.53	99.46	99.80
$Mg^{\#}$	0.682	0.683	0.667	0.728	0.731	0.758	0.705	0.769	0.763
$cr^{\#}$	0.469	0.496	0.485	0.422	0.399	0.438	0.445	0.380	0.394
X_{mt}	0.065	0.066	0.072	0.055	0.057	0.077	0.084	0.046	0.048
Fe^{2+}/Fe^{3+}	2.509	2.457	2.390	2.523	2.408	1.623	1.793	2.543	2.481

Sample	29-02	29-02	29-02	29-02	29-02	29-02	29-02	29-02	29-02	29-02
Olivine	260	260b	1	2	3	3b	4	4b	4c	5
SiO_2	39.36	39.87	40.66	40.23	40.76	40.49	40.00	39.25	39.60	40.52
Cr_2O_3	0.37		0.08	0.10	0.23	0.08	0.31	0.29	0.11	0.23
FeO	10.99	11.62	11.38	11.18	11.08	10.93	11.37	11.22	11.04	10.40
MnO	0.12		0.21	0.11	0.13	0.16	0.16	0.19	0.17	0.11
MgO	47.29	46.74	48.29	47.99	48.58	48.82	47.67	46.68	47.35	48.61
CaO	0.26	0.24	0.27	0.26	0.27	0.25	0.29	0.28	0.31	0.27
NiO	0.25		0.27	0.24	0.24	0.24	0.25	0.26	0.29	0.31
Sum	98.64	98.47	101.16	100.11	101.29	100.97	100.05	98.17	98.87	100.45
Fo	88.5	87.8	88.3	88.4	88.7	88.8	88.2	88.1	88.4	89.3
Spinel	260	260b	1	2	3	3b	4a	4b	4c	5
SiO_2	0.10	0.10	0.18	0.05	0.06	0.14	0.11	0.07	0.09	0.07
TiO_2	0.75	0.75	0.70	0.78	0.65	0.78	0.77	0.77	0.76	0.52
Al_2O_3	24.46	23.66	24.58	24.45	23.84	25.51	23.97	23.65	24.42	30.33
Cr_2O_3	39.13	38.72	39.12	39.74	40.81	38.50	39.67	39.80	39.14	35.65
Fe_2O_3	6.27	7.16	7.07	6.86	6.92	6.88	6.97	6.74	6.64	6.36
FeO	12.85	12.98	12.65	12.70	12.55	12.09	13.00	13.29	12.78	11.49
MnO	0.20	0.12	0.06	0.12	0.24	0.21	0.20	0.18	0.20	0.15
MgO	15.11	14.83	15.58	15.47	15.38	15.94	15.14	14.77	15.22	17.00
NiO	0.16	0.26	0.18	0.13	0.21	0.19	0.16	0.16	0.13	0.16
ZnO			0.03	0.11	0.12	0.12	0.09	0.12	0.05	0.10
Sum	99.03	98.58	100.15	100.42	100.77	100.36	100.08	99.54	99.42	101.83
$Mg^{\#}$	0.677	0.671	0.687	0.685	0.686	0.701	0.675	0.665	0.680	0.725
$cr^{\#}$	0.518	0.523	0.516	0.522	0.535	0.503	0.526	0.530	0.518	0.441
X_{mt}	0.073	0.084	0.082	0.079	0.079	0.079	0.081	0.079	0.077	0.070
Fe^{2+}/Fe^{3+}	2.278	2.014	1.988	2.057	2.015	1.953	2.073	2.191	2.139	2.008

North Fiji Basin-Hunter Ridge-Hunter fracture zone

IAT 1:

Sample	115/37	115/37	115/37	115/37	115/37	115/37	115/37	115/37	115/37	115/37
Olivine	39	50	52	68	72	74	81	92	95	98
SiO_2	40.32	40.45	40.35	41.29	40.07	40.76	39.91	40.10	40.84	39.90
FeO	12.81	12.38	13.57	7.99	12.25	9.58	13.90	10.27	9.55	11.86
MgO	46.60	46.85	45.92	50.02	46.63	48.80	45.18	48.47	49.28	46.83
CaO	0.22	0.26	0.24	0.23	0.24	0.33	0.24	0.26	0.29	0.24
Sum	99.95	99.94	100.08	99.53	99.20	99.47	99.23	99.10	99.95	98.83
Fo	86.6	87.1	85.8	91.8	87.1	90.1	85.3	89.4	90.2	87.6
Spinel	39	50	52	68	72	74	81	92	95	98
SiO_2	0.08	0.09	0.12	0.08	0.09	0.06	0.07	0.08	0.05	0.13
TiO_2	0.16	0.18	0.27	0.22	0.16	0.28	0.15	0.22	0.19	0.17
Al_2O_3	8.18	10.93	15.24	9.27	11.22	13.33	11.60	8.92	8.25	9.53
Cr_2O_3	55.63	50.98	41.76	57.32	50.39	49.69	47.29	56.56	57.76	53.87
Fe_2O_3	8.25	9.44	13.53	6.34	9.53	9.01	11.95	6.62	6.49	8.63
FeO	17.62	16.75	17.14	12.83	16.70	13.94	17.53	16.51	14.43	16.98
MnO	0.20	0.27	0.10	0.29	0.19	0.25	0.19	0.17	0.31	0.29
MgO	10.34	10.94	11.21	13.41	10.97	13.06	10.40	11.14	12.12	10.88
NiO	0.00	0.06	0.12	0.04	0.07	0.11	0.08	0.05	0.16	0.01
Sum	100.46	99.65	99.50	99.81	99.32	99.73	99.27	100.27	99.76	100.48
$Mg^{\#}$	0.511	0.538	0.538	0.651	0.539	0.625	0.514	0.546	0.600	0.533
$cr^{\#}$	0.820	0.758	0.648	0.806	0.751	0.714	0.732	0.810	0.824	0.791
X_{mt}	0.104	0.118	0.166	0.078	0.119	0.110	0.150	0.083	0.081	0.108
Fe^{2+}/Fe^{3+}	2.374	1.973	1.408	2.247	1.947	1.720	1.630	2.769	2.469	2.188

Sample	115/37	115/37	115/37	115/37	115/37	115/40	115/40	115/40	115/40	115/40
Olivine	100	106	109	111	114	21	26	41	47	63
SiO_2	40.28	40.59	39.83	40.56	40.43	40.28	39.78	39.96	40.78	39.98
FeO	9.98	9.96	12.78	10.46	11.78	11.55	13.89	12.48	11.31	11.74
MgO	48.04	48.72	46.28	48.53	47.17	47.00	45.15	45.79	47.95	47.41
CaO	0.22	0.24	0.23	0.24	0.23	0.28	0.28	0.25	0.24	0.26
Sum	98.53	99.51	99.12	99.79	99.61	99.11	99.11	98.46	100.28	99.40
Fo	89.6	89.7	86.6	89.2	87.7	87.9	85.3	86.7	88.3	87.8
Spinel	100	106	109	111	114	21	26	41	47	63
SiO_2	0.08	0.03	0.13	0.06	0.08	0.08	0.03	0.06	0.10	0.07
TiO_2	0.21	0.17	0.18	0.21	0.18	0.19	0.23	0.12	0.25	0.24
Al_2O_3	9.16	9.98	9.82	8.51	9.98	12.19	13.18	8.30	12.73	12.81
Cr_2O_3	55.72	54.84	52.59	57.01	52.41	48.93	44.80	55.31	47.97	48.90
Fe_2O_3	7.32	7.43	9.25	6.43	9.20	10.89	12.32	7.96	10.79	10.49
FeO	15.61	16.40	17.54	15.55	17.91	15.92	17.60	17.65	15.49	15.94
MnO	0.10	0.18	0.18	0.24	0.24	0.32	0.10	0.32	0.14	0.29
MgO	11.70	11.26	10.50	11.47	10.24	11.66	10.46	9.96	12.02	11.84
NiO	0.09	0.02	0.14	0.13	0.05	0.13	0.15	0.21	0.14	0.13
Sum	99.99	100.31	100.33	99.60	100.29	100.30	98.86	99.89	99.63	100.71
$Mg^{\#}$	0.572	0.550	0.516	0.568	0.505	0.566	0.514	0.501	0.580	0.570
$cr^{\#}$	0.803	0.787	0.782	0.818	0.779	0.729	0.695	0.817	0.717	0.719
X_{mt}	0.091	0.092	0.116	0.081	0.115	0.134	0.154	0.101	0.133	0.128
Fe^{2+}/Fe^{3+}	2.370	2.453	2.108	2.687	2.165	1.624	1.588	2.466	1.595	1.688

Sample	115/40	115/40	115/40	115/40	115/40	115/40	115/40	115/40	115/40	115/47
Olivine	70	85	92	106	112	115	117	120	127	3
SiO_2	40.01	40.26	40.59	40.26	40.08	39.87	40.44	40.13	39.85	40.40
FeO	13.15	12.21	10.44	11.65	11.56	11.41	11.41	12.48	11.32	10.19
MgO	45.77	46.85	48.64	46.85	47.20	47.58	47.46	45.63	47.15	48.60
CaO	0.25	0.27	0.25	0.27	0.26	0.26	0.28	0.23	0.26	0.26
Sum	99.18	99.58	99.91	99.03	99.09	99.13	99.59	98.48	98.57	99.44
Fo	86.1	87.2	89.3	87.8	87.9	88.1	88.1	86.7	88.1	89.5
Spinel	70	85	92	106	112	115	117	120	127	3
SiO_2	0.08	0.11	0.05	0.10	0.06	0.12	0.13	0.05	0.07	0.02
TiO_2	0.28	0.16	0.16	0.18	0.22	0.29	1.64	0.17	0.19	0.21
Al_2O_3	15.95	8.52	12.39	13.23	12.99	14.23	22.44	8.80	11.65	11.10
Cr_2O_3	42.38	56.12	51.19	47.09	46.82	46.48	31.54	54.27	50.14	53.86
Fe_2O_3	12.08	7.47	8.29	11.22	11.05	10.21	14.37	8.59	9.88	7.79
FeO	16.19	16.99	14.81	16.02	15.36	15.26	15.27	17.22	16.02	15.17
MnO	0.29	0.34	0.15	0.08	0.30	0.19	0.16	0.30	0.26	0.15
MgO	11.68	10.65	12.32	11.74	11.80	12.24	13.99	10.39	11.54	12.23
NiO	0.10	0.13	0.15	0.17	0.10	0.13	0.08	0.10	0.01	0.09
Sum	99.03	100.49	99.50	99.82	98.70	99.15	99.62	99.89	99.76	100.62
$Mg^{\#}$	0.563	0.528	0.597	0.566	0.578	0.588	0.620	0.518	0.562	0.590
$cr^{\#}$	0.641	0.815	0.735	0.705	0.707	0.687	0.485	0.805	0.743	0.765
X_{mt}	0.148	0.094	0.102	0.138	0.137	0.125	0.174	0.108	0.122	0.095
Fe^{2+}/Fe^{3+}	1.490	2.527	1.986	1.588	1.545	1.662	1.181	2.228	1.802	2.165

Sample	115/47	115/47	115/47	115/47	115/47	115/47	115/47	115/47	115/47	115/47
Olivine	4	5	6	10	20	30	48	67	71	78
SiO_2		41.23	40.33	40.99	39.15	40.87	40.55	40.40	40.06	39.30
FeO		10.41	10.68	10.48	12.19	11.22	10.64	10.34	13.80	15.46
MgO		49.32	48.71	48.60	46.03	48.72	49.03	48.87	47.43	44.52
CaO		0.25	0.29	0.30	0.22	0.28	0.24	0.28	0.20	0.23
Sum		101.21	100.00	100.38	97.58	101.10	100.46	99.90	101.48	99.51
Fo		89.4	89.0	89.2	87.1	88.6	89.1	89.4	86.0	83.7
Spinel	4	5	6	10	20	30	48	67	71	78
SiO_2	0.03	0.09	0.03	0.04	0.07	0.05	0.09	0.07	0.06	0.05
TiO_2	0.22	0.21	0.22	0.25	0.20	0.28	0.21	0.18	0.13	0.18
Al_2O_3	12.86	10.97	10.53	15.64	10.44	12.06	11.34	11.70	10.56	10.27
Cr_2O_3	47.80	52.78	54.64	47.33	50.54	52.31	52.38	51.86	51.89	48.60
Fe_2O_3	10.80	7.71	8.17	10.07	11.11	9.08	8.77	8.68	9.63	10.02
FeO	17.31	14.53	15.30	14.50	17.69	15.46	15.14	15.06	17.62	18.01
MnO	0.20	0.17	0.25	0.19	0.19	0.26	0.23	0.20	0.19	0.25
MgO	10.88	12.28	12.15	13.26	10.58	12.40	12.24	12.23	10.49	9.44
NiO	0.08	0.15	0.19	0.15	0.03	0.11	0.10	0.09	0.18	0.07
Sum	100.18	98.89	101.48	101.43	100.85	102.01	100.50	100.07	100.75	96.89
$Mg^{\#}$	0.528	0.601	0.586	0.620	0.516	0.588	0.590	0.591	0.515	0.483
$cr^{\#}$	0.714	0.763	0.777	0.670	0.765	0.744	0.756	0.748	0.767	0.760
X_{mt}	0.133	0.096	0.100	0.119	0.138	0.109	0.107	0.106	0.119	0.130
Fe^{2+}/Fe^{3+}	1.781	2.095	2.080	1.600	1.770	1.892	1.919	1.930	2.033	1.998

Sample	115/47	115/47	115/48	115/48	115/48	116/28	116/28	116/28	116/28	116/28
Olivine	99	98	39	51	103	74	102	99	98	94
SiO_2	40.99	40.62	38.92	39.40	39.08	40.47	40.32	40.41	40.01	40.36
FeO	10.74	10.26	15.53	13.54	13.70	8.90	10.10	9.92	10.49	8.68
MgO	49.63	49.46	43.85	45.48	45.68	49.45	47.93	48.49	48.21	49.45
CaO	0.27	0.27	0.26	0.14	0.17	0.32	0.30	0.34	0.20	0.22
Sum	101.63	100.60	98.56	98.56	98.62	99.13	98.64	99.16	98.91	98.71
Fo	89.2	89.6	83.4	85.7	85.6	90.8	89.4	89.7	89.1	91.0
Spinel	99	98	39	51	103	74	102	99	98	94
SiO_2	0.07	0.07	0.07	0.13	0.05	0.19	0.09	0.06	0.09	0.09
TiO_2	0.27	0.20	0.18	0.36	0.31	0.25	0.25	0.26	0.27	0.42
Al_2O_3	11.66	13.68	8.43	20.04	20.48	12.20	8.63	12.33	13.01	14.06
Cr_2O_3	49.91	50.22	52.26	34.41	37.46	54.35	53.00	49.33	47.70	49.30
Fe_2O_3	9.03	9.16	11.25	16.10	13.89	5.92	9.73	10.34	10.29	7.99
FeO	14.23	14.76	19.39	16.48	16.75	12.25	14.68	13.92	14.32	12.85
MnO	0.31	0.08	0.13	0.22	0.23	0.24	0.20	0.24	0.27	0.24
MgO	12.31	12.98	9.32	12.17	12.33	14.20	11.94	12.87	12.55	13.80
NiO	0.04	0.05	0.06	0.20	0.11	0.05	0.01	0.17	0.08	0.09
Sum	97.82	101.20	101.09	100.11	101.60	99.65	98.54	99.53	98.58	98.84
$Mg^{\#}$	0.607	0.611	0.461	0.568	0.568	0.674	0.592	0.622	0.610	0.657
$cr^{\#}$	0.742	0.711	0.806	0.535	0.551	0.749	0.805	0.729	0.711	0.702
X_{mt}	0.113	0.110	0.142	0.193	0.163	0.072	0.123	0.127	0.127	0.098
Fe^{2+}/Fe^{3+}	1.752	1.791	1.916	1.137	1.340	2.298	1.676	1.496	1.548	1.786

Sample	116/28	116/28	116/28	116/28	116/28	116/28	116/28	116/28
Olivine	122	163	156	168	171	172	178	184
SiO_2	40.00	39.25	39.91	39.52	39.96	40.23	39.42	38.77
FeO	11.65	16.01	11.48	11.54	10.96	8.36	14.03	15.88
MgO	47.06	43.85	47.48	47.50	47.74	49.75	45.46	43.62
CaO	0.28	0.23	0.27	0.30	0.27	0.19	0.21	0.24
Sum	98.98	99.34	99.14	98.86	98.93	98.52	99.12	98.50
Fo	87.8	83.0	88.1	88.0	88.6	91.4	85.2	83.0
Spinel	122	163	156	168	171	172	178	184
SiO_2	0.07	0.10	0.08	0.09	0.11	0.20	0.08	0.12
TiO_2	0.32	0.43	0.23	0.39	0.39	0.22	0.39	0.35
Al_2O_3	12.64	20.28	11.53	25.04	26.00	11.31	20.46	24.74
Cr_2O_3	47.22	32.31	51.71	33.22	31.85	55.01	35.84	23.48
Fe_2O_3	10.64	16.93	7.95	11.82	12.33	6.15	13.68	18.56
FeO	15.51	18.57	15.93	13.73	13.53	13.24	17.15	17.07
MnO	0.31	0.29	0.02	0.06	0.16	0.10	0.21	0.11
MgO	11.70	10.77	11.64	14.41	14.63	13.54	11.75	11.57
NiO	0.08	0.14	0.05	0.11	0.12	0.14	0.10	0.00
Sum	98.50	99.82	99.14	98.86	99.11	99.92	99.66	96.00
$Mg^{\#}$	0.573	0.508	0.566	0.652	0.658	0.646	0.550	0.547
$cr^{\#}$	0.715	0.517	0.751	0.471	0.451	0.765	0.540	0.389
X_{mt}	0.133	0.205	0.099	0.137	0.142	0.075	0.164	0.226
Fe^{2+}/Fe^{3+}	1.619	1.219	2.229	1.291	1.220	2.393	1.394	1.022

IAT 2:

Sample	87/5	87/5	87/5	87/5	87/5	87/21	87/21	113/5	113/5	113/5
Olivine	3	9	16	18	31	14	15	21	36	50
SiO_2	41.28	39.05	39.07	38.94	39.05	40.82	39.86	40.40	40.39	40.56
Cr_2O_3										
FeO	7.86	16.75	17.58	16.89	18.18	8.45	13.29	8.50	9.66	9.23
MnO										
MgO	50.68	43.11	41.65	43.27	42.01	50.49	46.40	49.52	49.40	49.81
CaO	0.29	0.15	0.22	0.17	0.18	0.26	0.26	0.22	0.26	0.31
NiO										
Sum	100.11	99.05	98.52	99.28	99.41	100.03	99.81	98.64	99.72	99.90
Fo	92.0	82.1	80.8	82.0	80.5	91.4	86.2	91.2	90.1	90.6
Spinel	3	9	16	18	31	14	15	21	36	50
SiO_2	0.02	0.05	0.03	0.09	0.05	0.05	0.03	0.10	0.12	0.03
TiO_2	0.22	0.12	0.16	0.16	0.18	0.20	0.32	0.14	0.19	0.16
Al_2O_3	6.18	6.06	11.24	6.10	8.96	7.41	20.80	8.64	10.26	9.14
Cr_2O_3	61.20	53.99	36.10	55.39	44.03	58.00	38.22	55.74	52.35	54.43
Fe_2O_3	5.80	10.86	21.64	9.11	17.41	6.85	12.05	7.69	8.56	7.82
FeO	11.90	21.03	21.07	20.90	21.63	13.96	15.41	13.57	13.50	13.85
MnO	0.06	0.28	0.36	0.28	0.22	0.12	0.20	0.13	0.20	0.16
MgO	13.59	7.67	7.63	7.76	7.56	12.36	12.90	12.65	12.69	12.35
NiO	0.16	0.03	0.05	0.07	0.08	0.09	0.19	0.14	0.14	0.02
Sum	99.13	100.09	98.28	99.86	100.11	99.04	100.13	98.80	98.01	97.96
$Mg^{\#}$	0.671	0.394	0.392	0.398	0.384	0.612	0.599	0.624	0.626	0.614
$cr^{\#}$	0.869	0.857	0.683	0.859	0.767	0.840	0.552	0.812	0.774	0.800
X_{mt}	0.073	0.141	0.280	0.119	0.224	0.086	0.142	0.096	0.107	0.099
Fe^{2+}/Fe^{3+}	2.277	2.152	1.082	2.549	1.381	2.265	1.421	1.961	1.752	1.968

Sample	113/6	113/6	113/6	113/6	113/6	113/6	115/3	115/3	115/3	115/3
Olivine	16	20	28	36	48	83	71	31	12	26
SiO_2	40.47	41.34	40.39	40.88	39.94	40.69	40.24	40.51	41.07	40.33
Cr_2O_3							0.02	0.03	0.02	0.09
FeO	9.03	7.14	10.75	7.63	11.95	8.00	14.33	13.48	11.56	12.72
MnO							0.18	0.21	0.25	0.16
MgO	49.60	51.65	47.85	50.86	47.38	50.39	45.66	47.16	47.33	46.93
CaO	0.25	0.20	0.26	0.26	0.27	0.27	0.22	0.27	0.29	0.26
NiO							0.19	0.17	0.24	0.14
Sum	99.35	100.33	99.25	99.63	99.54	99.34	100.84	101.83	100.76	100.63
Fo	90.7	92.8	88.8	92.2	87.6	91.8	85.0	86.2	87.9	86.8
Spinel	16	20	28	36	48	83	71	31	12	26
SiO_2	0.11	0.08	0.05	0.22	0.09	0.08				
TiO_2	0.24	0.13	0.17	0.16	0.15	0.08	0.37	0.33	0.43	0.42
Al_2O_3	8.58	8.19	9.20	9.04	7.30	8.42	15.98	13.44	12.70	12.96
Cr_2O_3	54.54	57.39	51.41	56.92	53.37	56.78	37.42	41.49	49.50	44.15
Fe_2O_3	7.38	6.74	10.53	5.73	8.79	6.77	16.14	14.49	13.12	13.44
FeO	13.81	12.45	15.21	11.90	16.31	12.95	17.59	16.99	17.66	16.37
MnO	0.16	0.17	0.25	0.29	0.21	0.12	0.28	0.25	0.24	0.18
MgO	12.21	13.28	11.47	13.73	10.25	12.91	10.66	10.63	11.85	11.36
NiO	0.11	0.06	0.04	0.00	0.02	0.07				
Sum	97.14	98.50	98.33	97.99	96.49	98.19	98.44	97.62	105.49	98.89
$Mg^{\#}$	0.612	0.655	0.573	0.673	0.528	0.640	0.519	0.527	0.545	0.553
$cr^{\#}$	0.810	0.825	0.789	0.809	0.831	0.819	0.611	0.674	0.723	0.696
X_{mt}	0.094	0.084	0.133	0.072	0.115	0.085	0.201	0.183	0.154	0.168
Fe^{2+}/Fe^{3+}	2.079	2.054	1.605	2.307	2.061	2.125	1.211	1.304	1.496	1.354

Sample	115/3	115/3	115/3	115/3	115/3	115/3	115/3	115/3	115/3	115/3
Olivine	69	40	23	7	8	38	10	35	16	2
SiO_2	40.66	40.41	41.54	40.43	41.11	41.64	41.30	41.50	41.45	41.79
Cr_2O_3	0.02	0.05	0.05	0.06	0.09	0.05	0.03	0.11	0.01	0.1
FeO	12.54	12.33	11.70	9.06	8.41	8.40	8.46	8.53	8.11	7.92
MnO	0.19	0.25	0.18	0.19	0.16	0.16	0.20	0.19	0.1	0.15
MgO	47.29	48.02	47.86	48.83	50.94	50.60	50.06	51.05	50.59	50.46
CaO	0.23	0.27	0.28	0.27	0.30	0.26	0.28	0.28	0.29	0.25
NiO	0.17	0.29	0.15	0.12	0.18	0.21	0.22	0.17	0.14	0.18
Sum	101.10	101.62	101.76	98.96	101.19	101.32	100.55	101.83	100.69	100.85
Fo	87.0	87.4	87.9	90.6	91.5	91.5	91.3	91.4	91.7	91.9
Spinel	69	40	23	7	8	38	10	35	16	2
SiO_2										
TiO_2	0.41	0.32	0.45	0.44	0.25	0.25	0.20	0.50	0.46	0.38
Al_2O_3	12.86	14.17	12.87	11.39	8.45	8.54	8.30	10.15	10.53	9.83
Cr_2O_3	43.91	45.25	44.70	49.29	55.01	55.71	56.76	51.32	52.06	55.08
Fe_2O_3	13.52	12.26	13.35	12.55	9.86	7.87	8.02	10.33	9.02	8.57
FeO	16.13	15.07	14.36	13.64	13.04	12.43	12.17	12.20	12.02	11.89
MnO	0.24	0.29	0.26	0.25	0.25	0.33	0.25	0.19	0.18	0.17
MgO	11.37	12.40	12.56	13.39	13.21	13.23	13.59	13.78	13.86	14.27
NiO										
Sum	98.43	99.76	98.55	100.96	100.07	98.36	99.29	98.47	98.13	100.19
$Mg^{\#}$	0.557	0.595	0.609	0.636	0.644	0.655	0.666	0.668	0.673	0.681
$cr^{\#}$	0.696	0.682	0.700	0.744	0.814	0.814	0.821	0.772	0.768	0.790
X_{mt}	0.169	0.149	0.166	0.153	0.122	0.099	0.099	0.129	0.112	0.105
Fe^{2+}/Fe^{3+}	1.326	1.366	1.195	1.208	1.470	1.754	1.686	1.313	1.482	1.542

Sample	115/3	115/3	115/3	115/3	115/3	115/3	115/3	115/3
Olivine	11	9	1	47	90	5	14	92
SiO_2	41.46	41.92	42.03	41.8	41.65	42.28	42.16	42.12
Cr_2O_3	0.01	0.1	0.14	0.07	0.15	0.06	0.1	0.06
FeO	7.29	6.24	5.79	5.88	5.72	5.99	5.88	5.73
MnO	0.09	0.1	0.14	0.11	0.1	0.13	0.12	0.08
MgO	50.86	52.57	51.95	52.36	52.93	51.86	52.68	52.23
CaO	0.27	0.2	0.18	0.2	0.21	0.21	0.2	0.19
NiO	0.28	0.34	0.36	0.27	0.38	0.35	0.23	0.19
Sum	100.26	101.47	100.59	100.69	101.14	100.88	101.37	100.60
Fo	92.6	93.8	94.1	94.1	94.3	93.9	94.1	94.2
Spinel	11	9	1	47	90	5	14	92
SiO_2								
TiO_2	0.35	0.16	0.17	0.28	0.20	0.21	0.23	0.18
Al_2O_3	10.50	9.77	10.07	9.99	9.83	10.30	10.30	10.40
Cr_2O_3	54.32	58.33	57.73	57.46	57.78	56.35	57.22	55.47
Fe_2O_3	8.69	5.16	6.46	6.46	6.33	6.81	5.76	6.76
FeO	11.66	10.31	9.83	9.84	9.68	9.29	9.23	8.31
MnO	0.11	0.18	0.19	0.12	0.12	0.15	0.11	0.19
MgO	14.50	14.91	15.47	15.51	15.51	15.65	15.69	15.94
NiO								
Sum	100.12	98.82	99.92	99.66	99.45	98.76	98.54	97.24
$Mg^{\#}$	0.689	0.721	0.737	0.737	0.741	0.750	0.752	0.774
$cr^{\#}$	0.776	0.800	0.794	0.794	0.798	0.786	0.788	0.782
X_{mt}	0.106	0.063	0.078	0.078	0.077	0.083	0.070	0.083
Fe^{2+}/Fe^{3+}	1.491	2.220	1.691	1.692	1.699	1.515	1.780	1.367

Boninite 1:

Sample	76/35	76/35	76/35	76/35	76/35	76/35	76/35	76/35	76/35	76/35
Olivine	6	11	13	16	40	55	62	64	68	79
SiO_2	41.32	40.42	40.70	40.72	40.82	40.64	40.90	40.74	40.43	40.86
FeO	8.52	10.71	10.61	9.60	10.03	10.30	10.91	8.79	10.44	9.11
MgO	50.53	48.05	47.56	49.13	48.45	48.15	47.72	50.32	47.89	49.52
CaO	0.14	0.15	0.17	0.15	0.13	0.19	0.19	0.18	0.18	0.19
Sum	100.50	99.34	99.03	99.61	99.43	99.27	99.71	100.02	98.94	99.68
Fo	91.4	88.9	88.9	90.1	89.6	89.3	88.6	91.1	89.1	90.6
Spinel	6	11	13	16	40	55	62	64	68	79
SiO_2	0.09	0.06	0.09	0.10	0.09	0.06	0.12	0.08	0.05	0.08
TiO_2	0.10	0.10	0.13	0.03	0.11	0.09	0.12	0.05	0.11	0.04
Al_2O_3	8.17	7.92	9.62	7.10	7.29	9.15	9.36	7.66	9.54	7.45
Cr_2O_3	60.01	58.24	55.72	60.13	59.20	56.11	55.81	59.63	55.50	59.55
Fe_2O_3	5.43	6.33	6.90	6.62	6.46	7.49	7.19	5.84	7.26	6.42
FeO	12.86	15.15	15.68	14.53	15.02	14.85	15.21	13.58	14.99	14.25
MnO	0.18	0.17	0.21	0.12	0.22	0.25	0.22	0.12	0.22	0.21
MgO	13.35	11.68	11.59	12.27	11.82	11.99	11.90	12.63	11.90	12.31
NiO	0.13	0.14	0.12	0.18	0.13	0.18	0.07	0.29	0.12	0.15
Sum	100.31	99.79	100.06	101.08	100.34	100.17	100.00	99.89	99.69	100.45
$Mg^{\#}$	0.649	0.579	0.568	0.601	0.584	0.590	0.582	0.624	0.586	0.606
$cr^{\#}$	0.831	0.831	0.795	0.850	0.845	0.804	0.800	0.839	0.796	0.843
X_{mt}	0.067	0.079	0.086	0.082	0.081	0.093	0.089	0.073	0.090	0.080
Fe^{2+}/Fe^{3+}	2.632	2.661	2.525	2.439	2.585	2.202	2.352	2.583	2.295	2.468

Sample	76/35	76/35	76/35	76/35	76/35	77/28	77/28	77/28	78/66	78/66
Olivine	86	90	99	112	119	32	52	62	1	8
SiO_2	40.55	40.30	40.43	40.59	40.84	41.29	41.37	41.71	40.77	40.56
FeO	10.86	10.59	10.60	10.12	10.32	8.79	8.34	7.99	9.69	11.49
MgO	47.89	48.21	47.93	48.57	48.37	49.61	49.75	50.03	48.57	47.32
CaO	0.20	0.18	0.16	0.18	0.20	0.18	0.17	0.20	0.18	0.19
Sum	99.49	99.28	99.12	99.47	99.73	99.87	99.63	99.94	99.22	99.56
Fo	88.7	89.0	89.0	89.5	89.3	91.0	91.4	91.8	89.9	88.0
Spinel	86	90	99	112	119	32	52	62	1	8
SiO_2	0.05	0.08	0.05	0.13	0.06	0.03	0.05	0.09	0.06	0.12
TiO_2	0.13	0.14	0.06	0.13	0.11	0.08	0.08	0.08	0.04	0.13
Al_2O_3	8.83	9.47	7.07	8.33	8.00	6.88	7.54	8.05	9.29	10.56
Cr_2O_3	57.20	54.67	59.89	58.28	58.59	60.41	60.14	59.39	58.78	54.80
Fe_2O_3	6.59	7.80	5.08	6.00	6.25	5.60	5.32	5.45	4.48	6.71
FeO	15.72	14.82	16.16	15.45	15.70	13.10	12.80	12.22	14.44	16.02
MnO	0.25	0.23	0.18	0.24	0.21	0.17	0.13	0.14	0.25	0.12
MgO	11.44	11.95	10.89	11.67	11.53	12.73	13.13	13.53	12.25	11.59
NiO	0.22	0.12	0.05	0.17	0.02	0.18	0.06	0.08	0.03	0.09
Sum	100.43	99.28	99.43	100.40	100.47	99.18	99.25	99.03	99.62	100.13
$Mg^{\#}$	0.565	0.590	0.546	0.574	0.567	0.634	0.646	0.664	0.602	0.563
$cr^{\#}$	0.813	0.795	0.850	0.824	0.831	0.855	0.843	0.832	0.809	0.777
X_{mt}	0.082	0.097	0.064	0.075	0.078	0.070	0.066	0.068	0.055	0.083
Fe^{2+}/Fe^{3+}	2.652	2.110	3.538	2.862	2.794	2.600	2.674	2.493	3.585	2.654

Sample	78/66	78/66	78/66	78/66	78/66	78/66	78/73	78/73	78/73	78/73
Olivine	9	64	70	75	118	122	3	6	33	28
SiO_2	40.73	41.02	40.59	40.89	40.55	40.81	40.99	40.75	41.04	40.28
FeO	10.45	10.84	11.39	11.71	10.52	9.46	9.64	10.23	8.38	10.60
MgO	48.29	48.46	47.91	47.87	47.59	49.62	49.30	48.18	50.41	48.10
CaO	0.15	0.14	0.18	0.19	0.17	0.14	0.16	0.17	0.15	0.20
Sum	99.62	100.46	100.06	100.66	98.83	100.03	100.08	99.34	99.98	99.18
Fo	89.2	88.8	88.2	87.9	89.0	90.3	90.1	89.4	91.5	89.0
Spinel	9	64	70	75	118	122	3	6	33	28
SiO_2	0.10	0.15	0.09	0.09	0.12	0.14	0.08	0.11	0.12	0.08
TiO_2	0.14	0.08	0.08	0.13	0.08	0.09	0.05	0.14	0.07	0.08
Al_2O_3	9.90	8.24	8.33	10.16	10.08	10.35	8.19	11.55	8.44	7.98
Cr_2O_3	55.71	58.53	58.65	55.04	54.84	56.17	59.27	52.20	59.56	58.91
Fe_2O_3	7.13	5.54	6.08	7.26	7.66	6.56	4.40	7.40	4.21	5.54
FeO	14.70	14.63	16.13	15.06	15.06	13.44	15.93	14.69	15.45	15.83
MnO	0.28	0.15	0.22	0.14	0.22	0.19	0.15	0.33	0.10	0.18
MgO	12.30	12.12	11.39	12.09	12.12	13.18	11.17	12.08	11.61	11.29
NiO	0.10	0.09	0.03	0.14	0.02	0.17	0.06	0.10	0.17	0.17
Sum	100.37	99.53	101.00	100.11	100.20	100.29	99.30	98.60	99.73	100.06
$Mg^{\#}$	0.599	0.596	0.557	0.589	0.589	0.636	0.556	0.594	0.573	0.560
$cr^{\#}$	0.791	0.827	0.825	0.784	0.785	0.785	0.829	0.752	0.826	0.832
X_{mt}	0.088	0.069	0.075	0.090	0.094	0.080	0.055	0.092	0.053	0.069
Fe^{2+}/Fe^{3+}	2.292	2.934	2.951	2.308	2.184	2.279	4.019	2.207	4.074	3.174

Sample	78/73	78/73	78/73	78/73	80/55	80/55	80/55	80/55	80/55	80/55
Olivine	22	38	39	55	7	23	26	28	32	35
SiO_2	40.87	40.94	40.00	40.42	40.04	40.66	40.52	41.59	40.17	40.50
FeO	8.34	7.94	12.00	11.03	10.52	10.57	10.48	10.42	10.74	9.80
MgO	50.12	50.91	46.89	48.01	48.69	48.49	48.77	48.99	48.76	48.90
CaO	0.19	0.17	0.19	0.18	0.15	0.13	0.13	0.15	0.13	0.17
Sum	99.51	99.97	99.08	99.64	99.40	99.85	99.90	101.14	99.81	99.36
Fo	91.5	91.9	87.4	88.6	89.2	89.1	89.2	89.3	89.0	89.9
Spinel	22	38	39	55	7	23	26	28	32	35
SiO_2	0.09	0.11	0.04	0.04	0.31	0.10	0.08	0.14	0.08	0.08
TiO_2	0.06	0.05	0.13	0.08	0.07	0.15	0.13	0.19	0.12	0.18
Al_2O_3	8.64	9.24	10.66	9.24	7.92	7.87	7.39	8.84	8.15	10.60
Cr_2O_3	59.45	59.31	52.45	55.94	55.40	56.47	57.37	56.23	56.00	52.97
Fe_2O_3	4.31	4.59	8.43	7.37	8.05	7.72	7.45	7.07	8.40	8.60
FeO	14.58	11.41	16.21	16.16	14.69	14.69	15.07	15.27	14.63	14.26
MnO	0.09	0.19	0.15	0.26	0.16	0.28	0.15	0.00	0.31	0.21
MgO	12.17	14.15	11.18	11.18	12.00	11.86	11.66	11.95	11.98	12.48
NiO	0.09	0.14	0.14	0.16	0.02	0.11	0.10	0.10	0.11	0.18
Sum	99.48	99.19	99.38	100.43	98.62	99.25	99.40	99.79	99.78	99.56
$Mg^{\#}$	0.598	0.688	0.551	0.552	0.593	0.590	0.580	0.583	0.593	0.609
$cr^{\#}$	0.822	0.812	0.767	0.802	0.824	0.828	0.839	0.810	0.822	0.770
X_{mt}	0.054	0.056	0.105	0.091	0.102	0.097	0.094	0.088	0.105	0.106
Fe^{2+}/Fe^{3+}	3.759	2.764	2.137	2.439	2.027	2.114	2.248	2.400	1.935	1.843

Sample	80/55	80/55	80/55	80/55	80/55	81/18	81/18	92/98	92/98	92/98
Olivine	36	38	43	45	56	10	24	1	14	168
SiO_2	40.57	40.73	40.15	41.09	39.51	40.82	40.68	41.28	40.92	41.03
FeO	9.89	11.51	13.65	11.27	13.72	8.11	8.32	10.38	10.35	10.46
MgO	48.59	47.64	46.18	47.86	45.28	49.66	48.99	48.86	48.65	48.22
CaO	0.19	0.17	0.21	0.14	0.15	0.18	0.17	0.20	0.17	0.20
Sum	99.25	100.05	100.19	100.37	98.67	98.77	98.16	100.72	100.08	99.91
Fo	89.7	88.1	85.8	88.3	85.5	91.6	91.3	89.4	89.3	89.1
Spinel	36	38	43	45	56	10	24	1	14	168
SiO_2	0.15	0.08	0.11	0.10	0.11	0.11	0.14	0.12	0.08	0.05
TiO_2	0.10	0.21	0.31	0.16	0.36	0.07	0.12	0.11	0.12	0.12
Al_2O_3	8.57	9.28	7.60	6.50	10.24	7.04	7.54	8.82	8.82	8.51
Cr_2O_3	56.36	53.95	52.22	58.91	45.13	60.68	58.90	55.48	56.85	56.32
Fe_2O_3	7.94	8.81	11.15	7.02	15.27	5.03	5.39	7.82	7.01	7.57
FeO	14.39	15.25	18.04	16.08	17.83	13.18	13.06	14.52	14.75	14.41
MnO	0.15	0.19	0.11	0.36	0.20	0.13	0.23	0.24	0.24	0.33
MgO	12.40	11.77	9.84	10.99	10.18	12.80	12.76	12.07	12.14	12.06
NiO	0.15	0.16	0.19	0.08	0.16	0.17	0.10	0.17	0.02	0.12
Sum	100.21	99.70	99.58	100.20	99.48	99.21	98.24	99.35	100.02	99.49
$Mg^{\#}$	0.606	0.579	0.493	0.549	0.504	0.634	0.635	0.597	0.595	0.599
$cr^{\#}$	0.815	0.796	0.822	0.859	0.747	0.853	0.840	0.808	0.812	0.816
X_{mt}	0.098	0.110	0.143	0.089	0.194	0.063	0.068	0.098	0.087	0.094
Fe^{2+}/Fe^{3+}	2.015	1.923	1.798	2.545	1.297	2.912	2.690	2.064	2.339	2.117

Sample	92/98	92/98	92/98	92/98	92/98	92/98	92/98	92/98	115/41	115/41
Olivine	174	18	20	30	39	108	98	91	44	46
SiO_2	41.34	40.40	41.31	40.37	40.98	41.13	40.68	40.43	40.21	40.37
FeO	9.84	10.62	7.52	10.27	10.56	10.10	10.31	10.43	12.23	11.50
MgO	49.50	48.44	50.08	48.02	48.07	48.37	48.58	48.02	48.82	49.56
CaO	0.16	0.15	0.17	0.18	0.21	0.13	0.16	0.19	0.21	0.23
Sum	100.84	99.61	99.07	98.83	99.82	99.73	99.73	99.07	101.47	101.65
Fo	90.0	89.0	92.2	89.3	89.0	89.5	89.4	89.1	87.7	88.5
Spinel	174	18	20	30	39	108	98	91	44	46
SiO_2	0.08	0.08	0.06	0.04	0.03	0.05	0.08	0.12	0.06	0.08
TiO_2	0.09	0.10	0.02	0.16	0.16	0.09	0.14	0.10	0.13	0.12
Al_2O_3	7.25	8.36	7.53	8.17	9.17	8.20	9.16	8.17	11.05	10.60
Cr_2O_3	59.61	56.57	60.73	57.47	55.63	57.46	55.64	55.67	50.29	53.30
Fe_2O_3	5.35	7.43	4.72	6.89	7.93	7.15	7.98	6.37	8.35	7.70
FeO	14.27	14.63	12.66	14.65	14.23	14.75	14.46	15.16	16.70	15.03
MnO	0.11	0.23	0.05	0.13	0.28	0.25	0.19	0.27	0.26	0.34
MgO	12.13	12.00	13.17	12.09	12.43	11.97	12.35	11.10	10.47	11.84
NiO	0.05	0.10	0.13	0.07	0.02	0.10	0.13	0.19	0.07	0.06
Sum	98.94	99.49	99.07	99.67	99.88	100.02	100.13	97.15	97.38	99.06
$Mg^{\#}$	0.603	0.594	0.650	0.595	0.609	0.591	0.604	0.566	0.528	0.584
$cr^{\#}$	0.847	0.819	0.844	0.825	0.803	0.825	0.803	0.821	0.753	0.771
X_{mt}	0.067	0.093	0.059	0.086	0.098	0.089	0.099	0.082	0.106	0.096
Fe^{2+}/Fe^{3+}	2.962	2.188	2.982	2.364	1.993	2.294	2.013	2.647	2.222	2.170

Sample	115/41	115/41	115/41	115/41	115/41	115/41	115/41	115/41	115/41	115/41
Olivine	52	54	59	61	62	66	69	75	82	104
SiO_2	40.20	39.72	40.43	40.13	40.44	40.46	41.04	40.65	40.52	40.46
FeO	11.30	11.62	12.33	11.50	10.52	11.34	10.79	11.18	11.88	12.71
MgO	48.13	47.14	47.87	48.25	48.65	48.66	49.96	48.65	48.26	47.04
CaO	0.20	0.18	0.18	0.18	0.21	0.24	0.24	0.24	0.23	0.20
Sum	99.83	98.65	100.81	100.05	99.82	100.70	102.03	100.72	100.88	100.41
Fo	88.4	87.9	87.4	88.2	89.2	88.4	89.2	88.6	87.9	86.8
Spinel	52	54	59	61	62	66	69	75	82	104
SiO_2	0.05	0.05	0.09	0.06	0.06	0.05	0.08	0.05	0.05	0.07
TiO_2	0.08	0.15	0.12	0.18	0.05	0.11	0.13	0.05	0.08	0.14
Al_2O_3	11.54	11.42	10.62	11.11	11.42	11.60	11.31	9.49	10.96	11.66
Cr_2O_3	53.68	52.66	51.90	53.30	52.61	54.20	51.58	55.82	51.96	50.70
Fe_2O_3	7.84	8.32	8.44	8.13	8.36	8.18	7.89	7.40	8.60	9.08
FeO	15.12	15.69	16.39	15.53	14.48	15.28	14.10	15.06	14.93	15.97
MnO	0.28	0.19	0.23	0.19	0.20	0.34	0.18	0.19	0.31	0.36
MgO	12.22	11.87	10.97	11.92	12.40	12.38	12.33	11.95	11.81	11.35
NiO	0.12	0.03	0.07	0.18	0.13	0.10	0.07	0.06	0.12	0.12
Sum	100.93	100.38	98.83	100.60	99.71	102.24	97.66	100.07	98.82	99.45
$Mg^{\#}$	0.590	0.574	0.544	0.578	0.604	0.591	0.609	0.586	0.585	0.559
$cr^{\#}$	0.757	0.756	0.766	0.763	0.756	0.758	0.754	0.798	0.761	0.745
X_{mt}	0.095	0.102	0.106	0.100	0.103	0.098	0.099	0.091	0.107	0.113
Fe^{2+}/Fe^{3+}	2.142	2.096	2.158	2.124	1.925	2.077	1.987	2.262	1.930	1.956

Sample	115/41	115/41	115/41	115/41	115/43	115/43	115/43	116/36	116/36	116/36
Olivine	130	116	115	139	33	52	64	1	2	5
SiO_2	40.69	39.71	40.49	40.31	39.44	40.02	39.97	40.12	39.79	33.88
FeO	14.07	11.62	11.24	11.49	12.14	11.69	11.33	11.36	11.50	12.41
MgO	46.50	47.12	49.32	48.44	47.35	46.94	47.59	47.41	48.14	43.25
CaO	0.21	0.20	0.20	0.18	0.21	0.23	0.25	0.19	0.16	0.18
Sum	101.47	98.65	101.25	100.42	99.15	98.88	99.14	99.08	99.60	89.72
Fo	85.5	87.8	88.7	88.3	87.4	87.7	88.2	88.2	88.2	86.1
Spinel	130	116	115	139	33	52	64	1	2	5
SiO_2	0.02	0.09	0.07	0.14	0.09	0.04	0.26	0.07	0.10	0.11
TiO_2	0.12	0.11	0.08	0.08	0.10	0.08	0.23	0.14	0.08	0.08
Al_2O_3	11.58	7.81	8.68	10.52	9.43	7.84	10.85	11.01	12.30	11.12
Cr_2O_3	51.44	58.58	58.00	53.09	54.68	57.11	52.32	50.47	49.89	51.29
Fe_2O_3	9.10	5.56	6.66	8.81	8.84	7.82	8.81	8.88	9.21	8.92
FeO	18.01	15.52	15.88	16.63	16.27	16.69	16.41	15.13	14.76	14.62
MnO	0.18	0.18	0.14	0.29	0.29	0.31	0.24	0.30	0.16	0.26
MgO	10.43	11.42	11.64	11.15	11.36	10.81	11.61	11.49	12.17	12.12
NiO	0.05	0.05	0.07	0.16	0.05	0.00	0.03	0.12	0.17	0.01
Sum	100.93	99.32	101.23	100.87	101.12	100.70	100.75	97.61	98.83	98.53
$Mg^{\#}$	0.508	0.567	0.566	0.544	0.554	0.536	0.558	0.575	0.595	0.596
$cr^{\#}$	0.749	0.834	0.818	0.772	0.796	0.830	0.764	0.755	0.731	0.756
X_{mt}	0.112	0.070	0.082	0.109	0.109	0.098	0.109	0.112	0.114	0.111
Fe^{2+}/Fe^{3+}	2.199	3.104	2.648	2.097	2.045	2.373	2.070	1.893	1.781	1.822

Sample	116/36	116/36	116/36	116/36	116/36	116/36	116/36	116/36	116/36	116/36
Olivine	8	24	29	30	33	59	57	54	88	87
SiO_2	40.37	39.78	39.78	40.60	39.92	40.01	40.00	40.02	39.89	40.24
FeO	10.98	10.73	11.18	10.39	10.55	10.04	10.85	10.48	11.24	11.36
MgO	47.72	48.15	47.34	48.58	48.05	48.91	48.25	48.26	47.53	47.57
CaO	0.21	0.21	0.20	0.20	0.19	0.21	0.19	0.19	0.24	0.21
Sum	99.28	98.87	98.50	99.77	98.70	99.17	99.28	98.96	98.90	99.39
Fo	88.6	88.9	88.3	89.3	89.0	89.7	88.8	89.1	88.3	88.2
Spinel	8	24	29	30	33	59	57	54	88	87
SiO_2	0.19	0.10	0.06	0.07	0.03	0.09	0.09	0.07	0.08	0.08
TiO_2	0.08	0.10	0.15	0.07	0.15	0.13	0.10	0.13	0.08	0.16
Al_2O_3	10.72	11.71	10.85	11.64	9.66	10.60	12.61	11.11	11.84	11.01
Cr_2O_3	51.44	50.69	52.06	51.11	54.47	53.14	48.82	51.91	51.23	52.73
Fe_2O_3	7.81	8.08	8.06	8.22	7.22	7.33	9.30	7.81	8.37	7.87
FeO	14.81	14.72	15.41	14.00	15.11	14.07	14.44	14.12	14.46	16.86
MnO	0.23	0.09	0.12	0.22	0.29	0.07	0.20	0.27	0.23	0.24
MgO	11.63	11.98	11.55	12.40	11.55	12.45	12.20	12.20	12.27	10.94
NiO	0.21	0.10	0.18	0.03	0.16	0.00	0.16	0.15	0.10	0.10
Sum	97.12	97.57	98.44	97.75	98.63	97.87	97.91	97.77	98.66	99.99
$Mg^{\#}$	0.583	0.592	0.572	0.612	0.577	0.612	0.601	0.606	0.602	0.536
$cr^{\#}$	0.763	0.744	0.763	0.747	0.791	0.771	0.722	0.758	0.744	0.763
X_{mt}	0.099	0.101	0.101	0.103	0.091	0.092	0.116	0.098	0.104	0.098
Fe^{2+}/Fe^{3+}	2.109	2.027	2.126	1.893	2.327	2.135	1.726	2.008	1.920	2.382

Boninite 2:

Sample	116/36	105/1	105/1	105/1	105/1	105/1	105/1	105/1	105/1	105/1
Olivine	76	1	2	4	6	8	9	10	14	16
SiO_2	39.86	39.54	40.77	40.78	39.91	40.69	40.94	41.08	40.48	40.46
FeO	11.96	14.12	10.13	12.31	13.55	10.49	9.75	9.43	9.96	10.26
MgO	46.39	45.66	49.64	49.02	46.63	48.98	50.14	50.19	49.60	48.78
CaO	0.21	0.25	0.23	0.22	0.20	0.21	0.21	0.23	0.18	0.22
Sum	98.42	99.56	100.77	102.34	100.29	100.37	101.03	100.92	100.21	99.72
Fo	87.4	85.2	89.7	87.6	86.0	89.3	90.2	90.5	89.9	89.4
Spinel	76	1	2	4	6	8	9	10	14	16
SiO_2	0.11	0.07	0.05	0.07	0.08	0.07	0.02	0.08	0.10	0.07
TiO_2	0.17	0.23	0.30	0.28	0.33	0.31	0.19	0.17	0.25	0.21
Al_2O_3	10.93	6.65	6.46	7.19	7.73	7.01	5.22	5.67	7.72	5.02
Cr_2O_3	51.31	56.65	59.01	56.27	54.67	57.34	59.96	59.12	58.15	60.54
Fe_2O_3	8.40	8.29	7.49	8.03	9.56	7.72	7.98	8.05	6.78	7.32
FeO	15.50	18.74	15.04	16.21	18.52	15.47	14.73	14.19	14.75	16.04
MnO	0.35	0.27	0.33	0.24	0.33	0.26	0.24	0.19	0.12	0.23
MgO	11.41	9.37	11.79	10.90	9.79	11.50	11.80	12.16	12.23	11.02
NiO	0.11	0.06	0.09	0.07	0.07	0.01	0.00	0.00	0.00	0.08
Sum	98.29	100.33	100.56	99.26	101.09	99.68	100.14	99.63	100.10	100.53
$Mg^{\#}$	0.567	0.471	0.583	0.545	0.485	0.570	0.588	0.604	0.597	0.551
$cr^{\#}$	0.759	0.851	0.860	0.840	0.826	0.846	0.885	0.875	0.835	0.890
X_{mt}	0.106	0.106	0.094	0.102	0.121	0.098	0.101	0.102	0.085	0.093
Fe^{2+}/Fe^{3+}	2.052	2.512	2.231	2.242	2.153	2.228	2.050	1.960	2.417	2.434

Sample	105/1	105/1	105/1	105/1	105/1	105/1	105/1	105/1	105/1	105/1
Olivine	24	26	30	32	33	35	38		51	53
SiO_2	40.49	40.79	40.47	40.63	40.64	40.30	39.40		40.64	40.19
FeO	11.65	9.24	11.32	11.31	11.85	10.70	13.06		10.29	12.51
MgO	47.97	50.25	48.70	48.68	47.82	49.08	45.95		49.32	47.28
CaO	0.18	0.26	0.23	0.22	0.23	0.21	0.19		0.25	0.20
Sum	100.30	100.54	100.72	100.84	100.55	100.29	98.60		100.50	100.18
Fo	88.0	90.6	88.5	88.5	87.8	89.1	86.2		89.5	87.1
Spinel	24	26	30	32	33	35	38	47	51	53
SiO_2	0.04	0.11	0.00	0.00	0.06	0.03	0.04	0.03	0.06	0.06
TiO_2	0.39	0.25	0.16	0.18	0.23	0.30	0.25	0.22	0.36	0.25
Al_2O_3	7.16	6.06	4.88	6.11	5.50	6.34	6.19	5.25	6.41	6.48
Cr_2O_3	54.76	58.93	60.00	58.39	58.96	58.17	58.73	59.23	56.87	57.16
Fe_2O_3	10.28	7.85	8.14	9.01	7.19	7.96	7.23	7.97	9.07	8.17
FeO	16.97	14.21	16.62	15.91	19.22	15.90	17.96	18.67	17.19	17.45
MnO	0.26	0.29	0.21	0.30	0.30	0.26	0.17	0.27	0.31	0.23
MgO	10.69	12.26	10.57	11.26	8.98	11.16	9.96	9.43	10.52	10.13
NiO	0.07	0.01	0.08	0.00	0.00	0.10	0.04	0.00	0.01	0.12
Sum	100.62	99.97	100.67	101.15	100.44	100.22	100.56	101.07	100.80	100.05
$Mg^{\#}$	0.529	0.606	0.531	0.558	0.454	0.556	0.497	0.474	0.522	0.509
$cr^{\#}$	0.837	0.867	0.892	0.865	0.878	0.860	0.864	0.883	0.856	0.855
X_{mt}	0.130	0.099	0.103	0.113	0.092	0.101	0.092	0.102	0.115	0.104
Fe^{2+}/Fe^{3+}	1.833	2.013	2.269	1.963	2.973	2.222	2.760	2.604	2.108	2.374

BABB 2

Sample	105/1	105/1	105/1	105/1	117/2	117/2	117/2	117/2	117/2	117/2
Olivine	58	67	74	82	48	48	48	4	5	6
SiO_2	39.92	40.88	40.51	40.23	40.43	40.43	40.43	40.46	40.28	40.37
FeO	12.60	10.08	10.28	10.66	11.17	11.17	11.17	9.72	10.94	10.55
MgO	47.13	50.14	49.19	48.37	48.16	48.16	48.16	48.86	47.61	48.61
CaO	0.23	0.20	0.19	0.19	0.25	0.25	0.25	0.28	0.31	0.31
Sum	99.87	101.30	100.17	99.46	100.00	100.00	100.00	99.33	99.14	99.84
Fo	87.0	89.9	89.5	89.0	88.5	88.5	88.5	90.0	88.6	89.1
Spinel	58	67	74	82	48a	48b	48c	4	5	6
SiO_2	0.05	0.04	0.04	0.04	0.16	0.11	0.12	0.12	0.09	0.16
TiO_2	0.20	0.23	0.23	0.22	0.28	0.32	0.29	0.30	0.32	0.44
Al_2O_3	5.86	4.74	6.15	5.59	42.45	42.95	42.63	41.26	44.36	40.12
Cr_2O_3	58.28	60.36	58.01	59.80	22.73	22.78	21.90	25.58	20.79	25.42
Fe_2O_3	8.21	7.92	7.82	6.53	4.68	4.33	5.02	4.29	4.87	5.86
FeO	17.46	15.56	18.69	18.91	9.58	9.81	9.39	9.51	10.17	10.35
MnO	0.28	0.22	0.26	0.25	0.09	0.08	0.23	0.00	0.06	0.14
MgO	10.09	11.26	9.41	9.22	18.94	18.89	18.88	19.14	18.85	18.70
NiO	0.13	0.09	0.06	0.04	0.22	0.27	0.19	0.30	0.25	0.28
Sum	100.56	100.42	100.67	100.60	99.13	99.53	98.64	100.50	99.76	101.48
$Mg^{\#}$	0.507	0.563	0.473	0.465	0.779	0.774	0.782	0.782	0.768	0.763
$cr^{\#}$	0.870	0.895	0.864	0.878	0.264	0.262	0.256	0.294	0.239	0.298
X_{mt}	0.104	0.101	0.100	0.084	0.049	0.045	0.053	0.045	0.051	0.061
Fe^{2+}/Fe^{3+}	2.363	2.185	2.655	3.217	2.277	2.517	2.079	2.467	2.319	1.963

Sample	117/2	117/5	123/1	123/1	123/1	123/1	123/1	123/1	123/1	123/1
Olivine	7	8	1	3	4	5	6	9	17	19
SiO_2	40.01	40.35	39.70	40.16	40.32	40.04	39.78	39.47	40.08	38.93
FeO	10.29	10.02	10.23	10.47	9.80	10.54	9.74	10.58	10.20	9.98
MgO	47.95	48.01	48.42	48.30	48.34	48.42	48.90	48.30	48.94	47.49
CaO	0.30	0.29	0.26	0.28	0.28	0.27	0.26	0.29	0.28	0.31
Sum	98.55	98.66	98.61	99.20	98.74	99.27	98.68	98.64	99.49	96.70
Fo	89.2	89.5	89.4	89.2	89.8	89.1	89.9	89.1	89.5	89.5
Spinel	7	8	1	3	4	5	6	9	17	19
SiO_2	0.10	0.13	0.10	0.11	0.09	0.11	0.15	0.10	0.13	0.14
TiO_2	0.33	0.30	0.33	0.37	0.46	0.43	0.41	0.39	0.42	0.45
Al_2O_3	45.29	43.89	37.43	34.67	35.49	36.20	37.68	35.33	35.55	35.51
Cr_2O_3	20.49	21.61	28.81	30.06	31.20	29.72	28.62	30.73	29.48	30.15
Fe_2O_3	4.55	4.76	4.96	5.79	4.58	5.03	5.31	5.36	4.77	4.73
FeO	9.94	9.59	9.78	11.62	10.61	10.60	9.46	11.67	10.19	10.15
MnO	0.02	0.08	0.08	0.14	0.01	0.04	0.18	0.18	0.15	0.04
MgO	19.29	19.19	18.49	16.97	17.97	17.96	18.90	17.27	17.72	18.00
NiO	0.14	0.27	0.25	0.17	0.21	0.21	0.24	0.14	0.28	0.28
Sum	100.15	99.82	100.23	99.89	100.62	100.29	100.95	101.18	98.69	99.45
$Mg^{\#}$	0.776	0.781	0.771	0.723	0.751	0.751	0.781	0.725	0.756	0.760
$cr^{\#}$	0.233	0.248	0.341	0.368	0.371	0.355	0.338	0.369	0.357	0.363
X_{mt}	0.047	0.049	0.053	0.063	0.049	0.054	0.056	0.058	0.052	0.051
Fe^{2+}/Fe^{3+}	2.428	2.237	2.191	2.232	2.577	2.342	1.979	2.417	2.374	2.383

E-MORB

Sample	123/1	123/1	123/1	92/37	92/37	92/37	92/37	92/37	92/37	92/37
Olivine	20	21	24	3	9	28	41	67	66	68
SiO_2	39.42	39.57	40.57	40.45	40.79	41.16	40.66	41.66	40.67	40.41
FeO	11.06	10.34	10.25	14.77	14.63	11.28	13.94	11.05	12.87	13.17
MgO	46.43	48.44	48.59	45.85	45.66	47.66	45.06	47.27	45.87	45.7
CaO	0.30	0.27	0.28	0.40	0.38	0.44	0.44	0.39	0.42	0.42
Sum	97.21	98.62	99.69	101.47	101.46	100.54	100.10	100.37	99.83	99.70
Fo	88.2	89.3	89.4	84.7	84.8	88.3	85.2	88.4	86.4	86.1
Spinel	20	21	24	3	9	28	41	67	66	68
SiO_2	0.13	0.12	0.13	0.25	0.38	0.26	0.20	0.23	0.26	0.29
TiO_2	0.46	0.31	0.48	0.91	0.79	1.00	1.08	0.98	1.00	1.01
Al_2O_3	35.69	36.96	35.05	30.26	34.07	27.10	25.36	26.24	25.79	24.02
Cr_2O_3	29.55	29.59	30.68	28.23	24.37	35.65	34.49	37.35	34.04	36.25
Fe_2O_3	5.77	5.61	4.85	9.33	8.08	6.36	8.55	5.47	7.46	6.40
FeO	11.75	11.01	10.72	14.30	14.47	12.83	15.82	13.52	14.70	15.01
MnO	0.24	0.24	0.21	0.17	0.21	0.15	0.17	0.24	0.22	0.20
MgO	17.22	17.88	17.57	15.00	15.11	15.91	13.81	15.28	14.15	13.66
NiO	0.17	0.28	0.32							
Sum	100.98	102.00	100.01	98.45	97.47	99.25	99.47	99.31	97.61	96.83
$Mg^{\#}$	0.723	0.743	0.745	0.652	0.651	0.689	0.609	0.668	0.632	0.619
$cr^{\#}$	0.357	0.349	0.370	0.385	0.324	0.469	0.477	0.488	0.470	0.503
X_{mt}	0.062	0.059	0.053	0.108	0.092	0.073	0.101	0.064	0.089	0.078
Fe^{2+}/Fe^{3+}	2.264	2.183	2.456	1.704	1.991	2.243	2.058	2.751	2.192	2.607

Sample	92/37	92/37	92/37	92/37	92/37	92/37	92/37	92/37	92/37	92/37
Olivine	74	75	7	12	13	21	27	31	35	40
SiO_2	41.4	41.21	39.75	39.78	39.65	39.58	40.39	40.06	39.67	39.57
FeO	12.13	13.31	14.40	13.92	12.63	14.34	11.18	12.85	14.16	12.84
MgO	46.96	46.24	45.78	45.60	46.59	44.92	47.88	46.14	44.51	46.40
CaO	0.39	0.42	0.44	0.39	0.43	0.39	0.35	0.40	0.40	0.35
Sum	100.88	101.18	100.36	99.69	99.30	99.23	99.80	99.45	98.73	99.16
Fo	87.3	86.1	85.0	85.4	86.8	84.8	88.4	86.5	84.8	86.6
Spinel	74	75	7	12	13	21	27	31	35	40
SiO_2	0.23	0.27	0.08	0.11	0.14	0.09	0.07	0.05	0.08	0.05
TiO_2	0.83	1.03	0.80	0.86	0.88	0.80	0.84	0.77	0.97	1.00
Al_2O_3	25.70	24.60	30.92	29.31	30.55	32.74	26.51	31.33	31.24	23.17
Cr_2O_3	37.31	34.58	29.86	31.42	31.35	26.49	37.59	31.56	30.26	38.85
Fe_2O_3	5.21	7.31	7.82	7.99	7.42	8.81	6.36	7.23	7.87	7.55
FeO	13.05	14.92	14.65	14.90	13.67	14.32	12.87	13.39	14.64	15.09
MnO	0.19	0.16	0.07	0.22	0.26	0.11	0.31	0.19	0.18	0.13
MgO	15.13	13.75	14.73	14.38	15.45	15.02	15.44	15.75	15.03	13.87
NiO			0.08	0.16	0.13	0.00	0.29	0.10	0.19	0.06
Sum	97.65	96.62	99.00	99.35	99.85	98.38	100.29	100.36	100.46	99.77
$Mg^{\#}$	0.674	0.622	0.642	0.632	0.668	0.651	0.681	0.677	0.647	0.621
$cr^{\#}$	0.493	0.485	0.393	0.418	0.408	0.352	0.488	0.403	0.394	0.529
X_{mt}	0.061	0.089	0.089	0.092	0.084	0.100	0.073	0.081	0.089	0.089
Fe^{2+}/Fe^{3+}	2.780	2.269	2.081	2.072	2.048	1.808	2.248	2.058	2.066	2.223

Sample	92/37	92/37	92/37	92/37	92/37	92/37	92/37	92/37	92/37	92/37
Olivine	46	49	53	79	T2:24	27	33	38	42	73
SiO_2	39.57	40.08	39.57	39.52	39.75	39.58	39.93	39.49	39.79	39.54
FeO	13.94	11.51	14.34	13.42	13.20	14.43	14.18	13.46	14.34	13.97
MgO	45.08	47.68	44.70	45.69	46.48	44.79	45.16	46.11	44.99	45.20
CaO	0.38	0.33	0.37	0.39	0.38	0.42	0.38	0.37	0.36	0.42
Sum	98.97	99.60	98.98	99.02	99.81	99.22	99.65	99.44	99.48	99.12
Fo	85.2	88.1	84.7	85.9	86.3	84.7	85.0	85.9	84.8	85.2
Spinel	46	49	53	79	24	27	33	38	42	73
SiO_2	0.09	0.06	0.16	0.08	0.10	0.08	0.13	0.11	0.08	0.05
TiO_2	0.78	0.83	0.93	0.87	0.71	1.04	0.91	0.99	0.81	0.87
Al_2O_3	39.33	26.29	32.35	26.90	29.59	26.76	32.08	25.39	35.28	25.95
Cr_2O_3	21.77	37.62	26.16	34.95	33.05	35.81	28.74	36.34	25.06	35.68
Fe_2O_3	8.13	6.07	8.06	7.30	6.76	7.34	8.49	7.45	8.58	8.05
FeO	13.10	13.08	14.72	14.80	14.24	15.38	14.41	14.82	14.12	15.39
MnO	0.19	0.07	0.22	0.11	0.03	0.22	0.15	0.16	0.12	0.07
MgO	16.73	15.39	14.45	14.31	14.96	14.28	15.26	14.18	15.60	13.96
NiO	0.17	0.10	0.15	0.10	0.10	0.09	0.20	0.21	0.17	0.12
Sum	100.29	99.51	97.20	99.42	99.54	101.01	100.37	99.66	99.82	100.14
$Mg^{\#}$	0.695	0.677	0.636	0.633	0.652	0.623	0.654	0.630	0.663	0.618
$cr^{\#}$	0.271	0.490	0.352	0.466	0.428	0.473	0.375	0.490	0.323	0.480
X_{mt}	0.088	0.070	0.093	0.085	0.077	0.084	0.095	0.087	0.095	0.093
Fe^{2+}/Fe^{3+}	1.791	2.392	2.030	2.253	2.341	2.330	1.887	2.211	1.829	2.124

101:

Sample	92/37	92/37	92/37	92/37	92/37	92/37	101/1	101/1	101/1	101/1
Olivine	72	70	76	92	89	96	11	14	20	21
SiO_2	40.29	40.04	39.88	39.85	39.72	39.64	39.80	40.38	40.53	40.66
FeO	13.18	12.51	11.89	14.31	14.81	12.99	12.15	10.98	11.16	11.49
MgO	46.92	47.21	47.40	45.63	45.45	46.81	47.53	48.09	48.29	48.11
CaO	0.40	0.41	0.38	0.37	0.41	0.37	0.22	0.20	0.22	0.22
Sum	100.78	100.17	99.55	100.16	100.39	99.80	99.69	99.66	100.20	100.48
Fo	86.4	87.1	87.7	85.0	84.5	86.5	87.5	88.6	88.5	88.2
Spinel	72	70	76	92	89	96	11	14	20	21
SiO_2	0.07	0.03	0.09	0.08	0.13	0.10	0.15	0.11	0.23	0.07
TiO_2	0.91	1.01	0.91	0.98	0.64	0.90	0.51	0.59	0.65	0.65
Al_2O_3	26.90	25.93	26.55	29.97	33.24	25.85	16.93	16.41	19.15	19.28
Cr_2O_3	36.32	37.60	37.47	31.99	28.56	37.73	44.27	44.64	42.36	41.99
Fe_2O_3	7.39	6.51	6.23	7.36	8.08	6.64	8.90	8.47	8.12	9.01
FeO	14.35	14.51	13.17	14.82	14.53	13.69	15.62	16.55	15.82	15.85
MnO	0.18	0.01	0.20	0.18	0.11	0.29	0.18	0.19	0.19	0.15
MgO	14.90	14.70	15.41	14.79	15.28	14.98	12.49	11.73	12.71	12.70
NiO	0.17	0.14	0.24	0.14	0.14	0.22	0.07	0.16	0.23	0.19
Sum	101.19	100.44	100.27	100.31	100.71	100.40	99.12	98.85	99.46	99.89
$Mg^{\#}$	0.649	0.644	0.676	0.640	0.652	0.661	0.588	0.558	0.589	0.588
$cr^{\#}$	0.475	0.493	0.486	0.417	0.366	0.495	0.637	0.646	0.597	0.594
X_{mt}	0.084	0.075	0.071	0.084	0.090	0.077	0.109	0.104	0.098	0.108
Fe^{2+}/Fe^{3+}	2.156	2.478	2.350	2.239	2.000	2.291	1.951	2.171	2.164	1.955

Sample	101/1	101/1	101/1	101/1	101/1	101/1	101/1	101/1	101/1	101/1
Olivine	22	23	28	6	8	10	11	14	16	18
SiO_2	40.90	40.68	40.49	40.31	40.52	40.35	40.51	40.66	40.51	40.59
FeO	9.45	11.70	11.87	12.38	12.42	12.66	11.69	9.34	12.52	11.43
MgO	49.61	47.79	47.56	47.87	47.30	47.42	47.94	49.91	47.23	48.00
CaO	0.14	0.19	0.19	0.25	0.21	0.18	0.19	0.19	0.22	0.20
Sum	100.10	100.37	100.11	100.81	100.45	100.61	100.34	100.09	100.48	100.22
Fo	90.3	87.9	87.7	87.3	87.2	87.0	88.0	90.5	87.1	88.2
Spinel	22	23	28	6	8	10	11	14	16	18
SiO_2	0.24	0.12	0.13	0.17	0.12	0.11	0.12	0.11	0.13	0.11
TiO_2	0.47	0.53	0.25	0.61	0.69	0.55	0.54	0.47	0.62	0.40
Al_2O_3	16.88	19.00	13.27	18.56	19.14	17.02	19.04	18.37	18.00	17.25
Cr_2O_3	48.19	42.36	49.71	42.95	40.96	43.88	42.41	43.97	41.96	46.07
Fe_2O_3	6.19	9.41	8.39	8.35	9.81	9.33	9.23	8.41	9.34	7.49
FeO	13.56	15.16	15.24	15.77	16.38	16.03	14.80	16.04	16.33	15.11
MnO	0.26	0.31	0.29	0.15	0.14	0.17	0.15	0.23	0.21	0.04
MgO	13.91	13.12	12.15	12.66	12.45	12.23	13.34	12.49	12.06	12.85
NiO	0.27	0.02	0.20	0.16	0.08	0.19	0.15	0.09	0.11	0.24
Sum	99.97	100.03	99.63	99.38	99.77	99.51	99.77	100.17	98.76	99.56
$Mg^{\#}$	0.646	0.607	0.587	0.589	0.575	0.576	0.616	0.581	0.568	0.603
$cr^{\#}$	0.657	0.599	0.715	0.608	0.589	0.634	0.599	0.616	0.610	0.642
X_{mt}	0.074	0.112	0.103	0.101	0.119	0.114	0.110	0.101	0.114	0.090
Fe^{2+}/Fe^{3+}	2.433	1.791	2.019	2.099	1.855	1.909	1.782	2.119	1.943	2.241

Sample	101/1	101/1	101/1	101/1	101/1	101/1	101/1	101/1	101/1	101/1
Olivine	30	36	37	50	58	59	X	2	5	6
SiO_2	40.65	40.22	40.64	39.98	40.32	40.66	40.47	40.20	40.54	40.39
FeO	11.99	12.07	11.97	12.86	12.23	10.46	11.51	11.72	10.42	11.44
MgO	47.63	47.04	48.25	46.98	47.80	47.91	47.39	47.40	49.37	47.40
CaO	0.21	0.20	0.19	0.23	0.20	0.21	0.18	0.21	0.17	0.19
Sum	100.48	99.53	101.04	100.05	100.56	99.23	99.56	99.53	100.51	99.42
Fo	87.6	87.4	87.8	86.7	87.4	89.1	88.0	87.8	89.4	88.1
Spinel	30	36	37	50	58	59	X	2	5	6
SiO_2	0.17	0.14	0.12	0.08	0.15	0.11	0.10	0.04	0.03	0.04
TiO_2	0.43	0.37	0.45	0.63	0.64	0.56	0.47	0.70	0.62	0.62
Al_2O_3	16.31	16.19	18.55	17.93	18.30	18.87	18.33	20.18	19.85	19.97
Cr_2O_3	45.43	45.30	43.07	42.21	41.83	43.61	43.13	41.77	41.98	41.79
Fe_2O_3	9.08	8.82	9.09	9.74	9.81	7.67	8.83	7.83	7.66	8.62
FeO	15.66	15.82	14.71	15.98	15.58	14.49	15.66	15.57	16.17	15.35
MnO	0.27	0.15	0.24	0.24	0.11	0.12	0.19	0.24	0.16	0.25
MgO	12.42	12.13	13.19	12.30	12.78	13.41	12.50	12.76	12.26	12.93
CaO								0.01	0.10	0.01
NiO	0.16	0.20	0.16	0.15	0.12	0.12	0.24	0.14	0.08	0.15
ZnO								0.14	0.11	0.10
Sum	99.93	99.12	99.58	99.27	99.32	98.96	99.44	99.36	99.01	99.83
$Mg^{\#}$	0.586	0.577	0.615	0.578	0.594	0.623	0.587	0.594	0.575	0.600
$cr^{\#}$	0.651	0.652	0.609	0.612	0.605	0.608	0.612	0.581	0.587	0.584
X_{mt}	0.110	0.108	0.109	0.119	0.119	0.092	0.107	0.094	0.092	0.103
Fe^{2+}/Fe^{3+}	1.918	1.994	1.798	1.822	1.766	2.100	1.970	2.211	2.346	1.980

Sample	101/1	101/1	101/1	101/1	101/1	101/1	101/1	101/1	101/1	101/1
Olivine	8	9			10	11	19	19A	20	21
SiO_2	40.01	40.41			40.27	39.94	40.51	40.28	40.31	40.54
FeO	12.20	11.47			11.55	12.16	9.69	10.99	11.43	10.09
MgO	46.77	47.29			47.06	46.94	48.99	47.62	47.50	48.76
CaO	0.20	0.19			0.22	0.17	0.18	0.22	0.21	0.19
Sum	99.17	99.36			99.11	99.20	99.37	99.11	99.46	99.58
Fo	87.2	88.0			87.9	87.3	90.0	88.5	88.1	89.6
Spinel	8	9	9a	9b	10	11	19	19A	20	21
SiO_2	0.00	0.03	0.08	0.07	0.04	0.04	0.08	0.08	0.04	0.03
TiO_2	0.67	0.60	0.54	0.55	0.65	0.69	0.44	0.40	0.49	0.55
Al_2O_3	18.21	20.44	18.85	19.54	19.81	18.78	19.12	17.11	17.17	18.98
Cr_2O_3	42.68	41.83	42.48	41.21	42.19	42.05	45.23	46.35	45.46	45.08
Fe_2O_3	7.78	7.74	8.01	8.45	7.74	8.55	6.74	7.14	7.87	6.75
FeO	16.37	16.35	16.43	16.05	16.30	15.86	13.60	15.90	14.99	13.80
MnO	0.18	0.16	0.24	0.25	0.23	0.23	0.18	0.23	0.31	0.10
MgO	11.75	12.30	11.81	12.15	12.27	12.31	13.93	12.17	12.64	13.74
CaO	0.00	0.01	0.08	0.04	0.02	0.04	0.06	0.00	0.04	0.01
NiO	0.12	0.20	0.12	0.12	0.10	0.13	0.09	0.09	0.11	0.26
ZnO	0.12	0.21	0.22	0.09	0.15	0.11	0.12	0.20	0.14	0.14
Sum	97.86	99.87	98.86	98.52	99.52	98.79	99.58	99.66	99.26	99.44
$Mg^{\#}$	0.561	0.573	0.562	0.574	0.573	0.580	0.646	0.577	0.601	0.640
$cr^{\#}$	0.611	0.579	0.602	0.586	0.588	0.600	0.613	0.645	0.640	0.614
X_{mt}	0.096	0.092	0.097	0.103	0.093	0.104	0.080	0.086	0.095	0.081
Fe^{2+}/Fe^{3+}	2.338	2.347	2.279	2.111	2.339	2.062	2.243	2.476	2.118	2.271

Sample	101/1	101/1	101/1	101/1	101/1	101/1	101/1	101/1	101/1	101/1
Olivine										
SiO_2										
FeO										
MgO										
CaO										
Sum										
Fo										
Spinel	103	103A	102	102A	102B	101	101A	101B	291	291A
SiO_2	0.05	0.09	0.09	0.07	0.06	0.06	0.10	0.08	0.08	0.83
TiO_2	0.54	0.44	0.36	0.30	0.31	1.04	1.05	1.07	0.27	0.29
Al_2O_3	16.25	14.08	14.99	15.68	15.02	26.11	26.02	25.95	12.32	12.70
Cr_2O_3	47.01	50.10	49.81	50.35	50.57	36.23	36.14	35.72	53.81	52.44
Fe_2O_3	6.80	6.31	6.25	5.08	5.22	6.79	6.40	6.74	5.52	5.51
FeO	16.46	16.88	16.85	16.49	16.54	15.77	15.90	15.84	14.49	14.94
MnO	0.19	0.19	0.27	0.23	0.20	0.24	0.15	0.17	0.20	0.17
MgO	11.69	11.32	11.50	11.72	11.58	13.53	13.53	13.49	12.54	13.16
CaO	0.02	0.01	0.00	0.02	0.02	0.08	0.03	0.02	0.03	0.02
NiO	0.17	0.12	0.13	0.07	0.08	0.10	0.14	0.10	0.17	0.06
ZnO	0.17	0.08	0.04	0.17	0.05	0.31	0.09	0.14	0.02	0.07
Sum	99.34	99.61	100.29	100.18	99.65	100.27	99.54	99.33	99.45	100.20
$Mg^{\#}$	0.559	0.545	0.549	0.559	0.555	0.605	0.603	0.603	0.607	0.611
$cr^{\#}$	0.660	0.705	0.690	0.683	0.693	0.482	0.482	0.480	0.746	0.735
X_{mt}	0.083	0.078	0.076	0.062	0.064	0.079	0.075	0.079	0.068	0.068
Fe^{2+}/Fe^{3+}	2.689	2.971	2.994	3.606	3.522	2.579	2.762	2.610	2.917	3.011

108:

Sample	101/1	108/5	108/5	108/5	108/5	108/5	108/5	108/5	108/5	108/5
Olivine		14	17	25	27	30	41	42	55	56
SiO_2		40.42	41.50	41.00	40.89	40.63	41.01	40.23	41.12	40.45
Cr_2O_3										
FeO		11.09	7.22	7.37	7.36	7.68	8.14	10.68	7.78	11.11
MnO										
MgO		47.27	50.83	50.77	49.97	49.59	49.38	47.56	51.00	47.75
CaO		0.17	0.19	0.22	0.15	0.17	0.18	0.22	0.20	0.18
NiO										
Sum		98.95	99.75	99.36	98.37	98.08	98.71	98.69	100.10	99.49
Fo		88.4	92.6	92.5	92.4	92.0	91.5	88.8	92.1	88.5
Spinel	291B	14	17	25	27	30	41	42	55	56
SiO_2	0.13	0.06	0.11	0.17	0.09	0.08	0.16	0.13	0.09	0.09
TiO_2	0.30	0.41	0.36	0.47	0.37	0.43	0.43	0.33	0.27	0.38
Al_2O_3	12.51	16.77	13.32	13.13	12.41	13.99	12.69	11.03	13.22	17.00
Cr_2O_3	53.19	46.37	53.87	54.11	53.87	51.06	51.94	54.25	54.46	45.47
Fe_2O_3	5.38	8.40	6.29	5.27	6.41	6.76	7.10	6.43	5.37	8.80
FeO	14.71	14.94	11.05	11.70	11.48	12.11	13.13	15.74	12.16	15.11
MnO	0.20	0.21	0.14	0.16	0.31	0.19	0.23	0.24	0.23	0.16
MgO	12.40	12.95	15.26	14.84	14.64	14.34	13.62	11.89	14.41	12.89
CaO	0.05									
NiO	0.13	0.16	0.20	0.14	0.08	0.14	0.21	0.04	0.10	0.08
ZnO	0.02									
Sum	99.02	100.27	100.60	99.99	99.66	99.10	99.51	100.07	100.31	99.98
$Mg^{\#}$	0.600	0.607	0.711	0.693	0.694	0.679	0.649	0.574	0.679	0.603
$cr^{\#}$	0.740	0.650	0.731	0.734	0.744	0.710	0.733	0.767	0.734	0.642
X_{mt}	0.067	0.101	0.075	0.064	0.078	0.082	0.087	0.080	0.064	0.106
Fe^{2+}/Fe^{3+}	3.037	1.977	1.954	2.470	1.992	1.991	2.055	2.720	2.517	1.909

Sample	108/5	108/5	108/5	108/5	108/5	108/5	108/5	108/5	108/5	108/6
Olivine	58	60	63	68	73	76	3	6	9	2
SiO_2	40.38	40.07	40.30	41.19	41.13	40.23	40.07	40.95	40.23	41.00
Cr_2O_3										
FeO	10.44	11.50	12.44	8.56	7.39	10.94	10.59	8.15	11.31	9.52
MnO										
MgO	48.02	47.15	46.44	49.71	51.33	47.33	47.91	50.90	48.16	49.86
CaO	0.20	0.17	0.16	0.20	0.12	0.22	0.20	0.20	0.18	0.22
NiO										
Sum	99.04	98.89	99.35	99.65	99.97	98.72	98.77	100.19	99.88	100.60
Fo	89.1	88.0	86.9	91.2	92.5	88.5	89.0	91.8	88.4	90.3
Spinel	58	60	63	68	73	76	108/5 3	6	9	2
SiO_2	0.08	0.07	0.24	0.29	0.11	0.07	0.04	0.07	0.08	0.11
TiO_2	0.28	0.43	0.39	0.46	0.51	0.46	0.40	0.29	0.41	0.29
Al_2O_3	10.76	13.30	16.16	13.02	13.59	17.16	13.20	13.62	13.71	12.36
Cr_2O_3	54.87	50.08	45.07	51.69	52.91	44.12	49.65	53.87	50.09	52.52
Fe_2O_3	6.16	7.63	9.44	6.60	5.61	9.04	7.87	5.69	8.51	7.35
FeO	15.56	15.74	16.14	13.74	11.56	14.92	15.18	12.10	14.89	15.28
MnO	0.13	0.07	0.21	0.28	0.13	0.32	0.16	0.07	0.31	0.15
MgO	11.90	12.06	12.23	13.47	14.80	12.71	12.12	14.59	12.74	12.30
CaO										
NiO	0.09	0.11	0.06	0.06	0.23	0.11	0.19	0.14	0.19	0.19
ZnO										0.10
Sum	99.83	99.49	99.94	99.61	99.45	98.92	98.81	100.43	100.93	100.65
$Mg^{\#}$	0.577	0.577	0.575	0.636	0.695	0.603	0.587	0.683	0.604	0.589
$cr^{\#}$	0.774	0.716	0.652	0.727	0.723	0.633	0.716	0.726	0.710	0.740
X_{mt}	0.076	0.094	0.115	0.081	0.068	0.110	0.098	0.068	0.103	0.090
Fe^{2+}/Fe^{3+}	2.804	2.293	1.900	2.315	2.287	1.835	2.143	2.365	1.944	2.310

Sample	108/6	108/6	108/6	108/6	108/6	108/6	108/6	108/6	108/6	108/6
Olivine	8	16	19	64	68	69	76	87	88	90
SiO_2	40.26	40.51	40.23	40.49	40.50	40.48	41.07	40.56	40.46	40.29
Cr_2O_3								0.09		
FeO	12.08	11.25	11.52	10.19	10.65	10.71	9.07	8.21	11.96	11.49
MnO								0.20		
MgO	47.83	47.99	48.06	48.45	48.11	48.47	49.96	49.39	47.33	47.85
CaO	0.20	0.20	0.20	0.21	0.22	0.19	0.22	0.23	0.20	0.20
NiO								0.30		
Sum	100.37	99.95	100.01	99.34	99.48	99.85	100.32	98.99	99.95	99.83
Fo	87.6	88.4	88.1	89.4	88.9	89.0	90.8	91.5	87.6	88.1
Spinel	8	16	19	64	68	69	76	87	88	90
SiO_2	0.08	0.12	0.06	0.09	0.07	0.06	0.10	0.75	0.06	0.08
TiO_2	0.34	0.38	0.38	0.39	0.52	0.40	0.30	0.38	0.40	0.41
Al_2O_3	13.38	13.36	15.34	14.31	14.17	12.57	13.06	11.02	15.01	12.12
Cr_2O_3	51.08	51.13	48.12	49.05	50.71	52.80	52.57	54.49	47.60	53.33
Fe_2O_3	7.73	7.06	8.23	7.58	7.04	6.89	6.89	4.61	8.39	6.14
FeO	15.77	15.19	15.20	14.07	15.09	15.05	13.13	14.01	15.45	15.84
MnO	0.27	0.27	0.20	0.16	0.13	0.31	0.23	0.29	0.24	0.17
MgO	12.10	12.36	12.65	13.06	12.78	12.52	13.70	13.17	12.26	11.92
CaO										
NiO	0.25	0.13	0.14	0.07	0.13	0.02	0.14	0.08	0.08	0.15
ZnO	0.00	0.13	0.00	0.02	0.11	0.09	0.02	0.25	0.10	0.04
Sum	101.00	100.13	100.32	98.80	100.76	100.71	100.14	99.05	99.59	100.21
$Mg^{\#}$	0.578	0.592	0.597	0.623	0.601	0.597	0.650	0.626	0.586	0.573
$cr^{\#}$	0.719	0.720	0.678	0.697	0.706	0.738	0.730	0.768	0.680	0.747
Xmt	0.094	0.086	0.099	0.093	0.085	0.084	0.083	0.058	0.102	0.076
Fe^{2+}/Fe^{3+}	2.267	2.390	2.052	2.063	2.381	2.427	2.116	3.373	2.046	2.865

Sample	108/6	108/6	108/6	108/6	108/6	108/6	108/6	108/6	108/6	108/6
Olivine	92	103	106	120	121	122	128	129	143	149
SiO_2	40.58	40.43	40.50	40.10	40.47	40.09	40.21	40.41	39.88	40.06
Cr_2O_3										
FeO	9.13	11.37	10.05	12.19	12.25	11.74	10.90	11.29	12.36	12.64
MnO										
MgO	49.62	47.79	49.36	47.19	47.19	47.70	47.98	48.32	47.37	46.65
CaO	0.22	0.22	0.23	0.19	0.17	0.20	0.22	0.18	0.19	0.19
NiO										
Sum	99.54	99.81	100.14	99.67	100.09	99.73	99.30	100.19	99.80	99.53
Fo	90.6	88.2	89.7	87.3	87.3	87.9	88.7	88.4	87.2	86.8
Spinel	92	103	106	120	121	122	128	129	143	149
SiO_2	0.08	0.05	0.09	0.10	0.08	0.10	0.03	0.06	0.07	0.07
TiO_2	0.32	0.40	0.35	0.39	0.47	0.45	0.46	0.42	0.41	0.39
Al_2O_3	12.37	13.38	11.69	14.81	13.59	15.93	12.71	12.04	17.03	15.95
Cr_2O_3	52.68	51.42	54.29	47.56	49.16	47.47	51.39	53.80	45.69	45.62
Fe_2O_3	6.47	7.33	6.17	8.52	8.29	7.73	7.25	6.32	8.76	9.22
FeO	14.34	15.57	14.74	15.56	16.33	15.53	15.30	15.57	15.66	16.01
MnO	0.29	0.28	0.27	0.25	0.27	0.13	0.23	0.20	0.18	0.34
MgO	12.60	12.22	12.49	12.11	11.68	12.50	12.25	12.20	12.58	11.98
CaO										
NiO	0.08	0.07	0.15	0.20	0.10	0.09	0.00	0.05	0.08	0.06
ZnO	0.14	0.19	0.11	0.11	0.07	0.18	0.05	0.10	0.11	0.06
Sum	99.37	100.91	100.35	99.61	100.04	100.11	99.67	100.76	100.57	99.69
$Mg^{\#}$	0.610	0.583	0.602	0.581	0.560	0.589	0.588	0.583	0.589	0.572
$cr^{\#}$	0.741	0.721	0.757	0.683	0.708	0.667	0.731	0.750	0.643	0.657
X_{mt}	0.080	0.089	0.076	0.104	0.102	0.094	0.089	0.077	0.105	0.112
Fe^{2+}/Fe^{3+}	2.465	2.359	2.656	2.030	2.189	2.232	2.345	2.738	1.988	1.931

Sample	108/6	108/6	108/6	108/6	108/6	108/6	108/6	108/6	108/6	108/6
Olivine	151	152	171	214	217/1	217/2	237	238	240	242
SiO_2	40.53	40.38	40.36	40.70	39.82	40.47	39.66	40.59	40.46	39.87
Cr_2O_3	0.19				0.21	0.14				0.09
FeO	7.67	10.48	11.17	10.09	7.25	7.54	12.37	10.08	10.08	11.02
MnO	0.14				0.12	0.11				0.13
MgO	49.93	48.81	47.69	48.64	50.19	50.48	46.95	48.70	48.71	47.39
CaO	0.18	0.20	0.18	0.20	0.18	0.17	0.19	0.20	0.26	0.19
NiO	0.43				0.32	0.34				0.19
Sum	99.06	99.88	99.40	99.64	98.09	99.26	99.17	99.58	99.51	98.87
Fo	92.0	89.2	88.4	89.6	92.5	92.2	87.1	89.6	89.6	88.5
Spinel	151	152	171	214	217/1	217/2	237	238	240	242
SiO_2	0.14	0.08	0.03	0.08	0.13	0.10	0.07	0.06	0.07	0.26
TiO_2	0.32	0.24	0.38	0.32	0.36	0.42	0.42	0.37	0.38	0.34
Al_2O_3	11.80	12.43	13.41	12.55	13.25	15.55	16.04	12.38	14.61	14.29
Cr_2O_3	53.62	51.77	50.93	53.34	53.21	50.79	45.67	53.09	49.34	49.44
Fe_2O_3	6.34	7.27	7.00	6.36	5.51	6.13	9.26	6.46	6.75	7.06
FeO	12.21	15.53	15.95	14.59	11.91	12.25	15.50	14.42	15.10	15.79
MnO	0.13	0.30	0.11	0.14	0.12	0.10	0.28	0.22	0.21	0.11
MgO	13.99	11.85	11.92	12.84	14.35	14.66	12.33	12.73	12.35	12.23
CaO										
NiO	0.13	0.18	0.10	0.02	0.26	0.22	0.10	0.13	0.11	0.15
ZnO	0.02	0.00	0.02	0.05	0.07	0.03	0.14	0.08	0.08	0.00
Sum	98.69	99.65	99.85	100.30	99.17	100.24	99.81	99.94	99.01	99.68
$Mg^{\#}$	0.671	0.576	0.571	0.611	0.682	0.681	0.587	0.611	0.593	0.580
$cr^{\#}$	0.753	0.736	0.718	0.740	0.729	0.687	0.656	0.742	0.694	0.699
X_{mt}	0.078	0.090	0.086	0.078	0.067	0.073	0.112	0.079	0.083	0.087
Fe^{2+}/Fe^{3+}	2.141	2.373	2.533	2.549	2.403	2.221	1.859	2.482	2.485	2.484

Sample	108/6	108/6	108/6	108/6	108/6	108/6	108/6	108/6	108/6	108/6
Olivine	242/2	244	250	252	261	268	273	273B	281	290
SiO_2	39.74	39.85	39.55	39.59	39.99	39.91	40.53	40.00	39.76	39.87
Cr_2O_3	0.06	0.12	0.17	0.12	0.11	0.07			0.02	0.10
FeO	11.07	8.90	11.35	11.61	11.63	10.52	11.50	11.92	11.83	10.77
MnO	0.23	0.12	0.15	0.19	0.10	0.12			0.19	0.14
MgO	46.76	48.68	46.88	46.67	47.02	48.23	47.75	47.50	47.29	47.58
CaO	0.23	0.22	0.16	0.18	0.17	0.20	0.19	0.18	0.18	0.19
NiO	0.16	0.24	0.16	0.21	0.19	0.15			0.19	0.26
Sum	98.24	98.14	98.43	98.56	99.20	99.19	99.97	99.60	99.45	98.91
Fo	88.3	90.7	88.0	87.8	87.8	89.1	88.1	87.7	87.7	88.7
Spinel	242/2	244	250	252	261	268	273	273B	281	290
SiO_2	0.11	0.07	0.08	0.05	0.07	0.06	0.06	0.06	0.09	0.06
TiO_2	0.42	0.43	0.33	0.37	0.43	0.40	0.46	0.43	0.37	0.43
Al_2O_3	15.90	13.09	12.90	12.34	11.87	13.71	15.77	15.10	13.79	12.66
Cr_2O_3	45.94	51.78	51.30	50.98	51.92	49.70	47.32	47.82	49.05	51.85
Fe_2O_3	7.57	5.69	6.99	7.73	6.74	7.35	7.97	7.81	8.03	7.01
FeO	15.22	13.19	15.75	16.17	16.08	14.68	14.97	15.34	15.81	15.61
MnO	0.26	0.09	0.22	0.16	0.23	0.06	0.20	0.12	0.20	0.16
MgO	12.19	13.27	11.88	11.54	11.47	12.59	12.71	12.42	11.93	12.10
CaO										
NiO	0.14	0.15	0.11	0.03	0.10	0.00	0.08	0.08	0.06	0.00
ZnO	0.00	0.13	0.02	0.14	0.03	0.16	0.15	0.00	0.07	0.18
Sum	97.75	97.89	99.58	99.51	98.93	98.71	99.69	99.18	99.40	100.06
$Mg^{\#}$	0.588	0.642	0.574	0.560	0.560	0.605	0.602	0.591	0.574	0.580
$cr^{\#}$	0.660	0.726	0.727	0.735	0.746	0.709	0.668	0.680	0.705	0.733
X_{mt}	0.094	0.071	0.086	0.096	0.084	0.091	0.097	0.096	0.099	0.086
Fe^{2+}/Fe^{3+}	2.233	2.580	2.503	2.325	2.652	2.220	2.087	2.182	2.187	2.475

Sample	108/6	108/6	108/6	108/6	108/6	108/6	108/6	108/6	108/6	108/6
Olivine	290/2	295	295	295/2	295/3	305	305B	305C	305D	305E
SiO_2	40.33	39.82	39.82	40.23	39.58	40.46	40.47	40.52	40.32	40.58
Cr_2O_3	0.11	0.06	0.06	0.10	0.06					
FeO	11.09	10.02	10.02	9.68	9.91	10.30	10.37	10.62	10.67	10.62
MnO	0.17	0.19	0.19	0.18	0.14					
MgO	47.73	48.05	48.05	48.31	48.49	47.99	48.35	48.45	48.16	48.17
CaO	0.20	0.22	0.22	0.21	0.20	0.19	0.20	0.21	0.18	0.17
NiO	0.21	0.18	0.18	0.28	0.25					
Sum	99.84	98.55	98.55	99.00	98.62	98.93	99.39	99.79	99.32	99.54
Fo	88.5	89.5	89.5	89.9	89.7	89.3	89.3	89.0	88.9	89.0
Spinel	290/2	295	295	295/2	295/3	305	305B	305C	305D	305E
SiO_2	0.08	0.06	0.05	0.06	0.07	0.08	0.10	0.03	0.06	0.11
TiO_2	0.43	0.48	0.44	0.33	0.37	0.33	0.28	0.34	0.31	0.46
Al_2O_3	16.41	13.25	13.26	13.23	13.13	13.23	12.67	12.75	12.69	13.55
Cr_2O_3	46.94	50.99	50.64	51.41	51.37	50.99	51.92	53.06	52.14	51.21
Fe_2O_3	7.83	7.03	6.96	6.94	6.60	6.95	6.84	6.38	6.57	6.47
FeO	15.04	14.79	14.54	14.15	14.12	14.42	14.01	14.98	14.46	15.37
MnO	0.22	0.13	0.34	0.30	0.11	0.15	0.12	0.16	0.23	0.12
MgO	12.76	12.69	12.49	12.85	12.86	12.69	12.88	12.54	12.50	12.44
CaO										
NiO	0.18	0.01	0.04	0.13	0.06	0.13	0.00	0.02	0.15	0.10
ZnO	0.06	0.07	0.15	0.00	0.14	0.02	0.23	0.12	0.14	0.00
Sum	99.95	99.49	98.91	99.39	98.83	99.00	99.04	100.38	99.26	99.83
$Mg^{\#}$	0.602	0.605	0.605	0.618	0.619	0.611	0.621	0.599	0.606	0.591
$cr^{\#}$	0.657	0.721	0.719	0.723	0.724	0.721	0.733	0.736	0.734	0.717
X_{mt}	0.095	0.086	0.086	0.085	0.081	0.086	0.084	0.078	0.081	0.079
Fe^{2+}/Fe^{3+}	2.135	2.337	2.324	2.265	2.378	2.305	2.275	2.609	2.444	2.638

Sample	108/6	108/6	108/6	108/6	108/6	108/6	108/6	108/6	108/6	108/6
Olivine	310	310/2	310/3	310/4	310/5	316	PX 32	PX10	B3	10
SiO2	39.46	40.01	39.79	39.75	39.70	40.22			40.35	40.31
Cr2O3	0.01	0.02	0.06	0.05	0.20	0.06			0.07	0.08
FeO	11.14	11.23	11.30	11.19	11.22	8.43			12.03	11.16
MnO	0.22	0.17	0.18	0.21	0.19	0.09			0.19	0.12
MgO	47.11	46.78	47.06	47.45	47.13	49.62			47.23	47.92
CaO	0.18	0.18	0.19	0.20	0.16	0.23			0.19	0.19
NiO	0.14	0.23	0.30	0.27	0.21	0.09			0.15	0.16
Sum	98.26	98.60	98.89	99.11	98.81	98.74			100.22	99.94
Fo	88.3	88.1	88.2	88.3	88.2	91.3			87.5	88.4
Spinel	310	310/2	310/3	310/4	310/5	316	32	10	3	10
SiO_2	0.08	0.91	0.11	0.04	0.07	0.08	0.13	0.07	0.16	0.10
TiO_2	0.48	0.50	0.33	0.38	0.31	0.43	0.53	0.48	0.42	0.33
Al_2O_3	14.65	16.63	14.57	14.65	13.58	14.76	16.32	14.34	14.15	15.51
Cr_2O_3	48.31	43.26	48.35	48.56	49.64	48.24	45.77	49.76	47.32	47.35
Fe_2O_3	7.50	7.09	7.73	7.81	7.41	7.82	9.27	7.83	9.38	8.74
FeO	15.45	16.63	15.25	15.32	15.39	12.59	16.00	13.87	16.62	14.97
MnO	0.17	0.17	0.19	0.16	0.25	0.15	0.25	0.25	0.17	0.35
MgO	12.24	12.01	12.28	12.24	11.93	13.98	12.49	13.47	11.66	12.66
CaO										
NiO	0.07	0.15	0.10	0.08	0.10	0.00	0.05	0.01	0.07	0.05
ZnO	0.09	0.09	0.03	0.22	0.10	0.03	0.00	0.04	0.06	0.16
Sum	99.04	97.44	98.93	99.46	98.77	98.08	100.81	100.11	100.01	100.22
$Mg^{\#}$	0.585	0.563	0.589	0.588	0.580	0.664	0.582	0.634	0.556	0.601
$cr^{\#}$	0.689	0.636	0.690	0.690	0.710	0.687	0.653	0.699	0.692	0.672
X_{mt}	0.092	0.090	0.095	0.096	0.092	0.096	0.112	0.095	0.115	0.106
Fe^{2+}/Fe_{3+}	2.289	2.605	2.194	2.178	2.309	1.788	1.920	1.969	1.969	1.902

Sample	108/6	108/7	108/7	108/7	108/7	108/7	108/7	108/7	108/7	108/7
Olivine	17	2A	3	4	4A	5	5A	10	10A	11
SiO_2	40.50	40.83	40.87	41.21	41.36	40.96	40.69	41.08	41.26	40.50
Cr_2O_3	0.09									
FeO	11.11	7.75	7.23	7.33	7.47	8.64	8.75	7.79	7.75	10.85
MnO	0.19									
MgO	48.00	50.91	51.63	51.62	51.73	49.87	49.99	50.82	50.89	48.05
CaO	0.16	0.16	0.16	0.16	0.16	0.22	0.26	0.16	0.19	0.18
NiO	0.21									
Sum	100.26	99.66	99.89	100.32	100.72	99.69	99.70	99.85	100.09	99.58
Fo	88.5	92.1	92.7	92.6	92.5	91.1	91.1	92.1	92.1	88.8
Spinel	17	2A	3	4	4A	5	5A	10	10A	11
SiO_2	0.12	0.08	0.08	0.08	0.11	0.05	0.15	0.07	0.04	0.06
TiO_2	0.45	0.32	0.35	0.34	0.37	0.39	0.42	0.31	0.33	0.46
Al_2O_3	16.78	11.74	13.89	12.71	12.99	13.02	13.15	12.04	11.85	17.07
Cr_2O_3	45.71	55.02	54.34	55.25	54.88	52.10	50.53	53.94	54.15	46.43
Fe_2O_3	8.74	5.46	4.44	4.06	4.09	6.76	6.92	6.23	5.84	6.85
FeO	15.43	12.27	11.25	12.42	11.71	13.50	13.07	11.99	12.59	14.92
MnO	0.17	0.20	0.24	0.08	0.22	0.23	0.15	0.15	0.19	0.19
MgO	12.77	13.81	14.86	14.07	14.41	13.35	13.49	14.13	13.66	12.68
CaO		0.05	0.01	0.01	0.01	0.02	0.00	0.00	0.01	0.07
NiO	0.04	0.20	0.25	0.11	0.09	0.06	0.06	0.13	0.12	0.14
ZnO	0.06	0.18	0.08	0.02	0.15	0.06	0.08	0.05	0.00	0.10
Sum	100.26	99.32	99.81	99.16	99.03	99.54	98.02	99.04	98.79	98.97
$Mg^{\#}$	0.596	0.667	0.702	0.669	0.687	0.638	0.648	0.677	0.659	0.602
$cr^{\#}$	0.646	0.759	0.724	0.745	0.739	0.729	0.720	0.750	0.754	0.646
X_{mt}	0.105	0.067	0.053	0.049	0.050	0.082	0.086	0.076	0.072	0.083
Fe^{2+}/Fe^{3+}	1.963	2.500	2.814	3.407	3.183	2.222	2.098	2.140	2.395	2.421

Sample	108/7	108/7	108/7	108/7	108/7	108/7	108/7	108/7	108/7	108/7
Olivine	18A	21	22	22A	32	34	35	35A	42	42A
SiO_2	41.15	40.93	41.01	40.85	40.95	39.91	40.66	40.72	40.39	40.61
Cr_2O_3										
FeO	8.15	7.09	8.96	8.78	8.96	11.91	10.33	11.19	9.47	9.34
MnO										
MgO	50.92	51.18	49.77	50.12	49.89	47.25	48.73	47.94	48.89	49.59
CaO	0.18	0.19	0.25	0.20	0.22	0.20	0.19	0.20	0.17	0.16
NiO										
Sum	100.41	99.39	100.00	99.96	100.02	99.27	99.91	100.05	98.92	99.71
Fo	91.8	92.8	90.8	91.1	90.8	87.6	89.4	88.4	90.2	90.4
Spinel	18A	21	22	22A	32	34	35	35A	42	42A
SiO_2	0.07	0.04	0.06	0.08	0.05	0.08	0.13	0.02	0.11	0.08
TiO_2	0.40	0.35	0.46	0.41	0.50	0.25	0.42	0.41	0.32	0.30
Al_2O_3	13.58	13.17	13.30	13.26	17.22	12.07	14.38	13.15	11.33	12.64
Cr_2O_3	53.58	55.00	51.09	50.94	45.53	53.10	48.46	51.84	55.32	54.80
Fe_2O_3	4.47	4.39	7.21	7.33	8.50	5.90	7.22	6.63	5.03	4.51
FeO	12.65	11.58	13.85	13.47	13.11	16.26	14.21	15.13	14.31	14.22
MnO	0.13	0.22	0.20	0.16	0.14	0.16	0.19	0.18	0.20	0.15
MgO	13.89	14.54	13.25	13.36	14.05	11.32	12.74	12.43	12.70	12.85
CaO	0.00	0.01	0.00	0.01	0.00	0.00	0.02	0.01	0.00	0.00
NiO	0.16	0.19	0.07	0.12	0.11	0.11	0.09	0.06	0.10	0.21
ZnO	0.08	0.06	0.00	0.05	0.13	0.20	0.13	0.00	0.00	0.10
Sum	99.01	99.55	99.50	99.19	99.33	99.44	97.99	99.85	99.43	99.86
$Mg^{\#}$	0.662	0.691	0.630	0.639	0.656	0.554	0.615	0.594	0.613	0.617
$cr^{\#}$	0.726	0.737	0.720	0.721	0.639	0.747	0.693	0.726	0.766	0.744
X_{mt}	0.055	0.053	0.088	0.090	0.102	0.073	0.090	0.081	0.062	0.055
Fe^{2+}/Fe^{3+}	3.144	2.936	2.136	2.042	1.714	3.066	2.186	2.537	3.159	3.502

Sample	108/7	108/7	108/7	108/7	108/7	108/7	108/7	108/7	108/7	108/7
Olivine	42SQ	43	43A	45	45A	46	46A	47	47A	49
SiO_2	40.64	41.04	40.65	40.93	41.23	40.66	40.22	41.33	41.42	41.04
Cr_2O_3										
FeO	9.73	8.59	9.59	7.94	7.90	11.19	11.45	8.08	7.70	7.36
MnO										
MgO	49.46	50.35	49.44	50.36	51.02	47.89	47.40	50.10	50.91	51.36
CaO	0.19	0.23	0.20	0.21	0.19	0.17	0.18	0.19	0.17	0.16
NiO										
Sum	100.01	100.22	99.87	99.44	100.33	99.91	99.25	99.71	100.20	99.92
Fo	90.1	91.3	90.2	91.9	92.0	88.4	88.1	91.7	92.2	92.6
Spinel	42SQ	43	43A	45	45A	46	46A	47	47A	49
SiO_2	0.08	0.08	0.13	0.23	0.06	0.09	0.09	0.07	0.10	0.06
TiO_2	0.37	0.32	0.39	0.35	0.33	0.40	0.39	0.32	0.32	0.31
Al_2O_3	14.21	12.23	13.91	12.82	13.54	14.62	15.99	12.05	13.48	12.36
Cr_2O_3	50.42	53.62	51.67	53.44	53.36	49.08	46.86	54.70	52.09	55.48
Fe_2O_3	5.78	5.29	5.37	5.08	5.05	6.78	7.48	5.25	5.78	4.21
FeO	13.51	13.12	15.19	13.40	12.20	15.44	15.41	12.55	13.38	11.85
MnO	0.21	0.27	0.25	0.13	0.14	0.20	0.20	0.14	0.18	0.16
MgO	13.04	13.10	12.39	13.48	14.12	12.15	12.26	13.73	13.30	14.20
CaO	0.01	0.01	0.01	0.01	0.02	0.00	0.01	0.00	0.03	0.00
NiO	0.13	0.19	0.09	0.11	0.17	0.07	0.04	0.18	0.20	0.16
ZnO	0.20	0.17	0.03	0.10	0.10	0.12	0.19	0.12	0.06	0.06
Sum	97.96	98.39	99.41	99.15	99.09	98.94	98.93	99.11	98.91	98.86
$Mg^{\#}$	0.633	0.640	0.593	0.642	0.674	0.584	0.587	0.661	0.639	0.681
$cr^{\#}$	0.704	0.746	0.714	0.737	0.726	0.693	0.663	0.753	0.722	0.751
X_{mt}	0.071	0.065	0.066	0.062	0.061	0.083	0.091	0.064	0.071	0.051
Fe^{2+}/Fe^{3+}	2.596	2.759	3.145	2.933	2.683	2.532	2.289	2.657	2.574	3.129

Sample	108/7	108/7	108/7	108/7	108/7	108/7	108/7	108/7	108/7	108/7
Olivine	50	58	62	65	75	80A	80B	81	81A	81B
SiO_2	41.22	41.24	40.16	41.32	40.43	40.59	40.34	41.24	40.71	40.69
Cr_2O_3										
FeO	8.06	7.24	11.59	7.26	10.00	11.74	11.85	7.59	9.15	8.10
MnO										
MgO	50.42	51.31	47.52	51.43	49.14	46.93	47.25	50.90	49.34	50.48
CaO	0.20	0.18	0.19	0.14	0.21	0.18	0.16	0.18	0.22	0.21
NiO										
Sum	99.90	99.97	99.46	100.16	99.79	99.44	99.60	99.91	99.42	99.49
Fo	91.8	92.7	88.0	92.7	89.8	87.7	87.7	92.3	90.6	91.7
Spinel	50	58	62	65	75	80A	80B	81	81A	81B
SiO_2	0.06	0.10	0.05	0.07	0.08	0.05	0.10	0.07	0.08	0.08
TiO_2	0.33	0.31	0.36	0.34	0.37	0.47	0.49	0.27	0.35	0.25
Al_2O_3	11.48	13.06	14.97	13.21	11.44	14.52	14.99	12.01	13.33	13.75
Cr_2O_3	54.53	54.98	48.96	54.52	54.22	47.68	47.71	54.76	50.80	51.61
Fe_2O_3	5.38	4.16	6.61	4.15	4.82	7.21	7.46	5.29	6.79	6.69
FeO	12.87	11.31	15.75	11.12	14.20	15.75	16.28	12.79	14.50	13.55
MnO	0.23	0.21	0.18	0.09	0.25	0.21	0.23	0.14	0.19	0.17
MgO	13.30	14.64	11.94	14.70	12.38	11.73	11.60	13.58	12.58	13.33
CaO	0.01	0.00	0.02	0.00	0.02	0.01	0.03	0.00	0.05	0.00
NiO	0.16	0.13	0.08	0.23	0.17	0.07	0.12	0.21	0.10	0.20
ZnO	0.05	0.13	0.14	0.12	0.02	0.03	0.26	0.03	0.00	0.06
Sum	98.42	99.03	99.06	98.56	97.97	97.74	99.26	99.14	98.76	99.70
$Mg^{\#}$	0.648	0.698	0.575	0.702	0.608	0.571	0.560	0.654	0.607	0.637
$cr^{\#}$	0.761	0.738	0.687	0.735	0.761	0.688	0.681	0.754	0.719	0.716
X_{mt}	0.067	0.050	0.081	0.051	0.061	0.090	0.092	0.065	0.084	0.081
Fe^{2+}/Fe^{3+}	2.660	3.023	2.649	2.978	3.270	2.429	2.426	2.688	2.373	2.249

Sample	108/7	108/7	108/7	108/7	108/7	108/7	108/7	108/7	108/7	108/7
Olivine	81D	84A	84B	91	91A	91B	91C	104	105	105A
SiO_2	41.30	41.19	41.11	41.09	41.48	41.13	40.80	40.51	40.88	40.77
Cr_2O_3										
FeO	7.88	7.83	7.86	7.55	7.73	7.65	8.57	9.11	8.23	8.19
MnO										
MgO	50.93	50.61	50.62	51.29	50.87	50.83	49.66	49.16	49.98	50.38
CaO	0.17	0.19	0.18	0.17	0.17	0.19	0.20	0.21	0.17	0.19
NiO										
Sum	100.27	99.82	99.77	100.11	100.25	99.81	99.22	98.99	99.27	99.54
Fo	92.0	92.0	92.0	92.4	92.1	92.2	91.2	90.6	91.5	91.6
Spinel	81D	84A	84B	91	91A	91B	91C	104	105	105A
SiO_2	0.06	0.07	0.10	0.07	0.06	0.06	0.05	0.08	0.10	0.23
TiO_2	0.42	0.34	0.27	0.36	0.33	0.28	0.35	0.36	0.31	0.33
Al_2O_3	12.35	12.05	12.08	14.95	12.21	13.13	13.07	12.29	12.40	13.97
Cr_2O_3	53.03	53.77	54.16	51.43	54.69	53.17	52.89	52.66	54.37	53.07
Fe_2O_3	6.41	5.50	5.51	5.90	4.49	5.22	5.25	4.88	4.85	4.23
FeO	12.19	12.36	11.92	11.40	12.06	12.05	13.07	14.39	13.24	12.47
MnO	0.21	0.16	0.18	0.19	0.09	0.16	0.08	0.09	0.09	0.17
MgO	13.97	13.65	14.00	14.86	13.94	14.01	13.41	12.30	13.35	14.02
CaO	0.00	0.02	0.01	0.02	0.00	0.04	0.01	0.00	0.04	0.04
NiO	0.19	0.15	0.14	0.22	0.16	0.15	0.20	0.16	0.18	0.24
ZnO	0.05	0.16	0.13	0.00	0.04	0.00	0.08	0.03	0.07	0.07
Sum	98.87	98.23	98.50	99.39	98.08	98.28	98.45	97.24	99.00	98.85
$Mg^{\#}$	0.671	0.663	0.677	0.699	0.673	0.675	0.647	0.604	0.643	0.667
$cr^{\#}$	0.742	0.750	0.750	0.698	0.750	0.731	0.731	0.742	0.746	0.718
X_{mt}	0.079	0.068	0.068	0.071	0.055	0.064	0.065	0.061	0.060	0.052
Fe^{2+}/Fe^{3+}	2.115	2.498	2.405	2.148	2.987	2.564	2.765	3.274	3.036	3.276

Sample	108/7	108/7	108/7	108/7	108/7	108/7	108/7	108/7	108/7	108/7
Olivine	116	121	122	123	128	131	142	148	148B	148C
SiO_2	40.29	40.73	40.99	40.54	40.19	41.26	40.48	40.90	41.26	40.96
Cr_2O_3										
FeO	10.83	9.13	8.32	11.74	11.55	7.97	9.55	10.00	8.14	8.01
MnO										
MgO	48.12	49.14	50.70	47.37	47.59	50.77	48.77	48.87	50.81	50.66
CaO	0.18	0.16	0.20	0.18	0.15	0.20	0.22	0.21	0.21	0.20
NiO										
Sum	99.42	99.15	100.21	99.83	99.48	100.19	99.02	99.98	100.42	99.82
Fo	88.8	90.6	91.6	87.8	88.0	91.9	90.1	89.7	91.8	91.9
Spinel	116	121	122	123	128	131	142	148	148B	148C
SiO_2	0.81	0.09	0.08	0.08	0.06	0.04	0.07	0.06	0.06	0.05
TiO_2	0.43	0.32	0.40	0.52	0.28	0.38	0.38	0.33	0.31	0.32
Al_2O_3	15.71	13.63	13.42	16.81	10.92	13.02	11.71	11.83	12.79	12.24
Cr_2O_3	47.90	52.40	53.75	45.83	54.20	54.10	55.61	53.10	53.84	54.05
Fe_2O_3	5.35	4.83	4.69	6.83	5.76	4.87	4.45	5.28	5.05	5.44
FeO	15.90	14.79	12.79	15.42	16.30	11.92	14.92	14.99	12.53	12.12
MnO	0.23	0.12	0.17	0.22	0.19	0.11	0.11	0.12	0.18	0.19
MgO	12.59	12.46	13.87	12.20	11.15	14.30	12.38	12.00	13.76	13.83
CaO	0.06	0.04	0.00	0.03	0.03	0.00	0.03	0.00	0.00	0.01
NiO	0.11	0.08	0.17	0.14	0.10	0.12	0.08	0.03	0.08	0.22
ZnO	0.08	0.09	0.05	0.17	0.06	0.06	0.20	0.01	0.14	0.15
Sum	99.17	98.86	99.38	98.26	99.04	98.92	99.95	97.75	98.74	98.61
$Mg^{\#}$	0.585	0.600	0.659	0.585	0.549	0.681	0.597	0.588	0.662	0.670
$cr^{\#}$	0.672	0.721	0.729	0.646	0.769	0.736	0.761	0.751	0.738	0.748
X_{mt}	0.067	0.060	0.057	0.084	0.072	0.059	0.055	0.066	0.062	0.067
Fe^{2+}/Fe^{3+}	3.306	3.401	3.033	2.508	3.147	2.722	3.727	3.157	2.762	2.475

Sample	108/7	108/7	108/7	108/7	108/7	108/7	108/7	108/7	108/7	108/7
Olivine	149	156	160	161	162	164	169	170	183	210
SiO_2	40.92	41.10	40.61	40.48	40.29	40.02	40.43	40.75	41.15	40.89
Cr_2O_3										
FeO	7.49	7.71	10.61	9.78	9.75	12.49	9.80	10.42	8.10	7.76
MnO										
MgO	50.88	51.32	48.52	49.43	49.39	46.98	48.88	48.49	50.47	50.88
CaO	0.14	0.21	0.21	0.16	0.18	0.18	0.18	0.20	0.20	0.19
NiO										
Sum	99.43	100.33	99.96	99.85	99.61	99.67	99.30	99.86	99.91	99.72
Fo	92.4	92.2	89.1	90.0	90.0	87.0	89.9	89.2	91.7	92.1
Spinel	149	156	160	161	162	164	169	170	183	210
SiO_2	0.09	0.08	0.08	0.06	0.08	0.07	0.08	0.47	0.12	0.11
TiO_2	0.51	0.29	0.40	0.26	0.33	0.42	0.30	0.41	0.37	0.39
Al_2O_3	12.86	11.03	12.82	12.12	13.07	14.43	12.19	13.57	12.44	13.89
Cr_2O_3	53.17	56.13	52.10	53.72	52.44	47.46	53.07	50.76	54.27	53.00
Fe_2O_3	4.74	4.66	5.76	4.62	5.48	7.75	5.08	5.18	4.45	4.55
FeO	12.03	13.29	15.06	15.10	14.31	16.33	14.95	16.23	12.35	12.57
MnO	0.17	0.18	0.19	0.19	0.19	0.11	0.20	0.20	0.22	0.08
MgO	14.08	13.09	12.22	11.93	12.60	11.47	12.03	11.73	13.78	14.02
CaO	0.00	0.06	0.00	0.05	0.00	0.04	0.04	0.22	0.04	0.02
NiO	0.15	0.09	0.07	0.02	0.16	0.08	0.06	0.08	0.09	0.21
ZnO	0.01	0.13	0.07	0.00	0.15	0.01	0.00	0.05	0.09	0.00
Sum	97.82	99.02	98.77	98.06	98.80	98.17	97.99	98.92	98.21	98.83
$Mg^{\#}$	0.676	0.637	0.591	0.585	0.611	0.556	0.589	0.563	0.666	0.665
$cr^{\#}$	0.735	0.774	0.732	0.748	0.729	0.688	0.745	0.715	0.745	0.719
X_{mt}	0.059	0.058	0.072	0.058	0.068	0.097	0.064	0.065	0.055	0.056
Fe^{2+}/Fe^{3+}	2.818	3.172	2.904	3.634	2.900	2.342	3.269	3.481	3.089	3.067

108 Cr-Al-spinel:

Sample	108/7	108/7	108/7	108/7	108/5	108/5	108/5	108/5	108/5	108/6
Olivine	335	259	A5 1	E4 4	4	6	83	5	N	37
SiO_2	41.26	40.00	39.61	40.28	40.23	39.89	40.12	40.06	40.25	40.10
Cr_2O_3			0.07	0.00					0.04	
FeO	7.96	12.16	11.76	11.85	11.78	11.84	12.30	13.23	11.99	13.23
MnO			0.18	0.21					0.20	
MgO	50.57	47.01	0.14	0.21	46.62	46.48	45.91	46.25	46.95	46.36
CaO	0.19	0.18	46.44	48.19	0.18	0.14	0.16	0.15	0.16	0.14
NiO			0.18	0.18					0.24	
Sum	99.98	99.35	98.38	100.92	98.81	98.35	98.48	99.70	99.83	99.82
Fo	91.9	87.3	87.6	87.9	87.6	87.5	86.9	86.2	87.5	86.2
Spinel	335	259	A5 1	E4 4	4	6	83	5	N	37
SiO_2	0.09	0.47	0.06	0.05	0.08	0.07	0.32	0.06	0.45	0.11
TiO_2	0.29	0.39	0.31	0.42	0.90	1.21	0.76	0.74	0.56	0.44
Al_2O_3	12.41	13.83	16.25	17.24	22.92	29.54	21.22	21.63	22.15	17.98
Cr_2O_3	54.07	48.03	45.69	44.76	35.85	27.34	37.53	35.91	37.66	40.87
Fe_2O_3	5.56	7.43	9.06	9.37	11.41	11.51	11.65	12.83	10.96	11.66
FeO	12.48	17.06	15.80	14.89	15.48	14.95	15.92	16.21	14.31	16.26
MnO	0.09	0.19	0.30	0.28	0.20	0.25	0.10	0.18	0.28	0.44
MgO	13.93	11.27	12.05	12.95	13.60	14.56	13.38	12.89	14.42	12.03
CaO	0.00	0.09								
NiO	0.11	0.06	0.16	0.16	0.12	0.11	0.20	0.10	0.13	0.12
ZnO	0.05	0.11	0.11	0.00					0.00	0.03
Sum	99.07	98.93	99.79	100.12	100.55	99.54	101.09	100.55	100.92	99.94
$Mg^{\#}$	0.665	0.541	0.576	0.608	0.610	0.635	0.600	0.586	0.642	0.569
$cr^{\#}$	0.745	0.700	0.654	0.635	0.512	0.383	0.543	0.527	0.533	0.604
X_{mt}	0.068	0.093	0.110	0.112	0.134	0.133	0.138	0.152	0.129	0.141
Fe^{2+}/Fe^{3+}	2.494	2.553	1.937	1.766	1.508	1.443	1.518	1.404	1.451	1.549

Sample	108/6	108/6	108/6	108/6	108/6	108/6	108/6	108/6	108/6	108/6
Olivine	37	37b	38	93	93	97	104	127	197	215
SiO_2	39.81	39.88	40.22	40.26	40.05	40.08	40.06	39.77	39.80	40.01
Cr_2O_3	0.00	0.02			0.01			0.00		
FeO	12.59	12.07	13.37	11.53	11.66	12.33	12.00	12.54	14.22	13.90
MnO	0.26	0.27			0.07			0.25		
MgO	45.96	46.64	46.50	47.82	47.59	47.40	47.58	46.35	45.81	45.47
CaO	0.17	0.18	0.15	0.19	0.19	0.18	0.19	0.20	0.17	0.16
NiO	0.23	0.20			0.19			0.15		
Sum	99.02	99.27	100.24	99.80	99.76	99.99	99.84	99.26	100.00	99.55
Fo	86.7	87.3	86.1	88.1	87.9	87.3	87.6	86.8	85.2	85.4
Spinel	37	37/2	38	93	93	97	104	127	197	215
SiO_2	0.18	0.11	0.07	0.12	0.14	0.10	0.08	0.36	0.06	0.09
TiO_2	0.46	0.71	0.86	2.50	2.31	0.70	0.80	1.33	0.92	0.76
Al_2O_3	18.15	21.82	22.23	46.47	46.43	36.98	28.81	30.31	20.33	17.03
Cr_2O_3	40.42	37.19	35.53	8.99	8.83	22.05	30.66	24.93	36.64	40.12
Fe_2O_3	11.14	10.61	11.78	11.23	10.74	10.17	10.41	11.99	12.59	12.99
FeO	16.21	15.49	15.92	11.99	11.62	12.65	13.51	14.43	17.33	18.05
MnO	0.23	0.18	0.11	0.17	0.20	0.14	0.14	0.11	0.13	0.24
MgO	12.06	13.15	13.00	19.25	19.04	16.59	15.21	15.15	12.06	11.12
CaO										
NiO	0.14	0.16	0.16	0.23	0.25	0.17	0.17	0.08	0.13	0.19
ZnO	0.10	0.00	0.13	0.15	0.24	0.03	0.20	0.18	0.03	0.10
Sum	99.10	99.42	99.79	101.09	99.80	99.58	99.99	98.87	100.22	100.69
$Mg^{\#}$	0.570	0.602	0.593	0.741	0.745	0.700	0.667	0.652	0.554	0.523
$cr^{\#}$	0.599	0.533	0.517	0.115	0.113	0.286	0.417	0.356	0.547	0.612
X_{mt}	0.136	0.127	0.140	0.120	0.116	0.111	0.119	0.140	0.152	0.159
Fe^{2+}/Fe^{3+}	1.617	1.622	1.502	1.186	1.203	1.383	1.442	1.338	1.529	1.544

Sample	108/6	108/6	108/6	108/6	108/7	108/7	108/7	108/7	108/7	108/7
Olivine	246	253/2	302	302/2	14	59	59A	59B	118	152
SiO_2	39.33	39.70	39.71	39.41	39.81	40.27	39.99	40.43	39.55	40.21
Cr_2O_3	0.06	0.02	0.08	0.04	0.06					
FeO	12.80	11.18	13.66	13.03	13.99	12.70	12.23	11.92	14.80	12.83
MnO	0.15	0.10	0.20	0.27	0.29					
MgO	46.05	47.13	45.44	45.82	45.43	46.18	47.16	47.83	45.01	46.64
CaO	0.20	0.17	0.18	0.16	0.15	0.14	0.13	0.17	0.17	0.16
NiO	0.15	0.13	0.13	0.15	0.18					
Sum	98.73	98.42	99.39	98.87	99.90	99.29	99.51	100.35	99.52	99.84
Fo	86.5	88.2	85.6	86.2	85.3	86.6	87.3	87.7	84.4	86.6
Spinel	246	253/2	302	302/2	14	59	59A	59B	118	152
SiO_2	0.11	0.12	0.11	0.11	0.12	0.03	0.11	0.12	0.05	0.07
TiO_2	0.67	3.66	0.69	1.18	0.98	1.27	0.83	0.71	0.55	0.84
Al_2O_3	21.69	35.70	21.38	24.02	19.54	23.46	20.63	20.79	21.67	23.97
Cr_2O_3	37.17	15.97	36.13	31.49	35.92	33.87	36.86	37.85	32.32	34.30
Fe_2O_3	10.58	11.76	11.05	12.40	13.46	10.82	10.81	10.62	14.52	10.02
FeO	15.65	14.02	16.09	15.79	18.08	16.61	15.76	15.56	17.18	15.34
MnO	0.21	0.17	0.23	0.16	0.09	0.21	0.23	0.22	0.19	0.21
MgO	12.95	17.02	12.38	13.16	11.40	12.70	12.55	12.75	11.52	13.06
CaO						0.06	0.02	0.04	0.01	0.04
NiO	0.06	0.16	0.11	0.14	0.21	0.20	0.14	0.20	0.09	0.20
ZnO	0.08	0.21	0.14	0.26	0.18	0.05	0.06	0.16	0.18	0.23
Sum	99.17	98.79	98.31	98.71	99.98	99.27	97.99	99.02	98.28	98.29
$Mg^{\#}$	0.596	0.684	0.578	0.598	0.529	0.577	0.587	0.593	0.544	0.603
$cr^{\#}$	0.535	0.231	0.531	0.468	0.552	0.492	0.545	0.550	0.500	0.490
X_{mt}	0.126	0.139	0.134	0.149	0.165	0.130	0.132	0.128	0.176	0.120
Fe^{2+}/Fe^{3+}	1.645	1.324	1.619	1.415	1.493	1.705	1.620	1.629	1.315	1.701

Sample	108/7	108/7	108/7	108/7	108/7	108/7	108/7	108/7	108/7	108/7
Olivine	171 A	171 B	176	191	206 A	206 B	206C	206 D	A5 2	E1 3
SiO_2	39.96	39.96	40.03	39.82	39.71	40.14	40.14	40.11	39.82	39.79
Cr_2O_3									0.18	0.08
FeO	13.14	13.14	12.60	13.51	13.17	12.99	12.99	13.11	12.09	11.30
MnO									0.19	0.19
MgO	46.88	46.88	46.50	45.65	46.17	46.83	46.83	46.26	0.10	0.03
CaO	0.17	0.17	0.16	0.14	0.16	0.17	0.17	0.15	46.43	47.75
NiO									0.18	0.19
Sum	100.15	100.15	99.30	99.13	99.21	100.13	100.13	99.63	99.00	99.33
Fo	86.4	86.4	86.8	85.8	86.2	86.5	86.5	86.3	87.3	88.3
Spinel	171 A	171 B	176	191	206 A	206 B	206 C	206 D	A5 2	E1 3
SiO_2	0.08	0.13	0.09	0.05	0.04	0.04	0.02	0.42	1.19	0.12
TiO_2	0.91	0.91	1.28	0.76	0.65	0.61	0.65	0.73	0.51	0.75
Al_2O_3	31.94	31.81	21.79	21.51	20.84	17.31	18.52	19.72	21.62	24.60
Cr_2O_3	24.65	24.85	34.00	36.71	37.47	42.16	40.91	38.63	37.70	34.80
Fe_2O_3	11.59	11.55	12.46	10.62	10.68	10.15	10.26	10.07	8.22	10.70
FeO	15.56	15.16	16.17	17.07	16.32	16.34	16.54	16.27	15.39	13.77
MnO	0.13	0.16	0.28	0.29	0.19	0.24	0.20	0.25	0.18	0.15
MgO	14.20	14.44	12.77	11.92	12.18	11.79	11.83	12.46	13.90	14.68
CaO				0.02	0.01	0.03		0.01		
NiO	0.12	0.18	0.12	0.15	0.14	0.13	0.22	0.17	0.04	0.15
ZnO	0.07	0.07	0.25	0.00	0.11	0.13	0.19	0.11	0.15	
Sum	99.26	99.28	99.19	99.10	98.62	98.93	99.35	98.85	98.89	99.72
$Mg^{\#}$	0.619	0.629	0.585	0.554	0.571	0.563	0.560	0.577	0.617	0.655
$cr^{\#}$	0.341	0.344	0.511	0.534	0.547	0.620	0.597	0.568	0.539	0.487
X_{mt}	0.132	0.132	0.151	0.128	0.129	0.124	0.125	0.123	0.101	0.125
Fe^{2+}/Fe^{3+}	1.492	1.459	1.442	1.785	1.697	1.788	1.792	1.796	2.081	1.430

108 Al-Ti-spinel:

Sample	108/7	108/7	108/7	108/7	108/6	108/6	108/6	108/6	108/6	108/6
Olivine	E1 1	T3 2	T3 1	T3 3	E4 1	E4 1	E4 2	E4 2	E4 5	Q
SiO_2	40.02	39.60	39.61	39.54	39.79	39.79	40.06	40.06	39.87	40.05
Cr_2O_3	0.06	0.08	0.04	0.15	0.04	0.04	0.06	0.06	0.00	0.04
FeO	11.77	13.10	13.13	13.29	11.73	11.73	11.89	11.89	12.03	13.76
NiO	0.21	0.19	0.17	0.20	0.15	0.15	0.24	0.24	0.29	0.31
MnO	0.21	0.16	0.11	0.22	0.14	0.14	0.16	0.16	0.28	45.50
MgO	47.57	46.22	46.38	46.21	47.81	47.81	47.05	47.05	47.86	0.15
CaO	0.20	0.18	0.16	0.17	0.19	0.19	0.20	0.20	0.18	0.13
Sum	100.04	99.52	99.60	99.77	99.85	99.85	99.66	99.66	100.50	99.94
Fo	87.8	86.3	86.3	86.1	87.9	87.9	87.6	87.6	87.6	85.5
Spinel	E1 1	T3 2	T3 1	T3 3	E4 1A	E4 1B	E4 2A	E4 2B	E4 5	Q
SiO_2	0.19	0.08	0.09	0.04	0.13	0.90	0.19	0.07	0.43	0.09
TiO_2	0.66	0.81	1.06	0.81	4.34	4.36	6.43	4.64	7.57	2.86
Al_2O_3	24.29	23.31	24.88	23.88	21.79	21.66	17.47	21.00	19.85	24.53
Cr_2O_3	35.20	34.09	31.46	34.88	29.02	28.53	28.80	29.46	22.23	26.40
Fe_2O_3	10.68	12.23	12.71	12.08	13.23	11.58	13.66	13.07	14.85	15.14
FeO	14.05	15.76	15.48	16.24	15.99	16.45	17.52	16.80	18.12	17.34
MnO	0.14	0.26	0.20	0.21	0.21	0.23	0.24	0.15	0.23	0.19
MgO	14.50	13.13	13.61	13.27	14.89	15.20	14.49	14.54	15.29	13.54
NiO	0.17	0.15	0.08	0.14	0.23	0.13	0.31	0.26	0.11	0.14
ZnO	0.00	0.13	0.25	0.07	0.20	0.06	0.23	0.00	0.12	0.15
Sum	99.88	99.96	99.82	101.62	100.02	99.10	99.34	99.99	98.80	100.38
$Mg^{\#}$	0.648	0.598	0.610	0.593	0.624	0.622	0.596	0.607	0.601	0.582
$cr^{\#}$	0.493	0.495	0.459	0.495	0.472	0.469	0.525	0.485	0.429	0.419
X_{mt}	0.125	0.145	0.150	0.140	0.170	0.153	0.192	0.170	0.214	0.186
Fe^{2+}/Fe^{3+}	1.462	1.432	1.354	1.494	1.343	1.579	1.425	1.428	1.356	1.273

Sample	108/7	108/7	108/7	108/7
Olivine	245/2	245	253	253
SiO_2	39.32	39.73	39.67	39.67
Cr_2O_3	0.03	0.06	0.06	0.06
FeO	12.79	12.53	11.74	11.74
NiO	0.23	0.18	0.22	0.22
MnO	45.73	46.47	47.05	47.05
MgO	0.15	0.13	0.20	0.20
CaO	0.15	0.18	0.21	0.21
Sum	98.40	99.29	99.15	99.15
Fo	86.4	86.9	87.7	87.7
Spinel	245/2	245	253	253
SiO_2	0.11	0.10	0.14	0.09
TiO_2	2.10	6.51	11.60	11.58
Al_2O_3	20.21	15.51	18.73	18.72
Cr_2O_3	32.06	28.79	7.53	7.49
Fe_2O_3	13.93	15.33	23.27	22.96
FeO	16.61	20.03	21.93	21.94
MnO	0.22	0.31	0.30	0.13
MgO	12.65	12.76	14.41	14.35
NiO	0.18	0.20	0.40	0.34
ZnO	0.17	0.11	0.13	0.14
Sum	98.23	99.66	98.44	97.74
$Mg^{\#}$	0.576	0.532	0.539	0.538
$cr^{\#}$	0.516	0.555	0.212	0.212
X_{mt}	0.176	0.219	0.384	0.382
Fe^{2+}/Fe^{3+}	1.325	1.452	1.048	1.062

Iceland

Sample	NO 42	NO 42	NO 42	NO 42	NO 42	NO 42	NO 42	NO 42	NO 42	NO 42
Olivine	1	2			3	4	5		7	
SiO_2	40.46	41.25			40.31	40.82	41.04		41.09	
Cr_2O_3										
FeO	9.59	7.79			11.57	8.19	8.22		7.84	
MnO										
MgO	48.84	50.89			47.86	50.14	50.80		50.90	
CaO	0.36	0.38			0.33	0.38	0.35		0.41	
NiO										
Sum	99.26	100.32			100.07	99.52	100.40		100.23	
Fo	90.1	92.1			88.1	91.6	91.7		92.0	

Spinel	1	2	2A	2B	3	4	5	6	7	8.0
SiO_2	0.15	0.17	0.13	0.13	0.09	0.15	0.18	0.11	0.15	0.11
TiO_2	0.24	0.22	0.23	0.20	0.16	0.22	0.24	0.20	0.22	0.22
Al_2O_3	22.65	23.09	23.21	23.20	39.19	23.23	22.61	23.27	23.13	22.80
Cr_2O_3	46.19	47.03	46.72	46.46	27.33	45.36	47.32	45.88	46.94	46.79
Fe_2O_3	4.20	3.43	4.00	3.12	5.48	3.55	3.25	4.85	4.41	5.12
FeO	10.76	9.46	10.12	10.75	10.83	12.26	10.51	8.91	9.96	9.14
MnO	0.00	0.08	0.03	0.14	0.17	0.23	0.14	0.07	0.09	0.12
MgO	16.59	17.40	17.15	16.46	18.16	15.44	16.68	17.78	17.40	17.73
NiO	0.15	0.30	0.25	0.16	0.13	0.15	0.25	0.22	0.16	0.29
ZnO										
Sum	100.93	101.17	101.84	100.61	101.54	100.60	101.18	101.29	102.46	102.32
$Mg^{\#}$	0.733	0.766	0.751	0.732	0.749	0.692	0.739	0.781	0.757	0.776
$cr^{\#}$	0.578	0.577	0.575	0.573	0.319	0.567	0.584	0.569	0.577	0.579
X_{mt}	0.048	0.039	0.045	0.035	0.057	0.041	0.037	0.054	0.049	0.057
Fe^{2+}/Fe^{3+}	2.849	3.067	2.812	3.834	2.197	3.835	3.593	2.043	2.511	1.984

Sample	NO 42	NO 42	NO 42	NO 42	NO 42	NO 42	NO 42	NO 42	NO 42	NO 42
Olivine	9	10			22	24	24B	27	27B	29
SiO_2	40.59	39.58			40.64	40.44	40.46	40.73	41	40.72
Cr_2O_3					0.15	0.15	0.18	0.17	0.34	0.21
FeO	7.88	12.97			7.48	8.14	7.95	7.49	7.53	7.46
MnO					0.13	0.14	0.09	0.09	0.16	0.13
MgO	50.19	45.98			50.84	50.35	50.46	50.52	50.39	51.48
CaO	0.45	0.37			0.39	0.35	0.35	0.38	0.39	0.38
NiO					0.38	0.29	0.23	0.43	0.41	0.26
Sum	99.11	98.90			100.01	99.86	99.72	99.81	100.21	100.62
Fo	91.9	86.3			92.4	91.7	91.9	92.3	92.3	92.5

Spinel	9	10	11	14	22	24	24B	27	27B	29
SiO_2	0.16	0.07	0.07	0.08	0.12	0.16	0.17	0.12	0.14	0.18
TiO_2	0.21	0.17	0.16	0.24	0.28	0.26	0.23	0.24	0.19	0.21
Al_2O_3	22.69	43.24	14.81	37.93	23.18	22.35	21.79	23.43	23.32	22.16
Cr_2O_3	46.54	23.06	54.22	27.83	45.36	45.76	45.76	45.17	45.39	46.32
Fe_2O_3	3.80	5.97	3.74	4.68	3.54	4.68	4.33	3.87	3.20	3.48
FeO	10.40	11.02	14.16	10.88	9.74	9.63	10.38	9.78	10.10	10.02
MnO	0.12	0.08	0.20	0.11	0.11	0.13	0.26	0.27	0.20	0.16
MgO	16.67	18.61	13.28	17.61	16.84	17.05	16.22	16.89	16.54	16.59
NiO	0.23	0.26	0.18	0.21	0.26	0.18	0.20	0.16	0.23	0.13
ZnO				0.03	0.04	0.01	0.00	0.01	0.00	0.01
Sum	100.82	102.48	100.82	99.60	99.47	100.21	99.34	99.94	99.30	99.26
$Mg^{\#}$	0.741	0.751	0.626	0.743	0.755	0.759	0.736	0.755	0.745	0.747
$cr^{\#}$	0.579	0.263	0.711	0.313	0.545	0.548	0.556	0.539	0.546	0.560
X_{mt}	0.043	0.061	0.045	0.050	0.040	0.053	0.050	0.044	0.037	0.040
Fe^{2+}/Fe^{3+}	3.040	2.053	4.206	2.585	3.058	2.287	2.665	2.808	3.510	3.197

Sample	NO 42	NO 42	NO 42	NO 42	NO 42	NO 42	NO 42	NO 42	NO 42A	NO 42A
Olivine	31	32	33	42	43	44	45	48	3	4
SiO_2	40.52	40.72	40.43	40.39	40.23	40	40.05	40.26	40.40	40.44
Cr_2O_3	0.16	0.24	0.21	0.19	0.07	0.13	0.08	0.13	0.27	0.22
FeO	8.25	7.46	7.54	7.41	9.42	10.31	10.58	10.12	7.89	7.96
MnO	0.13	0.09	0.07	0.07	0.2	0.15	0.11	0.17	0.01	0.19
MgO	50.12	50.56	50.51	50.54	49.02	48.43	47.53	48.44	50.05	50.54
CaO	0.37	0.36	0.35	0.37	0.35	0.29	0.32	0.34	0.43	0.35
NiO	0.28	0.32	0.44	0.34	0.29	0.31	0.29	0.3	0.29	0.40
Sum	99.83	99.74	99.54	99.32	99.58	99.61	98.97	99.75	99.33	100.10
Fo	91.5	92.4	92.3	92.4	90.3	89.3	88.9	89.5	91.9	91.9
Spinel	31	32	33	42	43	44	45	48	3	4
SiO_2	0.17	0.13	0.34	0.12	0.07	0.11	0.10	0.13	0.18	0.10
TiO_2	0.23	0.20	0.23	0.23	0.19	0.17	0.17	0.20	0.23	0.19
Al_2O_3	23.24	23.46	23.10	22.76	32.06	26.06	39.21	45.65	22.25	21.93
Cr_2O_3	44.09	45.47	45.68	45.24	34.53	41.05	27.06	21.51	45.83	45.78
Fe_2O_3	3.15	3.64	3.14	3.96	4.19	4.16	4.58	4.42	4.84	5.44
FeO	13.86	9.45	10.29	10.02	10.92	12.18	11.22	10.04	10.16	9.17
MnO	0.26	0.21	0.16	0.03	0.13	0.22	0.13	0.15	0.12	0.10
MgO	14.11	17.08	16.71	16.65	16.87	15.48	17.67	19.38	16.79	17.11
NiO	0.16	0.21	0.24	0.17	0.17	0.17	0.18	0.25	0.13	0.21
ZnO	0.03	0.03	0.04	0.01	0.02	0.05	0.00	0.02	0.03	0.17
Sum	99.30	99.87	99.93	99.19	99.15	99.66	100.32	101.74	100.56	100.19
$Mg^{\#}$	0.645	0.763	0.743	0.748	0.734	0.694	0.737	0.775	0.747	0.769
$cr^{\#}$	0.539	0.542	0.550	0.545	0.400	0.489	0.301	0.229	0.580	0.583
X_{mt}	0.037	0.041	0.036	0.045	0.046	0.047	0.048	0.045	0.055	0.062
Fe_{2+}/Fe^{3+}	4.895	2.884	3.640	2.815	2.899	3.250	2.724	2.525	2.331	1.873

Sample	NO 42A	NO 42A	NO 42A	NO 42A	NO 42A	NO 42A	NO 42A	NO 42A	NO 42A	NO 42A
Olivine	11	16	18	24	25	40	42A	42B	56	57
SiO_2	40.54	40.38	40.71	40.77	40.51	40.33	40.07	39.97	41.21	40.78
Cr_2O_3	0.16	0.28	0.18	0.16	0.21	0.15	0.11	0.15	0.20	0.21
FeO	9.09	8.52	7.88	7.87	9.09	9.90	11.13	11.34	7.95	7.83
MnO	0.11	0.12	0.14	0.20	0.15	0.03	0.17	0.18	0.12	0.09
MgO	49.13	49.48	50.61	50.72	49.30	48.96	47.12	47.32	50.61	50.14
CaO	0.32	0.46	0.34	0.35	0.34	0.34	0.34	0.32	0.33	0.34
NiO	0.25	0.43	0.32	0.36	0.18	0.29	0.28	0.25	0.24	0.36
Sum	99.60	99.66	100.18	100.42	99.77	100.00	99.23	99.53	100.66	99.75
Fo	90.6	91.2	92.0	92.0	90.6	89.8	88.3	88.2	91.9	91.9
Spinel	11	16	18	24	25	40	42A	42B	56	57
SiO_2	0.15	0.15	0.09	0.13	0.16	0.15	0.10	0.12	0.13	0.16
TiO_2	0.22	0.19	0.22	0.23	0.18	0.21	0.14	0.14	0.23	0.27
Al_2O_3	24.91	16.90	22.62	22.89	25.79	23.71	40.76	39.66	24.00	22.88
Cr_2O_3	42.24	51.25	46.36	46.23	41.87	44.67	24.41	26.28	44.26	46.01
Fe_2O_3	4.53	4.86	4.31	4.63	5.61	5.07	5.99	4.53	4.72	4.74
FeO	12.27	11.93	9.48	9.01	10.58	9.69	10.31	11.44	9.99	9.08
MnO	0.16	0.16	0.23	0.18	0.14	0.11	0.01	0.19	0.11	0.10
MgO	15.54	14.91	17.13	17.58	16.92	17.33	18.43	17.48	17.08	17.65
NiO	0.08	0.15	0.16	0.16	0.21	0.12	0.28	0.16	0.08	0.23
ZnO	0.12	0.24	0.00	0.12	0.12	0.03	0.01	0.00	0.06	0.01
Sum	100.21	100.74	100.60	101.15	101.58	101.09	100.44	100.00	100.66	101.12
$Mg^{\#}$	0.693	0.690	0.763	0.777	0.740	0.761	0.761	0.731	0.753	0.776
$cr^{\#}$	0.532	0.670	0.579	0.575	0.521	0.558	0.287	0.308	0.553	0.574
X_{mt}	0.051	0.057	0.049	0.052	0.062	0.057	0.063	0.048	0.053	0.053
Fe^{2+}/Fe^{3+}	3.011	2.726	2.444	2.164	2.096	2.127	1.910	2.804	2.352	2.130

Sample	NO 42A	NO 42A	NO 42A	NO 42A	NO 42A	NO 42A	NO 42A	NO 42A	NO 42A	NO 42A
Olivine	61	68	83	84	87C	96	119	120		128
SiO_2	40.06	40.00	40.62	40.72	39.25	40.69	39.96	40.55		40.32
Cr_2O_3	0.30	0.10	0.10	0.24	0.17	0.23	0.09	0.29		0.22
FeO	11.22	11.53	7.90	7.95	13.35	8.15	11.46	8.19		9.17
MnO	0.08	0.27	0.15	0.27	0.18	0.24	0.18	0.12		0.12
MgO	48.43	47.63	50.73	50.49	45.82	50.31	47.17	50.57		49.48
CaO	0.35	0.34	0.45	0.34	0.37	0.36	0.30	0.37		0.34
NiO	0.37	0.22	0.35	0.35	0.26	0.25	0.20	0.37		0.29
Sum	100.81	100.09	100.30	100.35	99.40	100.22	99.36	100.47		99.93
Fo	88.5	88.0	92.0	91.9	86.0	91.7	88.0	91.7		90.6
Spinel	61	68	83	84	87C	96	119	120	121	128
SiO_2	0.11	0.11	0.15	0.18	0.11	0.13	0.12	0.12	0.10	0.13
TiO_2	0.13	0.16	0.22	0.20	0.17	0.20	0.13	0.19	0.14	0.19
Al_2O_3	43.04	42.27	22.91	22.37	33.82	23.03	43.55	22.71	41.29	25.25
Cr_2O_3	22.92	23.23	45.49	46.90	31.25	45.24	22.17	46.10	25.11	42.48
Fe_2O_3	5.50	5.43	4.19	4.16	6.30	5.08	6.09	4.75	5.72	4.98
FeO	10.02	10.38	9.67	10.18	12.56	9.35	10.42	9.64	10.60	10.38
MnO	0.12	0.02	0.14	0.07	0.20	0.11	0.13	0.00	0.11	0.10
MgO	18.91	18.59	16.92	16.96	16.32	17.34	18.85	17.21	18.57	16.89
NiO	0.26	0.22	0.22	0.08	0.16	0.20	0.28	0.18	0.22	0.19
ZnO	0.04	0.01	0.12	0.04	0.00	0.00	0.00	0.08	0.00	0.00
Sum	101.05	100.42	100.03	101.14	100.89	100.68	101.74	100.98	101.86	100.59
$Mg^{\#}$	0.771	0.761	0.757	0.748	0.698	0.768	0.763	0.761	0.757	0.744
$cr^{\#}$	0.263	0.269	0.571	0.584	0.383	0.569	0.255	0.577	0.290	0.530
X_{mt}	0.057	0.057	0.048	0.047	0.068	0.057	0.062	0.053	0.059	0.056
Fe^{2+}/Fe^{3+}	2.022	2.125	2.563	2.719	2.215	2.048	1.903	2.257	2.061	2.313

Sample	NO 42A	NO 42A	NO 42A	NO 42A	NO 42A	NO 42A	NO 42A	NO 42A	NO 42A	NO 42A
Olivine	135A	135B	136	142A	142B	144	158A	158B	167	168
SiO_2	40.82	40.37	41.02	40.26	40.05	40.87	40.32	39.59	39.94	41.31
Cr_2O_3	0.13	0.51	0.24	0.14	0.17	0.30	0.34	0.32	0.00	0.21
FeO	7.99	7.96	8.46	8.92	8.88	8.13	7.91	7.75	11.50	7.90
MnO	0.17	0.23	0.05	0.06	0.03	0.13	0.12	0.06	0.19	0.08
MgO	51.40	50.43	50.43	49.71	49.62	51.08	50.57	49.85	47.22	51.03
CaO	0.36	0.41	0.36	0.37	0.39	0.37	0.34	0.38	0.34	0.37
NiO	0.36	0.39	0.27	0.47	0.43	0.38	0.44	0.16	0.25	0.39
Sum	101.21	100.32	100.83	99.94	99.56	101.27	100.04	98.12	99.44	101.29
Fo	92.0	91.9	91.4	90.9	90.9	91.8	91.9	92.0	88.0	92.0
Spinel	135A	135B	136	142A	142B	144	158A	158 B	167	168
SiO_2	0.15	0.14	0.14	0.11	0.17	0.12	0.10	0.09	0.11	0.14
TiO_2	0.25	0.17	0.18	0.18	0.22	0.18	0.21	0.25	0.14	0.25
Al_2O_3	22.89	22.49	21.56	21.74	22.13	22.72	22.61	22.00	54.72	22.53
Cr_2O_3	45.97	45.41	46.89	45.73	45.28	45.94	46.03	46.04	10.65	45.72
Fe_2O_3	4.07	5.47	4.56	4.77	4.80	4.52	4.47	4.68	5.74	4.51
FeO	9.93	9.08	11.74	11.61	12.44	9.32	9.06	9.27	8.70	9.55
MnO	0.09	0.17	0.27	0.01	0.25	0.10	0.11	0.07	0.21	0.06
MgO	17.02	17.32	15.65	15.65	15.23	17.27	17.37	16.96	21.03	17.10
NiO	0.14	0.17	0.16	0.08	0.10	0.17	0.16	0.30	0.30	0.21
ZnO	0.00	0.14	0.00	0.09	0.03	0.00	0.04	0.20	0.00	0.01
Sum	100.51	100.56	101.15	99.97	100.65	100.33	100.16	99.86	101.59	100.08
$Mg^{\#}$	0.753	0.773	0.704	0.706	0.686	0.768	0.774	0.765	0.812	0.761
$cr^{\#}$	0.574	0.575	0.593	0.585	0.579	0.576	0.577	0.584	0.115	0.576
X_{mt}	0.046	0.062	0.052	0.055	0.055	0.051	0.051	0.054	0.056	0.051
Fe^{2+}/Fe^{3+}	2.715	1.845	2.865	2.701	2.878	2.295	2.250	2.199	1.686	2.351

Sample	NO 42A	NO 42A	NO 42A	NO 42A	NO 42A	NO 42A	NO 42A	NO 42A	NO 42A	NO 58
Olivine	191	190	193B	196	213	217	218	221	234	2
SiO_2	40.62	40.38	40.57	39.98	40.73	39.93	40.16	40.35	39.55	40.12
Cr_2O_3	0.26	0.32	0.28	0.09	0.36	0.16	0.26	0.52	0.29	
FeO	7.79	10.40	9.52	11.28	8.24	11.52	7.88	8.09	11.01	10.12
MnO	0.03	0.17	0.16	0.18	0.17	0.25	0.11	0.13	0.12	
MgO	50.54	48.64	49.77	47.49	50.16	47.83	50.19	50.15	47.26	48.73
CaO	0.41	0.32	0.34	0.32	0.29	0.32	0.36	0.43	0.37	0.33
NiO	0.38	0.25	0.21	0.22	0.43	0.21	0.28	0.25	0.22	
Sum	100.02	100.50	100.84	99.56	100.36	100.22	99.24	99.92	98.82	99.31
Fo	92.0	89.3	90.3	88.2	91.6	88.1	91.9	91.7	88.4	89.6
Spinel	191	190	193B	196	213	217	218	221	234	2
SiO_2	0.11	0.11	0.13	0.09	0.15	0.06	0.12	0.09	0.11	0.09
TiO_2	0.26	0.20	0.22	0.12	0.22	0.16	0.24	0.26	0.15	0.18
Al_2O_3	22.31	40.80	24.37	57.34	25.03	38.01	23.34	22.87	42.09	31.88
Cr_2O_3	46.32	26.14	43.47	7.84	43.64	27.65	45.57	46.14	23.96	35.99
Fe_2O_3	4.73	4.92	5.04	5.14	4.71	6.01	4.61	4.82	5.58	4.00
FeO	9.44	10.13	11.17	8.09	8.88	10.70	9.38	9.42	10.03	11.19
MnO	0.17	0.16	0.19	0.12	0.15	0.17	0.05	0.03	0.13	0.14
MgO	17.14	18.72	16.33	21.52	17.90	17.85	17.49	17.47	18.81	17.05
NiO	0.32	0.29	0.23	0.29	0.21	0.24	0.10	0.14	0.25	0.09
ZnO	0.00	0.00	0.00	0.00	0.00	0.08	0.09	0.06	0.11	
Sum	100.80	101.47	101.16	100.55	100.89	100.92	100.98	101.29	101.22	100.61
$Mg^{\#}$	0.764	0.767	0.723	0.826	0.782	0.748	0.769	0.768	0.770	0.731
$cr^{\#}$	0.582	0.301	0.545	0.084	0.539	0.328	0.567	0.575	0.276	0.431
X_{mt}	0.054	0.051	0.057	0.050	0.052	0.064	0.052	0.054	0.058	0.044
Fe^{2+}/Fe^{3+}	2.218	2.288	2.462	1.748	2.094	1.978	2.263	2.171	1.997	3.116

Sample	NO 58	NO 58	NO 58	NO 58	NO 58	NO 58	NO 58	NO 58	NO 58	NO 58
Olivine		12	17	46	60	64	178	183	197	207
SiO_2		39.86	39.77	40.1	40.24	40.1	39.94	39.89	39.97	40.42
Cr_2O_3		0.1	0.07	0.12	0.17	0.17	0.1	0.24	0.16	0.15
FeO		9.85	10.56	9.87	9.01	9.88	10.78	10.71	10.1	10.38
MnO		0.22	0.19	0.17	0.16	0.13	0.17	0.2	0.11	0.18
MgO		48.08	47.01	47.69	48.28	47.16	46.98	46.77	46.99	48.34
CaO		0.34	0.34	0.33	0.3	0.34	0.34	0.39	0.33	0.34
NiO		0.24	0.23	0.3	0.35	0.28	0.26	0.32	0.31	0.39
Sum		98.69	98.18	98.57	98.51	98.06	98.58	98.52	97.96	100.2
Fo		89.7	88.8	89.6	90.5	89.5	88.6	88.6	89.2	89.2
Spinel	3	12	17	46	60	64	178	183	197	207
SiO_2	0.09	0.16	0.12	0.12	0.50	0.11	0.13	0.14	0.12	0.13
TiO_2	0.23	0.18	0.20	0.20	0.21	0.25	0.21	0.17	0.23	0.17
Al_2O_3	23.97	32.61	32.01	33.16	32.45	23.86	33.91	34.04	38.47	33.18
Cr_2O_3	38.91	33.64	32.74	34.13	35.11	40.98	33.57	33.15	26.71	33.62
Fe_2O_3	6.90	3.97	5.11	3.94	2.38	4.96	3.54	3.91	5.04	4.05
FeO	18.63	11.40	12.66	11.40	11.95	14.46	11.84	11.69	10.79	11.15
MnO	0.11	0.22	0.23	0.20	0.23	0.19	0.23	0.21	0.19	0.20
MgO	11.30	16.59	15.65	16.89	16.66	13.68	16.70	16.82	17.66	16.95
NiO	0.13	0.17	0.17	0.19	0.21	0.09	0.20	0.16	0.24	0.14
ZnO		0.02	0.03	0.03	0.03	0.00	0.01	0.02	0.01	0.01
Sum	100.27	98.96	98.92	100.25	99.73	98.58	100.33	100.31	99.45	99.60
$Mg^{\#}$	0.519	0.722	0.688	0.725	0.713	0.628	0.715	0.719	0.745	0.730
$cr^{\#}$	0.521	0.409	0.407	0.408	0.421	0.535	0.399	0.395	0.318	0.405
X_{mt}	0.081	0.044	0.057	0.043	0.026	0.058	0.038	0.043	0.054	0.044
Fe^{2+}/Fe^{3+}	3.002	3.189	2.752	3.219	5.573	3.243	3.723	3.320	2.381	3.060

Sample	NO 58	NO 58	NO 58	RE 36	RE 36	RE 36	RE 36	RE 36	RE 36	RE 36
Olivine	209		215	RE 36 1	2	3	4	5	6	7
SiO_2	39.3		40.24	41.19	42.19	40.78	41.63	40.61	41.29	40.72
Cr_2O_3	0.06		0.18							
FeO	11.08		10.4	10.30	10.57	10.74	10.20	8.72	9.61	9.94
MnO	0.21		0.18							
MgO	46.16		47.37	48.19	49.51	47.49	49.86	49.00	48.41	48.18
CaO	0.34		0.33	0.35	0.41	0.33	0.34	0.37	0.38	0.37
NiO	0.25		0.27							
Sum	97.4		98.96	100.03	102.69	99.35	102.02	98.71	99.69	99.20
Fo	88.1		89.0	89.3	89.3	88.7	89.7	90.9	90.0	89.6
Spinel	209	213	215	1	2	3	4	5	6	7
SiO_2	0.09	0.17	0.18	0.10	0.05	0.09	0.10	0.10	0.10	0.10
TiO_2	0.30	0.19	0.19	0.18	7.69	0.31	0.16	0.10	0.19	0.16
Al_2O_3	38.69	33.34	32.23	27.01	10.56	23.26	32.80	27.51	35.43	31.08
Cr_2O_3	25.75	34.65	34.19	38.01	37.25	36.29	31.91	39.21	32.30	35.81
Fe_2O_3	5.19	3.88	3.71	5.39	6.62	8.50	5.71	3.91	3.46	3.13
FeO	11.64	12.12	12.45	14.71	28.71	16.61	11.16	11.53	9.83	12.47
MnO	0.19	0.16	0.20	0.13	0.29	0.23	0.19	0.14	0.08	0.09
MgO	17.08	16.80	15.99	14.04	7.20	11.89	16.69	15.86	18.04	15.73
NiO	0.22	0.11	0.14	0.12	0.14	0.11	0.20	0.16	0.32	0.17
ZnO	0.04	0.03	0.02							
Sum	99.19	101.45	99.30	99.69	98.51	97.29	98.92	98.52	99.75	98.74
$Mg^{\#}$	0.723	0.712	0.696	0.630	0.309	0.561	0.727	0.710	0.766	0.692
$cr^{\#}$	0.309	0.411	0.416	0.486	0.703	0.511	0.395	0.489	0.379	0.436
X_{mt}	0.056	0.042	0.041	0.061	0.106	0.102	0.063	0.044	0.037	0.035
Fe_{2+}/Fe^{3+}	2.490	3.479	3.733	3.034	4.822	2.171	2.169	3.276	3.155	4.422

Sample	RE 36	RE 36	RE 36	RE 36	RE 36	RE 36	RE 36	RE 36	RE 36	RE 36
Olivine	9	10	11	12	13	14	15	18	19	41
SiO_2	40.88	40.90	40.73	40.35	40.02	41.63	41.04	40.52	40.81	40.32
Cr_2O_3										
FeO	8.99	10.29	10.55	9.92	12.67	9.47	10.03	10.71	9.49	11.24
MnO										
MgO	49.65	48.77	48.19	48.08	46.06	49.57	49.18	48.21	49.66	48.01
CaO	0.38	0.38	0.35	0.38	0.36	0.39	0.38	0.36	0.37	0.35
NiO										
Sum	99.89	100.35	99.82	98.73	99.11	101.06	100.62	99.80	100.33	99.91
Fo	90.8	89.4	89.1	89.6	86.6	90.3	89.7	88.9	90.3	88.4
Spinel	9	10	11	12	12	14	15	18	19	41
SiO_2	0.09	0.09	0.09	0.06	0.11	0.08	0.13	0.06	0.13	0.12
TiO_2	0.15	0.13	0.11	0.20	0.18	0.12	0.23	0.14	0.17	0.25
Al_2O_3	27.10	26.06	27.19	26.43	26.97	27.58	33.95	15.83	31.32	24.43
Cr_2O_3	40.39	39.07	38.49	37.03	35.44	38.38	31.81	47.22	35.34	37.08
Fe_2O_3	3.87	5.40	4.75	5.02	5.72	4.38	5.61	6.48	4.62	8.23
FeO	15.72	14.13	13.18	15.38	18.65	12.21	11.63	19.72	12.86	15.94
MnO	0.22	0.17	0.19	0.10	0.24	0.06	0.14	0.19	0.10	0.28
MgO	13.63	14.17	14.77	13.04	11.15	15.44	16.99	9.43	15.93	12.79
NiO	0.18	0.15	0.21	0.17	0.15	0.17	0.16	0.07	0.12	0.17
ZnO										
Sum	101.36	99.37	98.98	97.42	98.61	98.42	100.65	99.14	100.59	99.28
$Mg^{\#}$	0.607	0.641	0.666	0.602	0.516	0.693	0.723	0.460	0.688	0.589
$cr^{\#}$	0.500	0.501	0.487	0.484	0.469	0.483	0.386	0.667	0.431	0.505
X_{mt}	0.044	0.062	0.054	0.059	0.067	0.050	0.061	0.080	0.051	0.096
Fe^{2+}/Fe^{3+}	4.512	2.911	3.085	3.409	3.625	3.098	2.301	3.381	3.089	2.152

Sample	RE 36	RE 36	RE 36	RE 36	RE 36	RE 36	RE 78	RE 78	RE 78	RE 78
Olivine		44	65	99	109	121	1	2	4	5
SiO_2		40.83	40.70	40.91	40.06	41.22	40.04	40.89	40.91	41.12
Cr_2O_3										
FeO		9.90	11.57	10.36	13.59	9.36	14.55	10.49	10.23	10.13
MnO										
MgO		49.61	47.19	48.86	45.44	49.75	44.77	48.89	49.21	49.53
CaO		0.39	0.39	0.37	0.35	0.39	0.34	0.38	0.41	0.39
NiO										
Sum		100.72	99.84	100.50	99.44	100.72	99.69	100.65	100.76	101.17
Fo		89.9	87.9	89.4	85.6	90.5	84.6	89.3	89.5	89.7
Spinel	41A	44	65	99	109	121	1	2	4	5
SiO_2	0.47	0.07	0.09	0.10	0.11	0.07	0.06	0.11	0.12	0.14
TiO_2	0.37	0.17	0.15	0.16	0.17	0.17	0.26	0.16	0.21	0.17
Al_2O_3	24.35	33.38	27.74	27.97	27.83	28.46	23.61	31.12	32.17	33.50
Cr_2O_3	35.31	32.87	38.18	37.97	35.69	39.31	29.91	34.58	34.04	32.15
Fe_2O_3	8.29	4.91	4.63	4.79	6.06	4.54	17.32	5.85	5.47	5.77
FeO	15.66	11.44	15.30	15.39	19.71	12.43	18.79	11.25	10.83	10.80
MnO	0.10	0.23	0.20	0.17	0.20	0.15	0.18	0.07	0.19	0.14
MgO	13.16	16.75	13.77	13.86	11.07	15.93	11.23	16.83	17.23	17.33
NiO	0.16	0.22	0.12	0.07	0.14	0.18	0.20	0.14	0.15	0.22
ZnO										
Sum	97.87	100.04	100.18	100.48	100.98	101.25	101.55	100.12	100.41	100.22
$Mg^{\#}$	0.600	0.723	0.616	0.616	0.500	0.696	0.516	0.727	0.739	0.741
$cr^{\#}$	0.493	0.398	0.480	0.477	0.462	0.481	0.459	0.427	0.415	0.392
X_{mt}	0.099	0.054	0.053	0.054	0.070	0.050	0.202	0.064	0.060	0.063
Fe^{2+}/Fe^{3+}	2.097	2.588	3.667	3.573	3.613	3.043	1.205	2.137	2.203	2.078

Sample	RE 78	RE 78	RE 78	RE 78	RE 78	RE 78	RE 78	RE 78 B	RE 78 B	RE 78 B
Olivine	6	7	8	9	10	11	12	3	4	5
SiO_2	40.43	40.81	40.68	40.54	40.51	40.80	40.93	39.98	39.64	39.91
Cr_2O_3								0.15	0.09	0.08
FeO	11.03	9.89	10.11	9.68	9.84	10.00	9.73	10.32	10.29	10.25
MnO								0.17	0.23	0.15
MgO	47.46	49.08	49.14	49.57	49.25	49.51	48.29	47.56	48.1	47.88
CaO	0.34	0.42	0.37	0.37	0.35	0.36	0.39	0.35	0.35	0.37
NiO								0.25	0.18	0.22
Sum	99.27	100.20	100.31	100.17	99.96	100.67	99.34	98.78	98.89	98.85
Fo	88.5	89.8	89.6	90.1	89.9	89.8	89.8	89.1	89.3	89.3
Spinel	6	7	8	9	10	11	12	3	4	5
SiO_2	0.10	0.09	0.07	0.06	0.06	0.14	0.06	0.08	0.08	0.08
TiO_2	0.38	0.30	0.14	0.18	0.30	0.21	0.23	0.16	0.17	0.16
Al_2O_3	24.75	29.77	33.46	31.22	29.15	32.18	30.39	31.82	30.67	31.32
Cr_2O_3	36.33	35.70	32.18	36.26	37.79	34.16	36.83	35.04	34.45	35.24
Fe_2O_3	8.53	5.69	5.18	4.33	3.72	5.17	5.27	3.28	4.87	3.47
FeO	17.13	11.17	11.74	10.29	11.73	10.82	11.05	12.89	13.88	11.91
MnO	0.21	0.00	0.02	0.04	0.17	0.07	0.12	0.18	0.33	0.12
MgO	12.31	16.75	16.62	17.38	16.13	17.29	17.03	15.54	14.69	15.98
NiO	0.09	0.14	0.16	0.25	0.11	0.16	0.23	0.15	0.18	0.23
ZnO								0.02	0.01	0.03
Sum	99.82	99.61	99.57	100.01	99.15	100.20	101.22	99.16	99.33	98.55
$Mg^{\#}$	0.562	0.728	0.716	0.751	0.710	0.740	0.733	0.682	0.654	0.705
$cr^{\#}$	0.496	0.446	0.392	0.438	0.465	0.416	0.448	0.425	0.430	0.430
X_{mt}	0.100	0.063	0.057	0.047	0.042	0.057	0.058	0.036	0.055	0.039
Fe^{2+}/Fe^{3+}	2.233	2.182	2.519	2.640	3.506	2.324	2.330	4.377	3.168	3.812

Sample	RE 78 B	RE 78 B	RE 78 B	RE 78 B	RE 78 B	RE 78 B	RE 78 B	RE 78 B	RE 78 B	RE 78 B
Olivine	6	8	9	11	13	17	18	20	21	23
SiO_2	39.19	39.89	39.6	39.55	39.49	39.36	40.18	39.73	39.8	39.64
Cr_2O_3	0.09	0.04	0.08	0.09	0.09	0.04	0.11	0.04	0.2	0.08
FeO	9.97	10.43	9.91	9.83	9.86	9.7	9.88	10.36	9.46	9.98
MnO	0.28	0.13	0.16	0.13	0.13	0.12	0.11	0.13	0.16	0.16
MgO	47.86	47.94	47.87	47.9	47.54	47.34	48.3	47.85	48.08	47.56
CaO	0.41	0.39	0.39	0.37	0.36	0.38	0.36	0.37	0.38	0.38
NiO	0.29	0.28	0.26	0.3	0.24	0.17	0.3	0.25	0.31	0.26
Sum	98.09	99.09	98.28	98.18	97.72	97.1	99.23	98.73	98.38	98.06
Fo	89.5	89.1	89.6	89.7	89.6	89.7	89.7	89.2	90.1	89.5
Spinel	6	8	9	11	13	17	18	20	21	23
SiO_2	0.06	0.09	0.11	0.10	0.07	0.12	0.09	0.22	0.11	0.11
TiO_2	0.16	0.18	0.06	0.20	0.21	0.21	0.18	0.18	0.12	0.21
Al_2O_3	30.03	32.22	41.84	30.41	32.46	32.09	32.27	33.33	38.69	31.53
Cr_2O_3	36.30	33.85	24.15	34.34	33.72	32.96	33.55	31.78	28.04	33.42
Fe_2O_3	4.02	4.16	4.39	4.59	3.59	4.08	4.38	3.26	4.10	4.51
FeO	12.92	12.24	10.36	14.73	10.36	12.70	11.25	13.01	10.64	12.16
MnO	0.20	0.17	0.15	0.29	0.25	0.30	0.21	0.22	0.16	0.18
MgO	15.30	16.00	18.24	14.10	16.90	15.43	16.50	15.37	17.79	15.83
NiO	0.17	0.16	0.20	0.16	0.23	0.16	0.23	0.20	0.29	0.13
ZnO	0.00	0.03	0.03	0.02	0.02	0.03	0.02	0.00	0.05	0.00
Sum	99.15	99.11	99.53	98.94	97.81	98.08	98.68	97.58	99.99	98.08
$Mg^{\#}$	0.679	0.700	0.758	0.631	0.744	0.684	0.723	0.678	0.749	0.699
$cr^{\#}$	0.448	0.413	0.279	0.431	0.411	0.408	0.411	0.390	0.327	0.416
X_{mt}	0.045	0.046	0.046	0.052	0.040	0.046	0.049	0.037	0.043	0.051
Fe^{2+}/Fe^{3+}	3.578	3.267	2.623	3.563	3.201	3.464	2.850	4.428	2.889	2.994

Sample	RE 78 B	RE 78 B	RE 78 B	RE 78 B	RE 78 B	RE 78 B	RE 120	RE 120	RE 120	RE 120
Olivine	25	27	31	31B	31C	31D	1	2	3	4
SiO_2	39.07	39.73	39.79	39.98	39.8	39.89	40.49	40.54	40.94	40.23
Cr_2O_3	0.11	0.08	0.16	0.17	0.1	0.2				
FeO	9.51	10.14	9.35	9.56	10.28	10.53	10.91	9.98	9.88	10.18
MnO	0.1	0.22	0.12	0.12	0.16	0.17				
MgO	47.59	47.69	47.97	48.2	48.11	47.28	48.06	49.47	49.85	48.33
CaO	0.35	0.37	0.37	0.37	0.33	0.34	0.29	0.36	0.32	0.31
NiO	0.28	0.22	0.26	0.37	0.25	0.3				
Sum	97.01	98.44	98.01	98.76	99.03	98.72	99.75	100.35	101.00	99.05
Fo	89.9	89.3	90.1	90.0	89.3	88.9	88.7	89.8	90.0	89.4
Spinel	25	27	31	31B	31C	31D	1	2	3	4
SiO_2	0.10	0.07	0.08	0.05	0.11	0.11	0.13	0.13	0.15	0.13
TiO_2	0.18	0.13	0.16	0.12	0.14	0.11	0.13	0.07	0.08	0.55
Al_2O_3	36.60	32.03	32.46	35.36	36.80	36.96	34.45	31.62	27.60	38.16
Cr_2O_3	29.84	34.56	34.58	31.44	29.80	28.60	31.34	35.12	39.53	26.85
Fe_2O_3	3.41	4.10	3.75	3.98	3.64	4.54	5.58	4.76	5.05	5.10
FeO	10.45	11.18	10.74	10.45	11.27	11.58	10.92	10.94	10.77	9.79
MnO	0.18	0.15	0.19	0.18	0.12	0.24	0.12	0.10	0.15	0.17
MgO	17.45	16.63	16.97	17.37	17.11	16.88	17.34	16.91	16.71	18.52
NiO	0.25	0.18	0.18	0.27	0.27	0.14	0.20	0.29	0.21	0.21
ZnO	0.01	0.00	0.03	0.05	0.02	0.02				
Sum	98.47	99.03	99.15	99.27	99.28	99.17	100.21	99.94	100.25	99.47
$Mg^{\#}$	0.748	0.726	0.738	0.748	0.730	0.722	0.739	0.734	0.735	0.771
$cr^{\#}$	0.354	0.420	0.417	0.374	0.352	0.342	0.379	0.427	0.490	0.321
X_{mt}	0.037	0.045	0.041	0.043	0.039	0.049	0.060	0.052	0.056	0.055
Fe^{2+}/Fe^{3+}	3.410	3.033	3.184	2.921	3.436	2.838	2.175	2.552	2.370	2.136

Sample	RE 120	RE 120	RE 120	RE 120	RE 120	RE 120	RE 120	RE 120	RE 120	RE 120
Olivine	5	6	7	9	10	11	12	13	14	22
SiO_2	40.29	40.54	40.52	40.15	40.44	41.14	39.97	40.79	40.80	40.77
Cr_2O_3										0.19
FeO	11.73	9.67	10.31	12.15	9.97	11.04	11.78	9.82	11.14	9.43
MnO										0.21
MgO	46.87	49.05	48.75	47.13	48.56	47.77	46.39	48.80	47.59	49.44
CaO	0.31	0.35	0.33	0.33	0.30	0.35	0.33	0.38	0.35	0.32
NiO										0.31
Sum	99.20	99.61	99.90	99.76	99.26	100.29	98.48	99.80	99.88	100.67
Fo	87.7	90.0	89.4	87.4	89.7	88.5	87.5	89.9	88.4	90.3
Spinel	5	6	7	9	10	11	12	13	14	SP 22
SiO_2	0.10	0.14	0.32	0.12	0.10	0.11	0.10	0.12	0.80	0.15
TiO_2	0.18	0.15	0.18	0.13	0.05	0.17	0.20	0.20	0.44	0.19
Al_2O_3	30.66	27.21	28.35	27.85	26.53	31.00	25.11	31.33	24.25	32.45
Cr_2O_3	35.74	38.88	37.01	39.82	41.30	36.14	41.28	35.53	35.97	34.40
Fe_2O_3	4.60	4.67	4.76	4.66	4.54	4.43	4.89	4.96	6.51	4.97
FeO	13.00	13.90	14.28	11.33	11.66	12.19	15.40	10.73	21.30	10.37
MnO	0.13	0.17	0.05	0.05	0.06	0.18	0.29	0.18	0.23	0.01
MgO	15.66	14.56	14.73	16.46	16.07	16.27	13.56	17.15	10.12	17.56
NiO	0.09	0.24	0.12	0.36	0.23	0.12	0.14	0.28	0.16	0.29
ZnO										0.12
Sum	100.15	99.92	99.80	100.78	100.55	100.62	100.97	100.48	99.78	100.50
$Mg^{\#}$	0.682	0.651	0.648	0.721	0.711	0.704	0.611	0.740	0.459	0.751
$cr^{\#}$	0.439	0.489	0.467	0.490	0.511	0.439	0.524	0.432	0.499	0.416
X_{mt}	0.051	0.053	0.054	0.052	0.051	0.049	0.056	0.054	0.079	0.054
Fe_{2+}/Fe^{3+}	3.142	3.309	3.334	2.702	2.853	3.054	3.503	2.403	3.633	2.321

Sample	RE 120	RE 120	RE 120	RE 120	RE 120	RE 120	RE 120	RE 120	RE 120	RE 120
Olivine	24	26	31	18B	33	46	60	61	67	72
SiO_2	40.33	40.24	40.29	39.61	39.81	39.78	40.25	40.56	39.70	39.76
Cr_2O_3	0.05	0.26	0.15	0.09	0.13	0.17	0.34	0.11	0.20	0.22
FeO	9.76	9.70	9.73	11.79	9.76	11.12	10.73	10.42	9.89	10.93
MnO	0.15	0.26	0.16	0.20	0.15	0.11	0.16	0.27	0.05	0.19
MgO	48.97	48.31	48.93	47.09	48.48	46.93	48.12	48.39	48.59	47.74
CaO	0.35	0.29	0.37	0.31	0.33	0.32	0.28	0.32	0.32	0.31
NiO	0.33	0.36	0.40	0.31	0.35	0.29	0.35	0.41	0.33	0.24
Sum	99.95	99.42	100.01	99.39	99.01	98.73	100.21	100.47	99.08	99.39
Fo	89.9	89.9	90.0	87.7	89.8	88.3	88.9	89.2	89.8	88.6
Spinel	24	26	31	18B	33	46	60	61	67	72
SiO_2	0.17	0.13	0.12	0.11	0.14	0.10	0.05	0.22	0.14	0.16
TiO_2	0.16	0.15	0.15	0.16	0.16	0.14	0.16	0.22	0.15	0.23
Al_2O_3	32.17	31.58	28.90	27.46	36.62	32.61	32.99	30.47	29.81	26.73
Cr_2O_3	33.16	35.49	36.96	39.07	29.55	33.19	34.22	34.56	36.62	39.29
Fe_2O_3	5.55	5.28	6.05	4.65	5.81	5.25	5.41	6.43	5.52	4.89
FeO	10.49	10.70	11.21	13.85	9.54	11.28	10.54	12.38	11.14	14.19
MnO	0.01	0.22	0.08	0.00	0.21	0.00	0.15	0.05	0.14	0.11
MgO	17.34	17.35	16.60	14.82	18.54	16.81	17.44	16.27	16.69	14.56
NiO	0.10	0.14	0.19	0.10	0.15	0.20	0.12	0.16	0.23	0.06
ZnO	0.03	0.00	0.05	0.12	0.07	0.09	0.42	0.04	0.17	0.10
Sum	99.17	101.04	100.31	100.33	100.78	99.67	101.49	100.80	100.61	100.32
$Mg^{\#}$	0.747	0.743	0.725	0.656	0.776	0.726	0.747	0.701	0.728	0.647
$cr^{\#}$	0.409	0.430	0.462	0.488	0.351	0.406	0.410	0.432	0.452	0.496
X_{mt}	0.061	0.057	0.067	0.052	0.062	0.058	0.058	0.071	0.061	0.055
Fe^{2+}/Fe^{3+}	2.103	2.251	2.061	3.309	1.825	2.390	2.165	2.138	2.243	3.228

Sample	RE 120	RE 120	RE 120	RE 154	RE 154	RE 154	RE 154	RE 154	RE 154	RE 154
Olivine	73	78	79	1	2	5	6	7		
SiO_2	39.75	40.73	40.74	40.56	41.01	40.76	41.62	40.52		
Cr_2O_3	0.20	0.19	0.19							
FeO	10.78	8.28	9.12	11.08	9.67	11.36	9.42	9.95		
MnO	0.20	0.08	0.12							
MgO	47.90	50.46	49.93	47.36	49.54	47.61	50.13	48.55		
CaO	0.33	0.34	0.31	0.32	0.34	0.36	0.33	0.41		
NiO	0.36	0.44	0.42							
Sum	99.51	100.53	100.83	99.31	100.56	100.08	101.49	99.44		
Fo	88.8	91.6	90.7	88.4	90.1	88.2	90.5	89.7		
Spinel	73	78	79	1	2	5	6	7	8	8A
SiO_2	0.12	0.12	0.13	0.09	0.12	0.24	0.11	0.09	0.10	0.05
TiO_2	0.21	0.13	0.13	0.51	0.17	0.18	0.16	0.15	0.26	0.82
Al_2O_3	30.29	29.04	27.20	22.22	35.42	35.86	35.28	36.69	30.88	29.21
Cr_2O_3	36.99	39.74	40.81	39.99	30.23	28.35	31.64	29.87	34.05	34.76
Fe_2O_3	4.83	4.05	5.16	8.07	5.04	5.92	4.40	4.41	6.15	5.92
FeO	11.22	7.92	9.94	17.56	10.77	12.17	10.46	10.93	14.47	13.65
MnO	0.14	0.07	0.19	0.19	0.06	0.08	0.10	0.15	0.10	0.25
MgO	16.83	18.66	17.29	12.03	17.39	16.68	17.69	17.46	14.90	15.30
NiO	0.31	0.35	0.26	0.13	0.29	0.26	0.26	0.24	0.21	0.10
ZnO	0.00	0.00	0.14							
Sum	100.94	100.07	101.25	100.79	99.50	99.73	100.10	99.99	101.12	100.06
$Mg^{\#}$	0.728	0.808	0.756	0.550	0.742	0.710	0.751	0.740	0.647	0.666
$cr^{\#}$	0.450	0.479	0.502	0.547	0.364	0.347	0.376	0.353	0.425	0.444
X_{mt}	0.053	0.044	0.057	0.095	0.055	0.064	0.047	0.047	0.068	0.067
Fe^{2+}/Fe^{3+}	2.586	2.174	2.139	2.420	2.374	2.283	2.641	2.757	2.612	2.562

Sample	RE 154	RE 154	RE 154	RE 154	RE 154	RE 154	RE 154	RE 154	RE 154	RE 154
Olivine		11	22	23	23B	24	25	26	27	
SiO_2		40.59	40.54	40.18	40.18	40.32	40.55	40.39	40.54	
Cr_2O_3			0.11	0.09	0.09	0.16	0.15	0.16	0.09	
FeO		12.04	9.68	10.46	10.46	11.40	9.32	11.56	9.94	
MnO			0.19	0.14	0.14	0.27	0.20	0.29	0.17	
MgO		47.22	49.31	48.16	48.16	47.94	49.04	47.56	48.76	
CaO		0.39	0.34	0.34	0.34	0.34	0.34	0.37	0.33	
NiO			0.35	0.29	0.29	0.26	0.42	0.33	0.35	
Sum		100.24	100.52	99.66	99.66	100.69	100.01	100.66	100.16	
Fo		87.5	90.1	89.1	89.1	88.2	90.4	88.0	89.7	
Spinel	9	11	22	23	23B	24	25	26	27	28
SiO_2	0.12	0.07	0.13	0.09	0.12	0.35	0.12	0.11	0.11	0.80
TiO_2	0.21	0.26	0.15	0.18	0.16	0.45	0.16	0.27	0.15	0.24
Al_2O_3	34.61	32.74	36.77	35.91	37.73	31.69	38.50	35.24	35.16	35.21
Cr_2O_3	29.99	29.75	30.82	30.90	29.35	33.58	30.33	29.68	30.68	30.77
Fe_2O_3	6.69	8.34	3.75	3.68	3.75	4.92	3.21	5.39	5.43	2.87
FeO	13.97	13.52	10.51	11.89	11.05	13.17	10.73	12.82	11.89	13.42
MnO	0.14	0.16	0.18	0.24	0.18	0.15	0.12	0.25	0.23	0.23
MgO	15.71	15.52	17.83	16.68	17.49	16.00	18.12	16.14	16.79	16.34
NiO	0.13	0.18	0.26	0.22	0.29	0.23	0.30	0.19	0.21	0.17
ZnO			0.03	0.03	0.04	0.00	0.05	0.01	0.00	0.05
Sum	101.56	100.55	100.43	99.82	100.15	100.54	101.64	100.10	100.65	100.10
$Mg^{\#}$	0.667	0.672	0.752	0.714	0.738	0.684	0.751	0.692	0.716	0.685
$cr^{\#}$	0.368	0.379	0.360	0.366	0.343	0.415	0.346	0.361	0.369	0.370
X_{mt}	0.072	0.092	0.040	0.040	0.040	0.055	0.034	0.059	0.059	0.032
Fe^{2+}/Fe^{3+}	2.322	1.800	3.112	3.592	3.275	2.974	3.714	2.644	2.433	5.198

Sample	RE 154	RE 154	RE 154	RE 154	RE 154	RE 154	RE 154	RE 154	RE 154	RE 154
Olivine	29	30	31							42
SiO_2	40.03	39.89	40.36							40.93
Cr_2O_3	0.12	0.07	0.11							0.08
FeO	11.22	10.62	9.34							11.98
MnO	0.22	0.21	0.20							0.19
MgO	47.75	47.15	49.11							48.19
CaO	0.33	0.37	0.35							0.38
NiO	0.32	0.33	0.29							0.27
Sum	99.97	98.63	99.77							102.01
Fo	88.4	88.8	90.4							87.8
Spinel	29	30	31	112	M1	M2	M3	M4	GM1	42
SiO_2	0.08	0.73	0.14	0.51	0.06	0.11	0.08	0.10	0.08	0.11
TiO_2	0.17	0.36	0.14	0.62	0.40	0.21	0.38	0.26	0.19	0.19
Al_2O_3	37.85	32.45	38.07	20.67	32.35	32.75	33.37	33.53	35.44	36.80
Cr_2O_3	29.14	30.13	30.17	39.59	32.44	32.69	31.62	33.29	29.11	30.84
Fe_2O_3	3.55	4.66	3.11	5.46	5.58	5.21	5.47	4.96	5.50	5.00
FeO	11.59	16.07	10.25	23.61	14.35	14.29	14.23	10.95	13.56	10.13
MnO	0.22	0.25	0.09	0.45	0.14	0.15	0.25	0.32	0.28	0.14
MgO	17.07	14.09	18.21	7.77	15.06	15.10	15.22	17.28	15.55	18.41
NiO	0.27	0.15	0.27	0.13	0.15	0.16	0.17	0.18	0.14	0.28
ZnO	0.05	0.01	0.01	0.03	0.03	0.00	0.02	0.05	0.05	0.00
Sum	99.99	98.90	100.47	98.84	100.56	100.68	100.81	100.92	99.90	101.90
$Mg^{\#}$	0.724	0.610	0.760	0.370	0.652	0.653	0.656	0.738	0.672	0.764
$cr^{\#}$	0.341	0.384	0.347	0.562	0.402	0.401	0.389	0.400	0.355	0.360
X_{mt}	0.038	0.053	0.033	0.069	0.062	0.057	0.060	0.054	0.060	0.053
Fe^{2+}/Fe^{3+}	3.621	3.840	3.658	4.807	2.857	3.047	2.892	2.458	2.741	2.255

Sample	RE 154	RE 154	RE 154	RE 154	RE 154	RE 154	RE 154	RE 154	RE 154	RE 154
Olivine	7A	7B	11	13	27	29	43	46	49B	50
SiO_2	40.52	40.17	40.61	39.86	40.71	40.17	39.15	39.91	40.11	40.24
Cr_2O_3	0.25	0.17	0.11	0.11	0.25	0.15	0.08	0.17	0.19	0.16
FeO	9.24	9.86	10.41	11.16	12.41	9.83	15.16	10.57	9.72	9.51
MnO	0.20	0.23	0.09	0.19	0.22	0.16	0.26	0.07	0.27	0.16
MgO	49.12	48.84	48.63	48.09	47.46	49.53	44.67	48.07	49.48	49.51
CaO	0.39	0.35	0.34	0.33	0.38	0.31	0.35	0.36	0.33	0.36
NiO	0.33	0.41	0.41	0.34	0.27	0.29	0.16	0.37	0.41	0.26
Sum	100.04	100.02	100.61	100.08	101.71	100.44	99.82	99.51	100.50	100.21
Fo	90.4	89.8	89.3	88.5	87.2	90.0	84.0	89.0	90.1	90.3
Spinel	7A	7B	11	13	27	29	43	46	49B	50
SiO_2	0.08	0.12	0.13	0.13	0.11	0.11	0.06	0.16	0.10	0.12
TiO_2	0.17	0.24	0.20	0.15	0.46	0.13	0.38	0.17	0.16	0.19
Al_2O_3	37.52	35.61	37.88	36.37	22.27	37.39	20.27	35.70	36.50	36.45
Cr_2O_3	30.79	30.12	29.81	30.54	42.17	30.52	41.27	32.22	29.96	30.69
Fe_2O_3	4.61	6.23	3.86	5.29	6.57	4.91	7.50	4.72	5.02	5.26
FeO	8.16	11.79	10.40	10.63	15.60	9.74	19.99	9.56	10.09	9.56
MnO	0.16	0.19	0.08	0.15	0.23	0.07	0.25	0.23	0.11	0.27
MgO	19.54	17.00	18.19	17.94	13.29	18.67	9.73	18.53	18.06	18.42
NiO	0.30	0.29	0.25	0.15	0.15	0.24	0.11	0.33	0.27	0.27
ZnO	0.14	0.32	0.05	0.14	0.00	0.18	0.34	0.07	0.01	0.30
Sum	101.47	101.91	100.85	101.49	100.85	101.95	99.90	101.69	100.28	101.52
$Mg^{\#}$	0.810	0.720	0.757	0.751	0.603	0.774	0.465	0.776	0.761	0.775
$cr^{\#}$	0.355	0.362	0.346	0.360	0.560	0.354	0.577	0.377	0.355	0.361
X_{mt}	0.048	0.067	0.041	0.056	0.077	0.051	0.091	0.050	0.054	0.056
Fe^{2+}/Fe^{3+}	1.965	2.104	2.995	2.231	2.641	2.206	2.962	2.250	2.235	2.019

Sample	RE 154	RE 185	RE 185	RE 185	RE 185	RE 185	RE 185	RE 185	RE 185	RE 185
Olivine	52	1A	2A	3A	4A	5A	1	2		5
SiO_2	40.10			39.76	40.22	40.27	40.79	40.73		40.32
Cr_2O_3	0.14						0.09	0.20		0.19
FeO	9.22			8.46	9.21	9.46	9.75	9.66		10.36
MnO	0.23						0.15	0.15		0.06
MgO	49.82			47.06	47.73	46.98	49.14	48.56		48.34
CaO	0.34			0.32	0.34	0.36	0.38	0.36		0.37
NiO	0.35						0.26	0.31		0.27
Sum	100.21			95.59	97.50	97.08	100.56	99.95		99.91
Fo	90.6			90.8	90.2	89.8	90.0	90.0		89.3
Spinel	52	1A	2A	3A	4A	5A	1	2	4	5
SiO_2	0.11	0.08	0.11	0.11	0.07	0.07	0.08	0.12	0.11	0.11
TiO_2	0.17	0.13	0.11	0.16	0.12	0.11	0.19	0.09	0.12	0.13
Al_2O_3	35.96	28.04	31.49	30.58	29.91	36.15	30.24	30.45	30.53	27.02
Cr_2O_3	30.73	39.31	35.49	37.49	38.11	31.71	37.28	37.37	35.53	39.73
Fe_2O_3	5.44	4.84	4.84	3.93	4.60	4.75	3.94	3.49	5.01	3.83
FeO	9.52	10.38	10.74	11.35	10.47	10.80	10.97	10.76	10.71	13.41
MnO	0.12	0.16	0.15	0.08	0.20	0.12	0.19	0.02	0.18	0.19
MgO	18.38	16.93	17.12	16.83	17.17	17.85	16.71	16.94	16.74	14.74
NiO	0.26	0.23	0.20	0.16	0.27	0.23	0.22	0.16	0.24	0.17
ZnO	0.26						0.09	0.01	0.09	0.00
Sum	100.94	100.09	100.26	100.69	100.92	101.80	99.90	99.41	99.25	99.32
$Mg^{\#}$	0.775	0.744	0.740	0.725	0.745	0.747	0.731	0.737	0.736	0.662
$cr^{\#}$	0.364	0.485	0.431	0.451	0.461	0.370	0.453	0.452	0.438	0.497
X_{mt}	0.058	0.054	0.053	0.043	0.050	0.050	0.044	0.039	0.056	0.044
Fe^{2+}/Fe^{3+}	1.945	2.385	2.464	3.209	2.533	2.525	3.094	3.427	2.377	3.896

Sample	RE 185	RE 185	RE 185	RE 185	RE 185	RE 185	RE 185	RE 185	RE 185	RE 185
Olivine	6	7	9\1	9\2	10	11	11B	11C	12	13
SiO_2	40.49	40.80	40.71	40.80	40.71	40.57	40.80	40.50	40.75	40.60
Cr_2O_3	0.08	0.16	0.06	0.05	0.14	0.40	0.45	0.13	0.20	0.08
FeO	10.08	9.73	10.18	9.90	9.72	10.19	10.26	10.24	10.93	10.05
MnO	0.05	0.07	0.18	0.08	0.15	0.24	0.10	0.22	0.19	0.18
MgO	48.71	49.12	48.62	48.81	48.69	48.31	48.08	48.16	47.85	48.92
CaO	0.36	0.34	0.36	0.37	0.35	0.33	0.36	0.33	0.41	0.34
NiO	0.29	0.29	0.32	0.30	0.31	0.23	0.26	0.34	0.21	0.35
Sum	100.06	100.51	100.42	100.31	100.09	100.27	100.32	99.92	100.54	100.52
Fo	89.6	90.0	89.5	89.8	89.9	89.4	89.3	89.3	88.6	89.7
Spinel	6	7	9\1	9\2	10	11	11B	11C	12	13
SiO_2	0.26	0.15	0.22	0.11	0.11	0.12	0.09	0.12	0.11	0.15
TiO_2	0.09	0.16	0.10	0.10	0.10	0.13	0.11	0.11	0.26	0.24
Al_2O_3	32.39	31.08	36.39	32.91	38.58	30.55	30.30	31.28	28.71	28.91
Cr_2O_3	33.84	36.38	32.84	33.41	27.57	38.05	38.58	35.35	37.79	38.71
Fe_2O_3	3.74	3.94	5.63	4.47	4.58	1.58	1.05	4.62	4.75	4.42
FeO	11.00	10.30	9.10	10.33	11.23	10.99	11.91	11.22	12.30	10.72
MnO	0.19	0.17	0.09	0.08	0.15	0.17	0.14	0.04	0.14	0.12
MgO	16.75	17.26	19.66	17.29	17.41	16.46	15.78	16.75	15.91	16.96
NiO	0.17	0.25	0.17	0.21	0.23	0.19	0.25	0.18	0.15	0.29
ZnO	0.08	0.04	0.01	0.00	0.09	0.06	0.06	0.02	0.02	0.11
Sum	98.50	99.73	104.20	98.92	100.05	98.30	98.26	99.69	100.14	100.63
$Mg^{\#}$	0.731	0.749	0.794	0.749	0.734	0.727	0.703	0.727	0.698	0.738
$cr^{\#}$	0.412	0.440	0.377	0.405	0.324	0.455	0.461	0.431	0.469	0.473
X_{mt}	0.042	0.043	0.058	0.049	0.049	0.018	0.012	0.051	0.053	0.049
Fe^{2+}/Fe^{3+}	3.271	2.904	1.796	2.569	2.728	7.756	12.626	2.702	2.878	2.692

Sample	RE 185	RE 185B	RE 185B	RE 185B	RE 185B	RE 185B	RE 185B	RE 185B	RE 185B	RE 185B
Olivine	14	1	7	15A	15B	17	19A	19B	19C	21
SiO_2	40.91	40.44	39.58	39.95	39.88	40.18	39.99	39.89	39.73	39.73
Cr_2O_3	0.14	0.19	0.20	0.28	0.10	0.10	0.19	0.16	0.19	0.08
FeO	9.91	9.75	10.34	10.95	10.86	10.08	9.70	9.97	10.03	10.23
MnO	0.19	0.24	0.18	0.11	0.13	0.33	0.15	0.27	0.13	0.15
MgO	48.84	49.17	47.78	48.14	48.39	49.23	49.49	49.78	48.80	48.75
CaO	0.36	0.34	0.36	0.33	0.36	0.33	0.36	0.36	0.31	0.39
NiO	0.35	0.42	0.23	0.15	0.28	0.36	0.27	0.34	0.22	0.31
Sum	100.69	100.55	98.67	99.91	100.00	100.61	100.15	100.77	99.41	99.64
Fo	89.8	90.0	89.2	88.7	88.8	89.7	90.1	89.9	89.7	89.5
Spinel	14	1	7	15A	15B	17	19A	19B	19C	21
SiO_2	0.15	0.13	0.12	0.08	0.08	0.12	0.12	0.10	0.04	0.11
TiO_2	0.14	0.17	0.10	0.31	0.37	0.11	0.37	0.23	0.31	0.12
Al_2O_3	27.87	29.49	30.71	28.96	27.63	29.57	27.66	29.96	28.71	30.13
Cr_2O_3	40.04	39.06	35.74	37.35	39.55	33.95	39.15	36.92	38.35	36.99
Fe_2O_3	3.82	4.26	4.52	5.13	5.13	5.87	4.54	4.82	4.31	5.39
FeO	10.97	6.50	11.25	12.02	11.88	13.61	11.16	11.17	11.89	10.32
MnO	0.11	0.20	0.21	0.12	0.12	0.18	0.15	0.17	0.20	0.08
MgO	16.58	19.59	16.53	16.20	16.33	14.51	16.52	16.79	16.15	17.41
NiO	0.15	0.11	0.09	0.09	0.15	0.12	0.20	0.14	0.06	0.19
ZnO	0.13	0.07	0.00	0.02	0.09	0.26	0.05	0.00	0.02	0.00
Sum	99.95	99.58	99.28	100.30	101.32	98.29	99.94	100.31	100.05	100.74
$Mg^{\#}$	0.729	0.843	0.724	0.706	0.710	0.655	0.725	0.728	0.708	0.750
$cr^{\#}$	0.491	0.470	0.438	0.464	0.490	0.435	0.487	0.453	0.473	0.452
X_{mt}	0.043	0.047	0.050	0.057	0.057	0.067	0.051	0.053	0.048	0.059
Fe^{2+}/Fe^{3+}	3.194	1.693	2.764	2.605	2.574	2.576	2.731	2.578	3.068	2.128

Sample	RE 185B	RE 185B	RE 185B	RE 185B	RE 185B	RE 185B	RE 185B	RE 185B	RE 185B	RE 185B
Olivine	32	63	57	55	53	68	80	83	87	90A
SiO_2	40.18	39.61	40.35	39.69	39.96	40.06	39.90	39.82	39.78	40.34
Cr_2O_3	0.06	0.14	0.08	0.09	0.03	0.13	0.10	0.08	0.11	0.24
FeO	9.86	10.11	10.09	10.17	9.92	9.28	9.36	10.37	9.21	9.03
MnO	0.16	0.13	0.18	0.10	0.25	0.10	0.00	0.12	0.08	0.05
MgO	49.31	48.53	49.20	48.46	49.40	49.73	50.12	48.59	49.31	50.32
CaO	0.31	0.37	0.40	0.36	0.38	0.31	0.32	0.36	0.33	0.36
NiO	0.27	0.20	0.43	0.29	0.30	0.36	0.30	0.25	0.33	0.34
Sum	100.15	99.09	100.73	99.16	100.24	99.97	100.10	99.59	99.15	100.68
Fo	89.9	89.5	89.7	89.5	89.9	90.5	90.5	89.3	90.5	90.9
Spinel	32	63	57	55	53	68	80	83	87	90A
SiO_2	0.11	0.64	0.13	0.09	0.12	0.17	0.11	0.08	0.08	0.09
TiO_2	0.11	0.20	0.17	0.15	0.11	0.09	0.15	0.12	0.15	0.15
Al_2O_3	31.83	33.47	26.22	31.77	30.27	28.07	29.84	31.07	29.25	25.60
Cr_2O_3	36.23	31.23	41.65	34.60	37.03	40.64	37.05	35.87	38.95	42.80
Fe_2O_3	4.19	4.18	4.03	4.81	4.55	3.76	3.97	5.08	4.30	4.30
FeO	12.39	12.37	11.48	11.03	10.50	11.23	10.82	10.87	10.29	10.87
MnO	0.09	0.21	0.07	0.13	0.14	0.07	0.13	0.12	0.24	0.08
MgO	16.34	16.37	16.22	16.82	17.06	16.70	16.63	17.05	17.18	16.56
NiO	0.17	0.29	0.10	0.12	0.33	0.17	0.12	0.15	0.24	0.15
ZnO	0.15	0.08	0.04	0.16	0.00	0.00	0.16	0.02	0.01	0.08
Sum	101.59	99.05	100.10	99.69	100.11	100.91	98.97	100.43	100.68	100.68
$Mg^{\#}$	0.702	0.702	0.716	0.731	0.743	0.726	0.733	0.737	0.749	0.731
$cr^{\#}$	0.433	0.385	0.516	0.422	0.451	0.493	0.454	0.436	0.472	0.529
X_{mt}	0.045	0.047	0.045	0.053	0.050	0.042	0.044	0.056	0.047	0.048
Fe^{2+}/Fe^{3+}	3.289	3.287	3.165	2.546	2.570	3.318	3.033	2.380	2.657	2.810

Sample	RE 185B	RE 185B	RE 185B	RE 185B	RE 185B	RE 185B	RE 185B	RE 185B	RE 185B	RE 185B
Olivine	90B	91A	91B	91C	94	95	99A	99B	99B	213
SiO_2	40.29		39.81	39.61	39.59	39.85	40.03	40.13	39.92	
Cr_2O_3	0.26		0.23	0.15	0.17	0.07	0.12	0.21	0.15	
FeO	9.06		10.81	10.94	11.10	9.94	9.05	10.44	10.28	
MnO	0.18		0.20	0.19	0.21	0.11	0.20	0.08	0.21	
MgO	49.95		48.93	48.68	48.78	49.44	50.08	48.71	48.90	
CaO	0.32		0.34	0.34	0.38	0.33	0.36	0.42	0.34	
NiO	0.32		0.23	0.22	0.21	0.20	0.36	0.25	0.33	
Sum	100.38		100.55	100.13	100.44	99.94	100.20	100.24	100.13	
Fo	90.8		89.0	88.8	88.7	89.9	90.8	89.3	89.4	
Spinel	90B	90C	91A	91B	91C	94	95	99A	99B	213
SiO_2	0.11	0.08	0.08	0.08	0.11	0.11	0.09	0.09	0.07	0.07
TiO_2	0.12	0.13	0.27	0.32	0.35	0.12	0.15	0.11	0.09	0.44
Al_2O_3	26.24	25.98	27.56	27.63	27.12	31.28	25.92	32.80	31.29	27.10
Cr_2O_3	42.09	41.61	39.21	39.54	40.01	35.71	42.29	33.03	36.14	41.46
Fe_2O_3	4.60	4.01	5.25	4.88	3.80	4.63	4.56	5.10	5.61	4.32
FeO	10.18	10.72	11.75	11.83	12.94	11.11	10.83	12.69	10.39	9.66
MnO	0.20	0.19	0.07	0.10	0.26	0.16	0.07	0.38	0.08	0.19
MgO	16.96	16.31	16.23	16.17	15.34	16.78	16.55	15.88	17.56	17.79
NiO	0.27	0.18	0.13	0.27	0.08	0.25	0.22	0.06	0.13	0.00
ZnO	0.04	0.05	0.13	0.13	0.00	0.09	0.19	0.00	0.10	0.04
Sum	100.80	99.25	100.67	100.95	100.01	100.23	100.87	100.14	101.46	101.07
$Mg^{\#}$	0.748	0.731	0.711	0.709	0.679	0.729	0.731	0.691	0.751	0.767
$cr^{\#}$	0.518	0.518	0.488	0.490	0.497	0.434	0.523	0.403	0.437	0.506
X_{mt}	0.051	0.045	0.059	0.054	0.043	0.051	0.051	0.056	0.061	0.048
Fe^{2+}/Fe^{3+}	2.459	2.970	2.485	2.697	3.784	2.666	2.642	2.763	2.058	2.482

Sample	RE 185B	RE 185B	RE 185B	RE 185B	RE 217	RE 217	RE 217	RE 217	RE 217	RE 217
Olivine				1A	3A	4A	6A	9A	11A	1
SiO_2				39.76	39.89	40.36	39.95	40.52	40.04	40.17
Cr_2O_3										0.13
FeO				9.03	9.23	9.14	9.05	9.66	9.14	9.47
MnO										0.26
MgO				47.52	47.56	47.23	47.70	47.52	48.04	48.92
CaO				0.30	0.31	0.33	0.29	0.36	0.35	0.36
NiO										0.33
Sum				96.61	96.99	97.06	96.99	98.06	97.56	99.64
Fo				90.4	90.2	90.2	90.4	89.8	90.4	90.2
Spinel	214	215	216	1A	3A	4A	6A	9A	11A	1
SiO_2	0.09	0.13	0.07	0.10	0.12	0.15	0.13	0.11	0.10	0.11
TiO_2	0.15	0.13	0.10	0.15	0.14	0.16	0.16	0.13	0.11	0.17
Al_2O_3	25.59	26.25	23.86	32.95	37.69	36.81	37.35	34.66	37.58	34.51
Cr_2O_3	42.38	41.37	44.09	34.84	28.66	29.23	29.00	31.18	30.71	30.93
Fe_2O_3	5.00	4.93	4.87	4.88	4.51	5.00	4.14	5.41	5.39	2.43
FeO	10.37	10.24	10.30	10.50	11.14	12.50	8.92	13.54	9.27	11.07
MnO	0.12	0.12	0.04	0.08	0.07	0.19	0.08	0.22	0.07	0.21
MgO	16.91	17.02	16.64	17.74	17.47	16.69	18.68	15.78	19.24	16.31
NiO	0.10	0.14	0.18	0.20	0.33	0.21	0.20	0.21	0.23	0.25
ZnO	0.08	0.00	0.00							0.00
Sum	100.79	100.34	100.15	101.44	100.13	100.94	98.65	101.23	102.70	95.99
$Mg^{\#}$	0.744	0.748	0.742	0.751	0.736	0.704	0.789	0.675	0.787	0.724
$cr^{\#}$	0.526	0.514	0.553	0.415	0.338	0.348	0.342	0.376	0.354	0.376
X_{mt}	0.056	0.055	0.055	0.052	0.048	0.054	0.044	0.058	0.056	0.027
Fe^{2+}/Fe^{3+}	2.303	2.309	2.353	2.390	2.748	2.780	2.395	2.783	1.911	5.070

Sample	RE 217	RE 217	RE 217	RE 217	RE 217	RE 217	RE 217	RE 217	RE 217	RE 217
Olivine	2		4	5	6	7		8	10	11
SiO_2	40.49		40.18	40.44	40.39	40.36		40.23	40.21	40.54
Cr_2O_3	0.06		0.08	0.12	0.04	0.13		0.09	0.18	0.17
FeO	9.82		9.92	9.58	9.71	9.20		9.71	10.29	9.23
MnO	0.19		0.17	0.20	0.18	0.17		0.19	0.16	0.16
MgO	48.76		48.63	49.05	48.74	49.15		48.82	48.58	49.30
CaO	0.33		0.32	0.32	0.35	0.33		0.35	0.33	0.35
NiO	0.38		0.31	0.35	0.29	0.41		0.33	0.32	0.39
Sum	100.02		99.61	100.06	99.71	99.75		99.71	100.05	100.13
Fo	89.8		89.7	90.1	89.9	90.5		90.0	89.4	90.5
Spinel	2	3	4	5	6	7	9	8	10	11
SiO_2	0.17	0.13	0.10	0.14	0.12	0.12	0.14	0.16	0.12	0.08
TiO_2	0.15	0.15	0.13	0.17	0.18	0.17	0.15	0.16	0.12	0.17
Al_2O_3	37.62	38.41	36.80	38.91	38.12	37.36	35.78	36.73	36.35	37.95
Cr_2O_3	29.05	28.52	28.47	29.33	28.08	29.78	30.33	29.99	30.66	29.71
Fe_2O_3	4.02	3.47	4.42	2.95	3.59	3.46	4.25	3.79	4.37	3.85
FeO	10.79	11.58	12.60	9.41	11.64	10.54	11.74	11.25	11.24	10.75
MnO	0.15	0.21	0.29	0.22	0.13	0.13	0.25	0.15	0.06	0.19
MgO	17.67	17.20	16.11	18.71	17.03	17.76	16.73	17.30	17.45	17.84
NiO	0.29	0.22	0.22	0.27	0.22	0.23	0.22	0.18	0.16	0.25
ZnO	0.01	0.03	0.03	0.01	0.02	0.00	0.04	0.02	0.02	0.03
Sum	99.92	99.91	99.17	100.11	99.14	99.54	99.64	99.73	100.55	100.82
$Mg^{\#}$	0.745	0.726	0.695	0.780	0.723	0.750	0.717	0.733	0.735	0.747
$cr^{\#}$	0.341	0.333	0.342	0.336	0.331	0.348	0.363	0.354	0.361	0.344
X_{mt}	0.043	0.037	0.048	0.031	0.039	0.037	0.046	0.041	0.047	0.041
Fe^{2+}/Fe^{3+}	2.981	3.714	3.170	3.549	3.602	3.387	3.070	3.299	2.855	3.108

Sample	RE 217	RE 217	RE 217	RE 217	RE 217	RE 217	RE 217	RE 217	RE 217	RE 217
Olivine	12	13	14			17		19	20	21
SiO_2	40.16	40.31	39.98			40.38		40.37	40.04	40.12
Cr_2O_3	0.11	0.13	0.06			0.06		0.21	0.14	0.17
FeO	9.72	9.35	9.99			9.75		9.09	9.75	9.28
MnO	0.11	0.27	0.18			0.29		0.14	0.18	0.17
MgO	48.79	49.23	48.31			48.65		48.86	48.60	49.04
CaO	0.32	0.33	0.35			0.36		0.34	0.31	0.37
NiO	0.32	0.47	0.34			0.29		0.33	0.30	0.41
Sum	99.53	100.08	99.21			99.79		99.33	99.32	99.55
Fo	89.9	90.4	89.6			89.9		90.5	89.9	90.4
Spinel	12	13	14	15	16	17	18	19	20	21
SiO_2	0.12	0.25	0.20	0.11	0.14	0.14	0.13	0.23	0.11	0.12
TiO_2	0.14	0.18	0.18	0.17	0.12	0.13	0.14	0.17	0.15	0.13
Al_2O_3	36.97	28.15	34.86	37.34	38.56	37.88	38.33	32.79	37.25	36.05
Cr_2O_3	31.51	38.53	31.93	29.05	27.74	29.41	28.67	34.12	29.78	31.03
Fe_2O_3	2.67	3.39	3.38	3.90	4.37	3.45	4.02	3.37	4.10	3.85
FeO	11.04	13.33	12.14	12.24	10.35	11.23	10.11	10.73	10.51	9.90
MnO	0.16	0.29	0.17	0.26	0.14	0.18	0.14	0.20	0.11	0.16
MgO	17.52	14.99	16.52	16.64	18.00	17.38	18.17	17.07	17.84	17.96
NiO	0.21	0.16	0.21	0.21	0.23	0.29	0.28	0.23	0.27	0.24
ZnO	0.05	0.00	0.02	0.00	0.00	0.05	0.03	0.03	0.02	0.02
Sum	100.39	99.27	99.61	99.92	99.64	100.13	100.01	98.93	100.14	99.46
$Mg^{\#}$	0.739	0.667	0.708	0.708	0.756	0.734	0.762	0.739	0.752	0.764
$cr^{\#}$	0.364	0.479	0.381	0.343	0.326	0.342	0.334	0.411	0.349	0.366
X_{mt}	0.028	0.039	0.037	0.042	0.046	0.037	0.043	0.037	0.044	0.042
Fe^{2+}/Fe^{3+}	4.608	4.373	3.993	3.489	2.635	3.619	2.795	3.544	2.852	2.853

Sample	RE 286	RE 286	RE 286	RE 286	RE 286	RE 286	RE 286	RE 286	RE 286	RE 286
Olivine	1A	2A	3A	5A	6A	7A		9A	4	5
SiO_2	39.50	40.15	39.82	40.29	39.89	38.36		39.44	39.36	39.32
Cr_2O_3									0.21	0.12
FeO	14.64	14.75	14.59	15.96	17.76	15.58		15.11	14.99	15.39
MnO									0.23	0.26
MgO	44.58	45.28	44.88	44.47	43.07	42.97		44.51	44.81	44.68
CaO	0.31	0.32	0.28	0.31	0.27	0.26		0.33	0.32	0.30
NiO									0.25	0.25
Sum	99.02	100.50	99.57	101.03	101.00	97.18		99.39	100.17	100.32
Fo	84.4	84.6	84.6	83.2	81.2	83.1		84.0	84.2	83.8
Spinel	1A	2A	3A	5A	6A	7A	8A	9A	4	5
SiO_2	0.13	0.10	0.14	0.08	0.19	0.08	0.12	0.08	0.13	0.12
TiO_2	1.12	1.19	4.55	0.91	1.32	1.04	1.03	1.02	1.23	4.78
Al_2O_3	29.57	28.15	25.43	27.69	25.88	29.59	29.67	29.85	28.40	25.98
Cr_2O_3	29.17	29.68	26.75	30.42	31.04	30.21	28.56	28.84	29.27	26.55
Fe_2O_3	9.38	11.18	10.45	10.67	10.97	11.10	10.38	10.56	9.64	8.90
FeO	16.35	16.45	18.90	16.63	19.30	17.02	15.94	15.72	16.51	18.87
MnO	0.16	0.05	0.17	0.29	0.22	0.24	0.16	0.24	0.28	0.26
MgO	13.71	13.82	13.73	13.16	11.79	13.90	14.00	14.19	13.27	13.64
NiO	0.23	0.14	0.25	0.14	0.14	0.15	0.16	0.19	0.21	0.29
ZnO									0.06	0.02
Sum	99.82	100.76	100.37	99.99	100.85	103.33	100.02	100.70	99.00	99.42
$Mg^{\#}$	0.599	0.600	0.564	0.585	0.521	0.593	0.610	0.617	0.589	0.563
$cr^{\#}$	0.398	0.414	0.414	0.424	0.446	0.407	0.392	0.393	0.409	0.407
X_{mt}	0.109	0.129	0.133	0.124	0.130	0.124	0.119	0.121	0.114	0.115
Fe_{2+}/Fe^{3+}	1.937	1.636	2.010	1.732	1.955	1.704	1.707	1.654	1.904	2.355

Sample	RE 286	RE 286	RE 286	RE 286	RE 286	RE 286	RE 286	RE 286	RE 286	RE 286
Olivine	12	12B	14	13	13B	116	15	15B	16	17
SiO_2	39.60	39.39	38.87	39.36	38.95	39.32	39.13	39.03	38.61	39.10
Cr_2O_3	0.11	0.21	0.08	0.08	0.06	0.11	0.21	0.15	0.15	0.11
FeO	14.91	15.29	16.70	15.84	16.37	14.77	14.77	14.88	15.23	15.57
MnO	0.31	0.30	0.31	0.26	0.37	0.19	0.24	0.24	0.26	0.31
MgO	44.33	44.17	43.17	43.88	43.37	44.21	44.50	44.68	43.90	44.03
CaO	0.29	0.38	0.30	0.30	0.29	0.34	0.29	0.31	0.34	0.29
NiO	0.22	0.24	0.23	0.28	0.18	0.22	0.25	0.28	0.26	0.27
Sum	99.77	99.98	99.66	100.00	99.61	99.16	99.40	99.57	98.75	99.67
Fo	84.1	83.7	82.2	83.2	82.5	84.2	84.3	84.3	83.7	83.4
Spinel	12	12B	14	13	13B	116	15	15B	16	17
SiO_2	0.10	0.09	0.09	0.10	0.13	0.16	0.10	0.08	0.10	0.10
TiO_2	0.93	0.97	0.90	1.07	1.00	1.03	0.99	0.86	0.98	0.91
Al_2O_3	28.71	30.40	26.51	29.63	29.14	29.50	30.19	29.59	29.89	29.93
Cr_2O_3	30.23	28.16	31.32	28.68	28.18	29.07	29.10	28.88	28.06	28.34
Fe_2O_3	9.69	9.71	9.72	9.63	10.01	9.25	9.70	10.23	9.66	9.86
FeO	16.64	16.24	18.41	16.62	17.14	16.34	15.90	15.94	16.22	16.71
MnO	0.22	0.20	0.27	0.30	0.25	0.21	0.29	0.24	0.22	0.36
MgO	13.28	13.70	11.70	13.35	12.84	13.56	13.97	13.72	13.47	13.16
NiO	0.21	0.18	0.12	0.19	0.17	0.19	0.25	0.18	0.20	0.23
ZnO	0.06	0.03	0.05	0.03	0.02	0.02	0.09	0.03	0.03	0.05
Sum	100.07	99.68	99.09	99.61	98.88	99.32	100.58	99.75	98.83	99.65
$Mg^{\#}$	0.587	0.601	0.531	0.589	0.572	0.597	0.610	0.605	0.597	0.584
$cr^{\#}$	0.414	0.383	0.442	0.394	0.393	0.398	0.393	0.396	0.386	0.388
X_{mt}	0.112	0.112	0.116	0.112	0.117	0.108	0.111	0.118	0.112	0.114
Fe^{2+}/Fe^{3+}	1.909	1.858	2.104	1.918	1.904	1.964	1.822	1.732	1.867	1.883

Sample	RE 286	RE 286	RE 286	RE 286	RE 286	RE 286	RE 286	RE 286	RE 286	RE 286
Olivine	19	117	118	20	21	22	23	23B	24	112
SiO_2	39.00	38.76	38.95	38.96	39.56	39.16	39.05	39.18	39.56	39.18
Cr_2O_3	0.07	0.09	0.16	0.10	0.15	0.04	0.11	0.13	0.09	0.04
FeO	14.79	17.83	15.26	15.11	14.98	16.11	15.15	15.22	15.15	15.23
MnO	0.23	0.31	0.27	0.25	0.24	0.19	0.27	0.32	0.28	0.28
MgO	44.20	41.87	44.24	44.22	44.73	43.44	44.41	44.54	44.31	44.33
CaO	0.32	0.29	0.32	0.27	0.33	0.27	0.28	0.31	0.21	0.31
NiO	0.28	0.20	0.26	0.23	0.27	0.18	0.18	0.25	0.22	0.26
Sum	98.88	99.33	99.46	99.15	100.25	99.39	99.45	99.95	99.83	99.63
Fo	84.2	80.7	83.8	83.9	84.2	82.8	83.9	83.9	83.9	83.8
Spinel	19	117	118	20	21	22	23	23B	24	112
SiO_2	0.58	0.09	0.09	0.14	0.17	0.12	0.11	0.26	0.10	0.16
TiO_2	0.92	1.02	0.97	0.93	0.99	1.03	0.85	0.82	0.86	0.98
Al_2O_3	30.87	28.38	29.76	30.81	29.76	29.27	30.22	29.60	30.14	30.35
Cr_2O_3	28.50	28.33	28.71	27.76	29.07	27.67	28.60	28.21	28.53	28.04
Fe_2O_3	8.29	10.54	9.69	9.74	9.68	10.41	9.89	9.01	9.53	9.02
FeO	16.23	19.44	16.08	16.03	16.37	17.68	15.99	16.16	16.00	16.15
MnO	0.26	0.25	0.26	0.25	0.23	0.26	0.31	0.23	0.17	0.16
MgO	14.18	11.41	13.64	13.90	13.69	12.63	13.75	13.26	13.69	13.59
NiO	0.21	0.14	0.16	0.16	0.22	0.04	0.23	0.31	0.22	0.28
ZnO	0.03	0.01	0.06	0.01	0.04	0.04	0.02	0.01	0.01	0.04
Sum	100.07	99.61	99.42	99.72	100.22	99.15	99.97	97.87	99.25	98.78
$Mg^{\#}$	0.609	0.511	0.602	0.607	0.598	0.560	0.605	0.594	0.604	0.600
$cr^{\#}$	0.382	0.401	0.393	0.377	0.396	0.388	0.388	0.390	0.388	0.383
X_{mt}	0.096	0.124	0.112	0.112	0.111	0.122	0.113	0.106	0.110	0.105
Fe^{2+}/Fe^{3+}	2.176	2.051	1.844	1.829	1.880	1.887	1.797	1.995	1.866	1.990

Sample	RE 286	RE 286	RE 286	RE 286	RE 286	RE 286	RE 286	RE 286	RE 286	RE 286
Olivine	26		7A	7B	15	18	22	32	39A	39B
SiO_2	39.42		38.91	38.84	38.07	38.74	38.70	38.65	38.49	38.68
Cr_2O_3	0.07		0.08	0.04	0.06	0.11	0.08	0.19	0.16	0.11
FeO	14.71		15.43	15.47	17.11	15.52	15.43	15.78	15.16	15.03
MnO	0.21		0.36	0.30	0.15	0.22	0.17	0.20	0.20	0.36
MgO	44.47		44.90	44.78	42.86	44.71	44.79	44.67	45.02	44.67
CaO	0.30		0.33	0.28	0.29	0.30	0.26	0.32	0.27	0.28
NiO	0.27		0.30	0.26	0.23	0.31	0.21	0.25	0.36	0.12
Sum	99.45		100.31	99.97	98.77	99.91	99.64	100.06	99.66	99.25
Fo	84.3		83.9	83.8	81.7	83.7	83.8	83.5	84.1	84.1
Spinel	26	25	7A	7B	15	18	22	32	39A	39B
SiO_2	0.59	0.09	0.12	0.10	0.13	0.09	0.11	0.07	0.12	0.09
TiO_2	1.01	1.04	1.04	2.80	2.71	3.92	0.98	0.90	1.15	1.04
Al_2O_3	30.17	29.96	32.58	28.59	19.01	23.05	29.49	29.42	28.50	29.96
Cr_2O_3	28.25	28.34	28.09	26.24	32.05	29.80	29.75	28.73	29.55	29.65
Fe_2O_3	9.11	9.98	10.40	11.36	14.27	12.00	11.06	11.08	11.31	10.75
FeO	16.61	16.20	15.75	17.19	23.45	18.94	16.66	16.95	15.72	16.49
MnO	0.24	0.22	0.21	0.20	0.31	0.08	0.00	0.23	0.15	0.12
MgO	13.92	13.71	15.02	14.14	8.94	13.25	14.00	13.29	14.32	14.17
NiO	0.25	0.19	0.17	0.24	0.26	0.20	0.17	0.18	0.01	0.17
ZnO	0.04	0.04	0.18	0.11	0.20	0.18	0.08	0.05	0.09	0.00
Sum	100.19	99.77	103.56	100.96	101.33	101.50	102.30	100.91	100.94	102.43
$Mg^{\#}$	0.599	0.601	0.630	0.595	0.405	0.555	0.600	0.583	0.619	0.605
$cr^{\#}$	0.386	0.388	0.366	0.381	0.531	0.464	0.404	0.396	0.410	0.399
X_{mt}	0.106	0.115	0.114	0.136	0.184	0.151	0.125	0.127	0.130	0.121
Fe^{2+}/Fe^{3+}	2.026	1.804	1.683	1.681	1.827	1.753	1.674	1.700	1.545	1.704

Sample	RE 286	RE 286	RE 286	RE 286	RE 286	RE 286	RE 286	RE 286	RE 286	RE 286
Olivine	39C	41A	41B	45	46	50	58	69	74	75A
SiO_2	38.00	38.61	38.61	38.99	38.38	39.43	37.73	38.96	37.64	38.61
Cr_2O_3	0.10	0.07	0.16	0.07	0.06	0.11	0.10	0.12	0.12	0.27
FeO	15.85	15.55	15.08	16.09	15.39	15.20	19.48	15.79	18.81	15.52
MnO	0.11	0.31	0.20	0.16	0.28	0.23	0.19	0.33	0.10	0.27
MgO	44.16	45.27	45.01	44.11	44.06	45.70	41.09	44.45	41.06	43.91
CaO	0.28	0.30	0.32	0.29	0.29	0.31	0.34	0.31	0.36	0.29
NiO	0.25	0.36	0.16	0.06	0.19	0.22	0.25	0.31	0.36	0.24
Sum	98.75	100.47	99.54	99.77	98.65	101.20	99.18	100.27	98.45	99.11
Fo	83.3	83.8	84.2	83.0	83.6	84.3	79.0	83.4	79.6	83.5
Spinel	39C	41A	41B	45	46	50	58	69	74	75A
SiO_2	0.10	0.06	0.08	0.06	0.11	0.04	0.12	0.69	0.05	0.06
TiO_2	0.93	0.97	1.00	2.08	1.24	0.94	2.65	0.92	0.94	1.03
Al_2O_3	28.05	29.90	29.00	22.50	28.37	29.34	18.00	22.92	29.71	29.15
Cr_2O_3	30.39	29.06	29.58	31.16	30.40	29.40	34.31	35.40	29.24	30.25
Fe_2O_3	11.46	11.18	11.74	12.87	11.43	11.19	12.65	8.24	10.40	10.69
FeO	16.50	16.02	15.63	20.92	16.21	15.64	22.85	20.08	18.28	17.60
MnO	0.20	0.18	0.12	0.31	0.12	0.19	0.14	0.28	0.15	0.18
MgO	13.51	14.24	14.25	10.51	14.24	14.14	9.24	10.80	12.68	13.23
NiO	0.22	0.13	0.28	0.17	0.20	0.26	0.20	0.16	0.17	0.25
ZnO	0.23	0.02	0.28	0.15	0.11	0.13	0.00	0.14	0.04	0.04
Sum	101.58	101.76	101.95	100.74	102.43	101.26	100.16	99.62	101.65	102.49
$Mg^{\#}$	0.593	0.613	0.619	0.473	0.610	0.617	0.419	0.489	0.553	0.573
$cr^{\#}$	0.421	0.395	0.406	0.482	0.418	0.402	0.561	0.509	0.398	0.410
X_{mt}	0.131	0.126	0.133	0.159	0.130	0.127	0.164	0.101	0.119	0.121
Fe^{2+}/Fe^{3+}	1.599	1.592	1.480	1.806	1.575	1.553	2.008	2.709	1.954	1.829

Sample	RE 286	RE 286	RE 286	RE 291	RE 291	RE 291	RE 291	RE 291	RE 291	RE 291
Olivine	75B	81	87	1	2	3	4	5	7	8
SiO_2	38.38	38.60	37.22	40.87	40.13	40.72	40.23	41.03	40.19	40.61
Cr_2O_3	0.03	0.12	0.08							
FeO	16.70	15.59	19.47	9.73	9.29	9.71	9.63	9.91	9.44	9.14
MnO	0.35	0.16	0.20							
MgO	42.94	44.69	40.73	49.06	48.71	49.04	49.04	48.92	48.18	48.98
CaO	0.30	0.27	0.37	0.33	0.33	0.37	0.33	0.34	0.36	0.33
NiO	0.23	0.16	0.31							
Sum	98.93	99.59	98.38	99.99	98.46	99.85	99.22	100.20	98.17	99.07
Fo	82.1	83.6	78.9	90.0	90.3	90.0	90.1	89.8	90.1	90.5
Spinel	75B	81	87	1	2	3	4	5	7	8
SiO_2	0.06	0.07	0.16	0.09	0.05	0.09	0.07	0.05	0.05	0.11
TiO_2	2.23	2.01	2.63	0.14	0.24	0.14	0.11	0.17	0.19	0.15
Al_2O_3	21.16	30.18	18.11	28.92	26.13	28.53	31.73	30.54	32.12	30.12
Cr_2O_3	32.64	25.91	33.51	39.32	41.40	38.01	35.30	36.76	34.55	37.92
Fe_2O_3	12.07	11.95	13.65	4.84	4.16	5.16	4.78	4.86	4.80	4.72
FeO	21.11	16.26	22.75	10.71	11.00	10.49	10.31	10.68	10.53	10.75
MnO	0.22	0.24	0.25	0.08	0.04	0.16	0.09	0.05	0.00	0.28
MgO	10.22	14.50	9.33	17.16	16.39	16.87	17.37	17.20	17.30	17.13
NiO	0.15	0.23	0.15	0.24	0.15	0.14	0.20	0.12	0.22	0.24
ZnO	0.25	0.11	0.09							
Sum	100.11	101.47	100.64	101.49	99.56	99.59	99.96	100.43	99.76	101.42
$Mg^{\#}$	0.463	0.614	0.422	0.741	0.726	0.741	0.750	0.742	0.745	0.740
$cr^{\#}$	0.509	0.365	0.554	0.477	0.515	0.472	0.427	0.447	0.419	0.458
X_{mt}	0.152	0.138	0.177	0.053	0.047	0.057	0.052	0.053	0.052	0.051
Fe^{2+}/Fe^{3+}	1.944	1.513	1.853	2.458	2.944	2.260	2.400	2.443	2.441	2.532

Sample	RE 291	RE 291	RE 291	RE 291	RE 291	RE 291	RE 291	RE 291	RE 291	RE 291
Olivine	9	10	11	12	34	44	47	51	65	75
SiO_2	40.11	40.41	40.61	40.36	40.57	40.75	41.25	40.70	41.03	40.41
Cr_2O_3			0.13	0.15	0.13	0.10	0.07	0.07	0.11	0.12
FeO	9.71	9.91	10.24	10.03	9.66	10.01	9.86	9.81	9.57	9.82
MnO			0.16	0.13	0.17	0.06	0.19	0.10	0.16	0.20
MgO	48.60	48.65	49.12	49.37	49.29	49.06	49.52	49.13	49.15	48.85
CaO	0.35	0.36	0.34	0.37	0.34	0.37	0.38	0.36	0.35	0.32
NiO			0.25	0.32	0.34	0.33	0.34	0.31	0.28	0.30
Sum	98.77	99.33	100.86	100.73	100.50	100.67	101.62	100.48	100.65	100.02
Fo	89.9	89.7	89.5	89.8	90.1	89.7	90.0	89.9	90.1	89.9
Spinel	9	10	11 9	12	34	44	47B	51	65	75
SiO_2	0.09	0.11	0.13	0.15	0.31	0.09	0.09	0.51	0.12	0.11
TiO_2	0.16	0.10	0.14	0.17	0.22	0.14	0.20	0.20	0.16	0.19
Al_2O_3	25.73	32.86	32.28	29.10	29.84	30.72	26.19	30.79	30.41	31.71
Cr_2O_3	40.92	33.54	33.30	38.00	33.61	35.44	41.28	35.75	36.30	35.79
Fe_2O_3	4.89	4.73	3.25	4.05	3.52	4.03	3.88	3.70	4.82	3.80
FeO	10.97	10.10	13.24	10.74	10.98	10.94	10.76	10.87	10.04	10.51
MnO	0.18	0.13	0.15	0.16	0.09	0.12	0.11	0.25	0.19	0.16
MgO	16.16	17.48	15.05	16.73	15.83	16.48	16.35	16.98	17.24	17.18
NiO	0.22	0.20	0.24	0.24	0.24	0.20	0.14	0.34	0.33	0.25
ZnO			0.07	0.00	0.13	0.06	0.15	0.14	0.06	0.04
Sum	99.32	99.24	97.85	99.34	94.76	98.21	99.15	99.52	99.66	99.74
$Mg^{\#}$	0.724	0.755	0.670	0.735	0.720	0.729	0.730	0.736	0.754	0.744
$cr^{\#}$	0.516	0.406	0.409	0.467	0.430	0.436	0.514	0.438	0.445	0.431
X_{mt}	0.055	0.052	0.037	0.045	0.041	0.045	0.044	0.041	0.053	0.042
Fe_{2+}/Fe^{3+}	2.496	2.373	4.532	2.950	3.469	3.017	3.085	3.269	2.315	3.079

Sample	RE 291	RE 291	RE 291	RE 291	RE 291	RE 291	RE 291	RE 291	RE 291	RE 291
Olivine	75B	75C	76	76B	84	90		93	93B	94
SiO_2	41.11	40.54	40.47	40.83	40.49	40.61		40.34	40.68	40.51
Cr_2O_3	0.07	0.14	0.24	0.08	0.11	0.20		0.16	0.07	0.11
FeO	9.68	9.68	12.93	9.76	9.64	10.15		9.75	9.49	9.42
MnO	0.19	0.10	0.18	0.19	0.19	0.15		0.11	0.14	0.15
MgO	49.01	49.07	46.30	49.03	49.28	49.04		48.98	48.97	49.22
CaO	0.34	0.37	0.48	0.32	0.33	0.34		0.36	0.34	0.36
NiO	0.36	0.32	0.25	0.30	0.39	0.35		0.32	0.30	0.31
Sum	100.75	100.22	100.85	100.51	100.43	100.84		100.02	99.99	100.09
Fo	90.0	90.0	86.5	89.9	90.1	89.6		90.0	90.2	90.3
Spinel	75B	75C	76	76B	84	90	92	93	93B	94
SiO_2	0.11	0.03	0.05	0.10	0.50	0.10	0.13	0.12	0.13	0.19
TiO_2	0.10	0.15	0.20	0.23	0.26	0.25	0.20	0.15	0.15	0.09
Al_2O_3	31.33	32.43	30.15	32.52	30.44	32.47	30.63	31.84	32.10	32.66
Cr_2O_3	34.93	34.96	36.36	33.83	34.46	34.25	35.80	35.31	33.84	33.36
Fe_2O_3	4.68	3.61	4.73	4.53	3.25	3.82	4.52	3.91	4.29	4.63
FeO	10.22	10.83	10.15	10.26	14.27	10.78	10.53	10.91	10.35	9.85
MnO	0.13	0.08	0.15	0.08	0.13	0.15	0.05	0.08	0.18	0.09
MgO	17.11	16.94	17.07	17.43	14.71	17.01	17.02	16.93	17.06	17.54
NiO	0.17	0.24	0.25	0.19	0.14	0.23	0.30	0.19	0.16	0.26
ZnO	0.14	0.00	0.08	0.00	0.12	0.00	0.00	0.10	0.03	0.03
Sum	98.92	99.27	99.18	99.17	98.29	99.06	99.18	99.54	98.29	98.70
$Mg^{\#}$	0.749	0.736	0.750	0.752	0.648	0.738	0.742	0.734	0.746	0.760
$cr^{\#}$	0.428	0.420	0.447	0.411	0.432	0.414	0.439	0.427	0.414	0.407
X_{mt}	0.052	0.040	0.052	0.050	0.037	0.042	0.050	0.043	0.048	0.051
Fe^{2+}/Fe^{3+}	2.425	3.336	2.386	2.518	4.875	3.135	2.589	3.101	2.683	2.363

Sample	RE 291	RE 291	RE 291	RE 291	RE 291	RE 291	RE 291	RE 291	RE 291	RE 291
Olivine	102	111	111B	117	120	120B	134	134B	134C	137
SiO_2	40.57	40.41	40.58	41.02	40.42	40.32	41.15	40.24	40.42	40.55
Cr_2O_3	0.07	0.12	0.13	0.09	0.06	0.18	0.16	0.14	0.16	0.07
FeO	10.07	9.45	9.55	10.20	9.92	10.84	10.22	10.58	10.00	9.59
MnO	0.24	0.21	0.17	0.15	0.18	0.11	0.19	0.19	0.14	0.09
MgO	48.85	48.82	49.15	49.60	48.85	48.26	49.56	48.22	48.87	49.34
CaO	0.36	0.35	0.33	0.35	0.37	0.34	0.36	0.34	0.36	0.35
NiO	0.32	0.44	0.34	0.37	0.29	0.27	0.30	0.31	0.28	0.27
Sum	100.48	99.79	100.24	101.79	100.09	100.32	101.93	100.03	100.22	100.26
Fo	89.6	90.2	90.2	89.7	89.8	88.8	89.6	89.0	89.7	90.2
Spinel	102	111	111B	117	120	120B	134	134B	134C	137
SiO_2	0.10	0.12	0.23	0.10	0.12	0.08	0.09	0.11	0.08	0.12
TiO_2	0.16	0.18	0.15	0.16	0.16	0.12	0.19	0.20	0.16	0.12
Al_2O_3	31.77	30.79	31.60	30.83	33.10	33.70	26.31	26.42	26.24	33.55
Cr_2O_3	34.09	36.00	34.86	34.78	34.01	32.63	40.37	41.10	40.19	32.65
Fe_2O_3	3.81	4.30	4.80	4.29	4.12	4.61	4.75	4.45	4.98	4.71
FeO	10.83	10.04	10.14	11.06	10.36	10.46	10.86	11.81	10.77	9.77
MnO	0.09	0.10	0.16	0.14	0.13	0.02	0.24	0.19	0.13	0.09
MgO	16.60	17.26	17.48	16.40	17.44	17.36	16.14	15.86	16.27	17.72
NiO	0.24	0.25	0.23	0.19	0.16	0.20	0.30	0.27	0.23	0.19
ZnO	0.00	0.12	0.04	0.01	0.11	0.04	0.17	0.16	0.09	0.07
Sum	97.69	99.16	99.69	97.96	99.71	99.21	99.43	100.57	99.14	98.99
$Mg^{\#}$	0.732	0.754	0.754	0.726	0.750	0.747	0.726	0.705	0.729	0.764
$cr^{\#}$	0.419	0.440	0.425	0.431	0.408	0.394	0.507	0.511	0.507	0.395
X_{mt}	0.043	0.048	0.053	0.048	0.045	0.050	0.054	0.050	0.056	0.051
Fe^{2+}/Fe^{3+}	3.156	2.595	2.349	2.860	2.790	2.523	2.542	2.947	2.404	2.306

Sample	RE 291	RE 291	RE 291	RE 291	RE 291	RE 291	RE 291	RE 291	RE 291	RE 291
Olivine	163	166	166B	184	191	193	210	210	210	252
SiO_2	40.85	40.50	40.66	40.94	40.67	40.55	40.68	40.68	40.68	40.62
Cr_2O_3	0.05	0.10	0.13	0.15	0.11	0.23	0.16	0.16	0.16	0.17
FeO	10.06	10.48	9.75	9.88	9.60	9.85	9.78	9.78	9.78	9.63
MnO	0.10	0.14	0.21	0.23	0.15	0.24	0.16	0.16	0.16	0.08
MgO	49.43	48.42	49.35	49.47	49.37	49.03	48.99	48.99	48.99	49.22
CaO	0.33	0.34	0.35	0.36	0.36	0.35	0.34	0.34	0.34	0.36
NiO	0.42	0.24	0.28	0.31	0.26	0.26	0.29	0.29	0.29	0.28
Sum	101.24	100.24	100.73	101.34	100.51	100.50	100.39	100.39	100.39	100.35
Fo	89.8	89.2	90.0	89.9	90.2	89.9	89.9	89.9	89.9	90.1
Spinel	163	166	166B	184	191	193	210/1	210/2	210/3	252
SiO_2	0.14	0.09	0.10	0.09	0.06	0.10	0.08	0.09	0.17	0.11
TiO_2	0.15	0.19	0.18	0.17	0.22	0.21	0.18	0.18	0.25	0.16
Al_2O_3	33.14	28.94	30.68	26.86	28.54	30.34	30.41	28.63	30.48	30.89
Cr_2O_3	33.11	38.27	35.84	40.71	38.53	36.58	36.92	38.54	37.37	36.83
Fe_2O_3	4.25	3.84	4.93	4.46	3.30	4.53	4.17	4.64	3.82	4.38
FeO	10.45	10.43	10.24	10.85	11.23	10.36	10.68	10.56	11.00	10.63
MnO	0.17	0.08	0.15	0.13	0.18	0.08	0.09	0.19	0.09	0.09
MgO	17.24	16.80	17.21	16.48	16.10	17.16	16.99	16.79	17.07	17.21
NiO	0.17	0.26	0.22	0.28	0.18	0.24	0.19	0.19	0.20	0.18
ZnO	0.00	0.07	0.07	0.08	0.07	0.07	0.03	0.17	0.00	0.14
Sum	98.82	98.96	99.61	100.11	98.41	99.67	99.74	99.98	100.45	100.62
$Mg^{\#}$	0.746	0.742	0.750	0.730	0.719	0.747	0.739	0.739	0.734	0.743
$cr^{\#}$	0.401	0.470	0.439	0.504	0.475	0.447	0.449	0.475	0.451	0.444
X_{mt}	0.047	0.043	0.054	0.050	0.037	0.050	0.046	0.052	0.042	0.048
Fe^{2+}/Fe^{3+}	2.737	3.021	2.308	2.703	3.781	2.542	2.851	2.529	3.201	2.698

Sample	RE 291	RE 291A	RE 291A	RE 291A	RE 291A	RE 291A	RE 291A	RE 291A	RE 291A	RE 291A
Olivine	261	1	2	4	6	19	20A	20B	20C	20D
SiO_2	40.70	40.53	40.81	40.54	40.72	40.57	40.26	40.36	40.25	40.09
Cr_2O_3	0.16	0.18	0.14	0.18	0.13	0.14	0.17	0.17	0.03	0.06
FeO	9.55	9.56	9.56	9.77	9.09	9.52	9.51	9.73	9.62	9.72
MnO	0.21	0.16	0.10	0.17	0.15	0.21	0.24	0.19	0.15	0.24
MgO	49.00	48.83	48.95	48.84	49.19	49.36	48.73	49.23	48.80	48.70
CaO	0.36	0.36	0.34	0.39	0.37	0.33	0.36	0.34	0.40	0.39
NiO	0.31	0.32	0.25	0.33	0.32	0.25	0.26	0.31	0.34	0.35
Sum	100.29	99.94	100.15	100.22	99.97	100.38	99.53	100.33	99.59	99.55
Fo	90.1	90.1	90.1	89.9	90.6	90.2	90.1	90.0	90.1	89.9
Spinel	261	1	2	4	6	19	20A	20B	20C	20D
SiO_2	0.11	0.13	0.08	0.10	0.14	0.11	0.12	0.13	0.11	0.08
TiO_2	0.12	0.11	0.20	0.24	0.14	0.13	0.12	0.12	0.15	0.10
Al_2O_3	27.98	31.08	30.68	27.08	33.91	30.32	31.99	32.38	32.33	32.00
Cr_2O_3	38.89	35.98	35.96	39.67	32.87	36.21	34.94	34.19	33.92	34.73
Fe_2O_3	4.71	5.52	5.07	5.00	5.04	5.56	5.36	5.20	5.59	5.26
FeO	10.69	10.36	10.19	10.76	9.24	9.81	10.00	9.81	9.81	9.75
MnO	0.18	0.08	0.09	0.09	0.13	0.00	0.21	0.09	0.10	0.16
MgO	16.61	17.44	17.32	16.66	18.35	17.62	17.67	17.74	17.80	17.65
NiO	0.22	0.26	0.17	0.21	0.20	0.27	0.22	0.32	0.21	0.24
ZnO	0.01	0.14	0.14	0.00	0.00	0.00	0.04	0.00	0.01	0.12
Sum	99.52	101.09	99.89	99.81	100.01	100.00	100.67	99.98	100.02	100.07
$Mg^{\#}$	0.735	0.750	0.752	0.734	0.780	0.762	0.759	0.763	0.764	0.763
$cr^{\#}$	0.483	0.437	0.440	0.496	0.394	0.445	0.423	0.415	0.413	0.421
X_{mt}	0.053	0.060	0.056	0.056	0.054	0.061	0.058	0.057	0.061	0.057
Fe^{2+}/Fe^{3+}	2.518	2.087	2.235	2.393	2.037	1.963	2.074	2.098	1.951	2.060

Sample	RE 291A	RE 291A	RE 291A	RE 291A	RE 291A	RE 291A	RE 291A	RE 291A	RE 291A	RE 291A
Olivine	20E	20F	23	24	26A	26B	31	32	42	46
SiO_2	40.38	40.44	40.50	40.41	40.38	39.64	40.44	40.75	40.45	40.72
Cr_2O_3	0.16	0.05	0.10	0.45	0.10	0.47	0.20	0.09	0.18	0.16
FeO	9.64	9.81	9.30	9.77	9.75	13.56	9.70	9.79	9.46	9.58
MnO	0.17	0.22	0.05	0.04	0.39	0.20	0.23	0.13	0.16	0.08
MgO	48.94	48.89	49.01	49.33	48.97	45.80	48.33	49.26	49.23	49.27
CaO	0.34	0.38	0.35	0.39	0.37	0.36	0.34	0.34	0.37	0.33
NiO	0.35	0.34	0.26	0.29	0.24	0.29	0.37	0.36	0.39	0.30
Sum	99.98	100.13	99.57	100.68	100.20	100.32	99.61	100.72	100.24	100.44
Fo	90.1	89.9	90.4	90.0	90.0	85.8	89.9	90.0	90.3	90.2
Spinel	20 E	20F	23	24	26A	26B	31	32	42	46
SiO_2	0.10	0.10	0.12	0.10	0.09	0.10	0.08	0.13	0.11	0.15
TiO_2	0.17	0.17	0.16	0.17	0.09	0.19	0.17	0.08	0.17	0.21
Al_2O_3	32.02	33.17	34.47	33.38	32.73	31.53	32.91	39.58	30.50	32.00
Cr_2O_3	34.43	33.01	33.06	33.75	34.22	35.11	34.46	26.68	36.67	34.75
Fe_2O_3	5.01	6.11	4.35	4.44	4.93	5.07	4.71	5.24	4.79	5.37
FeO	10.17	9.57	10.11	10.85	10.31	10.39	10.17	9.25	10.43	10.12
MnO	0.00	0.23	0.10	0.10	0.14	0.18	0.11	0.12	0.06	0.08
MgO	17.40	18.11	18.01	17.22	17.46	17.25	17.66	18.87	17.32	17.78
NiO	0.27	0.16	0.14	0.16	0.19	0.26	0.25	0.24	0.19	0.23
ZnO	0.22	0.04	0.00	0.24	0.09	0.11	0.11	0.09	0.00	0.00
Sum	99.78	100.67	100.51	100.40	100.23	100.18	100.62	100.26	100.23	100.67
$Mg^{\#}$	0.753	0.771	0.761	0.739	0.751	0.747	0.756	0.784	0.748	0.758
$cr^{\#}$	0.419	0.400	0.391	0.404	0.412	0.428	0.413	0.311	0.446	0.421
X_{mt}	0.055	0.066	0.047	0.048	0.053	0.056	0.051	0.055	0.053	0.058
Fe^{2+}/Fe^{3+}	2.256	1.740	2.581	2.715	2.324	2.278	2.398	1.962	2.419	2.095

Sample	RE 291A	RE 291A	RE 291A	RE 291A	RE 291A	RE 291A	RE 291A	RE 291A	RE 291A	RE 291A
Olivine	55	61	64	65	66	67	74	81	86	86B
SiO_2	40.61	40.58	40.59	40.51	40.45	40.34	40.50	39.13	40.33	40.17
Cr_2O_3	0.13	0.25	0.15	0.15	0.05	0.08	0.06	0.34	0.15	0.25
FeO	9.23	9.99	8.99	9.90	9.40	9.84	9.32	9.40	9.55	9.50
MnO	0.12	0.09	0.19	0.19	0.01	0.13	0.14	0.09	0.05	0.14
MgO	49.01	48.81	50.09	48.68	48.52	48.67	49.31	48.12	48.89	48.86
CaO	0.36	0.32	0.33	0.34	0.31	0.37	0.38	0.33	0.40	0.35
NiO	0.25	0.28	0.26	0.34	0.38	0.28	0.44	0.28	0.27	0.27
Sum	99.71	100.32	100.60	100.11	99.12	99.71	100.15	97.69	99.64	99.54
Fo	90.4	89.7	90.9	89.8	90.2	89.8	90.4	90.1	90.1	90.2
Spinel	55	61	64	65	66	67	74	81	86	86B
SiO_2	0.09	0.08	0.11	0.09	0.10	0.30	0.11	0.09	0.05	0.77
TiO_2	0.22	0.14	0.13	0.19	0.94	0.15	0.16	0.22	0.20	0.13
Al_2O_3	30.49	26.96	33.50	26.04	34.20	30.99	34.24	31.24	25.90	26.86
Cr_2O_3	36.20	39.20	33.24	40.99	30.87	33.45	32.33	35.79	41.60	39.60
Fe_2O_3	5.65	5.31	5.07	5.04	5.44	7.26	4.53	4.40	4.88	3.84
FeO	10.03	11.41	9.36	11.24	10.00	9.11	9.48	10.39	10.91	11.72
MnO	0.16	0.18	0.14	0.08	0.00	0.23	0.06	0.00	0.08	0.05
MgO	17.48	15.91	18.12	16.21	18.39	18.09	18.01	17.32	16.43	16.63
NiO	0.29	0.25	0.31	0.19	0.25	0.25	0.30	0.22	0.29	0.03
ZnO	0.14	0.19	0.00	0.17	0.03	0.07	0.06	0.05	0.02	0.00
Sum	100.73	99.62	99.97	100.22	100.21	99.88	99.26	99.72	100.35	99.62
$Mg^{\#}$	0.757	0.713	0.775	0.720	0.766	0.780	0.772	0.748	0.729	0.717
$cr^{\#}$	0.443	0.494	0.400	0.514	0.377	0.420	0.388	0.435	0.519	0.497
X_{mt}	0.062	0.060	0.055	0.057	0.059	0.080	0.049	0.048	0.055	0.044
Fe^{2+}/Fe^{3+}	1.971	2.386	2.052	2.478	2.044	1.394	2.329	2.623	2.487	3.387

Sample	RE 291A	RE 291A	RE 291A	RE 291A	RE 291A	RE 291A	RE 291A	RE 291A	RE 291A	RE 291A
Olivine	86C	90	91	92	94	96	100			
SiO_2	40.44	40.35	40.56	40.53	39.95	40.10	40.12			
Cr_2O_3	0.13	0.24	0.06	0.16	0.09	0.06	0.18			
FeO	9.35	9.80	9.14	9.63	9.59	9.58	10.89			
MnO	0.29	0.12	0.15	0.13	0.11	0.12	0.18			
MgO	49.10	48.52	49.12	48.62	48.71	48.67	47.70			
CaO	0.36	0.36	0.38	0.37	0.36	0.31	0.35			
NiO	0.37	0.24	0.32	0.39	0.34	0.16	0.38			
Sum	100.04	99.63	99.73	99.83	99.15	99.00	99.80			
Fo	90.3	89.8	90.5	90.0	90.0	90.0	88.6			
Spinel	86C	90	91	92	94	96	100	206 C	206 RIM	207
SiO_2	0.12	0.04	0.07	0.23	0.11	0.14	0.10	0.12	0.08	0.12
TiO_2	0.13	0.16	0.21	0.18	0.05	0.17	0.46	0.20	0.24	0.21
Al_2O_3	32.58	31.50	33.68	33.38	37.99	31.10	24.25	26.22	25.99	25.75
Cr_2O_3	33.82	35.63	32.99	31.80	28.84	35.69	42.06	40.35	39.79	40.55
Fe_2O_3	5.36	5.33	4.66	3.89	5.23	4.70	3.95	5.15	5.26	4.84
FeO	10.01	10.15	9.76	15.45	9.31	10.71	14.01	12.00	13.84	12.37
MnO	0.11	0.14	0.21	0.19	0.17	0.21	0.20	0.14	0.22	0.23
MgO	17.69	17.53	17.80	14.14	18.67	17.06	14.31	15.72	14.50	15.29
NiO	0.22	0.18	0.15	0.18	0.29	0.16	0.11	0.23	0.20	0.17
ZnO	0.00	0.12	0.13	0.18	0.08	0.05	0.00	0.14	0.00	0.15
Sum	100.03	100.76	99.65	99.60	100.72	99.99	99.44	100.26	100.11	99.67
$Mg^{\#}$	0.759	0.755	0.765	0.620	0.782	0.740	0.645	0.700	0.651	0.688
$cr^{\#}$	0.411	0.431	0.396	0.390	0.337	0.435	0.538	0.508	0.507	0.514
X_{mt}	0.058	0.058	0.051	0.043	0.055	0.052	0.046	0.058	0.060	0.055
Fe_{2+}/Fe^{3+}	2.078	2.116	2.330	4.415	1.977	2.535	3.935	2.587	2.926	2.843

Sample	RE 291A	RE 291A	RE 291A	RE 291A	RE 291A	RE 291A	RE 291A	RE 291A	RE 291A	RE 291A
Olivine										
SiO_2										
Cr_2O_3										
FeO										
MnO										
MgO										
CaO										
NiO										
Sum										
Fo										
Spinel	208	209	210	211	212	213	214	215	216	217
SiO_2	0.12	0.10	0.09	0.11	0.11	0.13	0.09	0.06	0.08	0.09
TiO_2	0.22	0.19	0.16	0.15	0.19	0.18	0.18	0.18	0.44	0.15
Al_2O_3	30.76	30.64	30.42	28.79	28.30	22.55	26.86	26.20	21.17	27.82
Cr_2O_3	35.70	35.83	36.18	37.39	38.86	44.66	40.26	41.03	43.74	38.96
Fe_2O_3	4.75	4.93	5.11	5.12	4.92	4.20	4.57	5.29	6.08	5.32
FeO	9.98	10.15	10.26	10.25	10.39	11.35	9.99	10.28	12.87	10.17
MnO	0.15	0.15	0.07	0.22	0.19	0.12	0.10	0.18	0.18	0.14
MgO	17.43	17.22	17.30	16.93	16.91	15.62	16.97	16.84	14.64	17.01
NiO	0.14	0.29	0.18	0.15	0.28	0.15	0.22	0.19	0.09	0.17
ZnO	0.04	0.05	0.00	0.00	0.16	0.08	0.00	0.05	0.10	0.10
Sum	99.28	99.55	99.76	99.09	100.29	99.02	99.22	100.28	99.40	99.92
$Mg^{\#}$	0.757	0.752	0.750	0.746	0.744	0.710	0.752	0.745	0.670	0.749
$cr^{\#}$	0.438	0.440	0.444	0.466	0.480	0.571	0.501	0.512	0.581	0.484
X_{mt}	0.053	0.054	0.056	0.057	0.055	0.049	0.051	0.059	0.071	0.059
Fe_{2+}/Fe^{3+}	2.333	2.288	2.229	2.227	2.346	3.004	2.431	2.162	2.351	2.125

Sample	RE 291A	RE 291A	RE 291A	RE 291A	RE 291A	RE 291A	RE 291A	RE 291A	RE 291A	RE 291A
Olivine										
SiO_2										
Cr_2O_3										
FeO										
MnO										
MgO										
CaO										
NiO										
Sum										
Fo										
Spinel	218	219	219 RIM	206 C	206	206	206	206	206	206
SiO_2	0.06	0.09	0.07	0.06	0.09	0.08	0.09	0.05	0.15	0.09
TiO_2	0.17	0.17	0.37	0.23	0.19	0.24	0.20	0.24	0.21	0.21
Al_2O_3	27.28	29.13	24.34	26.12	26.10	26.33	26.24	26.25	26.24	26.20
Cr_2O_3	39.55	37.52	42.04	39.85	40.21	40.01	40.11	39.95	40.10	39.99
Fe_2O_3	5.10	5.16	5.07	5.15	5.14	5.42	4.84	5.07	4.80	4.86
FeO	10.35	10.05	13.11	12.08	12.06	12.03	12.35	12.80	12.96	13.00
MnO	0.10	0.05	0.17	0.13	0.21	0.25	0.06	0.27	0.17	0.14
MgO	16.90	17.22	15.00	15.50	15.59	15.65	15.48	15.17	15.04	15.00
NiO	0.09	0.19	0.14	0.27	0.17	0.28	0.20	0.08	0.23	0.23
ZnO	0.00	0.14	0.00	0.02	0.05	0.09	0.00	0.01	0.18	0.03
Sum	99.58	99.71	100.31	99.40	99.80	100.37	99.56	99.89	100.07	99.75
$Mg^{\#}$	0.744	0.753	0.671	0.696	0.697	0.699	0.691	0.679	0.674	0.673
$cr^{\#}$	0.493	0.464	0.537	0.506	0.508	0.505	0.506	0.505	0.506	0.506
X_{mt}	0.057	0.057	0.058	0.059	0.058	0.061	0.055	0.058	0.054	0.055
Fe^{2+}/Fe^{3+}	2.256	2.165	2.874	2.606	2.606	2.465	2.833	2.803	3.003	2.970

Sample	RE 291A	RE 291A	RE 291A	SU 18II	SU 18II	SU 18II	SU 18II	SU 18II	SU 18II	SU 18II
Olivine				2	4	6	7	8	9	10
SiO_2				39.63	39.71	39.23	39.63	39.16	39.51	39.59
Cr_2O_3										
FeO				15.88	15.12	15.61	15.73	15.78	15.66	15.28
MnO										
MgO				43.35	44.42	43.64	44.00	43.53	43.58	44.52
CaO				0.31	0.26	0.32	0.29	0.31	0.31	0.28
NiO										
Sum				99.17	99.51	98.80	99.65	98.77	99.05	99.66
Fo				82.9	84.0	83.3	83.3	83.1	83.2	83.9
Spinel	206	206	206 RIM	2	4	6	7	8	9	10
SiO_2	0.08	0.09	0.07	0.07	0.03	0.10	0.43	0.07	0.06	0.07
TiO_2	0.24	0.25	0.22	1.99	1.82	1.98	1.98	2.01	1.81	1.17
Al_2O_3	26.06	25.88	25.89	21.53	20.45	21.84	19.88	21.88	21.29	25.73
Cr_2O_3	40.08	39.49	39.19	30.83	32.89	30.06	29.41	30.90	32.49	31.96
Fe_2O_3	4.52	4.73	5.40	14.11	13.41	13.59	11.42	14.41	12.20	11.42
FeO	13.52	13.61	13.72	21.52	19.11	20.64	18.88	19.34	20.60	17.28
MnO	0.17	0.21	0.20	0.17	0.03	0.22	0.16	0.25	0.11	0.19
MgO	14.56	14.32	14.31	10.08	11.21	10.38	10.35	11.52	10.33	12.85
NiO	0.31	0.17	0.30	0.19	0.22	0.15	0.15	0.17	0.13	0.28
ZnO	0.01	0.22	0.06							
Sum	99.54	98.95	99.34	100.48	99.17	98.96	92.66	100.54	99.01	100.94
$Mg^{\#}$	0.657	0.652	0.650	0.455	0.511	0.473	0.494	0.515	0.472	0.570
$cr^{\#}$	0.508	0.506	0.504	0.490	0.519	0.480	0.498	0.486	0.506	0.455
X_{mt}	0.052	0.055	0.062	0.176	0.168	0.171	0.155	0.178	0.153	0.134
Fe_{2+}/Fe^{3+}	3.328	3.198	2.825	1.695	1.584	1.688	1.837	1.492	1.877	1.682

Sample	SU 18II	SU 18II	SU 18II	SU 18II	SU 18II	SU 18II	SU 18II	SU 18II	SU 18II	SU 18II
Olivine	11	12	13		15	17	18	19	20	21
SiO_2	39.58	39.44	38.94		39.16	39.77	39.16	39.88	39.30	39.59
Cr_2O_3										
FeO	16.10	15.81	17.17		17.45	15.69	15.69	15.50	15.88	16.27
MnO										
MgO	44.30	43.65	42.54		42.69	43.79	43.23	44.32	43.88	43.11
CaO	0.27	0.31	0.31		0.31	0.29	0.30	0.29	0.34	0.31
NiO										
Sum	100.25	99.21	98.96		99.61	99.54	98.39	100.00	99.41	99.26
Fo	83.1	83.1	81.5		81.3	83.3	83.1	83.6	83.1	82.5
Spinel	11	12	13	14	15	17	18	19	20	21
SiO_2	0.08	0.05	0.07	0.08	0.08	0.05	0.11	0.10	0.13	0.06
TiO_2	1.84	1.51	2.48	2.94	2.04	2.18	1.93	2.45	1.67	2.39
Al_2O_3	22.06	23.35	19.56	19.46	20.94	21.68	20.92	21.01	20.41	20.44
Cr_2O_3	31.55	32.15	30.39	29.10	31.71	29.98	30.98	29.99	33.69	29.92
Fe_2O_3	13.22	11.52	14.84	14.08	13.63	14.29	13.11	14.02	13.43	14.38
FeO	19.03	18.27	22.35	22.72	22.22	19.44	20.86	22.57	19.29	22.17
MnO	0.13	0.12	0.17	0.20	0.20	0.32	0.17	0.17	0.14	0.30
MgO	11.58	11.84	9.38	9.05	9.71	11.23	10.04	9.58	11.25	9.48
NiO	0.11	0.18	0.22	0.23	0.01	0.14	0.09	0.12	0.19	0.09
ZnO										
Sum	99.59	98.98	99.46	97.86	100.54	99.31	98.21	100.02	100.20	99.23
$Mg^{\#}$	0.520	0.536	0.428	0.415	0.438	0.507	0.462	0.431	0.510	0.433
$cr^{\#}$	0.490	0.480	0.510	0.501	0.504	0.481	0.498	0.489	0.525	0.495
X_{mt}	0.163	0.141	0.192	0.187	0.171	0.179	0.167	0.179	0.166	0.185
Fe^{2+}/Fe^{3+}	1.599	1.763	1.674	1.794	1.812	1.512	1.769	1.789	1.596	1.713

Sample	SU 18II	SU 18II	SU 18II	SU 18II	SU 18II	SU 18II	SU 18II	SU 24	SU 24	SU 24
Olivine	22		26	27	28	29	30	1	2	3
SiO_2	39.31		39.65	39.92	39.73	39.97	39.30	39.81	39.84	39.41
Cr_2O_3										
FeO	15.67		15.08	16.28	15.63	13.24	15.95	13.98	14.89	16.15
MnO										
MgO	43.63		44.42	43.94	43.23	45.95	42.87	45.31	44.42	42.99
CaO	0.33		0.29	0.32	0.29	0.29	0.32	0.25	0.26	0.30
NiO										
Sum	98.94		99.44	100.46	98.88	99.45	98.44	99.34	99.41	98.85
Fo	83.2		84.0	82.8	83.1	86.1	82.7	85.2	84.2	82.6
Spinel	22	24	26	27	28	29	30	1	2	3
SiO_2	0.07	0.18	0.10	0.07	0.08	0.10	0.07	0.07	0.12	0.06
TiO_2	2.02	3.34	1.15	1.77	1.59	0.99	1.91	1.05	0.98	1.86
Al_2O_3	20.86	18.49	26.37	20.97	20.68	27.19	20.77	28.63	28.09	21.93
Cr_2O_3	30.07	28.93	32.34	31.56	35.12	33.74	32.45	30.20	29.43	30.55
Fe_2O_3	13.93	15.20	10.56	13.72	12.25	8.56	13.41	9.95	11.11	13.72
FeO	21.15	22.74	16.88	18.66	19.80	15.05	21.79	15.05	15.58	17.93
MnO	0.27	0.11	0.22	0.05	0.15	0.16	0.20	0.15	0.17	0.18
MgO	9.81	9.47	13.27	11.46	11.07	14.37	9.76	14.38	13.89	11.97
NiO	0.07	0.26	0.18	0.08	0.05	0.16	0.23	0.15	0.25	0.11
ZnO										
Sum	98.26	98.72	101.07	98.34	100.80	100.32	100.59	99.64	99.62	98.30
$Mg^{\#}$	0.453	0.426	0.584	0.523	0.499	0.630	0.444	0.630	0.614	0.543
$cr^{\#}$	0.492	0.512	0.451	0.502	0.533	0.454	0.512	0.414	0.413	0.483
X_{mt}	0.178	0.204	0.123	0.172	0.150	0.099	0.168	0.115	0.129	0.171
Fe^{2+}/Fe^{3+}	1.687	1.662	1.777	1.512	1.796	1.953	1.805	1.681	1.558	1.453

Sample	SU 24	SU 24	SU 24	SU 24	SU 24	SU 24	SU 24
Olivine	4	5	6	7	8	9	10
SiO_2	39.60	39.71	39.38	39.36	39.50	39.42	39.25
Cr_2O_3							
FeO	16.25	16.15	16.88	15.49	16.10	16.49	16.30
MnO							
MgO	43.14	43.53	42.98	43.77	43.47	43.35	42.91
CaO	0.31	0.32	0.33	0.29	0.32	0.29	0.28
NiO							
Sum	99.30	99.73	99.56	98.92	99.39	99.56	98.74
Fo	82.6	82.8	81.9	83.4	82.8	82.4	82.4
Spinel	4	5	6	7	8	9	10
SiO_2	0.05	0.15	0.06	0.09	0.06	0.10	0.07
TiO_2	1.40	2.55	2.27	1.46	1.88	1.96	1.87
Al_2O_3	24.85	20.70	23.03	23.85	23.44	22.89	25.02
Cr_2O_3	29.99	29.57	26.17	30.79	30.01	28.23	27.51
Fe_2O_3	13.18	14.44	16.56	13.21	13.46	15.01	14.35
FeO	18.08	22.90	19.71	17.81	18.27	18.77	18.48
MnO	0.10	0.17	0.14	0.25	0.19	0.17	0.26
MgO	12.26	9.45	11.37	12.25	12.20	11.68	12.21
NiO	0.22	0.09	0.16	0.25	0.08	0.24	0.12
ZnO							
Sum	100.13	100.02	99.47	99.96	99.59	99.04	99.89
$Mg^{\#}$	0.547	0.424	0.507	0.551	0.544	0.526	0.541
$cr^{\#}$	0.447	0.489	0.433	0.464	0.462	0.453	0.424
X_{mt}	0.158	0.185	0.207	0.159	0.165	0.186	0.174
Fe^{2+}/Fe^{3+}	1.525	1.763	1.323	1.498	1.508	1.390	1.431

Appendix 5

Minor elements in olivine

Station 108, Hunter Ridge

Sample	108/7	108/7	108/7	108/7	108/7	108/7	108/7	108/7	108/7	108/7	108/7
Olivine	1	2	3	4	5	6	7	8	10	11	12
SiO_2	40.04	41.18	41.16	41.20	40.79	41.31	40.85	39.87	41.09	40.64	39.85
Cr_2O_3	0.011	0.107	0.137	0.129	0.077	0.121	0.046	0.028	0.101	0.060	0.006
FeO	14.23	8.05	7.25	7.44	9.39	7.66	11.50	12.06	7.78	10.57	14.49
MnO	0.259	0.146	0.139	0.140	0.182	0.151	0.218	0.225	0.157	0.195	0.276
MgO	45.99	50.78	51.21	51.05	49.36	50.88	47.34	47.12	50.69	47.83	45.32
CaO	0.169	0.190	0.180	0.165	0.223	0.193	0.171	0.183	0.201	0.194	0.149
NiO	0.194	0.313	0.403	0.404	0.244	0.379	0.229	0.189	0.416	0.234	0.114
Sum	100.89	100.77	100.48	100.53	100.27	100.69	100.35	99.67	100.43	99.72	100.21
Fo	85.2	91.8	92.6	92.4	90.4	92.2	88.0	87.5	92.1	89.0	84.8

Sample	108/7	108/7	108/7	108/7	108/7	108/7	108/7	108/7	108/7	108/7	108/7
Olivine	13	14	20	22	23	27	28	29	35	38	41
SiO_2	40.91	40.14	39.82	40.55	40.61	40.16	40.09	40.70	40.35	40.81	40.31
Cr_2O_3	0.077	0.039	0.004	0.115	0.087	0.027	0.067	0.094	0.049	0.108	0.053
FeO	8.87	11.87	14.21	9.04	10.54	12.95	11.33	9.59	11.35	8.88	11.22
MnO	0.181	0.218	0.276	0.176	0.199	0.262	0.217	0.184	0.220	0.156	0.212
MgO	49.82	47.07	45.07	49.17	48.14	46.18	47.23	49.14	47.59	49.67	47.93
CaO	0.220	0.194	0.162	0.218	0.214	0.160	0.207	0.215	0.219	0.165	0.178
NiO	0.205	0.198	0.145	0.220	0.247	0.194	0.211	0.292	0.199	0.377	0.228
Sum	100.28	99.73	99.69	99.49	100.04	99.93	99.35	100.21	99.98	100.17	100.13
Fo	90.9	87.6	85.0	90.7	89.1	86.4	88.1	90.2	88.2	90.9	88.4

Sample	108/7	108/7	108/7	108/7	108/7	108/7	108/7	108/7	108/7	108/7	108/7
Olivine	42	45	47	54	55	56	59	70	75	87	118
SiO_2	40.53	41.31	40.95	40.62	40.00	39.98	40.15	40.18	40.39	39.82	39.55
Cr_2O_3	0.117	0.167	0.114	0.068	0.028	0.025	0.048	0.021	0.102	0.011	0.027
FeO	9.82	7.66	7.60	10.07	12.72	13.02	11.67	12.18	9.93	13.99	14.80
MnO	0.182	0.142	0.145	0.187	0.242	0.237	0.241	0.236	0.189	0.251	0.290
MgO	49.25	50.80	50.80	48.89	46.45	45.85	47.13	46.50	48.79	45.59	45.01
CaO	0.202	0.186	0.172	0.198	0.171	0.167	0.160	0.168	0.216	0.180	0.171
NiO	0.295	0.386	0.342	0.252	0.184	0.219	0.248	0.182	0.237	0.176	0.134
Sum	100.40	100.65	100.12	100.29	99.80	99.50	99.65	99.47	99.85	100.02	99.98
Fo	89.9	92.2	92.3	89.6	86.7	86.3	87.8	87.2	89.7	85.3	84.4

Iceland

Sample	NO 42	NO 42	NO 42	NO 42	NO 42	NO 42	NO 42	NO 42	NO 42	NO 42	NO 42
Olivine	11	12	13	14	15	16	17	18	19	20	21
SiO_2	40.83	40.92	40.47	40.58	40.55	40.76	40.40	41.20	40.54	40.26	40.81
Cr_2O_3	0.126	0.151	0.039	0.072	0.035	0.156	0.026	0.148	0.083	0.038	0.167
FeO	9.28	7.89	10.65	9.86	10.10	8.31	11.29	7.88	10.22	10.95	8.50
MnO	0.177	0.150	0.203	0.182	0.195	0.155	0.214	0.151	0.194	0.207	0.156
MgO	49.38	50.03	48.06	48.74	48.87	49.61	47.25	50.25	48.10	47.85	49.55
CaO	0.339	0.369	0.334	0.368	0.402	0.484	0.327	0.367	0.341	0.333	0.386
NiO	0.279	0.380	0.279	0.299	0.244	0.344	0.256	0.375	0.279	0.271	0.294
Sum	100.41	99.89	100.04	100.10	100.40	99.82	99.76	100.37	99.76	99.91	99.86
Fo	90.5	91.9	88.9	89.8	89.6	91.4	88.2	91.9	89.3	88.6	91.2

Sample	NO 42	NO 42	NO 42	NO 42	NO 42	NO 42	NO 42	NO 42	NO 42	NO 42	NO 42
Olivine	22	23	24	25	26	27	28	29	30	31	32
SiO_2	41.02	40.96	40.79	40.95	40.92	40.90	40.45	40.77	40.99	40.93	41.03
Cr_2O_3	0.137	0.156	0.127	0.140	0.145	0.142	0.022	0.136	0.152	0.199	0.146
FeO	8.43	7.91	9.22	7.93	8.36	7.85	10.67	9.13	8.41	7.88	8.09
MnO	0.167	0.146	0.179	0.147	0.155	0.147	0.210	0.173	0.152	0.137	0.154
MgO	49.72	50.52	49.23	50.44	49.85	50.56	47.81	49.22	50.15	50.58	49.93
CaO	0.367	0.357	0.334	0.361	0.374	0.354	0.341	0.339	0.360	0.358	0.368
NiO	0.296	0.281	0.284	0.382	0.267	0.286	0.248	0.280	0.243	0.282	0.369
Sum	100.14	100.33	100.16	100.35	100.07	100.24	99.75	100.05	100.46	100.37	100.09
Fo	91.3	91.9	90.5	91.9	91.4	92.0	88.8	90.6	91.4	92.0	91.7

Sample	NO 42	NO 42	NO 42	NO 58	NO 58	NO 58	NO 58	NO 58	NO 58	NO 58	NO 58
Olivine	33	167	196	1	2	3	4	5	7	8	9
SiO_2	40.81	40.46	40.57	40.45	40.58	40.61	40.47	40.40	40.39	40.31	40.43
Cr_2O_3	0.064	0.026	0.026	0.061	0.057	0.003	0.069	0.060	0.050	0.060	0.060
FeO	9.00	11.37	11.33	9.99	9.88	9.88	10.10	9.94	11.10	9.93	11.34
MnO	0.176	0.213	0.212	0.183	0.177	0.199	0.187	0.189	0.221	0.192	0.214
MgO	49.07	47.36	47.26	48.23	48.53	48.24	48.00	48.14	47.59	48.36	47.38
CaO	0.390	0.322	0.323	0.332	0.344	0.273	0.399	0.344	0.343	0.346	0.337
NiO	0.314	0.253	0.282	0.286	0.291	0.010	0.290	0.293	0.265	0.286	0.293
Sum	99.82	100.00	100.00	99.53	99.86	99.22	99.52	99.37	99.96	99.48	100.05
Fo	90.7	88.1	88.2	89.6	89.8	89.7	89.4	89.6	88.5	89.7	88.2

Sample	NO 58	NO 58	NO 58	NO 58	NO 58	NO 58	NO 58	NO 58	NO 58	NO 58	NO 58
Olivine	10	11	12	13	14	15	16	17	18	19	20
SiO_2	40.39	40.34	40.39	40.35	40.02	40.46	40.41	40.61	40.58	40.21	40.60
Cr_2O_3	0.054	0.064	0.053	0.056	0.041	0.042	0.041	0.037	0.045	0.054	0.050
FeO	10.16	9.98	9.96	10.35	10.60	10.22	10.68	9.94	10.12	11.28	10.21
MnO	0.186	0.189	0.185	0.186	0.208	0.198	0.180	0.189	0.187	0.214	0.190
MgO	48.78	48.77	48.49	47.92	47.92	48.73	48.20	48.89	49.04	46.84	48.86
CaO	0.336	0.341	0.346	0.336	0.315	0.326	0.332	0.341	0.345	0.344	0.332
NiO	0.284	0.296	0.263	0.284	0.249	0.261	0.270	0.261	0.276	0.263	0.265
Sum	100.19	99.98	99.69	99.48	99.35	100.24	100.11	100.27	100.59	99.21	100.51
Fo	89.5	89.7	89.7	89.2	89.0	89.5	88.9	89.7	89.6	88.1	89.5

Sample	NO 58	NO 58	NO 58	NO 58	NO 58	NO 58	RE 36	RE 36	RE 36	RE 36	RE 36
Olivine	21	22	23	24	25	26	1	2	3	4	5
SiO_2	39.66	40.58	40.39	40.53	40.38	39.81	40.43	40.78	40.66	40.58	40.56
Cr_2O_3	0.009	0.060	0.038	0.057	0.070	0.076	0.083	0.067	0.073	0.060	0.053
FeO	13.61	10.02	10.73	10.00	10.09	11.64	9.76	9.69	9.19	9.33	10.21
MnO	0.261	0.192	0.203	0.189	0.189	0.214	0.189	0.176	0.179	0.179	0.209
MgO	45.38	48.40	47.55	48.47	48.27	46.84	48.89	49.50	49.08	49.24	48.04
CaO	0.313	0.339	0.319	0.347	0.347	0.365	0.400	0.383	0.381	0.369	0.381
NiO	0.155	0.286	0.261	0.285	0.284	0.272	0.298	0.337	0.326	0.323	0.284
Sum	99.39	99.88	99.49	99.88	99.63	99.22	100.05	100.93	99.89	100.08	99.74
Fo	85.6	89.6	88.8	89.6	89.5	87.8	89.9	90.1	90.5	90.4	89.3

Sample	RE 36	RE 36	RE 36	RE 36	RE 36	RE 36	RE 36	RE 36	RE 36	RE 36	RE 36
Olivine	6	7	8	9	10	11	12	13	14	15	16
SiO_2	40.32	40.34	40.48	40.48	40.55	40.68	40.24	40.61	40.42	40.83	40.62
Cr_2O_3	0.063	0.056	0.073	0.067	0.088	0.057	0.072	0.032	0.060	0.088	0.092
FeO	9.62	11.40	9.18	9.89	8.98	9.36	9.64	9.77	10.00	9.59	9.53
MnO	0.187	0.230	0.177	0.198	0.177	0.192	0.189	0.190	0.195	0.186	0.194
MgO	48.96	47.44	48.81	48.68	49.30	49.10	48.60	48.77	48.50	48.86	48.72
CaO	0.305	0.348	0.386	0.406	0.382	0.388	0.406	0.390	0.371	0.381	0.376
NiO	0.317	0.262	0.327	0.305	0.331	0.307	0.303	0.233	0.279	0.323	0.328
Sum	99.77	100.08	99.43	100.03	99.81	100.08	99.45	100.00	99.83	100.26	99.86
Fo	90.1	88.1	90.5	89.8	90.7	90.3	90.0	89.9	89.6	90.1	90.1

Sample	RE 36	RE 36	RE 36	RE 36	RE 36	RE 36	RE 36	RE 36	RE 36	RE 78	RE 78
Olivine	17	18	19	20	21	22	23	24	25	1	2
SiO_2	40.56	40.06	40.55	40.50	40.59	40.45	40.34	40.55	40.58	40.35	40.69
Cr_2O_3	0.115	0.060	0.072	0.107	0.070	0.072	0.064	0.070	0.060	0.045	0.064
FeO	9.51	12.01	9.13	9.14	9.46	9.27	9.45	9.83	9.61	10.19	10.55
MnO	0.191	0.220	0.179	0.177	0.185	0.186	0.178	0.191	0.185	0.196	0.204
MgO	48.53	46.68	49.02	49.00	48.86	48.76	48.87	48.31	48.63	48.29	47.82
CaO	0.488	0.383	0.350	0.396	0.403	0.382	0.389	0.346	0.381	0.388	0.388
NiO	0.282	0.269	0.249	0.328	0.305	0.313	0.302	0.316	0.317	0.257	0.248
Sum	99.68	99.68	99.55	99.65	99.87	99.43	99.59	99.61	99.76	99.72	99.96
Fo	90.1	87.4	90.5	90.5	90.2	90.4	90.2	89.7	90.0	89.4	89.0

Sample	RE 78	RE 78	RE 78	RE 78	RE 78	RE 78	RE 78	RE 78	RE 78	RE 78	RE 78
Olivine	3	4	5	6	7	8	9	10	11	12	13
SiO_2	40.27	40.67	40.53	40.60	40.42	40.43	40.59	40.54	40.59	40.45	40.61
Cr_2O_3	0.044	0.053	0.058	0.058	0.050	0.058	0.044	0.047	0.050	0.054	0.045
FeO	9.92	9.92	10.05	10.10	10.48	10.69	10.21	10.15	10.20	10.29	10.35
MnO	0.192	0.198	0.192	0.173	0.207	0.214	0.204	0.192	0.196	0.205	0.198
MgO	48.42	48.78	48.49	48.32	47.85	47.81	48.37	48.72	48.46	48.21	48.17
CaO	0.386	0.372	0.372	0.360	0.382	0.390	0.353	0.367	0.383	0.382	0.389
NiO	0.251	0.269	0.258	0.230	0.251	0.243	0.234	0.244	0.248	0.253	0.244
Sum	99.48	100.26	99.95	99.84	99.64	99.84	100.01	100.26	100.13	99.84	100.01
Fo	89.7	89.8	89.6	89.5	89.0	88.8	89.4	89.5	89.4	89.3	89.2

Sample	RE 78	RE 78	RE 78	RE 78	RE 78	RE 78	RE 78	RE 78	RE 78	RE 78	RE 78
Olivine	14	15	16	17	18	19	20	21	22	23	24
SiO_2	40.54	40.44	40.48	40.50	40.70	40.55	40.29	40.57	40.46	40.57	40.37
Cr_2O_3	0.051	0.054	0.048	0.063	0.045	0.045	0.050	0.054	0.045	0.047	0.056
FeO	10.06	10.69	10.29	10.18	10.00	9.97	12.24	9.94	10.05	9.90	10.08
MnO	0.199	0.204	0.198	0.201	0.199	0.196	0.239	0.203	0.191	0.186	0.198
MgO	48.71	48.11	48.79	48.33	48.86	48.72	46.82	48.78	48.99	49.18	48.75
CaO	0.389	0.381	0.376	0.392	0.374	0.390	0.378	0.383	0.378	0.369	0.390
NiO	0.252	0.244	0.248	0.238	0.260	0.256	0.275	0.262	0.270	0.260	0.248
Sum	100.20	100.12	100.43	99.90	100.44	100.13	100.29	100.19	100.38	100.51	100.09
Fo	89.6	88.9	89.4	89.4	89.7	89.7	87.2	89.7	89.7	89.9	89.6

Sample	RE 78	RE 120	RE 120	RE 120	RE 120	RE 120	RE 120	RE 120	RE 120	RE 120	RE 120
Olivine	25	1	2	3	4	5	6	7	8	9	10
SiO_2	40.35	40.39	40.60	40.21	40.37	40.35	40.19	39.90	40.10	40.53	40.31
Cr_2O_3	0.050	0.080	0.137	0.073	0.092	0.105	0.092	0.105	0.094	0.118	0.085
FeO	10.14	9.85	8.43	9.94	10.03	8.97	10.11	9.30	10.29	8.41	10.15
MnO	0.186	0.190	0.160	0.189	0.191	0.167	0.196	0.179	0.194	0.155	0.190
MgO	48.60	48.31	49.75	48.26	48.06	49.33	48.12	48.47	47.89	50.05	48.17
CaO	0.381	0.342	0.340	0.340	0.346	0.348	0.332	0.346	0.333	0.330	0.336
NiO	0.257	0.333	0.378	0.338	0.344	0.370	0.349	0.359	0.341	0.394	0.336
Sum	99.96	99.50	99.80	99.35	99.43	99.64	99.39	98.66	99.24	99.99	99.58
Fo	89.5	89.8	91.3	89.6	89.5	90.8	89.5	90.3	89.2	91.4	89.4

Sample	RE 120	RE 120	RE 120	RE 120	RE 120	RE 120	RE 120	RE 120	RE 120	RE 120	RE 120
Olivine	11	12	13	14	15	16	17	18	19	20	21
SiO_2	40.22	39.91	39.80	40.22	40.16	40.13	40.00	40.40	40.31	39.98	40.40
Cr_2O_3	0.082	0.076	0.077	0.098	0.080	0.082	0.088	0.064	0.096	0.107	0.145
FeO	10.07	10.47	10.22	10.04	10.04	10.02	9.83	11.01	9.76	9.90	7.93
MnO	0.194	0.192	0.195	0.192	0.189	0.192	0.194	0.200	0.189	0.195	0.151
MgO	48.17	47.51	47.42	48.02	48.17	48.31	48.06	47.71	48.53	48.30	49.89
CaO	0.344	0.330	0.323	0.341	0.334	0.339	0.343	0.333	0.340	0.343	0.340
NiO	0.337	0.349	0.338	0.330	0.355	0.341	0.350	0.326	0.345	0.345	0.400
Sum	99.42	98.84	98.37	99.24	99.33	99.41	98.87	100.04	99.57	99.17	99.26
Fo	89.5	89.0	89.2	89.5	89.5	89.6	89.7	88.6	89.9	89.7	91.8

Sample	RE 120	RE 120	RE 120	RE 120	RE 154	RE 154	RE 154	RE 154	RE 154	RE 154	RE 154
Olivine	22	23	24	25	1	2	3	4	5	6	7
SiO_2	40.13	40.30	40.23	39.66	40.27	40.62	40.64	40.09	40.40	40.16	39.67
Cr_2O_3	0.082	0.096	0.070	0.094	0.045	0.076	0.063	0.073	0.058	0.080	0.102
FeO	10.13	9.62	10.71	9.87	9.71	9.24	9.54	9.70	9.56	9.28	9.67
MnO	0.198	0.183	0.205	0.191	0.191	0.179	0.186	0.179	0.189	0.181	0.183
MgO	48.29	48.37	47.61	47.75	48.87	49.29	49.27	48.93	49.09	48.99	48.22
CaO	0.341	0.344	0.316	0.343	0.288	0.344	0.353	0.339	0.381	0.346	0.334
NiO	0.332	0.352	0.326	0.342	0.319	0.360	0.358	0.341	0.313	0.359	0.373
Sum	99.50	99.27	99.47	98.25	99.69	100.11	100.41	99.65	99.99	99.40	98.55
Fo	89.5	90.0	88.8	89.6	90.0	90.5	90.2	90.0	90.2	90.4	89.9

Sample	RE 154	RE 154	RE 154	RE 154	RE 154	RE 154	RE 154	RE 154	RE 154	RE 154	RE 154
Olivine	8	9	10	11	12	13	14	15	16	17	18
SiO_2	40.17	40.20	39.95	40.48	40.20	39.94	40.17	40.41	40.04	40.00	40.03
Cr_2O_3	0.044	0.095	0.079	0.083	0.089	0.034	0.089	0.079	0.066	0.088	0.089
FeO	10.73	9.40	9.71	9.47	10.18	9.13	9.99	9.62	12.11	9.66	9.37
MnO	0.209	0.173	0.187	0.189	0.200	0.192	0.189	0.185	0.241	0.186	0.181
MgO	47.88	49.00	48.64	49.05	48.63	48.94	48.56	48.85	46.97	48.59	48.56
CaO	0.257	0.325	0.357	0.337	0.341	0.280	0.341	0.340	0.361	0.343	0.337
NiO	0.277	0.360	0.337	0.346	0.349	0.345	0.352	0.341	0.284	0.327	0.342
Sum	99.57	99.55	99.26	99.96	99.99	98.86	99.69	99.83	100.07	99.19	98.91
Fo	88.8	90.3	89.9	90.3	89.5	90.5	89.7	90.1	87.4	90.0	90.3

Sample	RE 154	RE 154	RE 154	RE 154	RE 154	RE 154	RE 154	RE 154	RE 185	RE 185	RE 185
Olivine	19	20	21	22	23	24	25	46	1	2	3
SiO_2	40.16	40.30	40.16	40.35	40.42	40.48	40.27	40.11	40.67	40.26	40.53
Cr_2O_3	0.072	0.056	0.073	0.023	0.066	0.082	0.072	0.082	0.098	0.058	0.098
FeO	10.62	9.93	9.45	10.29	9.15	9.03	10.34	9.26	8.94	9.83	8.61
MnO	0.191	0.200	0.194	0.213	0.192	0.177	0.167	0.173	0.170	0.190	0.156
MgO	47.62	48.31	49.04	48.33	49.15	49.45	48.30	48.96	49.55	48.71	49.89
CaO	0.341	0.350	0.350	0.276	0.350	0.339	0.323	0.350	0.339	0.375	0.346
NiO	0.335	0.307	0.336	0.333	0.323	0.351	0.361	0.358	0.346	0.288	0.354
Sum	99.34	99.45	99.60	99.82	99.65	99.91	99.83	99.29	100.11	99.71	99.98
Fo	88.9	89.7	90.2	89.3	90.6	90.7	89.3	90.4	90.8	89.8	91.2

Sample	RE 185	RE 185	RE 185	RE 185	RE 185	RE 185	RE 185	RE 185	RE 185	RE 185	RE 185
Olivine	4	5	6	7	8	9	10	11	12	13	14
SiO_2	40.51	40.23	40.36	40.26	40.12	40.38	40.55	40.63	40.49	40.19	40.42
Cr_2O_3	0.056	0.066	0.083	0.069	0.056	0.079	0.070	0.099	0.077	0.057	0.073
FeO	9.87	9.71	9.60	10.24	10.29	9.16	9.86	8.58	9.42	10.01	9.71
MnO	0.183	0.182	0.177	0.201	0.195	0.173	0.186	0.161	0.177	0.182	0.190
MgO	48.96	48.85	49.08	48.05	48.35	49.64	48.74	49.93	49.29	48.61	49.04
CaO	0.367	0.379	0.354	0.386	0.378	0.369	0.381	0.350	0.355	0.392	0.374
NiO	0.302	0.296	0.317	0.285	0.272	0.303	0.295	0.349	0.322	0.288	0.294
Sum	100.25	99.71	99.97	99.49	99.66	100.10	100.08	100.10	100.13	99.73	100.10
Fo	89.9	90.0	90.1	89.3	89.3	90.6	89.8	91.2	90.3	89.6	90.0

Sample	RE 185	RE 185	RE 185	RE 185	RE 185	RE 185	RE 185	RE 185	RE 185	RE 185	RE 185
Olivine	15	16	17	18	19	20	21	22	23	24	25
SiO_2	39.95	40.00	40.51	40.28	40.63	40.52	40.11	40.39	40.57	39.92	40.19
Cr_2O_3	0.057	0.054	0.086	0.058	0.073	0.094	0.067	0.069	0.057	0.050	0.054
FeO	10.77	10.29	9.17	10.49	9.67	9.44	10.14	9.74	10.20	11.32	9.86
MnO	0.201	0.199	0.176	0.194	0.177	0.174	0.195	0.182	0.191	0.220	0.189
MgO	48.14	48.02	49.59	48.46	49.06	49.55	48.16	48.88	48.49	47.98	48.81
CaO	0.383	0.372	0.353	0.378	0.369	0.358	0.379	0.374	0.375	0.402	0.388
NiO	0.266	0.276	0.330	0.262	0.293	0.335	0.274	0.302	0.279	0.214	0.276
Sum	99.77	99.21	100.22	100.12	100.27	100.47	99.33	99.94	100.16	100.11	99.77
Fo	88.9	89.3	90.6	89.2	90.0	90.3	89.4	90.0	89.4	88.3	89.8

Sample	RE 217	RE 217	RE 217	RE 217	RE 217	RE 217	RE 217	RE 217	RE 217	RE 217	RE 217
Olivine	1	2	3	4	5	6	7	8	9	10	11
SiO_2	40.88	40.62	40.78	40.65	40.84	39.86	40.62	40.86	40.48	39.99	40.54
Cr_2O_3	0.083	0.089	0.076	0.076	0.073	0.026	0.076	0.072	0.064	0.057	0.047
FeO	9.42	9.70	9.37	9.20	9.71	13.65	9.22	9.43	9.63	11.96	9.33
MnO	0.183	0.183	0.183	0.177	0.187	0.275	0.176	0.183	0.187	0.210	0.187
MgO	49.38	48.85	48.99	49.02	49.03	45.20	49.08	49.08	48.27	46.53	48.71
CaO	0.336	0.339	0.339	0.336	0.341	0.180	0.337	0.337	0.348	0.350	0.315
NiO	0.356	0.350	0.349	0.344	0.345	0.241	0.360	0.351	0.340	0.276	0.330
Sum	100.64	100.13	100.09	99.80	100.53	99.43	99.87	100.31	99.32	99.37	99.46
Fo	90.3	90.0	90.3	90.5	90.0	85.5	90.5	90.3	89.9	87.4	90.3

Sample	RE 217	RE 217	RE 217	RE 217	RE 217	RE 217	RE 217	RE 217	RE 217	RE 217	RE 217
Olivine	12	13	14	15	16	17	18	19	20	21	22
SiO_2	40.34	40.64	40.61	40.68	40.63	40.66	40.55	40.56	40.67	40.55	40.56
Cr_2O_3	0.064	0.067	0.079	0.083	0.066	0.072	0.070	0.067	0.070	0.070	0.073
FeO	10.22	9.40	9.75	9.92	9.52	9.51	9.66	9.67	9.46	9.64	9.45
MnO	0.186	0.181	0.191	0.191	0.179	0.189	0.170	0.186	0.178	0.185	0.177
MgO	47.92	49.23	48.92	48.77	49.00	49.13	48.83	48.53	49.21	48.72	49.33
CaO	0.339	0.341	0.340	0.364	0.347	0.341	0.341	0.346	0.341	0.336	0.341
NiO	0.326	0.338	0.330	0.332	0.346	0.342	0.337	0.337	0.350	0.345	0.350
Sum	99.40	100.20	100.22	100.34	100.09	100.24	99.96	99.70	100.28	99.85	100.28
Fo	89.3	90.3	89.9	89.8	90.2	90.2	90.0	90.0	90.2	90.0	90.3

Sample	RE 217	RE 217	RE 217	RE 286	RE 286	RE 286	RE 286	RE 286	RE 286	RE 286	RE 286
Olivine	23	28	29	1	2	3	4	5	6	7	8
SiO_2	40.81	40.24	40.87	39.49	39.17	38.80	39.22	39.40	39.39	39.06	39.57
Cr_2O_3	0.069	0.069	0.102	0.036	0.040	0.042	0.031	0.045	0.039	0.039	0.032
FeO	9.27	9.59	8.94	15.10	15.03	14.74	14.94	14.80	14.79	15.14	15.11
MnO	0.178	0.186	0.169	0.279	0.269	0.270	0.265	0.269	0.267	0.275	0.267
MgO	49.25	48.67	49.36	44.55	44.58	44.33	44.78	44.79	44.64	44.20	45.09
CaO	0.340	0.339	0.319	0.308	0.305	0.299	0.294	0.306	0.299	0.301	0.311
NiO	0.352	0.342	0.389	0.259	0.253	0.247	0.247	0.249	0.252	0.237	0.242
Sum	100.27	99.44	100.15	100.02	99.65	98.73	99.78	99.86	99.68	99.25	100.62
Fo	90.5	90.1	90.8	84.0	84.1	84.3	84.3	84.4	84.3	83.9	84.2

Sample	RE 286	RE 286	RE 286	RE 286	RE 286	RE 286	RE 286	RE 286	RE 286	RE 286	RE 286
Olivine	9	11	13	14	15	16	17	18	19	20	21
SiO_2	39.22	39.34	39.43	39.19	39.13	39.41	39.57	39.23	39.03	39.19	39.34
Cr_2O_3	0.038	0.041	0.044	0.037	0.047	0.035	0.041	0.035	0.039	0.041	0.038
FeO	14.70	14.84	14.90	15.02	15.53	15.16	14.85	14.99	14.80	15.31	14.97
MnO	0.267	0.279	0.269	0.283	0.275	0.275	0.267	0.272	0.276	0.275	0.269
MgO	44.69	44.84	44.75	44.42	44.12	44.55	44.76	44.49	44.68	44.29	44.80
CaO	0.319	0.301	0.305	0.309	0.302	0.302	0.304	0.305	0.306	0.297	0.299
NiO	0.258	0.261	0.255	0.244	0.244	0.260	0.257	0.242	0.260	0.252	0.256
Sum	99.49	99.90	99.95	99.50	99.65	99.99	100.05	99.56	99.39	99.66	99.97
Fo	84.4	84.3	84.3	84.1	83.5	84.0	84.3	84.1	84.3	83.8	84.2

Sample	RE 286	RE 286	RE 286	RE 286	RE 286	RE 286	RE 286	RE 292	RE 292	RE 292	RE 292
Olivine	22	23	25	26	27	28	117	1	2	3	4
SiO_2	39.40	39.60	39.42	39.45	39.13	39.56	39.30	40.60	40.68	40.68	40.76
Cr_2O_3	0.038	0.041	0.039	0.037	0.035	0.048	0.038	0.066	0.073	0.057	0.067
FeO	14.88	14.92	14.90	14.91	15.61	14.94	15.20	9.74	9.53	10.35	9.52
MnO	0.269	0.280	0.275	0.275	0.279	0.283	0.283	0.186	0.176	0.203	0.178
MgO	45.09	44.78	44.89	44.92	44.18	44.74	44.34	49.04	49.09	48.52	49.35
CaO	0.304	0.302	0.306	0.308	0.301	0.339	0.301	0.350	0.354	0.309	0.360
NiO	0.248	0.265	0.256	0.251	0.258	0.253	0.242	0.319	0.319	0.270	0.310
Sum	100.23	100.19	100.09	100.15	99.79	100.16	99.70	100.30	100.22	100.39	100.55
Fo	84.4	84.3	84.3	84.3	83.4	84.2	83.9	90.0	90.2	89.3	90.2

Sample	RE 292	RE 292	RE 292	RE 292	RE 292	RE 292	RE 292	RE 292	RE 292	RE 292	RE 292
Olivine	5	6	7	18	19	20	21	22	23	24	25
SiO_2	40.68	40.86	40.84	40.92	40.69	40.72	40.74	40.88	40.84	40.88	40.83
Cr_2O_3	0.063	0.061	0.060	0.067	0.067	0.060	0.063	0.060	0.067	0.058	0.061
FeO	9.71	9.32	9.67	9.53	9.83	9.80	9.61	9.86	9.48	9.86	9.49
MnO	0.194	0.178	0.182	0.183	0.183	0.185	0.185	0.191	0.189	0.183	0.181
MgO	49.01	49.35	49.17	49.12	49.13	48.90	49.22	48.81	49.01	49.13	49.17
CaO	0.354	0.365	0.355	0.355	0.358	0.353	0.351	0.351	0.353	0.348	0.355
NiO	0.323	0.324	0.324	0.323	0.321	0.322	0.324	0.308	0.319	0.319	0.336
Sum	100.33	100.46	100.60	100.50	100.58	100.34	100.49	100.46	100.26	100.78	100.42
Fo	90.0	90.4	90.1	90.2	89.9	89.9	90.1	89.8	90.2	89.9	90.2

Sample	RE 292	RE 292	RE 292	RE 292	RE 292	RE 292	RE 292	RE 292	RE 292	RE 292	SU 18II
Olivine	26	27	28	29	30	31	32	33	34	35	1
SiO_2	40.48	40.94	40.91	40.82	40.81	40.70	40.73	40.76	40.76	40.83	39.67
Cr_2O_3	0.082	0.075	0.075	0.063	0.086	0.063	0.064	0.067	0.061	0.073	0.058
FeO	9.62	9.26	9.29	9.61	9.26	9.68	9.61	9.37	9.67	9.64	14.09
MnO	0.177	0.179	0.177	0.183	0.177	0.189	0.178	0.172	0.178	0.182	0.236
MgO	48.99	49.47	49.32	48.99	49.50	49.05	48.97	49.41	49.24	49.29	44.86
CaO	0.346	0.346	0.365	0.362	0.344	0.351	0.347	0.355	0.348	0.346	0.280
NiO	0.323	0.318	0.312	0.305	0.309	0.314	0.322	0.332	0.314	0.317	0.256
Sum	100.02	100.59	100.45	100.33	100.49	100.35	100.22	100.47	100.57	100.68	99.45
Fo	90.1	90.5	90.5	90.1	90.5	90.0	90.1	90.4	90.1	90.1	85.0

Sample	SU 18II	SU 18II	SU 18II	SU 18II	SU 18II	SU 18II	SU 18II	SU 18II	SU 18II	SU 18II	SU 18II
Olivine	2	3	4	5	6	7	8	9	10	11	12
SiO_2	39.63	39.44	39.33	39.27	39.67	39.36	39.19	39.06	39.17	39.33	39.46
Cr_2O_3	0.038	0.054	0.047	0.034	0.070	0.066	0.047	0.031	0.047	0.039	0.057
FeO	15.21	15.32	15.00	15.81	13.07	14.55	15.80	16.00	15.71	15.88	14.83
MnO	0.267	0.260	0.256	0.279	0.221	0.249	0.269	0.289	0.281	0.287	0.254
MgO	43.74	43.28	43.39	43.18	45.09	43.93	42.55	42.56	43.24	43.29	44.41
CaO	0.305	0.295	0.273	0.323	0.257	0.269	0.306	0.329	0.322	0.299	0.273
NiO	0.232	0.235	0.275	0.211	0.358	0.270	0.251	0.225	0.230	0.234	0.290
Sum	99.42	98.88	98.57	99.11	98.74	98.69	98.41	98.49	99.00	99.36	99.57
Fo	83.7	83.5	83.8	83.0	86.0	84.3	82.8	82.6	83.1	82.9	84.2

Sample	SU 18II	SU 18II	SU 18II	SU 18II	SU 18II	SU 18II	SU 18II	SU 18II	SU 18II	SU 18II	SU 18II
Olivine	13	14	15	16	17	18	19	20	21	22	23
SiO_2	39.46	39.62	39.41	39.26	39.39	39.79	39.24	39.20	40.07	39.42	39.59
Cr_2O_3	0.050	0.060	0.038	0.050	0.051	0.039	0.047	0.042	0.073	0.037	0.063
FeO	15.06	14.95	15.92	15.68	14.42	15.14	15.00	15.31	12.44	15.61	14.04
MnO	0.261	0.236	0.278	0.288	0.232	0.257	0.263	0.270	0.200	0.269	0.226
MgO	43.88	44.52	42.89	43.33	44.52	44.02	43.84	43.09	46.30	43.45	45.23
CaO	0.273	0.269	0.308	0.311	0.277	0.297	0.295	0.311	0.263	0.306	0.264
NiO	0.261	0.266	0.219	0.237	0.275	0.235	0.247	0.239	0.352	0.228	0.347
Sum	99.25	99.92	99.06	99.16	99.17	99.78	98.93	98.46	99.70	99.32	99.76
Fo	83.9	84.1	82.7	83.1	84.6	83.8	83.9	83.4	86.9	83.2	85.2

Sample	SU 18II	SU 18II
Olivine	24	25
SiO_2	39.16	39.63
Cr_2O_3	0.032	0.070
FeO	15.70	13.44
MnO	0.280	0.229
MgO	43.20	45.33
CaO	0.306	0.269
NiO	0.228	0.337
Sum	98.91	99.31
Fo	83.1	85.7